Reductie van golfoverslag door en golfkrachten op stormmuurtjes en promenades bovenaan gladde dijken. Een experimenteel onderzoek

Reduction of Wave Overtopping by and Wave-Induced Forces on Storm Walls and Promenades at Crest Level of Smooth Dikes. An Experimental Study

Koen Van Doorslaer

Promotoren: prof. dr. ir. A. Kortenhaus, em. prof. dr. ir. J. De Rouck
Proefschrift ingediend tot het behalen van de graad van
Doctor in de ingenieurswetenschappen: bouwkunde

UNIVERSITEIT GENT

Vakgroep Civiele Techniek
Voorzitter: prof. dr. ir. P. Troch
Faculteit Ingenieurswetenschappen en Architectuur
Academiejaar 2018 - 2019

ISBN 978-94-6355-190-8
NUR 956
Wettelijk depot: D/2018/10.500/108

Examination board

Supervisors:

em. prof. Julien De Rouck

prof. Andreas Kortenhaus

Coastal Engineering Research Group
Department of Civil Engineering
Faculty of Engineering and Architecture
Ghent University
Technologiepark 904
9052 Zwijnaarde, Belgium

Voting members:

em. prof. Luc Taerwe (chairman)	Ghent University
prof. Peter Troch (secretary)	Ghent University
prof. Mia Loccufier	Ghent University
prof. Leopoldo Franco	Uni Roma Tre (Italy)
prof. Jentsje van der Meer	Unesco-IHE Delft (The Netherlands)
dr. ir. Corrado Altomare	Ghent University
dr. ir. Hadewych Verhaeghe	Afdeling Maritieme Toegang (Belgium)

Acknowledgements

Over the past few years, I've spent more days at the seaside during a winter storm than in summertime enjoying a sunny day off. This has two reasons. First of all, as a coastal engineer I am just attracted by and interested in wave-structure interaction. It has something appealing to me, that partly scares me but even more attracts me and I want to know all about. The second reason is that during those summer holidays I was mostly behind my computer writing this manuscript, next to my fulltime employment at the DEME group. This combination has been really hard and stressful at times, but on the other hand also challenging and enriching. Now that I successfully reached this milestone, there is a few people that I want to thank gratefully since they have been there for me, each in their own way, but all indispensable.

The first person to express my gratitude is my promotor and also my mentor **Julien De Rouck**. My first steps as a coastal engineer were taken in your team and my interest in this field has grown under your guidance. You were my first boss, always busy but your door was always open for me. We had intense and interesting discussions on wave flume tests but after every weekend you started our Monday morning conversation about how my game of football over the past weekend had been. Much appreciated! Also after your retirement from University, as Emeritus Professor, you were there to answer every phone call or read my draft manuscripts to come back with very helpful guidance. Thanks for this! I know you had to wait a bit longer than expected to finish as a promotor of your final student, thanks for your patience! Your help in the last stressful weeks has been amazing.

Also my second promotor, professor **Andreas Kortenhaus** has meant a lot to me during the writing process of this manuscript. You pushed me to higher limits, I admire your very sharp view on data analysis. You brought more structure in my work, which is appreciated.

Professor **Peter Troch** was not directly involved in my PhD, but nevertheless I'd like to mention him in this word of thanks. Peter, you have made it possible for me to stay connected to university, by offering me the possibility to guide master thesis students and asking for input for new topics. I hope that we can continue this collaboration or even increase it in the near future.

Next, I'd like to thank my ex-colleagues and the current group of PhD students at the Coastal Engineering group of Ghent University. They showed a great interest for my topic, motivated me and shared their past struggles and positive experiences. Mainly the recently graduated doctors **David, Tim and Brecht**, thanks guys. We'll see each other at future coastal conferences! Also thanks to **Lien** and **Ellen** for the administrative support, during my years at AWW but also afterwards.

The technical staff – **Herman, Tom, Sam, Dave** – have been of major importance throughout my years at university for their never-ending help, but also for feeling me very welcome whenever I came back to their working spot to say hello after I left University. Sam, Dave, thanks for the many models you've built for me and operating so many tests. Herman, likewise, but an extra thanks for sharing an office for over 3 years and the many words of advice on life you've given me. Tom, one more word of thanks especially for you. Without your programming skills, I'd still be stuck with manual data-analysis until forever. A major thanks for the code you've written that made this process a little easier! Good luck to all, also with operating the new Coastal Basin in Ostend!

This work could not have been possible without the help of my thesis students on this topic. **Tobias & Gilles and Sarah & Valerie** have carried out a part of the data that was gathered for this PhD manuscript. Thanks for the hard work during your final year and for the fruitful discussions.

Also people outside Ghent University deserve to be in these acknowledgements. **Corrado Altomare**, my friend. Thanks for nice times we had in the many countries we have visited together, both work related and trips as friends. You are one of the few people that understand why I spend some hot summer days or Saturday nights behind my computer writing, since we share the same passion. Thanks for the insight on numerical models and for the many many discussions on overtopping! Good luck in Barcelona, and see you soon there ;-)

Also a word of thanks to **Jasper Vergaelen** (DEME) to help me improve some of the figures in this book. To my previous and current bosses at DEME, **Luc Van der Keere, Dirk Defloor, Marc Van Den Broeck** and also my previous boss who sadly passed away, **Martin Ockier**: thank you for always supporting me. Thank you for allowing me to take some long holidays or unpaid leave to work on this PhD manuscript. Your support and understanding has ment a lot to me.

Thanks to **Jentsje van der Meer** for providing me with the Harlingen dataset. I admire your passion and enjoy the nice discussions we have on wave overtopping. I'm looking forward for future collaborations and possibly working together on EurOtop live? :-)

The final professional colleagues to thank are the people in Rome, starting with **Alessandro Romano**. I especially went to Rome a few times to collaborate with you on the data analysis for the wave impacts. I'm grateful to have worked together with such a talented (your MATLAB skills are amazing!) and motivated young researcher. Also thank you **Giorgio Bellotti** and **Leopoldo Franco** for hosting me in Rome, for the dinners and the game of tennis.

Next to thanking my professional supporters, now is the time to thank my **family and friends**. To my **friends** I can (finally) answer your annoying question 'is your PhD still not yet ready?' with: Yes, it is finally ready! It took me a little longer since I didn't want to miss out on all the fun you were having in the meantime, but it was totally worth it!

To my **family** – with an extra major gratefulness to my sister and my mother – thank you for the past 34 years. Thanks for always believing in me, thanks for helping me through my bad days and for supporting me on my good days. The motivational messages in these last moths and weeks helped a lot in reaching my deadlines. Thanks for showing interest in what has occupied lots of my time for the past few years. I love you!

Zwijnaarde, December 2018

Koen Van Doorslaer

Table of contents

List of definitions used in this work

Dike	A dike is defined as a coastal defense structure with a slope on the seaward side and a promenade on top (see below). Whether this structure has a small or a wide crest, a landward slope or not, is of no importance in this work.
Dike slope	The dike slope is the seaward part of the dike between the toe of the structure and the crest of the structure, which is characterized by a slope angle α.
Smooth dike	A smooth dike is a dike where the seaward slope is covered with grass, concrete, pavement or other material which does not reduce the wave run-up due to roughness. For such structures, the reduction factor for the roughness γ_f is 1.
Crest	The crest is defined as the edge where the dike slope turns into a (quasi-)horizontal promenade. In the current research, the crest of the dike is located above the Still Water Level. Often the word crest is also used for whole upper part of the dike, however in this work the word "promenade" is used for that.
Promenade	A promenade is a (quasi-)horizontal area starting at the dike crest, by definition above the Still Water Level.
Promenade width	The promenade width is the horizontal distance between the top of the dike slope and the location where the overtopping is measured. This latter can be the geometrical end of the promenade, or at a storm wall if present on the promenade. In this case, the promenade width used for calculations can be smaller than the actual promenade. It is indicated in this work as G_c.
Berm	A berm is defined as a (quasi) horizontal part in between two seaward sloping parts of the dike, the lower or downward slope and the upper slope. A berm is often located near the SWL where it provides an optimal performance in reducing overtopping. When no berm is present, the reduction factor for berms γ_b becomes 1. In the new datasets presented in this work (UGent-1, UGent-2, Hydralab and GWK) no berms but promenades are present. In the existing dataset (Harlingen) a berm is present.

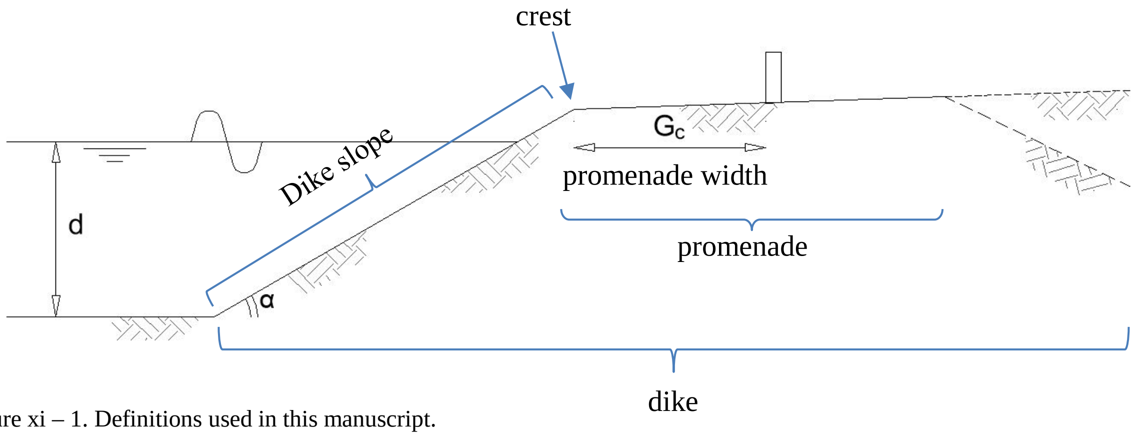

Figure xi – 1. Definitions used in this manuscript.

List of symbols

a	-	An empirical coefficient in the overtopping equation Eq. [2-19] from EurOtop (2016). Intersection with the Y-axis
A_c	[m]	Seaward freeboard. The vertical distance between the water level and the seaward crest of the dike. A_c was defined for rubble mound structures as the “armour freeboard” but is here linked to the seaward crest of the dike. $R_c = A_c + G_c \cdot \tan(\text{promenade slope}) + h_{wall}$
a_F	-	An empirical coefficient in the force equation Eq. [6-3]. Intersection with Y-axis
A_q	-	An empirical coefficient in the overtopping equation Eq. [2-10] from TAW (2002) and EurOtop (2007). Intersection with Y-axis
b	-	An empirical coefficient in the overtopping eqation Eq. [2-19] from EurOtop (2016). Slope of the trend-line
B	[m]	Berm width in between a lower slope and an upper slope, see EurOtop (2016)
b_F	-	An empirical coefficient in the force equation Eq. [6-3]. Slope of the trendline
b_{Owen}	-	An empirical coefficient in the overtopping equation by Owen (1980) Eq. [2-4]. Slope of the data in a semi-logarithmic plot
b'_{Owen}	-	An empirical coefficient in the overtopping equation by Owen (1980). $b'_{Owen} = b_{Owen} \cdot \sqrt{\frac{s_{0m}}{2\pi}}$
B_q	-	An empirical coefficient in the overtopping equation Eq. [2-10] from TAW (2002) and EurOtop (2007). Slope of the trend-line
b_1, b_2, b_3	[m]	The width of the 3 recording plates in the GWK experiments as defined in Figure 6-29
c	-	An empirical coefficient in the overtopping eqation Eq. [2-19] from EurOtop (2016). Power of the exponential function.
C_1	-	An empirical coefficient in Eq. [2-62]
C_5	-	An empirical coefficient in Eq. [2-63]
$c^*_{A,h}$	-	An empirical coefficient to quantify the flow depth in the run-up zone (zone A of Figure 2-12), Eq. [2-32]
$c^*_{A,U}$	-	An empirical coefficient to quantify the flow velocity in the run-up zone (zone A of Figure 2-12), Eq. [2-33]
$c^*_{C,h}$	-	An empirical coefficient to quantify the flow depth on the promenade/crest (zone C of Figure 2-12), Eq. [2-34]
$c^*_{C,U}$	-	An experimental coefficient to quantify the flow velocity on the promenade/crest (zone C of Figure 2-12), Eq. [2-35]
d	[m]	Water depth at the toe of the structure
d_b	[m]	The height of water level above the berm ($d_b > 0$) or below the berm ($d_b < 0$)

d_{br}	[m]	The breaker depth by SPM (1977), Figure 2-21
d_{B0}	[m]	Flow depth measured on the promenade with a storm wall in Eq. [2-64]
d_0	[m]	Flow depth at the beginning of the crest in Eq. [2-62]
f	-	Friction coefficient of the crest (f = 0.01 according to Schüttrumpf & van Gent (2003)
f’	-	Friction coefficient of the crest (f’ = 1 according to Bosman et al. (2008))
F	[N/m]	Impact force, peak value of the force recording over time of one impact
F_{dim}	[N/m]	Dimensionless individual impact $F_{dim} = F/(\rho \cdot g \cdot R_c^2)$
F_{dyn}		Dynamic impact, the first narrow peak in a force recording over time
F_h	[N/m]	The horizontal force measured on a structure. If the subscript ‘h’ is left out, also the horizontal force is ment
F_{H_GWK}	[N/m]	The total force on the horizontal recording plate in the GWK tests. $F_{H\_GWK} = F_{H1}+F_{H2}+F_{H3}$ with F_{H1}, F_{H2} and F_{H3} the total force of the 3 individual horizontal plates as defined in Figure 6-29
F_{max}	[N/m]	The maximum recorded impact over a test
F_{mean}	[N/m]	The mean value of all forces during a test, related to the number of overtopped waves. F_{mean} is calculated as the mean value from impact 1 to ‘impact’ number N_{ow}, with zero values for the numbers N_{im} to N_{ow}
F_{qs}	[N/m]	Quasi static impact, the second peak in a force recording over time
Fr	-	Froude number
F_v	[N/m]	The vertical force measured on a structure. The subscript ‘v’ always is mentioned when a vertical measured force is ment
F_{V_GWK}	[N/m]	The total force on a vertical recording plate in the GWK tests. $F_{V\_GWK} = (F_{V1}+F_{V2}+F_{V3}+F_{V4})/b_3$ with F_{V1}, F_{V2}, F_{V3} and F_{V4} the total force of the 4 individual sensors as defined in Figure 6-29
$F_{1/250}$	[N/m]	The average force value of the highest 1/250th of the total number of incoming waves in one test
$F_{x\%}$	[N/m]	The force value that is exceeded by x percentage of the waves
$F_{x/y}$	[N/m]	The average value of the highest x/y impacts, where x/y represents the noted fraction of the incoming waves
f(β)	-	A function of the dike slope and needs to be determined empirically in Eq. [2-62] by Chen et al. (2015).
$(Fr)_p$	-	Froude number in prototype dimensions
$(Fr)_m$	-	Froude number in model dimensions
g	[m/s²]	Gravity acceleration = 9.81m/s^2
G_c	[m]	Promenade width for dikes
h	[m]	Flow depth on the promenade. h = h_{max}, the peak of the flow depth recording of one individual bore
$h_{A,2\%}$	[m]	The flow depth in the run-up zone (zone A of Figure 2-12) exceeded by 2% of the incident waves

h_b	[m]	the depth of the toe of the wall below the SWL in Figure 2-16 by Den Heijer (1998). h_b is measured positive downward ($h_b > 0$ when toe of wall is below SWL, $h_b < 0$ when toe of wall is above SWL)
H_b	[m]	The wave breaker height by SPM (1977), Figure 2-21
h_c	[m]	The height of the wave crest, which is 0.78 H_b by SPM (1977), Figure 2-21
$h_{C,2\%}$	[m]	The flow depth on the promenade/crest (zone C of Figure 2-12) exceeded by 2% of the incident waves
$h_{front\ wall}$	[m]	Height of the seaward wall in a stilling wave basin
h_{max}	[m]	Maximum value of the flow depth in one *bore*, see Figure 2-11. In this manuscript further noted as h
h_{MAX}	[m]	Maximum value of all flow depths h in one *test*. Only the clear signals have been analyzed, so it is possible that h_{MAX} is not the actual maximum value that occurred during a test, but it's the maximum value of all analyzed values
H_{m0}	[m]	Spectral wave period at the toe of the structure
h_n	[m]	Height of the bullnose, see Figure 3-5
H_s	[m]	Significant wave height at the toe of the structure = $H_{1/3}$
h_{wall}	[m]	Height of the storm wall
h'	[m]	Flow depth of the water mass at the structure by SPM (1977), Figure 2-21
$H_{1/3}$	[m]	Significant wave height at the toe of the structure = H_s
i	-	The rank number of impacts, ordered from the highest to the lowest
k	-	Ratio of overtopping discharge over a structure with recurve wall to a structure without recurve wall, by Kortenhaus et al. (2003)
K_o	-	A proportionality constant in Eq. [2-62]
K_p	-	Reduction factor to account for slope porosity in Eq. [2-62] (K_p = 1 for impermeable slopes).
L	[m]	Length
L_{berm}	[m]	The horizontal distance from 1 wave height below the berm to 1 wave height above the berm
L_{0m}	[m]	Deep water wave length, calculated with the mean wave period T_m. $L_{0m} = \frac{g \cdot T_m^2}{2\pi}$
$L_{m-1,0}$	[m]	Deep water wave length, calculated with the spectral wave period $T_{m-1,0}$. $L_{m-1,0} = \frac{g \cdot T_{m-1,0}^2}{2\pi}$
L_{reg}	[m]	Local wave length (regular waves) at the dike toe in Eq. [2-63]
L_{0p}	[m]	Deep water wave length, calculated with the peak wave period T_p $L_{0p} = \frac{g \cdot T_p^2}{2\pi}$
M_{Fov}	[N/m]	Overtopping momentum flux

N_{im}	-	Number of impacts higher than the threshold value, Eq. [6-13]
N_L	[m]	Length of the bullnose by Coeveld et al. (2006)
N_{ow}	-	Number of overtopping waves over the dike crest A_c ($x_C = 0$). N_{ow} is calculated by multiplying the number of waves (N_w) by the probability of overtopping (P_{ov})
N_w	-	Number of waves in a storm/test
P_{int_rect}	[N/m]	The integrated pressure over the height by means of rectangular integration (Eq. [6-1])
P_{int_trap}	[N/m]	The integrated pressure over the height by means of trapezoidal integration (Eq. [6-2])
P_{ov}	-	The probability of an individual overtopping volume V_i to exceed a particular volume V. $P_{ov} = P[V_{ind}>V]$. P_{ov} is linked to the distribution of overtopping volumes (Eq. [2-45]) or to the distributions of impacts (Eq. [6-5])
q	[m³/m/s]	Average overtopping discharge
q_{crest}	[m³/m/s]	Wave overtopping discharge at the top of the dike slope, at the transition with the promenade. Measured at $x_C = 0$
$q_{effective}$	[m³/m/s]	Actual wave overtopping discharge at the required location
q_{ind}	[m³/m/s]	Individual discharge volume on the crest of the dike. $q_{ind} = U_{max} \cdot h_{max} = U \cdot h$
Q_{teo}	-	A theoretical generated normalized force based on estimated PDF-parameters, Figure 6-41. Normalized by dividing through the test-average force value
Q_{emp}	-	The measured force normalized by dividing through the test-average force value, Figure 6-41
Q^*	-	Dimensionless overtopping discharge according to TAW (2002), EurOtop (2007) and EurOtop (2016)
Q_*	-	Dimensionless overtopping discharge according to Owen (1980) Eq. [2-4]
Q'	-	Ratio of overtopping discharge over a rubble mound breakwater with parapet on the crown wall, to a crown wall without parapet, by Coeveld et al. (2006)
Q_0	-	An empirical coefficient in Eq. [2-4] by Owen (1980). Intersection with Y-axis.
Q_0'	-	An empirical coefficient. $Q_0' = Q_0 \cdot \sqrt{\frac{2\pi}{s_{0m}}}$
r_B	-	A factor for the width of the berm in Eq. [2-26]
R_c	[m]	Freeboard. The vertical distance between the water level and the landward highest point of the structure, the point where the water can no longer flow back to the sea. $R_c = A_c + G_c \cdot \tan(\text{promenade}) + h_{wall}$
r_{db}	-	A factor for the height of the berm in Eq. [2-26]
Re	-	Reynolds number
R_d	[N/m]	Dynamic force component in Eq. [2-67] (SPM, 1977), Figure 2-21

R_s	[N/m]	Static force component in Eq. [2-67] (SPM, 1977), Figure 2-21
R_t	[N/m]	Total impact force in Eq. [2-67] (SPM, 1977), Figure 2-21
$R_{u2\%}$	[m]	The calculated run-up height exceeded by 2% of the incident waves
R^*	-	Dimensionless freeboard according to TAW (2002), EurOtop (2007) and EurOtop (2016)
R_*	-	Dimensionless freeboard according to Owen (1980) Eq. [2-4]
s_{0m}	-	Wave steepness, calcultated with the mean wave period T_m. $s_{0m} = \frac{H_{m0}}{L_{0m}}$
s_{0p}	-	Wave steepness, calcultated with the peak wave period T_p. $s_{0p} = \frac{H_{m0}}{L_{0p}}$
$s_{m-1,0}$	-	Wave steepness, calcultated with the spectral wave period $T_{m-1,0}$. $s_{m-1,0} = \frac{H_{m0}}{L_{m-1,0}}$
T_m	[s]	Average wave period
$T_{m-1,0}$	[s]	Spectral wave period
T_p	[s]	Peak wave period related to the peak frequency of the wave spectrum
U	[m/s]	Flow velocity on the promenade/crest. $U = U_{max}$, the peak of the velocity recording of one individual bore
$U_{A,2\%}$	[m/s]	Wave run-up velocity in the run-up zone (zone A of Figure 2-12) exceeded by 2% of the incident waves
$U_{C,2\%}$	[m/s]	Wave run-up velocity on the promenade/crest (zone C of Figure 2-12) exceeded by 2% of the incident waves
U_{max}	[m/s]	Maximum value of the flow velocity in one *bore*, see Figure 2-11. In this manuscript further noted as U
U_{MAX}	[m/s]	Maximum value of all flow velocities U in one *test*. Only the clear signals have been analyzed, so it is possible that U_{MAX} is not the actual maximum value that occurred during a test, but it's the maximum value from all analyzed values
V	[m³]	Volume
V_{ind}	[m³/m]	Individual overtopped volume on the crest of the dike
v'	[m/s]	Velocity of the water mass at the structure by SPM (1977), Figure 2-21
W	[m]	The wall height defined by Tuan (2013), similar as h_{wall} which is the preferred parameter definition in this manuscript
x_A	[m]	The intersection of the seaward slope and the SWL. Start of the horizontal axis in the run-up zone (zone A of Figure 2-12)
x_C	[m]	Location on the promenade/crest (zone C of Figure 2-12), starting with $x_C = 0$ at the top of the dike slope = the start of the promenade/crest

x_Z	[m]	The horizontal distance between the location of interest and x_A (Figure 2-12)
z_A	[m]	The position on the seaward slope with respect to the SWL (Figure 2-12)
x_1	[m]	The horizontal distance from the still water line to the structure, by SPM (1977), Figure 2-21
x_2	[m]	The horizontal distance from the still water line to the limit of wave uprush, simplified as $2H_b\cot(\alpha)$ with α the foreshore slope (SPM, 1977), Figure 2-21
α	°	Slope angle of the dike
α_{avg}	-	Average slope slope angle to calculate the breaker parameter $\xi_{m-1,0}$ or ξ_{0p}
α_{wall}	-	Representing slope angle when a vertical wall is schematized by a slope, approach by EurOtop (2007) to account for the effect of a wave wall, Eq. [2-22]
γ	-	Reduction factor for wave overtopping
γ_b	-	Reduction factor for the influence of a berm
γ_f	-	Reduction factor for the influence of the roughness of the seaward slope of the dike
γ_{prom}	-	Reduction factor for the influence of a promenade at crest level
γ_{prom_v}	-	Reduction factor for the combined influence of a promenade and a storm wall at crest level
γ_s	-	Reduction factor for the influence of a small promenade before the wave wall according to Tuan (2013)
γ_{s0}	-	Reduction factor for the influence of wave steepness related to a bullnose
γ_v	-	Reduction factor for the influence of a vertical wall at the crest of the dike
γ_w	-	Reduction factor for the influence of a wave wall according to Tuan (2013)
γ_{ws}	-	Reduction factor for the influence of a wave wall at the end of a small promenade according to Tuan (2013) $\gamma_{ws} = \gamma_w \cdot \gamma_s$
γ_β	-	Reduction factor for the influence of oblique wave attack
γ_ε	-	Reduction factor for the influence of bullnose angle ε
γ_λ	-	Reduction factor for the influence of bullnose height ratio λ
ε	°	Angle of the bullnose, see Figure 3-5
κ_F	-	The shape parameter of a Weibull distribution of impact forces (Eq. [6-5])
κ_V	-	The shape parameter of a Weibull distribution of individual overtopping volumes (Eq. [2-45])
λ	-	Height ration of the bullnose to the wall height h_n/h_{wall}, see Figure 3-5

λ_F	-	The scale parameter of a Weibull distribution of impact forces (Eq. [6-5])
λ_V	-	The scale parameter of a Weibull distribution of individual overtopping volumes (Eq. [2-45])
λ_1	-	Experimental coefficient in Eq. [2-63]
μ	-	Average value of a normally distributed stochastic function
μ'	[Pa·s]	Dynamic viscosity
ν	[m²/s]	Kinematic viscosity (ν_{water}(20°C) = 1.10^{-6} m²/s)
ρ	[kg/m³]	Density
σ	-	Standard deviation
σ'	-	Relative standard deviation $\sigma' = \sigma/\mu$
$\xi_{m-1,0}$	-	The wave breaker parameter based on the spectral wave period $T_{m-1,0}$
ξ_{0p}	-	The wave breaker parameter based on the peak wave period T_p

List of abbreviations

ABPH	Honeywell pressure sensor
ADV	Acoustic Doppler Velocimeter
ANN	Artificial Neural Network
BIV	Bubble Image Velocimetry
CFD	Computational Fluid Dynamics
CIEM	Canal d'Investigació I Experimentació Marítima, the large wave flume at UPC, Barcelona
CLASH	Crest Level Assessment of coastal Structures by full scale monitoring, neural network prediction and Hazard analysis on permissible wave overtopping
DWL	Design Water Level (= Still Water Level)
EMF	Electromagnetic flow meter
GWK	Grosser WellenKanal, the large wave flume in Hannover, Germany
ICSP	Integrated Coastal Safety Plan
IPCC	Intergovernmental Panel on Climate Change
LIM	Laboratori d'Inginyeria Marítima. The laboratory at UPC where CIEM is located
NS	Navier Stokes
OVT	overtopping tank
PDF	Probability Distribution Function
PDCR	Druck/GE pressure sensor
PVC	Polyvinyl Chloride, a synthetic plastic polymer
SLR	Sea Level Rise
SPH	Smoothed Particle Hydrodynamics
SSP	Storm Surge Protection walls
SWASH	Simulating WAves till SHore (numerical model)
SWB	Stilling Wave Basin
SWL	Still Water Level (= Design Water Level)
UPC	Universitat Politècnica de Catalunya. The technical university in Barcelona, Spain
VOF	Volume Of Fluid

Summary

Low elevation coastal zones are under pressure of a rising sea level and increasing intensity of super storms on the one hand, and a population growth and enormous economic attraction on the other. The risk (probability times consequences) of a coastal disaster is thereby also increasing. Dike breaches or flooding due to wave overtopping are such possible disasters. Belgium is (or better, was) a textbook example of a country facing such a risk. Low elevated coastal dikes, highly populated coastal towns and limited space in height or width of the dikes to increase the safety level. In Belgium, this was resolved by a combination of beach nourishments and integrating crest modifications into the dike and/or installing (removable) storm walls on the promenade at crest level of the dike. In this PhD manuscript an extended database was set up and empirical formulae have been developed that allow for the design of crest modifications such as a storm wall with/without bullnose, a promenade, a promenade with storm wall with/without bullnose and a stilling wave basin.

Based on this practical coastal engineering application, three objectives were set in this work. A **first objective** was to determine the **overtopping reducing capacity** of each of the proposed geometrical crest modifications, and to develop new prediction formulae. A **second objective** was specified to geometries that have a promenade at crest level. The wave that overtops the dike travels over the promenade as a bore. It was the goal to study the **flow parameters** (flow depth and flow velocity) of this bore since they are dominant parameters in the physical process between wave overtopping and a wave-induced impact on a storm wall at the end of such a promenade. The **final goal** set in this work, was to study the **wave induced forces** to provide input for the structural design of the proposed overtopping reducing measures. How do forces need to be measured, how does the impact signal look like, what is the wave-induced force and how can it be linked to hydraulic conditions or flow parameters? These questions were answered in this PhD manuscript. The research is mainly specified on non-breaking waves, with intermediate to deep water in front of the dike.

First an **extended literature review** was performed on the three main topics (reduction of overtopping, overtopping flow parameters and wave-induced impacts). **Reduction of wave overtopping** is expressed by means of a reduction factor γ. This factor was analyzed here based on the overtopping equations as mentioned in EurOtop (2007). It was proven however that the developed reduction factors can also be used in the updated overtopping equations in EurOtop (2016). Quite some research has been performed in the past on overtopping reducing crest modifications, but few general methodologies have been developed from it. Most provide a reduction for a specific case study, without general formulae. For the existing formulae, the range of application was not ideal for the dikes studied in this manuscript, which was later confirmed by comparative data plots. The literature review on **overtopping flow parameters** showed a general trend, an exponential decay of the flow depth and the flow velocity over the width of the promenade/crest, but the empirical coefficients show a wide variation. Finally, for **wave-induced forces** the available information was mainly specified to vertical caisson breakwaters or rubble mound breakwaters with crown walls, which was proven later in this PhD as not to be useful for the geometries studied in this work: a smooth dike with promenade and storm wall. Recently, new information on similar geometries became available by Chen (2016) and Streicher et al. (2018). They work with (ver.) shallow foreshores and thereby broken waves, also their work is not yet finalized.

It was thereby decided to perform new research. Due to the new topics and specific geometries being studied in this PhD, it was not possible to work with numerical models or ANN (Artificial Neural Network) since both require validation/calibration before giving a reliable outcome. Therefore, in this work, **extensive experimental modelling** was carried out. A database of over 1100 new tests was set

up, spread over four different test campaigns in three different European laboratories, each working at a different scale:

- UGent-1 (overtopping and impacts, non-breaking waves)
- UGent-2 (overtopping, breaking waves)
- Hydralab (impacts, non-breaking waves)
- GWK (overtopping flow, impacts, non-breaking waves)

Also a fifth dataset, the existing Harlingen dataset, was reanalyzed to have a complete overview of the influence of a vertical wall on a dike to average overtopping discharges. This analysis has led to a flowchart how to calculate wave overtopping over a dike with vertical wall, presented in Figure 4-26 in this manuscript. For the cases with SWL above the foot of the vertical wall ($h_{wall}/R_c > 1$) the old procedure presented in EurOtop (2007) can be followed. For hydraulic situations with SWL below the storm wall, **two new reduction factors were presented to calculate wave overtopping on dikes with a storm wall**, caused by **breaking and non-breaking waves** respectively.

Based on the UGent-1 database (non-breaking waves), a **reduction factor γ** has also been presented for the **other overtopping reducing geometries at crest level of the dike**. The chapter on the reduction of wave overtopping contains a case study on all proposed reduction measures, where overtopping is calculated for three different wave heights. This exercise showed that the amount of reduction depends on the geometry and the hydraulic conditions, but reduction factors of 1.5 to very large numbers (factor 800) have been obtained.

To meet the second objective, **overtopping flow parameters** were measured in the (large scale) GWK test campaign. The flow parameters were measured on a promenade with storm wall at its end. The flow dephts were measured by means of a digital step gauge, and the flow velocities were determined by the time interval needed for a bore to travel in between two measured locations. By means of this discrete method, the maximum depth value and maximum velocity value were determined per overtopped wave (also known as 'bore'). Overtopping flow induced impacts on the storm wall gave reflection, leading to a bore travelling in the opposite direction which interfered with next incoming overtopping flows. No seperation method exists yet, so a manual analysis was required and only clear incoming waves were selected for analysis. The analysis showed that it was recommended not to measure in the beginning of the promenade, since there is a transition zone between the uprushing flow on the slope and the horizontal flow on the promenade where free surface irregularities and air entrainment disturbed good measurements. Also the middle of the promenade was no good measurement location, since too much interaction between incoming and reflected bores (after an impact) was noticed. The measurements for this work that were maintained for further analysis were carried out at 80% of the promenade length, **closest to the wall, showing to be the best possible measurement location**.

Besides some obvious trends (higher waves or smaller crest freeboard leads to increased flow parameters) and a low correlated trend between the flow parameters themselves, data plots did not provide extra information. A link with incoming overtopping volumes on the one hand, and with impact forces on the other hand, was investigated in the chapter on wave impacts.

In this chapter, first the wave impact recordings were studied. This showed that the force recording in the smallest scale tests (UGent-1) were influenced by resonance, and a low-pass filtering of about half of the structure's eigenfrequency had to be carried out to obtain more reliable result. The medium (Hydralab) and large scale (GWK) tests were not influenced by resonance. All impacts in a test were shown to be best represented by a Weibull Probability Distribution Function. The highest impacts of the distribution had a **church-roof shape**, charachterized by a first high dynamic peak value (short duration) and a second lower quasi-static peak value (longer duration). The lower impacts often showed a twin-peak shape, where both peaks had a similar magnitude. The higher peaks in the distribution –

with church-roof shape - determine $F_{1/250}$. The value $F_{1/250}$, based on the approach by Goda (1985), is the average force value of the highest $1/250^{th}$ of the number of incoming waves, and was proposed in this work as design value. Different ways to make the force dimensionless have been studied, and the best way showed to be by dividing F through $\rho g R_c^2$, where ρ is the mass density of the water, g the gravity acceleration and R_c the landward freeboard including the height of the stom wall. This was supported by available data and in line with findings by Pedersen (1996).

The main geometry to study the forces was 'a storm wall at the end of a promenade at crest level of a smooth dike'. New methodologies have been proposed to calculate wave induced forces on the storm wall. A first approach was defined where the **forces were linked to incoming wave parameters**. Approach 1a proposed an exponential relationship between the dimensionless impact force $F_{1/250}/\rho g R_c^2$ and the dimensionless freeboard R_c/H_{m0}. In approach 1b, the hydraulic parameters R_c and H_{m0} were used to determine the **shape and scale parameters of a Weibull force distribution**, from which the low exceedance value $F_{1/250}$ could be calculated. The second approach followed the steps of the physical process, by linking the (theoretically calculated) individual overtopping volumes to the measured flow parameters after which the **flow parameters were linked to the measured impact forces**. This approach 2 also allowed predicting a full distribution of impact forces, from which the low exceedance value $F_{1/250}$ could be calculated. A flowchart of the full procedure was given for each of the different approaches, from which it's clear that approach 1a is the preferred one. The different approaches were also compared to each other in a case study.

Besides the geometry of a smooth dike with promenade and storm wall, forces were also measured for the other geometries with a storm wall. The preferred approach, approach 1a, was worked out for all these geometries, and different empirical coefficients to the same exponential prediction formulae were presented. A comparison between the different geometries was also given in the case study.

At the end of this PhD manuscript a summary was given and some recommendations for future research on this topic. For wave overtopping, the advise for breaking waves on a smooth dike with a storm wall at crest level was based on little research and deserves more data for a more detailed investigation. For overtopping flows, a better method of analyzing and seperating incoming and reflected flow parameters is required, and it seems evident to study this in a numerical model. For impact forces, despite a large amount of data was collected and analyzed, new data with a variation in promenade width and wall height would be of interest to study the influence of the promenade width and/or wall height on the impact force. Those new data can be generated through experimental modelling, but also a Neural Network or numerical modelling approach is now feasible, since enough data already exists to train or validate the model.

Samenvatting

Laaggelegen kustzones staan onder druk. Enerzijds vanwege een stijgend zeeniveau en toenemende intensiteit van superstormen, anderzijds vanwege een toenemende aantrekkingskracht als woongebied en haar groot economisch potentieel. Het risico (kans maal gevolg) op een ramp neemt daardoor ook toe. Dergelijk mogelijke rampen zijn bijvoorbeeld dijkbreuken of overstromingen door golfoverslag. De Belgische kust is (of beter, was) een schoolvoorbeeld van een laaggelegen kustzone die blootgesteld staat (stond) aan dergelijk risico: dichtbevolkte kuststeden, relatief lage dijken en geen ruimte in hoogte of breedte om het veiligheidsniveau van de dijken op te trekken. In België is dit probleem opgelost door een combinatie van strandsuppleties en de kruinen van de dijken aan te passen, ingepast in de dijkhelling of door middel van mobiele stormmuurtjes op de promenade van de dijk. In dit doctoraat werd hiervoor een uitgebreide database opgesteld en werden empirische formules afgeleid om dergelijke aangepaste kruinen van dijken mee te ontwerpen. Onder aangepaste dijken verstaan we dijken met stormmuurtje (al dan niet met uitkragend “neusje”), een promenade, een promenade met stormmuurtje (al dan niet met uitkragend “neusje”) en een golfdempende uitbouw.

Gebaseerd op dit praktisch kustwaterbouwkundig vraagstuk werden drie objectieven afgeleid voor dit doctoraat. Een eerste objectief bestond erin de **reducerende capaciteit** van elke voorgestelde **geometrische kruinaanpassing** te bepalen, en een aangepaste rekenmethodiek te ontwikkelen. Een tweede objectief was toegespitst op geometrieën met een promenade bovenaan de dijk. De golf die over de kruin van de dijkhelling slaat, loopt vervolgens over de promenade met een bepaalde laagdikte en laagsnelheid. Het doel bestond erin om deze **laagdikte en -snelheid** te bepalen, omdat deze een dominante rol spelen in het **fysische proces tussen golfoverslag en de uiteindelijke golfimpact** op het stormmuurtje op het einde van zo’n promenade. Het laatste doel in dit doctoraat was het bestuderen van de **golfgeïnduceerde impacten**, om het **structureel ontwerp** van de voorgestelde geometrische maatregelen te kunnen uitvoeren. Hoe moeten golfgeïnduceerde krachten opgemeten worden, hoe ziet het impact signaal eruit, hoe groot is de kracht en hoe kan deze gelinkt worden aan de inkomende golfparameters of laagdikte en laagsnelheid? Deze vragen worden verder in het doctoraat beantwoord. Het onderzoek is vooral toegespitst op niet-brekende golven met relatief diep water aan de teen van de dijk.

Eerst werd een uitgebreid literatuuronderzoek uitgevoerd omtrent de drie grootste thema’s van dit doctoraat: reductie van golfoverslag, laagdikte/laagsnelheid van de overtopte golf, en golfgeïnduceerde krachten. Reductie van golfoverslag wordt uitgedrukt door middel van een invloedsfactor γ. Deze factor werd geanalyseerd middels de golfoverslag formules uit EurOtop (2007). Er werd echter aangetoond dat de ontwikkelde reductiefactoren ook kunnen gebruikt worden in de vernieuwde versie EurOtop (2016) met aangepaste golfoverslag formules. In het verleden is behoorlijk veel onderzoek gevoerd naar golfreducerende maatregelen, maar hieruit zijn weinig algemeen geldende formules of methodes ontwikkeld. Meestal ging het om een specifiek uitgewerkt voorbeeld, en daar waar een formule vermeld was bleek het toepassingsgebied niet in lijn met de geometrieën die in dit doctoraat onderzocht werden. De literatuurstudie over laagdikte en laagsnelheid gaven wel een algemene trend: een exponentieel dalende trend van beide parameters over de lengte van de promenade. Echter, hier gaven de empirische coëfficiënten uit de literatuur een grote variatie aan. Tot slot, voor golfimpacten bleek de beschikbare informatie vooral toepasbaar op verticale caissons in dieper water, of op stortsteengolfbrekers met een kruinmuur. Later in dit doctoraat werd aangetoond dat beiden niet toepasbaar bleken voor de huidige bestudeerde geometrieën (een gladde dijk met promenade en stormuurtje op het einde). Recent kwam nieuwe informatie beschikbaar waarin wel een gelijkaardige geometrie onderzocht was, maar hierbij

werden zeer ondiepe voorlanden beproefd met gebroken golven tot gevolg. Dit is buiten huidig toepassingsgebied, en bovendien betreft het nog lopend onderzoek.

Daarom werd beslist om zelf nieuw onderzoek uit te voeren. Gezien dit doctoraat zich op onbewandelde paden bevindt, was het niet evident om met numerieke modellen of neurale netwerken te werken. Beiden moeten immers gekalibreerd worden op bestaande data om betrouwbare uitkomsten te genereren. Vandaar werd in dit onderzoek **uitgebreid experimenteel onderzoek** uitgevoerd. Een database van **meer dan 1100 proeven** werd uitgevoerd, gespreid over vier verschillende test campagnes, in drie verschillende Europese laboratoria, elk op verschillende schaal:

- UGent-1 (golfoverslag en golfimpacten, niet-brekende golven)
- UGent-2 (golfoverslag, brekende golven)
- Hydralab (golfimpacten, niet-brekende golven)
- GWK (laagdikten en laagsnelheid, golfimpacten, niet-brekende golven)

Ook een vijfde dataset, de reeds bestaande Harlingen dataset, werd opnieuw geanalyseerd om een totaalbeeld te hebben van de invloed van een verticaal muurtje in een dijkhelling op gemiddelde golverslagdebieten. Deze analyse heeft geleid tot een flowchart (figuur 4-25) die aangeeft hoe golfoverslag kan berekend worden. Indien het water boven de voet van het muurtje staat ($h_{wall}/R_c > 1$) kan de oude procedure, zoals beschreven in EurOtop (2007), gevolgd worden. Zodra het muurtje volledig boven water zit, werd een nieuwe procedure voorgesteld, met twee nieuwe formules om de reductiefactor te bepalen, voor respectievelijk brekende en niet-brekende golven.

In de UGent-1 database werden ook andere reducerende geometrieën beproefd, waaruit voor elke geometrie een reductiefactor γ werd afgeleid. Op het einde van het hoofdstuk over de reductie van golfoverslag is een rekenvoorbeeld gegeven waarbij alle voorgestelde geometrieën doorgerekend zijn voor drie verschillende golfhoogtes. Hieruit blijkt dat de reductie in golfoverslag afhangt van de geometrie en de hydraulische randvoorwaarden, maar dat zeer grote reductiefactoren (factor 1.5 tot 800 en hoger) mogelijk zijn.

Voor het tweede luik van dit doctoraat werden laagdikten en laagsnelheiden van de overtopte golf op de promenade gemeten in de grootschalige GWK proeven. De metingen gebeurden telkens met een stormmuurtje op het einde van de promenade. De laagdikte werd gemeten met een digitale stappenbaak, en de laagsnelheid werd gemeten door het tijdsverschil te registreren waarbij de golf voorbij twee gekende punten passeerde. Met deze discrete methode werd telkens de maximum waarde per overtopte golf bepaald. De overtopte golf gaf aanleiding tot een impact op het stormmuurtje, waarna reflectie optrad, en de golf zich in de omgekeerde richting voortplantte en interfereerde met de volgende inkomende golf. Gezien er geen methode bestond om deze inkomende en gereflecteerde watertong van elkaar te scheiden, was een manuele analyse vereist en konden enkel duidelijk geïntentificeerde inkomende overtopte golven gebruikt worden in de analyse. Hieruit bleek ook dat de metingen in het begin van de promenade niet bruikbaar waren vanwege de overgang van een golven op een helling naar een horizontale beweging die met de nodige turbulentie gepaard ging. Ook de metingen in het midden van de promenade bleken niet bruikbaar, omdat daar veel interactie tussen inkomende en gereflecteerde golven werd opgemeten. De meest bruikbare metingen, die verder in dit werk gehanteerd werden, werden opgemeten op 80% van de lengte van de promenade, dichtst bij de muur.

Naast enkele voor de hand liggende relaties (grotere golven of kleinere vrijboorden leiden tot grotere laagdikte en laagsnelheid) en een scatterplot met grote spreiding tussen de laagdikte en de laagsnelheid, leidden deze figuren niet tot bijkomende informatie. Een link tussen de laagparameters en enerzijds de inkomende golfoverslagvolumes en anderzijds de golfkrachten werd in het volgende hoofdstuk onderzocht.

In dit hoofdstuk werd eerst het impact signaal in detail onderzocht. Hieruit werd afgeleid dat de golfkrachten die opgemeten werden in de proeven met kleinste schaal (UGent-1) onderhevig waren aan resonantie. Een lage doorlaat filter met een frequentie half zo groot als de eigenfrequentie van de structuur werd toegepast om een betrouwbaarder resultaat te bekomen. De proeven met middelgrote schaal (Hydralab) en grote schaal (GWK) bleken niet beïnvloed door resonantie. Alle golfkrachten opgemeten in één test bleken het best voorgesteld te kunnen worden middels een Weibull verdeling. De grootste krachten in deze verdeling bleken een typisch "church-roof" signaal te vertonen, waarbij eerst een kortstondige maar hoge piek (dynamische impact) werd geregistreerd, gevolgd door een langere lagere waarde (quasi-statische impact). De lagere krachten in de verdeling toonden eerder een tweetoppig krachtensignaal, waarbij de dynamische en quasi-statische impact van dezelfde grootteorde bleken. Het waren vooral de grootste krachten in de proef – met church-roof profiel – die samen de waarde $F_{1/250}$ bepaalden. $F_{1/250,}$ gebaseerd op het werk van Goda (1985), wordt bepaald door het gemiddelde kracht van de hoogste 1/250ste van het aantal inkomende golven. Deze waarde werd in dit werk vooropgesteld als ontwerpwaarde. Er werden ook verschillende manieren onderzocht om de kracht dimensieloos voor te stellen, en de beste manier hiertoe bleek door de kracht F te delen door $\rho g R_c^2$. Dit werd bewezen met behulp van data en bleek in lijn met literatuur.

Specifiek voor de geometrie met een promenade en een stormmuurtje werden verschillende methodes voorgesteld om de golfgeïnduceerde krachten uit te rekenen. In een eerste methodiek werden de golfkrachten gelinkt aan de inkomende golfparameters. Approach 1a stelde een exponentieel verband vast tussen de dimensieloze impact $F_{1/250}/\rho g R_c^2$ en de dimensieloze vrijboord R_c/H_{m0}. In approach 1b werden de hydraulische parameters R_c en H_{m0} gebruikt om de schaal en vormparameters van de Weibull verdeling van de krachten te bepalen, waaruit opnieuw de waarde $F_{1/250}$ bepaald kon worden. De tweede methode volgde meer het fysische proces: van de (theoretisch bepaalde) golfoverslagvolumes naar de opgemeten laagparameters, waarna deze laagdikte en laagsnelheid aan de opgemeten krachten gelinkt werden. Deze approach 2 liet ook toe om een Weibull verdeling van de krachten te bepalen, en hieruit de waarde $F_{1/250}$ af te leiden. Voor elke methode werd een flowchart opgemaakt, waaruit duidelijk bleek dat approach 1a de voorkeur geniet. De verschillende methodes werden met elkaar vergeleken in een rekenvoorbeeld.

Naast de geometrie met promenade en stormmuurtje werden de krachten ook opgemeten bij de andere geometrieën met een stormmuurtje. De voorkeursmethode, approach 1a, werd voor al deze geometrieën uitgewerkt en verschillende empirische coëfficiënten voor dezelfde exponentiele relatie werden hieruit afgeleid. Een vergelijking tussen alle geometriën werd opgenomen in het rekenvoorbeeld.

Dit doctoraat werd beëindigd met een samenvatting en enkele aanbevelingen voor toekomstig onderzoek. Voor golfoverslag loont het de moeite waard om het advies voor brekende golven op gladde dijken met een stormmuurtje bovenaan de helling te herevalueren op basis van een uitgebreider onderzoek. Voor de laagdikte en laagsnelheden van inkomende golven beter te kunnen scheiden van de gereflecteerde signalen moet een betere manier ontwikkeld worden. Numeriek modelleren lijkt hiervoor de meest geschikte weg. Voor golfkrachten tot slot, ondanks de zeer grote hoeveelheid data die reeds verzameld en geanalyseerd werd, blijkt het nuttig om nieuwe data te verzamelen waarbij een variatie van breedte van de promenade en hoogte van de stormmuurtjes wordt meegenomen, om hun invloed op de impacten in kaart te kunnen brengen. Deze nieuwe data kunnen in experimentele modellen worden bekomen, maar gezien er nu al een grote database bestaat waarop numerieke modellen gevalideerd of neurale netwerken kunnen getraind worden, opent dit deuren voor toekomstig onderzoek in deze omgevingen.

Key words

wave overtopping, sea dike, non-breaking waves, reduction factors, storm wall, bullnose, promenade, overtopping bore, flow depth, flow velocity, wave induced force, pressure.

List of relevant publications

Part of my research for this PhD has been published in journals and conference proceedings. A list of relevant publications is given below:

A1 Journal papers:

Van Doorslaer, K., De Rouck, J., Audenaert, S. and Duquet, V. (2015a). Crest modifications to reduce wave overtopping of non-breaking waves over a smooth dike slope. *Coastal Engineering*, *101*, 69–88. https://doi.org/10.1016/j.coastaleng.2015.02.004

Van Doorslaer, K., Romano, A., De Rouck, J. and Kortenhaus, A. (2017). Impacts on a storm wall caused by non-breaking waves overtopping a smooth dike slope. *Coastal Engineering*, *120*(November 2016), 93–111. https://doi.org/10.1016/j.coastaleng.2016.11.010

UGent master thesis:

Van Doorslaer, K. (2008). *Reduction of wave overtopping over dikes by means of a parapet (in Dutch. Orinal title: Reductie van golfoverslag over dijken door middel van een parapet*. Master thesis. Ghent University.

UGent master thesis, supervised by me:

Audenaert, S. and Duquet, V. (2012). *Wave overtopping over sea dikes and wave impacts on storm walls (In Dutch. Original title: Golfovertopping over zeedijken – krachten op stormmuur)*. Master thesis. Ghent University.

Boderé, T. and Vanhouwe, G. (2010). *Reduction of wave overtopping at smooth dike slopes. A combinaton of a promenade and a storm wall. (In Dutch. Original title: Reductie van golfoverslag bij een gladde dijk: combinatie van een berm en een stormmuur)*. Master thesis. Ghent University.

Conference proceedings

Van Doorslaer, K. and De Rouck, J. (2009a). Innovative crest design to reduce wave overtopping: Parapet and Stilling Wave Basin. In *Book of abstracts "An overview of marine research in Belgium anno 2009", 10th VLIZ Young Scientists' day* (p. 142). Ostend, Belgium.

Van Doorslaer, K., De Rouck, J. and Gysens, S. (2009b). Reduction of wave overtopping: from research to practice. In *Proceedings of the 4th International Short Conference on Applied Coastal Research (SCACR 2009)* (pp. 337–346). Barcelona.

Van Doorslaer, K. and De Rouck, J. (2010a). Reduction of wave overtopping on a smooth dike by means of a parapet. In *Proceedings of the 32nd International Conference on Coastal Engineering (ICCE 2010)*. Shanghai, China.

Van Doorslaer, K., De Rouck, J., Boderé, T., Vanhouwe, G. and Troch, P. (2010b). The influence of a berm and a vertical wall above SWL on the reduction of wave overtopping. In *Proceedings of the 3rd International Conference of the Application of Physical Modelling in Coastal and Port Engineering and Science (Coastlab10)*.

Ramachandran, K., Genzalez, R. R., Oumeraci, H., Schimmels, S., Kudella, M., Van Doorslaer, K., Trouw, K. (2012a). Loading of vertical walls by overtopping bores using pressure and force sensors - A large scale model study. In *Proceedings of the 33rd International Conference on Coastal Engineering (ICCE 2012)*. Santander, Spain.

De Rouck, J., Van Doorslaer, K., Versluys, T., Ramachandran, K., Schimmels, S., Kudella, M. and Trouw, K. (2012). Full scale impact tests of an overtopping bore on a vertical wall in the large wave flume (GWK) in Hannover. In *Proceedings of the 33rd International Conference on Coastal Engineering (ICCE 2012)*. Santander, Spain.

Van Doorslaer, K., De Rouck, J., Trouw, K., van der Meer, J. W. and Schimmels, S. (2012). Wave forces on storm walls, small and large scale experiments. *International Conference on Coastal and Port Engineering in Developing Countries (PIANC - COPEDEC VIII - 2012)*, 1–11. https://doi.org/10.13140/2.1.2319.1362

Ramachandran, K., Genzalez, R. R., Oumeraci, H., Schimmels, S., Kudella, M., Van Doorslaer, K., Trouw, K. (2012b). Loading of vertical walls by overtopping bores using pressure and force sensors – a large scale model study. In *Proceedings of the 4th International Conference of the Application of Physical Modelling in Coastal and Port Engineering and Science (Coastlab12)*. Ghent.

Trouw, K., Mertens, T., Vermander, J., Verwaest, T., Bolle, A., Van Doorslaer, K. and De Rouck, J. (2012). Design of storm return walls for the masterplan for coastal safety: from conceptual to detailed design. In *Proceedings of the 4th International Conference of the Application of Physical Modelling in Coastal and Port Engineering and Science (Coastlab12)*. Ghent.

Bellotti, G., Van Doorslaer, K., Romano, A., Baelus, L., Caceres, I., De Rouck, J. and Franco, L. (2014). Forces on (flood)walls and buildings by wave overtopping. In *Proceedings of the Hydralab IV Joint User Meeting*.

Van Doorslaer, K., Romano, A., Bellotti, G., Altomare, C., Cáceres, I., De Rouck, J., van der Meer, J. W. (2015b). Force Measurements on Storm Walls Due to Overtopping Waves: A Middle-Scale Model Experiment. In *Coastal Structures*. https://doi.org/10.1061/9780784480304.069

Van Doorslaer, K. and De Rouck, J. (2016a). Wave overtopping over sea dikes and impact forces on storm walls. In *International conference on coastal and port engineering in developing countries (PIANC - COPEDEC IX - 2016)*. Rio De Janeiro.

Van Doorslaer, K., De Rouck, J. and van der Meer, J. W. (2016b). The reduction of wave overtopping by means of a storm wall. In *Proceedings of the 35th International Conference on Coastal Engineering (ICCE 2016)* (Vol. 35). Antalya, Turkye.

Book

Part of this research has also been included in summary in the updated EurOtop (2016). Nevertheless, it belongs to the research of this PhD, and is written out in this manuscript.

EurOtop. (2016). *Manual on wave overtopping of sea defences and related structures An overtopping manual largely based on European research, but for worldwide application.* van der Meer, J. W., Allsop, W., Bruce, T., De Rouck, J., Kortenhaus, A., Pullen, T., Schüttrumpf, H., Troch, P., Zanuttigh, B. Retrieved from http://www.overtopping-manual.com/index.html

Database

In this work a new database of over 1100 new tests has been developed. This database has been made available for free download at www.koenvandoorslaer.com/phd

1 Introduction

1.1 *Effects of climate change on a global scale*

Global warming, climate change and sea level rise (SLR) are three very pressing issues of the 21st century. Climate change affects coastal areas in a variety of ways. According to the Intergovernmental Panel on Climate Change (IPCC), the global mean sea level has increased by 1.7mm per year between 1900 and 2010. Between 1971 and 2010 the increase was 2.0mm per year, and between 1993 and 2010 3.2mm per year. An increasing trend shows. All investigated scenarios by IPCC state that the SLR will continue in and beyond the 21st century and the rate of SLR will '*very likely*' exceed that of 1971-2010 in the upcoming centuries (Wong et al., 2014). The low emission scenario already predicts an average raise of 0.44m global mean SLR by 2100 (4.9mm/year averaged), where high emission scenarios predict average 0.74m SLR (8.2mm/year averaged), see Figure 1-1 and Table 1-1.

The causes for SLR are thermal expansion of the water by a warming ocean and increased losses of glaciers, ice caps and ice sheets of Antarctica and Greenland. The consequences of SLR are decreasing freeboards which can lead to inundation and erosion, but also wetland loss, increasing salinity of the ground water, and contamination of freshwater reserves and food crops are direct consequences of the SLR.

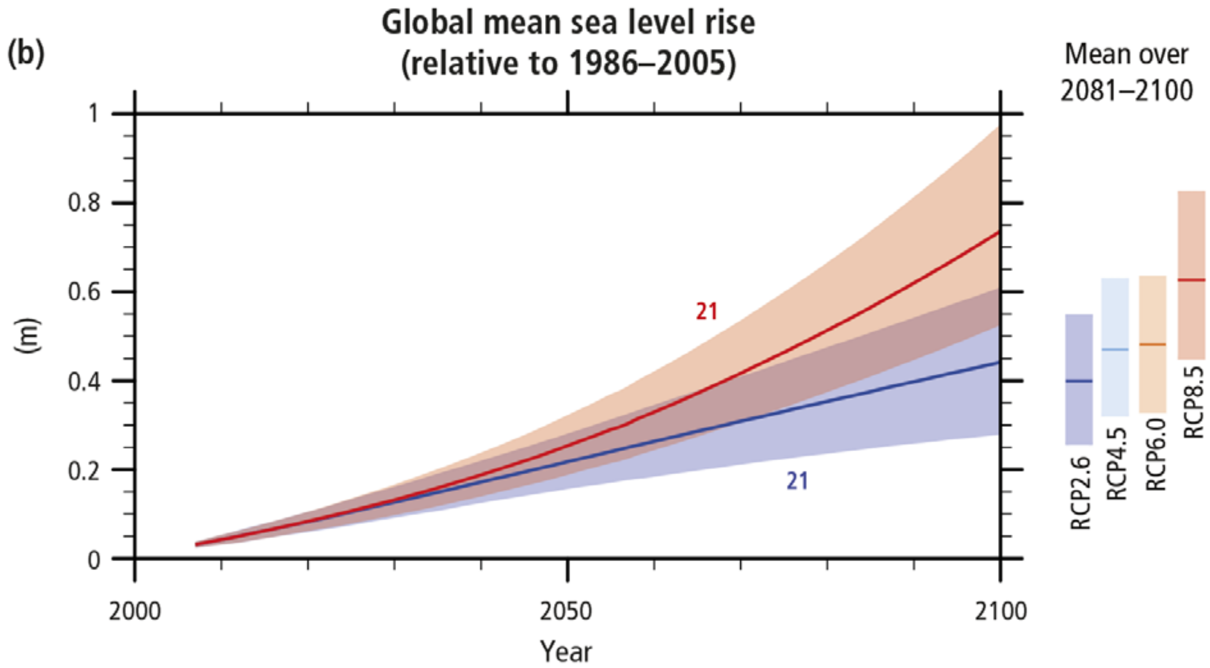

Figure 1-1. Global mean sea level rise according to different investigated scenarios 'RCP'. Figure by IPCC (2014).

Table 1-1. Predicted Sea Level Rise by 2100 and beyond for different emission scenarios. Table by Wong et al. (2014).

Table 5-2 | Projections of global mean sea level rise in meters relative to 1986–2005 are based on ocean thermal expansion calculated from climate models, the contributions from glaciers, Greenland and Antarctica from surface mass balance calculations using climate model temperature projections, the range of the contribution from Greenland and Antarctica due to dynamical processes, and the terrestrial contribution to sea levels, estimated from available studies. For sea levels up to and including 2100, the central values and the 5–95% range are given whereas for projections from 2200 onwards, the range represents the model spread due to the small number of model projections available and the high scenario includes projections based on RCP6.0 and RCP8.5. Source: WGI AR5 Summary for Policymakers and Sections 12.4.1, 13.5.1, and 13.5.4.

Emission scenario	Representative Concentration Pathway (RCP)	2100 CO_2 concentration (ppm)	Mean sea level rise (m)		Emission scenario	Mean sea level rise (m)		
			2046–2065	2100		2200	2300	2500
Low	2.6	421	0.24 [0.17–0.32]	0.44 [0.28–0.61]	Low	0.35–0.72	0.41–0.85	0.50–1.02
Medium low	4.5	538	0.26 [0.19–0.33]	0.53 [0.36–0.71]	Medium	0.26–1.09	0.27–1.51	0.18–2.32
Medium high	6.0	670	0.25 [0.18–0.32]	0.55 [0.38–0.73]	High	0.58–2.03	0.92–3.59	1.51–6.63
High	8.5	936	0.29 [0.22–0.38]	0.74 [0.52–0.98]				

Combined with (severe) land subsidence in many coastal areas (such as Tokyo, Indonesia e.g.) or the already low lying country (such as The Netherlands e.g.) the SLR is a huge potential threat for coastal towns. The IPCC estimates that the delta surface area vulnerable to flooding could increase by 50% for 33 deltas around the world under SLR as projected for 2100 in the low emission scenario.

Global warming has not only increased the water level but also has changed the frequency and intensity of the strongest tropical cyclones (hurricanes) since the 1970s. In the future, the frequency of tropical cyclones is *likely* to remain unchanged or slightly decrease according to the IPCC, but the frequency of the most intense tropical cyclones (such as the consecutive hurricanes Harvey, Irma, Jose and Katia in September 2017) is *likely* to increase. Also the intensity is *likely* to increase. The IPCC predicts that the extreme wind speeds, significant wave height in certain areas and extreme sea level are *likely* to *very likely* to increase. More trends and projections are given in Table 1-2.

Table 1-2. Trends and projections for the climate related drivers. Table by Wong et al. (2014).

Table 5-1 | Main climate-related drivers for coastal systems, their trends due to climate change, and their main physical and ecosystem effects.

Climate-related driver	Physical/chemical effects	Trends	Projections	Progress since AR4
Sea level	Submergence, flood damage, erosion; saltwater intrusion; rising water tables/impeded drainage; wetland loss (and change).	Global mean sea level *very likely* increase (Section 5.3.2.2; WGI AR5 Sections 3.7.2, 3.7.3).	Global mean sea level *very likely* increase (see Table 5.1; WGI AR5 Section 13.5.1). Regional variability (Section 5.3.2.2; WGI AR5 Chapter 13).	Improved confidence in contributions to observed sea level. More information on regional and local sea level rise.
Storms: tropical cyclones (TCs), extratropical cyclones (ETCs)	Storm surges and storm waves, coastal flooding, erosion; saltwater intrusion; rising water tables/ impeded drainage; wetland loss (and change). Coastal infrastructure damage and flood defense failure.	TCs (Box 5-1, WGI AR5 Section 2.6.3): *low confidence* in trends in frequency and intensity due to limitations in observations and regional variability. ETCs (Section 5.3.3.1; WGI AR5 Section 2.6.4): *likely* poleward movement of circulation features but *low confidence* in intensity changes.	TCs (Box 5-1): *likely* decrease to no change in frequency; *likely* increase in the most intense TCs. ETCs (Section 5.3.3.1): *high confidence* that reduction of ETCs will be small globally. *Low confidence* in changes in intensity.	Lowering of confidence of observed trends in TCs and ETCs since AR4. More basin-specific information on storm track changes.
Winds	Wind waves, storm surges, coastal currents, land coastal infrastructure damage.	*Low confidence* in trends in mean and extreme wind speeds (Section 5.3.3.2, SREX, WGI AR5 Section 3.4.5).	*Low confidence* in projected mean wind speeds. *Likely* increase in TC extreme wind speeds (Section 5.3.3.2, SREX).	Winds not specifically addressed in AR4.
Waves	Coastal erosion, overtopping and coastal flooding.	*Likely* positive trends in Hs in high latitudes (Section 5.3.3.2; WGI AR5 Section 3.4.5).	*Low confidence* for projections overall but *medium confidence* for Southern Ocean increases in Hs (Section 5.3.3.2).	Large increase in number of wave projection studies since AR4.
Extreme sea levels	Coastal flooding erosion, saltwater intrusion.	*High confidence* of increase due to global mean sea level rise (Section 5.3.3.3; WGI AR5 Chapter 13).	*High confidence* of increase due to global mean sea level rise, *low confidence* of changes due to storm changes (Section 5.3.3.3; WGI AR5 Section 13.5).	Local subsidence is an important contribution to regional sea level rise in many locations.
Sea surface temperature (SST)	Changes to stratification and circulation; reduced incidence of sea ice at higher latitudes; increased coral bleaching and mortality, poleward species migration; increased algal blooms.	*High confidence* that coastal SST increase is higher than global SST increase (Section 5.3.3.4).	*High confidence* that coastal SSTs will increase with projected temperature increase (Section 5.3.3.4).	Emerging information on coastal changes in SSTs.
Freshwater input	Altered flood risk in coastal lowlands; altered water quality/ salinity; altered fluvial sediment supply; altered circulation and nutrient supply.	*Medium confidence (limited evidence)* in a net declining trend in annual volume of freshwater input (Section 5.3.3.6).	*Medium confidence* for general increase in high latitudes and wet tropics and decrease in other tropical regions (Section 5.3.3.6).	Emerging information on freshwater input.
Ocean acidity	Increased CO_2 fertilization; decreased seawater pH and carbonate ion concentration (or "ocean acidification").	*High confidence* of overall increase, with high local and regional variability (Section 5.3.3.5).	*High confidence* of increase at unprecedented rates but with local and regional variability (Box CC-OA).	Coastal ocean acidification not specifically addressed in AR4. Considerable progress made in chemical projections and biological impacts.

SREX = IPCC 2012 Special Report on Managing the Risks of Extreme Events and Disasters to Advance Climate Change Adaptation.

On the one hand, coastal zones are facing these climate-related changes, on the other hand there is an increasing socioeconomic pressure: a deadly combination with continuously increasing risk. The IPCC reports in Wong et al. (2014) that despite the Low Elevation Coastal Zone only constitutes 2% of the world's land area, it contains 13% of the world's urban population, based on year 2000 estimates. 65% of the world's cities with populations of greater than 5 million people are located in these Low Elevation Coastal Zones. Many of these cities are even located below the 1-in-100-year extreme sea level. And these numbers only increase. From 1970 to 2010 the global population exposed to the 1-in-100-year extreme sea level has increased by 95%. Besides housing and working, coastal areas also generate huge social, economic, recreation and touristic, … revenues. It becomes very clear that the risk (risk = probability multiplied by consequence) of a coastal disaster is increasing.

Solutions to reduce the consequence are mainly socially and economically driven and thereby long term solutions. Solutions to reduce the probability however can be found on the short term. Not by reducing the SLR, that's long term, but by studying and improving the defense systems. Land is protected from the water and the waves by natural or men-made dikes, dunes, embankments, breakwaters, etc. With rising water levels and growing storm intensities the probability of wave overtopping over coastal dikes and embankments increases. This can be resolved by making the dikes higher or the dike crests wider. However, this requires space which is often not available. Finding a solution with space-limited crest modifications such as a storm wall or a stilling wave basin can be more feasible and economic. This is where this PhD manuscript focusses: how can wave overtopping over sea dikes be reduced dealing with the spatial restrictions in highly populated and economical/touristic areas? Are the existing guidelines to calculate wave overtopping over sea dikes sufficient to include the effect of overtopping reducing measures such as storm walls e.g.? What kind of wave induced forces are storm walls and other measures facing during high intensity storms? These questions will be answered in this work.

1.2 *An example case for the Belgian situation*

Although the Belgian coast only has a length of 67km, it is a densely populated area (500.000 inhabitants) of which every meter is intensively used, thereby similarly suffering the worldwide risk of a potential coastal disaster. From this perspective, extensive research has been carried out in Belgium (2005-2009) to evaluate the safety level of its coastal zone. These studies have shown that if a storm with a return period of 1000 years would have occurred at that moment, 1/3rd of the coastline would have been insufficiently protected, leading to overtopping, dike breaches, and flooding, and hence causing millions of euro’s structural and economical damage and the loss of many lives. Because of this conclusion, an Integrated Coastal Safety Plan (ICSP) was developed and approved by the Flemish government in 2011. This masterplan (Mertens et al., 2008) states that the Belgian coastal zones have to be protected against a storm with a return period of 1000 years, overtopping discharges have to be kept below 1l/m/s and (emergency) measures have to be taken immediately in vulnerable areas to protect them from a storm with a 100-year return period.

Before the approval of the ICSP, most of the Belgian coastline consisted of a sandy beach under a mild slope (1:100 - 1:50) followed by a smooth dike ($1.5 \leq \cot(\alpha) \leq 3$) and a quasi-horizontal part at crest level, further called “promenade”. Just next to this promenade, apartment buildings are present at several locations (Figure 1-2). With the geometry as presented in Figure 1-2 during nearly every winter storm the water reached the sea dike (Figure 1-3 to Figure 1-5) leading to a high probability of wave overtopping and resulting damage. These storms lead to erosion of the beach, causing a geometry like in Figure 1-4 with fairly deep water and non-breaking waves in front of the dike.

After the ICSP was approved, emergency beach nourishments were carried out to keep the high tide away from the dikes and protect the coastline against a 1-in-100-year storm. Dry beaches were nourished with a slope 1:35 to 1:50 in between the dike and the mild sloping foreshore (Figure 1-6). The storm water level doesn’t reach the dike and the promenade anymore (Figure 1-7). In the meantime, other permanent solutions to withstand a 1-in-1000-year storm were studied. The ICSP recommends both ‘soft’ and ‘hard’ measures to reduce wave overtopping. The soft measures are beach nourishments, where the hard measures can be new constructions on top of the smooth dike, of which an example is given in Figure 1-8.

This PhD manuscript is based on data collected between 2007 and 2011, the period when the ICSP was being written, and hard measures to reduce wave overtopping such as storm walls, bullnoses and others were studied. In 2007, most of the coastline in Belgium looked like Figure 1-2 and even Figure 1-4 and no structural dry beach nourishments had been carried out yet; the water level reached the dike during a storm. For this reason, the current work focusses on intermediate or deep water conditions near the toe of the dike (see Chapter 3).

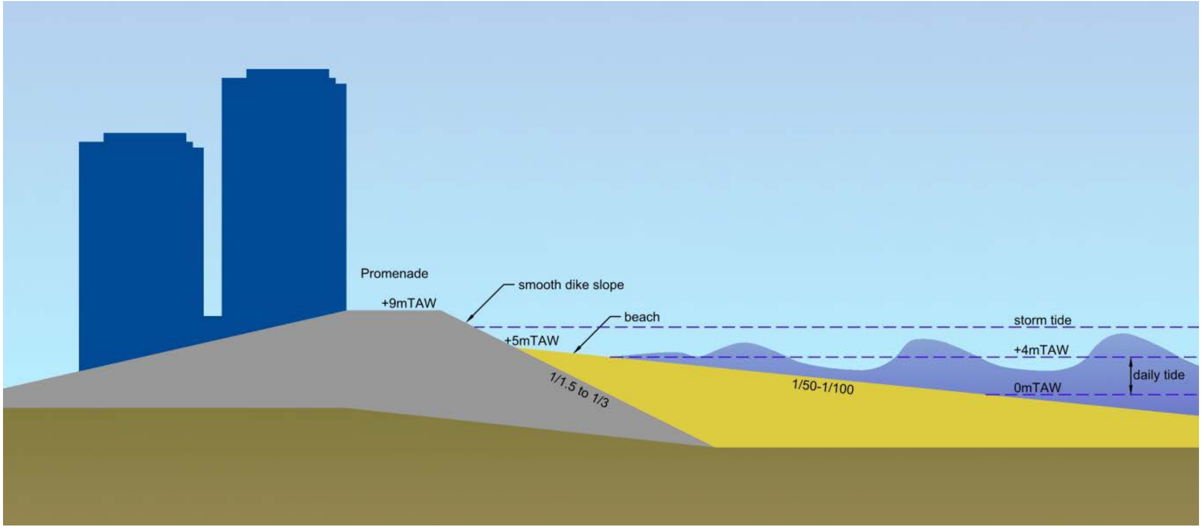

Figure 1-2. Typical cross section of the Belgian coastline **before** nourishments were carried out: mild sloping beach (1:50 to 1:100) in front of a smooth dike (1:1.5 to 1:3), a promenade and apartment buildings.

Figure 1-3. Storm water level reaching the dike in Ostend, Belgium. A situation before nourishments were carried out. (picture by Flemish Government – Coastal Division).

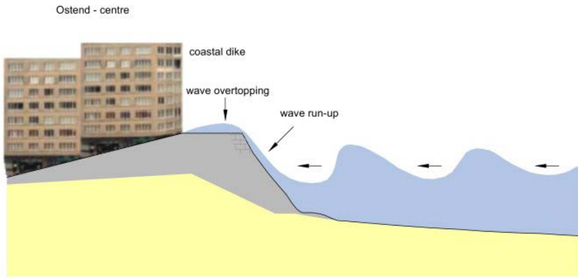

Figure 1-4. Eroded beach in front of the dike leading to deep water and non-breaking waves (picture: Masterplan Coastal Safety Belgium – Flemish Government – Coastal Division).

Figure 1-5. Sea dike in Ostend, at the Belgian coastline, during a winter storm before beach nourishments were carried out.

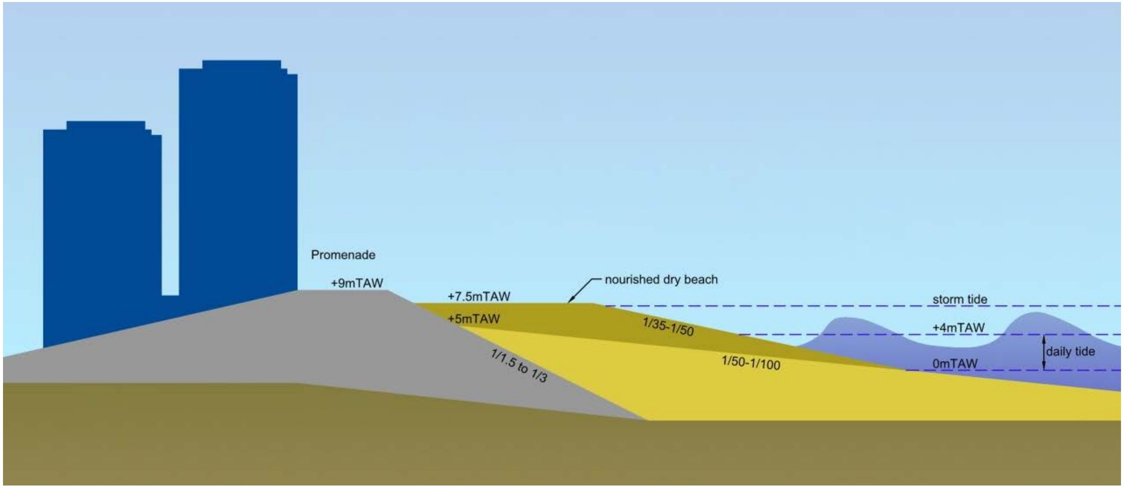

Figure 1-6. Typical cross section of the Belgian Coastline after nourishments were carried out: mild sloping beach (1:50 to 1:100), transition to shallow foreshore (1:35 to 1:50) in front of a smooth dike (1:1.5 to 1:3), a promenade and apartment buildings.

Figure 1-7. Aerial view of Oostende after beach nourishment (picture: Masterplan Coastal Safety Belgium – Flemish Government – Coastal Division).

Figure 1-8. Artist impression of a coastal dike, after implementation of overtopping reducing measures (promenade and storm wall) to reduce overtopping. Impression by 'Coastal Division, Flemish Government' for ICSP.

1.3 *Objectives*

Regardless which hard or soft measures are designed to increase the safety of the coastline, they have to take the strict spatial restrictions into account: increasing the height of the sea dike has to be limited due to visual implications for people living close behind the coastline, while a landward expansion of the promenade is often impossible due to the presence of existing apartments and buildings. The construction of permanent or mobile storm walls with or without bullnose, or the integration of a so called stilling wave basin in the crest of the sea dike are such crest modifications that reduce the overtopping discharges**. The design of hard measures at crest level to reduce the overtopping discharges forms one of the main topics of this PhD manuscript.** The outcome of this study leads to a reduction factor per geometry, function of a steering dimensionless parameter, to be included in the wave overtopping formulae.

Because this research started before the ICSP was implemented in Belgium, the focus was mainly on intermediate to deep water in front of the sea dikes and thus non-breaking wave conditions. Since 2016, Ghent University is doing ongoing research for similar dike constructions and crest modifications (storm walls e.g.) but with shallow foreshores (breaking and broken wave conditions), the situation after the beach nourishments were carried out (Streicher et al. (2016)). It's highlighted again that the research campaign from this PhD study worked with intermediate or deep water in front of a sea dike with slopes 1:2 to 1:3, leading to non-breaking waves.

Besides a geometrical design of storm walls and overtopping reducing measures, designers and contractors are also interested in how to design and build them. Very little information of this is yet available in literature. **What impacts these storm walls are facing during a design storm is a second question to be solved in this PhD manuscript**. This will allow the structural design of storm walls for practical application. Besides the impact value, it will also be investigated where and how to measure wave-induced forces, how an impact signal looks like, what the best representation of a distribution of all impacts in a storm is, and how to link the impacts at the storm wall to hydraulic parameters such as wave conditions or overtopping flow parameters.

In Figure 1-8, where an impression of a possible solution with a storm wall is given, the storm wall is not located directly at the seaward crest of the dike, but at the end of a promenade. It is thus not an actual sinusoidal wave impacting the storm wall, but an overtopped bore flowing over the promenade causing this impact. This 2nd order effect requires some **insight on the post overtopping process (flow depth, flow velocity)**. For a better understanding, this is already visualized in Figure 1-9 but will be dealt with in more detail in Chapter 5 of this PhD manuscript. The presence of the storm wall creates reflection which influences new incoming overtopped bores in zone 4 of Figure 1-9. This interaction is different from the existing knowledge on overtopping flow depths and velocities. The objective is to determine the individual incoming flow parameters and investigate their link with incoming waves or overtopping volumes (looking to the left of zone 4 in Figure 1-9) and with wave-induced impacts (looking to the right of zone 4 in Figure 1-9).

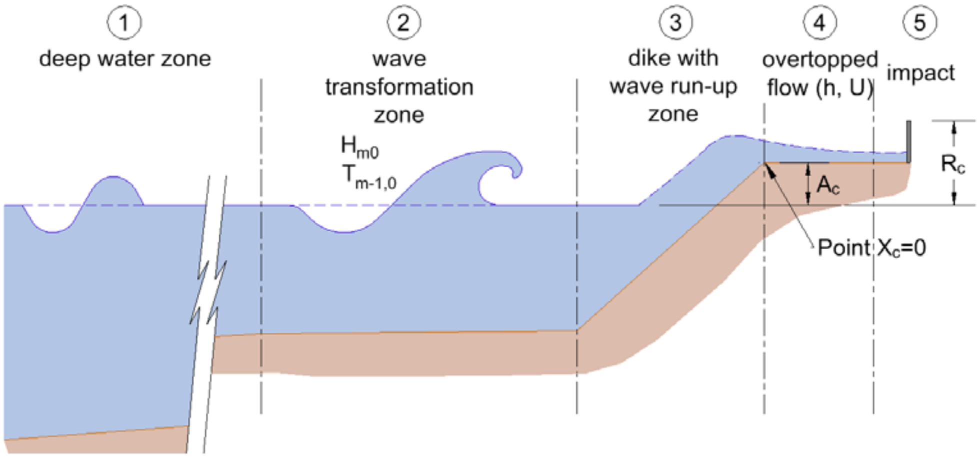

Figure 1-9. Evolution from deep water waves to the post overtopping process of a bore impacting a storm wall at the end of a promenade.

1.4 *Methodologies*

The database for this PhD found its origin in practical questions for real life coastal engineering problems. Many tests in the wave flume of Ghent University were performed for the ICSP, originally for site specific conditions. Along the way, similar questions for different sites were asked to the coastal engineering laboratory at Ghent University and by doing more experimental tests a more complete database on overtopping and impacts was gathered. The site specific questions were answered, but the elaborated database at Ghent University with a wide range of parameters still had lots of unanalyzed potential. Three research questions, highlighted in bold in the previous section 1.3, were set and additional analysis was carried out on this dataset. Besides this newly developed database at Ghent University, more tests were carried out in different laboratories. The combination of carrying out more experimental research and an intensive analysis ensures that the objectives from section 1.3 are met.

Chapter 3 gives an overview of the different research campaigns. The current section explains the methodology followed for each of the three mentioned research goals, since they all differ. However, the constant is that this work is based on experimental modelling: physical model tests lead to a dataset from which empirical or semi-empirical formulae were determined.

1.4.1 *Reduction of wave overtopping*

Different structures were built in the wave flume, waves were generated and wave overtopping was measured. The equipment for each of these wave flume tests will be described in Chapter 3.

It was important to start with overtopping tests on a reference case, since the analysis works in a relative way: how much less overtopping comes over a structure with adapted crest compared to the reference case. Generic formulae from literature could have been used for the reference case, but for an ideal comparison it was chosen to build the reference situation in the wave flume and run some tests on it.

A database of over 1000 new overtopping tests, with similar parameters as in the well-known CLASH database, was set up. Overtopping tests are generally analyzed by plotting the data in a log-linear plot: dimensionless freeboard R_c/H_{m0} on the horizontal linear axis, dimensionless overtopping $q/(g{\cdot}H_{m0})^{0.5}$ on the vertical logarithmic axis, see Figure 1-10. Results are described by the experimental formula Eq. [1-1], where a, b and c are empirical coefficients.

$$\frac{q}{\sqrt{g \cdot H_{m0}^{3}}} = \mathrm{a} \cdot \exp\left(-b \cdot \frac{R_c}{H_{m0}}\right)^{c} \qquad [1\text{-}1]$$

How much a geometry with modified crest reduces the wave overtopping compared to its reference situation can be seen from such plots. When different measures (e.g. a dike with a storm wall versus a dike with a promenade, see Chapter 3) are plotted together it can be evaluated which one has the least overtopping for specific hydraulic conditions. In Figure 1-10 a preview is given on the analysis in Chapter 4, to explain and visualize the methodology. The black data represent overtopping over the reference structure, a smooth dike. The blue data represent a dike with a storm wall (Section 4.1) and are below the black data and thus show lover overtopping. Finally the green data are from a dike with wall and bullnose (see 4.2.1) are generally even lower and show a better reduction in wave overtopping.

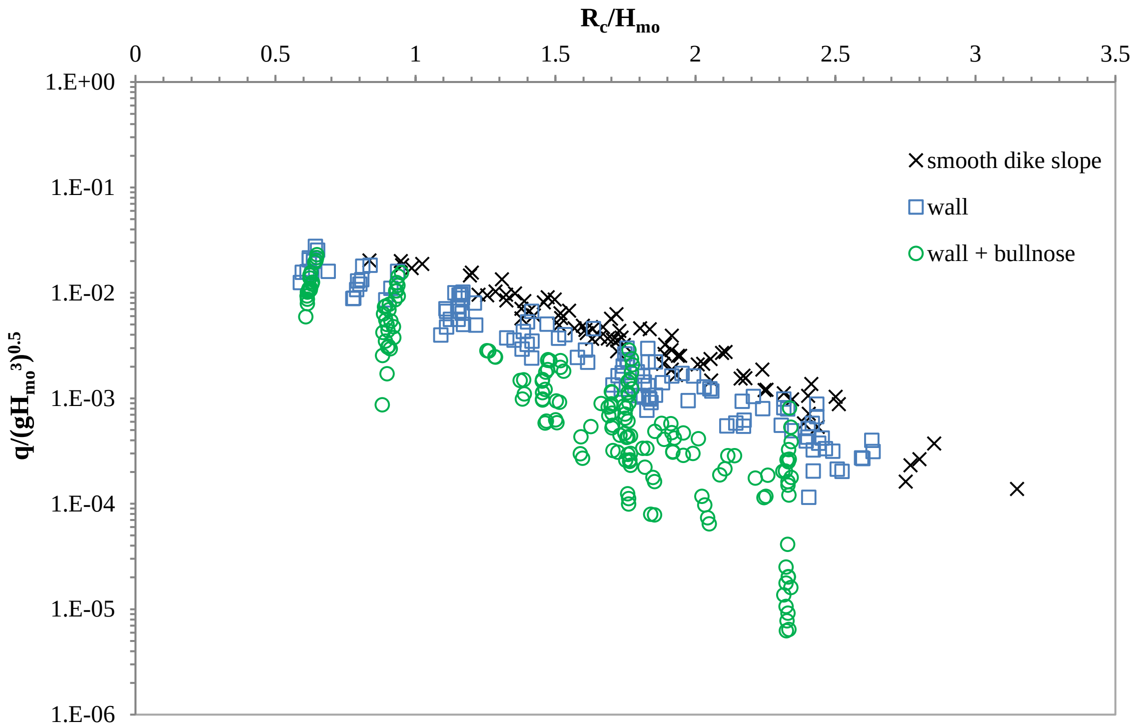

Figure 1-10. Classic representation of average wave overtopping discharges, with the dimensionless freeboard R_c/H_{m0} on the horizontal linear axis and the dimensionless discharge $q/(g \cdot H_{m0})^{0.5}$ on the vertical logarithmic axis. Dataplot shows the overtopping over the reference case (black data), and reduction due to adding a wall (blue data) and a bullnose (green data).

The amount of reduction that can be analyzed from the graphs is expressed as a reduction factor γ, and is different per geometry. This factor, smaller than 1 when overtopping is reduced compared to the reference situation, appears in the denominator of the dimensionless freeboard $R_c/(H_{m0} \cdot \gamma)$. It can thereby also be seen as a virtual increase of the freeboard R_c. The smaller the value of γ, the better its geometry reduces overtopping, the less overtopping discharge over the structure is measured.

Through the plotted data, an exponential trendline can be fitted, see Figure 1-11. The coefficients a (intersection with Y-axis) and c (curve in the trendline) are considered to be constant as will be explained in Section 2.2. The coefficient b indicates the slope of the trendline and differs for different datasets, see Figure 1-11. From the ratio of these factors b of the different trendlines, the average reduction from the blue or the green data in Figure 1-11 towards the reference case (black data) can be expressed. This reduction or the ratio in b-coefficients is expressed as the factor γ in the exponential part of Eq. [1-1]. As an example for the figure below, the average reduction for a storm wall would be

2.281/2.657 = 0.858 and for the storm wall with bullnose 2.281/3.46 = 0.659. Note that these values are averaged reduction factors, which were deducted from an average trendline analysis through the whole dataset.

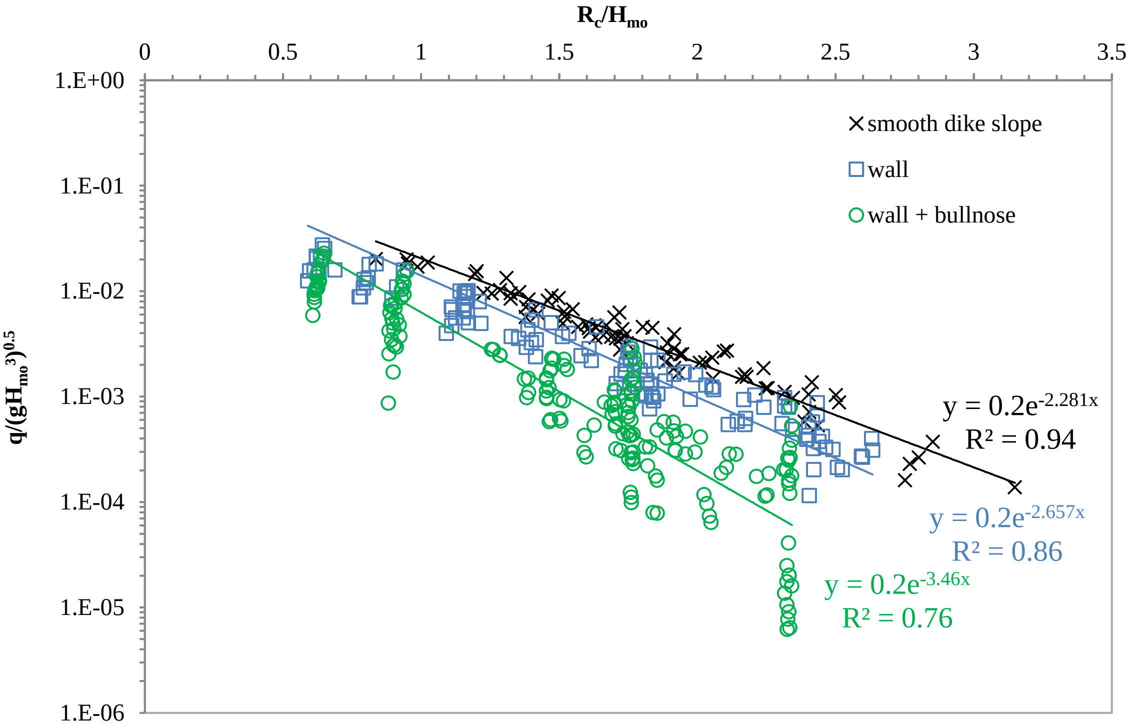

Figure 1-11. Repetition of Figure 1-10 where now the average trendlines per dataset have been added.

Different in this work, compared to this trendline analysis which was generally done before, is that a point-by-point analysis is carried out in Chapter 4 to obtain the reduction factor. Instead of comparing trendlines, in this work b and thus γ are calculated for every single data point. Then a relation between these calculated γ-values and their geometrical dimensionless parameter which causes the reduction (such as dimensionless wall height, or dimensionless promenade width) are sought. This is carried out for each of the studied geometries.

This new method is more precise and more transparent than the trendline analysis where data are plotted in groups of "more or less the same values". The new point-by-point methodology is explained in Chapter 4.

Per geometry, per modification that is made to the dike crest, a reduction factor γ is determined in Chapter 4. These reduction factors, that depend on their geometrical parameters, allow the user to calculate average overtopping discharges over structures with a modified crest, or allow to design a structure to meet the overtopping requirements (e.g. 1 l/m/s which is often the limiting value).

The first objective of this manuscript is to define the overtopping reducing capacity of crest modifications of smooth dikes, and present prediction formulae for each of those modified crests. Sumarized, the following steps are proposed to achieve this research goal:

- Use of new hydraulic model tests
- Define (and test) a reference case
- Use mean wave overtopping data, relative to the reference case
- Use a point-to-point analysis rather than a trendline comparison, and investigate different influences that might affect the reduction
- Introduce a reduction factor γ in the dimensionless freeboard $R_c/(H_{m0}\cdot\gamma)$ for each geometry

1.4.2 *Flow depths and flow velocities*

Figure 1-9 schematizes one of the possible crest modifications of a dike, where a storm wall has been added to the end of a promenade at crest level to reduce wave overtopping. A wave that overtops the dike crest continues over the promenade as an overtopping bore which is then blocked by the storm wall. Such a bore or overtopping flow is characterized by a flow depth and a flow velocity. The zone of interest to study these overtopped flow parameters is the promenade at crest level of the dike, indicated in Figure 1-9 as zone 4.

The flow depth and flow parameters are studied by running and analyzing hydraulic model tests, since literature review in Chapter 2 shows big differences between different consulted sources. It was not possible to measure these flow parameters in all tests that have been carried out for this research. In Chapter 3 it's explained in more detail how and in which test campaigns the flow parameters were recorded.

Nevertheless, for the tests where flow measurements took place, flow parameters were measured at different locations over the promenade length by means of different equipment. These flow depth and flow velocity measurements were new in the facilities where the tests took place, so different equipment from other fields of coastal engineering or different purpose tests (e.g. sand transport in the swash zone) have been tried. In the analysis, the evolution of the flow parameters over the promenade is studied at and the flow parameters at the optimal location are selected. The interaction between incoming and reflected bores after an impact is crucial in this analysis.

The incoming flow parameters are individual values per overtopped bore. By means of data plots a relation between these individual flow parameters and the incoming hydraulic parameters (zone 2 in Figure 1-9) is looked for. Since the hydraulic parameters are test-averaged values, a good fit with individual flow parameters is not straightforward. Also the internal relations between flow depth and flow velocity are investigated based on literature. Finally, the individual flow parameters, both separate and combined, are linked to the individual flow induced impacts by means of data plots.

Summarized, the following methodology is followed to obtain a better insight in overtopping flow parameters:

- Use of new hydraulic model tests
- Measure at multiple locations, identify incoming bores and select optimal location
- Data plots to find relationships: between flow depth and flow velocity internally, with hydraulic test averaged conditions and with individual flow induced forces.

1.4.3 *Wave induced forces*

According to the literature study in Chapter 2, studying wave induced loads was done less in the past, and not on geometries like the ones in this work. Impacts on other geometries were studied by means of experimental modelling with an empirical formula as output. This approach is followed too in the current work.

In a set of newly developed tests, the storm walls with and without bullnose are equipped with pressure sensors and force sensors. To have a good understanding of the recordings, the forces are analyzed and compared to the integrated pressure, and the effect of different set-ups (horizontal plates versus vertical plates, recording sections at the left or the right side of the storm wall) is also investigated.

A new force database is set up, and three approaches are followed:

- a low exceedance force value $F_{1/250}$ is determined per test and directly linked to the wave conditions per test (empirical approach).
- a probability distribution function of the impact forces where the shape and scale parameters are linked to wave conditions. From this PDF the value $F_{1/250}$ is determined (empirical and statistical approach).
- a theoretical distribution of individual overtopping volumes is linked to a distribution of overtopping flow parameters, which on its turn in linked to a distribution of individual impacts. Also here, the low exceedance force value $F_{1/250}$ is determined (physical and statistical approach).

Unlike for overtopping discharges, the dimensionless parameters to plot forces are yet unknown and form part of the analysis. All approaches lead to empirical formulae that allow the designer to answer the 3rd objective: what wave induced impacts do the overtopping reducing measures face during a storm?

1.5 *PhD outline*

The next chapter in this PhD manuscript gives an overview of related literature and research. The available formulae to calculate wave overtopping discharges are given, together with the knowledge on the relevant reduction factors. Next, flow depths and flow velocities are studied, the distribution of individual waves are explained and the available information on impacts is given.

Chapter 3 explains the tested geometries, the different test set-ups and parameters that are measured. The range of application is listed in parameter tables. Tests are carried out in three different laboratories over Europe, with different goals (measuring overtopping, impacts and post-overtopping flow parameters). Which tests are used for which purpose is indicated in this third chapter.

The 4th chapter deals with the reduction of wave overtopping and the different crest modifications studied. In a first subsection, a detailed analysis is given on the reduction by means of a storm wall. Also a comparison with literature is carried out here. Next subsections are repeating the developed procedure for the different overtopping reducing measures: storm wall with bullnose, promenade, promenade with storm wall, promenade with storm wall and bullnose, stilling wave basin. Chapter 4 is concluded with a case study.

In Chapter 5, the analysis of the flow depth and flow velocity of the post overtopping flow on the promenade is given.

Chapter 6 deals with the impacts on a storm wall. It's first investigated whether literature describes the measured data accurately. When this seems not to be the case, a detailed look at the impact recordings is carried out in Section 6.2 and compared for different ways of testing: force recordings versus pressure recordings, measurement plates of different height and width and recording sections left and right at the storm wall are discussed and a way forward is proposed. Section 6.3 introduces three different approaches (approach 1a, 1b and 2) to describe impact forces. Section 6.4 then analyses these three approaches for the most common geometry: the storm wall located at the end of the promenade at crest level. Section 6.5 gives the preferred methodology (approach 1a) for impacts on all other geometries (storm wall, storm wall with bullnose, promenade with storm wall, promenade with storm wall and bullnose). Chapter 6 is concluded with a case study.

The conclusions of the PhD manuscript are given in Chapter 7. The recommendations for continued research are given in the last Chapter 8.

2 Literature study

A literature review is given in this chapter, containing the existing knowledge relevant for the present work. As mentioned in the introduction, the starting point of the present work is a situation with intermediate to deep water in front of the smooth dikes related to the wave height, leading to non-breaking waves. Shallow water waves and breaking waves are not the main subject of the present PhD manuscript.

To meet the objectives listed in Section 1.3, the main topics that were studied are wave overtopping and wave impacts. The link between both are individual overtopping volumes, leading to an overtopped bore with a certain flow depth and flow velocity (see Figure 1-9). All these topics are described here in the literature review.

2.1 *Different ways of modelling*

Wave overtopping is a well-studied subject in coastal engineering. Experimental modelling, numerical modelling, Artificial Neural Networks (ANN) and field studies are the main options to investigate overtopping, all of them with numerous publications and research projects. For studying overtopping flow characteristics and wave induced loads, the same models exist except for ANN. The most important items of the four categories, related to this PhD research, are summarized below.

2.1.1 *Experimental modelling*

"A physical model is a physical system reproduced (usually at a reduced size) so that the major dominant forces acting on the system are presented in the model in correct proportion to the actual physical system" (Hughes, 1993). EurOtop (2016) adds the following related to the development of semi-empirical prediction formulae: "The equation form is based on physical insight in the governing parameters, but additional empirical constants are required, which have been determined by fitting to experimental data from physical model testst". Physical modelling has some advantages such as: cost effective, good understanding of the processes due to visual observation, data quality, controlled environment, the ability to test problems that can't be solved theoretically/mathematically,… Physical modelling also has some disadvantages such as possible scale and model effects, the unabillity of obeying all similarity laws which makes it impossible to scale all acting forces (gravity, viscosity, surface tension …) simulteanously, the unability of including wind or current or other hydraulic forces in the model, the limited size of the test matrix, discrete measurements, …

In a physical model, simplifications have to be made. Bathymetries or geometries are simplified and the model is tested on its dominant hydraulic forces, often individual forces (such as wave action or currents only) and not combined forces (such as wave and wind action, or wave and current action). However, physical models are improving and the combination of hydraulic forces becomes more common to test. Despite models are improving, the unability to have perfect similarity will always remain. Geometric (length scaling) and kinematic (time scaling) similarity between prototype and scale model are easily achieved, but dynamic similarity (a constant model-to-prototype ratio of all masses and forces acting on the system) is impossible to achieve. No fluid is known that will satisfy all force ratio requirements if the model is smaller than the prototype (Hughes, 1993). In coastal engineering, systems with fluids and free water surface, gravity and inertia are the dominant forces. It's thereby important that the Froude number, the square root of the ratio between intertial force and gravitational force, is the same for prototype as for model:

$$Fr = \sqrt{\frac{intertial\, forces}{gravity\, forces}} = \sqrt{\frac{\rho L^2 V^2}{\rho L^3 g}} = \frac{V}{\sqrt{gL}} \qquad [2\text{-}1]$$

$$(Fr)_p = (Fr)_m \rightarrow \left(\frac{V}{\sqrt{gL}}\right)_p = \left(\frac{V}{\sqrt{gL}}\right)_m \qquad [2\text{-}2]$$

where ρ is the density, L the length, V volume and g gravity acceleration. Subscript p stands for prototype and m for scale model.

When the Froude scale law (Eq. [2-2]) is obeyed, other scale laws such as Reynolds (viscosity), Weber (surface tension), Cauchy (elastic force) … are disobeyed. The forces related with surface tension and elastic forces are known to be small in coastal problems, the viscosity effects can sometimes play a role of importance: e.g. wave propagation in a shallow harbor, wave propagation through the porous rubble mound armour and filter layers. It is therefore important to verify that the Reynolds number (Eq. [2-3]), the ratio between the inertial force and the viscous force, is larger than 10^{-4}. Reynolds numbers above this value represent turbulent flow, for which the scale effects due to kinematic viscosity are negligible.

$$Re = \frac{intertial\, force}{viscous\, force} = \frac{\rho L^2 V^2}{\mu' V L} = \frac{\rho L V}{\mu'} = \frac{LV}{\nu} \qquad [2\text{-}3]$$

where ρ is the density, L the length, V volume, μ' is the dynamic viscosity and ν the kinematic viscosity.

Experimental modelling will be used throughout the present work, as explained in section 2.1. Froude scaling is used since the here investigated topics relate to open water gravitational problems and viscosity does not play an important role. Reynolds numbers are well above 10^{-4}. A structure will be built in the flume, data is collected, (semi) empirical formulae are set up and the experimental coefficients are determined by curve fitting on data plots.

The European research project CLASH (De Rouck et al., 2009) investigated scale effects between prototype and scale model overtopping measurements. Prototype measurements were carried out at three real life coastal structures: an antifer breakwater in Zeebrugge, Belgium, a rubble mound breakwater at Ostia, Italy, and a vertical seawall with rubble mound toe protection in Samphire Hoe, UK. These three structures were also built in different wave flumes (2D) and wave basins (3D) at different scales: Zeebrugge 2D 1:30, Ostia 2D 1:20 and 3D 1:40, Samphire Hoe 2D 1:40 and 3D 1:20. Comparison of the prototoype and small scale data has led to a scale factor for wave overtopping. This factor is dependent on:

- the roughness: smooth dikes do not show significant scale or model effects, in contrast to rubble mound structures;
- the slope: scale effects have only been observed for sloping structures, not for vertical ones. The rougher the slope, the larger the scale effect;
- the mean overtopping discharge (upscaled to prototype): tests with discharges smaller than 1l/m/s (upscaled to prototype) have the largest scale effects. Above 1l/m/s (10^{-3}m³/m/s) prototype there is no (significant) scale effect.

The tests in the current research have smooth dikes and are thereby the overtopping results are not influenced by scale effects. Small scale tests will provide reliable results. Nevertheless, the smallest overtopping discharges, which represent (almost) zero-overtopping in real life, are most vulnerable to scale or model effects, despite being collected on smooth dikes. Overtopping of below 10^{-6}m³/m/s in model scale is disregarded in the data analysis of the UGent overtopping tests.

2.1.2 *Numerical modelling*

Numerical models for CFD (Computational Fluid Dynamics) are nowadays powerful tools to study phenomena of interaction between sea waves and coastal structures. Mesh-based methods (e.g. VOF) and mesh-free schemes (e.g. SPH) have been more and more intensively used in the last decade to study coastal engineering problems. Numerical methods can be employed especially to extend and extrapolate the main results from existing literature and experimental campaigns towards out-of-range parameter values or other more complex structures and, at the same time, they can overcome drawbacks of physical models such as model and scale effects and limitations in measurement technique. Numerical models also provide much more detailed information. EurOtop (2016) mentions for e.g. overtopping flow that both instantaneous parameters like velocities, pressures and free surface configuration, and integrated parameters like forces or individual and average overtopping volumes, can be obtained from a numerical model.

Nevertheless, numerical methods cannot completely replace experimental modelling. First, any numerical model does need to be validated against experimental results especially if the phenomenon under study has been never analyzed before with it. Second, numerical models are a quite accurate representation of the fluid dynamics, but none of the models is capable of treating all relevant physical processes all together in one model. They fall into main categories: Boussinesq models (Stansby, 2003), non-linear shallow water models, e.g. SWASH (Zijlema et al., 2011), and Navier Stokes (NS) equation models, both mesh-based (e.g. OpenFoam: Jensen et al. (2014)) and mesh-free (e.g. SPH: Dalrymple et al. (2001)). Any model has its own capabilities and disadvantages. For example, non-linear shallow water models are fast and very accurate for wave propagation and wave transformation problems, but they cannot cope with complex geometries (storm walls, stilling wave basins) because they are vertically integrated. On the other hand, NS models, both mesh-based and mesh-free, solve the whole governing equations of fluid but are quite computationally expensive (in obtaining a large amount of data). Mesh refinement techniques and coupling with less computational expensive models are possible solutions to increase the efficiency of NS models, however they still require high modelling skills and further validations.

Overtopping and post-overtopping processes are very complex, turbulent, stochastic, non-uniform, multi-scale and multi-phase phenomena that require accurate modelling and intense calculations if, as in the present study, the goal is to get new insight on complex fluid dynamics and fluid-structure interaction that haven’t fully been studied before. Therefore, numerical modelling is not the most viable and reliable way to proceed in the framework of this PhD. Later, in a detailed design study, numerical models can be very useful however.

2.1.3 *Field data*

Doing field measurements requires (super) storms to collect meaningful data. Most of the measures described in the current work are built along coastlines to prevent overtopping and flooding during super storms with a return period of e.g. 1000 years. This means that these measures statistically have a very low probability of being overtopped or experience impacts during their lifetime. The amount of data that could be collected would be too low for research purpose. In the European CLASH project prototype measurements were carried out, but the CLASH project ran for 4 years and only 132 data points were collected in 3 different prototype test set-ups. This is limited compared to the possibilities in a wave flume. For these reasons, collecting field data on prototype dikes was not an option. However, also in a flume large scale data can be obtained. Reference is made to Section 3.2.

2.1.4 *Neural Network*

A second goal of the CLASH project mentioned in Section 2.1.1 was to collect a large database of small-scale tests and train an artificial Neural Network (ANN) to predict wave overtopping. Over 10.000 tests on a variety of coastal structures were collected and identified by 31 (geometrical and hydraulic) parameters (van der Meer et al., 2009). A first ANN is described by van Gent et al. (2007) and is trained on data with overtopping dischargers larger than zero. An updated ANN by Verhaeghe et al. (2008) is trained on the same CLASH database but includes tests with small/zero overtopping. A two-phase procedure is introduced by Verhaeghe et al. (2008), where overtopping is first classified as significant or negligible (classifier phase) before it's calculated (quantifier phase).

In general the prediction quality of overtopping discharges by both ANN's is good, but it all depends on the geometry. If the tested geometry is in line with datasets for which the ANN was trained, the outcome is good, even outside the parameter validity interval of the original data. Unfortunately, the geometries in this PhD research were not part of the original ANN dataset and thus prediction of overtopping on modified crests by ANN shows poor results. Only few tests in the CLASH-database consisted of dikes with wave walls, no other crest modifications were available.

With the update to EurOtop (2016) the database is enlarged to over 13.500 overtopping tests and the predicting ANN has been improved (Formentin et al. (2014), Zanuttigh et al. (2016) and Zanuttigh et al. (2018)). Part of the database from this PhD has been used to train the new ANN, so the prediction for modified crests with the updated ANN will be better than with the previous ANN, although it is still ongoing work.

To date, wave induced forces cannot be predicted by means of the existing ANN's, because no network has ever been trained for such data.

2.2 *Wave Overtopping*

2.2.1 *Wave overtopping over coastal dikes*

The oldest method to quantify wave overtopping discharge over a sea defense structure is by means of semi-empirical prediction formulae, which have been set up by testing a scale model of a structure in a wave flume or wave tank. In the beginning, only regular waves were investigated, while since the 1970s datasets using irregular waves were produced leading to a more realistic simulation of sea states. A chronological overview of some important sources is given in this section for overtopping over smooth mild sloping structure. The review on overtopping is focused on the geometries studied in the present PhD research. Very steep or very gentle dike slopes, shallow foreshores, vertical structures and rubble mound structures are no part of this PhD research however steep slopes and vertical structures are briefly mentioned for a comparison later in this work.

Owen 1980

One of the first well-known overtopping formulae was developed by Owen (1980) and included in the British guidelines for sea defense structures. The formula is based on experimental modelling with random waves on simple dike slopes. The general way of presenting overtopping is by means of equation [2-4]:

$$Q_* = Q_0 \cdot exp(-b_{Owen} \cdot R_*) \qquad [2\text{-}4]$$

with Q_* the dimensionless overtopping discharge, R_* the dimensionless freeboard and Q_0 and b_{Owen} two empirical constants. The dimensionless values are given by equations [2-5] and [2-6] .

$$Q_* = \frac{q}{T_m \cdot g \cdot H_s} = \frac{q}{\sqrt{g \cdot H_s^3}} \cdot \sqrt{\frac{s_{0m}}{2\pi}} \quad [2\text{-}5]$$

$$R_* = \frac{R_c}{T_m\sqrt{g \cdot H_s}} = \frac{R_c}{H_s} \cdot \sqrt{\frac{s_{0m}}{2\pi}} \quad [2\text{-}6]$$

where q ($m^3/m/s$) is the average overtopping discharge over the structure, T_m the mean wave period, g the gravity acceleration ($9.81m/s^2$), H_s the significant wave height at the toe of the structure, R_c the crest freeboard and s_{0m} the wave steepness ($s_{0m} = H_s/L_m$ with L_m the wavelength equal to $g \cdot T_m^2/(2 \cdot \pi)$).

When substituting [2-5] and [2-6] in [2-4], this leads to equation [2-7] and its more known form equations [2-8] or [2-9].

$$\frac{q}{T_m \cdot g \cdot H_s} = Q_0 \cdot exp\left(-b_{Owen} \cdot \frac{R_c}{T_m\sqrt{g \cdot H_s}}\right) \quad [2\text{-}7]$$

$$\frac{q}{\sqrt{g \cdot H_s^3}} = Q_0 \cdot \sqrt{\frac{2\pi}{s_{0m}}} \cdot exp\left(-b_{Owen} \cdot \frac{R_c}{H_s} \cdot \sqrt{\frac{s_{0m}}{2\pi}}\right) \quad [2\text{-}8]$$

$$\frac{q}{\sqrt{g \cdot H_s^3}} = Q_0{}' \cdot exp\left(-b'_{Owen} \cdot \frac{R_c}{H_s}\right) \quad [2\text{-}9]$$

The coefficients Q_0 and b_{Owen} are given in Owen (1980). For simple dike slopes of 1:1, 1:2 and 1:4, the values of Q_0 and b_{Owen} were determined experimentally for the following range of parameters:

$0.05 < R_* < 0.30$
$10^{-6} < Q_* < 10^{-2}$
$1.5 < d/H_s < 5.5$
$0.035 < s_{0m} < 0.055$

where d is the water depth at the toe of the structure. The coefficients Q_0 and b_{Owen} depend on the slope of the dike. The derived coefficients Q_0' and b'_{Owen} from Eq. [2-9] depend on the slope of the dike and on the wave period T_m.

TAW 2002

Since the 1970s, a lot of research was carried out on wave run-up and wave overtopping at Delft Hydraulics (today: Deltares) in The Netherlands. In the 1990s results were published in a form that is still known today:

$$Q^* = A_q \cdot exp(-B_q \cdot R^*) \quad [2\text{-}10]$$

This is a little different than Owen's approach (Eq. [2-4]) due to different notation of dimensionless overtopping Q^* (Eq. [2-11]) and dimensionless freeboard R^* (Eq. [2-12]).

$$Q^* = \frac{q}{\sqrt{g \cdot H_{m0}^3}} \quad [2\text{-}11]$$

$$R^* = \frac{R_c}{H_{m0}} \quad [2\text{-}12]$$

Van der Meer (1993) published results from the experiments at Delft Hydraulics, and van der Meer & Janssen (1994) brought together results from the Delft Hydraulics tests (van der Meer, 1993), British tests (Owen, 1980) and German tests. Based on this, Dutch guidelines for wave run-up and wave overtopping on dikes were published in 2002 (TAW, 2002). In this report more data with a large variation in hydraulic and geometrical boundary conditions was brought together. A dimensionless plot of the available data is given with a regression formula that allows calculating average wave overtopping over a sloping structure. Difference is made for breaking and non-breaking waves, see Figure 2-1. The range of application for R_c/H_{m0} can be read from the graphs.

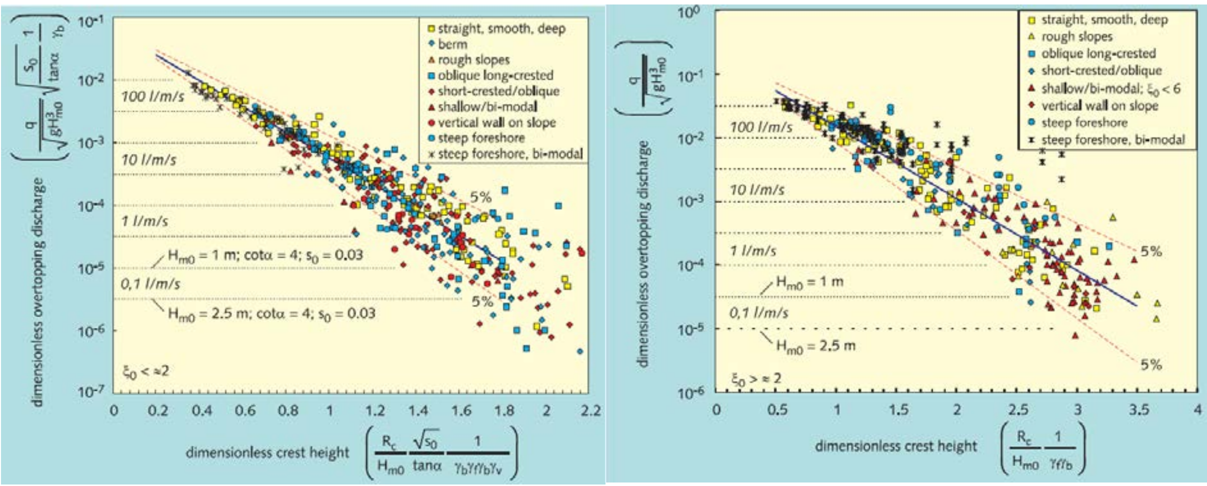

Figure 2-1. Dimensionless plot of breaking waves (left) and non-breaking waves (right).

The average overtopping discharge for **breaking waves** on a sloping dike is:

$$\frac{q}{\sqrt{g \cdot H_{m0}^3}} = \frac{0.067}{\sqrt{tan\alpha}} \cdot \gamma_b \cdot \xi_{m-1,0} \cdot exp\left(-4.75 \cdot \frac{R_c}{H_{m0}} \cdot \frac{1}{\xi_{m-1,0} \cdot \gamma_b \cdot \gamma_f \cdot \gamma_\beta \cdot \gamma_v}\right) \qquad [2\text{-}13]$$

with a maximum for **non-breaking waves**:

$$\frac{q}{\sqrt{g \cdot H_{m0}^3}} = 0.2 \cdot exp\left(-2.6 \cdot \frac{R_c}{H_{m0}} \cdot \frac{1}{\gamma_f \cdot \gamma_\beta}\right) \qquad [2\text{-}14]$$

where α is the slope angle of the dike, $\xi_{m-1,0}$ the wave breaker parameter based on the spectral wave period $T_{m-1,0}$, and γ a reduction factor for the influence of a berm (γ_b), roughness of the slope (γ_f), a vertical wall on top of the slope (γ_v) or oblique wave attack (γ_β). The distinction between breaking and non-breaking is made by calculating both values q from Eq. [2-13] and [2-14], and the minimum defines whether the waves are breaking or non-breaking. Experience has shown that the limit between both can be found at a breaker parameter of about $\xi_{m-1,0} = 1.82$ or $\xi_{0p} = 2$. Eq. [2-13] (breaking waves) is used until a maximum is reached in Eq. [2-14] (non-breaking waves). In a log-linear graph, both equations give a straight line, as shown in Figure 2-1.

The test range for breaking waves was $0.3 < \frac{R_c}{H_{m0}} \cdot \frac{1}{\xi_{m-1,0} \cdot \gamma_b \cdot \gamma_f \cdot \gamma_\beta \cdot \gamma_v} < 2.2$. The factor 4.75 in Eq. [2-13] is the average value of a normally distributed stochastic function, with a standard deviation $\sigma = 0.5$ ($\sigma' = \sigma/\mu = 0.10$) The test range for non-breaking waves was $0.5 < \frac{R_c}{H_{m0}} \cdot \frac{1}{\gamma_f \cdot \gamma_\beta} < 3.7$. The factor 2.6 from Eq. [2-14] is the average value, with a standard deviation $\sigma = 0.35$ ($\sigma' = \sigma/\mu = 0.13$).

γ is located in the denominator of the exponent. A γ-value lower than 1 shows a virtual increase of the crest freeboard, leading to a reduction of the overtopping discharge. When a certain influence is not present, the reduction factor γ is equal to one. With all γ-factors equal to one in the above formulae, Eq.

[2-13] and [2-14] are representing average overtopping discharge over a smooth impermeable dike with a simple slope and perpendicular wave attack.

There are some important differences between Owen (1980) formula [2-7] and TAW (2002) formulae [2-13] and [2-14]:

- There is no distinction between breaking waves and non-breaking waves in the Owen formula [2-7]. Owen’s formula probably overestimates overtopping for steep slopes (non-breaking waves).
- According to Owen, wave overtopping discharge is influenced by the wave period by means of the wave steepness $s_{0,m}$ over the full range from breaking to non-breaking, while in TAW through the wave steepness (the breaker parameter) a distinction is made between breaking and non-breaking but the non-breaking waves don’t show an additional dependency of the wave period: there is no s_{0m} or $\xi_{m-1,0}$ in Eq. [2-14].
- The dike slope angle is another active parameter according to Owen (different coefficients Q_0 and b_{Owen} for different slopes) while formula [2-14] shows no dependency for non-breaking waves.

Besides Owen, also the final report of the Dike-3D project (Kortenhaus et al., 2006) mentions a possible influence of the wave period, and they include a correction factor γ_{s0} to account for the wave steepness in the non-breaking formula. This in contrast to Eq. [2-14] where the wave period is not additionally included in the prediction formulae besides it’s classification between breaking and non-breaking waves.

Based on the above, it will be studied in the newly developed data whether the wave period and/or slope angle have an influence on average wave overtopping discharges in the tested range of parameters.

EurOtop 2007

In 2007 European coastal engineers published an assessment manual (EurOtop, 2007) that replaces the German, Dutch and British guidelines. The manual is more elaborate that only overtopping over smooth dikes, and also contains guidelines on tolerable discharges, run-up, overtopping over rubble mound slopes and vertical walls. For the calculation of overtopping over smooth dikes, the formulae of TAW (2002) and Owen (1980) are mentioned both, but the most recent research (TAW, 2002) is recommended since it is based on the largest database and also includes Owen’s original data. From 2007 on, Eq. [2-13] and [2-14] are used most often for overtopping over smooth dike calculations.

Victor 2012

Victor (2012) studied overtopping behavior on steep dike slopes and low crest freeboards. In his work he also investigated the influences of slope angle and the wave period.

The test range of Victor (2012) was limited to non-breaking waves with rather steep slopes (1V:2.75H to 3V:1H)[1]. For the mildest slopes in Victor’s tests (1:1 up to 1:2.75), a weak dependency of the slope angle on the overtopping discharges shows. For the most steep slopes (1:1 up to 3:1) the dependency is larger. In the tested range of slopes (1:2.74 to 3:1) the mildest slopes give the most

[1] Slopes in this work are always mentioned as V:H. A slope with $\cot(\alpha)=3$ is noted as 1:3, meaning 1 vertical, 3 horizontal

overtopping. Based on this slope dependency, Victor found a transition between the formula for non-breaking waves (Eq. [2-14]) and the overtopping formula over vertical walls.

Victor (2012) also shows that the influence of the wave period on the overtopping discharges is non-existent on first sight. Detailed study however has shown that there is an influence but it's limited compared to the effect of the relative crest freeboard and the slope angle. For the mildest slopes he tested (< 1:2.2) the largest wave period has the largest overtopping. For slopes 1:2 to 1:1 there is no influence, and for the steeper slopes 2:1 and 3:1 the smallest wave period leads to the largest overtopping. The influence of the wave period is small to negligible, but dependent on the slope angle.

Victor defined different formulae for the coefficients A_q and B_q in Eq. [2-10], where the influence of the slope angle and wave period is taken into account.

The current work uses slopes 1:2 and 1:3, where there is a weak slope dependency and negligible dependency of the wave period.

EurOtop 2016

Van der Meer & Bruce (2014), based on data by Victor (2012), a revision of early Dutch work from the 1970s and other datasets from the CLASH database, have modified the equations [2-13] and [2-14] to the following set of equations, valid for $\cot(\alpha) \geq 2$:

$$\frac{q}{\sqrt{g \cdot H_{m0}^3}} = \frac{0.023}{\sqrt{tan\alpha}} \cdot \gamma_b \cdot \xi_{m-1,0} \cdot exp\left[-\left(2.7 \cdot \frac{R_c}{H_{m0}} \cdot \frac{1}{\xi_{m-1,0} \cdot \gamma_b \cdot \gamma_f \cdot \gamma_\beta \cdot \gamma_v}\right)^{1.3}\right] \qquad [2\text{-}15]$$

with a maximum of: $$\frac{q}{\sqrt{g \cdot H_{m0}^3}} = 0.09 \cdot exp\left[-\left(1.5 \cdot \frac{R_c}{H_{m0}} \cdot \frac{1}{\gamma_f \cdot \gamma_\beta}\right)^{1.3}\right] \qquad [2\text{-}16]$$

These equations are also included in EurOtop (2016), with only one difference: the influence factor γ^* is included in the exponential part of the formula for non-breaking waves to account for the overtopping reduction by storm walls or promenades at crest level of the dike, based on Van Doorslaer et al. (2015a) and Van Doorslaer et al. (2016b). These papers are the results of the present work which will be explained later in this manuscript (Section 4.1). Consequently, the equations given in EurOtop (2016) are Eq. [2-15] and [2-17], with only changes in the formula for non-breaking waves (addition of γ^*), valid for $\cot(\alpha) \geq 2$ and $R_c/H_{m0} \geq 0$:

$$\frac{q}{\sqrt{g \cdot H_{m0}^3}} = \frac{0.023}{\sqrt{tan\alpha}} \cdot \gamma_b \cdot \xi_{m-1,0} \cdot exp\left[-\left(2.7 \cdot \frac{R_c}{H_{m0}} \cdot \frac{1}{\xi_{m-1,0} \cdot \gamma_b \cdot \gamma_f \cdot \gamma_\beta \cdot \gamma_v}\right)^{1.3}\right] \qquad [2\text{-}15]$$

with a maximum of: $$\frac{q}{\sqrt{g \cdot H_{m0}^3}} = 0.09 \cdot exp\left[-\left(1.5 \cdot \frac{R_c}{H_{m0}} \cdot \frac{1}{\gamma_f \cdot \gamma_\beta \cdot \gamma^*}\right)^{1.3}\right] \qquad [2\text{-}17]$$

Due to the exponent 1.3, Eq. [2-15] and [2-17] no longer give a straight line in the log-linear graph but give a slight curved trend. For sloping structures with dimensionless freeboards $R_c/H_{m0} > 0.5$ the difference between these new formulae and the ones from EurOtop (2007) is small. The improvement from Eq. [2-13] and [2-14] to Eq. [2-15] and [2-17] is mainly in the area of very low freeboards, including zero freeboard: $0 \leq R_c/H_{m0} \leq 0.5$. The previous equations [2-13] and [2-14] were only valid for $R_c/(H_{m0} \cdot \xi_{m-1,0} \cdot \gamma) > 0.3$ (breaking waves) or $R_c/(H_{m0} \cdot \gamma) > 0.5$ (non-breaking waves) but were often (mis)used for smaller freeboards too. It can be seen in Figure 2-2 for breaking waves that in this zone of small freeboards the largest differences occur. Almost identical conclusions can be seen in Figure 2-3 for non-breaking waves. The difference between old (EurOtop, 2007) and new (EurOtop, 2016) is explained in EurOtop (2016) and lies within the range +/- 30%. It is concluded that this difference is much smaller than the reliability of overtopping predictions. The reliability is a factor 2.5 for the largest overtopping discharges to a factor 20 for the smallest overtopping discharges, based on the 90% confidence interval of the measured data.

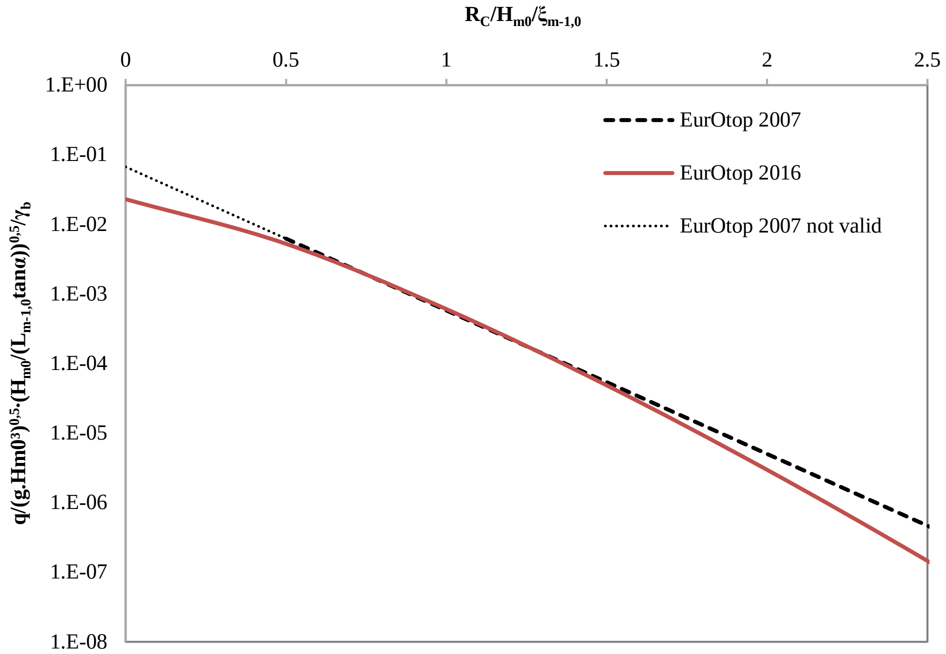

Figure 2-2. Comparison of EurOtop (2007) formula for breaking waves with the new formula in EurOtop (2016).

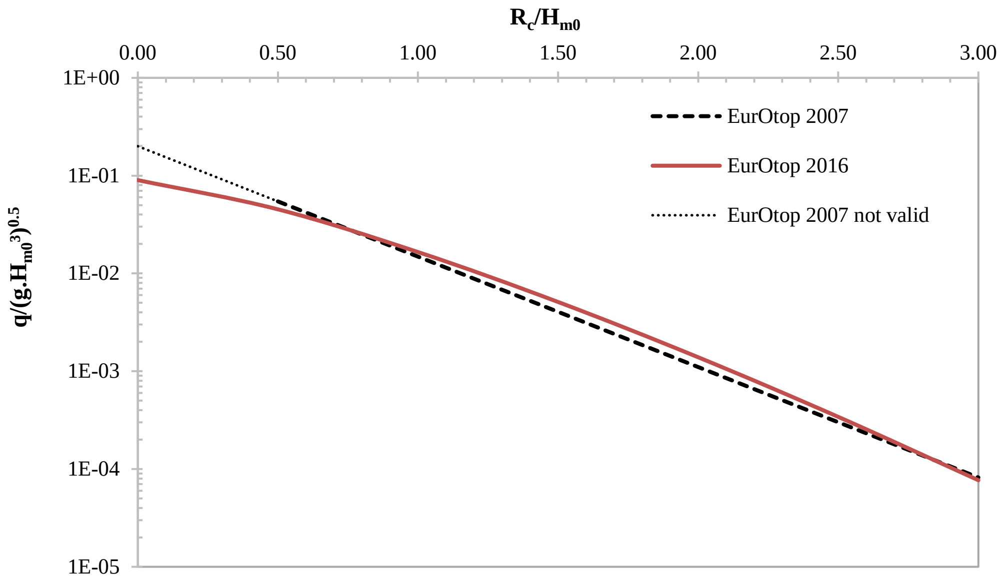

Figure 2-3. Comparison of EurOtop (2007) formula for non-breaking waves with the new formula in EurOtop (2016).

It was mentioned that Eq. [2-15] and [2-17] are valid for $\cot(\alpha) \geq 2$. For steeper slopes, the constant coefficients 0.09 and 1.5 change and become function of the dike slope angle (see Eq. 5.18 in

EurOtop (2016)), based on research by Victor (2012). Also Goda (2009) defined prediction formulae that cover the range from sloping dikes to vertical structures where the empirical coefficients depend on the slope angle and the wave height at the toe of the structure. However, since the dike slopes in the present study are $\cot(\alpha)$ = 2 to 3, the constant coefficients 0.09 and 1.5 from Eq. [2-15] and [2-17] can be used.

Gallach Sanchez 2018

The work by Victor (2012) was continued and improved by Gallach Sanchez (2018) for low-freeboard cases and steep dike slopes. Based on new data for very small and zero freeboards, Gallach Sanchez (2018) published an empirical coefficient c = 1.1 instead of c = 1.3 by EurOtop (2016), which brings the trendline almost back to a straight instead of a curved line. Since the current research has parameter range for $R_c/H_{m0} > 0.5$, the prediction equations by Gallach Sanchez (2018) are however not used in this work.

Equations to be used in the present work

The EurOtop formulation is used in the present work, since this is the most recent recommendation (EurOtop, 2016) and based on the largest database (including the one from Owen (1980)).

The study on the influence of a wave wall on the overtopping of non-breaking waves started in 2008 and dates from before van der Meer & Bruce (2014) published their improved equations [2-15] and [2-16]. This means that the reduction factors γ for non-breaking waves have been derived with the former formula [2-14] from EurOtop (2007).

Eq. [2-18] shows the shape of the equations as in EurOtop (2007), with the reduction factor in the exponential part of the formula.

$$\frac{q}{\sqrt{g \cdot H_{m0}^3}} = A_q \cdot exp\left(-B_q \cdot \frac{R_c}{H_{m0}} \cdot \frac{1}{\gamma}\right) \qquad [2\text{-}18]$$

After the update by van der Meer & Bruce (2014), the formula has been changed to the shape Eq. [2-19] in EurOtop (2016). The reduction factor γ in the exponential part of the formula is thus also underneath the power c = 1.3.

$$\frac{q}{\sqrt{g \cdot H_{m0}^3}} = a \cdot exp\left[-\left(b \cdot \frac{R_C}{H_{m0} \cdot \gamma}\right)^c\right] \qquad [2\text{-}19]$$

Although mathematically different equations, the reduction factor γ derived in Eq. [2-18] can still be used in Eq. [2-19]. Molines & Medina (2015) have selected over 1000 tests in the CLASH database for different armour units, and have recalculated the reduction factor for slope roughness, γ_f, for Eq. [2-18] and Eq. [2-19]. The obtained differences in γ are minimal. By using a reduction factor that has been developed based on Eq. [2-18] in Eq. [2-19], the difference on q is smaller than the uncertainties on the overtopping formulae [2-18] or [2-19]. This justifies the use of γ derived in Eq. [2-18] to be used in Eq. [2-19].

An example case is given in Table 2-1 where overtopping is calculated over a steep smooth sloping structure, non-breaking waves (Eq. [2-14] resp. [2-17]). The freeboard R_c is 2m, the wave height H_{m0} = 1.5m.

Table 2-1. Example case: absolute values of old formula versus new formula change, but the amount of reduction remains the same regardless of which formula is used.

q for R_c = 2m, H_{m0} = 1.5m	Old formula EurOtop (2007) (Eq. [2-14])	New formula EurOtop (2016) (Eq. [2-17])	% difference
Reference situation, smooth dike: No reduction factor	35.9 l/m/s	44.1 l/m/s	18.6%
Reducing geometry with reduction factor γ = 0.7	8.1 l/m/s	10.3 l/m/s	21.4%
% reduction	77.4%	76.6%	0.8%

The absolute values for both the reference situation and the situation with reduction element are different when using the EurOtop (2016) formula (Eq. [2-17]) compared to the old formula (Eq. [2-14]); reading the horizontal lines in Table 2-1 shows a difference of 18.6 resp. 21.4% more overtopping when using the new formula. This can also be seen in Figure 2-3 for dimensionless freeboard of 1.33. These differences are smaller than the uncertainties on the overtopping formulae.

Despite this absolute difference, the reducing capacity is the same regardless which formula is used: reading the vertical columns in Table 2-1 shows a reduction of 77.4% by the old formula, where the new formula shows a reduction of 76.6%. A similar conclusion is found for non-breaking waves Eq. [2-13] vs Eq. [2-15].

The conclusion of this example is that the reduction factors as derived with the old formulae can be used in the new overtopping formulae [2-15] and [2-17]. This is also shown in EurOtop (2016) in its Figure 5.16.

2.2.2 *Wave overtopping over vertical structures*

The topic of this PhD manuscript is related to smooth dikes and reduction of wave overtopping over such smooth dikes, e.g. by a storm wall at the crest level of a dike. Adding a storm wall to the crest of the dike makes the average slope steeper. Victor (2012) studied steep dike slopes and provided slope dependent A_q and B_q coefficients in Eq. [2-18]. The extreme boundary of a steep dike slope is a vertical wall. Analysis of vertical wall data without foreshore slope by van der Meer & Bruce (2014) shows that for small freeboards (R_c/H_{m0} < 0.91) Eq. [2-22] by Allsop et al. (1995) and for large freeboards (R_c/H_{m0} > 0.91) Eq. [2-21] by Franco et al. (1994) should be used.

$$\frac{q}{\sqrt{g \cdot H_{m0}^3}} = 0.05 \cdot exp\left(-2.78 \cdot \frac{R_c}{H_{m0}}\right) \qquad \text{For } R_c/H_{m0} < 0.91 \qquad [2\text{-}20]$$

$$\frac{q}{\sqrt{g \cdot H_{m0}^3}} = 0.2 \cdot exp\left(-4.3 \cdot \frac{R_c}{H_{m0}}\right) \qquad \text{For } R_c/H_{m0} > 0.91 \qquad [2\text{-}21]$$

Eq. [2-20] and [2-21] and Victor (2012)'s approach for a dike slope 1:1 will be plotted along with the data over dikes with a storm wall later in Section 4.1.2b)

2.3 *Reduction factors for wave overtopping*

In this section, the existing literature on crest modifications to reduce wave overtopping over smooth dikes is described.

2.3.1 *Storm wall and bullnose*

EurOtop (2007) includes a section on the effect of wave walls on sloping structures. It is stated that the knowledge on this geometry is limited and only a few model studies were available, and therefore it's recommended to use the Neural Network from van Gent et al. (2007) or Verhaeghe et al. (2008) for more reliable calculations. However, in Section 2.1.4 is shown that these ANN's have not been trained on much data for dikes with wave walls, so that statement in EurOtop (2007) is questionable. The procedure to calculate the reduction due to wave walls in EurOtop (2007) is based on van der Meer (1997) and contains the following steps: a first step is to calculate the average slope α_{avg} by changing the vertical wall by a 1:1 slope (Figure 2-4). This allows to calculate the wave breaker parameter ξ_{0p} deciding whether the breaking ($\gamma_b\xi_{0p} < 3$) or non-breaking ($\gamma_b\xi_{0p} \geq 3$) overtopping formula should be used. Notice that the transition is at $\xi_{0p} = 3$ for dikes with storm wall, which is different than in Section 2.2 for plain dikes where the transition is at $\xi_{0p} = 2$. Next, EurOtop (2007) introduces Eq. [2-22] :

$$\gamma_v = 1.35 - 0.0078 \cdot \alpha_{wall} \qquad [2\text{-}22]$$

where α_{wall} is the angle of the wall in degrees (between 45° for a 1:1 slope and 90° for a vertical wall), which leads to $\gamma_v = 0.65$ when a vertical wall is present, and $\gamma_v = 1$ when no wall is present. The last step in the procedure is that data with $\gamma_b\xi_{0p} \geq 3$ have to be calculated with Eq. [2-14] without a γ_v in the equation, and data with $\gamma_b\xi_{0p} < 3$ have to be calculated with Eq. [2-13] where γ_v according to Eq. [2-22] is included.

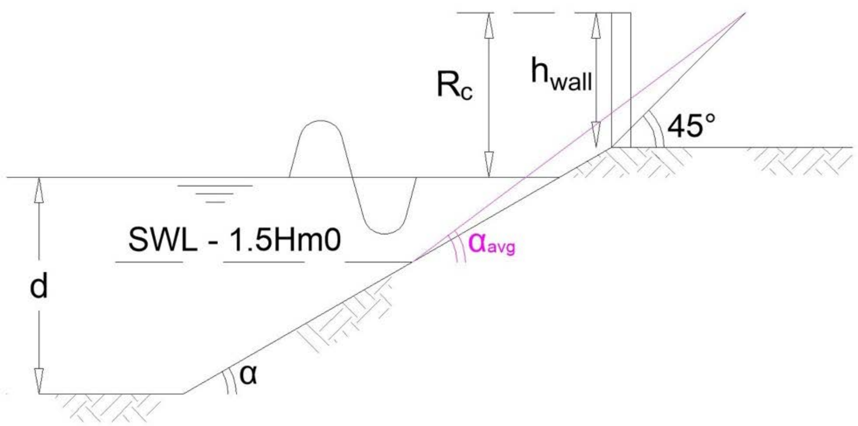

Figure 2-4. Determination of the average slope α_{avg} from $1.5H_{m0}$ below SWL to the run-up height or top of the construction. The vertical wall is replaced by a 1:1 slope.

The procedure and analysis behind Eq. [2-22] was based on a dataset from 1994 for Harlingen in The Netherlands. It will be explained in more detail in Section 3.5 and will be reanalyzed in Section 4.1 together with the present dataset on wave walls on top of a smooth sloping structure.

New work by Tuan (2013) was published which gives an approach to calculate the reduction due to crown-walls on low crested sea dikes. Tuan defined a reduction factor for the influence of a vertical wall on top on the slope in the breaking wave equation Eq. [2-13] and in the non-breaking formula [2-14]:

$$\gamma_w = \frac{1}{1 + 1.60 \cdot \frac{W}{A_c} \frac{1}{\xi_{m-1,0}}} \qquad [2\text{-}23]$$

where W is the wall height and A_c is the difference between the toe of the storm wall (= top of the slope) and the still water level, see Figure 2-5. Tuan (2013) also uses A_c instead of R_c in Eq. [2-14], thereby changing it into Eq. [2-24]. He compiles the effect of the wave wall fully in the reduction factor γ_w and excludes it from the freeboard by using A_c instead of R_c.

$$\frac{q}{\sqrt{g \cdot H_{m0}^3}} = 0.2 \cdot exp\left(-2.6 \cdot \frac{A_c}{H_{m0}} \cdot \frac{1}{\gamma_f \cdot \gamma_\beta \cdot \gamma_w}\right) \qquad [2\text{-}24]$$

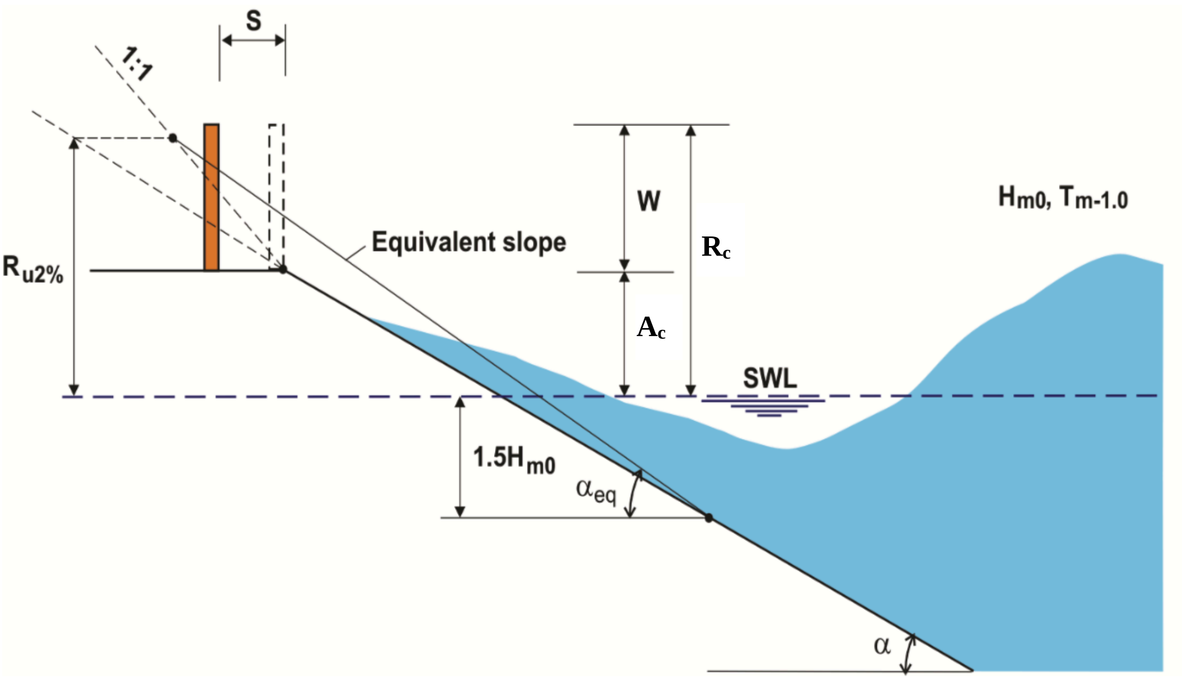

Figure 2-5. Definition of parameters by Tuan (2013), slightly modified to fit the parameter definition in this manuscript.

Furthermore, Tuan (2013) advises to use the actual slope angle α instead of the equivalent slope angle α_{eq} as is done in EurOtop (2007).

The approach by EurOtop (2007) and the approach by Tuan (2013) will be used for the dike with storm wall and compared with the current data set.

Kortenhaus et al. (2001) discuss Storm Surge Protection (SSP) walls (see Figure 2-6 left), which will be treated in section 2.3.3 as geometry ‘promenade + wall’. In the SSP project, the focus is mainly on impact forces on the wall, but the authors also deal with the overtopping reduction shortly. It is mentioned that a so-called overtopping reducer (Figure 2-6 right), comparable to the bullnose investigated in this PhD, is an efficient method to further reduce wave overtopping, especially for dimensionless freeboards $R_c/H_{m0} > 1.2$.

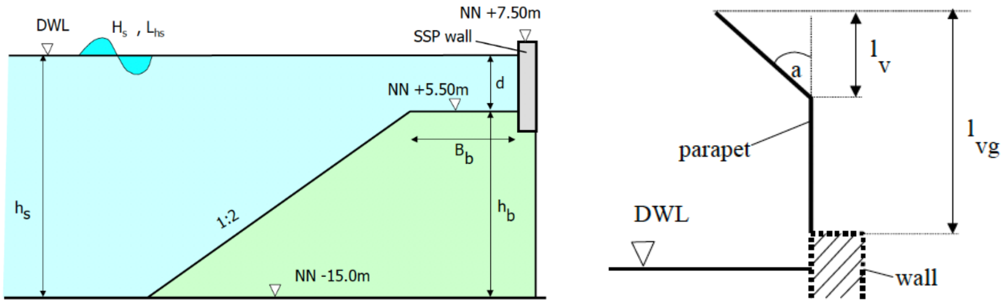

Figure 2-6. Storm Surge Protection (SSP) walls by Kortenhaus et al. (2001). A bullnose is added (right) to reduce the wave overtopping discharges.

Cornett et al. (1999), Kortenhaus et al. (2003) and Pearson et al. (2004) discuss the reduction for overtopping on vertical walls (caisson, quay wall, …) and not on sloping structures. Cornett et al. (1999) studied a caisson with 3 angles of overhanging wall geometry: 30°, 45° and 60°. They found a γ-factor starting from 0.9 up to 0.7. Even a relatively modest overhang inclined 30° with respect to vertical can reduce overtopping discharges by a factor of 10 or more. The extent of the decrease in overtopping discharges at the overhanging wall was found to be highly variable, depending on the water level and wave conditions. No generic method is proposed in Cornett et al. (1999) to calculate the reduction factor. Kortenhaus et al. (2003) and Pearson et al. (2004) developed a generic method to determine a k-factor defined as the ratio of overtopping discharge with parapet to the overtopping discharge without parapet. This method is unfortunately not applicable here since the present study always has a sloping dike which does not fit the used parameters by Kortenhaus et al. (2003) and Pearson et al. (2004). Following to these works, very new information recently became available by Castellino et al. (2018), numerical research, and Martinelli et al. (2018), experimental research. Both also investigated a recurve parapet added to a caisson breakwater, where the parapet has a curved angle and varies between 0° and 90° (see Figure 2-7). A continued reduction of overtopping can be seen for larger angles, and the k-factor by Pearson et al. (2004) has been confirmed.

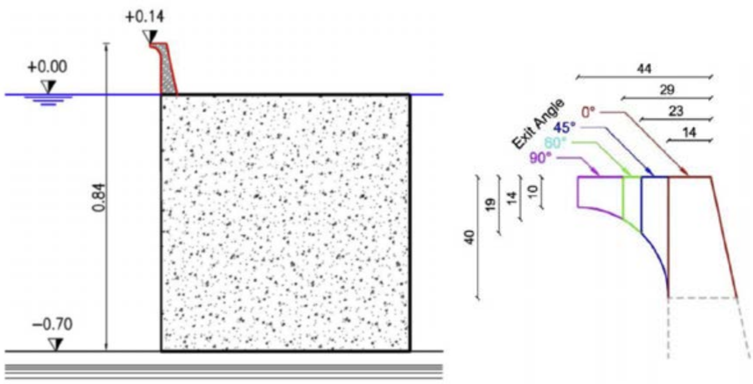

Figure 2-7. Vertical structures with curved parapets by Castellino et al. (2018) and Martinelli et al. (2018)

Some studies exist with a storm wall with or without parapet on top of a rubble mound breakwater, which is a sloping structure. Coeveld et al. (2006) define a parameter Q’ which is similar to the k-factor by Kortenhaus et al. (2003): the ratio of overtopping discharge of a breakwater with crest element to one without crest element. This ratio Q’ depends on a number of parameters:

- an exponential decreasing trend for increasing R_c/H_{m0} was found;
- no relationship between Q’ and the wave period was found;
- a decrease of Q’ was observed for an increase in nose length;
- a decrease of Q’ was observed for an increase in crest width;

The ratio Q' is defined as

$$Q' = 1.55 \cdot e^{-4\frac{h_{wall}}{H_{m0}} - 0.4\frac{G_c}{H_{m0}} - 2\frac{N_L}{H_{m0}}} \qquad [2\text{-}25]$$

where h_{wall} is the wall height, G_c the crest width and N_L the length of the bullnose. The authors believe that the ratio filters out the roughness of the rubble mound breakwater and is therefore also applicable on smooth slopes with and without storm wall with bullnose. However, Coeveld et al. (2006) state that their data show bad comparison with Eq. [2-14]. A better comparison was found to compute the overtopping over the rubble mound breakwater without storm wall with the Neural Network approach, and then using Eq. [2-25] to include the effect of the storm wall with bullnose. Eq. [2-25] will be tested on the data used in this thesis.

2.3.2 *Promenade*

As defined in the list of definitions in the beginning of this manuscript, the (quasi) horizontal part at crest level is called promenade. It contains a gentle slope of 1% to 2%, to stimulate drainage from rainfall and overtopped water towards the sea. A promenade is different than what is meant by the term "berm" in the EurOtop manual. A berm is a (quasi) horizontal part in the dike slope and often located around the design water level, to reduce the average slope and thereby reduce wave overtopping discharges. The promenade in this study is at crest level, clearly above SWL. Thereby, the reduction coefficient as presented in EurOtop (2007) might not be the best prediction tool for promenades. Nevertheless, it will be checked with the data used here.

The EurOtop (2007) and EurOtop (2016) equations for the presence of a berm are given in Eq. [2-26] to [2-28].

$$\gamma_b = 1 - r_B(1 - r_{db}) \text{ for } 0.6 \leq \gamma_b \leq 1.0 \qquad [2\text{-}26]$$

with r_B a factor for the width of the berm (B is the actual berm width, L_{berm} is the horizontal distance from 1 wave height below the berm to 1 wave height above the berm, see Fig 5.40 in EurOtop (2016)):

$$r_B = \frac{B}{L_{berm}} \qquad [2\text{-}27]$$

and r_{db} a factor for the height of the berm (d_b is the height of the berm above or below the SWL and $R_{u2\%}$ is the calculated run-up height):

$$r_{db} = 0.5 - 0.5cos\left(\pi\frac{d_b}{R_{u2\%}}\right) \qquad [2\text{-}28]$$

EurOtop (2007) also mentions that if the overtopping is not measured at the end of the slope, but a few meters backwards the hazard effect of overtopping will reduce. As a rule of thumb, a reduction $q_{effective} = q_{crest}/x_C$ where x_C is the backwards distance between 5 and 25, is mentioned. This is however not based on measurements, but just an indication that the promenade can reduce wave overtopping effects. A factor 5 to 25 is probably too much (and the advice is also not maintained in EurOtop (2016)), but this will be further studied with the present data set.

Tuan (2013) also introduces a reduction factor for a (small) crest width:

$$\gamma_s = \frac{1}{1 + \frac{1}{8} \cdot \frac{S}{H_{m0}} \cdot \frac{1}{\xi_{m-1,0}}} \qquad [2\text{-}29]$$

where S is the distance between the top of the slope and the location of the wall. It's similar to the promenade width G_c in Figure 1-9, but much smaller. The experiments in Tuan (2013) are based on typical Vietnamese coastal dikes which have less space between the crest of the dike slope and the wave wall (1m-2m prototype) than the promenades in this PhD (10m-20m prototype) and therefore out of the range of this study. A second remark is that Tuan (2013) did not test individual small crests, but always in combination with a wave wall at the end of his crest (see Eq. [2-32]). He calculated the reduction due to the crest width as the fraction between the combined promenade-wall reduction factor and the reduction factor of the wall only.

2.3.3 *Promenade with storm wall at the end*

As mentioned in the previous section, Tuan (2013) measured overtopping over a wave wall at the end of a very short crest width S (1 to 2m prototype). The following equations were given for the reduction factor of the combined influence of a wave wall and the crest width:

$$\gamma_{ws} = \gamma_w \cdot \gamma_s \qquad [2\text{-}30]$$

$$\frac{q}{\sqrt{g \cdot H_{m0}^3}} = 0.2 \cdot exp\left(-2.6 \cdot \frac{A_c}{H_{m0}} \cdot \frac{1}{\gamma_f \cdot \gamma_\beta \cdot \gamma_{ws}}\right) \qquad [2\text{-}31]$$

Eq. [2-30] implies that the total reduction factor can be achieved by multiplying individual factors. For the work by Tuan (2013), that statement is true because he only has data of the combined geometry "crest width with storm wall at the end" and no independent data for the crest width alone; the Vietnamese crests (1-2m prototype) are too small for investigating the separated influences of crest or storm wall. However, the general statement that reduction factors can always be multiplied to account for a combined effect of individual influences is investigated in Section 4.2.

Kortenhaus et al. (2001) discuss Storm Surge Protection (SSP) walls, which is a similar geometry compared to the dike with promenade and storm wall in Figure 1-9. In the current PhD research, the promenade is always above the SWL, while in the SSP-project there is a considerable water depth on the promenade, which is a different hydraulic situation (see Figure 2-8). The horizontal platform is then a berm, not a promenade. Instead of an overtopping bore (like in the current study), waves face the SSP wall directly.

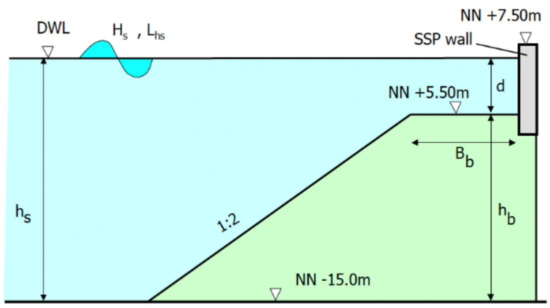

Figure 2-8. Generalised cross section of storm surge protection walls. Figure by Kortenhaus et al. (2001).

It is mentioned in the SSP project that the wave period has a significant influence on the overtopping rates for the tested geometries (dike with berm and storm wall). Also Pearson et al. (2004), who studied the effectiveness of bullnoses on vertical walls, claim to see a clear dependency of the wave period on the overtopping discharges. However, both papers don't establish a generic method to account for this dependency. As mentioned in the previous section, the dependencies of the wave period will be verified in the current data set.

2.3.4 *Stilling Wave Basin*

A stilling wave basin (SWB) is a construction of a storm wall at the crest level of the dike, followed by an overspill basin and a second storm wall, see Figure 2-9. The incoming waves hit the first wall, are projected upward and drop in the basin before hitting the landward wall. By dropping in the basin and by running back and forth between the walls, the energy of the incoming wave is heavily reduced and much less overtopping occurs over the seaward wall. Some literature is available on these topics ((Beels (2005), Geeraerts et al. (2006) and Geeraerts & De Rouck (2008)), but it all belongs to the research project of Ghent University on reduction of wave overtopping, and is thereby included in this work (Section 4.2.5). Specifically on the Stilling Wave Basin, some external literature (not from Ghent University) was found on overspill basins in rubble mound breakwaters (Aminti & Franco (2001), Burcharth & Lykke Andersen (2006), Cappietti & Aminti (2012)). The latter show that a storm wall and an overspill basin can have similar behavior in terms of reducing average overtopping discharges, but the overspill basin acts twice as good than the storm wall regarding individual wave overtopping events. Both measures can decrease the average discharge up to a factor of 2 under the tested conditions (Aminti & Franco, 2001). Further, it is stated that the volume of the overspill basin plays a role, but the freeboard remains the most important parameter. A last important finding is that the water in the basin should be allowed rapid drainage in order to maintain the efficiency of the basin. This latter condition is confirmed by Burcharth & Lykke Andersen (2006). Therefore, openings in the seaward wall(s) are recommended.

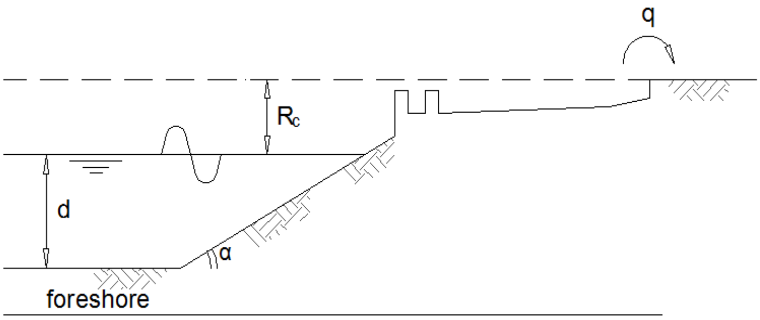

Figure 2-9. A stilling wave basin with a (double) front wall, an overspill basin and a second storm wall before the waves can overtop the structure.

In the SSP project by Kortenhaus et al. (2001) the implementation of "underwater barriers" on the promenade (Figure 2-10 right) was also described as overtopping reducing measure. This is similar to an SWB but again with the difference that the SWB in the present study is located above the SWL and in the SSP project it's located under water. One of the conclusions by Kortenhaus et al. (2001) is that a certain horizontal space should be available between the underwater barrier and the SSP wall, to allow wave energy dissipation.

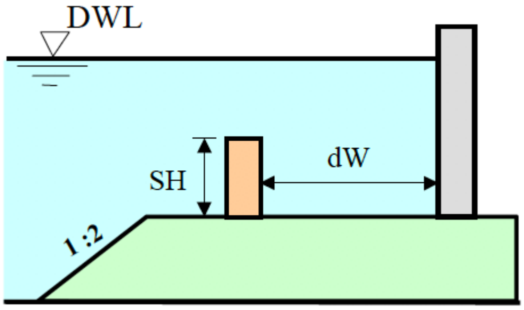

Figure 2-10. Constructional measures to reduce wave overtopping and loading of storm surge protection walls by creating an underwater barrier. Figure by Kortenhaus et al. (2001).

2.3.5 *Other influences*

There are several other influences that reduce wave overtopping: roughness of the dike slope, artificial roughness elements such as blocks or steps, porosity of the structure, oblique wave attack, a berm intermediate in the slope, … EurOtop (2016) describes all these influences in detail and expresses reduction factors. They are however not studied in the current work, and therefore not reported in this literature overview. In all tests carried out for this work, smooth impermeable dike slopes ($\gamma_f = 1$) without berms ($\gamma_b = 1$) were tested with perpendicular incoming waves ($\gamma_\beta = 1$).

2.4 *Flow depth and flow velocity*

The overtopped wave on the dike crest will be referred to as overtopped bore in this thesis. When a wave overtops the seaward slope of a dike, it could be considered as a breaking wave propagating across the flat seabed in the form of a spilling breaker. The turbulence, and therefore also the propagation and energy dissipation process, is qualitatively similar to the process of a bore (Chen, 2016). This bore is characterized by two important flow parameters (flow depth and flow velocity), that have an influence on the successive impact of an overtopped bore on a storm wall. A summary of available literature on these flow parameters is given in this section.

Since dike failures and breaches often occurred due to erosion of the landward slope of the dike initiated by overtopped waves, Schüttrumpf and van Gent have independently studied the overtopping flow parameters (Schüttrumpf (2001), Schüttrumpf et al. (2002), van Gent (2001) and van Gent (2002)). They both notified that the failures could not be described by an average approach, since it are mainly extreme events with a low exceedance probability that cause failure. Both authors gave formulae for the flow depth $h_{2\%}$ and flow velocity $U_{2\%}$, each only exceeded by 2% of the waves. For their research, they divided the structure in three zones: a seaward slope, the crest (= the promenade) and the landward slope, see Figure 2-12. The last zone is not of interest for this work, and will therefore not be further discussed.

The flow velocity U is actually the discrete value U_{max}, the maximum value of the velocity recording of one bore. Similar for the flow depth h, short for h_{max}, which is the maximum of the flow depth recording of one bore (Figure 2-11). U_{max} and h_{max} are individual bore related values, and not the maxima over a longer duration test. $U_{2\%}$ and $h_{2\%}$ are then the values of U_{max} and h_{max} that are only exceeded by 2% of the recorded values. If the maximum values within a full test are meant, the subscript is written in capital letters: h_{MAX} and U_{MAX}.

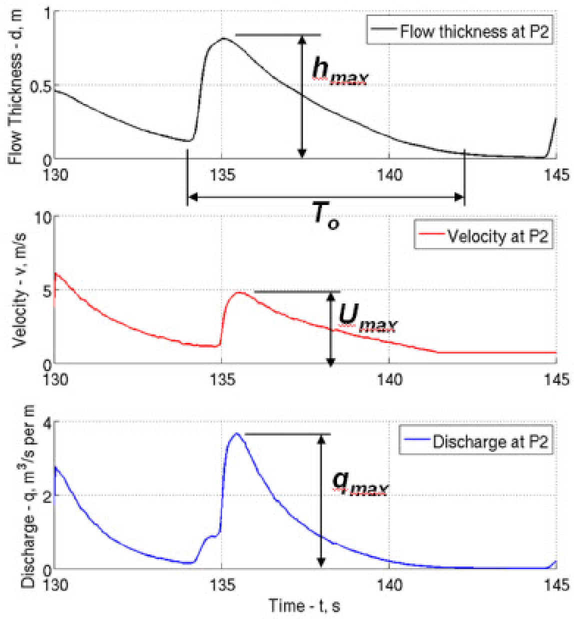

Figure 2-11. Definition of flow depth h_{max} = h and flow velocity U_{max} = U. Figure by Hughes et al. (2012).

Schüttrumpf and Van Gent found similar formulae but different experimental coefficients for the flow parameters on the seaward slope and on the crest. Other researchers have performed extra tests or did extra analysis on the existing data sets, of which a summary is provided below.

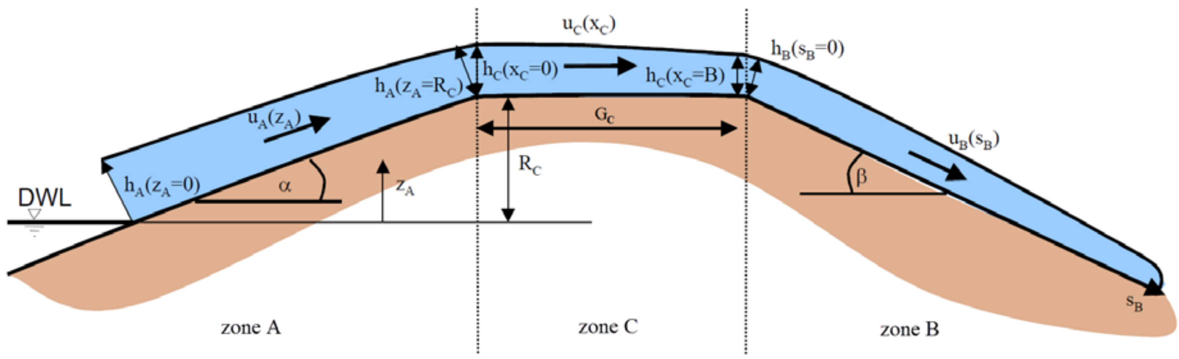

Figure 2-12. Definition of the overtopping flow parameters by Schüttrumpf & van Gent (2003). In accordance with EurOtop (2016), the crest width is renamed (G_c instead of B in the original figure).

The layer thickness in the run-up slope (zone 3 in Figure 1-9; zone A in Figure 2-12) can be calculated by assuming a linear decrease of the layer thickness from SWL to the highest point of the wave run-up:

$$\frac{h_{A,2\%}}{H_s} = c^*_{A,h}\left(\frac{R_{u,2\%} - z_A}{H_s}\right) \qquad [2\text{-}32]$$

where $h_{A,2\%}$ is the flow depth on the seaward slope exceeded by 2% of the incident waves, H_s the significant wave height, $c^*_{A,h}$ an empirical coefficient, $R_{u,2\%}$ the run-up height on a very high slope exceeded by 2% of the incident waves and z_A the position on the seaward slope with respect to the SWL. Some authors also express $h_{A,2\%}$ in terms of $(x_Z – x_A)$, which is the difference on the horizontal axis and only differs from the vertical difference $(R_{u,2\%} - z_A)$ by $\tan(\alpha)$.

The wave run-up velocity is defined as the front velocity of the run-up tongue. It is determined by a simplified energy equation:

$$\frac{U_{A,2\%}}{\sqrt{gH_S}} = c^*_{A,U} \cdot \sqrt{\frac{R_{U,2\%} - z_A}{H_S}} \quad [2\text{-}33]$$

where $U_{A,2\%}$ is the wave run-up velocity exceeded by 2% of the incident waves, g the gravity acceleration and $c^*_{A,U}$ an experimental fitting coefficient.

On the dike crest (zone 4 in Figure 1-9, zone C in Figure 2-12), the flow parameters depend on the incoming flow depth and flow velocity at the transition between the seaward slope and the crest. This is found by substituting $z_A = A_C$ (A_C is the seaward crest freeboard as indicated in Figure 1-9) in [2-32] and [2-33]. Eq. [2-34] and [2-35] show an exponential decay of the flow parameters over the crest width.

$$\frac{h_{C,2\%}(x_C)}{h_{C,2\%}(x_C = 0)} = exp\left(-c^*_{c,h}\frac{x_C}{G_c}\right) \quad [2\text{-}34]$$

$$\frac{U_{C,2\%}(x_C)}{U_{C,2\%}(x_C = 0)} = exp\left(-c^*_{c,U}\frac{x_C \cdot f}{h_{C,2\%}(x_C)}\right) \quad [2\text{-}35]$$

where $h_{c,2\%}$ and $U_{c,2\%}$ respectively are the flow depth and flow velocity on the crest exceeded by 2% of the incident waves. x_C is the location on the crest, starting with 0 at the seaward side of the crest. G_c is the width of the dike crest (Figure 2-12), f is the friction coefficient of the crest (f = 0.01 for smooth slopes) and $c^*_{C,h}$ and $c^*_{C,U}$ are empirical coefficients.

Van Gent (2001) observed that the maximum thickness of the water layer does not necessarily occur at the same time as the maximum velocity. These maxima can be 'within the same overtopping wave at different positions of time' but can also be 'within different waves'.

After the research of Schüttrumpf and Van Gent in 2001 and 2002, a joint paper was published (Schüttrumpf & van Gent, 2003). This was followed by Schüttrumpf & Oumeraci (2005) and EurOtop (2007) who all published different empirical coefficients for Eq. [2-32] to [2-35]. These coefficients are summarized in Table 2-2.

Also Bosman et al. (2008), Van der Meer et al. (2012), Lorke et al. (2012), Hughes et al. (2012) and Hughes (2015) have published research results on overtopping flow parameters, with some modifications to the above mentioned equations and constants.

Bosman et al. (2008) reanalyzed the data by van Gent and Schüttrumpf and assigned the difference between both approaches to the slope angle of the dike. He proposed the same Eq. [2-32] and [2-33] where the empirical constants depend on the slope: $c^*_{A,h} = \frac{9 \cdot 10^{-3}}{sin^2(\alpha)}$ and $c^*_{A,U} = \frac{0.30}{sin(\alpha)}$. He also introduced a transition zone at the beginning of the crest, a turbulent zone where it's hard to distinguish the run-up layer thickness from the horizontal flow depth. The exponential decay of the flow parameters starts behind this transition zone, where new formulae (Eq. [2-36] and [2-37]) are valid. Unfortunately, the length of this transition zone is not specified by Bosman.

$$\frac{h_{C,2\%}(x_C)}{h_{C,2\%}(x_C = 0)} = 0.81 \cdot exp\left(-15 \cdot \frac{x_C}{f' \cdot L_0}\right) \quad [2\text{-}36]$$

$$\frac{U_{C,2\%}(x_C)}{U_{C,2\%}(x_C = 0)} = exp\left(-0.042\frac{x_C}{f' \cdot h_{C,2\%}(x_C)}\right) \quad [2\text{-}37]$$

The slope friction f' is 1 for a smooth dike. Bosman also introduced the wave length L_0 instead of the crest width G_C in the exponential part of Eq. [2-36].

Analysis of new experiments in the Flowdike project (Lorke et al., 2012) confirm that the coefficients in the flow depth equations depend on the slope angle and that both the flow depth and flow velocity decrease along the crest of the dike. Lorke compared her data with the approach by Schüttrumpf & van Gent (2003) (Eq. [2-32]) and found $c^*_{C,h}$= 0.35 for 1:3 slope and 0.54 for 1:6 slope, and with the approach by Bosman et al. (2008) (Eq. [2-36]) and found a constant value 0.89 (slope 1:3) and 3.25 (slope 1:6) instead of 15. Despite similar general conclusions were found, again other empirical coefficients were identified.

Van der Meer et al. (2010) proposed simplified Eq. [2-32] and [2-33] for the flow depth and the flow velocity at z_A=R_c (equal to x_c = 0):

$$h_{A,2\%}(R_c) = 0.26 \cdot (R_{u,2\%} - R_c) \quad [2\text{-}38]$$

$$U_{A,2\%}(R_c) = 0.35 \cdot cot(\alpha) \cdot \sqrt{g(R_{U,2\%} - R_c)} \quad [2\text{-}39]$$

At the dike crest, the equations become:

$$h_{C,2\%}(x_c = 0) = 0.13 \cdot (R_{u,2\%} - R_c) \quad [2\text{-}40]$$

$$U_{c,2\%}(x_c) = U_{c,2\%}(x_c = 0) \cdot exp\left(-1.4 \cdot \frac{x_C}{L_{m-1,0}}\right) \quad [2\text{-}41]$$

The denominator of the exponent in Eq. [2-41] has the wave length instead of the flow depth in earlier equations [2-35] and [2-37], and the friction factor f = 0.01 is left out. It's remarked by the author that Eq. [2-41] might no longer be valid for wide promenades. The flow depth is no longer decreasing over the length of the slope or promenade. Also the velocity in the run-up zone is a constant according to van der Meer.

Van der Meer et al. (2012) summarized all preceding literature and advised to use equations [2-32] and [2-33] with coefficients $c_{A,h2\%}$ = 0.20 for slopes of 1:3 and 1:4 and $c_{A,h2\%}$ = 0.30 for a 1:6 slope. The intermediate slope 1:5 gave an interpolated value of 0.25. For $c_{A,U2\%}$ the advice was to use 1.4 to 1.5 for slopes between 1:3 and 1:6. The paper also concluded that 'all research that is compared is not always consistent. This may be due to the fact that measurements of velocities and flow depths on structures is not easy. (…) Or that assumptions, like a linear decrease, are not correct. Moreover, many measurements were performed at a transition between slope and crest, where the wave changes from up-rushing to horizontal. This could also give some extra scatter.' Van der Meer et al. (2012) does not give new advice for flow parameters on the crest, but refers to van der Meer et al. (2010).

The research by Hughes et al. (2012) was performed with negative freeboards (submerged dike) and principally outside the range of interest for this publication. However, they selected 9 from the 27 tests with smallest negative freeboards (prototype equivalent -0.29m) where the crest of the structure became dry between the successive overtopping waves and therefore relate to the current work (with positive freeboards $R_c > 0$) after all. These tests were used in Hughes et al. (2012) to study the flow depth and flow velocity of the individual overtopping waves. For the purpose of the current thesis, the most important conclusions of the work by Hughes et al. (2012) are given below:

- The flow depth U and flow velocity h on the crest are Rayleigh distributed, and also their multiplication ($q_{ind} = U \cdot h$) is Rayleigh distributed
- 2% exceedance values of flow thickness and velocity are most probably not to occur in the same (overtopping) wave volume. This confirms the findings by Van Gent (2002), Lorke et al. (2010) and other authors on the flow parameters.

- Despite $h_{2\%}$ and $U_{2\%}$ not occurring in the same wave, they are both expressed by means of the same parameters. Substitution of Eq. [2-39] into [2-40] or vice versa leads to a relationship between the 2% exceeded flow depth and the 2% exceeded flow velocity. Combining these equations with the coefficients proposed by Lorke et al. (2010) leads to Eq. [2-42] and experimental data by Hughes (2015) leads to Eq. [2-43]. The lower coefficient by Hughes (cotα = 4.25, the slope in Hughes's experiments would give 4.12 instead of 1.53) could not be explained, but location where U and h are measured certainly plays a role due to decreasing velocities and flow depths.

$$U_{2\%} = 0.97 \cdot \cot\alpha \cdot (g \cdot h_{2\%})^{0.5} \quad [2\text{-}42]$$

$$U_{2\%} = 1.53 \cdot (g \cdot h_{2\%})^{0.5} \quad [2\text{-}43]$$

The advice in EurOtop (2016) is the same as in van der Meer et al. (2012) for the run-up zone. For the crest, EurOtop (2016) states that in the beginning of the crest a decrease of flow depth occurs to about 2/3rd of its value and then remains more or less constant. This decrease is due to a transition zone from slope to horizontal (undefined in length). For the flow velocity, the following equation is proposed, with the wave length in the exponent:

$$\frac{U_{C,2\%}(x_C)}{U_{C,2\%}(x_C = 0)} = exp\left(-1.4\frac{x_C}{L_{m-1,0}}\right) \quad [2\text{-}44]$$

Table 2-2: Coefficients from equations [2-32] to [2-35] provided by different researchers.

	Slope	$c^*_{A,h}$	$c^*_{A,U}$	$c^*_{C,h}$	$c^*_{C,U}$
Schüttrumpf (2001)	1:4	0.22	0.94	0.75	0.50
	1:6	0.21	0.94	0.75	0.50
Schüttrumpf et al. (2002)	1:6	0.33	1.55**	1.11	0.50
Van Gent (2002)	1:4	0.15	1.30	0.40	0.50
Schüttrumpf & van Gent (2003)	1:6	0.33	1.37*	0.89***	0.50
	1:4	0.15	1.30	0.40	0.50
Schüttrumpf & Oumeraci (2005)	1:3 to 1:6	0.33	0.94	0.75	0.50
EurOtop (2007)		$0.055cot(\alpha)$	1.55	0.89/1.11***	0.5
Bosman et al. (2008)	1:4 and 1:6	$\frac{0.01}{sin^2(\alpha)}$	$\frac{0.30}{sin(\alpha)}$	Use [2-36] and [2-37]	
van Der Meer et al. (2010)		0.26	$0.35cot(\alpha)$	Use [2-40] and [2-41]	
Lorke et al. (2010)	1:3			0.20	$0.35cot(\alpha)$
	1:6			0.29	$0.35cot(\alpha)$
Lorke et al. (2012)	1:3			0.35	
	1:6			0.54	
Van der Meer et al. (2012)	1:3 to 1:4	0.20	1.4	Use [2-40] and [2-41]	
	1:6	0.30	1.5		
EurOtop (2016)	1:3 to 1:4	0.20	1.4	$2/3h_A(R_c)$ constant	Eq. [2-44]
	1:6	0.30	1.5		

Note*: $c^*_{A,U}$=1.37 according to Schüttrumpf belongs to 10% exceeding value instead of 2% exceeding value. The 2% exceeding value is 1.55.
Note**:Bosman et al. (2008) states that $c^*_{A,U}$ should have been 1.64 instead of 1.55 in Schüttrumpf et al. (2002).
Note***: 0.89 for TMA spectra. 1.11 for natural wave spectra.

Due to the difficuluties in theoretical prediction of the flow depths and flow velocities, Chen (2016) also measured flow characteristics in her PhD. "Due to the breaking waves on the foreshore or dike slopes, the overtopped waves on the dike are highly aerated and turbulent. This complexity limits the accuracy of the measurement of the overtopping wave. Thus, choosing a proper technique is necessary." Bubble Image Velocimetry (BIV) is used. Besides BIV, they also installed flow meters at x_C = 0.025 which might still be in the transition zone. From these recordings, Chen (2016) noticed a difference between flow depths on promenades without storm walls and promenades with storm walls.

Comparison of the different prediction formulae for flow parameters

Different researchers have studied flow depths and flow velocities from overtopping waves. During their tests, the overtopped bore was unobstructed, no impact on a storm wall with consequently a reflected bore was taken into account. Table 2-2 gives an overview of different equations and empirical constants. The values of the empirical coefficients show large spreading.

Figure 2-13 gives a graphical comparison of the flow depth for an example with H_s = 1.2m, R_c = 2m, $T_{m-1,0}$ = 9s. On the horizontal axis, the run-up zone is shown from 0 to 2m (z_A = 0 to z_A = R_C = 2m). From 2m to 12m the crest is shown: x_C = 0 is located at 2m, x_C = 10m is located at 12m.

The flow depth at the beginning of the crest is the same as the flow depth at the end of the run-up zone, except for the lines by Bosman et al. (2008) and EurOtop (2016). They identify a transition zone, so actually these formulae are only valid outside the (unknown) transition zone. In the run-up zone, differences of a factor 2.5 to 4 are noticed for this example, on the crest from 3 to 6 between the extremes.

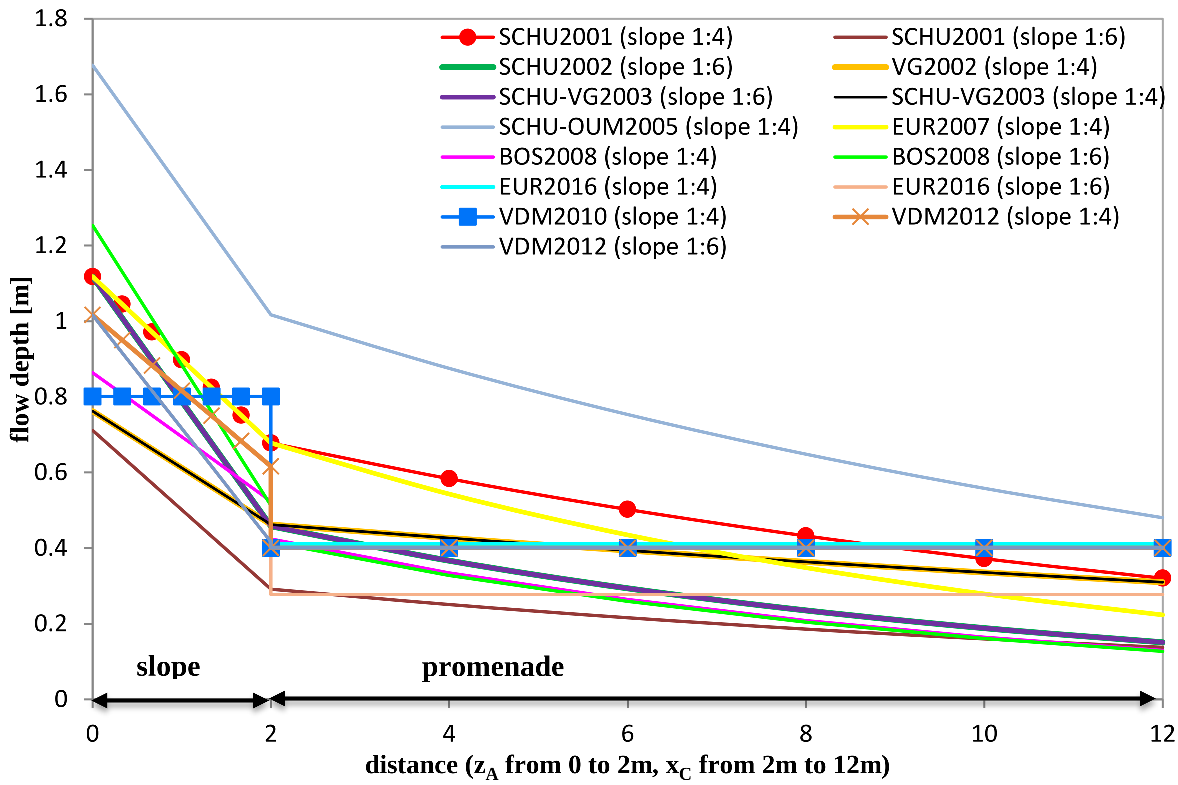

Figure 2-13. Graphical comparison of flow depths based on different research (H_s = 1.2m, R_c = 2m, $T_{m-1,0}$ = 9s).

A similar graph for the flow velocity is given in Figure 2-14. In the run-up zone differences of a factor 2 to 2.5 are found, on the crest the difference is between 2.5 and 3.5 when Bosman is not taken into account.

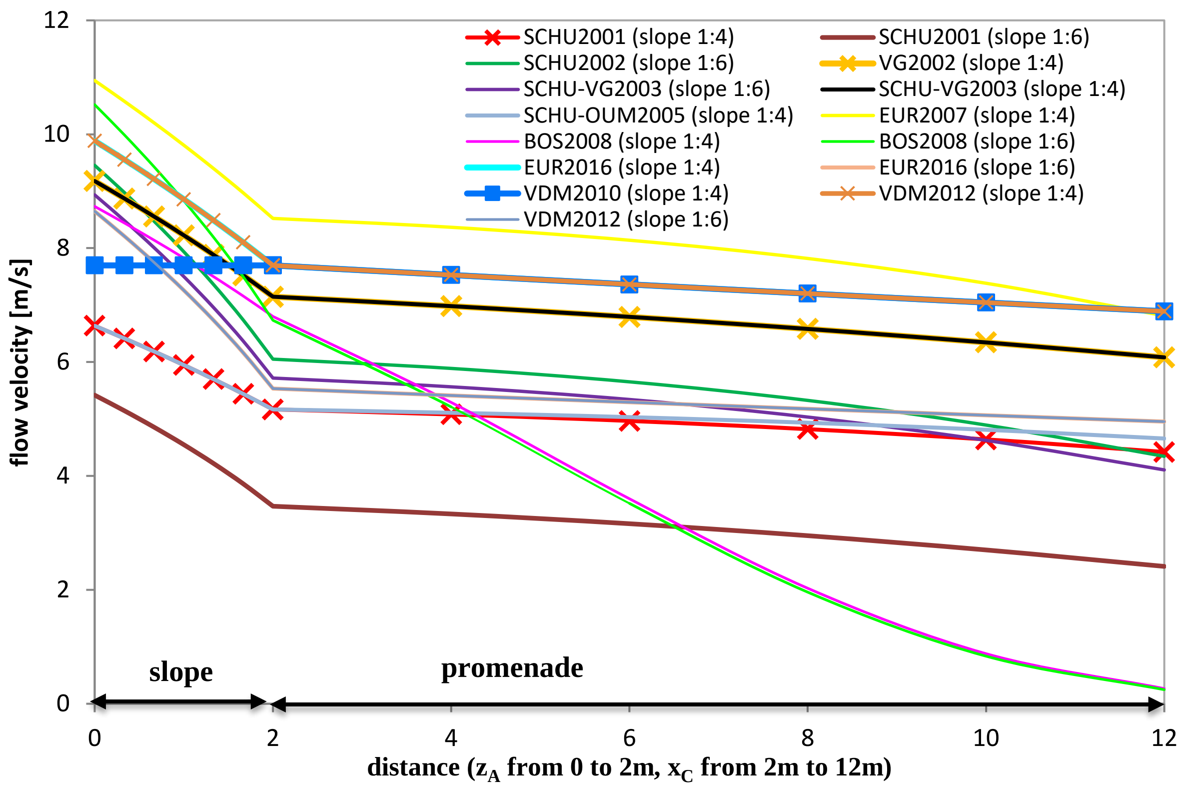

Figure 2-14. Graphical comparison of flow velocities based on different research (H_s = 1.2m, R_c = 2m, $T_{m-1,0}$ = 9s).

This graphical comparison shows that there has been a lot of research on this matter, but it's still unclear what the correct empirical formulae are. The trends are confirmed by most of the authors, but the absolute values differ significantly. The most important conclusions from the above literature overview are that:

- Different empirical formulae exist to calculate the overtopping flow parameters. It is unclear which coefficients perform best, and a theoretical estimation of the flow depth and flow velocity on the crest is thus not straightforward. Measurements are recommended above a theoretical approach. However, measuring flow depths is difficult and must be analyzed with great care. Chen (2016) used BIV, equipment that was not available for the current work.
- There is a transition zone at the beginning of the crest, so care should be taken to measure flow depths and velocities in this transition zone since it may lead to wrong results. The length of the transition zone is unknown.
- An (exponential?) decay of both flow depth and flow velocity was observed over the length of the promenade. U and h reduce over the promenade. To obey the mass conservation law, the recordings of both flow depth and flow velocity will show longer time duration at the end of the promenade compared to in the beginning of the promenade.
- The maximum of the flow depth and the maximum of the flow velocity does not necessarily take place in the same wave. This makes it difficult to predict which combination of flow depth and flow velocity gives the highest (or any low exceedance value) impact.

2.5 *Distribution of individual waves*

The overtopping flow is initiated by individual overtopping volumes at $x_C = 0$ in Figure 1-9, which will be discussed in this section.

The overtopping flow parameters are induced by waves overtopping the crest of the dike. Individual overtopping volumes can be described by a two-parameter Weibull distribution (EurOtop, 2007). The probability P_{ov} of an individual overtopping volume V_{ind} to exceed a particular volume V is given in Eq. [2-45], based on Hughes et al. (2012) and Victor (2012). Reworked, the distribution of individual volumes can be calculated by using Eq. [2-46].

$$P_{ov} = P[V_{ind} > V] = exp\left(-\left(\frac{V}{\lambda_V}\right)^{\kappa_V}\right) \quad [2\text{-}45]$$

$$V = \lambda_V\left(-ln(P_{ov})\right)^{\frac{1}{\kappa_V}} \quad [2\text{-}46]$$

with $\lambda_V > 0$ being the scale parameter and $\kappa_V > 0$ the shape parameter. For exponential distributions $\kappa_V = 1$, and for Rayleigh distributions $\kappa_V = 2$. EurOtop (2007), based on the work by van der Meer & Janssen (1994), gives values for the shape and scale parameters: $\kappa_V = 0.75$ and λ_V is a function of the average overtopping discharge q, the probability of overtopping P_{ov} and the average wave period T_m.

$$\lambda_V = 0.84 \cdot T_m \cdot \frac{q}{P_{ov}} \quad [2\text{-}47]$$

$$P_{ov} = exp\left(-\left(\sqrt{-ln0.02}\,\frac{A_C}{R_{U,2\%}}\right)^2\right) \quad [2\text{-}48]$$

$$R_{U,2\%} = H_{m0} \cdot 1.65 \cdot \xi_{m-1,0} \quad [2\text{-}49]$$

with a maximum of $R_{U,2\%} = H_{m0}\left(4.0 - \frac{1.5}{\sqrt{\xi_{m-1,0}}}\right)$ [2-50]

During the design process of the US Overtopping Simulator, van der Meer et al. (2011) and Hughes et al. (2012) looked into the distribution of individual overtopping volumes. Van der Meer et al. (2011) proposed an update for λ_V, Hughes et al. (2012) proposed an update for both κ_V and λ_V. Also Victor (2012) proposed new formulae for κ_V and λ_V, based on data on smooth dikes with $0.4 \leq cot(\alpha) \leq 2.75$ and $0.1 \leq A_c/H_{m0} \leq 2.0$, which is in line with the current parameter range. When the analysis for this PhD research was carried out, Victor's work was the most recent and was also carried out in the UGent wave flume. For this reason, his formulae for κ_V and λ_V are further used in this thesis.

$$\kappa_V = exp\left(-2.0\frac{A_C}{H_{m0}}\right) + 0.56 + 0.15cot(\alpha) \quad [2\text{-}51]$$

$$\lambda_V = 1.13\tanh(1.32\kappa_V) \cdot \frac{q \cdot T_m}{P_{OV}} \quad [2\text{-}52]$$

$$P_{ov} = exp\left[-\left((1.4 - 0.30cot\alpha)\frac{A_C}{H_{m0}}\right)^2\right] \quad [2\text{-}53]$$

Van der Meer & Janssen (1994) stated that the Weibull fitting was particularly accurate for the higher values of the distribution. Thereby, the Weibull parameters of van der Meer et al. (2011) and

Victor (2012) were derived for $V_i > V_{mean}$. Hughes et al. (2012) even only used the upper 10% of the values for his fitting.

Hughes et al. (2012) extended the study of flow parameters to individual overtopping volumes. The multiplication of U (m/s) and h (m) is the individual discharge q_{ind} ($m^3/m/s$). For each overtopping wave a volume V_{ind}, a flow depth h_{max} (=h) and flow velocity U_{max} (=U) were measured. A relationship between V_{ind} and q_{ind} was then presented:

$$q_{ind} = U \cdot \mathrm{h} = 0.184 \cdot g^{0.5} \cdot V_{ind}^{0.75} \qquad [2\text{-}54]$$

Note that this involves individual parameters V_{ind}, U, h and q_{ind}.

Hughes (2015) updated the relationship between V_{ind} and q_{ind} based on data coming from Flowdike1 (1:3 slope, Lorke et al. (2010)) and Flowdike2 (1:6 slope, Lorke et al. (2010)), The dike slope angle and the wave period are now included in the following relationship:

$$q_{ind} = 7.405 \frac{V_{ind}\sqrt{tan\alpha}}{T_{m-1,0}} \qquad [2\text{-}55]$$

2.6 *Wave impacts*

Overtopping volumes (at $x_C = 0$ in Figure 2-15) lead to an overtopped bore with a certain flow depth and flow velocity, of which an overview of the existing literature was given in the previous Section 2.4. If this bore contains sufficient energy, it will impact the storm wall. The available literature on wave impacts on storm walls is given in this section. The process was already visualized in Figure 1-9 and is repeated here in Figure 2-15.

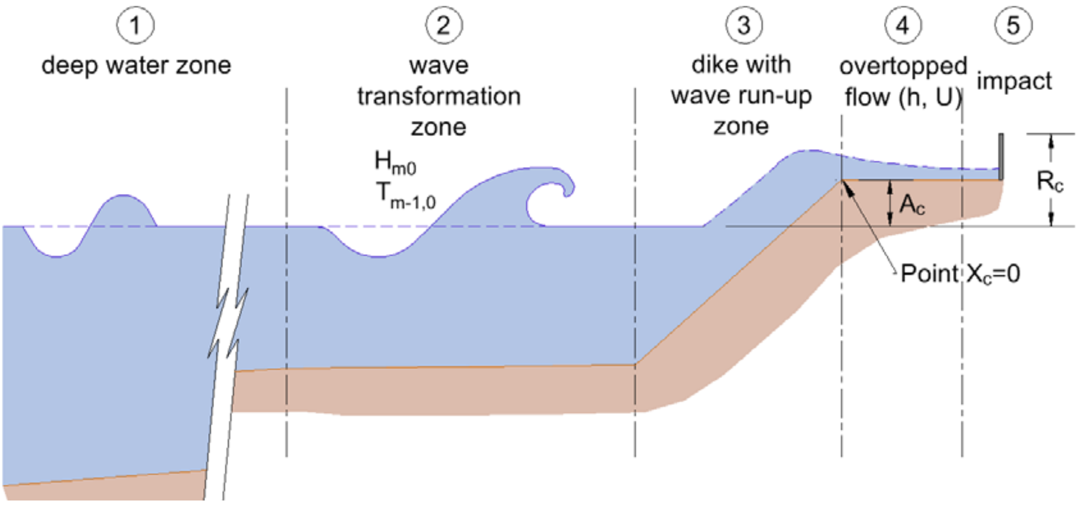

Figure 2-15: Evolution from deep water waves to the post overtopping process of a bore impacting a storm wall.

Limited information is available regarding impacts on a geometry as sketched in Figure 2-15. Therefore, also other bore or flow impacts are studied.

Some studies from the 1960's on tsunami surge forces (Cumberbatch, 1960) and water wedge impacts (Cross, 1967) indicate that the impact is proportional to both the bore height and the flow velocity squared:

$$F_h = \frac{1}{2}\rho g h^2 + C_F \rho h u^2 \qquad [2\text{-}56]$$

with C_F an empirical coefficient proportional to the water wedge angle.

In the 1990's, research was done in the Netherlands on vertical water retaining structures to quantify wave overtopping and wave impacts. The investigated storm walls were located at the end of quay constructions or at the end of a slope (with and without 'berm'), see Figure 2-16. Results were published in Den Heijer (1998).

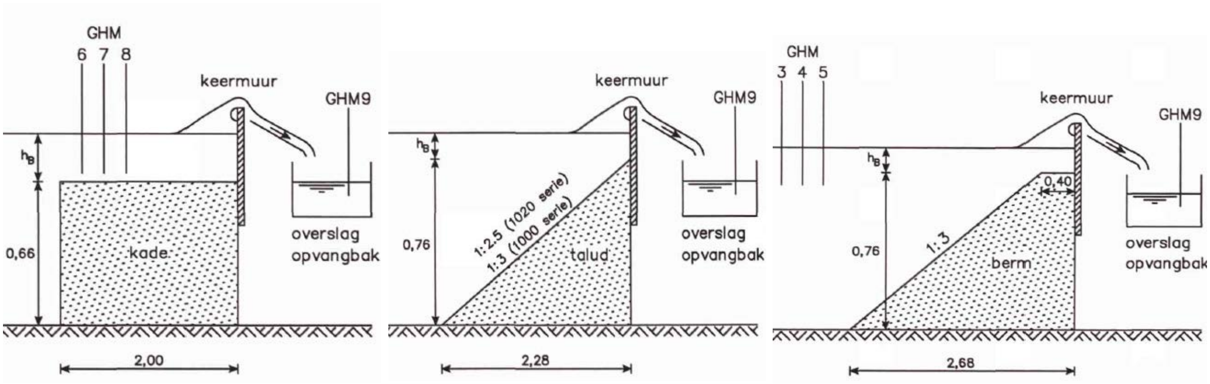

Figure 2-16. Three investigated geometries in Den Heijer (1998) to quantify overtopping and wave impacts.

The main difference in in Den Heijer (1998) is the still water level which is already against the storm wall, where in the current PhD research the crest of the dike is dry and the storm wall only faces impacts when waves first overtop the dike crest and continue over the promenade as a bore.

Den Heijer (1998) mentions that wave induced forces have a stochastic nature, and it's impossible to determine the maximum force. There is always a chance, regardless how small, that a larger force occurs. Nevertheless, the maximum recorded values in tests with 3000 waves were used to set up experimental formulae. Results on the quay wall were separated from results on the dike. Tests with and without berm at the top of the dike slope were analyzed together.

For the quay wall Eq. [2-57] to [2-59] are valid for $0.8 < h_b/H_s < 2$, with h_b the difference between the base of the wall and the SWL, see Figure 2-16.

$$\frac{F_{max}}{\rho g H_s^2} = 15 \qquad \text{for } s_{0p} < 0.0051 \qquad [2\text{-}57]$$

$$\frac{F_{max}}{\rho g H_s^2} = 16.5 - 294 \cdot s_{0p} \qquad \text{for } 0.0051 < s_{0p} < 0.022 \qquad [2\text{-}58]$$

$$\frac{F_{max}}{\rho g H_s^2} = 10 \qquad \text{for } s_{0p} > 0.022 \qquad [2\text{-}59]$$

For dikes, Eq. [2-60] and [2-61] are valid for $-1.2 < h_b/H_s < 1$.

$$\frac{F_{max}}{\rho g H_s^2} = 1.62 + exp\left(3\frac{h_b}{H_s}\right) \qquad \text{for } h_b/H_s \leq 0.78 \qquad [2\text{-}60]$$

$$\frac{F_{max}}{\rho g H_s^2} = 12 \qquad \text{for } h_b/H_s > 0.78 \qquad [2\text{-}61]$$

These equations are the upper boundary of Den Heijer's dataset, which makes them design equations and not data-averaged fitted curves. Den Heijer (1998) does not explain why the forces were made dimensionless by dividing through $\rho g H^2$; this will be studied in Chapter 6 where also the formulae [2-57] to [2-61] will be tested on the current dataset.

At Flanders Hydraulics Research in Belgium, researchers also worked on bore impacts, but so far only published specific case studies (Veale et al. (2012), Altomare et al. (2014)) or numerical modeling results (Altomare et al., 2015) without providing generic design formulae. Ghent University is nowadays performing research on a similar geometry as presented in the current thesis, but with a mild sloping beach in front of the dike leading to a very shallow foreshore conditions. Under these conditions, only broken waves reach the crest of the dike, and are therefore different to the non-breaking waves in the present work. First results of the shallow foreshore case are given in Streicher et al. (2016). No generic formulae do exist yet. Finally, also Delft University carried out research on wave impacts on buildings along the Belgian/Dutch coastlines (Chen et al. (2014), Chen et al. (2015) and Chen (2016)). Similar to Streicher's research, shallow foreshores and broken waves have been tested there, which is different from the non-breaking deepwater waves at the toe of the dikes in the current work. But these papers contain a generic approach which will be summarized here.

In Chen et al. (2014) the process of wave impacts is studied for regular waves. Due to different air entrainment and the turbulent overtopped bore, the impacts show irregular behavior. It's shown that an impact has a kind of churchroof profile with a first short duration dynamic peak and a second quasi-static peak with longer duration. This corresponds with the "breaking wave impact" by Oumeraci et al. (1993) and Kortenhaus & Oumeraci (1998) in Figure 2-17, who classified breaker types for wave loads on vertical structures in the European project PROVERBS (Oumeraci et al., (1999). However for overtopping bores, the dynamic peak and quasi-static peak don't always obey the ratio 2.5 from Figure 2-17. Even more, the dynamic peak can be higher than the quasi-static, but not always. Two examples of impacts measured by Chen et al. (2014) are shown in Figure 2-18, where the red line respresents the total force on the storm wall and the other coloured lines the individual pressure sensors (P_1 the lowest, P_4 the highest). The upper panel in Figure 2-18 shows an impact where the quasi-static peak is higher than the dynamic one, the lower panel shows the opposite although the difference in magnitude between the peaks is rather small. They are more "twin-peaks" rather than church-roof profiles. The lowest impact sensor (P_1) recorded more a church-roof shape , since this sensor is feeling the dynamic impact the most.

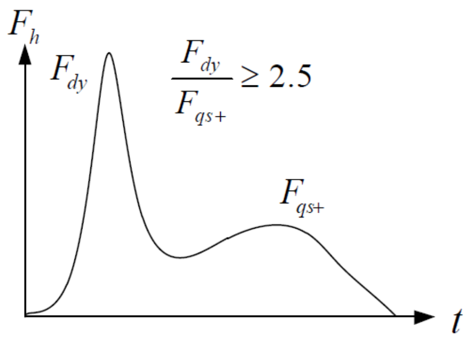

Figure 2-17. Churchroof profile for "breaking wave impact": dynamic peak at least 2.5 times the dynamic peak, by Oumeraci et al. (1993) and Kortenhaus & Oumeraci (1998).

For a <u>single bore impacting the wall</u>, the process was divided in four stages by Chen et al. (2014), see Figure 2-18:

- Pre-impact, where the bore approaches the wall with a wedge shape leading edge.
- Initial impact stage. When the irregular bore front touches the wall, a rapidly rising tip forms a vertical jet (see indication "jet impact" in Figure 2-18). This happens a little earlier than the main wedge touching the wall (see indication "initial impact" in Figure 2-18), and dampens the main impact during this stage.
- Deflection stage: the main wedge continues rising up the wall until it reaches its maximum run-up. Kinetic energy is converted into potential energy.

- Reflection stage: water starts falling down onto the remaining unsplashed part of the incident wave, and is advancing seawards. The quasi-static peak (see indication “quasi-static impact” in Figure 2-18) is generated during this stage.

For multiple consecutive bore impacts on the wall, studied by Chen (2016) for irregular waves, there can be interaction between the consecutive overtopping bores in the form of catching up or collision:

- When the catching up happens far from the wall, a new bore forms with an impact like a single event.
- When the catching up happens at the wall, an impulsive impact with large magnitude for short duration is noticed.
- When the collision between the reflected bore and a next incoming bore happens just in front of the wall, the incoming bore can “jump” over the reflected bore and induce an impulsive violent impact at a higher location. This comes from a trapped air cavity in between the incoming and the reflected bore, which reacts similar as the “breaking wave impact” defined in Figure 2-17.
- When the collision between the reflected bore and a next incoming bore happens far away from the wall, the incoming velocity is reduced and the impact is dampened.

Chen (2016) studied 39 irregular wave tests and selected the highest 3 impacts per test. 48% of those impacts were due to single wave impact, 23% by catching up and 29% by collision.

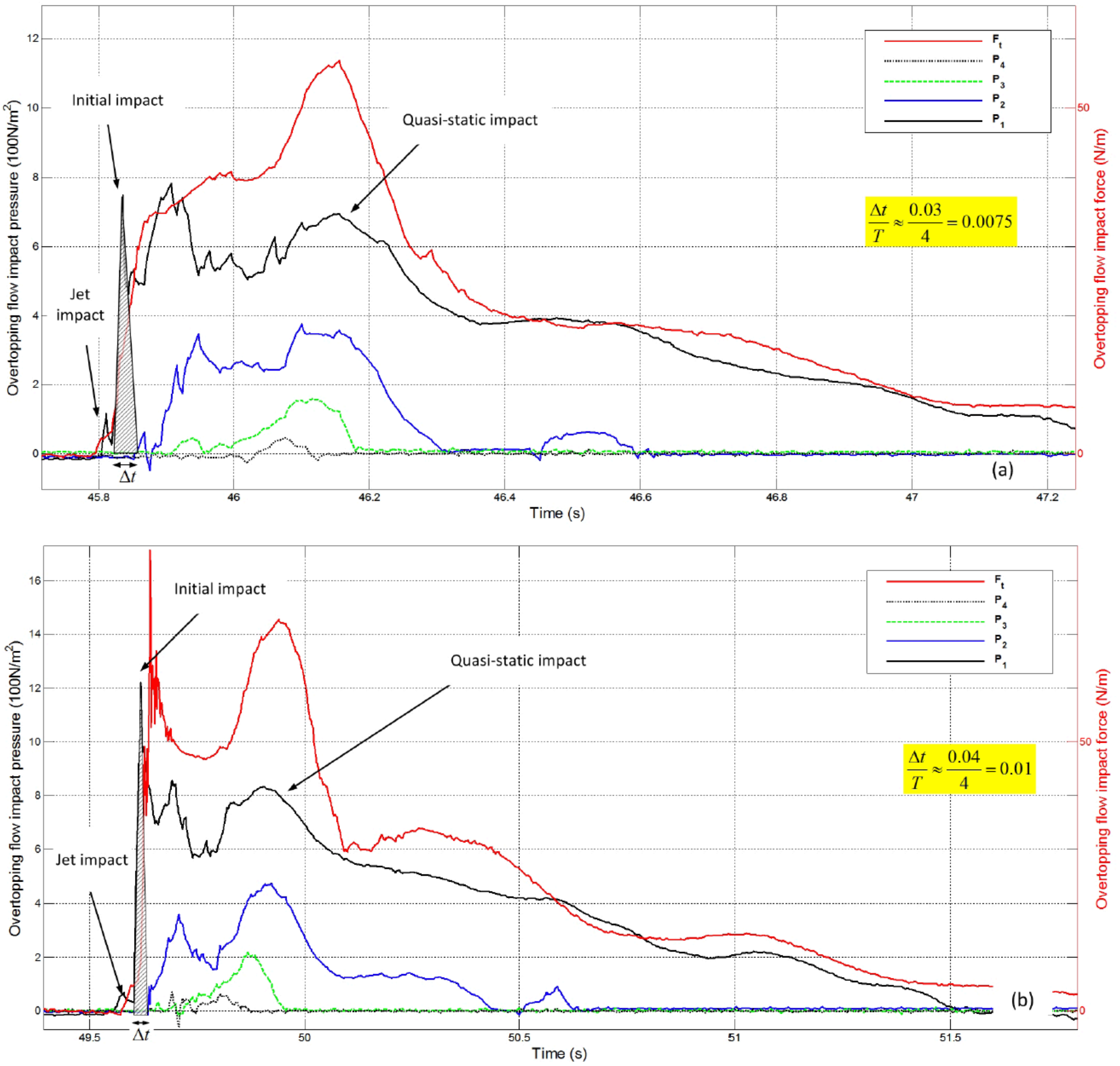

Figure 2-18. Total force recording (red) and pressure recordings (black, blue, green, dotted blue) of a bore impact on a storm wall by Chen et al. (2014).

The single overtopping wave approach is described in Chen et al. (2015) where only regular waves were tested to better understand the process of overtopped bores and impacts. Results are presented by means of the overtopping Momentum Flux which is proportional to the water mass contained in the overtopping wedge, written as a function of R_c and R_u. The flow depth d_0 at the beginning of the crest was also defined in terms of these same parameters, which makes the momentum flux a function of the flow depth.

$$M_{Fov} = \frac{\rho g}{2} \frac{K_o}{K_p C_1^2} d_0^2 f(\beta) \qquad [2\text{-}62]$$

where M_{Fov} is the overtopping momentum flux (N/m), K_o is an unknown proportionality constant and K_p is a reduction factor to account for slope porosity (K_p = 1 for impermeable slopes). C_1 is an empirical coefficient, d_0 is the flow depth at the beginning of the crest and f(β) is a function of the dike slope and needs to be determined empirically.

Further simplification of Eq. [2-62] by Chen et al. (2015), combined with including the exponential decay of the flow depth over the crest width has led to Eq. [2-63]:

$$\frac{F_t}{C_5 f(\beta)\rho g d_0^2} = exp\left(-\lambda_1 \frac{G_c}{L_{reg}}\right) \quad [2\text{-}63]$$

where G_c is the promenade width (or crest width), λ_1 and C_5 are experimental coefficients, and L_{reg} is the local wave length (regular waves) at the dike toe. After fitting of Eq. [2-63] with the data, the experimental coefficients are filled in:

$$\frac{F_t}{\rho g d_{B0}^2} = 1.7\cot(\alpha)exp\left(-3.08\cot(\alpha)\frac{G_c}{L_{reg}}\right) \quad [2\text{-}64]$$

with d_{B0} the flow depth measured on the promenade with a storm wall. Chen measured flow depths on the promenade with and without a wall, and noticed that the flow depth is influenced by the wall. Her measurements of the flow depth are carried at at x_C = 0.025m, close to the beginning of the crest and might thus be in the "transition zone" as defined by Bosman et al. (2008). This might not have been the best location to measure flow depths.

Eq. [2-64] is based on regular wave data, shallow foreshore and broken waves, and contains the flow depth d_{B0} on a location that other authors have remarked as doubtful. It's questionable that this approach will give good results for the data in the current work, but it will be tested nevertheless in Chapter 6. The main conclusion from Chen et al. (2015) is that the impact force depends on the slope angle, the flow depth squared and the crest width.

Chen (2016) studied impacts by consecutive bores, based on tests with irregular waves on shallow foreshores. A (rather complex) 7 step procedure is given to calculate the Generalized Pareto distribution of the impacts. From this distribution the maximum or any other low-exceeded value can be calculated. Chen states that also Weibull, Gamma and Exponential distributions perform well in describing the impacts. There is no influence of the wall height or promenade width in the procedure, which means results are only valid for the range of parameters tested. In the 7 step procedure, force results are made dimensionless by dividing them through $\rho g R_c H_{m0}$. For the data analysis in her work, a low pass filter 50Hz was used, which reduced the unfiltered force peaks by 10 to 20%. This is stated to be fair for impacts on objects with large inertia. It's also stated that fresh water and small scale overestimates the impact pressure because less entrained air is present. Finally, the report by Chen uses force recordings over pressure recordings.

Remarkably both approaches by Chen make the force F dimensionless by means of other coefficients: $\rho g d_0^2$ in Chen et al. (2015) versus $\rho g R_c H_{m0}$ in Chen (2016). Also the crest width is included in one, and left out in the other formula. Den Heijer (1998) made the force dimensionless by $\rho g H_s^2$, yet another coefficient.

The latest information published on wave impacts on storm walls is by Streicher et al. (2018). Comparable to Chen et al. (2014), he also found a "twin-peak" shape, where the dynamic peak is lower compared to the church-roof profile by Oumeraci et al. (1993) and Kortenhaus & Oumeraci (1998). In his observations, the quasi-static peak is just as important as the dynamic one. If the dynamic peak (F_{dyn}) is larger than 1.2 times the quasi-static peak (F_{qs}), Streicher classifies impacts as impulsive or dynamic (see Figure 2-19). In the other case, he classifies waves as quasi-static. In his tests with shallow foreshores, he found that the majority of the impacts (about 70%) is quasi-static.

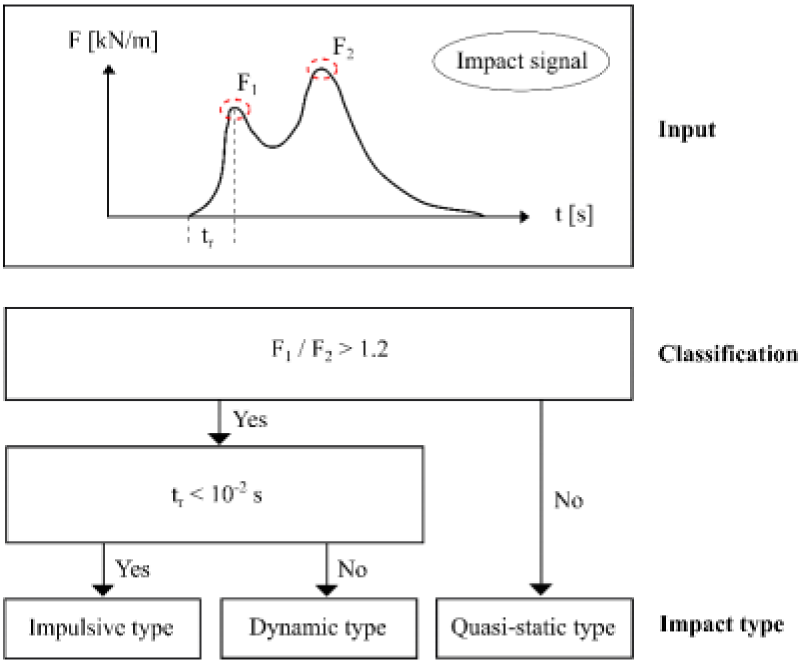

Figure 2-19. Classification of the breaker type by Streicher et al. (2018).

When stepping aside from the same geometry (smooth dikes), some information is available from research at Aalborg University, to estimate impacts on the crown walls of a rubble mound breakwater. The slope, promenade and storm wall still are similar, but the roughness and permeability of the structure are different. Some parameters have the same influence on the impacts, other parameters lead to a different behavior.

Pedersen (1996) measured wave impacts on breakwater crown walls and compared his results to other research in that field. He referred to Jensen (1984) who found that the measured horizontal force on a crown wall was directly proportional to the ratio H_s/A_c, and also increasing wave periods lead to an increased wave load on the crown wall. Hamilton & Hall (1992) showed that the wave load increased with an increasing wave height, but as soon as the crown wall is overtopped further increasing of the wave height did not affect the wave load anymore. A horizontal asymptote was approached. Hamilton & Hall (1992) further confirmed the influence of the wave period according to Jensen, and assumed to see a dependency of the slope angle on the impact forces. Günbak & Ergin (1983), Jensen (1984) and Burcharth (1993) each provided a simplified methodology to calculate wave impacts, but none of them seemed to be generic and different formulae (with different coefficients) were given for similar geometries. Since no generic approach existed, Pedersen (1996) carried out own model experiments. He noticed that

a) The force recording has a church-roof shape like Figure 2-20.
b) The maximum impact ($F_{h,peak}$) is reached in a short time interval ($0.01s < t_{rise} < 0.1s$), after which the force value decays over a longer time interval ($0.1s < t_{decay} < 0.25s$) to a value $F_{h,static}$ which holds on somewhat longer (see Figure 2-20).
c) Pedersen (1996) did not work with maximal values, but values with low exceedance probability (such as $F_{1\%}$, $F_{0.1\%}$, …) were presented to avoid the uncertainty that comes along with maximal values in a stochastic process.
d) Increasing wave height gives increasing force (for a constant freeboard).
   Increasing freeboard (for a constant wave height) gives decreasing force.
e) For overtopped wall heights, wave forces have a horizontal asymptote when the wave height increases.

Non-overtopped wall heights do not show asymptotic behaviour and impacts increase with increasing wave height.

f) The impact force is proportional to the wall height squared, but increasing the wall height beyond the threshold point between overtopping and no overtopping, does not further increase the wave load.
g) Longer waves (higher wave periods) lead to higher impact forces.
h) The wave loading on the crown wall decreases with decreasing slope angle (flatter slope).
i) The low probability exceedance wave forces are governed by wave impact pressures. Pressure contributions from the hydrostatic head are so small that they can be ignored.

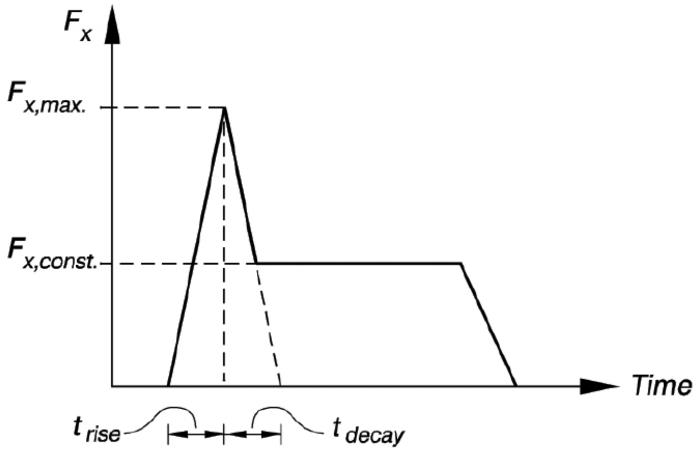

Figure 2-20. Schematized wave force evolution (by Pedersen (1996)).

A final source that can be mentioned regarding wave impacts on storm walls is the SPM (1977). Breaking wave forces on vertical walls are treated there, and also a subsection on broken waves on a (foreshore) slope with a wall on top is mentioned. The proposed geometry lacks a promenade; the vertical wall is directly at the slope. Despite these differences in comparison with the current geometry, the approach by SPM (1977) is often used as a rough first estimation of what wave impact forces to be expected.

A distinction between the wall seaward of the still water line (submerged foot) and the wall landward of the still water line (emerged foot) is given. Only the latter part is used here, see Figure 2-21.

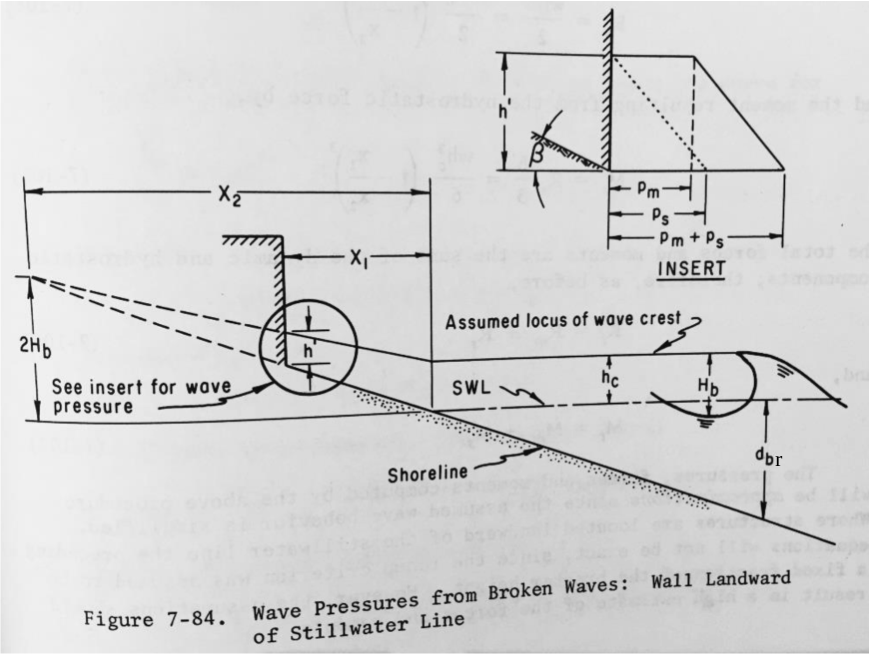

Figure 2-21. Scan of the original drawing by SPM (1977) on calculating wave forces on vertical walls landward of the still water line.

The velocity v' and flow depth h' of the water mass at the structure is calculated by Eq. [2-65] and [2-66].

$$v' = \sqrt{g d_{br}}\left(1 - \frac{x_1}{x_2}\right) \tag{2-65}$$

$$h' = h_c\left(1 - \frac{x_1}{x_2}\right) \tag{2-66}$$

with d_{br} the breaker depth, h_c the height of the wave crest, which is 0.78 times the wave breaker height H_b. x_1 is the distance from the still water line to the structure, and x_2 is the distance from the still water line to the limit of wave uprush, simplified as $2H_b\cot(\alpha)$ with α the foreshore slope.

The total impact force (R_t) is than given by Eq. [2-67] which is the sum of a dynamic component (R_d) and a static component (R_s). This is the same dependency of flow depth and flow velocity as in Eq. [2-56] by Cross (1967).

$$R_t = R_d + R_s = h' \cdot \left(\frac{\rho g v'^2}{2g}\right) + \frac{\rho g h'^2}{2} \tag{2-67}$$

A comparison of Eq. [2-67] with measurements is provided in Chapter 6.

2.7 *Model and scale effects*

2.7.1 *Model and scale effects for measuring wave overtopping*

In the CLASH project (De Rouck et al., 2009) it was concluded that measuring wave overtopping on smooth dikes and smooth vertical structures is not influenced by scale effects in the range of parameters tested.

To also exclude model effects, it was decided to do overtopping tests on a reference case (a smooth dike) to be able to compare all future crest modifications to this reference case. Overtopping tests have only been carried out in one laboratory and have been analyzed in a relative way. Results on the reference case are also compared to a selection from the CLASH database with similar hydraulic and geometrical conditions and show no difference (see Chapter 4). For these reasons, it's believed that the model effects don't influence the overtopping results.

2.7.2 *Model and scale effects for measuring flow parameters and wave induced forces*

To avoid Reynolds effects due to viscosity problems in the (Froude scaled) UGent experiments where a thin (order few mm to few cm) water layer flows over the crest promenade, flow parameters were only recorded in the tests with the largest scales (GWK tests, section 3.2, and Hydralab tests, section 3.3). Then, Reynolds numbers are large enough ($> 10^{-4}$) not to cause viscosity problems.

Besides the viscosity problems in small scales, there is also the effect of air bubbles. Small scale tests contain less air bubbles, which lead to higher impacts because the air (mixed in a water layer) has a cushioning effect (Bullock et al., 2001). Bullock's investigation also shows that air bubbles that form in fresh water tend to be larger than those which form in seawater and they fuse more easily, which leads to a quicker escape from the air bubbles in fresh water compared to sea water. Using fresh water in small scale tests would thereby overestimate the impacts measured, however this could not be confirmed by measurements. To conclude, Bullock et al. (2001) also claim that the influence of small quantities of air does not seem to be as dramatic as simple estimates of its effect on compressibility might suggest.

Steendam et al. (2018) mentions a factor of 2 of difference on the impact forces between small scale tests and full scale tests, where the small scale tests gave the largest results. Just like Bullock et al. (2001), they lay this difference to both the scale effect (small scale gives less air bubbles and higher impacts) and the model effect (fresh water lets air escape more easily and gives larger impacts than salt water tests).

A model or scale effect can also be induced by the stiffness of the structure and the recording frequency of the force or pressure sensors. It's important to record values with a high sampling rate, mainly for impacts which have a very short rise time. The measuring frequencies for the different equipment are given in Chapter 3. When impacts on a storm wall are in the same frequency range as the natural frequency of the storm wall, resonance can occur and artificial high values will be registered. More information on the filtering can be found in Section 6.2.1.

This shows that Froude scaling, large scale tests and filtering are important for the current work. Other model effects are specific for this work, and are treated in Chapter 3 on the test set-up and Section 6.4.4 in the analysis.

2.8 *Conclusions from literature review*

The literature study started with a comparison between the four possible models to meet the objectives stated in Section 1.3: experimental modelling, numerical modelling, an artificial neural network and field data. Given the circumstances, **experimental modelling** is the most viable and reliable way to proceed since:

- at the start of this PhD research, there was no(t yet enough) experimental data available to validate the numerical models. The process of overtopping reduction by specific crest geometries, overtopping flows and consequent wave induced impacts was not yet understood well enough.
- the wave transformation from deep water to nearshore to run-up must be modelled well, as well as the wave overtopping, post-overtopping process and impacts. This requires a large grid and possibly combination between different numerical models, which makes numerical modelling complex and computational expensive. This was not the goal of the current PhD.
- the original neural network was not trained with a lot of data on dikes with modified crests;
- no neural network has ever been trained for predicting wave impacts;
- it requires real life (super)storms to collect field data which don't come on request and cannot be controlled.

Section 2.2 on <u>wave overtopping</u> showed that the current approach by EurOtop (2016) can be used to present the measured data by means of Eq. [2-15] and [2-17]. The literature study has shown that any **reduction factor that was calculated based on the older formulae by EurOtop (2007) can still be used in EurOtop (2016)**.

The overtopping reducing measures were described in Section 2.3. Quite some literature is available, but all of it was based on tests with different hydraulic and/or geometrical conditions. The applicability on the data in the current PhD is expected to be low, but this will be verified in Chapter 4 with the current dataset. Only if the available literature is not sufficient to answer the first research question (is the existing literature sufficient to predict wave overtopping over dikes with modified crest, and if not; how to modify the equations?), new equations will be defined by means of experimental data and curve fitting in data plots to find semi-empirical coefficients.

In Section 2.4 a comparison of the extended literature on <u>flow depths and flow velocities</u> was made. It seems that **nearly all formulae have a similar shape, but there is a large spreading on the empirical coefficients**. **Measurements are better than a theoretical calculation** for the current PhD. However, measuring flow parameters is not straightforward and location dependent. First of all there is interaction between the bores of consecutive overtopped waves that reflect on the storm wall. There also is a transition zone, in the beginning of the crest where the water goes from a slope to a horizontal surface, in which the flow depth is affected by free surface variation and air entrapment and measurements provide unreliable results. And finally, there's an (exponential?) decay of the flow depth and flow velocity over the promenade. The measurement equipment and location of measuring is important and is described in Chapter 3. This should lead to knowledge on the individual overtopping flow parameters (2nd research objective), which in a later stage can be linked to wave impacts.

On <u>the distribution of individual waves</u> (Section 2.5), more consistency between the different research was found. The shape and scale parameters for the **Weibull distribution** used in this work are to be calculated by Eq. [2-51] and [2-53] by Victor (2012). The distribution of overtopping volumes can be transformed into a **distribution of overtopping dicharges** based on Eq. [2-55] by Hughes (2015).

The available literature on wave impacts was discussed in Section 2.6. Similar to the literature on wave overtopping, some information on wave impacts is available but it's all based on tests with different hydraulic and/or geometric conditions. Some overall general findings were given, like the **churchroof shape of the force recording**, working with **low exceedance values instead of F_{max}**, the relationship between the force and the flow depth squared and flow velocity squared, and finally the **proportionality of the force with the wave height, inverse crest freeboard and wave period**. One of the questions that arose from the literature is how to make the force dimensionless, since different approaches have been found. This all will be further studied in Chapter 6 to answer the 3rd objective: which wave induced forces do storm walls at crest level face under storm conditions?

Care should be taken with results from (really) small scale. The flow depths or flow velocities might be affected by viscosity effects when Froude scaling is applied but Reynolds numbers are too low. Also the air content in fresh water overtopped bores seems to be less in small scale compared to seawater and large scales, which possibly results in higher impacts in the laboratory. Finally, filtering of the force recordings to avoid resonance is of importance in this work.

Based on the above findings, it's clear that the three objectives set in Section 1.3 remain. Some points of attention are added to the methodology as defined in Section 1.4:

- Reduction of wave overtopping discharges over smooth dikes by means of crest modifications will be investigated through experimental modelling. A reference case will be tested and compared to different geometries. The reduction factors however will be deducted from the EurOtop (2007) formulae, since the research and analysis took place before van der Meer & Bruce (2014) published updated formulae for wave overtopping. Nevertheless, the achieved reduction factors are valid to be used in the EurOtop (2016) formulae.
  As mentioned earlier, a point-by-point analysis will be used to obtain the reduction factors as a function of their dominant dimensionless parameter. This method is new compared to what is usually done, and is explained in more detail in Chapter 4.
- Flow depths and flow velocities cannot be obtained from literature, but should be measured. However, due to the interaction of the bores and the unknown length of the transition zone, care should be taken in where to measure the flow parameters. To avoid problems due to entrained air and viscosity effects, a large scale should be chosen where possible.
- Also wave induced forces are recorded in the experimental model. The way to present dimensionless forces is to be studied and also here, care should be taken for the scale and/or model effects. The methodologies however, to link low exceedance force values to test average wave parameters on the one hand, and link individual overtopping volumes to flow parameters to individual impacts, remain as explained in Section 1.4.

3 Test campaigns

Within the framework of this PhD research, four new test campaigns have been carried out and the existing data of one external test campaign have been added and reanalyzed. The present chapter describes the wave flume and test set-up per campaign, the different geometries tested, and the measurement equipment used to collect the required data. The excel databases can be downloaded from www.koenvandoorslaer.com/phd

The four new test campaigns were carried out in four different wave flumes of different European laboratories, at different sizes and thus different scales. Froude scales are mentioned for each test campaign, related to possible prototype values. Results in the following chapters are presented in model scale values.

3.1 *UGent-1 dataset*

3.1.1 *Test set-up*

The first and most elaborate of all test campaigns, set up in the framework of the current PhD research, was carried out between 2008 and 2011 in the wave flume of the Coastal Engineering Department of Ghent University. In this campaign, over 1000 new scale model tests on a wide variety of structures have been carried out, a first part focusing on overtopping reduction and a second part on impact forces. The collected data from this campaign is hereafter referred to as the “UGent-1” dataset. This database became a part of the update of EurOtop (2016) and the updated Neural Network (Formentin et al., 2017).

The wave flume of UGent (Figure 3-1) has a length of 30.00m, a width of 1.00m, and a height of 1.20m, respectively. Waves are generated using a piston type wave paddle, and the steering of this paddle features active wave absorption. Each tested time series contained approximately 1000 incoming waves, mostly with a Jonswap (γ = 3.3) spectrum creating irregular waves. A few tests were repeated with another single peak spectrum, Pierson-Moskowitz. No influence of the spectrum on the overtopping volumes was noticed for the range of dimensionless freeboards and tested spectra in the current data set. Since it is a 2D flume, only perpendicular wave attack (γ_β = 1) was tested.

Figure 3-1. Pictures of the wave flume at Ghent University, 30m x 1m x 1.2m

At the opposite end of the wave paddle, different structures (see section 3.1.2) were built in the flume. They all consisted of a smooth dike (γ_f = 1). Both a dike slope 1V:2H and 1V:3H were tested. A few of the data with breaker parameter $\xi_{m-1,0}$, calculated with the actual dike slope α, just above 1.82 gave results that could not be identified as “non-breaking waves” with full confidence. Therefore, in the current UGent-1 data set, the limit was set on $\xi_{m-1,0} \geq 2.1$ to clearly define a test as non-breaking.

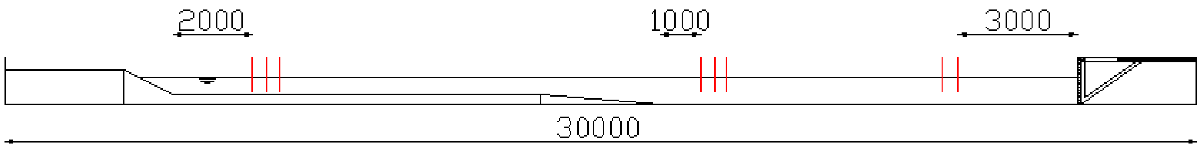

Figure 3-2. Position of wave gauges in the wave flume of Ghent University (distances in mm). Right, the wave paddle is shown, left the smooth dike.

To upscale the present test set-up to a prototype sea dike, a factor 10 to 15 could be used for the impact tests and 10 to 25 for the overtopping tests. However, the user could also use other scale factors. The results in the present work are given in model scale values and/or dimensionless.

3.1.2 *Tested geometries and parameter range*

a) *Reference case: smooth dike ($\gamma_f = 1$)*

Before any overtopping reducing measure is studied, it was decided to test a reference case instead of using literature formulae. In that way, all model effects are excluded in the relative analysis of the overtopping reducing measure compared to the reference case, because both have been tested in the same wave flume with the same boundary conditions, the same equipment, the same analysis software and even the same operators.

The smooth dike ($\gamma_f = 1$) serves as a reference case. A sketch of this reference geometry is given in Figure 3-3, the arrow with indication ‘q’ shows where the overtopping is measured.

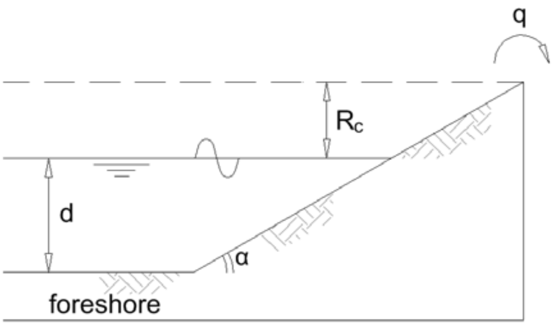

Figure 3-3. Cross section of the reference case: smooth dike.

80 new tests were performed on this geometry. The range of parameters of these 80 tests is summarized in model values in Table 3-1.

Table 3-1. Summary of the characteristics of the UGent-1 tests (non-breaking waves) on a smooth dike (scale model values).

UGent-1		Tests overtopping	Tests impacts
Slope angle of the smooth dike	$\cot(\alpha)$	2 and 3	Not applicable for this geometry
Mean spectral wave period	$T_{m-1,0}$	1.16 – 2.34 s	
Dimensionless freeboard	R_c/H_{m0}	0.83 – 3.15	
Freeboard (top of structure to SWL)	R_c	0.13 – 0.27 m	
Spectral wave height	H_{m0}	0.066 – 0.168 m	
Water depth at toe of the structure	d	0.35 – 0.49 m	
Wave steepness	$s_{m-1,0}$	0.004 – 0.055	
Wave breaker parameter	$\xi_{m-1,0}$	2.10 – 7.81	

b) *Smooth dike with storm wall*

A first measure to reduce wave overtopping is by placing a vertical storm wall (with height h_{wall}) on the dike. In this way, incoming waves are projected upwards and less water overtops the dike crest. Note that the crest level of the dike (dashed line in Figure 3-4) can be maintained by placing the storm wall seaward on the slope (Figure 3-4, left side), or can be increased by placing the storm wall on top of the original crest (Figure 3-4, right side). The developed reduction factors for wave overtopping are of course generally applicable. The only difference is that the situation on the right in Figure 3-4 has a larger freeboard R_c (larger X-value on the log-linear graph) in comparison with the X-value of the original smooth dike. The situation on the left of Figure 3-4 has the exact same X-value and allows for direct comparison. In the present research, the situation on the left in Figure 3-4 was built in the wave flume, to be able to keep the overtopping collector at the same level.

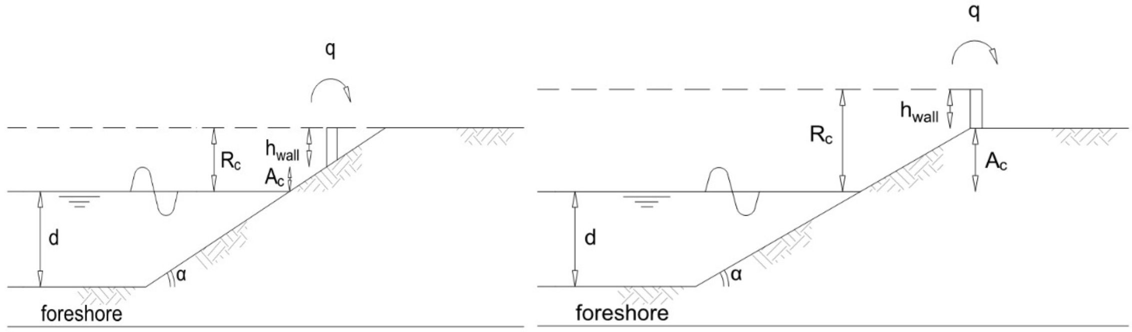

Figure 3-4. Cross section of a smooth dike with a vertical wall (h_{wall}) including the definition of the freeboard R_c.

A total of 117 tests were performed for a range of storm conditions and different heights of the storm wall in order to investigate its overtopping reducing capacity. In 27 of these tests wave impacts were measured by 2 load cells (54 data points) on a fixed wall height. Table 3-2 provides a summary of the parameters of the test program on this geometry.

Table 3-2. Summary of the characteristics of the UGent-1 tests on a smooth dike with storm wall (scale model values).

UGent-1		Tests overtopping	Tests impacts
Slope angle of the smooth dike	$\cot(\alpha)$	2 and 3	2 and 3
Mean spectral wave period	$T_{m-1,0}$	1.06 – 3.31	1.56 – 3.31
Dimensionless freeboard	R_c/H_{m0}	0.59 – 2.63	1.15 – 2.60
Wall height	h_{wall}	2, 4, 5, 6 and 8 cm	8cm
Freeboard (top of structure to SWL)	R_c	0.05 – 0.29 m	0.16 – 0.29 m
Dimensionless wall height	h_{wall}/R_c	0.08 – 1.00*	0.27 – 0.50
Spectral wave height	H_{m0}	0.07 – 0.18 m	0.07 – 0.18 m
Water depth at toe of the structure	d	0.36 – 0.57 m	0.36 – 0.51 m
Wave steepness	$s_{m-1,0}$	0.007 – 0.052	0.007 – 0.040
Wave breaker parameter	$\xi_{m-1,0}$	2.20 – 4.80	2.27 – 4.80

* additionally 2 tests with $h_{wall}/R_c = 1.60$, the other 115 tests have $h_{wall}/R_c \leq 1$, meaning an emerged wall. Also in the rest of the UGent-1 dataset, the SWL is always below the foot of the wall.

Note that for the impact tests, a fixed wall height has been used.

c) *Smooth dike with storm wall with bullnose*

Wave overtopping can be further reduced, without increasing the height of the wall, by adding a “nose” to the vertical wall. This is also known as a recurve wall or parapet (Pearson et al. (2004), Kortenhaus et al. (2001)), but in this work further referred to as *bullnose*. Due to the presence of the bullnose, waves are not only projected upward, but also back towards the open sea. A sketch of the tested geometry as well as the definition of the used parameters in the formulae is given in Figure 3-5.

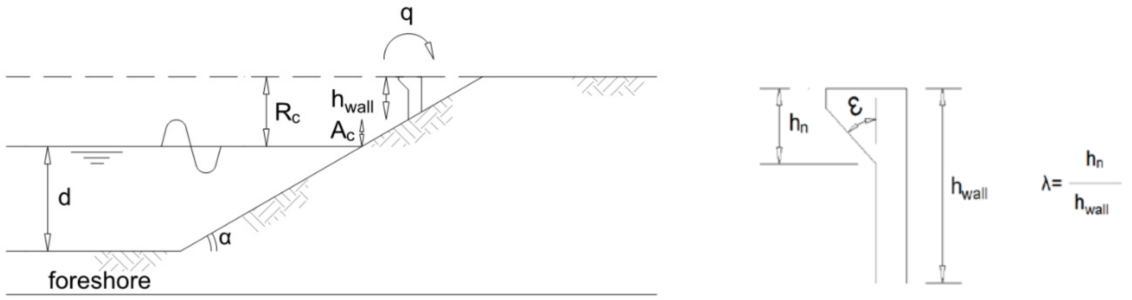

Figure 3-5. Cross section of a smooth dike with storm wall (h_{wall}) and bullnose and definition of the used parameters ε and λ.

175 tests have been carried out on a smooth dike with storm wall and bullnose, divided in 2 phases. A first phase (92 tests) only focused on wave overtopping, where the influence of the geometrical parameters such as the height of the wall and the nose (h_{wall} and h_n) and the angle ε of the bullnose were investigated in order to find an optimal geometry. The range of the parameters of the 92 tests from phase 1 is given in Table 3-3. In the second phase of the research on storm walls with bullnose, the influence of the wave period and slope angle on overtopping was investigated on two optimal parapet geometries, based on 83 new tests. These optimal bullnoses have $\varepsilon = 30°$ or $\varepsilon = 45°$, keeping λ constant at 0.375. In the 2nd phase, also wave impacts were measured. A summary of the test program from phase 2 is given in Table 3-3.

Table 3-3. Summary of the UGent-1 test program on a smooth dike with storm wall and bullnose (phase 1, scale model values).

UGent-1		**Tests overtopping (phase 1)**	**Tests overtopping (phase 2)**	**Tests impacts (phase 2)**
Slope angle of the smooth dike	cot(α)	2	2 and 3	2 and 3
Mean spectral wave period	$T_{m-1,0}$	1.10 – 1.45 s	1.53 – 2.30 s*	1.53 – 2.30 s*
Dimensionless freeboard	R_c/H_{m0}	0.60 – 2.35	1.25 – 2.26	1.25 – 2.26
Wall height	h_{wall}	2, 5 and 8 cm	8cm	8cm
Freeboard (top of structure to SWL)	R_c	0.09 – 0.18 m	0.16 – 0.29 m	0.16 – 0.29 m
Dimensionless wall height	h_{wall}/R_c	0.11 – 0.90	0.28 – 0.50	0.28 – 0.50
Spectral wave height	H_{m0}	0.08 – 0.15 m	0.09 – 0.18 m	0.09 – 0.18 m
Water depth at toe of the structure	d	0.44m – 0.53m	0.36 – 0.51m	0.36 – 0.51m
Wave steepness	$s_{m-1,0}$	0.04 – 0.05	0.01 – 0.04	0.01 – 0.04
Wave breaker parameter	$\xi_{m-1,0}$	2.28 – 2.51	2.20 – 4.61	2.20 – 4.61
Height of the nose	h_n	1, 2 and 3 cm	3 cm	3 cm
Height ratio parapet (h_n/h_{wall})	λ	0.125 – 1	0.375	0.375
Nose angle parapet (in degrees)	ε	15°, 30°, 45° 60°	30° and 45°	30° and 45°

*the wave period in phase 2 was chosen considerably larger than in phase 1 in order to investigate the influence of this parameter on the overtopping discharge over the optimal parapet geometry.

Note that for the impact tests, a fixed wall height and height of the nose have been used.

d) *Smooth dike with promenade*

Many coastal zones have a (touristic) promenade at crest level of their dikes. Besides knowing the amount of overtopping coming onto the promenade, it can also be of relevance to know the amount of overtopping discharge at the end of the crest width, because this is the overtopping that is flowing towards the hinterland. As stated in the literature review, as soon as the width of the promenade reaches a considerable width, it should have a reducing effect on the overtopping discharge or the volume that is reaching buildings at the end of the promenade. 62 tests have been carried out with 3 different promenade widths to study its influence.

The promenade had a 1% or 2% slope to stimulate drainage from overtopping water or rainfall back towards the sea. The freeboard R_c is defined as the difference in height between the highest point of the dike and the still water level, and is thus measured at the back of the promenade. The slope of the promenade is included in R_c, see Figure 3-6. The parameters as tested for this geometry are given in Table 3-4. Obviously, no impact tests were carried out.

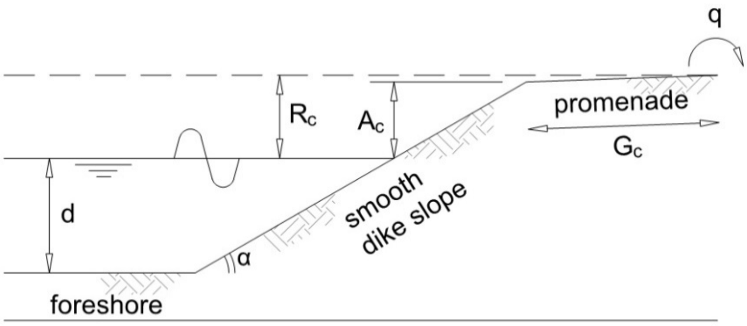

Figure 3-6. Cross section of a smooth dike with promenade (G_c).

Table 3-4. Summary of the characteristics of the UGent-1 tests on a smooth dike with promenade (scale model values).

UGent-1		Tests overtopping	Tests impacts
Slope angle of the smooth dike	cot(α)	2 and 3	Not applicable for this geometry
Mean spectral wave period	$T_{m-1,0}$	1.1 – 2.22 s	
Dimensionless freeboard	R_c/H_{m0}	0.85 – 2.68	
Length promenade	G_c	33.3, 66.7 and 100 cm	
slope promenade	-	1% and 2%	
Freeboard (top of structure to SWL)	R_c	0.10 – 0.28 m	
Seaward freeboard (top of slope to SWL)	A_c	0.093 – 0.26 m	
Dimensionless promenade length	$G_c / L_{m-1,0}$	0.045 – 0.5	
Spectral wave height	H_{m0}	0.07 – 0.17 m	
Water depth at toe of the structure	d	0.28 – 0.53m	
Wave steepness	$s_{m-1,0}$	0.009 – 0.050	
Wave breaker parameter	$\xi_{m-1,0}$	2.2 – 4.2	

e) *Smooth dike with promenade and storm wall*

Overtopping can be further reduced by building a storm wall at the end of a promenade, see Figure 3-7. 136 tests were carried out with different wall heights and promenade widths to quantify the reduction in wave overtopping. 27 of these tests also had force measurements on the storm wall. These 27 tests had a fixed promenade width (1m) and wall height (8cm), selected as optimal overtopping reducing measure, and therefore also tested on impacts. R_c again includes the slope of the promenade and the height of the storm wall. The level from the SWL to the crest of the dike is called A_c (Figure 3-7). It is however R_c that is further used in the analysis of wave overtopping reduction. The parameter A_c becomes more important for impact analysis, since this value is related to the overtopping bore characteristics (flow depth and flow velocity) on the promenade. The relationship between those parameters is as follows: $R_c = A_c + G_c \cdot \tan(\text{promenade}) + h_{wall}$.

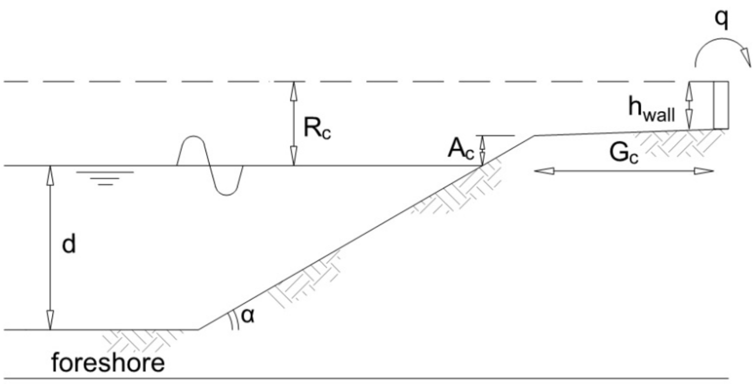

Figure 3-7. Cross section of a smooth dike with promenade (G_c) and storm wall (h_{wall}). The seaward freeboard A_c is also indicated.

The range of the parameters of the test program on a smooth dike with promenade and storm wall is listed in Table 3-5. A typical prototype geometry, e.g. along the Belgian coastline, has promenade widths of 10 to 15m and a storm wall height of about 1m. To achieve this, the model values from UGent can be scaled to prototype using a scale factor of 10 to 15.

Table 3-5. Summary of the characteristics of the UGent-1 tests on a smooth dike with promenade and storm wall (scale model values).

UGent-1		Tests overtopping	Tests impacts
Slope angle of the smooth dike	cot(α)	2 and 3	2 and 3
Mean spectral wave period	$T_{m-1,0}$	1.12 – 2.25 s	1.60 – 2.25 s
Dimensionless freeboard	R_c/H_{m0}	0.85 – 2.56	0.90 – 2.07
Freeboard (top of structure to SWL)	R_c	0.10 – 0.28 m	0.12 – 0.22 m
Seaward freeboard (top of slope to SWL)	A_c	0.013 – 0.24 m	0.03 – 0.13 m
Spectral wave height	H_{m0}	0.075 – 0.17 m	0.078 – 0.159 m
Length promenade	G_c	33.3, 66.7 and 100cm	100 cm
slope promenade	-	1% – 2%	1%
Dimensionless promenade width	$G_c/L_{m-1,0}$	0.05 – 0.41	0.127 – 0.252
Wall height	h_{wall}	2, 4, 6 and 8 cm	8cm
Dimensionless wall height	h_{wall}/R_c	0.07 – 0.80	0.364 – 0.667
Water depth at toe of the structure	d	0.36 – 0.55 m	0.41 – 0.51 m
Wave steepness	$s_{m-1,0}$	0.010 – 0.050	0.010 – 0.036
Wave breaker parameter	$\xi_{m-1,0}$	2.26 – 4.80	2.32 – 4.80

Note that for impact tests, a fixed promenade width and wall height have been used.

f) *Smooth dike with promenade and storm wall with bullnose*

The storm wall at the end of the promenade can also have a bullnose to further reduce the overtopping discharge, see Figure 3-8. 100 tests were carried out to study the extra reducing effect of the bullnose compared to the previous geometry with a storm wall at the end of the promenade. In 64 of these tests, forces were recorded; horizontal forces in 32 tests and vertical forces in a repetition of these 32 tests. For the force measurements, again no variation in promenade width (1m) and wall height (8cm) was tested. The range of parameters tested is given in Table 3-6.

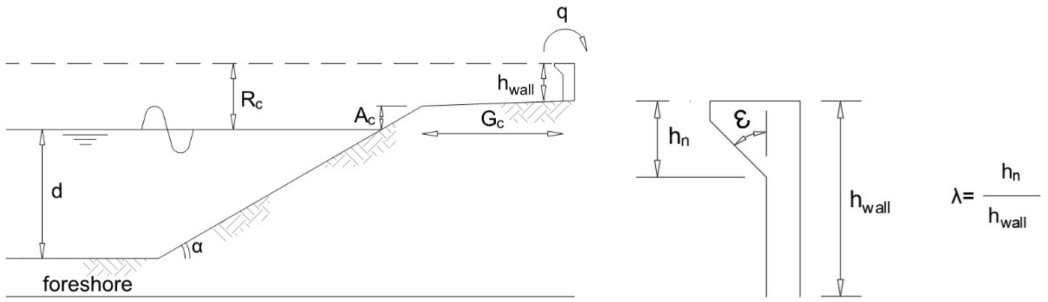

Figure 3-8. Cross section of a smooth dike with promenade (G_c) and storm wall (h_{wall}) with bullnose (λ,ε).

Table 3-6. Summary of the characteristics of the UGent-1 tests performed on a smooth dike with promenade, storm wall and parapet (scale model values).

UGent-1		Tests overtopping	Tests impacts
Slope angle of the smooth dike	cot(α)	2 and 3	2 and 3
Mean spectral wave period	$T_{m-1,0}$	1.25 – 2.25 s	1.60 – 2.25 s
Dimensionless freeboard	R_c/H_{m0}	0.7 – 1.9	0.92 – 1.80
Freeboard (top of structure to SWL)	R_c	0.08 – 0.24 m	0.12 – 0.22 m
Spectral wave height	H_{m0}	0.08 – 0.17 m	0.08 – 0.16
Length promenade	G_c	33.3, 66.7 and 100 cm	100 cm
slope promenade	-	1% – 2%	1%
Dimensionless promenade length	$G_c/L_{m-1,0}$	0.04 – 0.40	0.13 – 0.25
Wall height	h_{wall}	4, 6, 8 cm	8 cm
Dimensionless wall height	h_{wall}/R_c	0.17 – 0.80	0.36 – 0.67
Height ratio parapet	ε	30°, 45°	30° and 45°
Nose angle parapet (in degrees)	λ	0.25 – 0.375	0.375
Water depth at toe of the structure	d	0.40 – 0.55 m	0.41 – 0.51 m
Wave steepness	$s_{m-1,0}$	0.010 – 0.040	0.010 – 0.036
Wave breaker parameter	$\xi_{m-1,0}$	2.14 – 4.77	2.14 – 4.77

Note that for impact tests, a fixed promenade width, wall height and nose height have been used.

g) *Smooth dike with Stilling Wave Basin*

A last measure proposed in this thesis to reduce wave overtopping by modifying the existing crest of a dike, is the so-called Stilling Wave Basin (SWB). The concept already existed for rubble mound breakwaters (Aminti & Franco, 2001) and has been introduced on a smooth dike by Beels (2005), Geeraerts et al. (2006) and Geeraerts & De Rouck (2008). The latter tests were carried out at Ghent University some years ago and have been added here to give a complete overview of overtopping reducing measures at smooth dikes.

The SWB is made up of a seaward wall, a basin and a landward wall. The seaward wall is partially permeable to allow the evacuation of the water in the basin. It may consist of a double row of shifted walls (Figure 3-10) or a single wall with some gaps. This innovative crest design is based on the principle of energy dissipation: the incoming wave hits the seaward wall and is projected upward, then drops in the basin before hitting the landward wall. At that moment, most of its energy is already dissipated. Consequently, the landward wall is overtopped less in comparison with an unmodified crest, even though the crest height has not been increased.

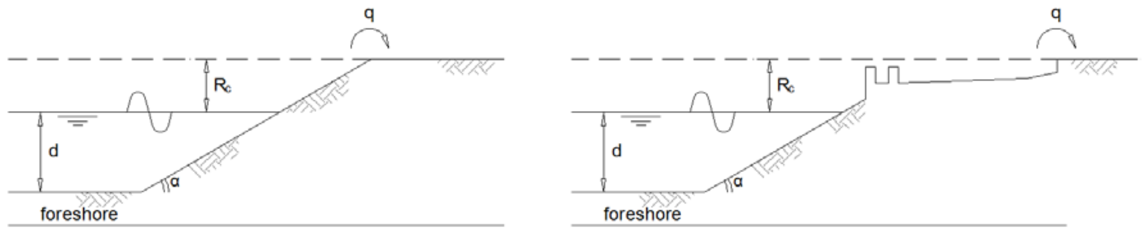

Figure 3-9. Cross section of a simple smooth dike (left) compared to a dike with SWB built in the crest (right).

Many geometrical variations of the SWB have been tested, with over 300 tests with non-breaking wave conditions by Geeraerts and Beels. The range of hydraulic parameters and geometric variations is listed in Table 3-7 and is illustrated in Figure 3-10 and Figure 3-11. No impacts were measured in these tests.

Table 3-7. Summary of the characteristics of the tests performed on a smooth dike with SWB (scale model values) by Beels (2005) and Geeraerts et al. (2006).

UGent-1		Overtopping tests	Impact tests
Slope angle of the smooth dike	cot(α)	2; 2.5; 3	Not measured for this geometry
Mean spectral wave period	$T_{m-1,0}$	1.16 s – 2.33 s	
Dimensionless freeboard	R_c/H_{m0}	0.56 – 2.7	
Freeboard (top of structure to SWL)	R_c	0.10 – 0.27 m	
Spectral wave height	H_{m0}	0.08 – 0.18 m	
Length basin	L_{basin}	48, 36, 24 and 12 cm	
slope basin	-	2%	
Wall height	$h_{front\ wall}$	48, 72, 96, 120 and 144mm	
Distance between front walls	-	4cm	
Water depth at toe of the structure	d	0.30 – 0.52 m	

The front wall of the SWB varied in height from 48mm to 144mm, in which the 48mm above the SWB floor was kept constant over all variations tested. In Figure 3-10 a total wall height of 96mm is shown; it's the 48mm below the SWB floor which has been varied between 0mm and 96mm. To upscale to prototype, a scale factor of 25 is proposed, related to a prototype front wall of 1.2m (48mm x 25) which is a perfect height to lean on, like a railing.

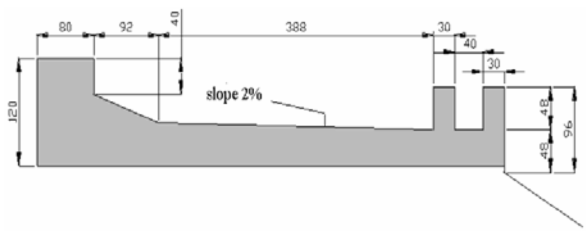

Figure 3-10. Side view of Stilling Wave Basin (dimensions in mm), figure by Geeraerts et al. (2006).

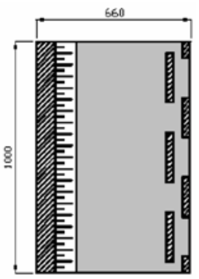

Figure 3-11. Plan view of Stilling Wave Basin (dimensions in mm), figure by Geeraerts et al. (2006).

3.1.3 *Measurementes and equipment*

a) *Waves*

Waves were measured using resistance type wave gauges with a measurement frequency of 40Hz. The wave gauges were positioned as shown in Figure 3-2: two gauges in front of the wave paddle (on behalf of the active wave absorption), three at deeper water, and three in front of the structure (at a distance of $0.4L_{0p}$ from where the SWL reached the structure). By means of these groups of gauges, incident and reflected wave conditions could be separated from each other and the incoming wave height could be determined, using the method by Mansard & Funke (1980). The wave height H_{m0} near the toe of the structure is used throughout the analysis of the UGent-1 data. Wave gauges were mounted to a frame over the flume, making them able to measure the waves in the center of the 1m wide flume, see Figure 3-12.

Figure 3-12. wave gauges in the UGent large wave flume.

b) *Wave overtopping*

Wave overtopping was captured by a 0.30m wide tray on top of the smooth dike, and lead to a 30 liter basin that was constantly weighed on a balance. When the basin was full, water was pumped back to the back of the wave flume in order to maintain the correct water level in the flume during the test. Total overtopping volume could be deducted from the balance's weight registration in time. The measurement frequency of the balance was 7.5 Hz. Pictures are given in Figure 3-13 and Figure 3-14.

For all tests in the UGent-1 dataset, average overtopping discharges have been determined. No individual values were analyzed.

Figure 3-13. Wave overtopping tray (left) and balance with pumping system (right) in the UGent-1 set-up.

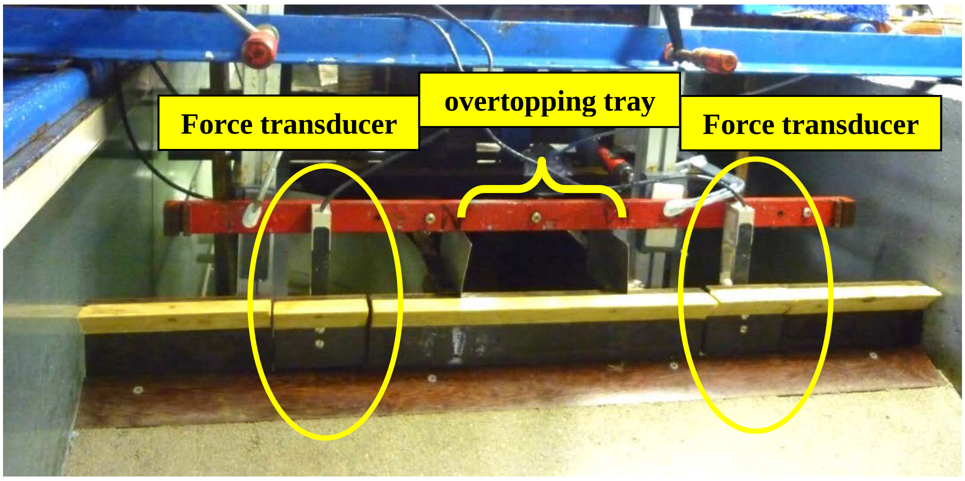

Figure 3-14. Frontal view of the top of the structure, with the central overtopping tray flanked by two force transducers (see further, subsection 3.1.3d).

c) *Overtopping flow parameters*

As shown in Section 3.1.2, some geometries in the UGent-1 database have a promenade at crest level where overtopped bores can flow. However, the UGent-1 dataset does not contain recordings of the overtopping flow (flow depth and flow velocity). Some attempts have been made, without successful results for the turbulent bores at the small scale, as could be expected based on Section 2.7.2. Therefore, these attempts are not further treated here.

d) *Impacts*

Most of the geometries in Section 3.1.2 had a storm wall as overtopping reducing measure. In some cases, this storm wall had a bullnose to further decrease the overtopping discharges. For all these overtopping reducing measures in the UGent-1 database, wave impact measurements had been carried out. This was done by measuring the impact force by means of force transducers. A photo of geometry 'dike + promenade + wall' is given in Figure 3-15, but measuring devices and techniques for impact recordings were similar for the other geometries.

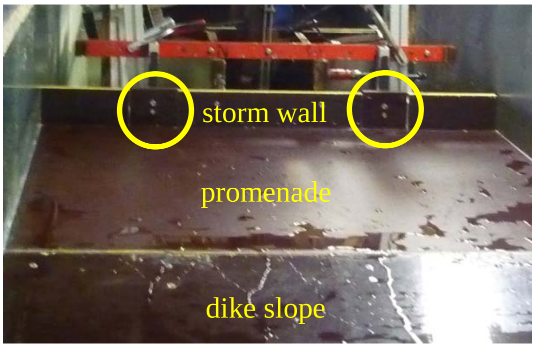

Figure 3-15. Geometry of the smooth dike with promenade and storm wall built in the wave flume of UGent (left). Detail of the part of the storm wall attached to the force transducer (right).

The storm wall consisted of two sections (each 10cm wide) attached to force transducers (see yellow circles in Figure 3-15). The force transducers were mounted to a rigid structure (the red bar in Figure 3-15), and the storm walls – a loose section – was screwed to the force transducer. No openings were left between the recording sections, but a continuous wall was built. Force sensors with a range up to 5kg were used. Forces were recorded at 1000Hz sampling frequency and analyzed with a bandstop filter between 49.9Hz and 50.1Hz to filter out a peak of the net frequency. During the analysis, also a low-pass filter of 50Hz was used to avoid resonances near the eigenfrequency of the storm wall (90Hz) which would disturb the analysis. Also a More information on the filtering and resonance is given in Section 6.2.1

In case a bullnose or parapet nose was attached to the storm wall, tests were run twice: a first run with the storm wall attached to the force transducers measuring the horizontal force (Figure 3-16, left), a repetition of the tests with the bullnose attached to the force transducers measuring the upward, vertical force (Figure 3-16, right).

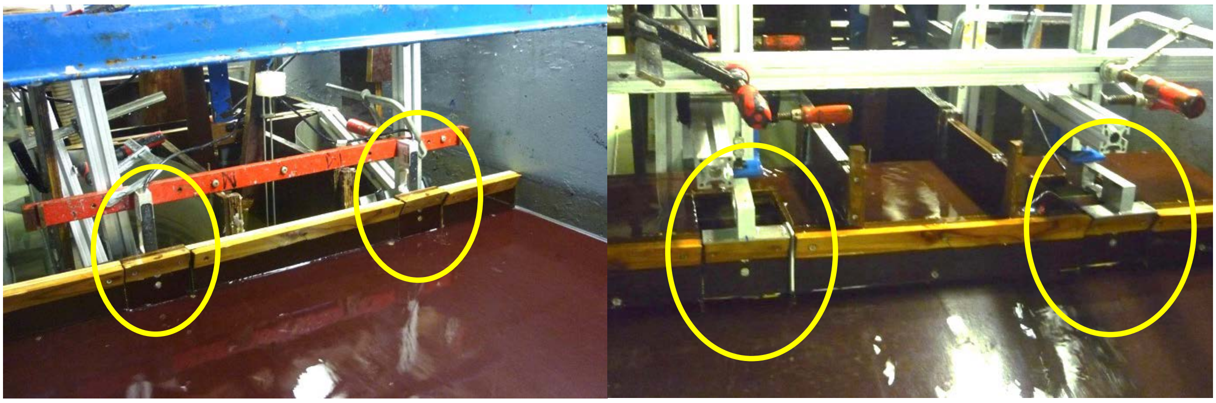

Figure 3-16. Force transducers measuring horizontal forces (left) versus vertical forces (right) on a wall with bullnose.

3.2 *GWK dataset*

3.2.1 *Test set-up*

A second new test campaign was performed in the summer of 2011 in the Grosser Wellenkanal (GWK) in Hannover, Germany, at a large scale. This dataset is hereafter referred to as the GWK dataset. The GWK wave flume has a length of 300m, is 5m wide and 7m high (Figure 3-17). In the beginning of the project, a few tests with regular waves have been run to better understand the process of overtopping bores on a promenade impacting a storm wall, but the majority of the tests has been run with a Jonswap (γ = 3.3) wave spectra. The wave paddle in GWK is equipped with active wave absorption. A dike with a slope of 1:3 and a crest height of 6.5m, constructed of interlocked concrete tiles (an almost smooth surface), was built in the flume to test the stability of the interlocking revetment blocks, see Gier et al., (2012). Since the geometry of this dike was close to the required geometry, and since there was only a limited amount of time available in the laboratory for testing (2 weeks, including set-up), it was decided to use the dike as it was despite it's rather high crest level (large A_c) in relation to the maximum achievable water depth and wave height in the GWK. This also means that some restrictions were faced during the test campaign, which are described later in this section.

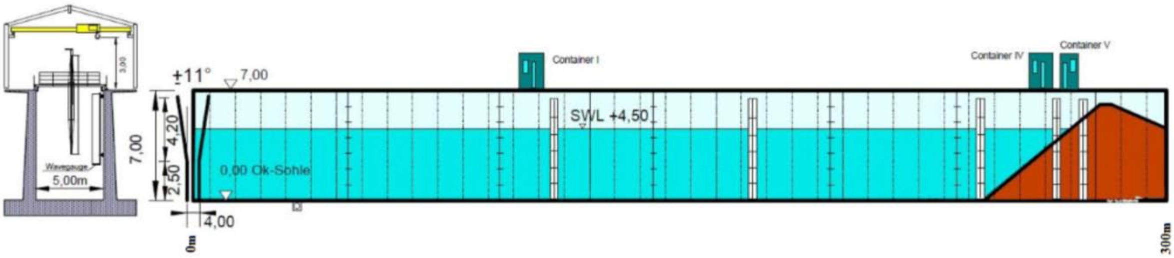

Figure 3-17. Cross section over the width (left side) and length (right side) of GWK.

3.2.2 *Tested geometry and parameter range*

Only one geometry was tested, see Figure 3-18. A (relatively) smooth dike slope 1:3 with a promenade of 10m wide at crest level and a storm wall of 1.7m high. This is comparable to the geometry ‘Smooth dike with promenade and storm wall’ as in section 3.1.2e) from the UGent-1 dataset upscaled with a factor 10. The experiments at GWK can therefore be considered as (nearly) full scale (1:1) tests.

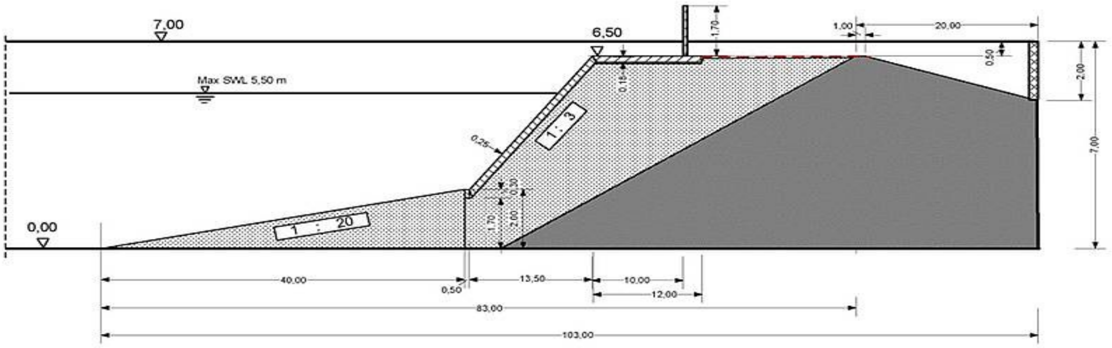

Figure 3-18. Cross section of the GWK experiments: 1:3 smooth dike with promenade and storm wall. Sketch with distorted scale. Figure by De Rouck et al. (2012).

21 tests with irregular waves, Jonswap spectrum $\gamma = 3.3$, were carried out. The water level of these tests was 4.5m and 5.0m, giving a seaward crest freeboard A_c of 2m and 1.5m, respectively. The wave heights H_{m0} varied from 0.85m to 1.5m, with wave periods T_p in the range of 6.0s to 12.0s. In combination with the 1:3 dike slope, non-breaking waves were found. The test program for the GWK tests is summarized in Table 3-8, note that a fixed promenade width and wall height have been used.

Table 3-8. Characteristics of the GWK dataset on a smooth dike with promenade and storm wall (large scale tests).

GWK			Flow parameter & impact tests
Number of tests (Jonswap 3.3)	-	-	21
Slope angle of the smooth dike	$\cot(\alpha)$	-	3
Promenade length (=crest width)	G_c	(m)	10 m
Dimensionless promenade length	$G_c/L_{m-1,0}$	-	0.07 – 0.22
Promenade slope	-	(%)	0 %
Wall height	h_{wall}	(m)	1.50m (hor), 1.70m (vert)
Dimensionless wall height	h_{wall}/R_c	-	0.43 – 0.50
Water depth at toe of the structure	d	(m)	4.5 – 5.0 m
Freeboard (seaward side)	A_c	(m)	2.0 – 1.5 m
Dimensionless freeboard	A_c/H_{m0}	-	1.11 – 2.35
Freeboard (landward side)	R_c	(m)	3.5 – 3.0 m
Dimensionless freeboard	R_c/H_{m0}	-	2.22 – 4.42
Mean spectral wave period (incoming)	$T_{m-1,0}$	(s)	5.36 – 9.716 s
Spectral wave height (incoming)	H_{m0}	(m)	0.68 – 1.474 m
Wave breaker parameter	$\xi_{m-1,0}$	-	1.89 – 4.38
Wave steepness	$s_{0,\ m-1,0}$	-	0.006 – 0.031

3.2.3 *Measurements and equipment*

In the GWK test campaign the incident wave parameters (water level, wave height, wave period), post-overtopping characteristics of the bore (flow depth, flow velocity) and impacts on the storm wall (impact forces, impact pressures) were measured at several locations in the flume, on the crest and at the wall respectively. The overtopping discharges and individual overtopping volumes were not recorded in this test campaign.

a) *Waves*

3 sets of resistive wave gauges were installed over the length of the flume. A first set of three gauges near the wave paddle (deep water conditions), a set of three gauges at 2/3rd of the used length of the flume (to observe the evolution of the wave parameters over the length of the flume) and a set of four in front of the toe of the dike. A wave gauge at the wave paddle is controlling the active wave absorption. The wave gauges near the toe of the dike were used for analysis.

The wave gauges were double wired and positioned along one side of the flume. The sampling frequency was 100Hz.

Figure 3-19. Wave gauges in GWK, attached to the side of the flume.

b) *Wave overtopping*

Wave overtopping discharges have not been measured in the GWK test campaign, not at the seaward crest of the dike (A_c), and not over the storm wall (R_c).

c) *Overtopping flow*

Due to the large scale, it became more feasible to measure flow parameters of the overtopped bore, namely flow depth and flow velocity. Several methods have been used, but not all of them gave good results. All measurement systems at the crest of the dike were storing data at a sampling frequency of 2000 Hz.

To measure the **flow depth** of the overtopping bore on the crest, three digital step gauges were installed at different locations on the promenade: at 0.5m, 3.8m and 7.9m starting from the seaward edge of the promenade (x_C = 0 in Figure 1-9), see Figure 3-20. A digital step gauge is a PVC rod with in our case a sensor every 2cm in height indicating whether it is wet or dry. The highest sensor indicating that it's wet indicates the flow depth. These step gauges could also be used to determine the **flow velocity** of the front of the overtopping bore. By knowing the exact distance in between two different step gauges, and by the time difference of these two sensors reacting to an incoming overtopping bore, the front velocity of this bore in between the two step gauges can be calculated.

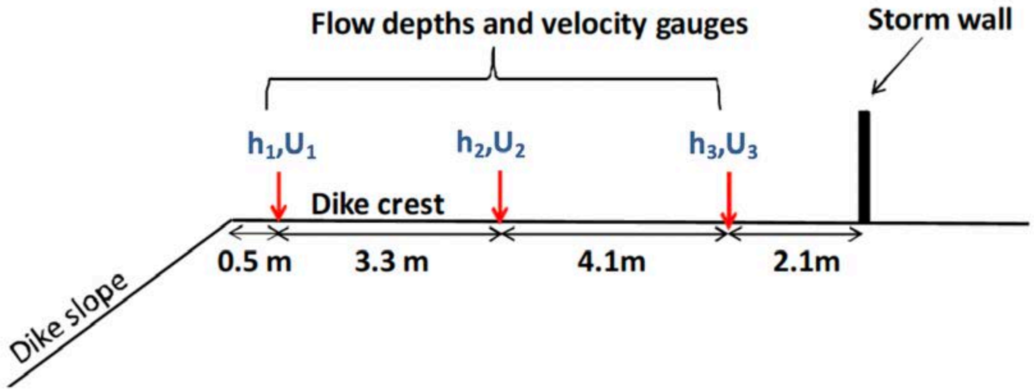

Figure 3-20. Indication of flow parameters recordings at the promenade in the GWK experiments.

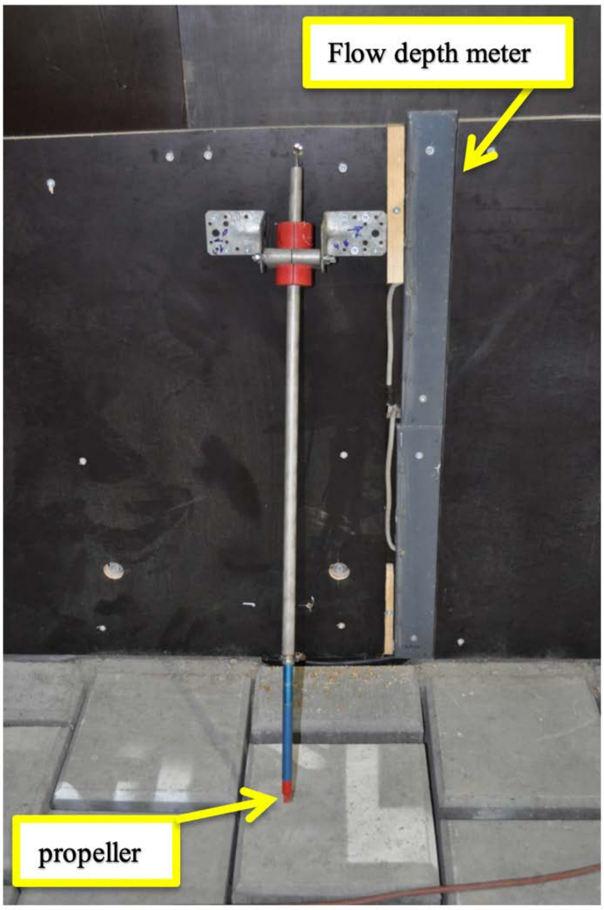

Figure 3-21. Digital step gauge to measure flow velocity and flow depth, propeller to measure flow velocity.

This method can be verified by means of video analysis. At different positions along the promenade, video cameras were installed mainly to get a better understanding of the physical behavior of impacts, run-up, splash, etc. Horizontal lines with 1m interval were painted on the promenade, see Figure 3-23. Ideally, the video images could also be used to determine which distance a wave front has covered in a certain time frame, with that providing the front velocity of the overtopping bore. Unfortunately, video analysis could not be automated since the cameras were not calibrated and have therefore only been used for verifying some individual results obtained by the previous method. Also no particle image velocity or bubble image velocity measurements were available in the GWK tests. Another possibility to measure velocities of the overtopping bore, was by installing a micro-propeller at the same location of each step gauge (see Figure 3-21). After calibration, the rotation speed of the propeller's blade is linked to the velocity of the overtopping bore at a certain point in the velocity profile over the height of the bore. This easy method was however not working well, since small grains and dirt particles in the water (pumped into the flume from the nearby canal) often blocked the propeller during a test, disturbing the velocity recording. It is advisable to use propellers with a larger casing in future test campaigns to avoid blocking by sand particles in the water. A detail of the narrow housing is shown in Figure 3-22. Another disadvantage of this micro propeller was that the rotational direction could not be distracted from the output signal, which made it impossible from this recording to see whether an incoming or a reflected bore (after an impact) was measured.

Figure 3-22. Detail of the micro propeller in the GWK set-up.

Since video analysis and the propeller did not provide good results, it was decided to use the three step gauges along the promenade to measure both flow depth and the flow velocity of the bore front passing from one step gauge to another. As will be explained in Chapter 5, also this analysis had to be done manually and was very time consuming, but gave reliable results. A link between the overtopping flow parameters and the impact forces was the most important realization in this test campaign.

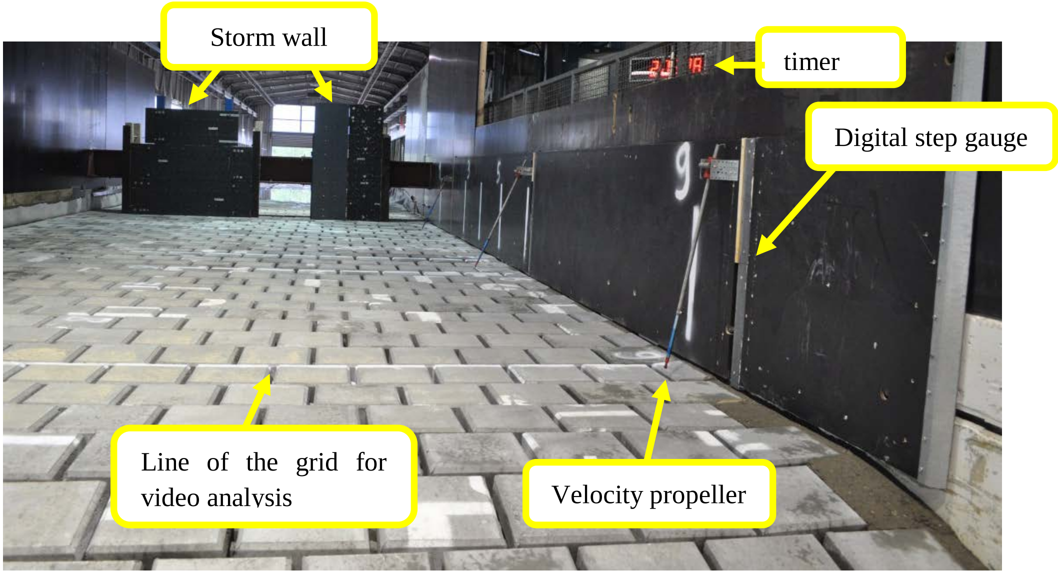

Figure 3-23. Overview of the measurement equipment on the 10m horizontal promenade during the GWK tests.

d) *Impacts*

Due to a short preparation time, the set-up was built with material available at Ghent University, where the construction of the storm wall was prepared and transported to Hannover. There, the storm walls were attached to frame which was bolted to a steel beam, which on its turn was connected to the rigid side walls of the flume, and not to the dike itself. A very stiff structure was created to minimize vibrations and resonance effects in the measurements. Some pictures of the installation are given in Figure 3-24 to Figure 3-26. The finished construction is shown in Figure 3-27.

Figure 3-24. Installation of the steel beem to the rigid side walls of the flume.

Figure 3-25. steel beam attached to the sides of the flume, installation of the blue supporting frame.

Figure 3-26. View on the blue supporting frames attached to the steel beam.

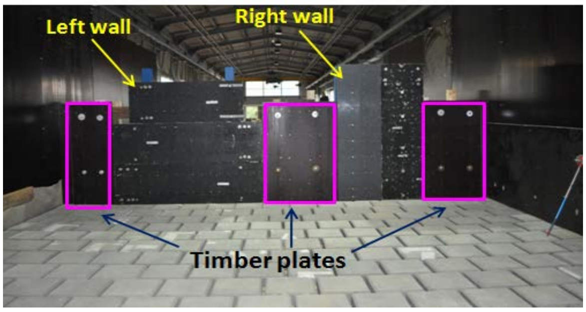

Figure 3-27. Closed storm wall (left side) vs opened storm wall with only measurement plates (right side) in the GWK tests.

During the first 4 experiments, the storm wall was closed (Figure 3-27, left side). Two measurement sections were foreseen in this storm wall: the left wall and the right wall in Figure 3-27, left side. The left wall had 3 horizontal plates (with a total height of 1.50m), each plate equipped with 4 force sensors. The right wall had 2 vertical plates (with a height of 1.70m), one to measure forces with 4 force sensors, one to measure pressures with 2 rows of 8 pressure transducers: see Figure 3-28.

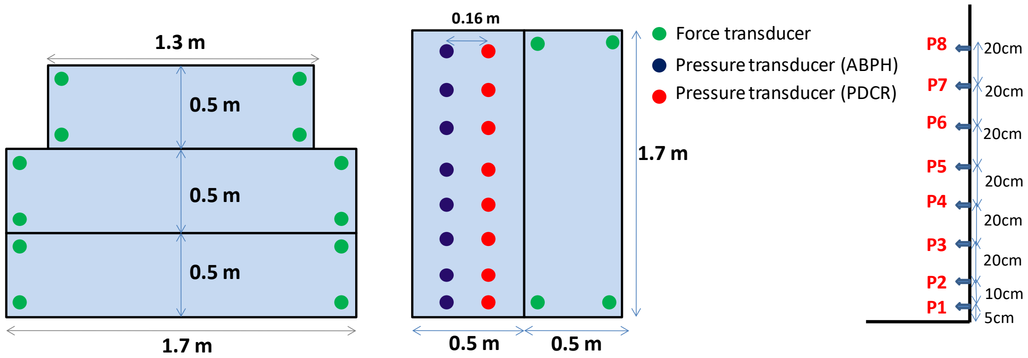

Figure 3-28. Installation of force and pressure sensors at the left and right storm wall, and their position in height (Figure byRamachandran et al. (2012a)).

The pressure sensors were installed at 2 vertical rows, each row with 8 sensors and positioned according to Figure 3-28. The left row were ABPH sensors (Honeywell pressure sensors), the right row were PDCR sensors (Druck/GE pressure sensors), both installed flush mounted on the storm wall (see detail in Figure 3-29). The ABPH sensors however were influenced by temperature variation and forces exerted on the housing of the sensors during the impacts and did not give reliable results. They were further excluded from the analysis, and only the PDCR sensors were used for comparison with force measurements.

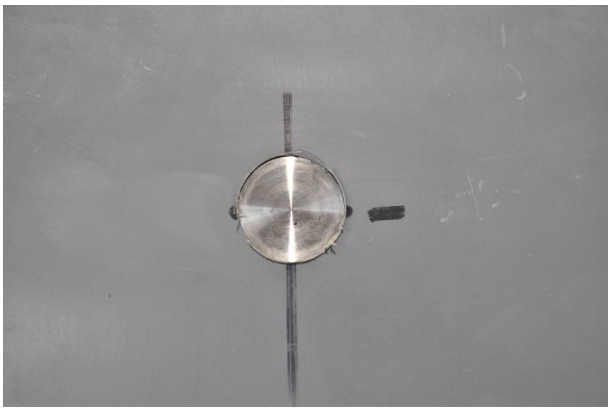

Figure 3-29. Detail of the flush mounted ABPH installed pressure sensor.

The force transducers (500kg, 1ton and 2 ton sensors from Tedea Huntleigh) were located in the 4 corners of each plate. Each sensor was mounted to the frame, and the storm wall (a steel plate) was attached to the 4 sensors. This is shown in Figure 3-30 to Figure 3-32. The impacts on the plate were passed along to the transducers, who recorded the impact.

Figure 3-30. Blue supporting frame bolted to the rigid steel beam.

Figure 3-31. Black storm wall attached to the force sensors, who on their turn are attached to the supporting frame.

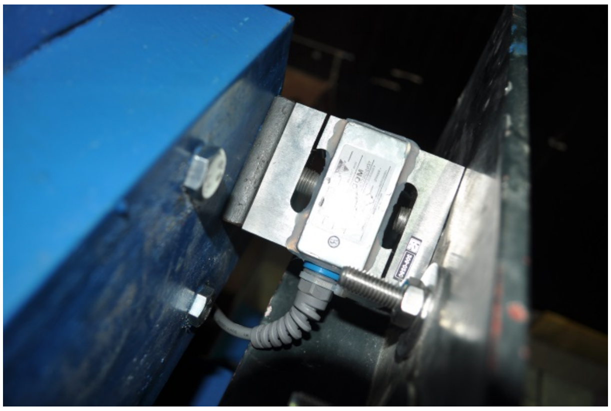

Figure 3-32. Detail of Figure 3-31: black storm wall attached to a force sensor, who on its turn is attached to the blue supporting frame.

Forces and pressures were recorded at 2000Hz and filtered at 1000Hz. A hammer test on the plates with force sensors showed that the structure's eigenfrequency was much higher, so no resonance was noticed during the tests. More information on resonance and filtering is found in Section 6.2.1.

During these first experiments with closed wall (Figure 3-27, left side), it became clear that a large residual water layer remained in front of the storm wall (up to 50 cm and more) which heavily damped each of the following incoming waves. This was not realistic, since waves are not this long crested in reality and overtopping water can run off in all directions during a real storm. Furthermore, the crest in the GWK was horizontal, no seaward slope of 1 or 2% as in the UGent-1 experiments was foreseen. Consequently, it was decided to create some openings in the storm wall, whereas the measurement plates remained in place. The overtopping water was now allowed to run off between the plates (Figure 3-27, right side). In this way, higher, undamped impacts could occur. Only the tests with opening in between the recording sections are withheld for further analysis in this work.

Behind the storm wall, at the end of the flume, a basin was present with two pumps pumping the water back towards the flume (Figure 3-33). Due to the distance from the walls, and the lack of recording equipment in the basin, it could not be used for measuring overtopping discharges, but it was just a buffer to collect water and pump back to the flume. The size of the overtopping basin however, was not adapted to this large amount of water to be collected after making the aforementioned openings in the wall (Figure 3-27, right side). The pumps were not strong enough to empty the overtopping basin during the tests. The tests had to be stopped when the overtopping basin was full, or in contrary, when the wave overtopping at the seaward crest was too low and no impacts were measured. Hence, the number of waves of each test varied between 40 and 200 and the impacts varied between 5 to 60% of those numbers, being too few to have complete force distributions as could be expected during a storm lasting a few hours. Nevertheless, recent work by Romano et al. (2015) showed that reliable overtopping parameters are obtained for wave sequences shorter than 1000 waves, and that the seeding number affects mainly small overtopping discharge. Since the GWK experiments had large overtopping discharges over the crest, and overtopping flow is the main driver of wave impacts, the impact tests can be considered reliable despite the low number of waves. The force values are reliable, but no full distribution for statistical analysis could be derived.

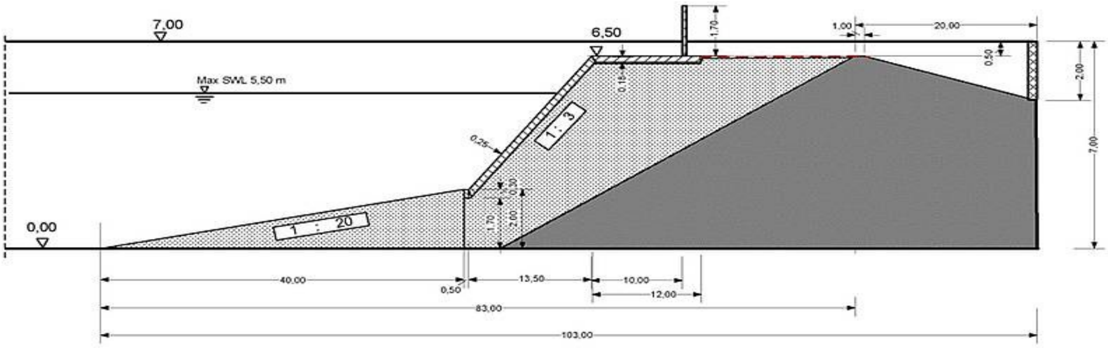

Figure 3-33. Overtopping basin at the end of the GWK flume.

Despite some disadvantages, this test campaign had the advantage that it was at large scale and that high quality measurements of the overtopping flow process were performed.

More information on the test set-up and the measurement equipment can be found in De Rouck et al. (2012), who gave a preliminary analysis of the tests with irregular waves, and in Ramachandran et al. (2012a), where regular waves were discussed. Only the 21 tests with irregular waves are considered further in this manuscript.

3.3 *Hydralab dataset*

3.3.1 *Test set-up*

The third new test campaign to study wave impacts on storm walls was carried out in the Canal d'Investigació I Experimentació Marítima (CIEM), at the Universitat Politècnica de Catalunya (UPC, Barcelona, Spain) within the HYDRALAB IV framework (www.hydralab.eu). This dataset is further referred to as the Hydralab dataset. The CIEM wave flume is 100.0 m long, 3.0 m wide, 5.0 m deep and is equipped with a wedge type wave generator. No active wave absorption was available throughout the experiments in Barcelona. Time series of approximately 1000 waves were generated with Jonswap ($\gamma = 3.3$) spectrum.

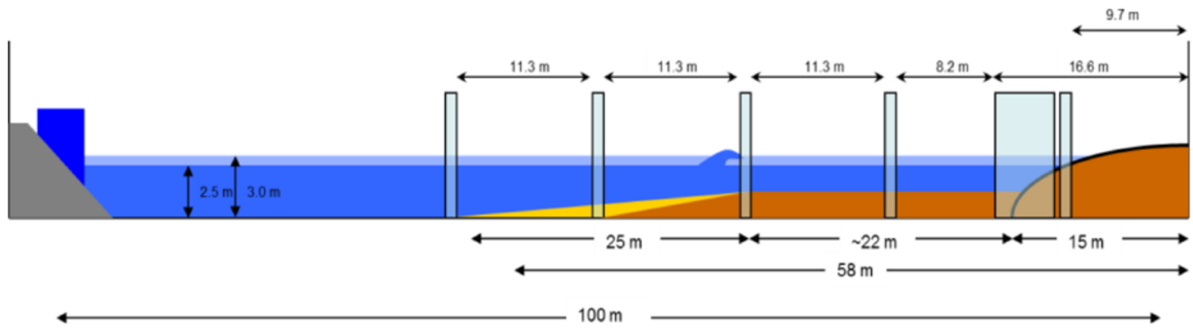

Figure 3-34. Cross section of the CIEM wave flume in Barcelona.

Within the Hydralab IV projects in Barcelona, several other projects related to sandy beaches were carried out. In the planning by LIM (Laboratori d'Inginyeria Marítima, who operate the CIEM wave flume) both before and after the experiments for this research, a lot of sand had to be used in the flume. Taking all sand out to have the largest possible available water depths, and putting it all back in afterwards would have reduced the available time window for testing too much, after which LIM decided to leave all sand in the flume, and create a kind of foreshore with it. The lower possible water levels in combination with the ability of the wave maker, changed the foreseen large scale testing into mid-scale testing with a Froude scale of 1:6 compared to a prototype dike and the 1:1 scaled GWK tests.

3.3.2 *Tested geometry and parameter range*

In the Hydralab experiments, the focus was on measuring impacts on a storm wall at the end of a promenade on a dike. The geometry consisted of a smooth dike slope 1:3 with a promenade width of 1.69m and a storm wall of 0.20m high. This storm wall was built similarly to the UGent-1 experiments: a continuous wall over the entire width of the flume with two measurement sections where one section was used to measure pressures, and the other to measure forces.

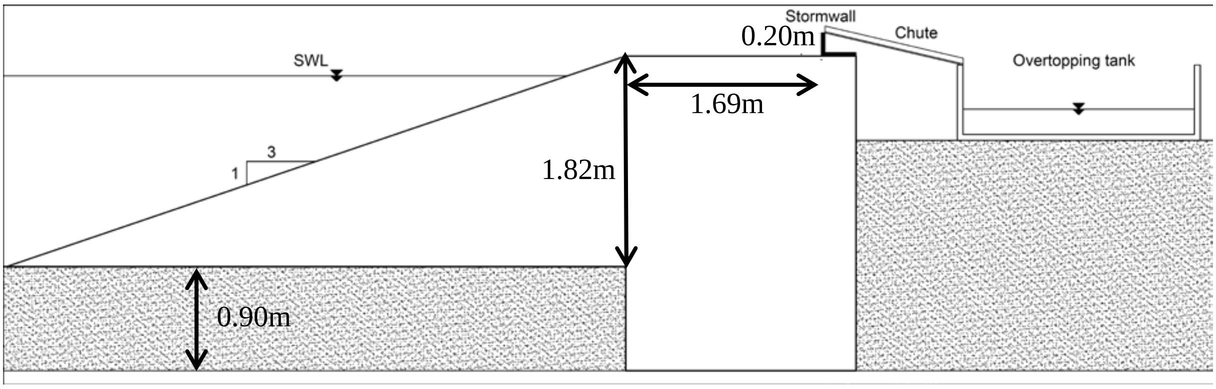

Figure 3-35. Cross section of the 1:3 smooth dike with a 1.69m wide promenade and 0.2m high storm wall in the Hydralab tests in Barcelona.

The total height of the structures, measured from the top of the 0.90m thick sand layer which was present in the flume and acted as a foreshore, is 1.82 m. Three water levels at the toe of the structure have been used (1.49m, 1.65m and 1.82m). Wave height at the toe of the structure was between 27cm and 36cm. Also here, non-breaking waves were tested. A summary of the test program is given in Table 3-9. Note that a fixed promenade width and wall height have been used in the Hydralab dataset.

Table 3-9. Characteristics of the Hydralab dataset on a smooth dike with promenade and storm wall (dimensional values are model scale values).

Hydralab tests			**Flow parameter & impact tests**
Number of tests (Jonswap 3.3)	-		14
Slope angle of the smooth dike	cot(α)	-	3
Promenade length (= crest width)	G_c	(m)	1.69
Dimensionless promenade length	$G_c/L_{m-1,0}$	-	0.077 – 0.159
Promenade slope	-	(%)	1.8
Wall height	h_{wall}	(m)	0.20
Dimensionless wall height	h_{wall}/R_c	-	0.357 – 0.87
Water depth at toe of the structure	d	(m)	1.49; 1.65; 1.82
Freeboard (seaward side)	A_c	(m)	0.33; 0.17; 0
Dimensionless freeboard	A_c/H_{m0}	-	0 – 1.235
Freeboard (landward side, incl. stormwall)	R_c	(m)	0.56; 0.40; 0.23
Dimensionless freeboard	R_c/H_{m0}	-	0.644 – 2.097
Mean Spectral Wave period (incoming)	$T_{m-1,0}$	(s)	2.61 – 3.74
Spectral Wave height (incoming)	H_{m0}	(m)	0.267 – 0.362
Wave breaker parameter	$\xi_{m-1,0}$	-	1.83 – 2.84
Wave steepness	$s_{0,\ m-1,0}$	-	0.13 – 0.033

3.3.3 *Measurements and equipment*

a) *Waves*

12 resistance type wave gauges and 4 pore pressure sensors placed along the wave flume have been used to record the free surface elevation time series. All wave gauges were installed at one side of the flume and were placed at regular distances along the flume. The last 4 wave gauges can be used to determine the incoming wave height at the toe of the structure by means of a reflection analysis. The pore pressure sensors were not further used.

b) *Wave overtopping*

The overtopping discharge and volumes were measured by collecting overtopping over the storm wall in a concrete tank (cross section in Figure 3-35, details in Figure 3-36), equipped with 3 pressure sensors to measure the volume. It was expected that very large overtopping would take place during tests with the lowest freeboards and really small volumes would be collected under other conditions. In order to improve the overtopping measurement (expected inaccuracy problems would occur if overtopping volumes were too small with respect to the volume of the measuring tank) a modular volume system was implemented, by reducing the funnel (in case of large overtopping, allowing less water in the tank) or by using a separate much smaller tank (in case of small overtopping, increasing the accuracy).

The maximum volume of the overtopping tank (OVT) was 2.5m^3. In order to allow bigger overtopping volumes a set of two pumps with an average capacity of up to 300l/min each was installed in the overtopping tank. Once the water reached a certain level (visually observed) the pumps were (manually) activated and the volume of extracted water was measured by an electromagnetic flow meter (EMF) installed in the circuit returning the water to the flume.

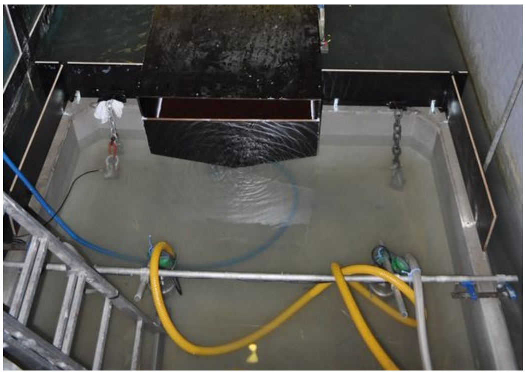 

Figure 3-36. Concrete overtopping tank (left) with 2 submerged pumps. An Electromagnetic Flow Meter (right) measures the water that is pumped out of the overtopping tank and is returned back to the flume.

Unfortunately, some problems were observed with the overtopping measurements during the tests:

- The connections to lift the overtopping tank (OVT) in the flume broke during the first attempt. These holes remained in the OVT and caused problems at a later stage.
- The OVT was installed on top of the leftover sand at the end of the flume, see Figure 3-35. During the first tests, the sand showed differential settling which caused the OVT to tilt forward. The tank was too heavy to lift and repair this; recording water levels in the OVT which is tilted requires some extra steps to calculate the volumes.
- Due to the tilting, the front wall became too low and water was running out of the OVT back to the flume (without passing the EMF). Water also leaked through the holes from the (broken) lifting mechanism. Duct tape and wooden panels could not fix this problem.
- The width of the OVT covered almost 90% of the flume width. In the 10% remaining width of the flume, there was a water set-up through which water entered the tank.
- The worst problem was that the pipes to return the water level back to the flume after being pumped out of the OVT, did not have a check valve. The water in the flume was higher than the water in the OVT, so often water was flowing in the opposite direction through the pipes filling instead of emptying the OVT. From the recordings of the EMF, this could not be filtered out: the signal in voltage did no show in which direction the water was flowing.

Due to these issues and too short preparation time, it was not possible to use any of the wave overtopping data. An important goal of the Hydralab project was thereby not met. The UGent-1 dataset thus remained the only dataset with reliable overtopping measurements.

c) *Overtopping flow*

Four acoustic wave gauges at 1m above the promenade and four Acoustic Doppler Velocimeter (ADV) at a few cm above the promenade were installed to measure flow depths and flow velocities of the overtopped waves. LIM had good experience with the use of these equipment in measuring flow velocities and flow depths in swash zone of beach run-up. Unfortunately, for this project, not only the ADV recorded signals proved not to be reliable, but also the acoustic wave gauges often failed or gave a noise which was larger than the recording. Therefore, no overtopping flow parameters could be used from these experiments, and the focus for the analysis of this dataset is therefore on the relationship between the wave parameters and the impact forces (similar to the UGent-1 dataset).

d) *Impacts*

The storm wall was built to cover the entire width of the flume, but in different panels. Two panels were equipped with measuring sensors. One panel (width of 0.5 m) was instrumented to measure the impact forces. In total 4 force sensors were fixed to a rigid supporting structure and the panel was attached to these sensors (see Figure 3-37). The other panel was firmly fixed to the supporting structure and 3 pressure sensors were installed, flush mounted and aligned along a vertical line (see Figure 3-37 and Figure 3-38). The height of the heart of the pressure sensors, from the base of the storm wall, is 2.5cm, 10cm and 17.5cm. Pressure and force analysis will be compared, and also the impact profile over the height will be given in Chapter 6.

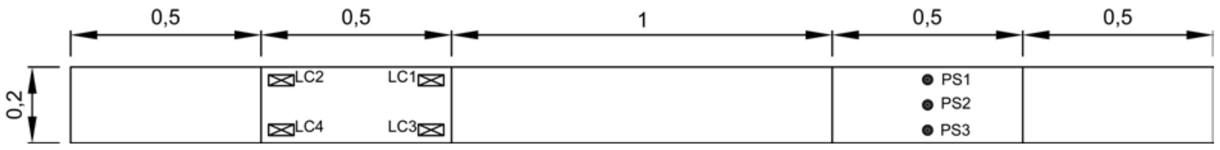

Figure 3-37. Front view of the storm wall in the 2.5m wide flume of Barcelona. The 2nd panel to the left is equipped with force sensors, the 2nd panel to the right is equipped with pressure sensors.

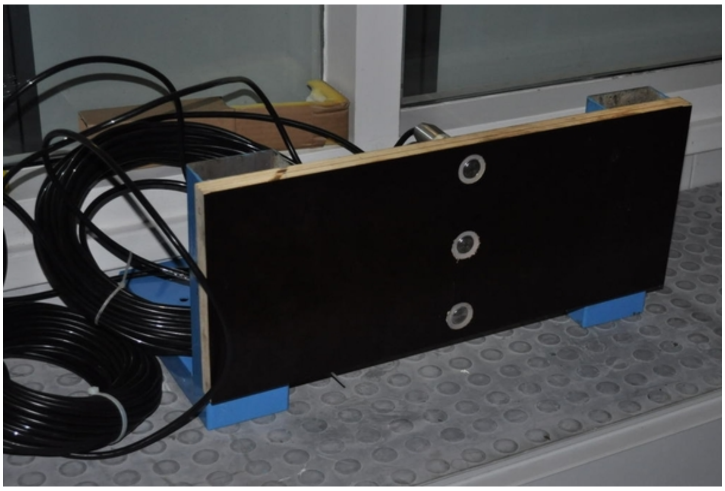

Figure 3-38. Detail of the storm wall in the CIEM wave flume of Barcelona with pressure transducers in one vertical line.

Pressures were recorded at 2400Hz, forces at 4800Hz. Analysis has shown that the structure had an eigenfrequency of 88Hz, but the impacts gave mainly values between 0 and 20Hz. No low pass filtering to filter out resonance was needed. See Section 6.2.1 for more information on resonance and filtering.

3.4 *UGent-2 dataset*

After a new procedure was developed for the reduction of wave overtopping by non-breaking waves on smooth dikes with measures at crest level (UGent-1), it was decided to run a few tests on breaking waves. In the small flume of Ghent University, the influence of a storm wall on the overtopping of breaking waves (slope 1:6) was studied by means of a small scale database.

3.4.1 *Test set-up*

A new dataset was collected in the small wave flume of Ghent University (Figure 3-39). This flume has a length of 15m, a width of 0.35m and a height of 0.60m, more or less half the size of UGent's primary wave flume used in Section 3.1.The small wave flume also has a piston type wave paddle and is equipped with active wave absorption.

Figure 3-39. Small wave flume at Ghent University: 15m x 0.35m x 0.60m.

Each tested time series contained approximately 1000 incoming waves, all with an irregular Jonswap (γ = 3.3) wave spectrum. Only perpendicular incoming waves (γ_β = 1) and smooth dike (γ_f = 1) were tested. In this test campaign, a smooth dike with slope cot(α) = 6 was used. Same as for section 3.1 also intermediate/deep water in front of the structure was tested. However, due to the mild sloping dike, the breaker parameter ξ_{m0} was much lower than 2 and the test results were always in the zone of breaking waves.

3.4.2 *Tested geometries and parameter range*

Tests in the small flume represent prototype situations at a very small scale; a Froude scale 1:50 related to a prototype situation. At such a small scale, viscous effects are not scaled down properly by using Froude scale laws. Thin overtopping layers might be affected by that and not give reliable results. Therefore, tests with a promenade at crest level were eliminated from the test program. Only tests with the reference situation (a smooth dike) and tests with a smooth dike with storm wall have been tested for overtopping measurements. Forces were not recorded in the UGent-2 tests.

Table 3-10. Parameter range for the UGent-2 tests in the small wave flume of Ghent University.

UGent-2		**Wave overtopping tests (breaking waves)**	
		Smooth dike (reference)	Smooth dike with storm wall
Slope angle of the smooth dike	cot(α)	6	6
Wave breaker parameter	$\xi_{m-1,0}$	0.80 – 1.01	0.77 – 0.96
Dimensionless freeboard	R_c/H_{m0}	0.56 – 1.50	0.46 – 1.61
Dimensionless wall height	h_{wall}/R_c	no wall	0.08 – 0.60
Number of tests	-	19	31

3.4.3 *Measurements and equipment*

a) *Waves*

The waves were recorded with the same wave gauges at a same sampling frequency as explained in Section 3.1.3a). Similar to Figure 3-2, three groups of wave gauges were installed along the flume. The last group closest to the structure was used to determine the incoming wave height H_{m0} at the toe of the structure.

b) *Overtopping*

Overtopping discharges were measured at the same way as for the UGent-1 tests in the large flume of Ghent University (Section 3.1.3b). The only difference is that a smaller tray (10cm instead of 30cm) was used to collect the overtopping since the flume is smaller.

No other parameters were measured in these experiments.

3.5 *Harlingen dataset*

Besides doing new overtopping tests (UGent-1 and UGent-2 datasets in Sections 3.1 and 0 respectively) to study the existing advice on storm walls, also the existing dataset that formed the base of EurOtop (2007)'s advice on overtopping reduction due to storm walls, was added to this PhD research to have a complete overview of reduction due to vertical walls on dikes. This dataset, the Harlingen dataset, is treated here.

3.5.1 *Test set-up*

The "Harlingen dataset", named after its location in the North of the Netherlands, was the result of a request by the Dutch government (Rijkswaterstaat) to study modifications to the coastal defense system in Harlingen but also to develop general design formulae for wave run-up and overtopping for wave walls on top of a structure. The Harlingen dataset is the dataset which has eventually led to Eq. [2-22] introducing a reduction factor for breaking waves only in the overtopping Equations [2-13] and [2-15]. A series of tests has been carried out in 1994 at Delft Hydraulics' (currently named Deltares) wave flume 'Scheldegoot', partly tests with a quay and partly tests with a dike. The background of these tests is given in report H2014 by Den Heijer (1998), the analysis of the tests with a dike is redone in report H2458 by van der Meer (1997). The Harlingen dataset was part of a wider test program on wave run-up and overtopping at dikes, which formed the basis of the TAW (2002) manual and later also included in EurOtop (2007).

The 'Scheldegoot' is a wave flume which is 55m long, 1m wide and 1.2m deep. Irregular waves with a JONSWAP spectrum were generated and the wave paddle was equipped with active wave absorption. Three sets of wave gauges were installed along the flume: one near the wave paddle for the active absorption, one set 5m in front of the dike and one close to the toe of the dike. The sampling frequency of the measuring instruments was 50Hz.

3.5.2 *Tested geometries and parameter range*

38 tests of the Harlingen dataset, the ones with a dike, are of interest for the present scope. They can be found in the CLASH database, series 223. Series 223 can be split up in 3 different geometries

- Smooth slope $\cot(\alpha) = 2.5$ with wave wall, see Figure 3-40 (4 tests)
- Smooth slope $\cot(\alpha) = 3.0$ with wave wall, see Figure 3-40 (16 tests)
- Smooth slope $\cot(\alpha) = 3.0$ with a small berm of 0.40m in front of a wave wall, see Figure 3-41 (18 tests)

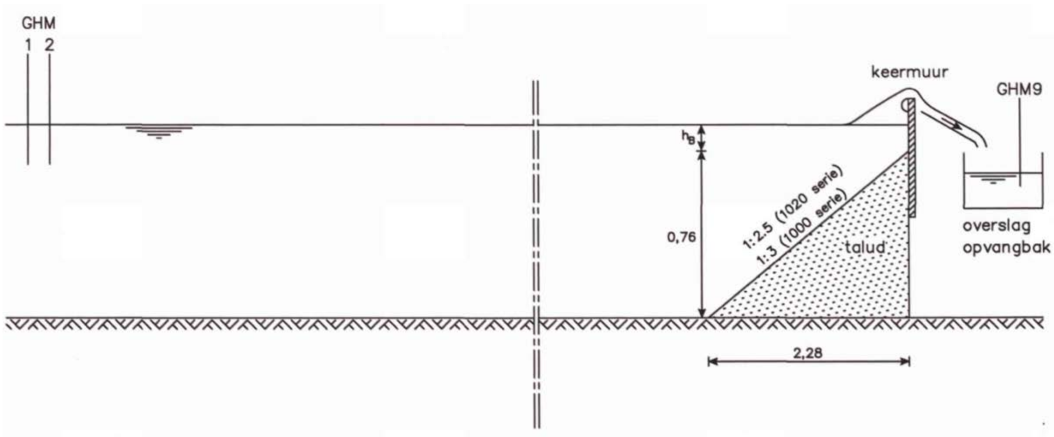

Figure 3-40. Smooth dike ($\cot(\alpha)$ = 2.5 or 3) with a vertical wall. Figure by Den Heijer (1998).

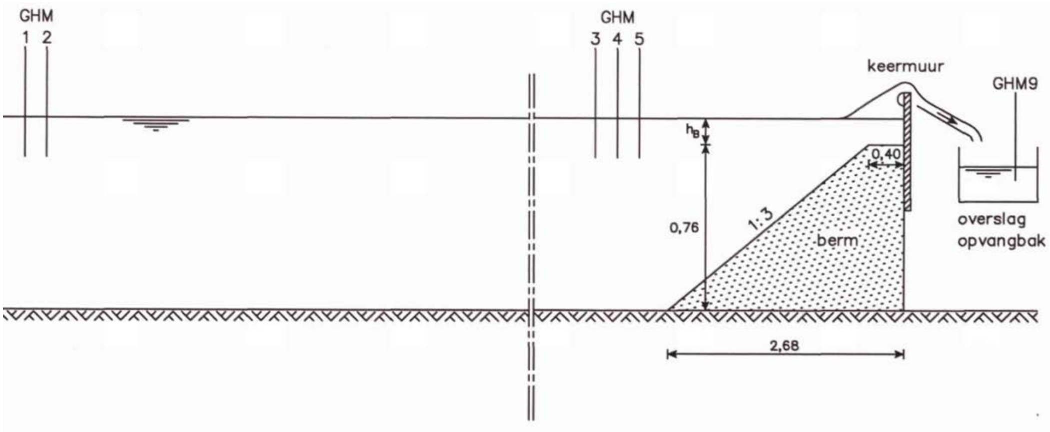

Figure 3-41. Smooth dike (cot(α) = 3) with a berm (0.4m wide) and a vertical wall. Figure by Den Heijer (1998).

The Harlingen dataset was carried out within the following range of parameters:

- Dimensionless freeboard $1.5 \leq R_c/H_{m0} \leq 3.0$
- The foot of the wall was between 1.2 times the wave height above the still water level SWL (dry berm) and 1.2 times the wave height below SWL (submerged berm, see Figure 3-42).
- The relative length of the berm, B/L_{0p}, was between 0.05 and 0.08. The ratio B/H_{m0} was between 2 - 3.
- The minimal height of the wall was about 0.5 times H_{m0}, the maximal height was about 3 times H_{m0}.
- The wave steepness with the peak period s_{op} was between 0.02 and 0.04.
- The height of the wall was between 10% and 40% of the structure's total height, and between 0.43 to 3.3 times the wave height, which is considerably larger than the storm walls in the UGent data.

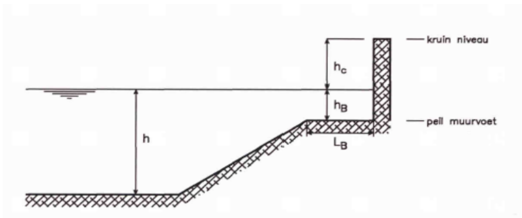

Figure 3-42. Example of the Harlingen dataset with a small berm in front of the wall, but more important a submerged berm (below the water level).

3.5.3 *Measurements and equipment*

a) *Waves*

9 resistive type wave gauges were installed in the Scheldegoot, of which 5 were active for recording water level elevations during the tests: 2 wave gauges near the wave paddle and 3 wave gauges near the toe of the structure. Water level elevations were recorded at a sample frequency of 50Hz.

b) *Wave overtopping*

The water overtopping the storm wall was captured and led by a tray into an overtopping tank. The tank had a surface of 0.354m^2 and contains 1 wave gauge to measure the increasing water level in the tank. This wave gauge also recorded at 50Hz.

No other parameters were measured in these experiments.

3.6 *Comparison of test set-ups*

The PhD manuscript is divided into 3 main topics (see Section 1.3): reduction of wave overtopping, overtopping flow parameters, and impact forces on storm walls. This means different test campaigns also had different goals and parameters to measure. Besides incoming wave parameters, the following things were measured in the different test campaigns:

- UGent-1: wave overtopping & wave impacts — treated in Chapters 4 & 6
- GWK: flow parameters & wave impacts — treated in Chapters 5 & 6
- Hydralab: wave impacts — treated in Chapter 6
- UGent-2: wave overtopping — treated in Chapter 4
- Harlingen: wave overtopping — treated in Chapter 4

All these datasets, except for the Harlingen dataset, are newly set up data sets for the present PhD research. Only the Harlingen dataset was set up by others (Den Heijer (1998) and van der Meer (1997)) but will be reanalyzed in Chapter 4.

The Excel databases of the 4 new test campaigns are made available for free download at www.koenvandoorslaer.com/phd.

This section 3.6 highlights some important differences between the different test campaigns.

The **wave overtopping** data from UGent-1, UGent-2 and Harlingen will be analyzed in Chapter 4. Table 3-11 gives a comparison of some important differences between these three different data sets. In Section 4.1 the reduction by a storm wall will be investigated for the three data sets for a range of both breaking and non-breaking waves. Section 4.2 treats the other reduction measures, and is only based on non-breaking waves from the UGent-1 database. The scale factors have not been mentioned in Table 3-11, since literature study (Section 2.7.1) has shown that no scale effects are to be expected for overtopping tests on smooth dikes.

Table 3-11. Comparison of the test campaigns on wave overtopping reduction.

Test campaign	Slope cot(α)	Number of tests	Wave regime	h_{wall}/R_c	Overtopping reducing measures
UGent-1	2 and 3	> 1000	Non-breaking (NB)	0.08 – 1.00*	Smooth dike, Storm wall, storm wall with bullnose, promenade, promenade with storm wall, promenade with storm wall and bullnose
UGent -2	6	50	Breaking (B)	0.08 – 0.60	Smooth dike, Storm wall
Harlingen	2.5 and 3	38	both	0.27 – 1.50	Storm wall, (small) promenade with storm wall

*2 exceptions with $h_{wall}/R_c > 1.00$: $h_{wall}/R_c = 1.60$, see Figure 4-20.

One of the main differences between UGent-1/-2 and the Harlingen data is that UGent experiments (nearly) only have data with $h_{wall}/R_c \leq 1$, where more than 60% of the Harlingen data have $h_{wall}/R_c > 1$. The SWL below the crest of the dike ($h_{wall}/R_c \leq 1$) gives an essential difference in overtopping behavior, which will be shown in Section 4.1.

Another difference is that UGent works with small walls (2 to 9% of the total structures height and 10 to 110% of the incoming wave height), where the Harlingen data works with considerably larger walls (10% to 40% of the total structures height and 43% to 330% of the wave height).

The GWK test campaign was the only one where **flow parameters** were recorded and provided reliable results. These flow parameters will be analyzed in Chapter 5.

The **wave induced impact** tests are carried out in three different test campaigns (UGent-1, GWK, Hydralab). The analysis is given in Chapter 6, an overview of the different parameters that were measured is given in Table 3-12. UGent-1 and Hydralab tests have good wave and force measurements, whereas the GWK tests provide good data with respect to flow characteristics and force measurements. Different approaches are given in Sections 0 and 6.4 for calculating the impacts on a smooth dike with promenade and storm wall. The other geometries from the UGent-1 database are dealt with in Section 6.5.

Table 3-12. Overview of the measured parameters in the different zones (Figure 1-9) and for different test campaigns. All tests used here are in the non-breaking regime.

Test campaign	Wave regime	Scale	Number of tests	Number of waves per test	d, H_{m0}, T_p (zone 2)	V, q (x_c = 0 in zone 3/4)	U, h (zone 4)	P or F (zone 5)
UGent-1	NB	10 to 15	203	ca. 1000	Yes	No	No	only F
Hydralab	NB	6	14	ca. 1000	Yes	No	Bad recordings	P and F
GWK	NB	1	21	37 to 204	Yes	No	Yes	P and F
UGent-1	Smooth dike, Storm wall, storm wall with bullnose, promenade with storm wall, promenade with storm wall and bullnose							
Hydralab	Promenade with storm wall							
GWK	Promenade with storm wall							

The comparison of some key dimensional and dimensionless parameters for the analysis of the impacts on a storm wall is given in Table 3-13. This gives the validity interval of the formulae in Chapter 6.

Table 3-13. Range of key test parameters and some dimensionless parameters for the different set-ups.

	UGent-1	Hydralab	GWK
Dike cot(α)	2 and 3	3	3
$G_c/L_{m-1,0}$	0.127 – 0.252	0.077 – 0.159	0.07 – 0.22
Promenade slope	1.0%	1.80%	0.0%
h_{wall}/R_c	0.364 – 0.667	0.357 – 0.87	0.43 – 0.50
h_{wall}/H_{m0}	0.50 – 1.02	0.55 – 0.75	1.02 – 2.21
A_c/H_{m0}	0.226 – 1.224	0 – 1.235	1.11 – 2.35
R_c/H_{m0}	0.906 – 2.072	0.644 – 2.097	2.22 – 4.42
$\xi_{m-1,0}$	2.235 – 4.793	1.83 – 2.84	1.89 – 4.38
$s_{0,\ m-1,0}$	0.010 – 0.036	0.013 – 0.033	0.006 – 0.031
N_w (number of waves)	1080 - 1415	920 - 1029	37 – 204
N_{ow} (number of overtopping waves)	730 – 1278	555 – 965	27 - 130
N_i (number of impacts)	253 - 864	118 - 760	9 - 75
Type of storm wall	Closed	Closed	Open

UGent-1 and Hydralab datasets show a wide range of overlapping parameters. The main differences in the range of the parameters can be observed from the GWK set-up and are highlighted in grey in Table 3-13. The difference mainly comes from using an existing structure in the flume (higher freeboard, no promenade slope). As explained in section 3.2.3d), a remaining water layer on the promenade was observed during the first tests, after which openings in the storm wall were created, otherwise the residual water layer was obstructing the impact tests too much. This was not the case for the UGent-1 and Hydralab set-up, where a closed wall could be used for all tests. There were different reasons for this:

- Hydralab (1.8%) and UGent-1 (1.0%) had a mild slope on the promenade stimulating the drainage of the water back to the flume, where the promenade in the GWK tests had no slope (0.0%);
- The test program of Hydralab and UGent-1 showed smaller dimensionless landward freeboards (A_c/H_{m0}) with larger waves and smaller freeboards, which also led to overtopping over the storm wall (small h_{wall}/H_{m0}). In GWK this was not the case (large A_c/H_{m0}), thereby keeping most of the water in front of the storm wall leading to an unrealistic high residual water layer obstructing the incoming bore. In a 3D situation in reality, also this water would have ran off.

As mentioned earlier, making openings in the storm walls in the GWK solved the problem of the residual water layer, but filled up the overtopping basin at the back of the flume too fast so that tests had to be aborted after a short number of waves. This caused the number of overtopping waves and impacts also to be highly different in the GWK dataset compared to the other two datasets.

Due to the mentioned differences, datasets in Table 3-13 will be treated separately depending on the approach. UGent-1 and Hydralab data are used to link impact forces to hydraulic parameters (Section 6.4.1 and 6.4.2). The GWK dataset mainly serves for an indirect approach where overtopping flow parameters are linked to the impact forces (see Section 6.4.3).

Despite having (too) short time series and slightly different hydraulic conditions, the GWK data will also be compared with the other two datasets to discuss potential scale and model effects as introduced in Section 2.7.2. In Section 6.4.4, force estimations by the three different approaches are compared.

4 Reduction of wave overtopping

In this chapter, the analysis of overtopping discharges is discussed, focusing on reduction of wave overtopping over smooth dikes. The advice on the influence of wave walls has been updated between EurOtop (2007) and EurOtop (2016). This update results from the research presented here, and was published in Van Doorslaer et al. (2015a) and Van Doorslaer et al. (2016b). First, the reduction by means of a storm wall is discussed (Section 4.1). Other overtopping reducing measures are discussed in Section 4.2.

4.1 *Reduction by means of a storm wall*

As mentioned in the literature study, EurOtop (2007) briefly discusses the 'effect of wave walls' on wave overtopping over coastal dikes in its section 5.3.5. EurOtop (2007) provides a procedure which was based on the analysis of the Harlingen dataset. This will be explained in the next Section 4.1.1. The new data from the current research will be plotted according to this EurOtop (2007) methodology, as well as with other prediction formulae from literature. Where improvements can be made, a new methodology for the specific geometries in this research will be developed. This will be done in Section 4.1.2 for the new UGent-1 data (non-breaking waves) and in Section 4.1.3 for the new UGent-2 data (breaking waves). In Section 4.1.4 the new procedure for the geometries in this work will be used for the Harlingen data, to see if it is also applicable outside the parameter ranges for which it has been developed. A summary and conclusion is given in Section 4.1.5

4.1.1 *The Harlingen dataset*

The Harlingen test set-up and different geometries are explained in Section 3.5. It is the dataset on which EurOtop (2007) based its advice on the reducing effect of wave walls.

Van der Meer & Janssen (1994), TAW (2002) and EurOtop (2007), all based on this dataset (extended with other data), work with the average slope to calculate the wave breaker parameter which defines whether to use the formula for breaking or non-breaking waves. The average slope is calculated between 1.5 times the wave height below the still water level and the run-up height above the still water level or the top of the structure, as shown in Figure 4-1. If a wall is present, the average slope is calculated between $1.5H_{m0}$ below the SWL and the top of the wall.

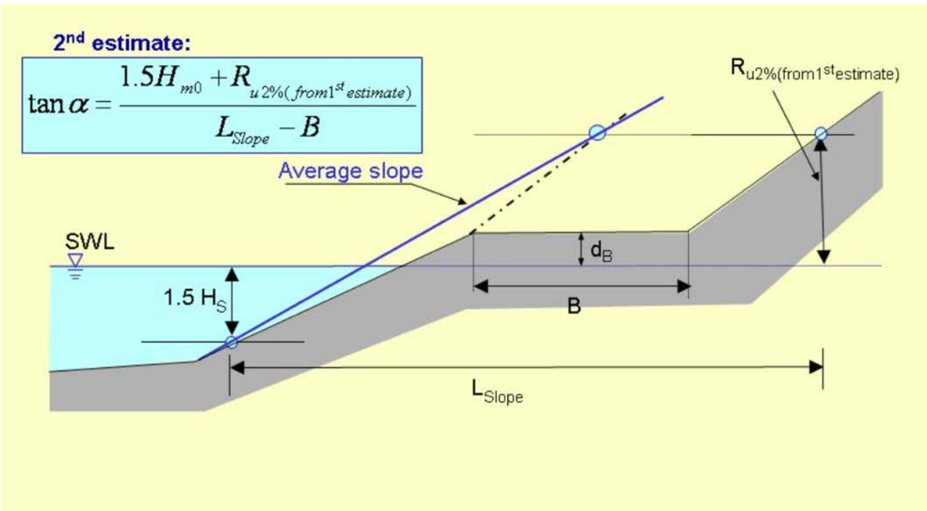

Figure 4-1. Definition of average slope. Figure by EurOtop (2007).

In the Harlingen dataset, the (sometimes large) wall on top lead to steep average slopes and breaker parameters larger than two by the above procedure in Figure 4-1. As a consequence, the waves were classified as non-breaking, regardless of the actual slope angle and the fact that the wall sometimes was high above the still water line and did not influence the breaking of the waves on the dike.

When the data on the three different geometries with wave wall (Figure 3-40 and Figure 3-41) were plotted in a log-linear diagram they showed to be mainly below EurOtop (2007)'s reference line for non-breaking waves Eq. [2-14], see Figure 4-2.

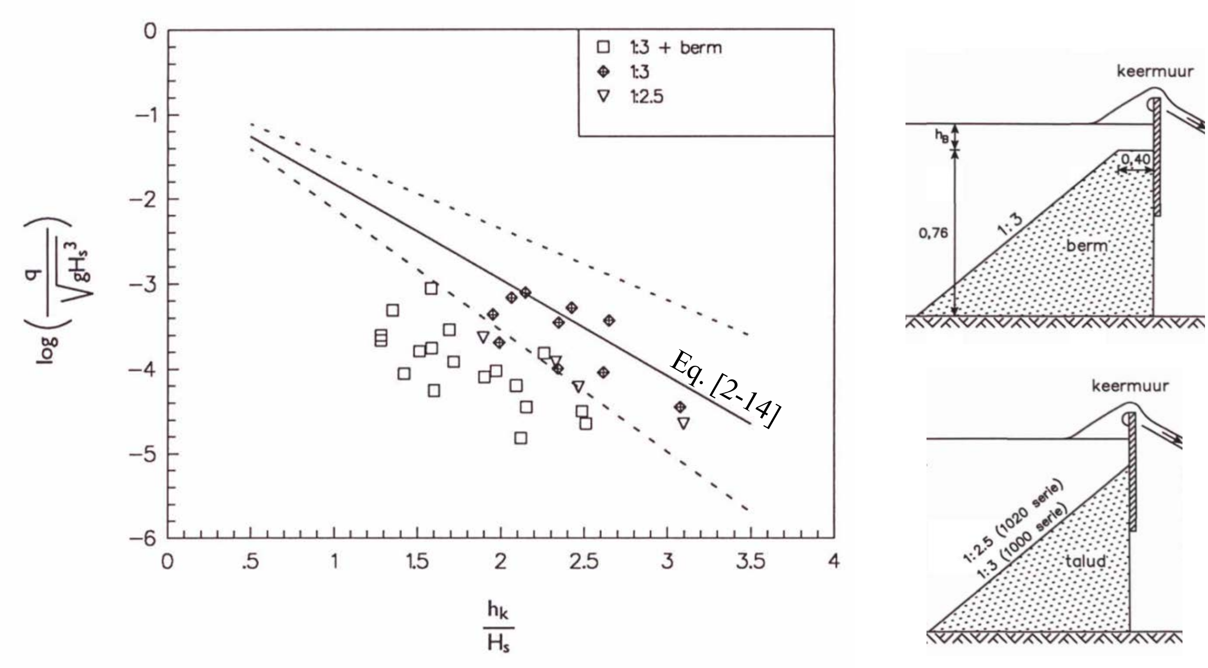

Figure 4-2. All tests in the Harlingen dataset (slope 1:2.5 with wave wall, lower right, slope 1:3 with wave wall, lower right, and slope 1:3 with berm and wave wall, upper right) plotted in the non-breaking overtopping graph are mostly below EurOtop (2007) line Eq. [2-14]. Figure by van der Meer (1997).

It was investigated in report H2458 by van der Meer (1997) if, by introduction of a reduction factor for the wave wall, the existing prediction formulae [2-13] and [2-14] could better predict the data.

Therefore, the report H2458 investigated the replacement of the vertical wall by a certain slope to calculate the average slope and consequently the wave breaker parameter for a better representation of the data. Best results showed by replacing the vertical wall by a 1:1 slope to calculate the (milder) average slope, see Figure 4-3 and Figure 4-4.

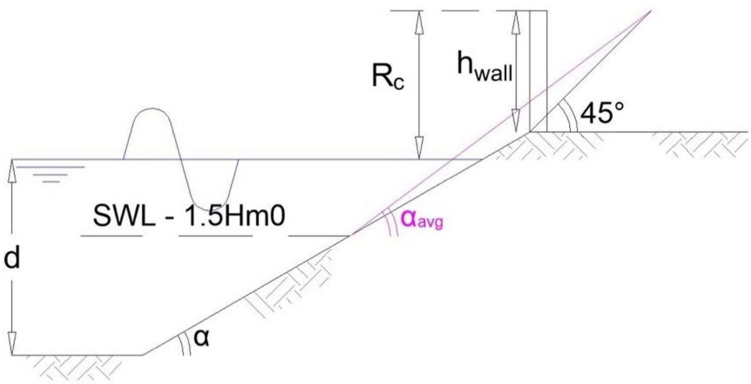

Figure 4-3. Average slope calculation when only a wall, no berm is present (Repetition of Figure 2-4).

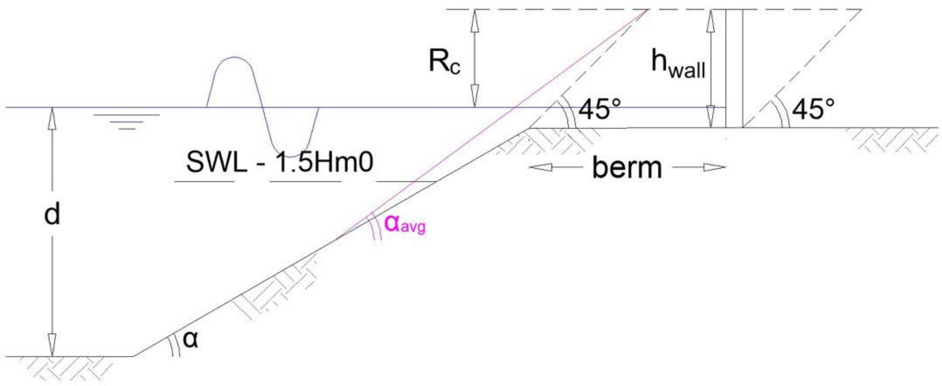

Figure 4-4. Average slope calculation when a wall and a berm are present.

A second step in the procedure was to change the transition between breaking and non-breaking from $\gamma_b\xi_{0p} = 2$ to $\gamma_b\xi_{0p} = 3$. By doing so, quite some data points moved from the non-breaking regime to the breaking regime, see Figure 4-5. The ones in the non-breaking graph (Figure 4-5, left) were presented well – within the confidence band – and did not need any further improvement according to the authors. The ones in the breaking graph (Figure 4-5, right) were below the confidence interval but were well grouped so that a trendline could be fitted through the data and a reduction factor could be extracted so that the data points move closer to the prediction line.

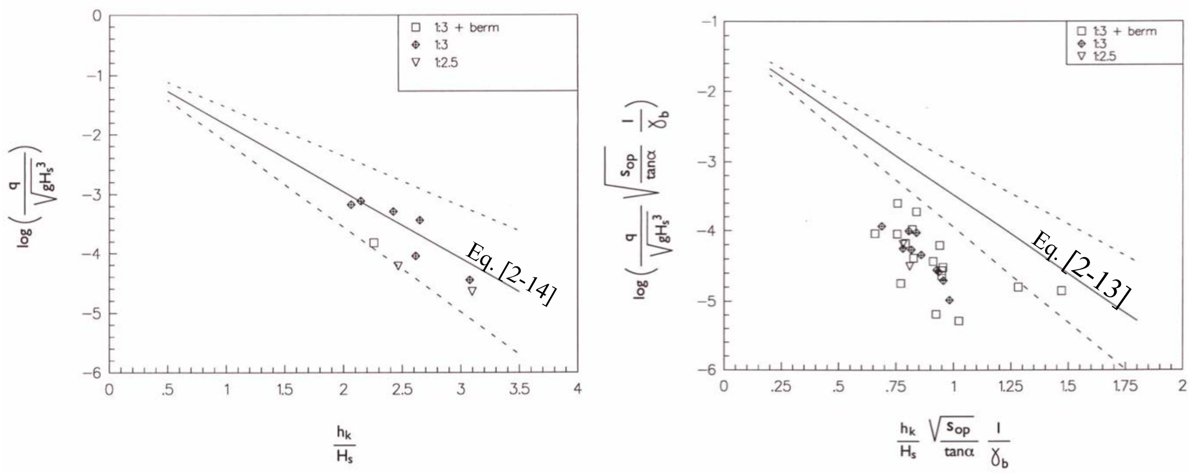

Figure 4-5. Harlingen dataset with equivalent slope calculation by changing the vertical wall into a 1:1 slope. The boundary between the non-breaking waves (left) and breaking waves (right) is at $\gamma_b\xi_{0p} = 3$. Figures by van der Meer (1997).

The trendline fitted through the data in Figure 4-5 (right side) led to a reduction factor $\gamma_v = 0.65$. When including this in the denominator of the horizontal axis (increasing the virtual freeboard), the data points were presented better by the formula for breaking waves, see Figure 4-6. They are now mostly within the confidence band.

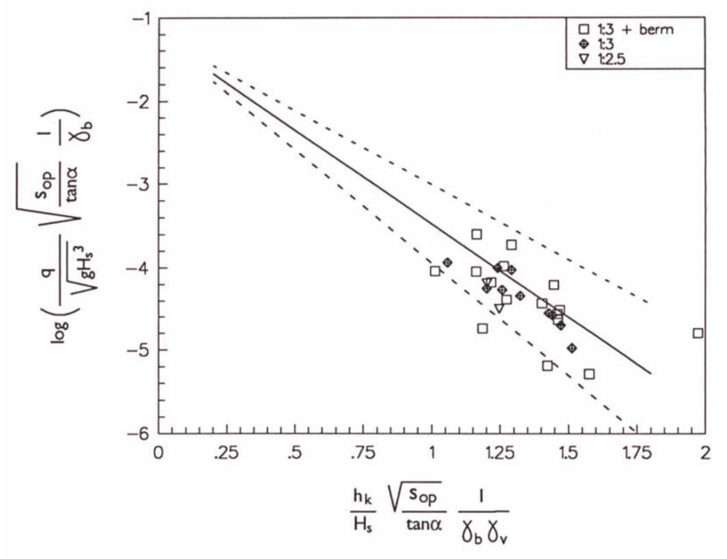

Figure 4-6. Breaking waves of the Harlingen dataset by replacing the vertical wall into a 1:1 slope, by setting the boundary of breaking waves at $\gamma_b\xi_{0p} \leq 3$ instead of 2, and by introducing a reduction factor $\gamma_v = 0.65$ on the horizontal axis. Figure by van der Meer (1997).

The Harlingen data are now represented well in Figure 4-5 (left side, non-breaking waves, $\gamma_b\xi_{0p} \geq 3$) and in Figure 4-6 (breaking waves, $\gamma_b\xi_{0p} \leq 3$). Just like γ_b also γ_v is only included in the breaking formula since a geometrical variation in a dike is felt more by breaking waves than by non-breaking waves.

4.1.2 *UGent-1 dataset for non-breaking waves*

The analysis of the UGent-1 dataset is based on the shape of Eq. [2-18] but as explained in Section 2.2 the obtained reduction factors γ can also be used in Eq. [2-19] without losing relevant accuracy.

$$\frac{q}{\sqrt{g \cdot H_{m0}^3}} = A_1 \cdot exp\left(-B_1 \cdot \frac{R_c}{H_{m0}} \cdot \frac{1}{\gamma}\right) \qquad [2\text{-}18]$$

$$\frac{q}{\sqrt{g \cdot H_{m0}^3}} = a \cdot exp\left[-\left(b \cdot \frac{R_C}{H_{m0} \cdot \gamma}\right)^c\right] \qquad [2\text{-}19]$$

a) *Reference situation*

A smooth dike without storm walls was first tested in the wave flume of UGent acting as a reference situation before a smooth dike with storm wall was tested. 80 new tests with non-breaking waves were performed for the reference situation. A sketch of this reference geometry is given in Section 3.1.2a) Figure 3-3 and repeated below in Figure 4-7. The arrow with indication ‘q’ shows where the overtopping was measured.

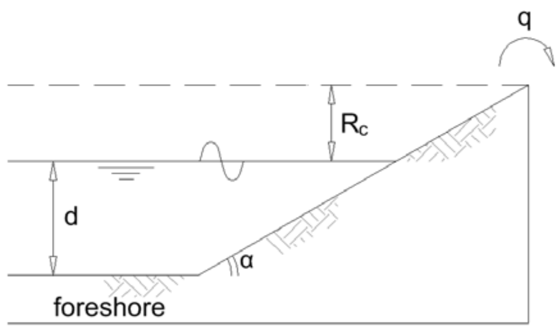

Figure 4-7. Reference situation for UGent-1 model tests, smooth dike.

In the analysis, the measured data of the dike with storm wall are not compared to literature for non-breaking waves on smooth dikes (Eq. [2-14]), but to the trendline which is determined from these 80 reference tests on the smooth dike as shown in Figure 4-7. In this way, the test set-up, measuring devices and -techniques are the same for the reference case as for cases with overtopping reducing measures, which guarantees a good comparison and avoids difficulties in comparing data from different hydraulic models. The test program on the reference dike was given in Table 3-1 in Section 3.1.2a).

The results from the 80 reference tests (non-breaking waves) are plotted in a semi-logarithmic diagram with the dimensionless freeboard (R_c/H_{m0}) on the horizontal axis and the dimensionless overtopping discharge ($q/\sqrt{gH_{m0}^3}$) on the vertical axis. An exponential trend line is fitted through the data and gives the reference formula to calculate the average overtopping discharge on a smooth dike under non-breaking wave conditions, Eq. [4-1].

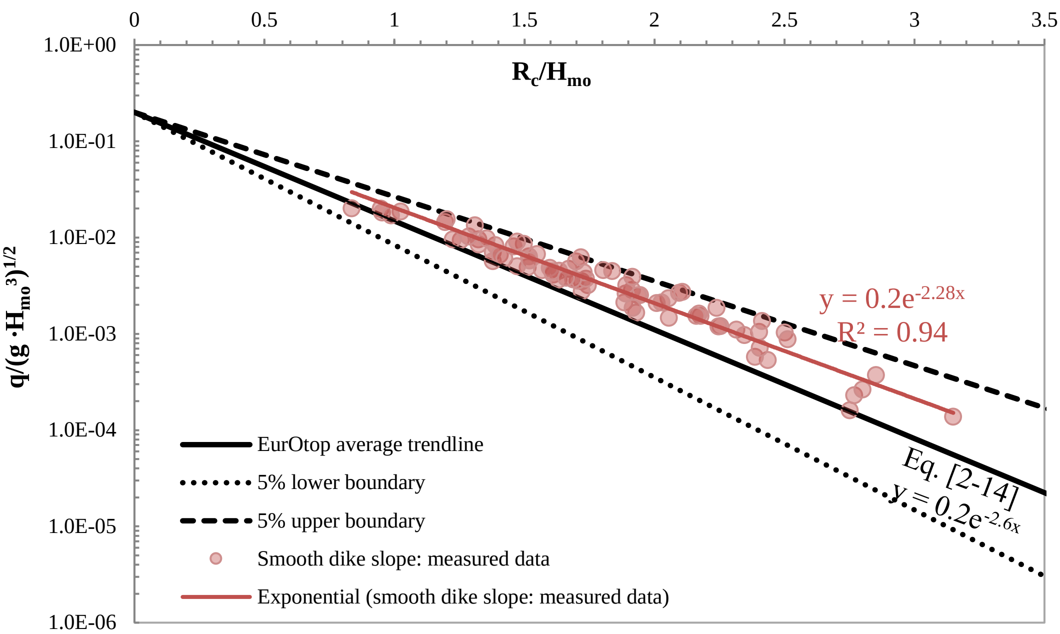

Figure 4-8. Reference data set of non-breaking waves on a smooth dike for the UGent-1 data set.

$$\frac{q}{\sqrt{g \cdot H_{m0}^3}} = 0.2 \cdot \exp\left(-2.28 \cdot \frac{R_c}{H_{m0}}\right) \qquad [4\text{-}1]$$

It can be noticed that the scatter around this trend line is small. When taking the exponential coefficient as normally distributed stochastic variable, the mean value is 2.28 with a standard deviation $\sigma = 0.15$ (relative standard deviation $\sigma' = 0.07$). Almost all results are located above the EurOtop (2007) average trend line Eq. [2-14], resulting in a higher trend line and thus a smaller coefficient in the exponent: 2.28 instead of 2.6.

If the CLASH dataset is used, but limited to the data with similar geometry

- $\beta = 0°$ for perpendicular wave attack,
- $\gamma_f = 1$ for smooth slopes,
- $1.5 \leq \cot(\alpha) \leq 3.0$ for the dike slope,
- $R_c > 0$ for positive crest freeboards,
- $B = 0$ for the absence of berms,
- and $G_c = 0$ for the absence of promenades at crest level; overtopping is measured direct at the crest of the dike)
- $\xi_{m-1,0} \geq 2.1$ like in the present database, in order to only work with non-breaking waves,

only 472 of the 10532 tests remain. When in addition the reliability factor is set to RF = 1, 255 data points remain, which are shown in Figure 4-9. The average trend line through these 255 tests has a coefficient of 2.29, very close to the reference line of the data shown in Figure 4-8. The data from Figure 4-8 are plotted together with the considered CLASH data in Figure 4-9, and they are in line with each other, meaning that the UGent-1 data are in line with results from other laboratories with similar boundary conditions. The CLASH data show larger scatter, probably due to the fact that they are found in different laboratories all over the world.

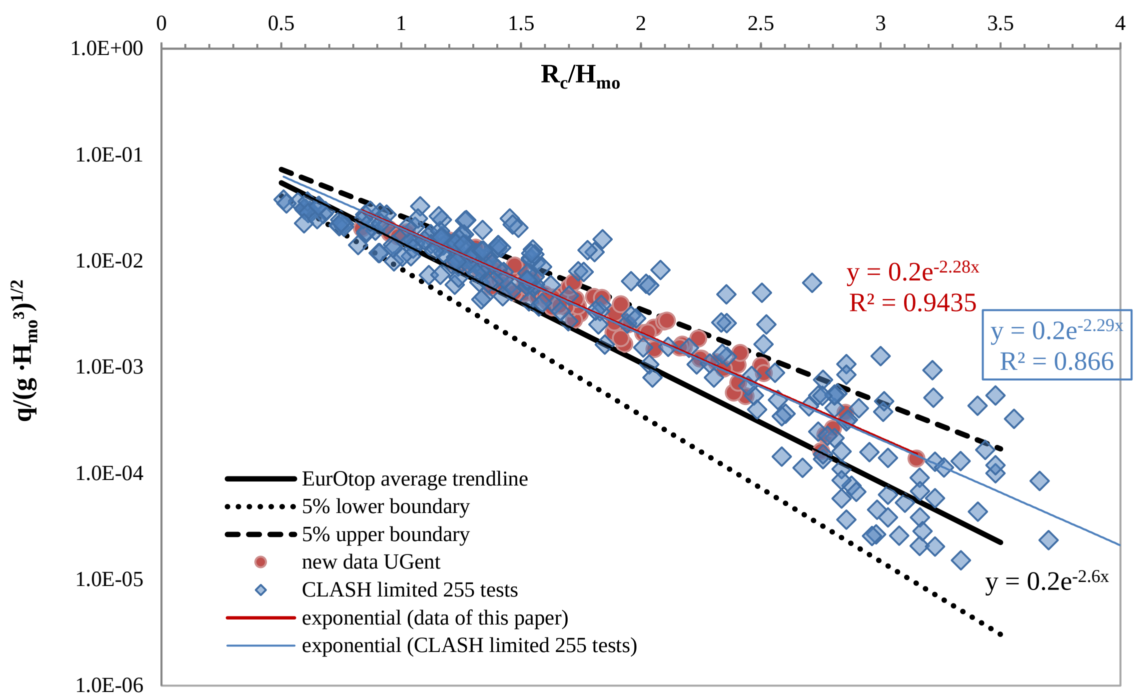

Figure 4-9. Comparison between UGent-1 data set and CLASH database on a smooth dike.

The coefficient 2.6 in equation [2-14] is the average coefficient (normally distributed with a standard deviation $\sigma = 0.35$ and relative standard deviation $\sigma' = 0.13$) of all different geometries and hydraulic conditions for non-breaking waves over sloping structures. For reasons of comparison, the storm wall and all other overtopping reducing measures further in this work will be referred to Eq. [4-1]

with coefficient 2.28. The 90% confidence bounds around this reference line however will be plotted using the standard deviation $\sigma = 0.35$.

The distinction between breaking and non-breaking waves is based on the wave breaker parameter ξ_{0p} who contains both the wave period and the slope angle. However, as mentioned in the literature review some authors (Owen (1980), Kortenhaus et al. (2006)) introduce extra influence factors for the wave period or slope angle in the range of non-breaking waves. Other authors such as Victor (2012) show that these influences are negligible for the range of parameters used in the present work. Nevertheless, the 80 new data points are subjected to a detailed analysis on the influences of slope angle and wave period on the mean overtopping discharge. Figure 4-10 shows data on the smooth dike focusing on the slope angle and wave period. The red trend line is the same as in Figure 4-8 based on all 80 data points. Note that this plot contains dimensions for the wave period, which is only for visualization purposes. If a (dimensional) influence is seen in the graph, a detailed dimensionless analysis will be carried out.

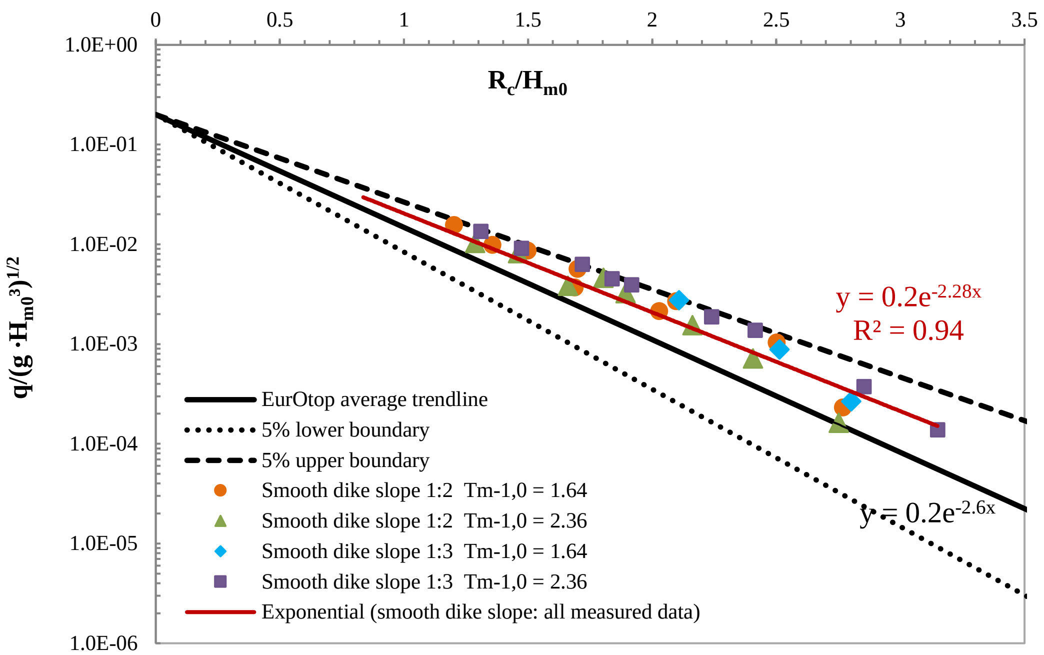

Figure 4-10. 29 data points on a smooth dike split up by wave period and slope angle α.

The following observations can be made:

- Slope angle: only slopes 1V:2H and 1V:3H were tested. When comparing the slope angles $\cot(\alpha) = 2$ versus $\cot(\alpha) = 3$ the mildest slope is slightly more overtopped (purple squares higher than green triangles, blue diamonds slightly higher than orange circles) since this slope reflects less energy and allows more overtopping. Another explanation is that the layer thickness of the “tongue” of the overtopping wave which is somewhat larger for milder slopes, giving a larger overtopping discharge (Bosman et al., 2008). The difference between both slopes is however almost negligible in the obtained data, from which it can be concluded that the slope angle only has very limited influence within the used range of tested parameters. This finding is similar to what was found by Victor (2012); wave overtopping has a weak dependency on the slope angle for mild dike slopes ($1.5 \leq \cot \alpha \leq 3$).
- Wave period: on a slope of 1:2 there is no influence of the wave period on the average overtopping discharge, while on a slope of 1:3 a minor difference exists: an increase of wave

overtopping occurs for increasing wave period. This is in line with the findings by Victor (2012); a (minor) influence of the wave period on wave overtopping exists, but its influence is limited compared to the effect of the relative crest freeboard.

Due to the minor differences in overtopping discharge for tests in the current data set with different wave periods or different slope angles, similar to what was found by Victor (2012) in the same parameter range, it can be concluded that parameters $T_{m-1,0}$ (or $s_{m-1,0}$) and α do not need to be additionally included in the non-breaking overtopping formula for smooth mild dike slopes with $1.5 \leq \cot(\alpha) \leq 3$. Eq. [4-1] is an accurate description of the data found in Figure 4-8.

b) *Reduction factor γ_v*

Wave overtopping can be reduced by placing a vertical storm wall (with height h_{wall}) on the dike. In this way, incoming waves are projected upwards. The geometry as tested is given in Figure 3-4 and repeated below in Figure 4-13. The test program of 117 new tests was given in Table 3-2 in section 3.1.2b).

In Figure 4-11, the overtopping results are grouped by the height of the wall and plotted in different symbols and colors. The different wall heights (2cm to 8cm model dimensions) are shown in the legend. This dimensional plot is only for visualization purposes, if a trend can be concluded from the plot, it will be further analyzed to achieve dimensionless presentation. The reference formula Eq. [4-1] is plotted as a solid red line, the 90% confidence band using the standard deviations by EurOtop (2007) is plotted as black dashed line, the 90% confidence band using the standard deviations found in the UGent-1 data on the reference situation is plotted as a dotted line.

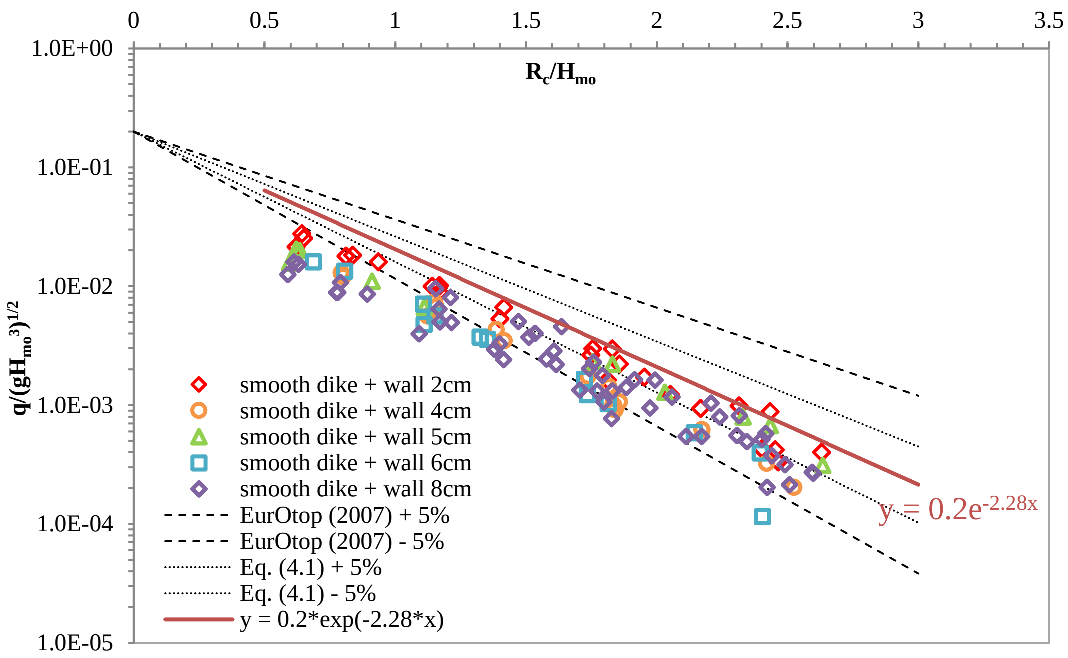

Figure 4-11. Data plot of the 117 tests of the UGent-1 dataset on smooth dikes with storm walls.

All data are located below the red reference line and most data is located outside the 90% confidence band from the UGent-1 dataset. Comparison to the 90% confidence band from EurOtop (2007) shows that about 2/3rd of the data are within the confidence band and thus predicted fairly well, with about 1/3rd of the data still outside the confidence band. More detailed analysis shows that mainly the data with low freeboards and/or highest storm walls are outside the 90% confidence band. Overal, it can be said that a reduction in overtopping volume due to the storm walls can be noticed since all data are below the reference line. When comparing data for an equal dimensionless freeboard R_c/H_{m0}, it can be seen that the higher the storm wall the more the overtopping discharge is reduced despite the same absolute value of R_c. Hence, the height of the storm wall has an influence on the reduction.

As mentioned in the literature review, the data will be compared to prediction formulae for smooth steep dike slopes cot(α) = 1 by Victor (2012) and for overtopping over a vertical wall (Eq. [2-20] and [2-21]), see Figure 4-12 (dashed-dotted and dashed line, respectively). The data show that the storm wall on top of a sloping dike does not increase the virtual slope that much that it can be considered as a vertical structure (dashed black line). The purple data points in Figure 4-12 (overtopping over a smooth dike with storm walls of 8cm) comes close to the steep dike slope cot(α) = 1 (dash-dotted line). However, the dash-dotted line of the steep dike 1V:1H is overpredicting the discharge for some tests with R_c/H_{m0} < 1, and under predicting for all tests with higher freeboards. Calculating the overtopping over a smooth dike with a storm wall as if it was overtopping over an increased virtual steeper slope seems not to describe the measured data properly.

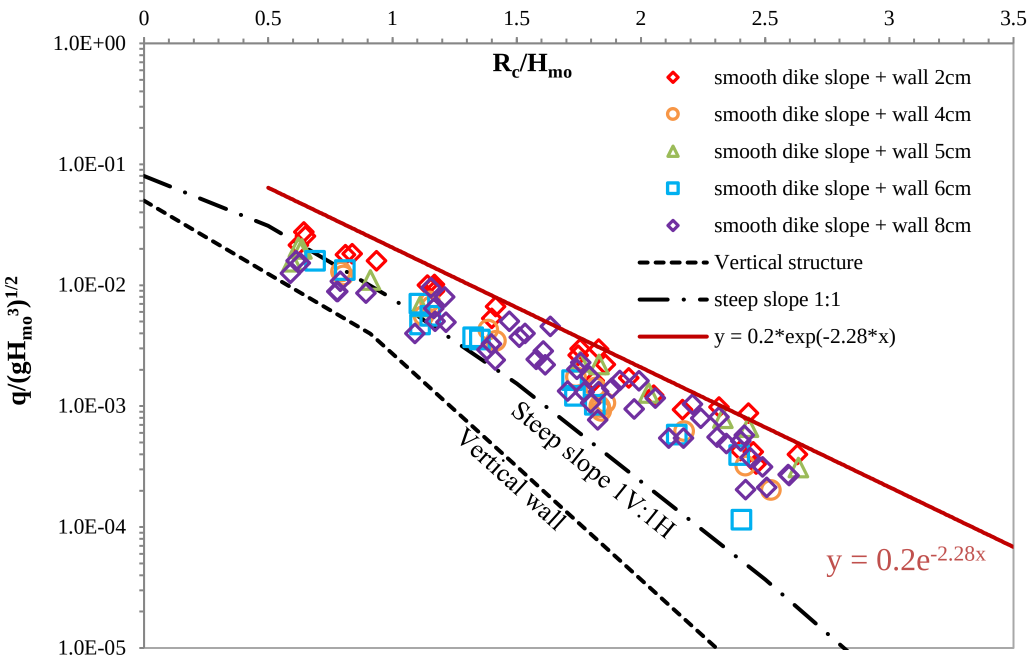

Figure 4-12. Data from UGent-1 data set on a smooth dike with storm wall - measured values. Wall heights given in model dimensions. Comparison with reference situation (red line), vertical wall (dashed line), steep dike slope cot(α)=1 (dash-dotted line).

In the following, it is investigated if the approach as explained in Section 4.1.1 and included in EurOtop (2007) gives better results for the data on smooth dikes with a storm wall in the UGent-1 dataset. In summary, this approach is as follows:

- Calculate the average slope where the wall is replaced by a 1:1 slope (Figure 4-13)
- Calculate the wave breaker parameter based on this average slope
- If $(\gamma_b)\xi_{0p} > 3$ the data remains non-breaking and have to be plotted in the non-breaking graph. No reduction factor is required. Note that $\gamma_b = 1$ in the current dataset.
- If $(\gamma_b)\xi_{0p} < 3$ the data become breaking, and a constant reduction factor $\gamma_v = 0.65$ must be applied to the data. Note that $\gamma_b = 1$ in the current dataset.

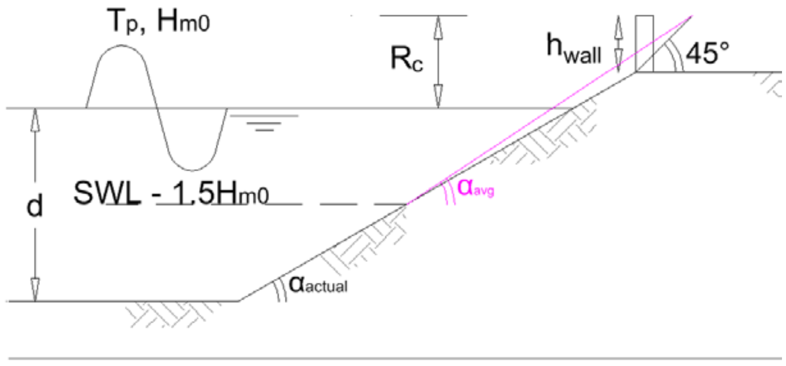

Figure 4-13. Cross section of a smooth slope with a crown wall in the UGent data set. The storm wall has to be replaced by a 1:1 slope to calculate the average slope.

The UGent-1 dataset contains 117 data points on smooth dikes with storm wall, which all have a breaker parameter $\xi_{m-1,0}$ (calculated with the actual slope) larger than 2.1 and were thereby originally classified as all non-breaking. Due to the average slope approach and the shifted transition, 80/117 data points have $\xi_{0p} > 3$ and thus remain non-breaking. Those are shown in Figure 4-14, together with the reference line for the smooth dike.

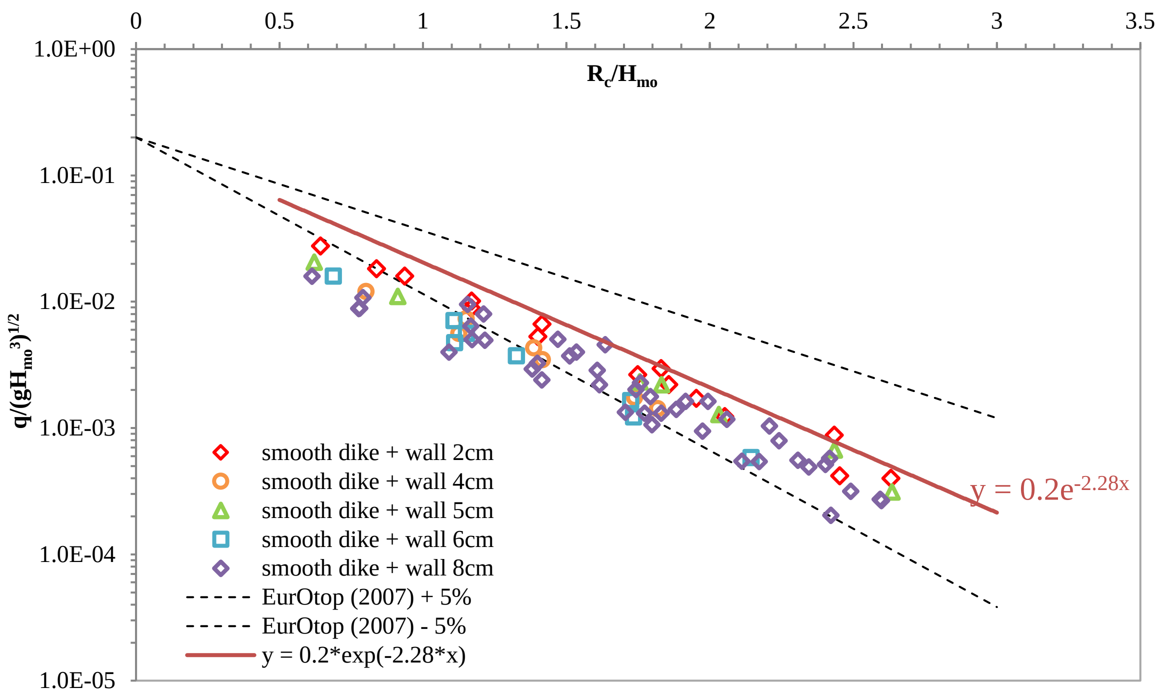

Figure 4-14. 80/117 data points on smooth dikes with storm wall from the UGent-1 dataset that remain non-breaking with ξ_{0p} > 3.

Figure 4-14 shows that all data points with storm wall are located below the trendline of the reference case Eq. [4-1] that was deducted in Section 4.1.2.a), and that about 1/3rd of the data (26 out of 80 points) are outside the 90% confidence bound calculated with the standard deviation from EurOtop (2007). The EurOtop (2007) approach has no further option to correct these data and bring these data closer to the trendline of the reference case. The dependency on the wall height that was already seen in Figure 4-11 is still visible, since this graph is just another representation of the majority of the same data (80/117).

Next to the 80 data points that remain non-breaking, also 37/117 data points shift to the breaking graph since $\xi_{0p} < 3$. These 37 points are shown in Figure 4-15 together with the reference line for a smooth dike slope 1:6 that will be explained further in Section 4.1.3.

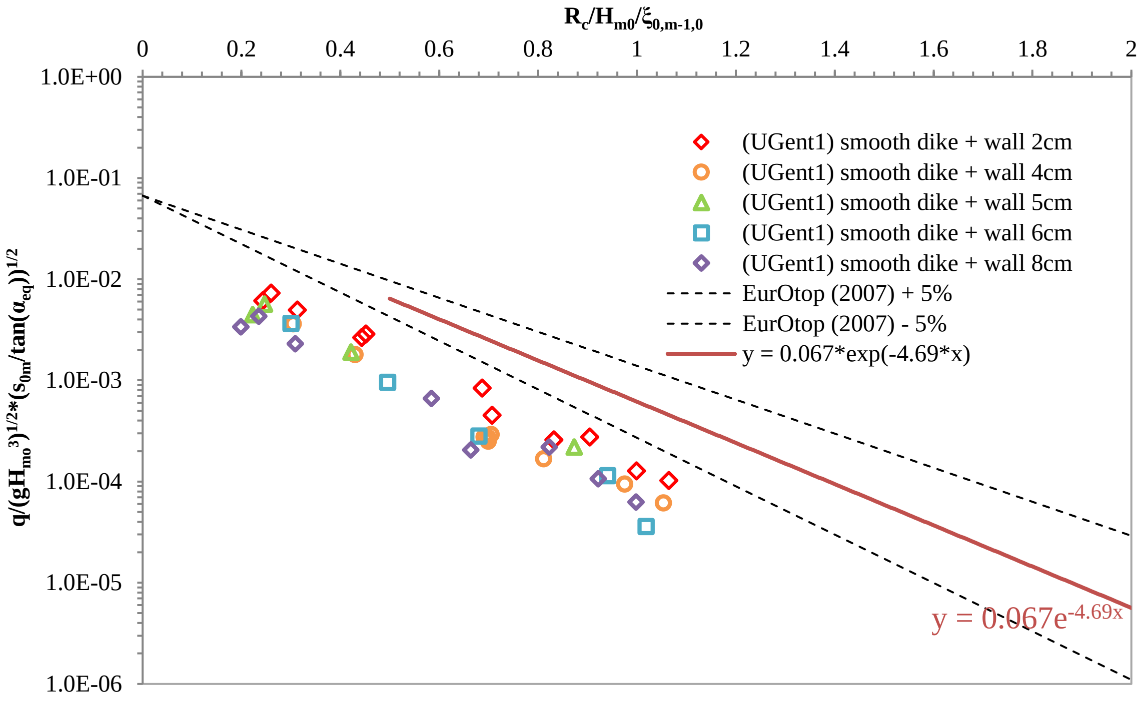

Figure 4-15. 37/117 data points from the UGent-1 dataset on smooth dike with storm wall have shifted to the breaking graph since $\xi_{0p} < 3$.

These 37 data points with storm walls are located under the non-breaking reference trendline. For breaking waves EurOtop (2007) provides a correction factor $\gamma_v = 0.65$ to implement on the horizontal axis. This leads to Figure 4-16.

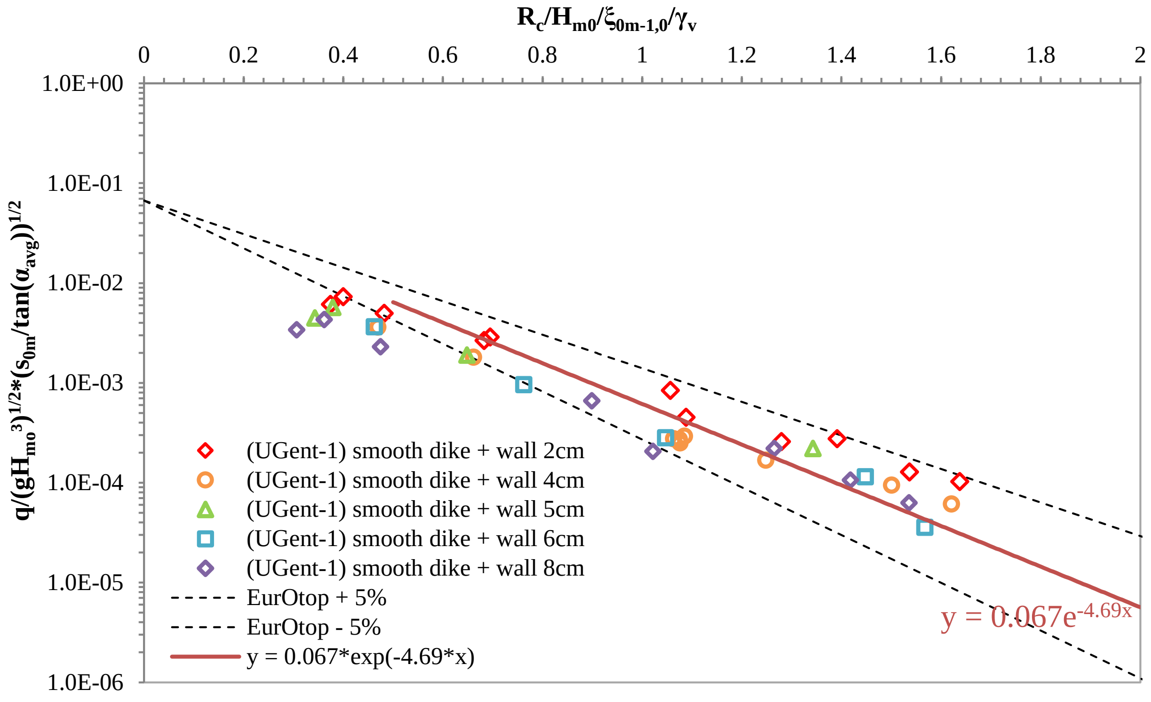

Figure 4-16. Data from Figure 4-15 corrected by $\gamma_v = 0.65$.

Most of the data (25 out of 37 ≈ 2/3rd) are within the 90% confidence band, but for small freeboards the correction was not enough and the data are under the 90% confidence band. Also for larger freeboards, despite being inside the 90% confidence band, the correction by γ_v = 0.65 is not optimal since the data are (slightly but consistent) above the red reference line.

The above Figure 4-14 and Figure 4-16 show that the original procedure from EurOtop (2007) used to predict the 117 data points of the UGent-1 dataset (ξ_{0p} > 2.1) provides results, 2/3rd of which are within the 90% confidence band, and about 1/3rd – mainly data with small freeboard – are below the 90% confidence band. Non-breaking waves (with ξ_{0p} > 3 according to EurOtop (2007)) are consistently below the reference line. For breaking waves data with small freeboards are below the reference line, data with large freeboards are aboven the reference line. Also the influence of the wall height is not included in the existing procedure.

In the following figures, two more approaches from the Literature study in Chapter 2 are tried:

- Tuan (2013) in Figure 4-17.
- Coeveld et al. (2006) in Figure 4-18 and Figure 4-19.

Tuan's approach (using Eq. [2-23] in Eq. [2-24]) works with the freeboard A_c and is indicated by the blue markers in Figure 4-17. Compared to the data plotted in Figure 4-11, the data have shifted to the left away from the trendline and are now significantly below the red reference line. This is probably due to the fact that Tuan has used A_c instead of R_c to calculate the overtopping discharge and this creates a stronger overtopping increasing prediction than the introduction of γ_w can counter with a reducing effect. If γ_w is calculated by Eq. [2-23], then introduced into Eq. [2-14] which uses R_c instead of A_c, the green markers in Figure 4-17 result and are a better prediction than the blue markers. Related to the EurOtop 90% confidence band most of the green data fall within the interval. However, there still is some of data outside of the confidence interval set-up with standard deviations around Eq. [4-1]. Detailed analysis has shown that these are the data with the largest wall heights, which are most far outside Tuan's range of application.

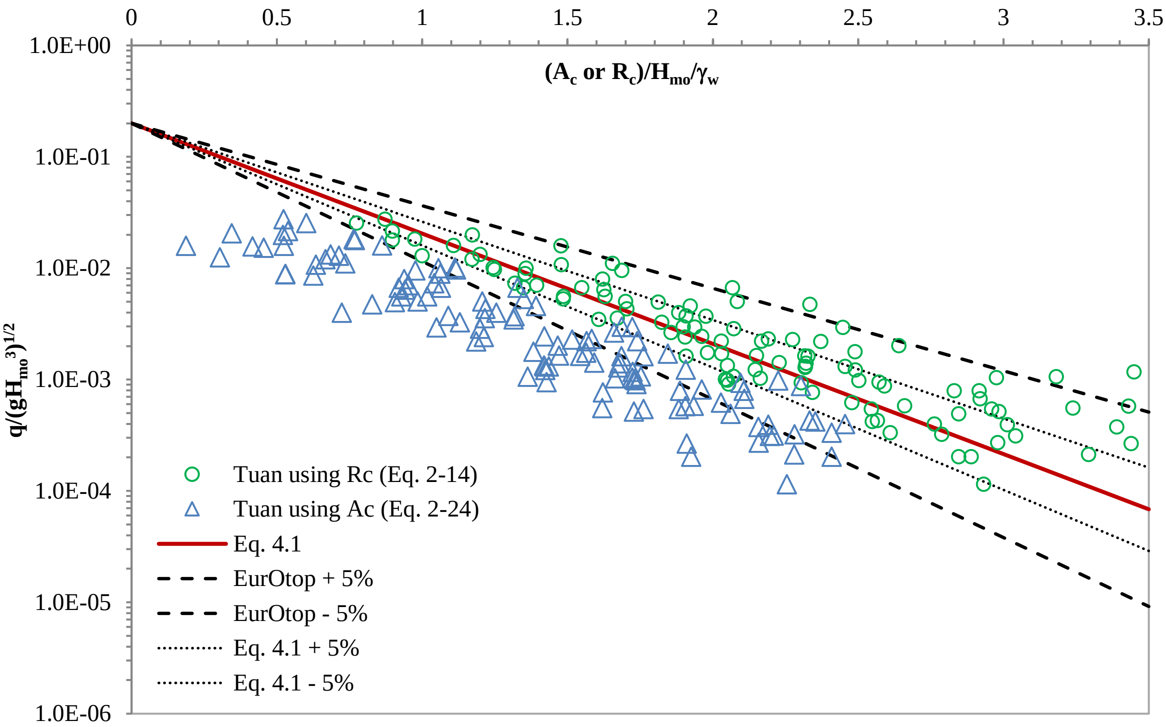

Figure 4-17. Correction of the measured data by means of Tuan (green and blue).

The final approach is carried out by using Eq. [2-25] by Coeveld et al. (2006), where no reduction factor γ is proposed but a ratio Q' between the discharges over slopes with/without wall. The overtopping over a smooth dike with wall is calculated from the overtopping prediction over the smooth dike without wall (Eq. [4-1]) to which the ratio Q' (Eq. [2-25]) is applied. These predictions are then compared to the actual measured data for smooth dikes with a wall, see Figure 4-18. Most datapoints are below the 45° line, showing that the measured values are larger than the predictions. Another visualization of the same attempt is given in Figure 4-19 where the predictions according to Coeveld et al. (2006) show smaller values than the actual measurements. Note that in Figure 4-19 no reduction or correction factor is included in the horizontal axis (unlike Figure 4-17) so the interpretation here is different.

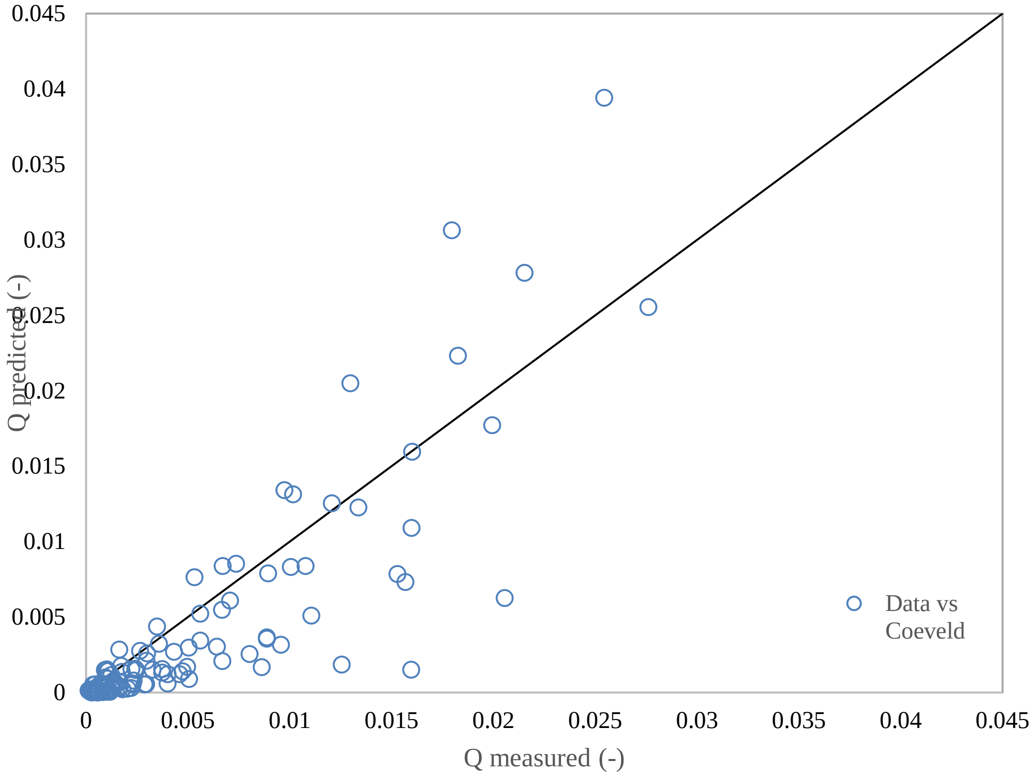

Figure 4-18. Comparison of predicted data by Coeveld et al. (2006) with the measured data (dimensionless plot).

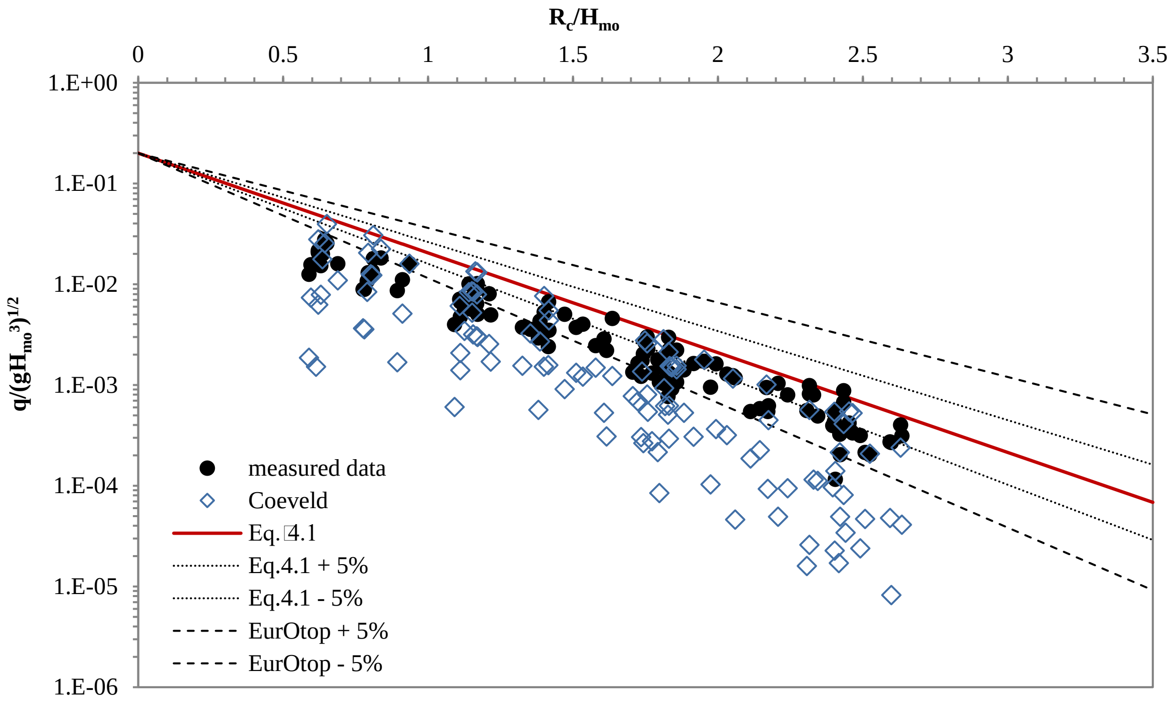

Figure 4-19. Comparison of predicted data by Coeveld et al. (2006) with the measured data (loglinear plot).

The analysis depicted in Figure 4-12 to Figure 4-19 shows that it is necessary to develop a new methodology specificly for the studied geometries in this work: smooth dikes with small storm walls at crest level. A reduction factor will be included in Eq. [4-1] to account for the reduction by a storm wall and other overtopping reducing measures.

Since all other overtopping reducing measures will be analyzed in the same way as the influence of the storm wall will be analyzed, and since all those measures from the current work are located at crest level of the dike, clearly above SWL, where the influence of the breaking process is no longer physically present, it was decided to work with the actual slope in the analysis of the UGent-1 data and setting the transition between non-breaking and breaking waves back to $\xi_{0p} = 2$. Since UGent-1 data have $\xi_{m-1,0} > 2.1$, they are all classified as non-breaking.

Note that no berms have been tested in UGent-1, so the choice of using the actual slope is only valid within the boundaries of the current test program, being smooth dikes without berms.

Based on the findings by Victor (2012), and similar to what is done in Figure 4-10 for smooth dikes, first the influence of the slope angle and the wave period is studied in the data set of smooth dike with storm walls from Figure 4-11. The figures of this analysis can by found in Audenaert & Duquet (2012), a master thesis in the framework of this PhD. The conclusions are given below:

- Slope angle: the difference between slope $\cot(\alpha) = 2$ and $\cot(\alpha) = 3$ is again minor, but in contrast to the dike without storm wall, the steepest slope gives slightly larger overtopping discharges. The reason for this is that on a steeper slope, the vertical velocity component of the run-up is larger compared to a milder slope, which leads to slightly larger overtopping discharges. Nevertheless, detailed data analysis shows that the difference is again negligible, and no component α will be included in the formula.
- Wave period: no difference between small and large wave periods was distinguished this time.

To take the reducing effect of the storm wall into account, Eq. [4-1] is adjusted to Eq. [4-2] by introducing a reduction factor γ_v, which is independent of slope angle and wave period as stated above.

This reduction factor, a value smaller than one, is introduced in the exponential part of the formula. γ_v can now be calculated for every single test, by isolation from Eq. [4-2] as is done in Eq. [4-3]. The outcome of Eq. [4-3] represents the amount of virtual increase of the dimensionless freeboard. In the graphical representation, it shows how much every data point needs to be shifted on the horizontal axis of Figure 4-11 to be exactly on the reference line and would thus give perfect prediction of the overtopping discharge by using Eq. [4-2].

$$\frac{q}{\sqrt{g \cdot H_{m0}^3}} = 0.2 \cdot \exp\left(-2.28 \cdot \frac{R_c}{H_{m0}} \cdot \frac{1}{\gamma_v}\right) \qquad [4\text{-}2]$$

$$\gamma_v = \frac{-2.28 \cdot \frac{R_c}{H_{m0}}}{ln\left(\frac{q}{0.2 \cdot \sqrt{g \cdot H_{m0}^3}}\right)} \qquad [4\text{-}3]$$

This is done for each of the 117 tests on smooth dikes with a vertical wall in the UGent-1 dataset. A gamma value lower than one means reduction of overtopping. The lower the value, the larger the reduction, or the lower the resulting overtopping discharge is. All values of γ_v are now plotted versus a dimensionless parameter to find a best fitting curve. As could be seen in Figure 4-11, the height of the wall has an important influence: for a similar freeboard, the higher the wall the lower the overtopping discharge. Different dimensionless wall heights (h_{wall}/R_c, h_{wall}/H_{m0}) have been investigated in the framework of this PhD manuscript and have been reported in Boderé & Vanhouwe (2010). The best dimensionless parameter for this situation was h_{wall}/R_c. The reduction factor γ_v is thus a function of the dimensionless wall height h_{wall}/R_c, which expresses which portion of the freeboard is used by the wall height. This dimensionless parameter h_{wall}/R_c is plotted on the horizontal axis in Figure 4-20. It can be seen, that the decrease of γ-value (or increasing reduction) slows down towards higher dimensionless wall-heights, which is better expressed by an exponential relationship than by a linear one. With only 2 data points with $h_{wall}/R_c > 1$ (the toe of the wall is below the still water level) the trendline should not be extrapolated. However, these data points indicate that no extra reduction occurs when the toe of the wall becomes submerged. For $h_{wall}/R_c > 1.24$ the reduction coefficient becomes constant.

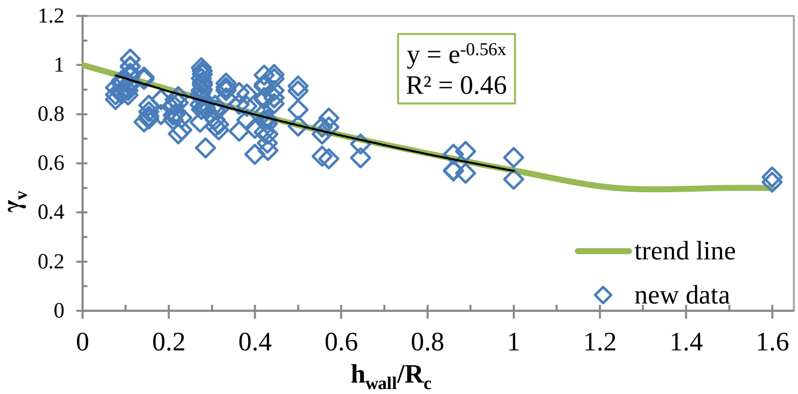

Figure 4-20. Calculated γ_v as a function of h_{wall}/R_c.

The reduction factor γ_v is defined in Eq. [4-4].

$$\gamma_v = \exp\left(-0.56 \cdot \frac{h_{wall}}{R_c}\right) \qquad \text{for } \frac{h_{\text{wall}}}{R_c} < 1.24$$
$$\gamma_v = 0.5 \qquad \text{for } \frac{h_{\text{wall}}}{R_c} \geq 1.24 \qquad [4\text{-}4]$$

Due to the uncertainty for $h_{wall}/R_c > 1$ (too few data points), it would be advised to use Eq. [4-4] only up to $h_{wall}/R_c \leq 1$.

In the following the data of Figure 4-11 are corrected by means of Eq. [4-2] and [4-4] and plotted in Figure 4-21. This leads to a good prediction of wave overtopping over smooth dikes with a storm wall as shown in Figure 4-21.

All data points in Figure 4-21 are now close to the reference line, all within EurOtop's confidence band and even mostly within the more narrow confidence band set-up with standard deviations from Eq. [4-1]. The exponential coefficient $2.28/\gamma_v$ is taken as a normally distributed stochastic value with a mean value $\mu = 2.82$ and a standard deviation of $\sigma = 0.41$. The relative standard deviation σ' becomes 0.15 which has the same order of magnitude as the relative standard deviation on Eq. [2-14] as mentioned in EurOtop (2007): 0.35/2.6 = 0.13. Despite the low R^2 value in Figure 4-20, this relative standard deviation is in range with similar prediction formulae.

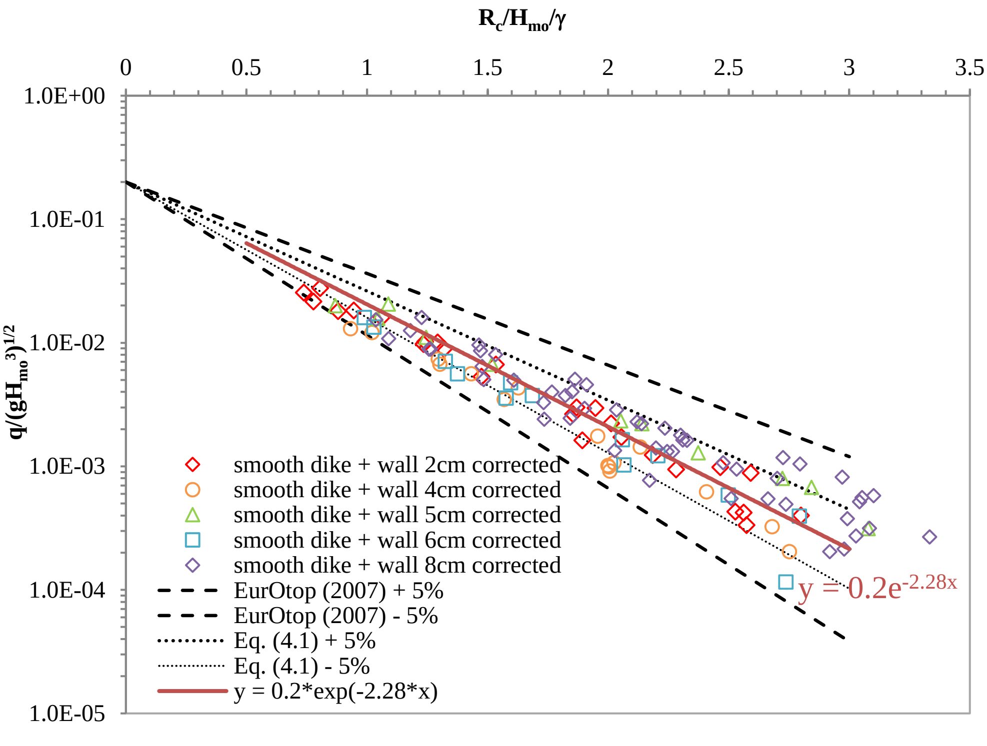

Figure 4-21. Data set on a smooth dike with storm wall - corrected values.

4.1.3 *UGent-2 dataset for breaking waves on a smooth dike slope 1/6*

A similar analysis for the UGent-2 data set of breaking waves is performed as in section 4.1.2 for non-breaking waves. Again the actual slope α is used for calculating the breaker parameter since a relatively small wave wall on the crest of the dike does not influence the breaking process on the slope.

a) *Reference situation*

A reference situation, a smooth dike without wave wall, was tested first. Results are presented in Figure 4-22 together with Eq. [2-13] from EurOtop (2007) and the 90% confidence interval.

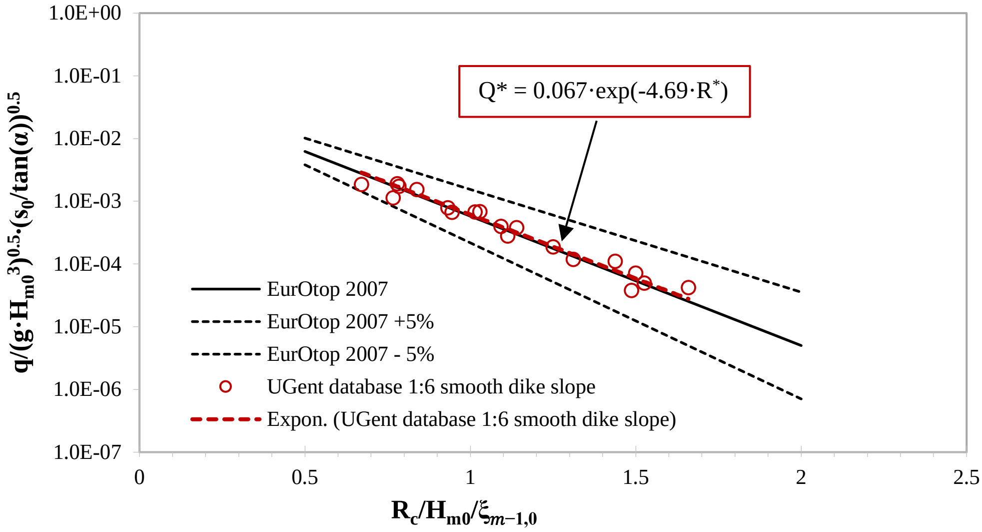

Figure 4-22. Measured data over a smooth dike slope 1:6, breaking waves, UGent-2 data set.

$$\frac{q}{\sqrt{g \cdot H_{m0}^3}} = \frac{0.067}{\sqrt{tan\alpha}} \cdot \gamma_b \cdot \xi_{m-1,0} \cdot exp\left(-4.69 \cdot \frac{R_c}{H_{m0}} \cdot \frac{1}{\xi_{m-1,0} \cdot \gamma_b \cdot \gamma_f \cdot \gamma_\beta \cdot \gamma_v}\right) \quad [4\text{-}5]$$

Even though the data are very close to EurOtop (2007)'s reference line, the coefficient 4.69 (σ = 0.088, σ' = 0.02) from this new trendline is used instead of 4.75 from Eq. [2-13] in the further analysis of γ_v, to provide the best possible analysis of the reduction factor.

b) *Reduction factor γ_v*

When the 31 tests of the UGent-2 data set with a wave wall at crest level are plotted in Figure 4-23, it can be seen that they are (nearly) all located a little below the red dashed reference line found in Figure 4-22, showing the (small) overtopping reducing effect from the wave wall on top of a gentle sloping dike. When using the existing procedure by EurOtop (2007), those data are classified as breaking waves since $\xi_{m-1,0} < 1$ in the UGent-2 dataset and thus clearly in the breaking zone $\xi_{0p} < 3$. Based on Figure 4-23, applying a reduction factor $\gamma_v = 0.65$ would overcompensate the data. Like was done for the UGent-1 data, the same new procedure is thereby also followed for the UGent-2 data: using the actual dike slope and the transition between breaking and non-breaking at $\xi_{0p} = 2$. Nevertheless, the UGent-2 data remain breaking also in this new procedure.

It is noted that the UGent-2 tests were carried out in a small wave flume, small scale and with small model sized wall heights. Also, the test program was more limited compared to the UGent-1 dataset. Results are therefore only orienting and require a wider range of parameters and more analysis.

Three different wall heights have been tested, but due to the limited amount of reduction, no clear difference is found between them. The reduction factor γ_v seems to be constant and independent on the wall height. The wave breaking on the slope already dissipates a lot of energy, so that the height of the wall does not make the big difference any more, unlike for non-breaking waves in the previous section.

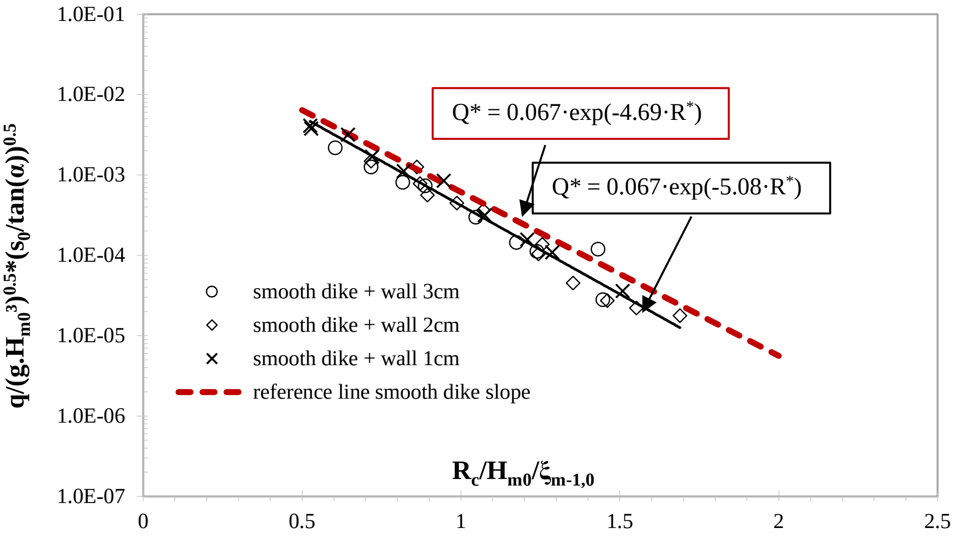

Figure 4-23. Measured data on a smooth dike slope 1:6 with wave wall, breaking waves, UGent-2 data set. Wall heights given in model scale (1:50).

The ratio of the exponential coefficients of the reference line (4.69) and the trendline through the data on the dike with wall (5.08) gives $\gamma_v = 0.92$ ($\sigma = 0.01$), the reduction factor for breaking waves on a mild sloping dike ($\cot(\alpha) = 6$) with a wave wall. This reduction factor can be introduced in Eq. [2-13] or [2-15] for breaking waves. Note that this reduction factor is remarkably higher (which gives lower reduction) than the factor found in the Harlingen analysis.

4.1.4 *Reduction factor for wave walls, a procedure based on all available data.*

The analysis in Sections 4.1.1 to 0 has shown some differences between the different datasets:

- In the Harlingen dataset, the wall formed an important part of the geometry and the toe was located both above and below the SWL. In the analysis of the UGent datasets, the wall was considerably smaller and was located above the still water level.
- The actual slope α was used in the UGent data analysis to determine the wave breaker parameter and the selection between breaking and non-breaking waves. The analysis of the Harlingen data used the average slope α_{avg} where the vertical wall section is replaced by a 1:1 slope.
- In the Harlingen data set the transition between breaking and non-breaking was moved to $\gamma_b\xi_{0p} = 3$, where for the UGent datasets the transition is left at $\xi_{0p} = 2$ ($\gamma_b = 1$, no berms were tested).
- The Harlingen methodology introduces a reduction factor for breaking waves, being $\gamma_v = 0.65$, where for non-breaking waves the geometrical influences didn't have to be included through a reduction factor. The UGent datasets on the other hand show a reduction factor both for non-breaking waves (Eq. [4-4]) and for breaking waves ($\gamma_v = 0.92$).

It is now investigated if the new procedure developed for storm walls at the crest of the dike also works for the Harlingen data with both high and lower walls, breaking and non-breaking waves. Note that one of the three geometries in the Harlingen dataset contains a berm, so for these data the reduction factor γ_b by Eq. [2-26] is included in Figure 4-24 and Figure 4-25

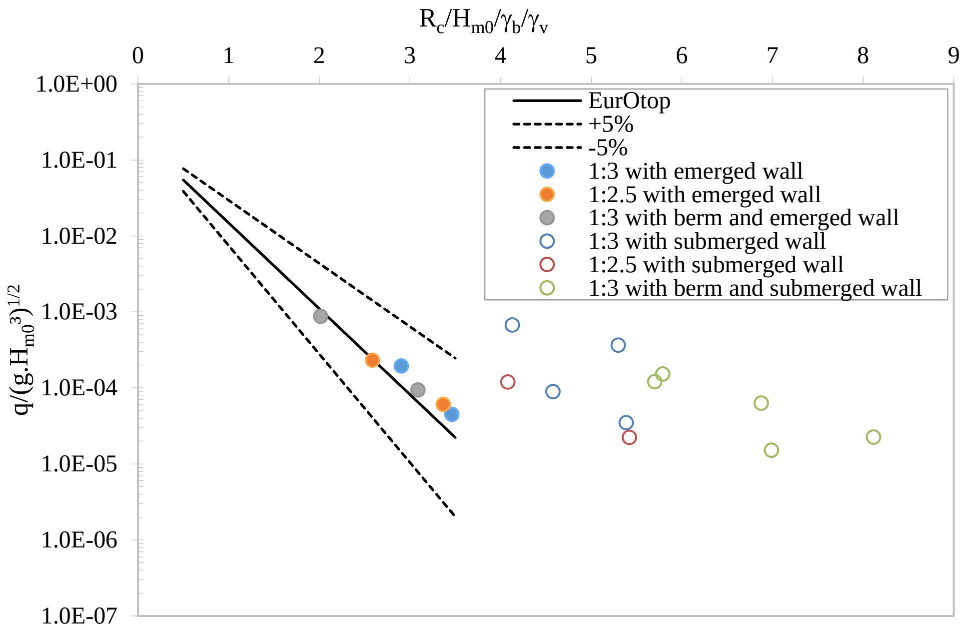

Figure 4-24. All non-breaking waves from the Harlingen dataset, using the new procedure: using the actual slope α and $\xi_{0p} \geq 2$. Data points are corrected by γ_v from Eq. [4-4] and where necessary also by γ_b from Eq. [2-26].

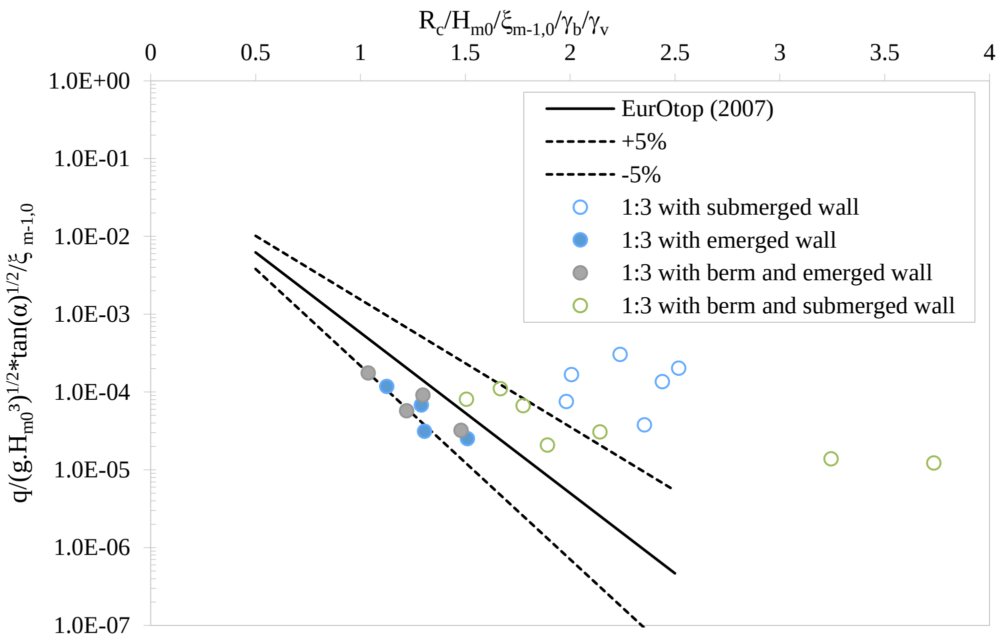

Figure 4-25. All breaking waves from the Harlingen dataset, using the new procedure: using the actual slope α and $\xi_{0p} < 2$. Data points are corrected by $\gamma_v = 0.92$ and where necessary also by γ_b from Eq. [2-26].

The data in Figure 4-24 and Figure 4-25 have been split between an emerged wall (toe of the wall above SWL) in full markers and a submerged wall (toe of the wall below SWL) in open markers. It can be seen that by using the newly developed procedure on the Harlingen data in Figure 4-24, the full markers are predicted very well but the open markers are outside (above) the 90% confidence interval. For Figure 4-25 a similar conclusion can be derived, besides that the correction by $\gamma_v = 0.92$ is still a slight underprediction of the full markers however they are mostly within the 90% confidence band. The reason for this difference is that Harlingen has a 1:2.5 to 1:3 slope where UGent-2 was developed for a 1:6 slope, where more breaking on the slope occurs. Overal, the data for emerged wall (full data mark) are predicted fairly well by the black reference line, where the data for a submerged wall (open data mark) are mostly outside the 90% confidence interval and thus not predicted well.

4.1.5 *Summary and procedure*

According to EurOtop (2007), overtopping over sloping structures can be calculated by means of Eq. [2-13] and [2-14]:

$$\frac{q}{\sqrt{g \cdot H_{m0}^3}} = \frac{0.067}{\sqrt{tan\alpha}} \cdot \gamma_b \cdot \xi_{m-1,0} \cdot exp\left(-4.75 \cdot \frac{R_c}{H_{m0}} \cdot \frac{1}{\xi_{m-1,0} \cdot \gamma_b \cdot \gamma_f \cdot \gamma_\beta \cdot \gamma_v}\right) \quad [2\text{-}13]$$

$$\frac{q}{\sqrt{g \cdot H_{m0}^3}} = 0.2 \cdot exp\left(-2.6 \cdot \frac{R_c}{H_{m0}} \cdot \frac{1}{\gamma_f \cdot \gamma_\beta}\right) \quad [2\text{-}14]$$

The reduction factor for wave walls γ_v, 0.65 for breaking waves and 1 for non-breaking waves, was based on the analysis of the Harlingen dataset from 1994. This procedure uses an average slope where the storm wall is replaced by a 1:1 slope, and defines the transition between breaking and non-breaking waves at $\gamma_b\xi_{0p} = 3$.

It was shown that specific geometries investigated in this work (smooth dike slope (1:2 to 1:3) with small wall at crest level of the dike) were not predicted very well with this procedure. For these specific geometries, a new methodology was set up using the actual dike slope and transition between breaking and non-breaking waves at $\xi_{0p} = 2$. Here, both breaking and non-breaking equations contain the reduction factor γ_v. For non-breaking waves ($\xi_{0p} > 2$), γ_v as a function of h_{wall}/R_c was defined in Eq. [4-4]. For breaking waves ($\xi_{0p} < 2$) γ_v seemed to be a constant value 0.92 developed for mild slopes 1:6.

The new methodology for storm walls at crest level is used to predict the Harlingen data, which seems to work satisfying for emerged walls and does not work for submerged walls. The boundary between both is at $h_{wall}/R_c = 1$. For submerged walls, the procedure by EurOtop (2007) would be advised, for emerged walls the procedure as developed in this work can be used. Of course each procedure can also be used in his own parameter interval, where the range of data of the Harlingen data is overlapping somewhat with the UGent data range.

Wave wall with submerged foot $h_{wall}/R_c > 1$, breaking and non-breaking waves

Based on the Harlingen dataset: replace the vertical wall section by a 1:1 slope and calculate the average slope. With this average slope, calculate the wave breaker parameter ξ_{0p}.

- $\gamma_b\xi_{0p} < 3$ gives breaking waves. In Eq. [2-13] for breaking waves, a reduction factor $\gamma_v = 0.65$ has to be included
- $\gamma_b\xi_{0p} > 3$ gives non-breaking waves. In Eq. [2-14] for non-breaking waves, no reduction factor is required ($\gamma_v = 1$).

This application is limited to slopes between cot(α) = 2.5 and 3, and the foot of the wall is between $-1.2 \cdot H_{m0}$ below SWL and the SWL. The wall is thus always submerged.

Wave wall with emerged foot $h_{wall}/R_c < 1$, breaking waves

Based on UGent-2 dataset with cot(α) = 6: use the actual dike slope, calculate the breaker parameter ξ_{0p}. For $\xi_{0p} < 2$, use Eq. [2-13] or [2-15] with a reduction factor $\gamma_v = 0.92$.

Wave wall with emerged foot $h_{wall}/R_c < 1$, non-breaking waves

Based on UGent-1 dataset with $\cot(\alpha) = 2$ and 3: use the actual dike slope, calculate the breaker parameter ξ_{0p}. For $\xi_{0p} \geq 2$, use Eq. [2-14] or [2-17] with a reduction factor γ_v depending on the dimensionless wall height, according to Eq. [4-4]:

$$\gamma_v = \exp\left(-0.56 \cdot \frac{h_{wall}}{R_c}\right) \qquad \text{for} \frac{h_{\text{wall}}}{\text{R}_c} < 1 \qquad [4\text{-}4]$$

A summary of the procedure to include the effect of a storm wall on a dike is given in the flowchart in Figure 4-26.

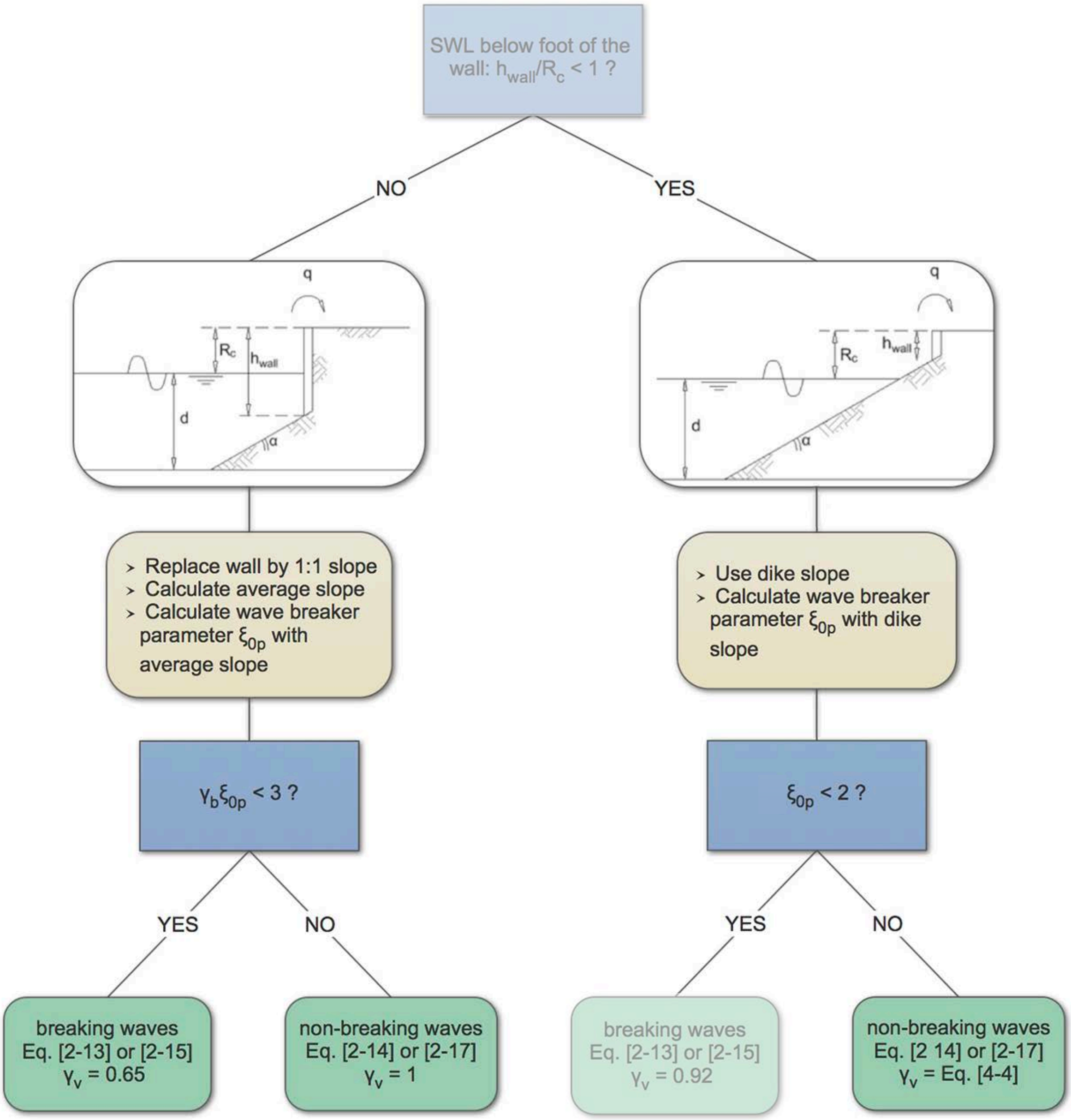

Figure 4-26. Flowchart of the use of a reduction factor for a wall in the overtopping equations.

It can be seen that two boxes in the flowchart have a lighter colour, since they require further research:

- Top of the flowchart, the splitting $h_{wall}/R_c = 1$. When looking at both Harlingen and UGent datasets, this seems an obvious difference between both datasets. But also the location of the toe of the wall related to the SWL, or the height of the wall related to the total height of the structure is a difference between both datasets. This could be investigated further.
- Bottom line of the flowchart, right side (UGent procedure) for breaking waves. $\gamma_v = 0.92$ is valid for a mild sloping dike 1:6 and was developed with a limited test matrix in a (very) small wave flume. The value of the reduction factor is orienting but requires more research to be confirmed. When using this value to the breaking waves of the Harlingen dataset (with steeper dike slopes) it already seems that the reduction factor might be a little lower than 0.92.

4.2 *Other overtopping reducing measures*

Similar to Section 4.1.2 equations shape Eq. [2-18] according to EurOtop (2007) is used for analysis since that was the relevant equation at time of analysis, but results can be used in shape Eq. [2-19] according to EurOtop (2016). Only the UGent-1 database contains experiments on other overtopping reducing measures, so this section 4.2 exclusively deals with non-breaking waves ($\xi_{0p} \geq 2$).

4.2.1 *Smooth dike with storm wall and bullnose*

Wave overtopping can be further reduced, without increasing the height of the wall, by adding a "nose" to the vertical wall. Several names for this nose are found in literature (parapet, bullnose, recurve wall). The name "bullnose" is maintained in the current work. Due to the presence of this bullnose, waves are not only projected upward, but also back towards the open sea. A sketch of the tested geometry as well as the definition of the used parameters in the formulae are given in Figure 3-5 and repeated below in Figure 4-27.

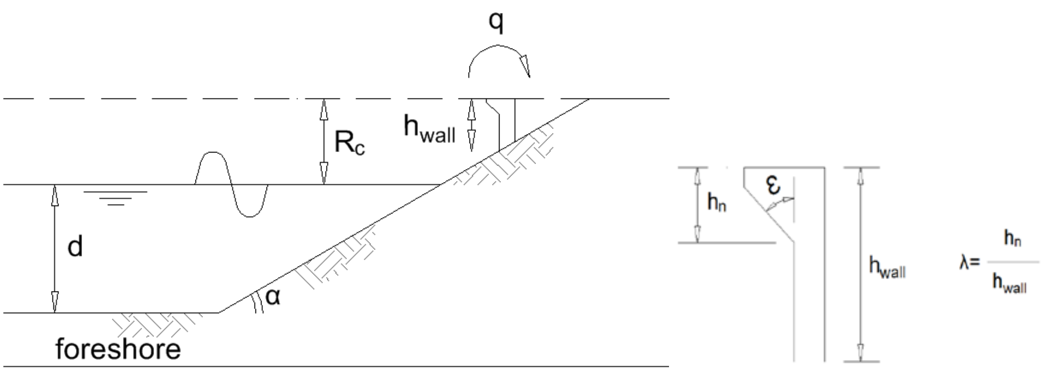

Figure 4-27. Sketch of a smooth dike with storm wall and bullnose and definition of the used parameters ε and λ.

The working principle is shown in the photo sequence in Figure 4-28, the waves coming from the right are clearly being projected back towards the sea (wave flume), reducing the amount of water overtopping the crest of the dike.

Figure 4-28. Bullnose on top of a vertical wall showing the reduction of wave overtopping (incoming waves from the right).

175 tests have been carried out on a smooth dike with storm wall and bullnose, divided in two phases. In the first phase, 92 tests on storm walls of 2, 5 and 8cm (model scale values) to find the optimal

shape of the bullnose. In the second phase, 83 tests on a storm wall of 8cm (model scale value) to test the influence of the slope angle and the wave period, see Table 3-3.

a) *Phase 1: Influence of nose angle ε and height ratio λ*

The data for the first phase are plotted in Figure 4-29 to Figure 4-31, respectively, for different heights h_{wall} of the storm wall. Despite the dimensions shown in Figure 4-29 to Figure 4-31 the analysis is carried out in a dimensionless way, these graphs are for visualization purposes only. For every graph, there are different geometries of the bullnose (different ε, different λ), which explains the large scatter among the green data points.

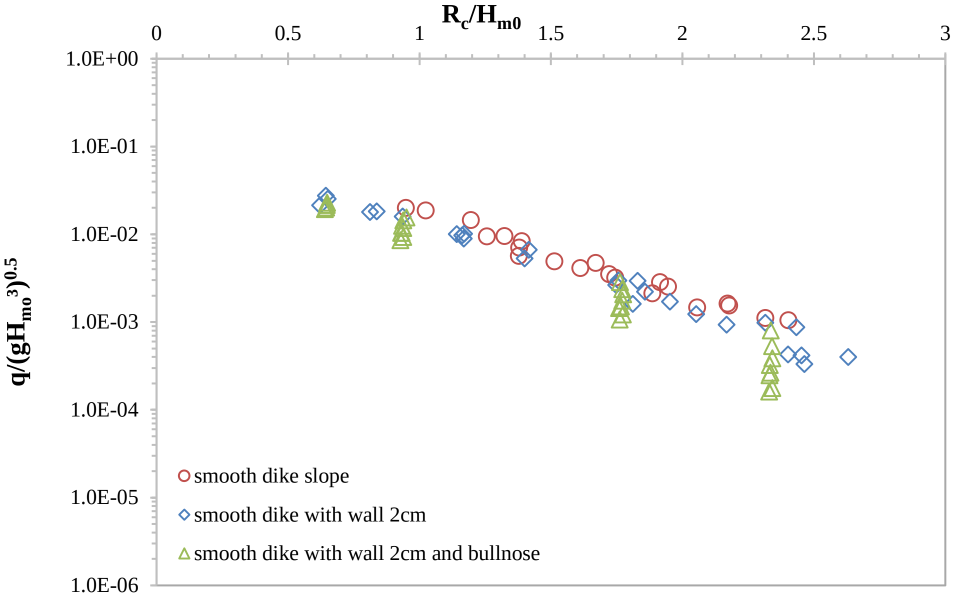

Figure 4-29. Overtopping results of the smooth dike (red) with a 2cm wall (blue) and a 2cm wall with bullnose (green). Wall height in model scale.

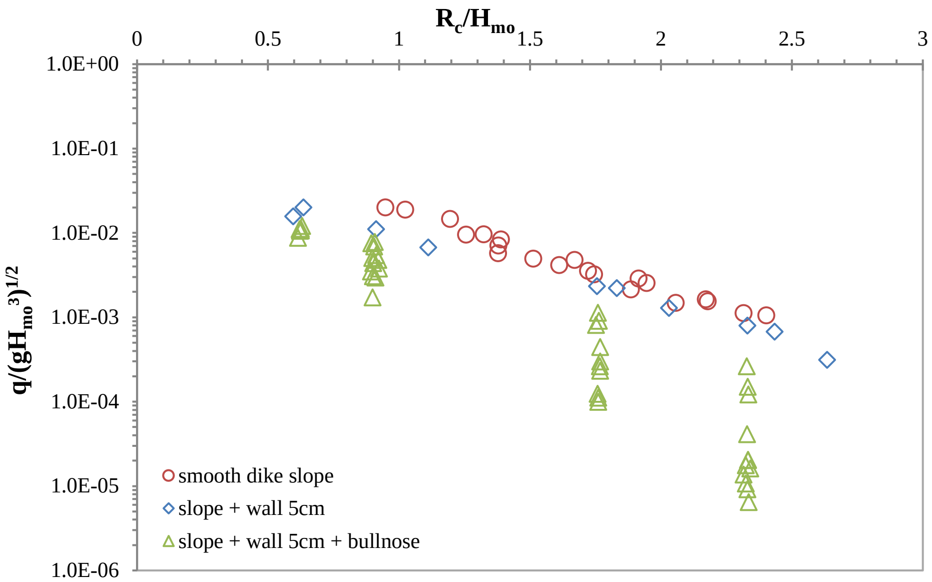

Figure 4-30. Overtopping results of the smooth dike (red) with a 5cm wall (blue) and a 5cm wall with bullnose (green). Wall height in model scale.

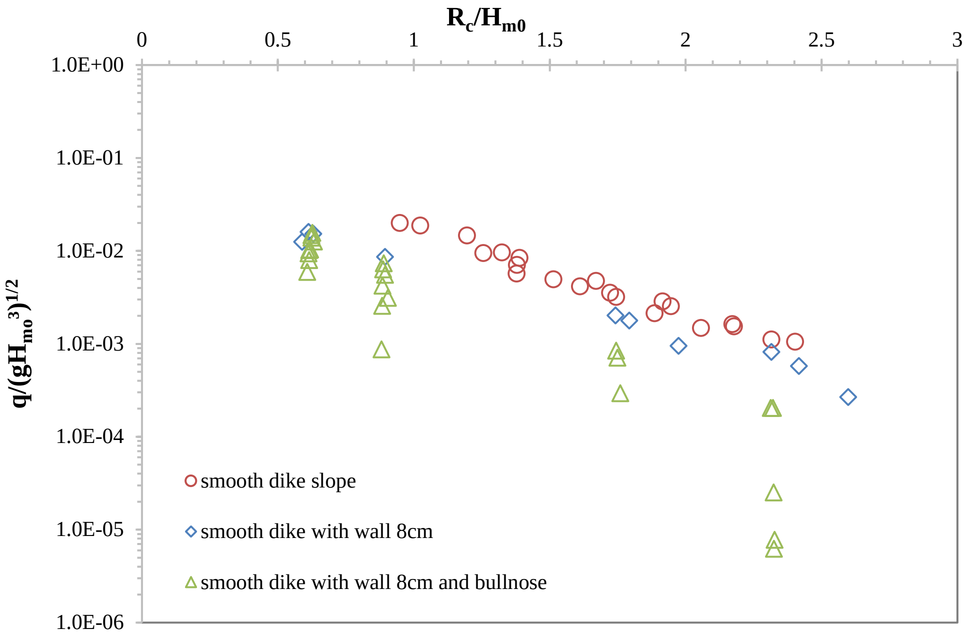

Figure 4-31. Overtopping results of the smooth dike (red) with a 8cm wall (blue) and a 8cm wall with bullnose (green). Wall height in model scale.

The red data points show the overtopping over the reference situation, a smooth dike. The blue data points include a storm wall of 2, 5 or 8cm (model scale) respectively, and the green data points include the same wall heights, but different bullnose angles ε and different height ratios λ have been added. The reduction between the red (reference case) and blue (wall) data has been explained in the previous section, this section solely investigates the extra reduction due to the bullnose. This extra reduction can clearly be seen since all green data are below the blue and red data. Big scatter among the green data was already mentioned, there is up to a factor 100 of difference between data with a similar dimensionless freeboard. This is due to the different geometries of the bullnose; the reduction of wave overtopping strongly depends on both parameters ε and λ.

A reduction factor due to the height of the storm wall already exists (γ_v Eq. [4-4]), a new reduction factor γ_{bn} is introduced here to describe the influence of the bullnose. Multiplication of both reduction factors (γ_v and γ_{bn}), gives the full reduction of a bullnose compared to the reference case, a smooth dike. γ_{bn} on its own only gives the influence of adding a nose to the wall. The principle is sketched in Figure 4-32.

To determine γ_ε and γ_λ, the average trend line approach is used, since it is easy and straightforward to group the data per values of the dimensionless parameters ε and λ. A point-per-point methodology is evaluated to be impossible for defining the influence ε and λ since the dataset did contain too many variables to fix all-but-one parameters (geometric (ε, λ, α, h_{wall}/R_c) and hydraulic (s_{0m})) and look for the influence of this one parameter. Once γ_ε and γ_λ are analyzed, the point-per-point method is used to determine γ_{bn}.

The final equation to plot data on a smooth dike with storm wall and bullnose is Eq. [4-6].

$$\frac{q}{\sqrt{g \cdot H_{m0}^3}} = 0.2 \cdot \exp\left(-2.28 \cdot \frac{R_c}{H_{m0}} \cdot \frac{1}{\gamma_v} \cdot \frac{1}{\gamma_{bn}}\right) \quad [4\text{-}6]$$

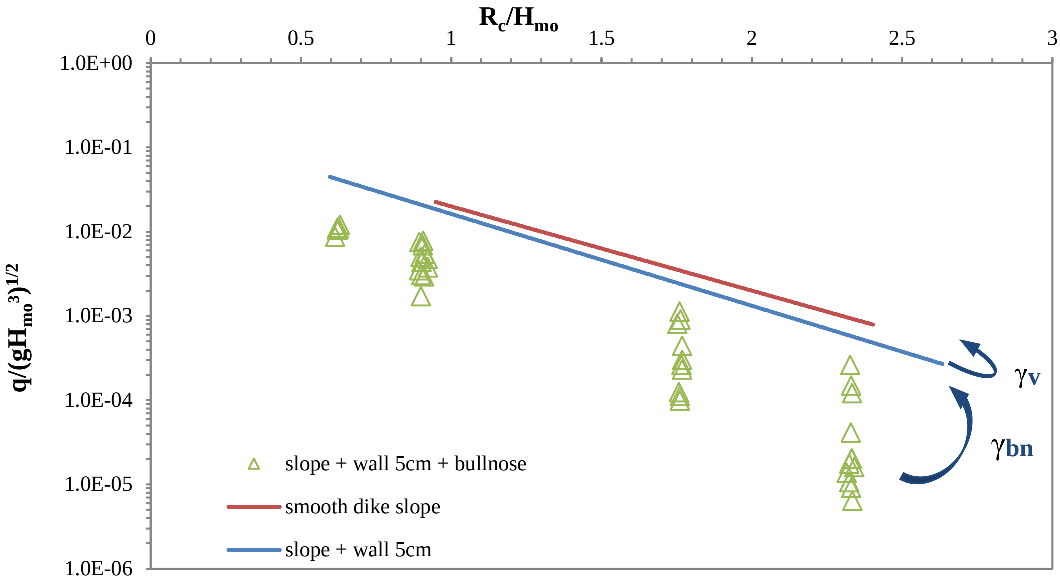

Figure 4-32. Principal explanation of the effect of γ_{bn} and γ_v. The combination of both represents the reduction due to a storm wall with bullnose.

The results in the above graphs are now grouped per nose angle ε or height ratio λ. First, the influence of the bullnose's angle ε is investigated. The data are thereby grouped per angle, see Figure 4-33 for h_{wall} = 5cm as an example case. The higher the value of the bullnose angle becomes, the lower the data points are located, meaning the overtopping discharge over such a structure is lower. The scatter among data within a group of fixed ε is due to the variation of the other geometrical parameter λ that still exists.

A trendline can be fitted through each group of data points, from which the reduction towards the blue trendline (smooth dike with 5cm storm wall) can be calculated. It's chosen not to refer the green data to the red line but to the blue line, since the influence between the blue line and the red line was already explained through γ_v in Eq. [4-4]. An example for the 30° bullnose is given (green data points in Figure 4-33): the reduction due to the bullnose compared to the dike with storm wall is calculated as the ratio of its exponential coefficient (-3.80) to the exponential coefficient of the dike with wall 5cm (-2.51): 2.51/3.8 = 0.66. This ratio represents the reduction from a bullnose only indicating how much more a storm wall of 5cm with a bullnose of 30° reduces the wave overtopping as compared to a storm wall of 5cm without bullnose.

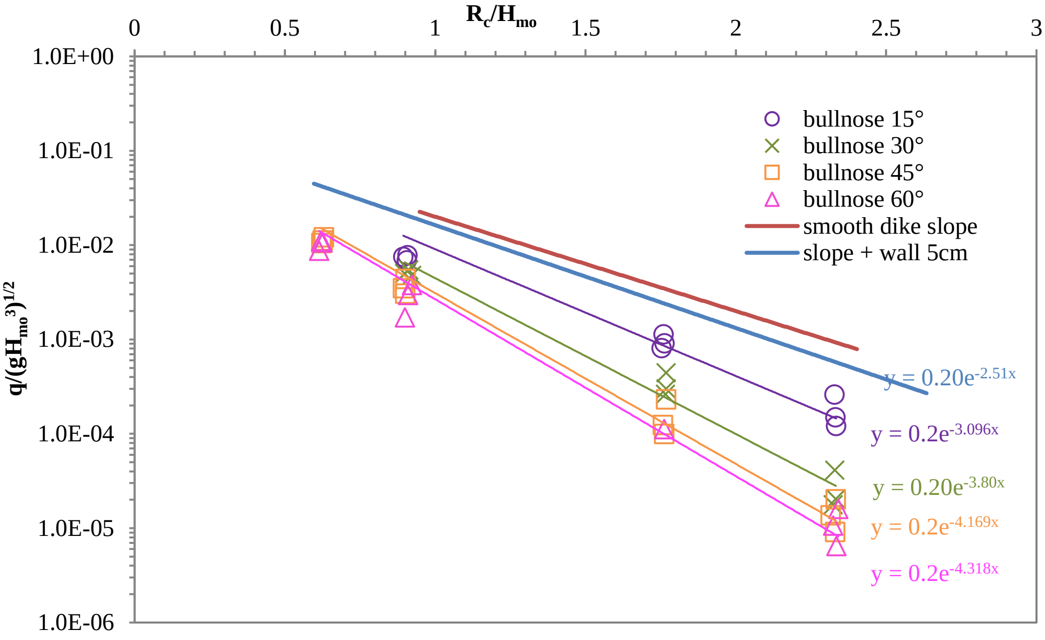

Figure 4-33. Data on a dike with wall 5cm and bullnoses of different angles ε and height ratios λ. Data are grouped per nose angle ε, and show lower overtopping discharge for increasing ε.

The same is done for the other data points grouped per nose angle ε, for all tests with wall height 2cm, 5cm or 8cm. The values are named 'γ_ε', the influence of the bullnose's angle. It's visually noticed during the experiments and seen in the data analysis afterwards that a very small storm wall (2cm in model scale) behaves differently than the larger walls 5cm and 8cm. Dimensionless, the transition between a small and a large wall is found at $h_{wall}/R_c = 0.25$. For $h_{wall}/R_c > 0.25$, γ_ε is plotted in Figure 4-34. The aforementioned value of 0.66 can be found in Figure 4-34 for ε = 30° for a storm wall of 5cm (diamond symbol).

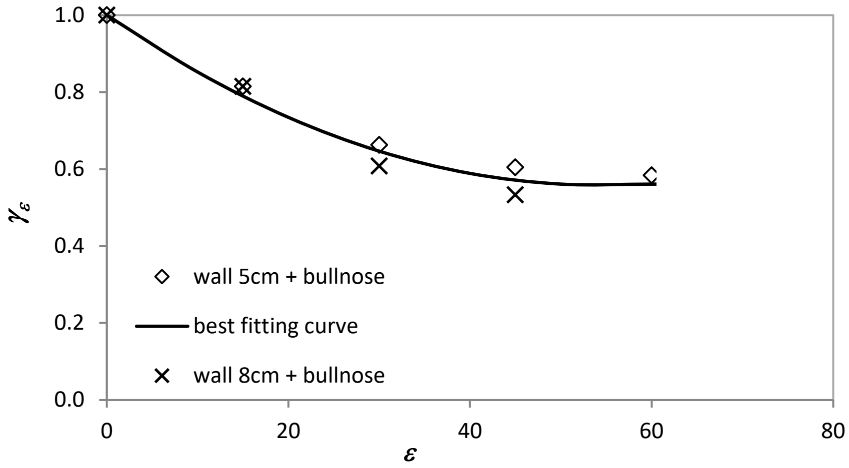

Figure 4-34. Reduction factor γ_ε of the bullnose angle for all tests on the storm wall $h_{wall}/R_c > 0.25$.

The trendline that is the best fitting curve for these data is a quadratic descending function up to ε = 50°. From that point on, an increasing bullnose angle seems to not further increase the reduction (or thus decrease the overtopping) within the tested parameter range. Castellino et al. (2018) and Martinelli et al. (2018) report continuously increasing reduction also for larger tested angles, however their angle definition is different compared to this work (see Figure 2-7). The curve in Figure 4-34 starts at $\gamma_\varepsilon = 1$

for ε = 0°, i.e. no nose gives no extra reduction of overtopping compared to a storm wall. The function description of the trendline is given in Eq. [4-7]. This trendline is valid for the tests with $h_{wall}/R_c > 0.25$.

$$\gamma_\varepsilon = 1.53 \cdot 10^{-4} \cdot \varepsilon^2 - 1.63 \cdot 10^{-2} \cdot \varepsilon + 1 \qquad for \qquad 15° \leq \varepsilon \leq 50°$$
$$\gamma_\varepsilon = 0.561 \qquad for \qquad 50° \leq \varepsilon \leq 60° \qquad [4\text{-}7]$$

A similar analysis has been made for all tests of h_{wall} = 2cm, which corresponds with $h_{wall}/R_c \leq 0.25$. The height of the nose h_n in these tests was 1cm or 2cm, leading to λ = 0.5 or 1. They are analyzed separately because visual observation during the experiments and data analysis have shown that this low storm wall with bullnose physically behaves differently compared to higher walls with bullnose. The upward projection of the incoming wave is much less or even absent for the little wall heights. The wave thereby more easily fills the space underneath the bullnose, after which the rest of the incoming water can overtop more easily. There is still a reduction, but it's not as dominant as shown by Eq. [4-7] in Figure 4-34.

The results for $h_{wall}/R_c \leq 0.25$ are shown in Figure 4-35, grouped per bullnose angle ε. The exponential coefficient 2.478 for the smooth dike with a 2cm wall, divided by the exponential coefficients of the trendlines through the data with bullnoses of different angles ε (2.535, 2.709, 2.89 and 2.976) gives again the obtained values γ_ε, this time for $h_{wall}/R_c \leq 0.25$. The outcome is plotted in Figure 4-36 and is characterized by Eq. [4-8]:

$$\gamma_\varepsilon = 1 - 0.003 \cdot \varepsilon \qquad for \qquad 15 \leq \varepsilon \leq 60° \qquad [4\text{-}8]$$

As explained, the overtopping reducing effect is still there but less pronounced than for $h_{wall}/R_c > 0.25$. Values up to 0.83 (for ε = 60°) are reached here instead of 0.58 in Figure 4-34.

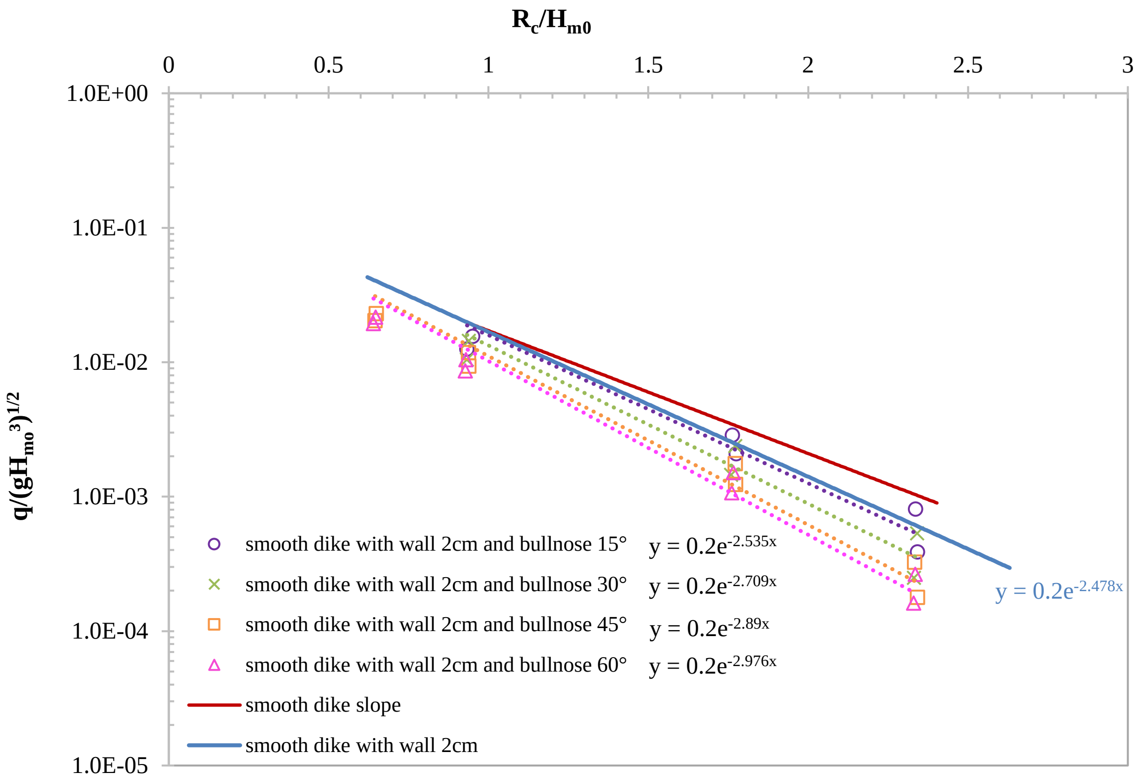

Figure 4-35. Data of all tests with a wall height of 2cm split and for different bullnose angles ε.

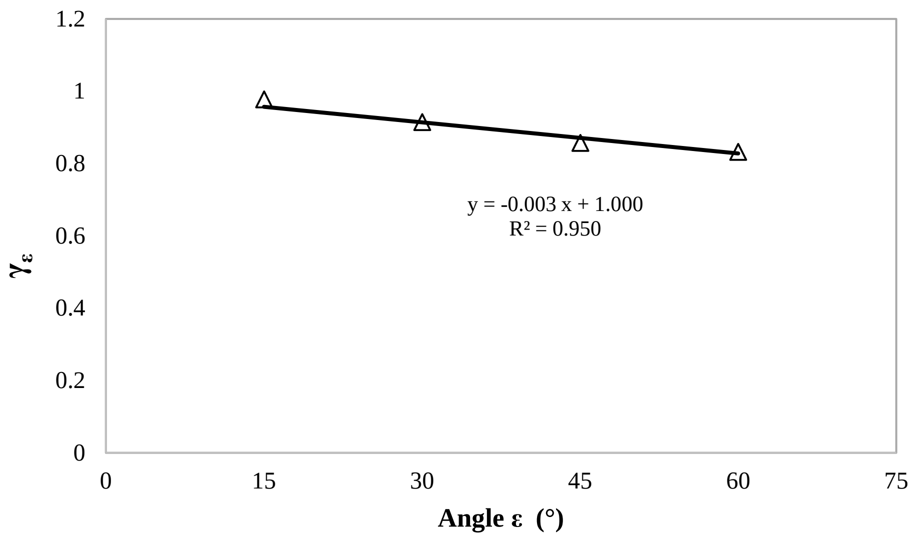

Figure 4-36. Reduction factor γ_ε of the bullnose angle for all tests on the storm wall $h_{wall}/R_c \leq 0.25$.

Although the parameter ε is the dominant geometric variable, wave overtopping also decreases when the height of the bullnose h_n is more prominent, and thus when λ increases. The influence of the bullnose' height ratio λ is now investigated. A similar analysis as in Figure 4-33 to Figure 4-36 has been performed with the data grouped per constant value of λ (see Van Doorslaer (2008)). Trendlines are fitted through the data with constant λ, and the ratio of their exponential coefficients and the exponential coefficient of the reference situation's trendline gives the values γ_λ. The outcome for the tests on walls of $h_{wall}/R_c > 0.25$ (walls of 5cm and 8cm) are plotted in Figure 4-37, the outcome for $h_{wall}/R_c \leq 0.25$ (h_{wall} = 2cm) is plotted in Figure 4-38; however it's not ideal to plot a line through only two datapoints (λ = 0.5 and 1), a small descending trend is noticeable.

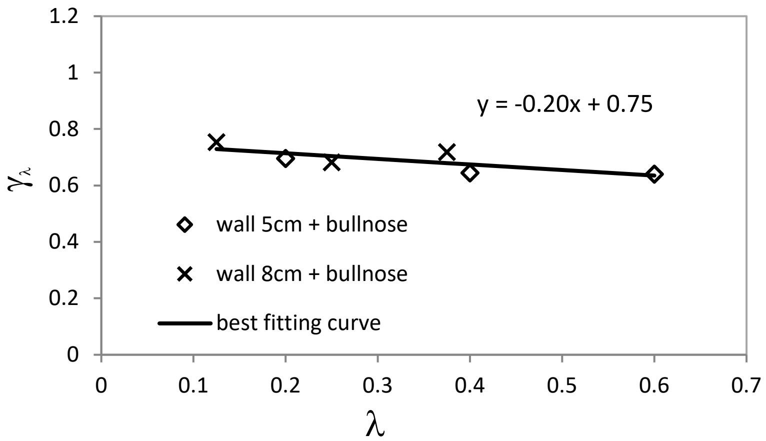

Figure 4-37. Reduction factor γ_λ of the height ratio λ for all tests on the storm wall $h_{wall}/R_c > 0.25$.

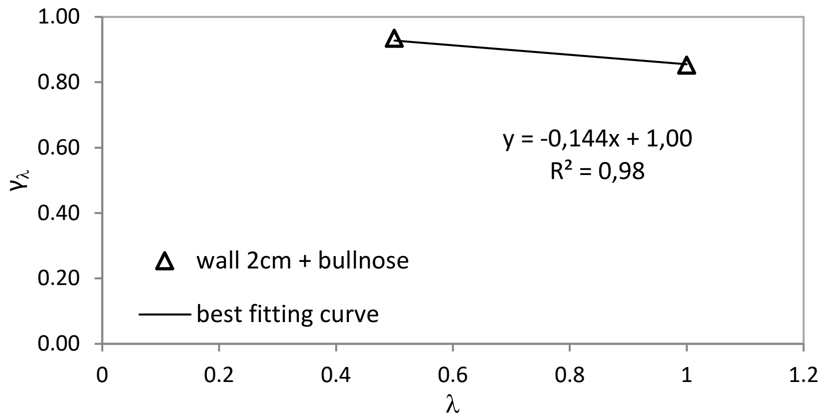

Figure 4-38. Reduction factor γ_λ of the height ratio λ for all tests on the storm wall $h_{wall}/R_c \leq 0.25$.

The trendlines in Figure 4-37 for $h_{wall}/R_c > 0.25$ and in Figure 4-38 for wall heights $h_{wall}/R_c \leq 0.25$ determine the reduction factor γ_λ, which gives the reduction for the height ratio of the nose.

$$\text{If } \frac{h_{wall}}{R_c} > 0.25\text{: } \gamma_\lambda = 0.75 - 0.20 \cdot \lambda \qquad for \qquad 0.125 \leq \lambda \leq 0.6 \tag{4-9}$$

$$\text{if } \frac{h_{wall}}{R_c} \leq 0.25\text{: } \gamma_\lambda = 1 - 0.144 \cdot \lambda \qquad for \qquad 0.5 \leq \lambda \leq 1 \tag{4-10}$$

Two separate reduction factors γ_ε and γ_λ have now been analyzed. However, both ε and λ are inseperable for a storm wall with bullnose, which makes independent treatment of their influence not possible: γ_ε is influenced by λ and vice versa. Consequently, a simple multiplication of γ_ε and γ_λ leads to a too low value of the overall reduction factor γ_{bn} meaning an overestimation of the reduction. This is shown in Figure 4-39 for $h_{wall}/R_c > 0.25$, where the simple multiplication $\gamma_\varepsilon \cdot \gamma_\lambda$ is given on the vertical axis, whereas the value γ_{bn}, isolated from Eq. [4-6] by means of Eq. [4-11], is given on the horizontal axis.

$$\gamma_{bn} = \frac{-2.28 \cdot \frac{R_c}{H_{m0}} \cdot \frac{1}{\gamma_{v\_calculated}}}{ln\left(\frac{q}{0.2 \cdot \sqrt{g \cdot H_{m0}^3}}\right)} \tag{4-11}$$

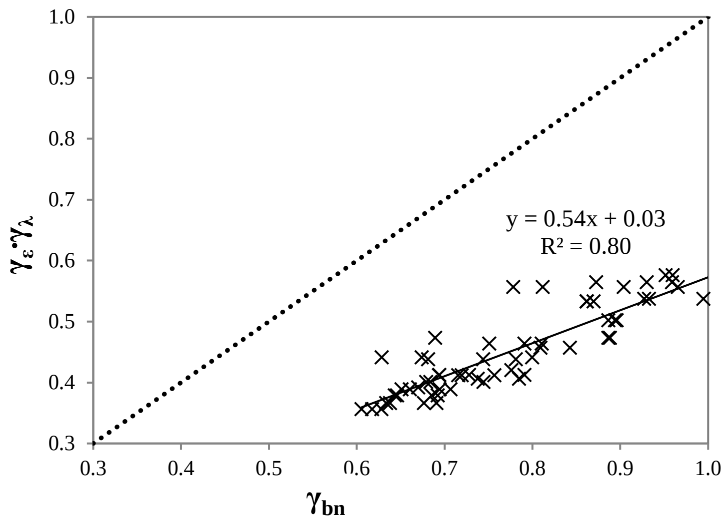

Figure 4-39. Comparison of the simple multiplication of γ_ε and γ_λ and the actual γ_{bn} for all data $h_{wall}/R_c > 0.25$.

As was already expected, the multiplication of both factors γ_ε and γ_λ gives much lower (more reducing) values than the actual reduction γ_{bn}. Since the data in Figure 4-39 are grouped well together, the final formulae to calculate γ_{bn} for $h_{wall}/R_c > 0.25$ can be derived from this trendline.

$$\gamma_\varepsilon \cdot \gamma_\lambda = 0.54 \cdot \gamma_{bn} + 0.03 \Rightarrow \gamma_{bn} = \frac{(\gamma_\varepsilon \cdot \gamma_\lambda - 0.03)}{0.54} \approx 1.8 \cdot \gamma_\varepsilon \cdot \gamma_\lambda \qquad [4\text{-}12]$$

When a similar analysis is performed for the data $h_{wall}/R_c \leq 0.25$, the final formula becomes

$$\gamma_{bn} = 1.8 \cdot \gamma_\varepsilon \cdot \gamma_\lambda - 0.53 \qquad [4\text{-}13]$$

Summarized, the following formulae are valid to account for wave overtopping calculations for smooth dikes with storm wall and bullnose:

$$\frac{q}{\sqrt{g \cdot H_{m0}^3}} = 0.2 \cdot \exp\left(-2.28 \cdot \frac{R_c}{H_{m0}} \cdot \frac{1}{\gamma_v \cdot \gamma_{bn}}\right) \qquad [4\text{-}5]$$

For $h_{wall}/R_c > 0.25$:

$$\gamma_{bn} = 1.80 \cdot \gamma_\varepsilon \cdot \gamma_\lambda \qquad [4\text{-}12]$$

with	$\gamma_\varepsilon = 1.53 \cdot 10^{-4} \cdot \varepsilon^2 - 1.63 \cdot 10^{-2} \cdot \varepsilon + 1$	if	$15° \leq \varepsilon \leq 50°$	[4-6]
	$\gamma_\varepsilon = 0.56$	if	$\varepsilon \geq 50°$	[4-6]
	$\gamma_\lambda = 0.75 - 0.20 \cdot \lambda$	if	$0.125 \leq \lambda \leq 0.6$	[4-8]

For $h_{wall}/R_c \leq 0.25$:

$$\gamma_{bn} = 1.80 \cdot \gamma_\varepsilon \cdot \gamma_\lambda - 0.53 \qquad [4\text{-}12]$$

with	$\gamma_\varepsilon = 1 - 0.003 \cdot \varepsilon$	if	$15° \leq \varepsilon \leq 60°$	[4-7]
	$\gamma_\lambda = 1 - 0.15 \cdot \lambda$	if	$0.5 < \lambda \leq 1$	[4-9]

A few remarks to be made here:

- γ_{bn} only takes into account this extra reducing effect of the bullnose, as shown in Figure 4-32. Consequently, γ_{bn} always has to be combined with γ_v of the vertical wall to calculate the overtopping discharge over a structure with a storm wall and a bullnose.
- Note that γ_λ in [4-9] is not equal to one when λ is zero (see Figure 4-37), and γ_{bn} in [4-12] or [4-13] are also not one for $\gamma_\varepsilon \cdot \gamma_\lambda = 1$. There is not enough data in the regions of very small noses (very small values of λ or ε), since that was outside the scope of this research. The formula [4-7]

to [4-13] can thereby not be used outside the mentioned intervals. In case λ or ε are really small, the wall with bullnose is not much more beneficial than a vertical wall. In that case, the formula [4-4] for a vertical wall is recommended for a conservative design approach.

- The reduction factor due to a bullnose has to be below one.

b) *Phase 2: influence of the wave period and dike angle*

In the second phase of the research on walls with bullnose, the influence of the wave period and slope angle is investigated on two optimal bullnose geometries, based on 83 tests with h_{wall} = 8cm (model value). These optimal walls with bullnose have ε = 30° or ε = 45°, keeping λ constant at 0.375. This leads to γ_{bn} = 0.79 respectively γ_{bn} = 0.70 for $h_{wall}/R_c > 0.25$ according to formulae [4-12], [4-7] and [4-9]. The test matrix for phase 2 is given in Table 3-3.

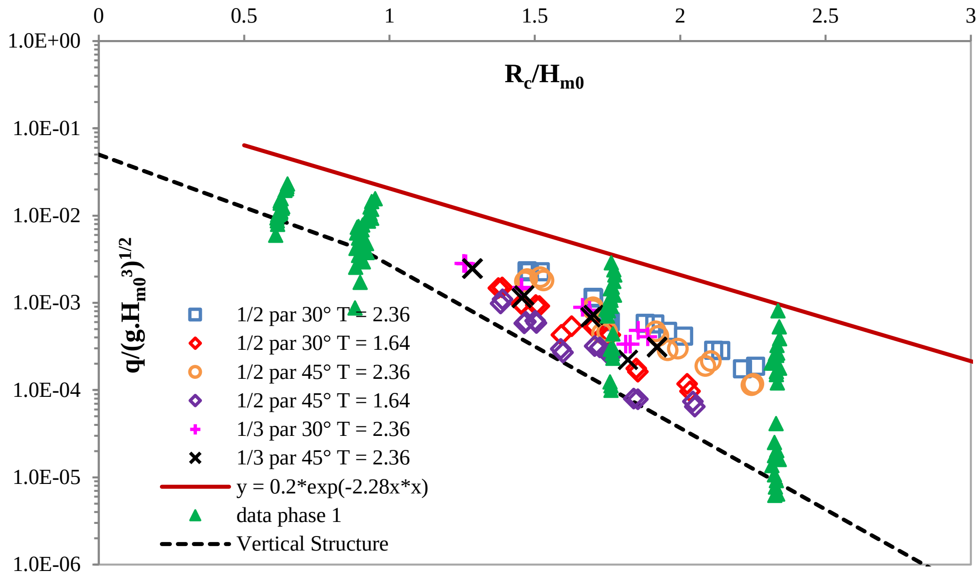

Figure 4-40. Data set on a smooth dike with storm wall and bullnoses – measured values, UGent-1 data set.

Data of the 2nd phase on dike slope 1:2 are plotted in Figure 4-40, together with the data of phase 1. The green triangles in Figure 4-40 are the same green triangles as in Figure 4-31. Some conclusions can be drawn from this graph:

- Data of phase 2 are amongst the data of phase 1, which is expected since apart from a larger wave period the range of parameters in phase 2 is similar to phase 1.
- All data of both phase 1 and 2 are clearly below the reference line. In some tests with small freeboards, even lower overtopping discharges then vertical structures with equal dimensionless freeboards are noticed. This indicates that a storm wall with bullnose is a very good measure to reduce wave overtopping for non-breaking waves over smooth dikes.
- When looking at the data of dike slope 1:2 and ε = 30° (blue and red data points), the blue squares with the largest wave period show more wave overtopping than the red diamonds. For the data of dike slope 1:2 and ε = 45° (orange and purple data points) the same observations are made: the orange circles have the largest wave period and give more wave overtopping than the purple triangles.

  For a dike slope of 1:3 no such comparison could be made, because all tests with wave period $T_{m-1,0}$ = 1.64s lead to breaking waves ($\xi_{0p} < 2$). Based on the data on dike slope 1:2, there is a clear influence of the wave period for the geometry with bullnose. This confirms what was found in Kortenhaus et al. (2001) and Pearson et al. (2004). It is visually observed in Pearson et al. (2004) and Van Doorslaer (2008) that long waves, who have a larger volume of water under the crest of a wave, first "fill" the space underneath the bullnose, after which it acts as a normal storm wall which is more easily overtopped than a wall with (empty) bullnose. The influence of the wave period should thus be included for this kind of geometry.

- When comparing data sets with the same dike slope cot(α) and the same wave period, such as red diamonds versus purple triangles (cot(α) = 2, $T_{m-1,0}$ = 1.64s) or blue squares versus orange circles (cot(α) = 2; $T_{m-1,0}$ = 2.36s) or black cross versus pink plus (cot(α) = 3; $T_{m-1,0}$ = 2.36s), they only have a different nose angle ε. Here the conclusion is that ε = 45° gives a little lower overtopping volumes than storm walls with a bullnose of 30°. This confirms what was found in phase 1 in Figure 4-34.
- When comparing data sets with the same nose angle ε and the same wave period, only the dike slope cot(α) varies. For example, black crosses versus orange circles (ε = 45°, $T_{m-1,0}$ = 2.36s) or pink plus versus blue squares (ε = 30°, $T_{m-1,0}$ = 2.36s), there is a small difference. The mildest dike slope is overtopped the least since the run-up on the mildest slope has more horizontal velocity and less vertical velocity to overcome the structure. The influence is nevertheless again small and the number of different slopes in this data set too limited to deduct an reduction factor for the slope.

Summarizing for the storm wall with bullnose, it can be concluded that together with γ_v to include the effect of the height of the storm wall, and γ_{bn} to include the reducing effect of the nose angle ε and the height of the nose λ, also a correction factor to account for the wave period must be included. It was decided to maintain the already evaluated γ_v and γ_{bn} and to add a factor $\gamma_{s0,bn}$, accounting for the wave period by means of the dimensionless wave steepness $s_{0,m-1,0}$. The suffix 'bn' is added, since later in this work it shows that the wave period only has its influence on storm walls with bullnose located directly at the end of the dike. Eq. [4-6] is thus extended to Eq. [4-14]:

$$\frac{q}{\sqrt{g \cdot H_{m0}^3}} = 0.2 \cdot \exp\left(-2.28 \cdot \frac{R_c}{H_{m0}} \cdot \frac{1}{\gamma_v \cdot \gamma_{bn} \cdot \gamma_{s0,bn}}\right) \qquad [4\text{-}14]$$

From Eq. [4-14] $\gamma_{s0,bn}$ can be isolated as follows:

$$\gamma_{s0,bn} = \frac{-2.28 \cdot \frac{R_c}{H_{m0}} \cdot \frac{1}{\gamma_{v\_calculated}} \cdot \frac{1}{\gamma_{bn\_calculated}}}{ln\left(\frac{q}{0.2 \cdot \sqrt{g \cdot H_{m0}^3}}\right)} \qquad [4\text{-}15]$$

When this value is plotted against the wave steepness, a descending trendline can be seen in Figure 4-41. This point-by-point analysis leads to a reduction factor $\gamma_{s0,bn}$ as given in Eq. [4-16]:

$$\gamma_{s0,bn} = 1.33 - 10 \cdot s_{m-1,0} \qquad [4\text{-}16]$$

This gamma-factor can become larger than one for low steepness (long waves), which means the overtopping discharge will become higher than for tests with high steepness (short waves). This however does not mean that a bullnose is not reducing. Eq. [4-16] always has to be combined with γ_{bn} and γ_v and the combination has to be below one. γ_{bn} or $\gamma_{s0,bn}$ cannot be used individually.

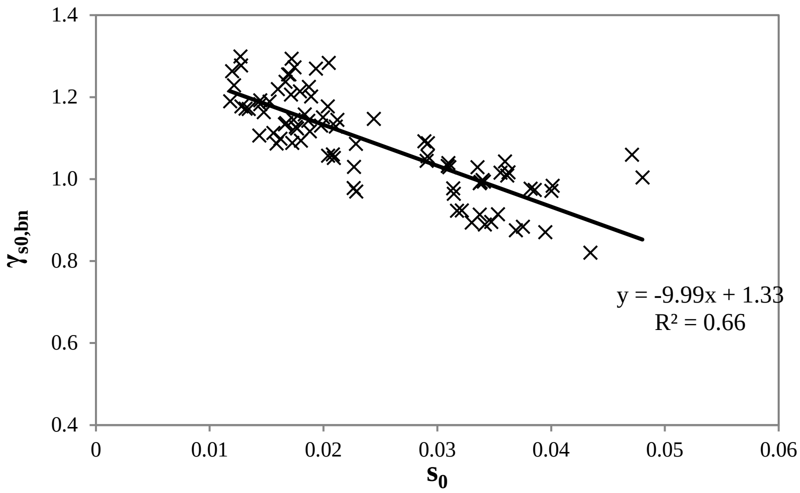

Figure 4-41. Reduction factor $\gamma_{s0,bn}$ to account for the wave period.

Equation [4-14] in combination with Eq. [4-16] for $\gamma_{s0,bn}$, [4-12] or [4-13] for γ_{bn} and [4-4] for $\gamma_{v,}$ have to be used to calculate the overtopping discharge over a dike with a storm wall and bullnose. After introduction of the correction factors γ_v, γ_{bn} and $\gamma_{s0,bn}$ on the horizontal axis, all data points from Figure 4-40 shift well to the average line given by Eq. [4-14]: see Figure 4-42. This means Eq. [4-14] is a good prediction line for the measured overtopping values over a smooth dike with storm wall and bullnose within the parameters listed in Table 3-3. The exponential coefficient $2.28/(\gamma_v \cdot \gamma_{bn} \cdot \gamma_{s0,bn})$ is taken as a normal distributed stochastic variable, with a mean value of 3.62 and a standard deviation σ of 0.65. This gives a relative standard deviation σ' of 0.18, in line with EurOtop findings and other chapters in this research.

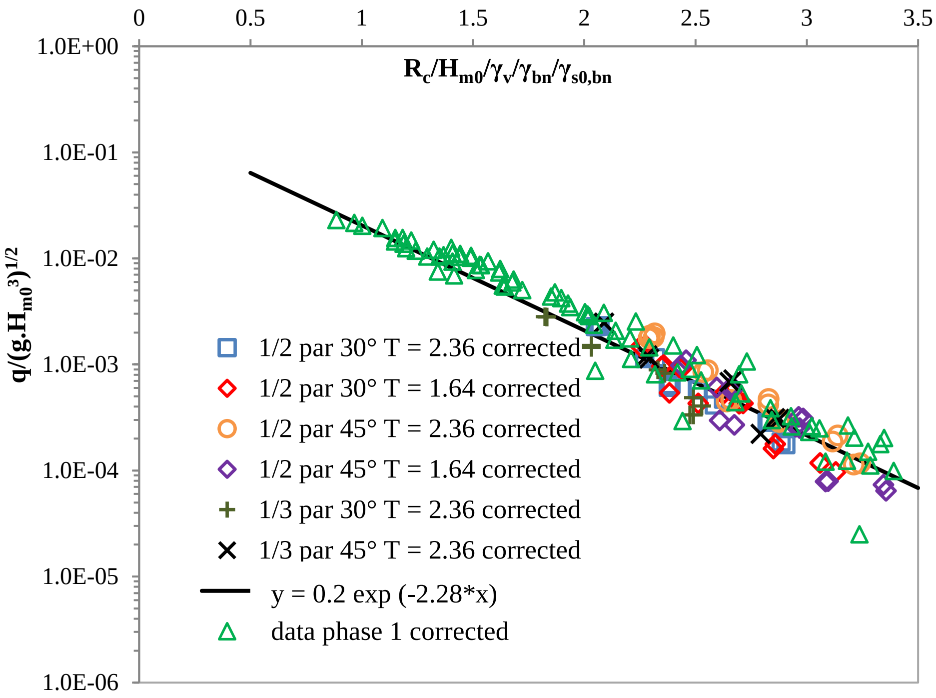

Figure 4-42. Data set on a smooth dike with storm wall and bullnose – corrected values, UGent-1 data set.

4.2.2 *Smooth dike with promenade*

Geometries exist where the dike has a wide promenade at crest level, examples of those can be found along the Belgian coastline but also in harbours of river embankments worldwide. As before, the freeboard R_c is defined as the difference in height between the highest point of the dike and the still water level, including the promenade slope. The geometry was given in Figure 3-6 and is repeated below in Figure 4-43. The test program for this type of wall is summarized in Table 3-4.

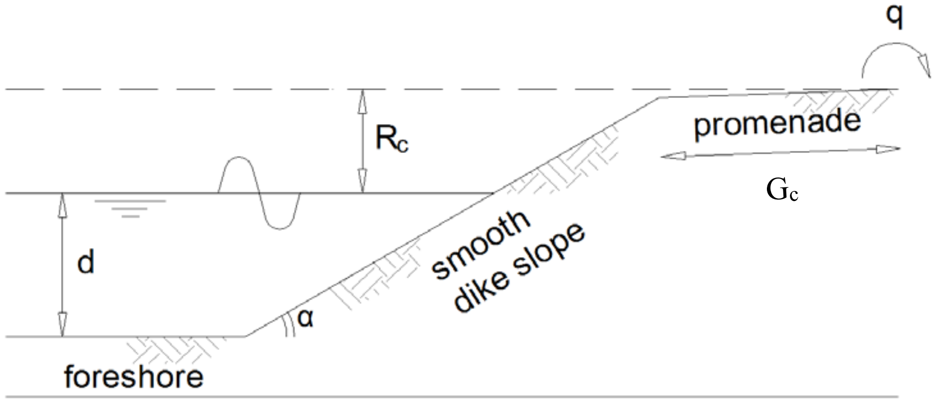

Figure 4-43. Smooth dike with promenade and used parameters.

Figure 4-44 shows in blue the data as measured, where it can be seen that all of them are located a bit below the reference line. Since the data are consistent on the lower side of this confidence band, it shows that a promenade offers a reduction but it's limited since data are still within the 90% confidence band so the reduction is smaller than the uncertainty on the formulae. In this same Figure 4-44, three attempts are made to correct these data according to reduction factors found in literature. In green, Eq. [2-26] based on EurOtop (2007) is tried, although this approach was developed for berms, not for promenades. It can be seen in Figure 4-44 that this approach is overcompensating the data, which means that a berm around the SWL is better reducing the overtopping than a promenade at crest level. The 2nd attempt in Figure 4-44 is shown in red, based on Eq. [2-29] by Tuan (2013) introduced in Eq. [2-31] using freeboard A_c. A third and final attempt is using this same reduction factor Eq. [2-29] by Tuan (2013) but introducing it in Eq. [2-14] using freeboard R_c, this is shown in purple. Also both attempts by using Tuan (2013) (slightly) overcompensate the effect of a promenade and shift the data to above the average trendline.

Since the approaches from literature are not appropriate for the geometry as in Figure 4-43, a new reduction factor is developed here.

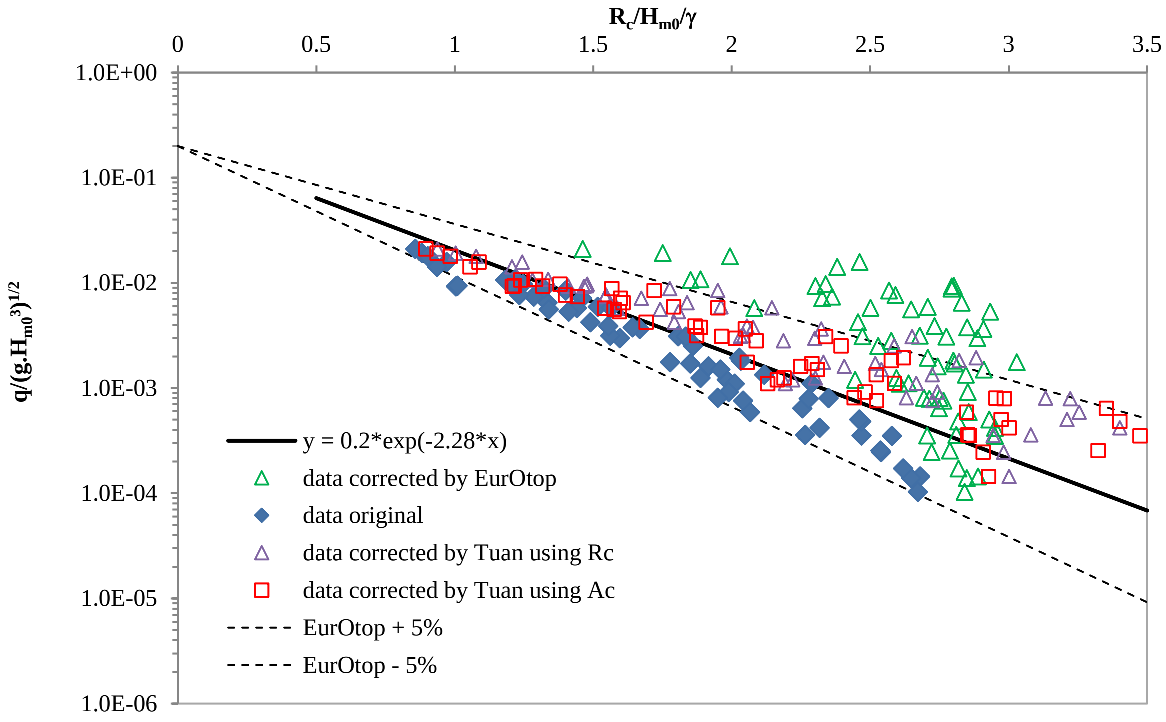

Figure 4-44. Data on a smooth dike with promenade (blue) and corrected by EurOtop (2007) reduction factor for a berm (green).

The blue data were therefore analyzed, with extra attention paid to the wave period and slope angle, see Figure 4-45 for slope angle (left) and wave period (right). Dimensional plots are only for visualization purposes only. If an influence of one of the visualized parameters is found, a dimensionless analysis will be carried out. Similar conclusions as for the reference case (smooth dike) were found:

- Slope angle, Figure 4-45 left: a minor difference in overtopping, where the mildest slope (green data) is overtopped slightly more due to the thicker layer thickness of the incoming wave on milder slopes.
- Wave period, Figure 4-45 right: the largest wave period gives slightly more wave overtopping. When looking at the data even more in detail, there is no influence of the wave period on slope 1:2, and on slope 1:3 there is a minor difference with the most overtopping for large wave periods.

Overall, both influences were not very strong and were therefore not further considered here.

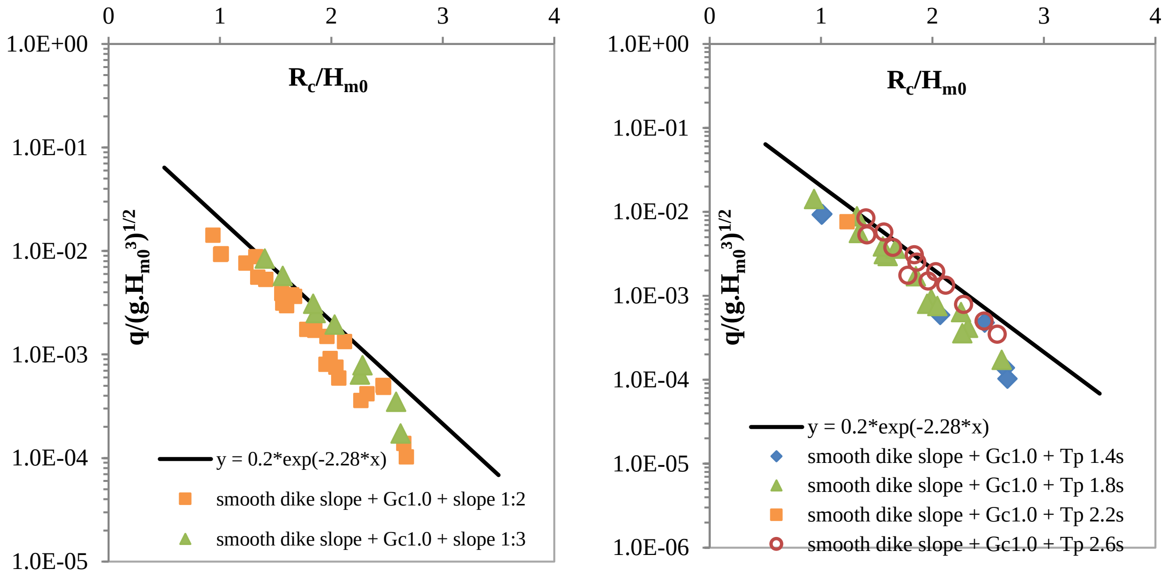

Figure 4-45. Influence of slope angle (left) and wave period (right) on the wave overtopping discharge on smooth dikes with promenade at crest level.

The blue data in Figure 4-44 or the colored data in Figure 4-45 show that the presence of a promenade has a reducing effect on wave overtopping, since data are below the reference line, but not as strong as a storm wall. The effect is slightly increasing with the length G_c of the promenade. This can be evaluated from Figure 4-46. Again, the dimensional plot is only to visualize the effect of the promenade length on a repeated set of tests. A (small) influence can be seen – longer promenades (orange data G_c = 1m) are slightly below the shorter promenades (blue data G_c = 0.33m model scale). This influence is now studied in a dimensionless way.

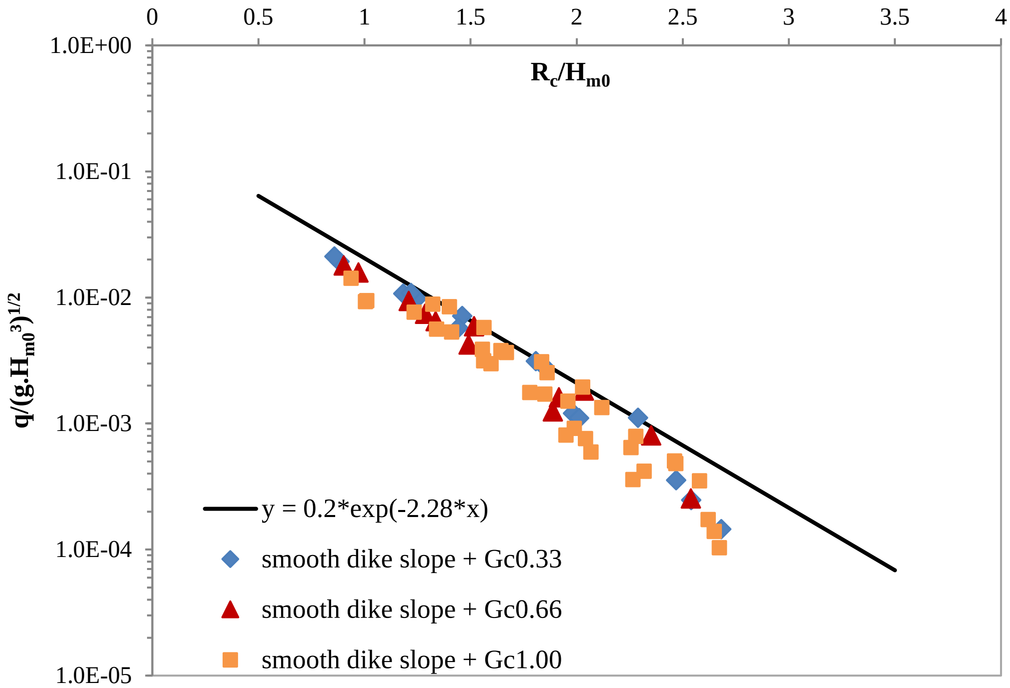

Figure 4-46. Smooth dike with promenade – measured values. Promenade length indicated by Gc in model values.

Similar to the previous sections, a reduction factor for the promenade width is introduced in Eq. [4-17].

$$\frac{q}{\sqrt{g \cdot H_{m0}^3}} = 0.2 \cdot \exp\left(-2.28 \cdot \frac{R_c}{H_{m0}} \cdot \frac{1}{\gamma_{prom}}\right) \qquad [4\text{-}17]$$

By isolating γ_{prom} from Eq. [4-17], its value can be calculated for every data point and plotted against its dominating dimensionless parameter; the dimensionless promenade length, made dimensionless by division through the deep water wave length. Other parameters have been studied, but were less satisfying, see Audenaert & Duquet (2012).

The trendline through the data gives the reduction factor for the influence of a promenade at crest level of the dike.

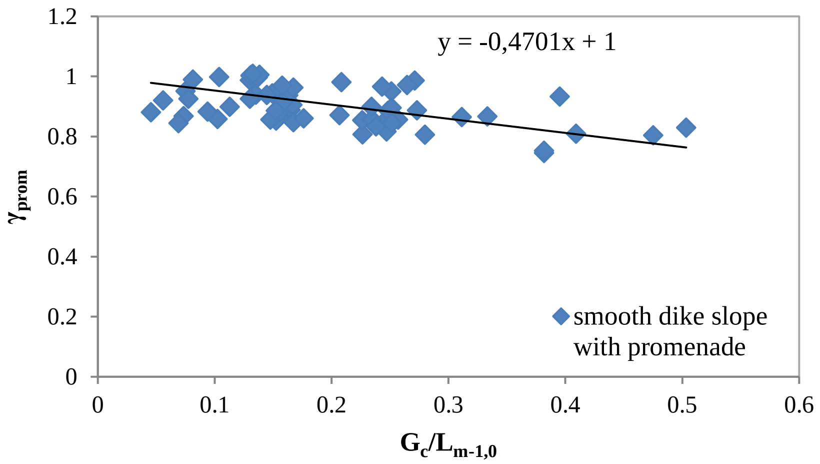

Figure 4-47. Reduction factor for the promenade length on the overtopping discharge.

$$\gamma_{prom} = 1 - 0.47 \cdot \frac{G_c}{L_{m-1,0}} \qquad [4\text{-}18]$$

In Figure 4-48 the data from Figure 4-46 are corrected by means of Eq. [4-17] and Eq. [4-18]. All points are now closer to the reference line with little scatter and all within the 90% confidence bands. This proves that Eq. [4-18] describes the overtopping reduction accurately. The exponential coefficient $2.28/\gamma_{prom}$ is taken as a normally distributed stochastic variable and has a mean value of 2.55 with a standard deviation $\sigma = 0.19$, resulting in a relative standard deviation σ’ of 0.07.

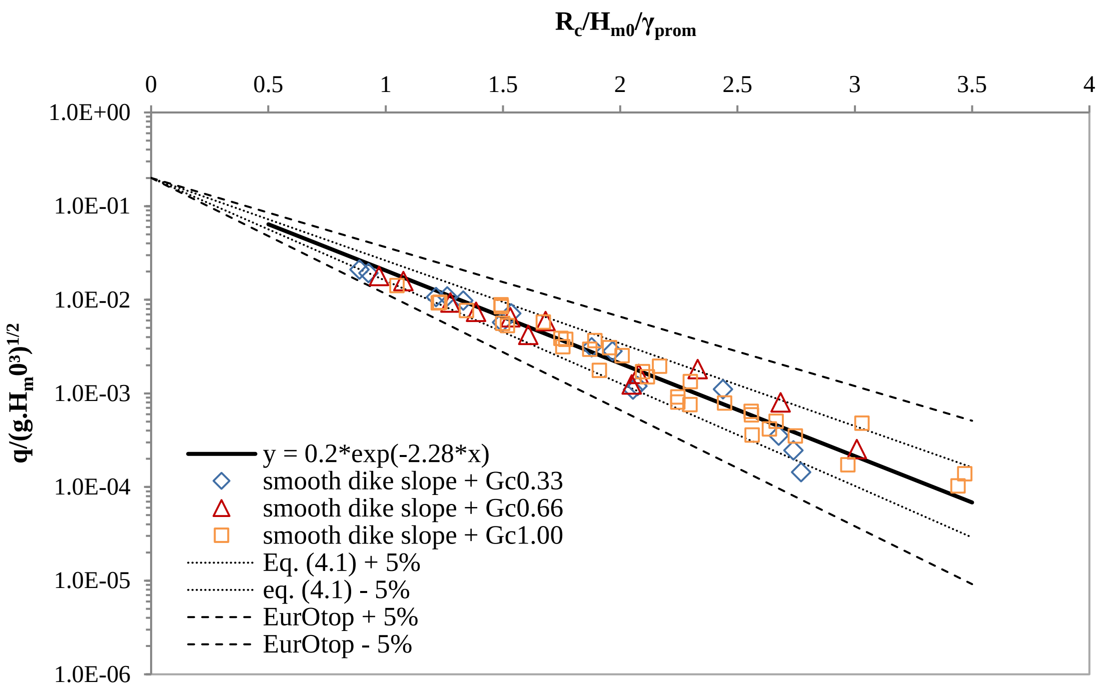

Figure 4-48. Smooth dike with promenade- corrected values.

4.2.3 *Smooth dike with promenade and storm wall*

In Eq. [2-30] it is suggested that the reduction factors of a wall and a promenade can be multiplied with each other to account for their combined influence. However, that statement is from Tuan (2013) who always investigated the combined geometry promenade/crest with storm wall, and never the independent influence like was done in the previous sections. The physical process of a wave hitting a wall might be different when a promenade is present in between the top of the dike and the wall. For this reason, 136 model tests were performed on geometries with both a promenade and a wall. The geometry was presented in Figure 3-7 and repeated below in Figure 4-49. The test program consisted of 136 tests and was summarized in Table 3-5. Remind that $R_c = A_c + G_c \cdot \tan(\text{promenade}) + h_{wall}$.

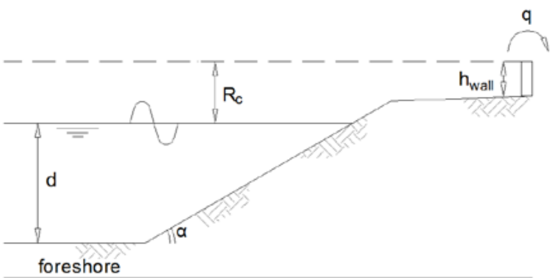

Figure 4-49. Sketch of a smooth dike with a promenade and a storm wall.

Results are plotted in Figure 4-50 for all combinations of geometric variation (wall heights, promenade widths, slope angles) and sea state parameters (water level, wave period, wave height). The use of a promenade with a storm wall clearly leads to small wave overtopping discharges, which makes this geometry a very efficient measure to reduce wave overtopping.

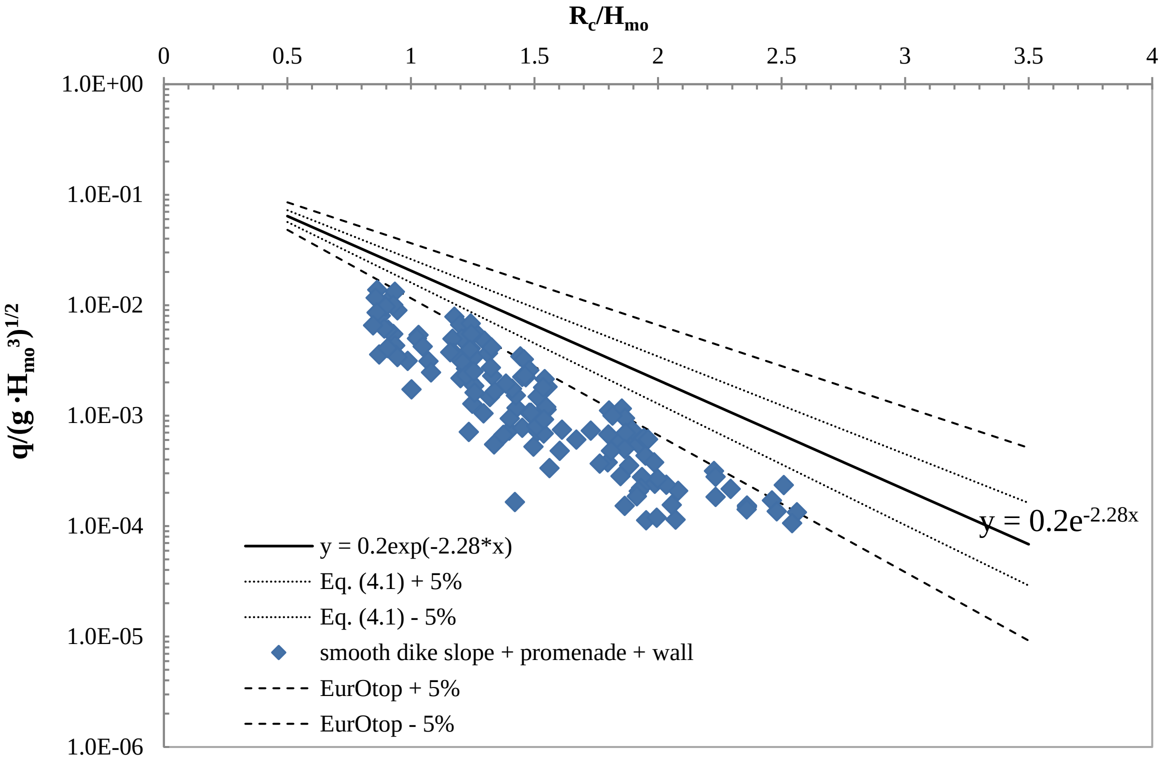

Figure 4-50. Reduction due to a promenade and storm wall.

A first attempt to better describe these data is by using Eq. [2-30] and [2-31] by Tuan (2013). This is done in Figure 4-51 in the green data and does not work well. When using Eq. [2-30] in Eq. [2-14] by using R_c instead of A_c the red data show. A better approach, but still not fully satisfying. New analysis on the blue data is carried out to have a better prediction for wave overtopping on smooth dikes with a promenade and a wall.

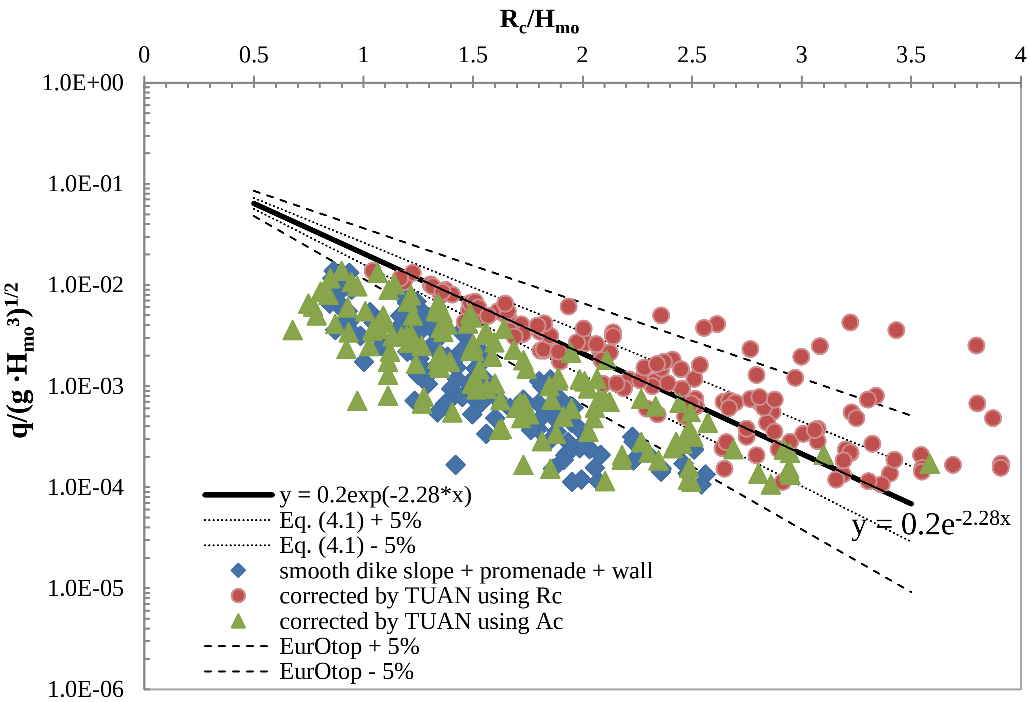

Figure 4-51. Correction of the data by introducing Eq. [2-30] by Tuan (2013) on the horizontal axis.

Data analysis has shown that there is again no clear influence of the wave period or the slope angle noticed. General findings for all data are given here, an example case for one geometry (G_c = 1m and h_{wall} = 8cm model values) is given in Figure 4-52:

- Slope angle: mildest slope 1:3 is slightly more overtopped compared to 1:2, due to the thicker water layer. The influence is however too weak to be included in the reduction factors.
- Wave period: for both slopes, there was just a little more overtopping measured for the longest wave periods. This is due to the larger layer thickness of the water on the promenade as a consequence of the larger volume of water under the crest of longer waves. Also here, the influence will not be included in the reduction factors since the difference in overtopping measured was too small.

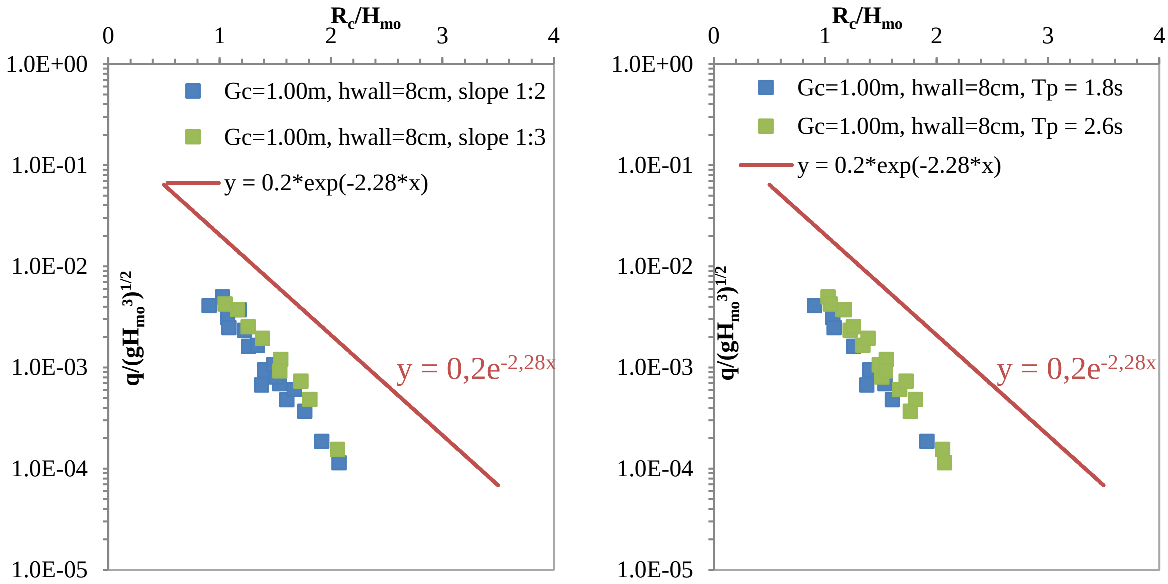

Figure 4-52. Influence of slope angle (left) and wave period (right) on the wave overtopping discharge on smooth dikes with promenade at crest level and a storm wall at its end. Example case for G_c = 1m and h_{wall} = 8cm.

In a first attempt to account for the reducing effect by a promenade and a storm wall, the combination of both individual reduction factors γ_{prom} and γ_v are included in the horizontal axis of Figure 4-50. This is shown in Figure 4-53. The data are shifted closer to the trendline of the reference case, however not yet enough. The reducing effect of the combination of a wall and a promenade is stronger than the multiplication of both influences separately.

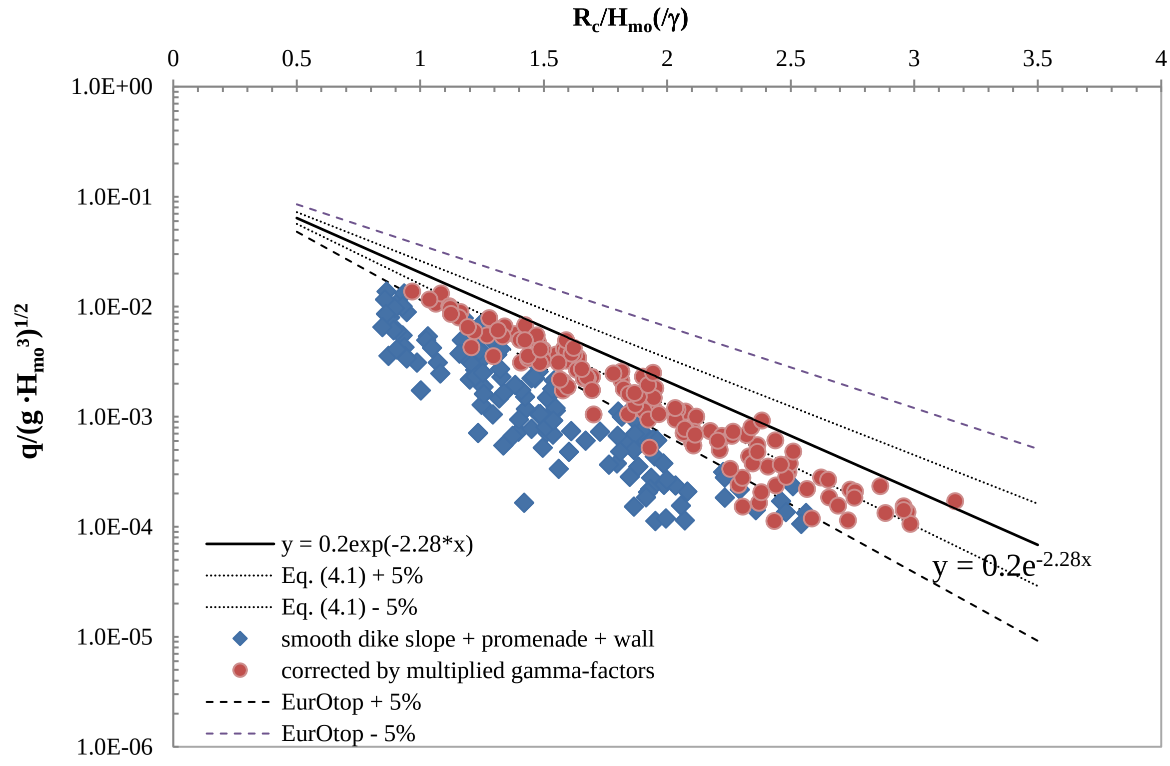

Figure 4-53. Smooth dike with promenade and storm wall– original (blue) and corrected values with the multiplication of the 2 individual reduction factors γ_{prom} and γ_v (red).

A new parameter is introduced: γ_{prom_v}.

$$\frac{q}{\sqrt{g \cdot H_{m0}^3}} = 0.2 \cdot \exp\left(-2.28 \cdot \frac{R_c}{H_{m0}} \cdot \frac{1}{\gamma_{prom\_v}}\right) \qquad [4\text{-}19]$$

From isolation from Eq. [4-19], γ_{prom_v} can be calculated for each data point and plotted against the calculation of $\gamma_{prom} \times \gamma_v$ (Eq. [4-18] × Eq. [4-4]), see Figure 4-54. As expected from Figure 4-53, γ_{prom_v} is smaller than $\gamma_{prom} \times \gamma_v$.

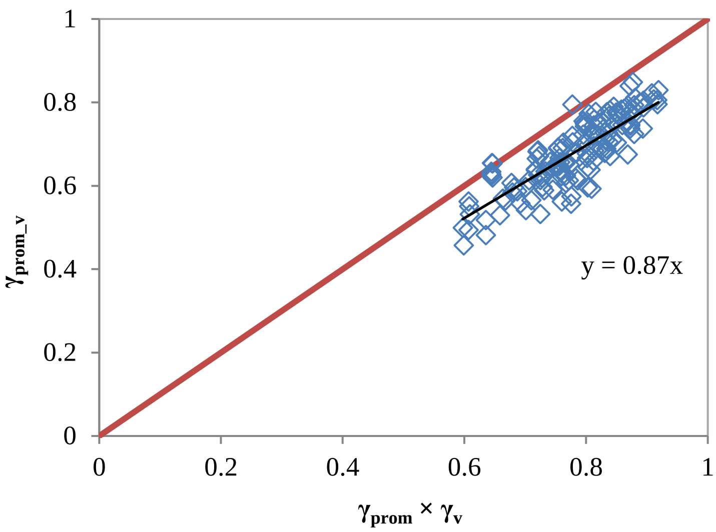

Figure 4-54. Deduction of γ_{prom_v} as a function of γ_{prom} and γ_v

The trendline defines the reduction factor as a function of γ_{prom} and γ_v

$$\gamma_{prom\_v} = 0.87 \cdot \gamma_{prom} \cdot \gamma_v \tag{4-20}$$

with γ_{prom} as defined in Eq. [4-18] and γ_v in Eq. [4-4]. Note that this formula Eq. [4-19] is only usable when both a promenade and a storm wall are present. When one of both is missing, Eq. [4-17] (promenade) or Eq. [4-2] (wall) should be used.

In Figure 4-55 the blue values are corrected by means of Eq. [4-20], which leads to a high correlation to the trend line meaning that a good prediction is obtained. The exponential coefficient $2.28/\gamma_{prom\_v}$ has a mean value of 3.42 with a standard deviation $\sigma = 0.46$, resulting in a relative standard deviation $\sigma' = 0.13$.

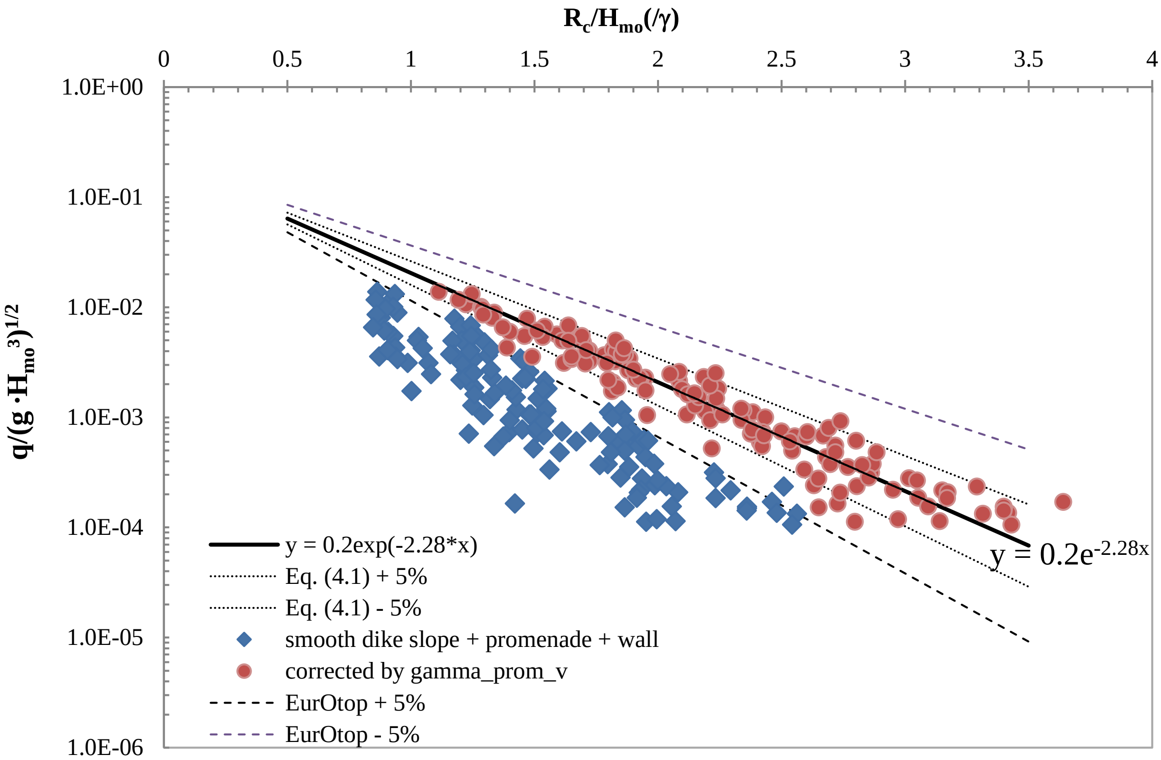

Figure 4-55. Smooth dike with promenade and storm wall– original (blue) and corrected values with factor γ_{prom_v} (red).

This section has shown that reduction factors can not always be multiplied with each other, when they were developed for individual influences that, when combined, can have other physical behavior. The reason why Tuan (2013) a simple multiplication did work was that both promenade and wall height had always been tested together. In this PhD manuscript the original promenade and wall height influence were studied separately.

4.2.4 *Smooth dike with promenade, storm wall and bullnose*

Even though the combination of a promenade and a vertical wall is already a very efficient measure, wave overtopping can be further reduced without increasing the height of the wall by adding a bullnose to the wall. This combined effect has been investigated by means of 100 tests with geometric variation (wall height, bullnose angles, bullnose height ratios, promenade width and slope angle) and varying sea state parameters (water level, wave height, wave period). A sketch of this geometry is given in Figure 3-8 and repeated below in Figure 4-56. The test program was already summarized in Table 3-6.

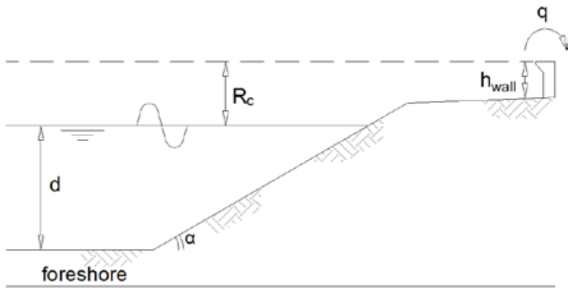

Figure 4-56. Sketch of a smooth dike with promenade, storm wall and bullnose.

Results are plotted in Figure 4-57. As expected, the data are clearly below the reference line of a smooth dike.

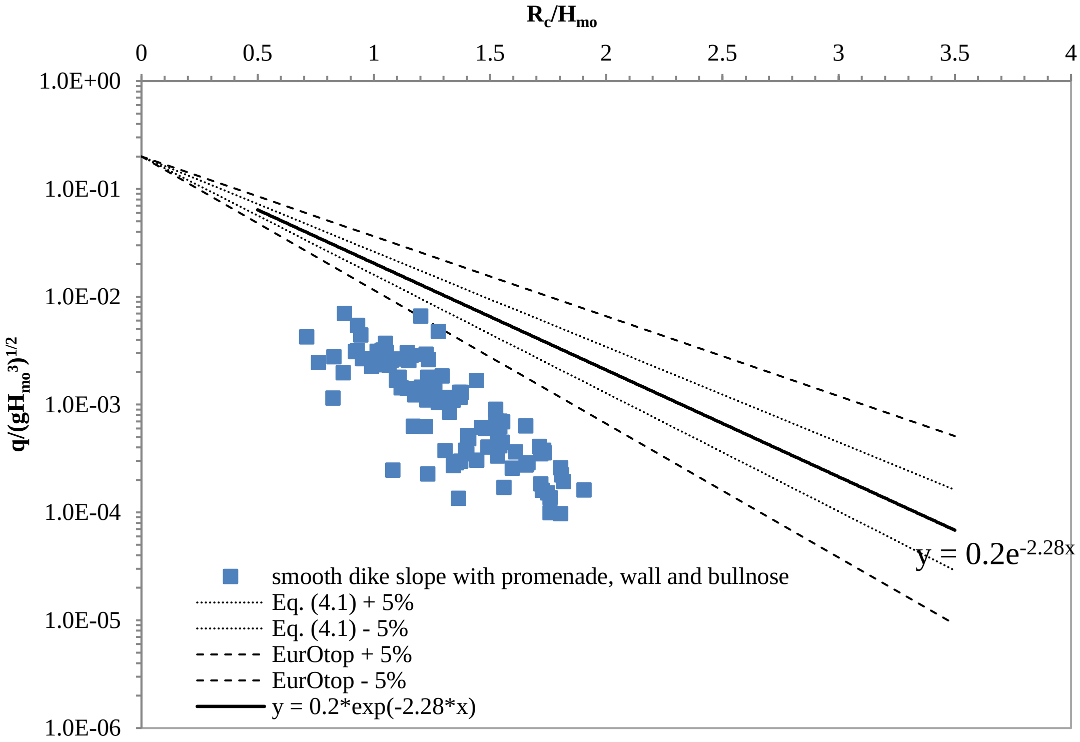

Figure 4-57. Reduction due to a promenade with storm wall and bullnose, UGent-1 data set.

Similar as for the other data, the influence of the wave period and slope angle seems rather weak. General findings for all data are given here, an example plot for one geometry (G_c = 1m and h_{wall} = 8cm) is shown in Figure 4-58:

- Slope angle (Figure 4-58 left): the mildest slope 1:3 is slightly more overtopped compared to 1:2, due to the thicker water layer. The influence is however too weak to include in the reduction factors.
- Wave period (Figure 4-58 right): for both slopes, there was just a little more overtopping measured for the longest wave periods. This is due to the larger layer thickness of the water on the promenade as a consequence of the larger volume of water under the crest of longer waves. The difference between the tests with the longer and shorter wave period are of the same order of magnitude as for the previous geometry (promenade + storm wall without bullnose); the bullnose does not increase this difference, unlike for the geometry with the storm wall with bullnose directly at the end of the slope. The promenade filters out this dependency.

  Therefore, the hydrodynamic behavior on this type of dike with promenade, storm wall and bullnose are different than for sloping structures, and result in wave overtopping which is not strongly dependent on the wave period. The storm wall with bullnose at the end of the promenade reflects the incoming water layer equally for long as for short waves with only very little difference due to the larger layer thickness on the promenade of long waves overtopping the dike. This is similar to the geometry dike with promenade and storm wall.

  The influence $\gamma_{s0,bn}$ will not be included for the current geometry, unlike for the geometry dike with storm wall and bullnose.

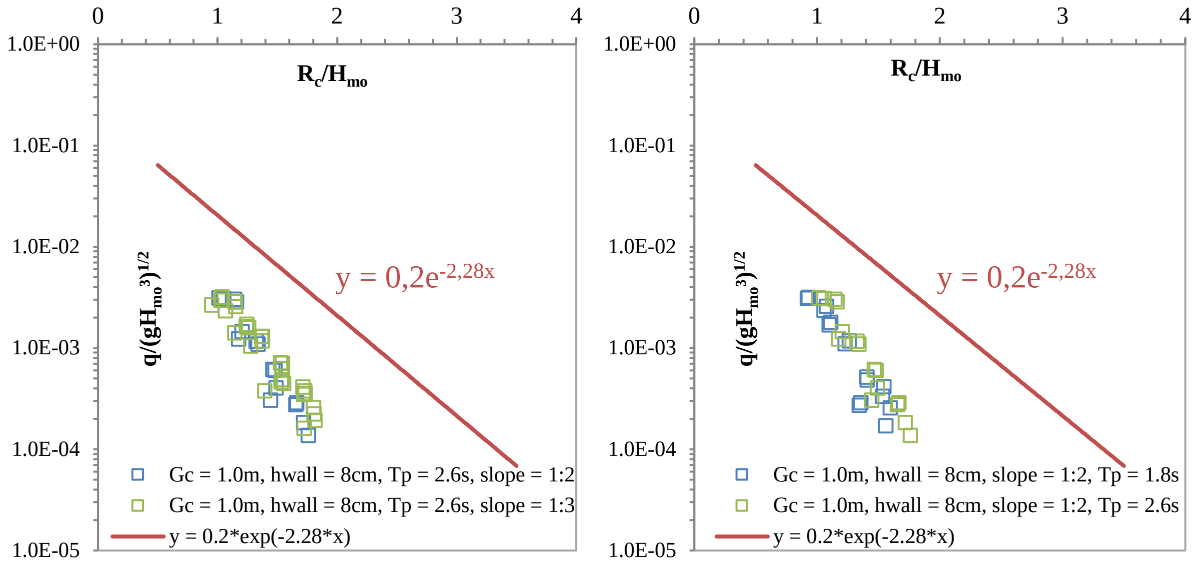

Figure 4-58. Influence of slope angle (left) and wave period (right) on the wave overtopping discharge on smooth dikes with promenade at crest level and a storm wall with bullnose at its end. Example case for G_c = 1m and h_{wall} = 8cm.

The data are corrected by introducing the existing reduction factors for promenade and wall (γ_{prom_v}) and bullnose (γ_{bn}) on the horizontal axis, see Figure 4-59. It can be seen, that the data are overcorrected; the effect of $\gamma_{prom\_v} \times \gamma_{bn}$ is too strong. Adding a bullnose to the wall still increases the reducing effect, although it is not as effective as for a storm wall located more seaward at the end of the slope. In such a situation, the wall and bullnose take benefit of the upward motion of the water tongue, whereas when the storm wall with bullnose is located at the end of a promenade the water tongue has a more horizontal motion. Adding a bullnose to the wall has therefore less effect compared to its seaward position.

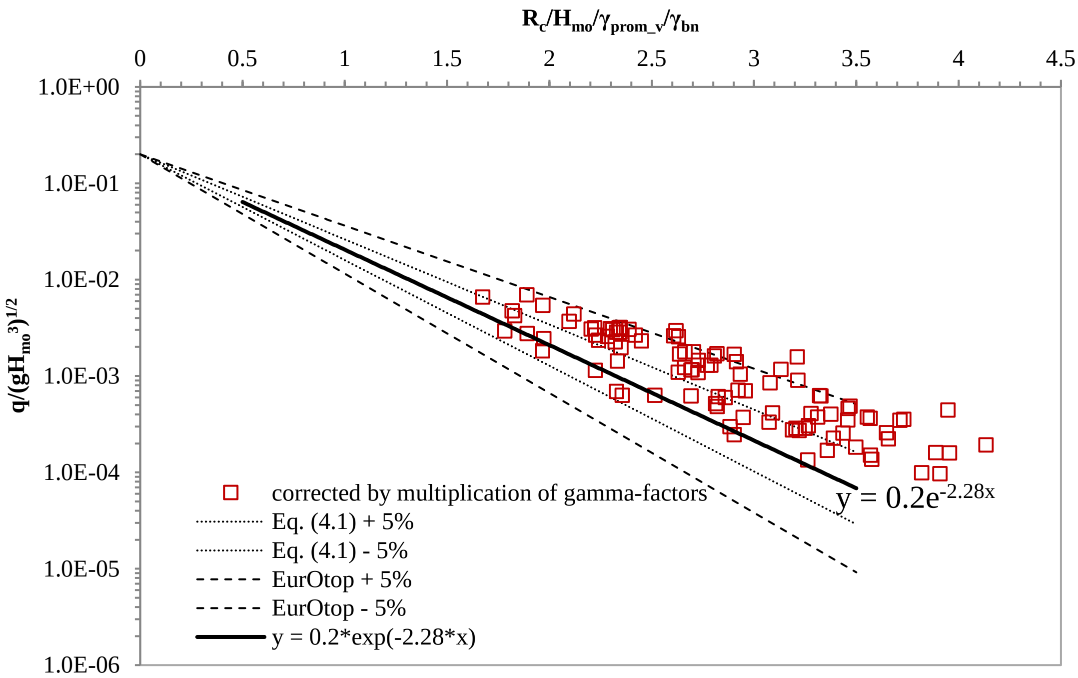

Figure 4-59. Correction of the data by introducing γ_{prom_v} and γ_{bn} on the horizontal axis.

As shown in Figure 4-59, the multiplication of γ_{prom_v} and γ_{bn} overestimates the actual reduction in wave overtopping. A new factor $\gamma_{prom\_v\_bn}$ is introduced, see Eq. [4-21].

$$\frac{q}{\sqrt{g \cdot H_{m0}^3}} = 0.2 \cdot \exp\left(-2.28 \cdot \frac{R_c}{H_{m0}} \cdot \frac{1}{\gamma_{prom\_v\_bn}}\right) \qquad [4\text{-}21]$$

This factor $\gamma_{prom\_v\_bn}$ can be calculated for every data point by isolation from Eq. [4-21], and plotted against the multiplication of Eq. [4-20] and [4-12] or [4-12]: $\gamma_{prom\_v} \times \gamma_{bn}$. The result is given in Figure 4-60.

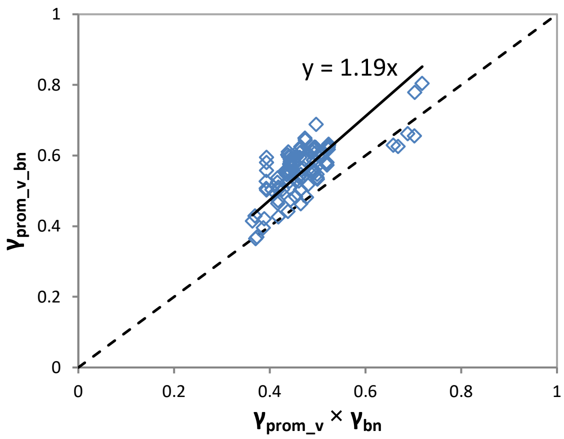

Figure 4-60. Deduction of $\gamma_{prom\_v\_bn}$ as a function of γ_{prom_v} and γ_{bn}.

As expected, $\gamma_{prom\_v\_bn} > \gamma_{prom\_v} \times \gamma_{bn}$ since the latter was too low (overestimating the real reduction). This does not mean that adding the bullnose to the storm wall will not further reduce the overtopping discharges; it only means that the new parameter $\gamma_{prom\_v\_bn}$ is not as effective as the multiplication of γ_{prom_v} and γ_{bn}. A wall with bullnose functions best directly on a slope, since it takes benefit of the upward motion of the water to reflect it back towards the sea. The following reduction factor can be concluded from Figure 4-60:

$$\gamma_{prom\_v\_bn} = 1.19 \cdot \gamma_{prom\_v} \cdot \gamma_{bn} \qquad [4\text{-}22]$$

Combining Eq. [4-22] with Eq. [4-20], the reduction factor can also be calculated as:

$$\gamma_{prom\_v\_bn} = 1.03 \cdot \gamma_{prom} \cdot \gamma_{v} \cdot \gamma_{bn} \qquad [4\text{-}23]$$

The underestimation of $\gamma_{prom\_v} \times \gamma_{bn}$ almost neutralizes the overestimation of $\gamma_{prom} \times \gamma_{v}$, and the final reduction factor $\gamma_{prom\_v\_bn}$ seems to be 3% less efficient than the product of all individual measures. This seems to be a coincidence. The advise still is that **reduction factors cannot be just multiplied with each other without detailed study**, especially **in situations** like these **where the physical behavior changes** from a wave overtopping a structure, to an overtopping bore on the promenade overtopping a storm wall.

When one or more of the above parts are missing in the geometry, like no bullnose or no promenade, Eq. [4-22] or Eq. [4-23] cannot be used. The user should then use the correct geometry as mentioned in earlier sections in this work.

In Figure 4-61 the blue values are corrected by means of Eq. [4-22] or Eq. [4-23] introduced in the horizontal axis from Figure 4-57. As can be seen, a good prediction is obtained. The exponential coefficient $2.28/\gamma_{prom\_v\_bn}$ is taken as a normally distributed variable, and has a mean value of 4.13 with a standard deviation of 0.59. The relative standard deviation is then 0.14.

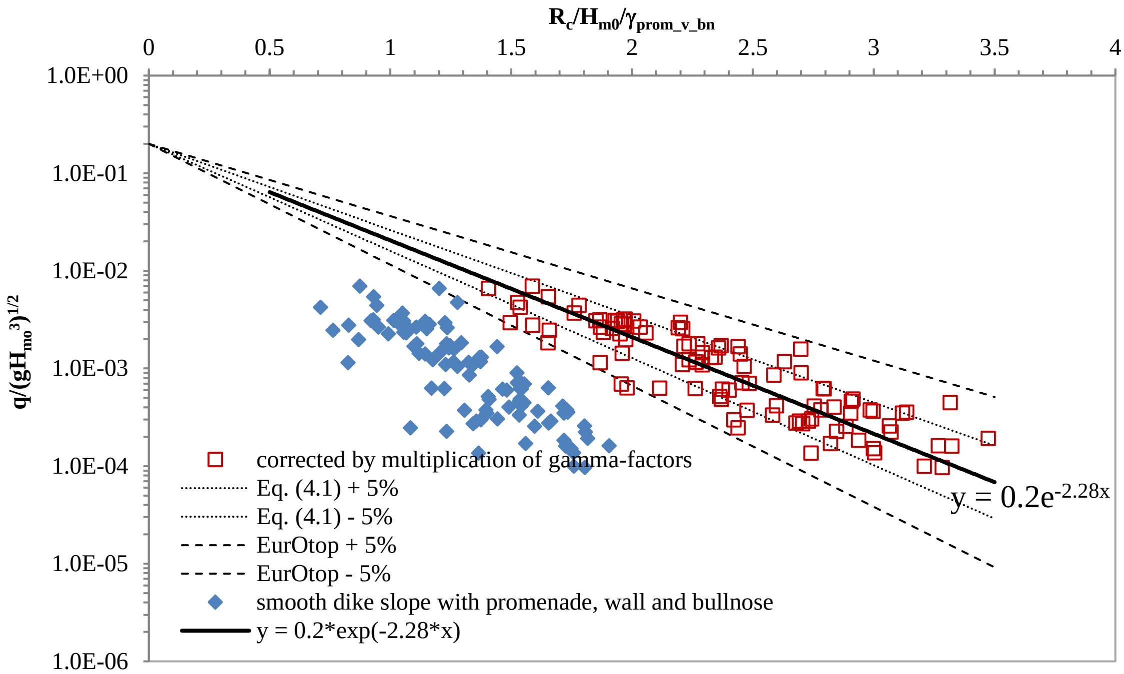

Figure 4-61. Smooth dike with promenade, storm wall and bullnose – original (blue) and corrected values (red).

4.2.5 *Stilling Wave Basin (SWB)*

A last measure proposed in this manuscript to reduce wave overtopping by modifying the existing crest of dikes, is the so-called Stilling Wave Basin (Beels (2005) and Geeraerts et al. (2006)). The construction is described in Figure 3-9 to Figure 3-11 and repeated below in Figure 4-62. The test program was provided in Table 3-7.

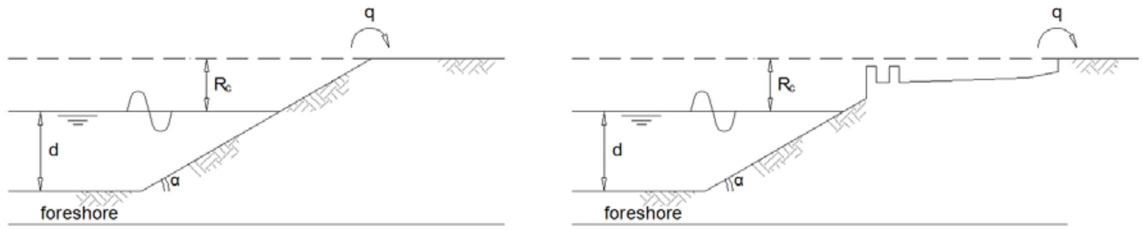

Figure 4-62. Simple smooth dike (left) compared to a dike with SWB built in the crest (right).

The analysis of the data lead to the following conclusions:

- The blocking coefficient, which is the ratio between the open and the closed part of each row of shifted walls, has an important influence on the wave overtopping over the landward wall. An optimum between inflow (as low as possible) and outflow (as high as possible) was a subject of the study. A blocking coefficient of 50% for the most seaward wall, and 65% of the 2nd row wall has been found optimal. To avoid that the wave flows directly into the basin, 20% of each wall part of the first row overlaps with a wall part from the second row. To encourage the drainage back towards the sea, the basin has been given a 2% slope.

- The two separate overlapping walls may be replaced by one wall with small gaps just above the floor of the basin. This has also been constructed in the city of Ostend (Belgium), where the engineered and architectural design go hand in hand (Figure 4-63).
- The height of the front wall and the length of the basin have been studied. While the effect of γ_{prom} is smaller than the effect of γ_v (see section 4.2.2), a similar conclusion can be drawn for the SWB: the variation of height of the front wall is dominant, while the effect of the basin's length is present but less pronounced.
- The slope angle and the wave period have a minor influence on the reduction in wave overtopping. As for the vertical wall (γ_v) and promenade above SWL (γ_{prom}), both influences are not strong enough to be included in the formula of the reduction coefficient.

Since so many variations in the geometry of the SWB are possible, one uniform reduction formula as a function of the dominant geometrical variable could not be determined. The blocking coefficient, the distance in between the double row walls, the slope near the landward wall, the length of the basin and the height of the front wall all have their influence on the reduction of wave overtopping. The basic geometry (L_{basin} = 48cm, $h_{front\ wall}$ = 96mm) with the optimal blocking coefficient of 50% (1st row) and 65% (2nd row) has been tested in full detail. A reduction factor of 0.48 is found for this specific geometry, and can be used to quantify wave overtopping over a dike with SWB. In case a specific geometry is required, it is suggested to determine the reduction capacity by means of scale model tests.

$$\frac{q}{\sqrt{g \cdot H_{m0}^3}} = 0.2 \cdot \exp\left(-2.28 \cdot \frac{R_c}{H_{m0}} \cdot \frac{1}{\gamma_{SWB}}\right) \qquad [4\text{-}24]$$

$$\gamma_{SWB} = 0.48 \text{ (for the selected geometry)} \qquad [4\text{-}25]$$

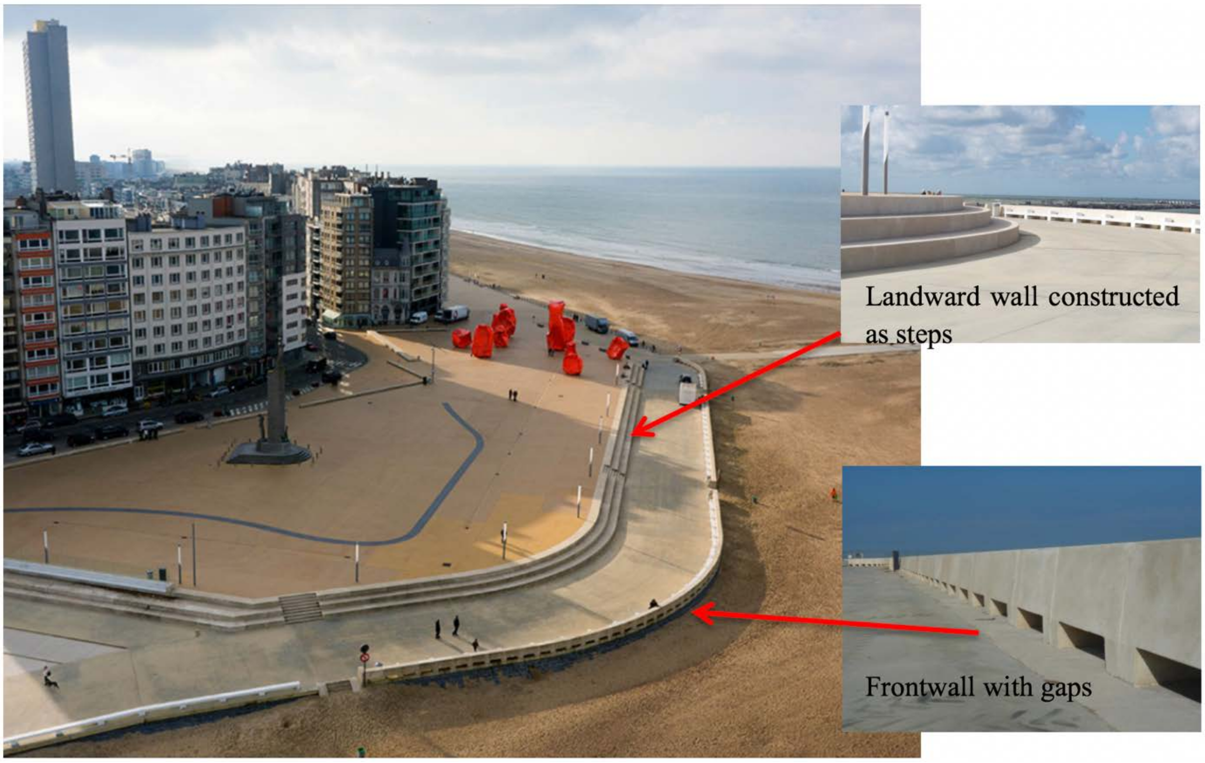

Figure 4-63. Stilling wave basin as constructed in the city of Ostend. Picture taken during low tide ©airmaniacs.be.

4.3 *Case study*

The previous sections 4.1 and 4.2 explained the overtopping reducing capacity and gave design formulae for the different geometries. For non-breaking waves, a reference table of the reduction factors is given in Table 4-1.

Table 4-1. Overview of the reduction factors in the UGent-1 database, for NON-BREAKING waves.

Smooth dike with storm wall	γ_v	$f(h_{wall}/R_c)$	Eq. [4-4]
Smooth dike with storm wall and bullnose	$\gamma_v \cdot \gamma_{bn} \cdot \gamma_{s0,bn}$	$f(h_{wall}/R_c, \varepsilon, \lambda, s_{m-1,0})$	Eqs. [4-4], [4-7], [4-8], [4-9], [4-10], [4-12], [4-13], [4-16]
Smooth dike with promenade	γ_{prom}	$f(G_c/L_{m-1,0})$	Eq. [4-18]
Smooth dike with promenade and storm wall	γ_{prom_v}	$f(h_{wall}/R_c, G_c/L_{m-1,0})$	Eq. [4-20]
Smooth dike with promenade, storm wall and bullnose	$\gamma_{prom\_v\_bn}$	$f(h_{wall}/R_c, G_c/L_{m-1,0}, \varepsilon, \lambda, s_{m-1,0})$	Eq. [4-22] or [4-23]
Smooth dike with SWB	γ_{SWB}	Geometry specific	Eq. [4-25]

It's important to note that the coefficients from Table 4-1 are only valid for the geometries and the parameter ranges that belong to the tests on those geometries. More information on the geometry and parameter range can be found in Chapter 3.

It's not straightforward to conclude which of the presented geometries is best in reducing wave overtopping. The overtopping reducing effect of each measure is dependent on the hydraulic boundary conditions and the geometry of the structure. For example, a promenade above the SWL will reduce the small overtopping volumes (large R_c/H_{m0}) better than the large overtopping volumes (small R_c/H_{m0}). Large overtopping volumes are best reduced by a storm wall with bullnose, or by a combination of a promenade and a storm wall (with/with bullnose), or by an SWB. The SWB combines the effect of a promenade and a storm wall, but is capable of reducing the incoming energy even further by means of the double row of front walls and a spilling basin. This reflects in the low reduction coefficient γ_{SWB} = 0.48 for the presented geometry.

An example is worked out below to demonstrate the overtopping reducing capacity for all proposed measures under 3 different wave heights. The other parameters, such as R_c, $T_{m-1,0}$ and $\cot(\alpha)$ remain the same throughout the whole example. As was explained in section 2.1, the reduction factors have been developed based on the EurOtop (2007) shape (Eq. [2-18]) with coefficients analyzed from own data (Eq. [4-2]), but can be used in the EurOtop (2016) shape (Eq. [2-19]).

Based on the **probabilistic design approach** according to EurOtop (2016), the basic formula to calculate wave overtopping discharge over a smooth dike for **non-breaking waves** is

$$\frac{q}{\sqrt{g \cdot H_{m0}^3}} = 0.09 \cdot exp\left[-\left(1.5 \cdot \frac{R_C}{H_{m0}} \cdot \frac{1}{\gamma^*}\right)^{1.3}\right] \qquad [2\text{-}17]$$

with γ^* the reduction factor for the different geometries.

For the coefficients in Eq. [2-17] and for all reduction measures further on in this case study, the standard deviations deducted in this paper are not included. It is up to the reader to decide which safety level is required.

Table 4-2. Overtopping over a smooth dike.

Cot(α)		2		
SWL	mTAW	7.00		
crest level	mTAW	9.00		
R_c	m	2.00		
$T_{m-1,0}$	s	8.2		
H_{m0}	m	2.00	1.33	1.00
R_c/H_{m0}	-	1.00	1.50	2.00
q	l/m/s	146.5	24.6	4.4

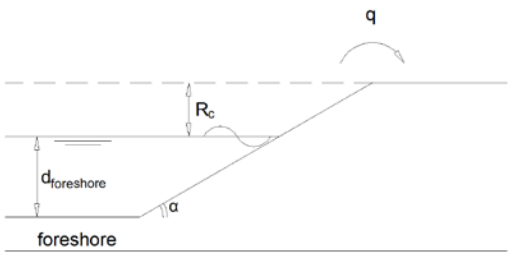

Wave overtopping over a smooth dike with crest level at +9.00mTAW and water level at +7.00mTAW is calculated by means of Eq. [2-17] with $\gamma^* = 1$. A mean overtopping discharge of 146.5, 24.6, and 4.4 l/m/s, respectively, is found for a storm with H_{m0} = 2.0m, 1.33m, and 1.0 m, respectively, at the sketched smooth dike.

When a storm wall of 1.25m height is added to the slope of the dike, γ^* in Eq. [2-17] accounts for the storm wall γ_v. The formula now becomes

$$\frac{q}{\sqrt{g \cdot H_{m0}^3}} = 0.09 \cdot exp\left[-\left(1.5 \cdot \frac{R_C}{H_{m0}} \cdot \frac{1}{\gamma_v}\right)^{1.3}\right] \qquad [4\text{-}26]$$

with γ_v calculated using Eq. [4-2]. By placing the storm wall in the dike, the freeboard R_c remains the same as in Table 4-2. The mean overtopping discharges reduce to 55.21, 4.7 and 0.39 l/m/s, respectively which is 2.65, 5.22 or 11.2 times less than without the storm wall and the same crest freeboard.

Table 4-3. Overtopping over a smooth dike with storm wall.

Smooth dike with storm wall **h_{wall} = 1.25m; h_{wall}/R_c = 0.625**				
H_{m0}	m	2.00	1.33	1.00
γ_v	-	0.705	0.705	0.705
q	l/m/s	55.2	4.7	0.39
Ratio to smooth dike	-	2.65	5.22	11.2

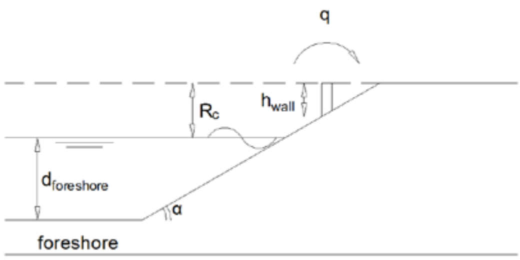

Further, a bullnose is added to the same storm wall with ε = 45° and λ = 1/3. Again, no change in crest freeboard R_c. The average discharge can be calculated by means of Eq. [4-27].

$$\frac{q}{\sqrt{g \cdot H_{m0}^3}} = 0.09 \cdot exp\left[-\left(1.5 \cdot \frac{R_C}{H_{m0}} \cdot \frac{1}{\gamma_v \cdot \gamma_{bn} \cdot \gamma_{s0,bn}}\right)^{1.3}\right] \qquad [4\text{-}27]$$

With γ_v calculated using Eq. [4-4], γ_{bn} using Eq. [4-12] and $\gamma_{s0,bn}$ using Eq. [4-16]. A reduction ratio of 6.3, 14.8 or 38.5 is achieved in comparison to a smooth dike under the same hydraulic conditions. The effect of a bullnose is most prominent for larger dimensionless freeboards, which was also concluded by Kortenhaus et al. (2001) in the SPP-project. Reductions up to a factor of 10 and higher are possible, just like the study by Kortenhaus et al. (2003) and Pearson et al. (2004).

Table 4-4. Overtopping over a smooth dike with a storm wall and a bullnose.

Smooth dike with storm wall and bullnose **h_{wall} = 1.25m; h_{wall}/R_c = 0.625** **bullnose ε = 45°, λ = 1/3**				
H_{m0}	m	2.00	1.33	1.00
$\gamma_v * \gamma_{bn} * \gamma_{s0,bn}$	-	0.521	0.569	0.617
q	l/m/s	23.4	1.7	0.11
Ratio to smooth dike	-	6.3	14.8	38.5

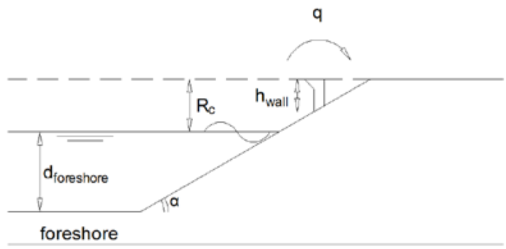

When a promenade at crest level is taken into account, it is explained in Section 4.2.2 to include a reduction factor γ_{prom} in the exponential part of the formula, which now becomes

$$\frac{q}{\sqrt{g \cdot H_{m0}^3}} = 0.09 \cdot exp\left[-\left(1.5 \cdot \frac{R_C}{H_{m0}} \cdot \frac{1}{\gamma_{prom}}\right)^{1.3}\right] \qquad [4\text{-}28]$$

γ_{prom} is calculated by using Eq. [4-18]. The promenade in this case study is 15m wide and has a 1% slope, leading to an increased crest height of +9.15mTAW. To maintain the freeboard R_c constant at 2m (for direct comparison), the water level in this (theoretical) case study is also increased by 15cm.

The table below shows the reduced mean overtopping discharges. The effect of a promenade is much lower than the effect of other measures. Nevertheless, the overtopping is reduced by a factor of 1.2, 1.3, and 1.5, respectively.

Table 4-5. Overtopping over a smooth dike with promenade.

Smooth dike with promenade **Promenade width = 20m, slope 2%**				
H_{m0}	m	2.00	1.33	1.00
γ_{prom}	-	0.93	0.93	0.93
q	l/m/s	124.7	18.7	2.9
Ratio to smooth dike	-	1.2	1.3	1.5

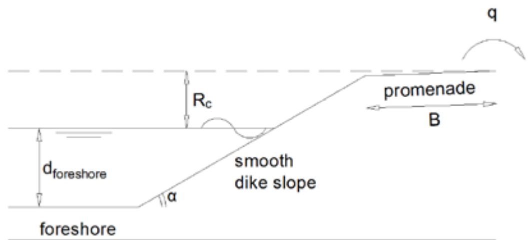

When a storm wall of 1.25m height is present at the end of the promenade, the crest height of the structure is increased to +10.40mTAW. To maintain the same crest freeboard R_c = 2m for reasons of comparison, the water level is also increased up to +8.40mTAW. The mean overtopping discharge is now calculated using the formula

$$\frac{q}{\sqrt{g \cdot H_{m0}^3}} = 0.09 \cdot exp\left[-\left(1.5 \cdot \frac{R_C}{H_{m0}} \cdot \frac{1}{\gamma_{prom\_v}}\right)^{1.3}\right] \qquad [4\text{-}29]$$

with γ_{prom_v} according to Eq. [4-20].

Table 4-6. Overtopping over a smooth dike with promenade and storm wall.

Smooth dike with promenade and storm wall **Promenade width = 15m, 1% slope** **Storm wall 1.25m high. R_c = 2m, h_{wall}/R_c = 0.625**				
H_{m0}	m	2.00	1.33	1.00
γ_{prom_v}	-	0.57	0.57	0.57
q	l/m/s	24.0	1.2	0.05
Ratio to smooth dike	-	6.1	21.5	86.2

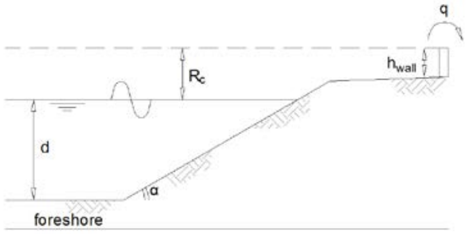

This geometry is capable of reducing the wave overtopping discharge to a minimum so far, with reduction ratio of 6.1, 21.5 and 86.2 compared to the discharge over smooth dikes with the same freeboard R_c. Therefore, this geometry is applied a lot at the Belgian coastline to reduce wave overtopping. The storm wall can be constructed as a mobile wall which is only set up when there is a risk of wave overtopping during a storm, see Figure 4-64 and Figure 4-65. When the high tide and storm surge have passed, this mobile wall can be deconstructed and the promenade regains its original function as a touristic promenade, without disturbing the open view at the sea.

Figure 4-64. Firemen installing a mobile storm wall on the promenade by the seaside in Ostend, Belgium.

Figure 4-65. Installation of a mobile storm wall, panels slide in between vertical anchored piles.

The discharge can be reduced even further, by adding a parapet to the above structure, with ε = 45° and λ = 1/3. The formula becomes

$$\frac{q}{\sqrt{g \cdot H_{m0}^3}} = 0.09 \cdot exp\left[-\left(1.5 \cdot \frac{R_C}{H_{m0}} \cdot \frac{1}{\gamma_{prom\_v\_bn}}\right)^{1.3}\right] \qquad [4\text{-}30]$$

with $\gamma_{prom\_v\_bn}$ according to Eq. [4-22] or Eq. [4-23].

Table 4-7. Overtopping over a smooth dike with promenade and storm wall with bullnose.

Smooth dike with promenade and storm wall and bullnose Promenade width = 15m, 1% slope Storm wall 1.25m high. R_c = 2m, h_{wall}/R_c = 0.625 Bullnose ε = 45°, λ = 1/3				
H_{m0}	m	2.00	1.33	1.00
$\gamma_{prom\_v\_bn}$	-	0.48	0.48	0.48
q	l/m/s	10.1	0.3	0.01
Ratio to smooth dike	-	14.6	93.3	729.6

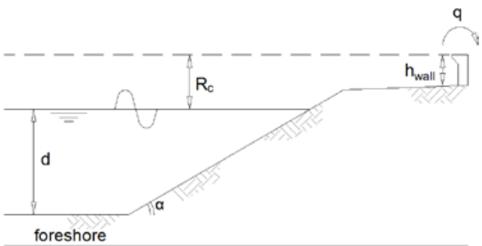

The overtopping discharge is dropped again with a factor of more than 2.5 compared to Table 4-6, which leads to average overtopping discharges of 10.1, 0.3 and 0.01 l/s/m respectively.

To conclude, also an SWB with the standard geometry as presented in Figure 3-10 is included in this (theoretical) comparison. The average overtopping discharge now has to be calculated by using

$$\frac{q}{\sqrt{g \cdot H_{m0}^3}} = 0.09 \cdot exp\left[-\left(1.5 \cdot \frac{R_C}{H_{m0}} \cdot \frac{1}{\gamma_{SWB}}\right)^{1.3}\right] \qquad [4\text{-}31]$$

Table 4-8. Overtopping over a smooth dike with Stilling Wave Basin.

Stilling Wave Basin **L_{basin} = 12m** **$h_{front\ wall}$ = 2.4m**				
H_{m0}	m	2.00	1.33	1.00
γ_{SWB}	-	0.48	0.48	0.48
q	l/m/s	9.8	0.3	0.01
Ratio to smooth dike	-	14.9	97.7	780.0

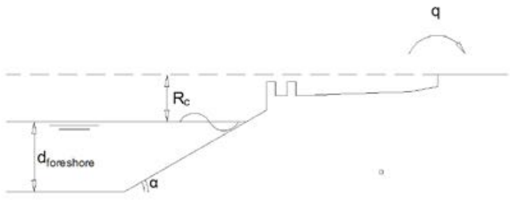

The overtopping discharge now is reduced to 9.8, 0.3 and 0.01 l/m/s respectively, which is about the same as for Table 4-7. The boundary conditions such as wave conditions, space, crest height, etc. will have to decide what kind of crest modification is the most efficient to reduce wave overtopping.

To conclude this example, overtopping over a rubble mound breakwater and a vertical caisson breakwater are added to this comparison. Since the γ-factor for the roughness of the rubble mound comes close to the values of reduction factors for SWB or dike with promenade and wall with/without parapet, similar reduction in wave overtopping is achieved. The vertical wall on the other hand reduces more than a dike with wall or parapet, since the slope is much steeper, but doesn't reduce wave overtopping as affective as an SWB or a dike with promenade and storm wall does for the presented hydraulic conditions. This proves again that even for a smooth dike, very good reducing crest geometries can be built.

Table 4-9. Overtopping over rubble mound breakwater and caisson breakwater.

Rubble mound breakwater: γ_f = 0.50				
H_{m0}	m	2.00	1.33	1.00
q	l/m/s	12.31	0.37	0.01
Ratio to smooth dike	-	11.9	66.4	445.6
Caisson breakwater (vertical wall)				
H_{m0}	m	3.00	2.00	1.00
q	l/m/s	24.0	1.5	0.12
Ratio to smooth dike	-	6.1	16.2	37.7

5 Flow depths and flow velocities

After waves overtopped a dike (see Chapter 4), the wave overtopping bore travels over the promenade towards a vertical wall or storm wall (see Figure 5-1). This chapter deals with flow depths and flow velocities of the wave-induced bore on the promenade whilst wave impacts will be studied in Chapter 6.

In some of the geometries tested, the storm wall was located at the beginning of the promenade, in other geometries at it's end. Due to the presence of a promenade, the physics change from a wave impacting a structure to an overtopped bore travelling over the promenade with a certain flow depth and flow velocity before impacting the structure.

The aforementioned flow characteristics have only been measured properly in the large-scale tests in the GWK, see Section 3.2 for the test set-up. In the other datasets, the scale was either too small to measure the overtopping bore or the measurements turned out to be inaccurate.

In Figure 2-11 it was explained that the maximum recorded flow depth in one bore is noted as h, and the maximum recorded flow velocity in one bore is noted as U.

5.1 *Principle and location of measurements*

A principal sketch of the kinematics of the overtopping bore is shown in Figure 5-1.

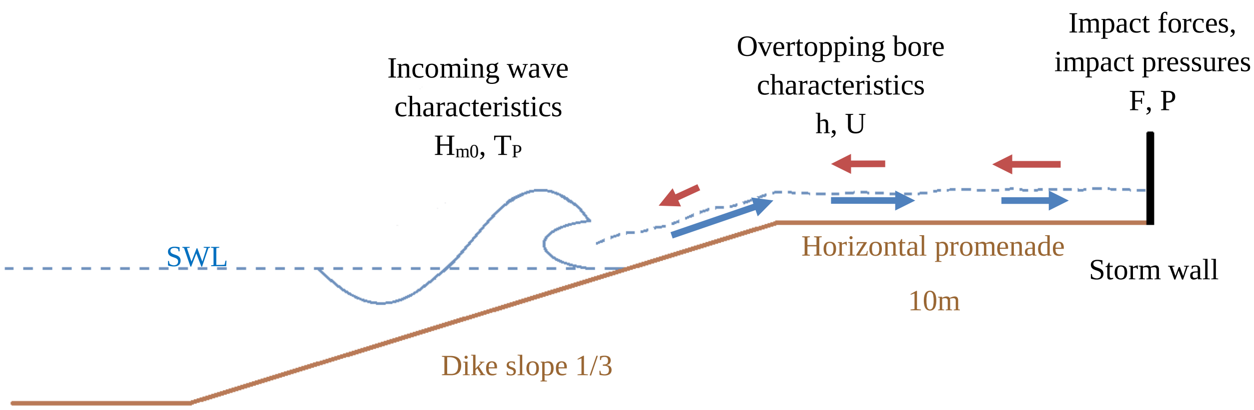

Figure 5-1. Hydrodynamic processes associated with the impact of the overtopping bore on the dike crest.

If the promenade is in the wave run-up zone ($A_c < R_{u2\%}$), wave overtopping over the dike crest on the promenade occurs. The overtopping bore has a certain flow depth and horizontal velocity on the promenade while progressing towards the storm wall. After an impact occurs, this incoming overtopped bore reflects and progresses back towards the sea. If at that moment a new overtopping event over the dike crest occurs, the incoming and reflected bore meet each other. The result of this collision is a reduction in flow velocity of the incoming wave and a local increase of the flow depth. It is assumed that the consecutive impact on the storm wall will thereby be reduced, since a part of the energy of the incoming overtopping bore is lost in the collision with the reflected bore.

As explained in Section 3.2.3d), the first test set-up in the GWK experiments had a continuous storm wall without openings along the flume width. Due to a lot of wave overtopping over the dike crest (at A_c), there was no time for the water on the promenade to evacuate, which resulted in a residual water layer of some decimeters (even up to 50cm, scale 1:1) remaining on the promenade. This water layer highly dampened the wave impacts measured on the storm wall. However, in reality, a 3D situation, the water would also evacuate along the sides with a higher probability of an empty promenade by the time the next wave overtops the dike crest. It was expected that a wave impact on the wall would be higher with an empty promenade, and the worst-case scenario needed to be investigated. Thereby it was decided to create openings in between the recording sections of the wall and let the water evacuate through the gaps. A 10cm wide timber plate remained at the sides of the recording sections, trying to minimize the side effects which could occur when water was passing through these gaps, see Figure 5-2.

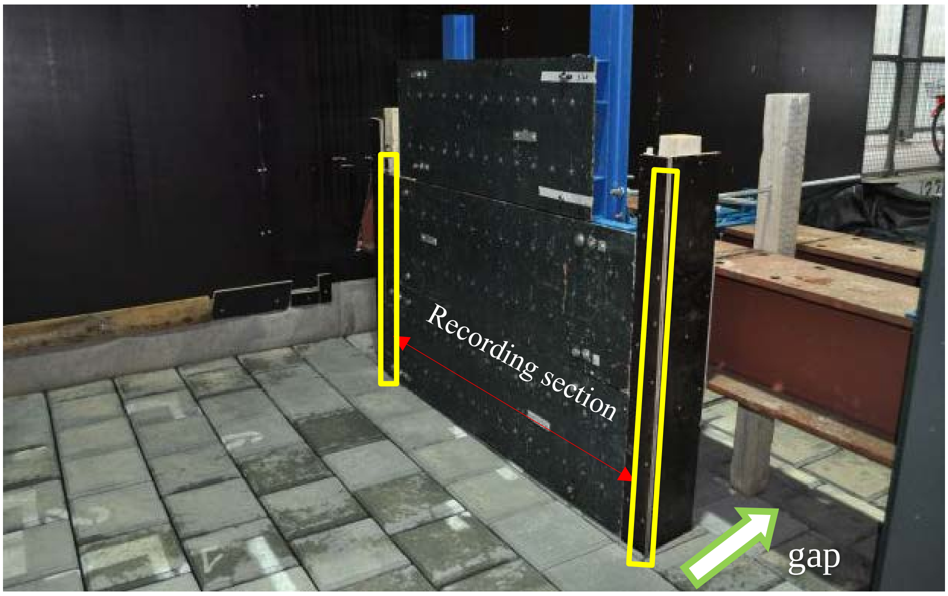

Figure 5-2. The recording section on the left storm wall (red arrow), flanked by 10cm wide timber plates (yellow) for minimizing the side effect, GWK data set. The water can evacuate through the gap indicated by a green arrow.

Even by creating gaps in between the recording sections of the storm wall, the bore hitting the wall itself always reflected. Interaction with the next incoming overtopping bore was inevitable.

In the wave flume test, incoming wave parameters are separated from the reflected waves by means of the method by Mansard & Funke (1980). This cannot be done for overtopping flow on the crest since a non-constant incoming flow is totally different than a superposition of mathematically describable sinusoidal waves as assumed by Mansard & Funke (1980). In some cases, the overtopped bores were separated a little in time (see Figure 5-3: discrete peaks of the 3 different flow depth meters), which allows for analyzing the flow depth and flow velocity for individual bores. In other cases, where the reflecting water was clearly interfering with the incoming bore, it becomes very difficult if not impossible to analyze the flow parameters (see Figure 5-4). Consequently, it is decided to only analyze clear and distinct flow depth signals and to avoid flow depth recordings where incoming and reflected bores interfered.

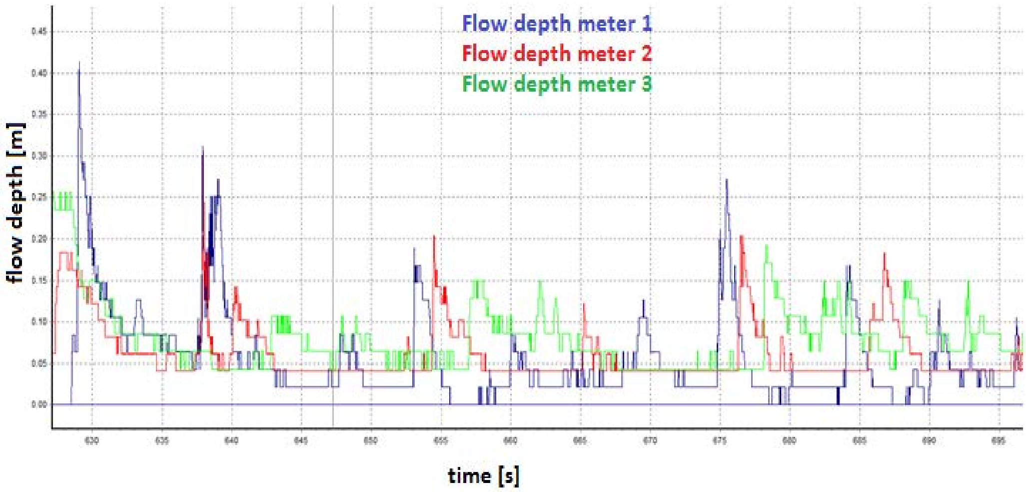

Figure 5-3. Recordings of the flow depth meters 1 (x_C = 0.5m), 2 (x_C = 3.8m) and 3 (x_C = 7.9m) on the 10m long promenade: clearly separated overtopping bores.

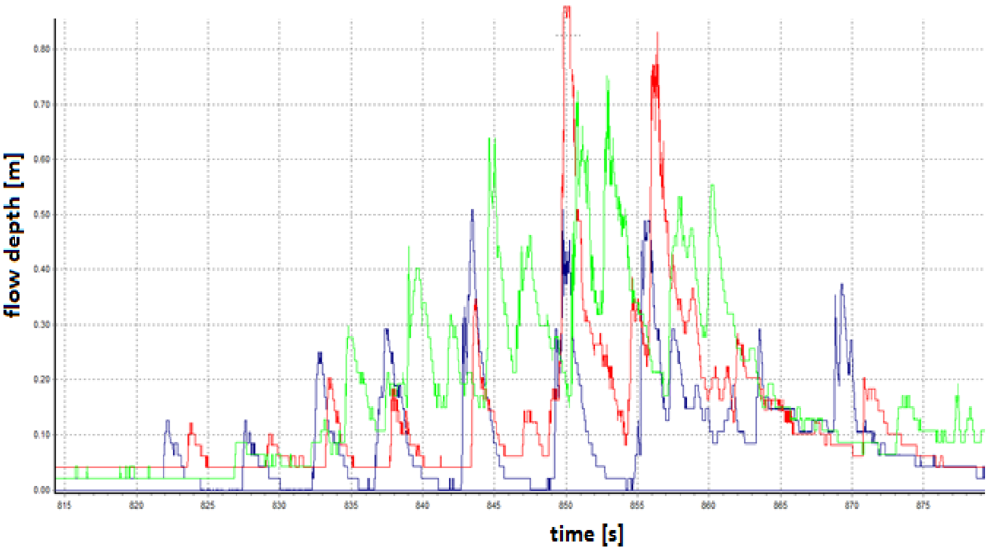

Figure 5-4. Recordings of the flow depth meters 1 (x_C = 0.5m), 2 (x_C = 3.8m) and 3 (x_C = 7.9m) on the 10m long promenade: large interference of reflected bores in between the next incoming bores.

In Figure 5-3 near the middle of the horizontal time axis, a clear example of the wave progressing and reflecting on the promenade can be seen. This figure is repeated in Figure 5-5 with indication of the response of the flow depth meters.

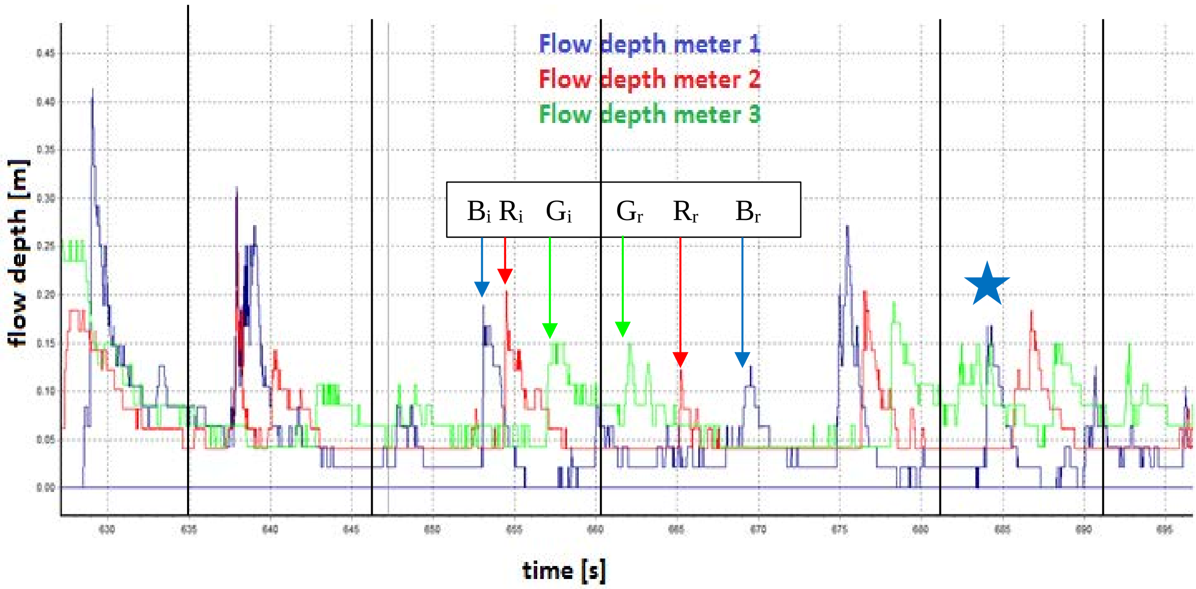

Figure 5-5. Repitition of Figure 5-3 with indication of the moment of registration by the digital step gauge (blue-red-green) and the moments of impact (black line).

First, a signal was recorded by the first digital step gauge (blue), then the 2nd flow depth meter (red) responded, a few milliseconds later the 3rd flow depth meter (green) responded. Shortly after, the impact was measured (black line). The bore reflected and the flow depth meters responded in reversed order (green, red, blue) indicating the reflecting bore. When considering the next incoming wave in Figure 5-5 that was approaching the wall, the following order shows: blue – red – green – impact with reflection (black vertical line) – green – red – blue although this bore was already disturbed by a next incoming wave indicated by the blue star: there is a blue incoming recording between the 2nd green recording and the 2nd red recording. The red recording after the blue star is higher than the blue recording, which indicates a local increase in flow depth due to the collision between incoming and reflecting bore. For this latter example, analysis and separation between incoming and reflective bore is impossible with the available equipment.

As was mentioned in Section 3.2.3c), the flow depth was measured with 3 digital step gauges installed at the side of the flume: h_1 measured at 0.5m, h_2 at 3.8m and h_3 at 7.9m counting from the start of the promenade. The flow depth recording over time h(t) shows a triangular recording (see detail in Figure 5-6). The flow depth is defined as the maximum value of the flow depth recording, which is the layer thickness of the bore front passing the sensor (see Figure 2-11 and circles indicated in Figure 5-6). It is assumed here that the flow depth remains a constant (maximum) value from its recording location to the next recording location.

Also mentioned in Section 3.2.3c), the flow velocity recordings with propellers did not give good results due to blocked propeller blades and the video-recording was for informative purposes only. The flow velocity is determined from the time signals of the digital step gauges. A detail of the flow depth recording is given in Figure 5-6. The moment when the bore front passed a step gauge is marked by a black vertical line. Dividing the distance interval by the time difference in between two signals leads to the flow velocity in between the two considered locations: $U = \Delta x/\Delta t$.

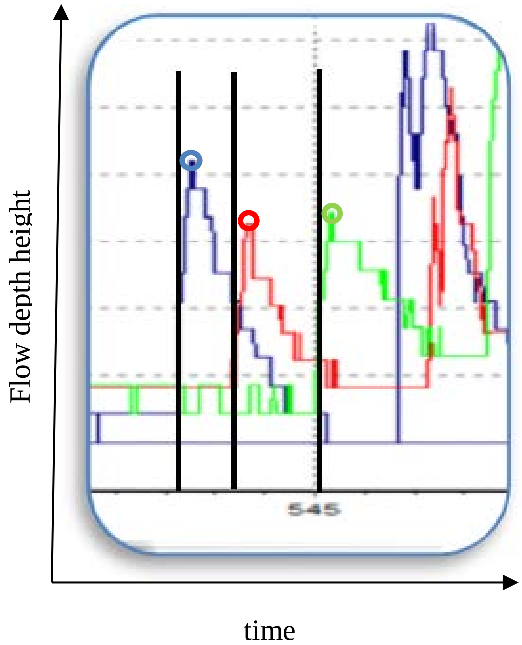

Figure 5-6. Time interval between the flow depth recordings, with known distance interval between the sensors to determine the flow velocity. The black lines indicate the moment when the bore front passes the flow depth meter, the blue-red-green circles indicate the values h_1 (blue), h_2 (red) and h_3 (green).

This is a reliable but very time-consuming (manual) way to determine the flow velocity U of discrete overtopping bores (without interference between incoming and reflective bores) at certain locations on the promenade. By means of the 3 step gauges, two velocities can now be determined: U_1 between flow depth meter 1 and 2, and U_2 between flow depth meter 2 and 3. If the force or pressure recording at the wall (x_C = 10m) is included as a 4th measurement location, in the same way as the step gauges record the moment when the overtopping bore front reaches the measurement location, also a 3rd velocity can be determined: U_3 between flow depth meter 3 and the wall. This method implicitly assumes that the flow velocity is constant in between its two measured locations. This is not fully correct, but due to the short distance interval in between the step gauges, it is assumed to be a good approximation. This assumption was also confirmed by Schüttrumpf & Oumeraci (2005) which stated that the velocity of overtopping bores on short dike crests with rather smooth surface only decreases slightly.

Table 5-1 shows an example for the geometry of the dike and wave conditions used in the GWK experiments: slope tan α = 1:3, crest freeboard R_c = 2.0m, wave height H_s = 1.2m and wave period T_p = 10s, promenade width G_c = 10m and the roughness f = 0.01 for smooth slopes. The flow parameters at the beginning of the promenade ($z_A = R_c$ equal to $x_C = 0$ in Figure 2-12) can be calculated by Eq. [2-32] and [2-33]. The formulae to calculate the decaying flow depth and flow velocity on the crest of a dike were given in Eq. [2-34] and [2-35], respectively. Table 2-2, Figure 2-13 and Figure 2-14 showed that there are different coefficients leading to large differences in flow depths and flow velocities. For this example it is chosen to use the coefficients by Schüttrumpf & van Gent (2003) with a slope 1:4 since these equations don't lead to the extremes but to average values in Figure 2-13 and Figure 2-14. Using these coefficients leads to Eq. [5-1] and [5-2] for the flow parameters on the promenade.

$$\frac{h_{C,2\%}(x_C)}{h_{C,2\%}(x_C=0)} = exp\left(-0.40 \cdot \frac{x_C}{G_c}\right) \quad [5\text{-}1]$$

$$\frac{U_{C,2\%}(x_C)}{U_{C,2\%}(x_C=0)} = exp\left(-0.5\,\frac{x_C \cdot f}{h_{C,2\%}(x_C)}\right) \quad [5\text{-}2]$$

The decrease in flow depth is related to the distance along the promenade, while the decrease in flow velocity depends on both the distance along the promenade and the flow depth at that position. According to Table 5-1 the flow velocity decreases 1 to 7% in between the different locations, which is small. The assumption that the flow velocity is constant over a short distance (between 2 flow depth meters) can thus be accepted. The flow depth decrease is a little bigger but still not large (up to 15%) based on the equations by Schüttrumpf & van Gent (2003).

Table 5-1. Theoretical flow depth and flow velocity on the dike, for wave conditions Hs = 1.2m, Tp = 10s, using Eq. [5-1] and [5-2].

Distance at crest (position of sensors)	Flow depth	% difference with previous	Flow velocity	% difference with previous
0m (Eq. [2-32] and [2-33])	0.46m		7.14m/s	
0.5m	0.45m	-2%	7.11m/s	-1%
3.8m	0.40m	-12%	6.81m/s	-4%
7.9m	0,34m	-15%	6.36m/s	-7%
10m	0,31m	-8%	6.08m/s	-4%

The descending trend in both flow depth and flow velocity seems to be in contradiction to the continuity equation. The values in Table 5-1 result from the maximum values in the profiles of h(t) and U(t). These maxima decrease over the length of the promenade, due to friction and dispersion, but the recording of the flow parameters over time has a longer duration. This can be seen in Figure 5-6 where the green flow depth recording is wider (longer time duration) than the blue one. This is explained further in Figure 6-75. If the integral of the product of h(t) and U(t) over time is taken, continuity equation will be fulfilled.

Another difficulty with this descending trend is that the location of measurements becomes important, certainly if the flow parameters will be linked to the incoming waves or to the wave impacts. As explained in Section 2.3, there is a transition zone at the beginning of the crest going from a slope to a horizontal surface. It is unknown how long this transition zone is (Bosman et al., 2008). It is thus unsure if the first flow depth meter (located at 0.5m from the beginning of the promenade) measured correct flow depths since it was located in a zone where the flow is very turbulent. h_1 and U_1 are not further used in the analysis. At the second flow depth meter (3.8m away from the beginning of the promenade), it was often noticed that the reflection of a first overtopping bore encountered an incoming second overtopping bore and this collision makes it impossible to distinguish the incoming flow depth from the reflected one. The value h_2 was thereby sometimes higher than h_1 which is physically impossible. H_2 and U_2 are not further used in the analysis. The last flow depth meter (at 7.9m from the beginning of the crest and thus 2.1m before the storm wall) gave clean signals and the most reliable flow depths. It was also the location closest to the wall and thus the preferred location to link the flow depth to the impacts. Thereby, h_3 and U_3 are used in the analysis.

5.2 *Analysis of flow parameters*

A manual analysis is carried out for the 21 GWK experiments, which contain a total of 2413 waves. Not every wave overtopped the crest of the dike, not every overtopped bore gave an impact on the storm wall, and due to reflection from the impact on the storm wall and disturbing new incoming overtopped bores not every bore gave clean flow depths h_3 and flow velocity signals U_3. A total of 621 overtopped bores with a good signal of flow depth, flow velocity and impact force are obtained through manual analysis.

These 621 flow depths h_3 and flow velocities U_3 are individual values from irregular waves overtopping the crest of the dike and resulting into these individual overtopped bores. It is thus not logic to link the individual flow parameters to the incoming wave height H_{m0} which is one value representing the full wave train, a test-averaged value. This is however done in Figure 5-7 and Figure 5-8, to show the order of magnitude of the different values: flow depths between 0.06m and 0.70m, flow velocities between 0.5m/s and 7m/s. Lower velocities and flow depths were not measured at the end of the promenade and/or did not lead to an impact higher than the threshold value (see Chapter 6). The plots also show that higher waves lead to higher flow depths and flow velocities. A similar graph could be made by plotting the flow parameters versus the dimensionless seaward freeboard A_c/H_{m0}: lower freeboards leads to higher values of the flow parameters. But also in such a graph, no relationship can be withdrawn.

A better way of presenting the flow depths and flow velocities is by linking them to individual wave overtopping. This was however not measured in the current research. Linking the individual flow parameter to other individual values such as overtopped bores or impacts will be carried out in Chapter 6.

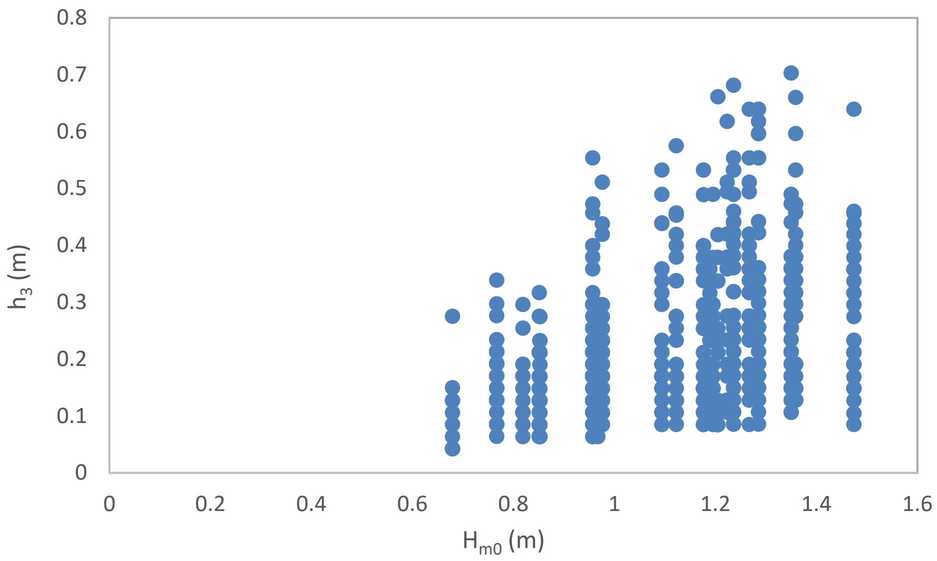

Figure 5-7. Flow depth h_3 (measured at 7.9m from the beginning of the crest) versus incoming wave height H_{m0} in the GWK experiments (model values). 621 clean flow depth signals from 21 tests.

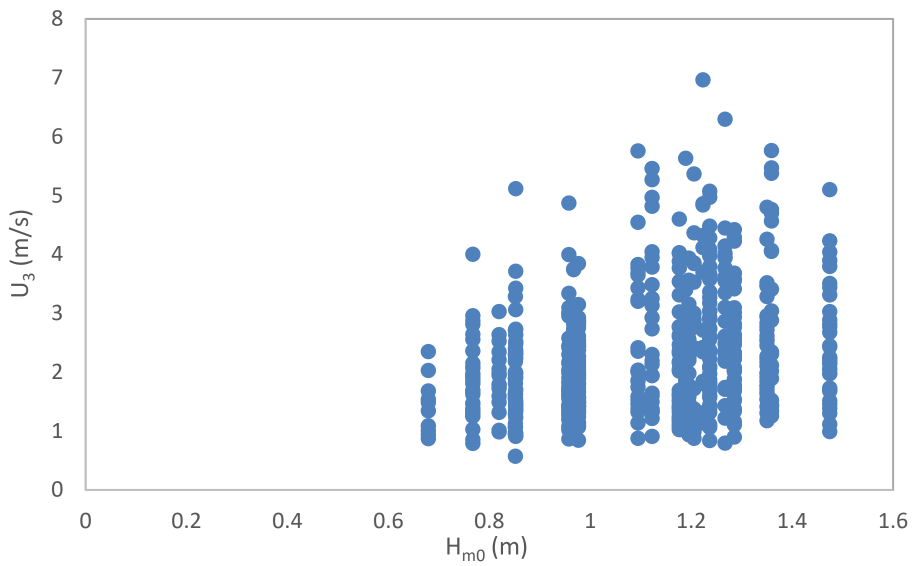

Figure 5-8. Flow velocity U_3 (measured at 7.9m from the beginning of the crest) versus incoming wave height H_{m0} in the GWK experiments (model values). 621 clean flow velocity signals from 21 tests.

5.3 *Comparison with literature*

The example given in Table 5-1 showed a flow depth $h_{2\%}$ = 0.34m and a flow velocity $U_{2\%}$ = 6.36m/s at location x_C = 7.9m for hydraulic conditions H_{m0} = 1.2m and T_p = 10s. These values are verified with the tests carried out in the GWK test campaign. Four tests had comparable hydraulic conditions, and the maximum analyzed flow parameters in these four test are given:

- Test 2208: H_{m0} = 1.236m, $T_{m-1,0}$ = 7.216s => h_{MAX} = 0.68m, U_{max} = 5.07m/s
- Test 2303: H_{m0} = 1.195m, $T_{m-1,0}$ = 8.483s => h_{MAX} = 0.49m, U_{max} = 3.94m/s
- Test 2304: H_{m0} = 1.189m, $T_{m-1,0}$ = 8.29s => h_{MAX} = 0.36m, U_{max} = 5.63m/s
- Test 2305: H_{m0} = 1.122m, $T_{m-1,0}$ = 9.046s => h_{MAX} = 0.58m, U_{max} = 5.46m/s

The analyzed highest flow depths in these four tests vary between 0.36m and 0.68m, which is higher than the prediction by Schüttrumpf & Oumeraci (2005). On the other hand, the flow velocities are lower than the predicted results. Section 2.4 has shown that the predictions from literature show large differences. When looking at Figure 2-13 and Figure 2-14, the values from the 4 mentioned tests are within the largest predicted values (with exception of h_{MAX} = 0.68m).

For the 621 analyzed bores with a distinct flow depth and impact signal resulting from 21 tests it becomes obvious that a comparison of these results resulting from individual waves with test-averaged values such as H_{m0} is not sufficient.

Another attempt follows from analysis by Lorke et al. (2010) and Hughes (2015), who found a relationship between the flow depth and the flow velocity. Figure 5-9 shows the relation between both flow parameters (h_3 and U_3) of each overtopped bore where the flow depth is plotted on the horizontal axis and the flow velocity is plotted on the vertical axis. There is still a large scatter, but the figure shows that small discharges ($q = h \cdot U$) are typically related to small flow velocities and small flow depths, while large overtopped discharges are related to a large flow velocity and/or a large flow depth.

Hughes (2015), Van Gent (2002) and others stated that the maximum velocity and maximum flow depth do not necessarily occur in the same wave. Figure 5-9 confirms this statement. All 621 analyzed flow depths and flow velocities are plotted in blue markers. The 21 red squares in Figure 5-9 are the ones related to the highest analyzed velocities over the 21 tests (noted as h3_MAX). The 21 green circles are the ones having the highest analyzed flow depth in each of the 21 tests (noted as U3_MAX). The green and red symbols indicate that the highest analyzed flow depths and flow velocities did not necessarily occur in the same wave.

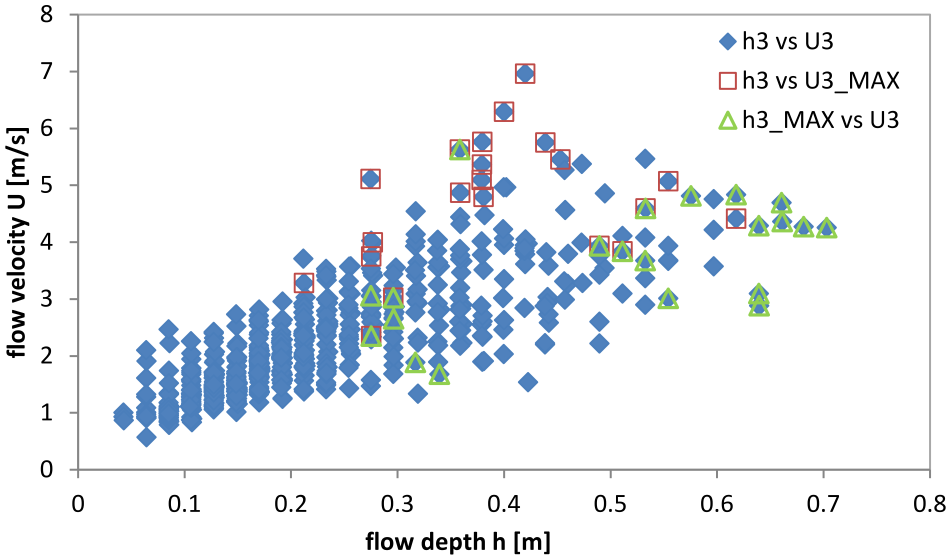

Figure 5-9. Relation between the flow depth and flow velocity measured in every of the 621 overtopped bores.

Eq. [2-42] by Lorke et al. (2010) and Eq. [2-43] by Hughes (2015) (Section 2.4) also gave a relationship between $U_{2\%}$ and $h_{2\%}$. In their work, $U_{2\%}$ and $h_{2\%}$ represent the 2% exceeding values of all flow depths and flow velocities that occurred on the crest during their tests. Both authors stated that the values $U_{2\%}$ and $h_{2\%}$ do not necessarily belong to the same bore. The equations [2-42] and [2-43] are plotted together with the analyzed data from the GWK experiments in Figure 5-10. The blue marks show again the same 621 individual bores as in Figure 5-9 with clean results for h_3 and U_3. Since not all overtopping bores gave clean signals (mainly due to wave groups and/or reflection as was explained in the previous section 5.1), it's impossible to determine the 2% exceeding values in the current dataset. Therefore, another low-exceedance value is plotted in red squares: U_{3_MAX} vs h_{3_MAX}, which is the combination of the maximum of all analyzed flow velocities U_3 and the maximum of all analyzed flow depths h_3. 21 red squares for 21 tests. Since it is only possible to analyze clear recording signals and a lot of bores were disturbed by reflection and wave grouping, it is unsure whether U_{3_MAX} and h_{3_MAX} were physically the highest waves that have occurred during the test, but it are the highest values that can be analyzed. Nevertheless, the red marks represent a low exceedance value just like the theory by Lorke et al. (2010) and Hughes (2015) do. They can't be compared directly to a 2% exceeding value but a similar trend shows in Figure 5-10. Note that the red marks, with maximum analyzed flow depth h_{MAX} and maximum analyzed flow velocity U_{MAX} from the 21 experiments mainly did not occur in the same bore, and thereby mainly do not correlate with a blue marker from one of the 621 actual bores which gives flow depth and flow velocity from the same bore.

Based on Figure 5-10, it can be stated that the prediction by Lorke et al. (2010) serves as an upper bound for the measured data and the predictions by Hughes (2015) serve as a mean value. With both relations from literature, the flow depth can be calculated based on the flow velocity or vice versa. However, the scatter in the data is too big so it is decided to not use these relationships, and further use the measured flow values to link with wave impact forces in the next chapter.

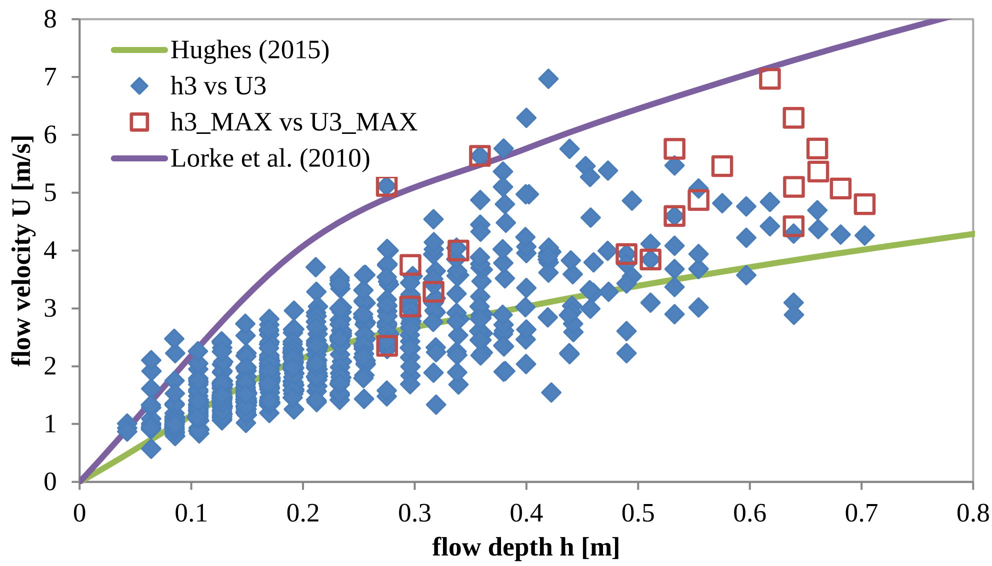

Figure 5-10. Relation between the flow depth and flow velocity, compared with theoretical Eq. [2-42] and [2-43].

5.4 *Summary*

This chapter provides an analysis of flow parameters on the promenade of the dike after waves overtop the dike crest and travel over the promenade with a certain flow depth and flow velocity. Only data from the large-scale tests in the GWK were used for this analysis. During these tests, openings were made between the recording sections of the storm wall at the end of the promenade, to avoid damping of the incoming waves by a large residual water layer. This was considered to be more in line with a 3D situation in the field and regarded a conservative approach. Unlike for waves, no separation method exists for overtopped bores to determine incoming and reflected flow parameters. Therefore, only data of isolated bores were used which do not show any interference of incoming and reflected bores. Those bores were manually detected and flow parameters were analyzed.

Three flow depth meters were installed along the promenade, resulting in three flow depth measurements (h) and three flow velocities (U) where the latter were determined based on the known distance between the meters and the moment in time when the bore front passes them. The analysis has shown that the recording closest to the storm wall, sensor number 3 at x_C = 7.9m, showed the most reliable results and was therefore used to determine the flow depth h_3 and flow velocity U_3. This has led to 621 individual values of flow depths and flow velocities from 21 tests. In comparison to available literature results, these data are within the extremes of Figure 2-13 and Figure 2-14.

Both U and h did not show any relation with the test averaged values such as H_{m0} or A_c/H_{m0}, apart from the principal trend that larger waves or smaller freeboards result in larger flow parameters. A trend between U and h of each bore could be identified, as already introduced by Lorke et al. (2010) and Hughes (2015). The results by Lorke et al. (2010) provides an upper bound prediction, the relationship by Hughes (2015) is close to the average of the data used here. This analysis has also shown that the maximum flow velocity and the maximum flow depth do not (necessarily) occur in the same overtopped bore. Nevertheless, presenting the data in such a way shows a lot of scatter which is not good for design purposes. A better way of presenting the bore characteristics is by linking them to other individual parameters such as impact forces or individual overtopping volumes. This will be shown in the next chapter.

6 Wave impacts

The previous chapters have dealt with the issue of average wave overtopping and possibilities to reduce the overtopping discharges were suggested. Also a better understanding of the flow parameters of overtopped bores was established. But what is the damage that can occur due to such overtopped bores? The literature study in Chapter 2 has shown that some knowledge is available on impacts on crown walls on top of rubble mound breakwaters. Also, there is information on damages of grass and clay covers at the landward side of overtopped dikes. Unfortunately, for the crest of smooth sloping dikes few information is available, besides the very recent study by Chen (2016) and the currently ongoing study by Streicher et al. (2018), both for breaking and broken waves in very shallow foreshore conditions.

What happens when (non-breaking) waves overtop a smooth sloping sea dike, and buildings or other structures are situated at the crest level of this dike? Do these structures provide sufficient strength against structural failures during storms with severe wave overtopping over the sea dike? When storm walls are built on a promenade to protect the structures behind them or to prevent flooding of the low-lying hinterland: what impacts will these storm walls face during their lifetime? What are the governing processes leading to such impacts? Which wave overtopping volumes lead to which impacts on sea walls, storm walls, flood walls, buildings or any other type of structure on the promenade or on top of the dike? Most of these questions are still fully or partly unanswered.

Therefore, the impacts on storm walls are studied in this chapter. First, it's investigated whether the relationships from literature describe the measured data well. This is done in Section 6.1. Section 6.2 focusses on the impact recordings themselves. What was measured in the different test campaigns and are there differences between the different recordings? Also the statistical distributions, the low-exceedance values and a way to present the forces dimensionless will be discussed here. In Section 6.3 three different methodologies to calculate overtopping impact forces are given. Two storm wall locations were distinguished. For the first location, the storm wall was located at the end of the dike (dike crest), with and without bullnose. For the second location the storm wall was located at the end of a promenade at crest level, again with and without bullnose. A geometry with strong overtopping reducing capacity is a storm wall at the end of a promenade. This latter geometry will thus be treated first (Section 6.4), while the other geometries will be treated in section 6.5. A case study is given at the end of this Chapter in Section 6.6.

Similar to Chapter 5 on flow parameters, this analysis is dealing with **individual values** and not with test-averaged values like in Chapter 4 on wave overtopping. Wave impacts are used in stability design, where **low-exceedance force values** are of interest since those values can cause the instability or damage of storm walls or buildings.

6.1 *Comparison with literature*

In the literature review in Section 2.6, the analysis has shown that limited design formulae exist for a smooth dike with a storm wall (Den Heijer (1998) and SPM (1977), Figure 6-1), and for a smooth dike with promenade and storm wall (Den Heijer (1998), Cross (1967), Chen et al. (2015), Figure 6-5 right). In this section, the data obtained in this PhD on these two geometries will be plotted according to the equations from literature to verify their applicability.

6.1.1 *Smooth dike with storm wall*

Den Heijer (1998) developed Eq. [2-60] and [2-61] for the impacts on a storm wall situated at the end of a dike, although the water level in his tests was much higher than in the current research. The dike slope and the toe of the storm wall were often submerged in his tests (Figure 6-1). This is expressed by means of the value h_b, which is the difference between the foot of the wall and the SWL: $h_b = h_{wall} - R_c$. In Den Heijer's tests, the range of tests went from $-1.2 < h_b/H_s < 1$. In the current dataset from this PhD, the range was always negative ($-1.9 < h_b/H_s < -0.6$), meaning that the foot of the wall was always above the SWL in the current research.

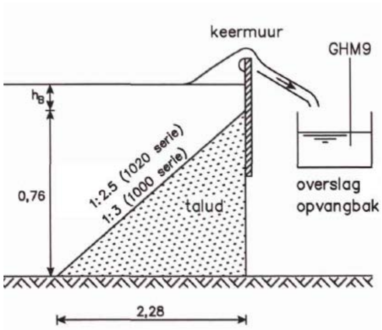

Figure 6-1. One of the geometries tested by Den Heijer (1998) for which Eq. [2-60] and [2-61] have been developed.

Eq. [2-60] and [2-61] by Den Heijer (1998) were given in Chapter 2 and are repeated here:

$$\frac{F_{max}}{\rho g H_s^2} = 1.62 + exp\left(3\frac{h_b}{H_s}\right) \qquad \text{for } h_b/H_s \leq 0.78 \qquad [2\text{-}60]$$

$$\frac{F_{max}}{\rho g H_s^2} = 12 \qquad \text{for } h_b/H_s > 0.78 \qquad [2\text{-}61]$$

These equations are plotted in a black dotted line in Figure 6-2 and Figure 6-3 together with the data of the UGent-1 experiments on a similar geometry (a smooth dike with storm wall). The theory by Den Heijer predicts impact forces in the same range as in the current study, however the scatter is rather large, caused by F_{max} and/or making the force dimensionless by $\rho g H_s^2$.

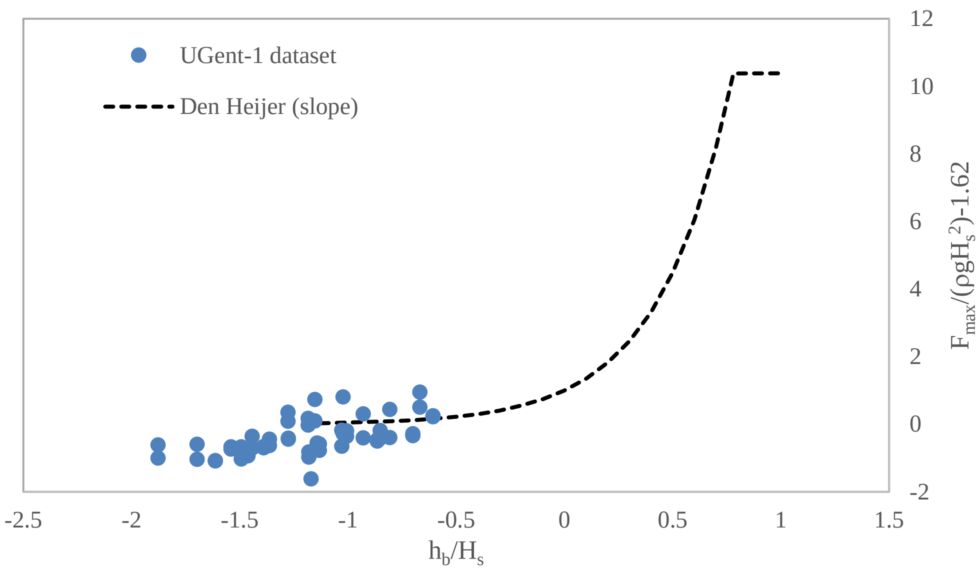

Figure 6-2. Comparison of the UGent-1 data to the predcitions by Den Heijer (1998).

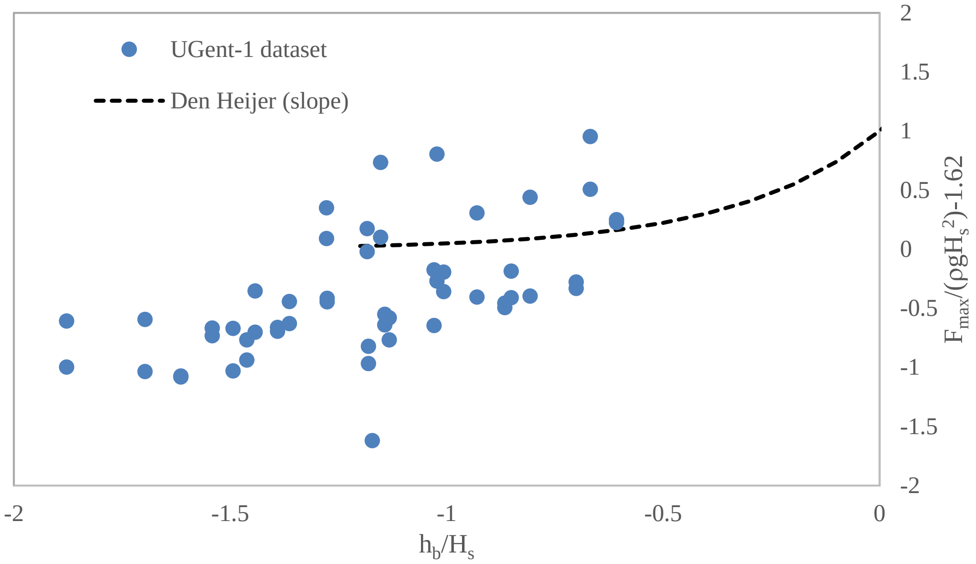

Figure 6-3. Repitition of Figure 6-2, zoomed in on the range of the UGent-1 dataset.

The same dataset (UGent-1, smooth dike with storm wall) is also plotted according to the approach by SPM (1977) Eq. [2-67], see Figure 6-4.

$$R_t = R_d + R_s = h' \cdot \left(\frac{\rho g v'^2}{2g}\right) + \frac{\rho g h'^2}{2} \qquad [2\text{-}67]$$

The Shore Protection Manual consistently overpredicts the impacts. For this comparative exercise, the water depth at the toe of the structure is used for d_b, the ratio between the breaker height and the breaker depth is 1.3 (d_{br} = 1.3H_b) and the theoretical wave breaker height which is defined as 0.77 times the breaker depth. Since this value is unknown, the water depth at the toe of the dike is used instead, however this value is probably much larger than the intended breaker height. Logically, a too large wave breaker height leads to an overestimation of the calculated impacts. Better knowledge on the wave breaker height is required to properly use Eq. [2-67].

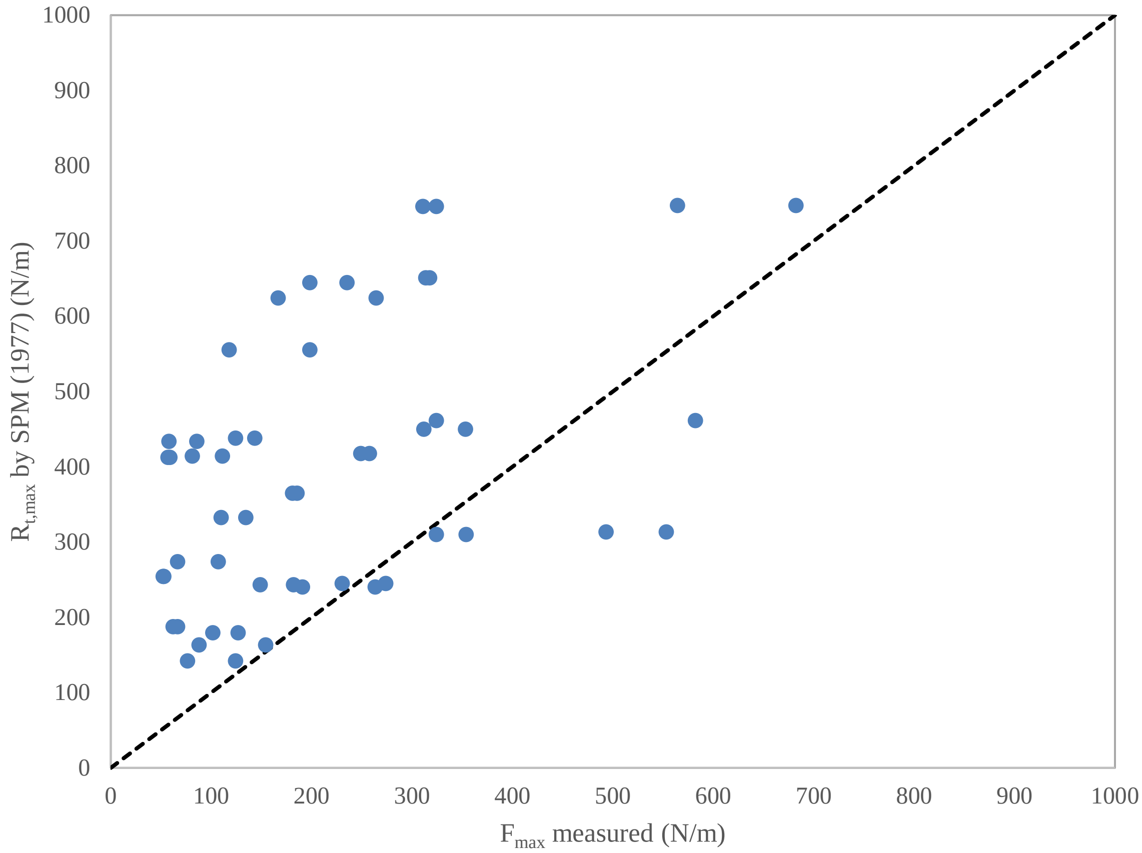

Figure 6-4. Comparison of the UGent-1 data to the prediction by SPM (1977).

6.1.2 *Smooth dike with promenade and storm wall*

Den Heijer (1998) also developed formulae for a situation with a promenade/crest in front of the storm wall. One with quay wall (Figure 6-5 left), the other with a dike and a short promenade (Figure 6-5 right). Den Heijer used a rather high water level with $-1.2 < h_b/H_s < 1$. Again not perfectly comparable to the current research ($-1.3 < h_b/H_s < -0.3$), but the Eqs. [2-57] to [2-59] (quay wall) and [2-60] with [2-61] (dike) are tested nevertheless, see Figure 6-6 and Figure 6-7.

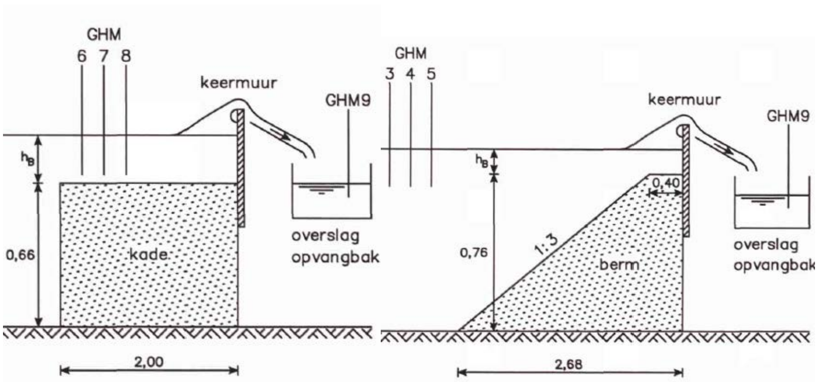

Figure 6-5. Quay wall (left) and smooth dike (right) with a promenade and storm wall from the tests by Den Heijer (1998).

Eqs. [2-60] and [2-61] for the slope were repeated in the previous section, Eqs. [2-57] to [2-59] for the quay wall are repeated here:

$$\frac{F_{max}}{\rho g H_s^2} = 15 \qquad \text{for } s_{0p} < 0.0051 \qquad [2\text{-}57]$$

$$\frac{F_{max}}{\rho g H_s^2} = 16.5 - 294 \cdot s_{0p} \qquad \text{for } 0.0051 < s_{0p} < 0.022 \qquad [2\text{-}58]$$

$$\frac{F_{max}}{\rho g H_s^2} = 10 \qquad \text{for } s_{0p} > 0.022 \qquad [2\text{-}59]$$

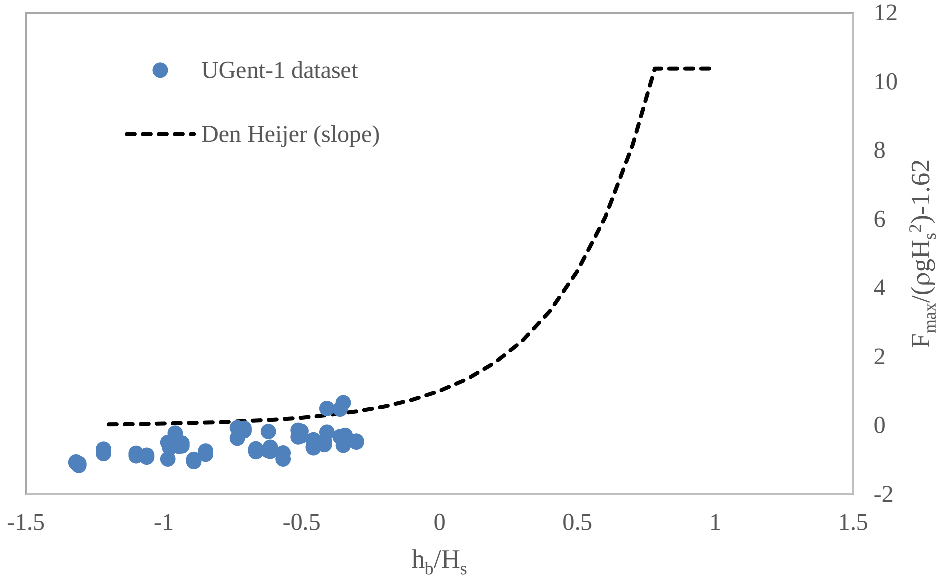

Figure 6-6. Comparison of the UGent-1 data with Eq. [2-57] to [2-59] (slopes) by Den Heijer (1998).

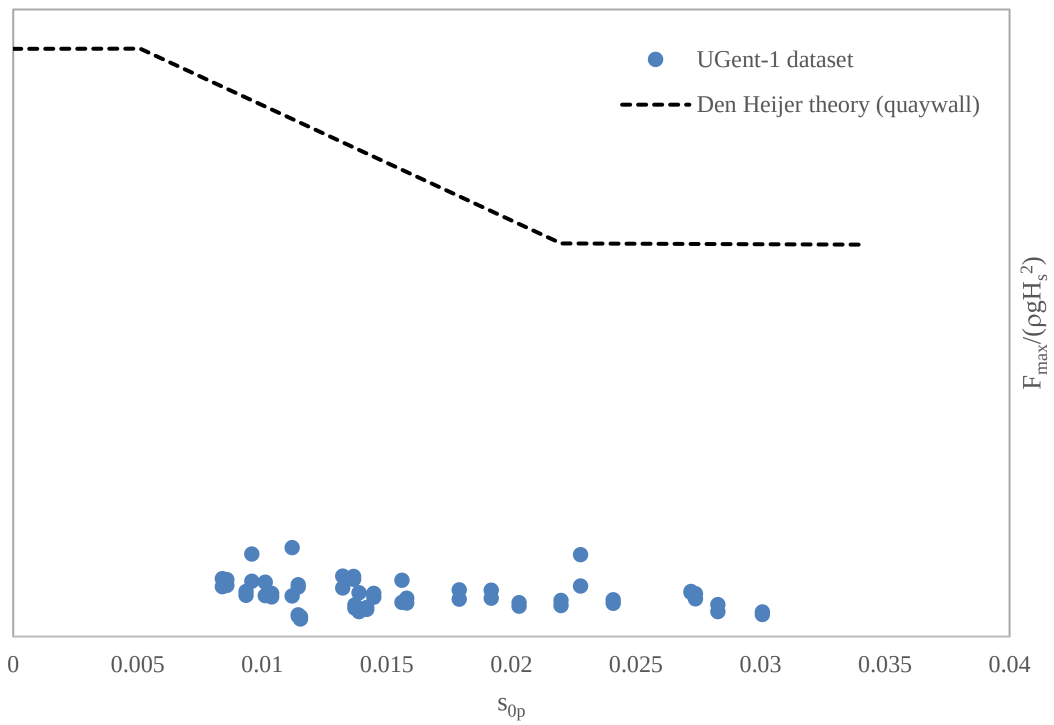

Figure 6-7. Comparison of the UGent-1 data with Eq. [2-60] and [2-61] (slopes) by Den Heijer (1998).

Both predictions show a (very) large overestimation of the impact force. Due to the much lower water levels in the current research, wave run-up and the overtopping bore travelling over the promenade gives energy dissipation that leads to lower impact forces related to the research by Den Heijer (1998) where the still water level was mostly against the storm wall leading to more violent wave impacts.

The approach by Cross (1967) was set-up for tsunami impacts, and uses the flow depth and the flow velocity. Therefore, only the GWK data can be compared to Eq. [2-56].

$$F_h = \frac{1}{2}\rho g h^2 + C_F \rho h u^2 \qquad [2\text{-}56]$$

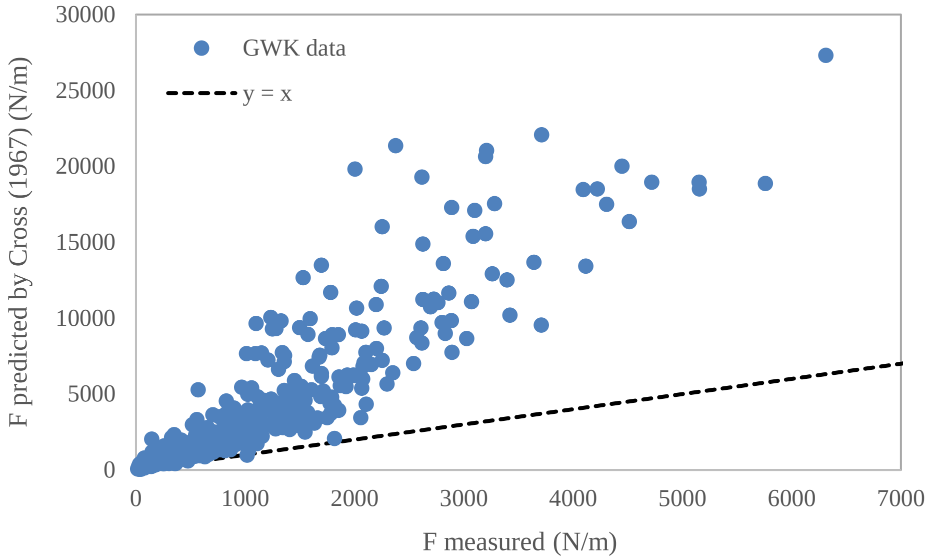

Figure 6-8. Comparison of the GWK data to the tsunami impact force predictions by Cross (1967). The black line y = x shows the 45° line.

Figure 6-8 shows the predicted forces by using Eq. [2-56] on the vertical axis, assuming a water wedge angle of 20°, and the measured forces on the horizontal axis. The tsunami-theory by Cross (1967) is significantly overpredicting the measured impact forces by a factor 4 to 9. It can be concluded that this theory is not applicable to predict random wave overtopping induced forces.

A final attempt to predict the measurements by means of formulae from literature is by using the equations derived by Chen et al. (2015). In her tests, regular waves and a very shallow foreshore were used. The force is made dimensionless by division through $\rho g d_{b0}^2$, with d_{b0} being the flow depth, and related to the dimensionless promenade width. A comparison is given in Figure 6-9. The order of magnitude is similar, but the scatter is big (a factor of 2 to 3 in both over and underprediction).

$$\frac{F_t}{\rho g d_{B0}^2} = 1.7\cot(\alpha) exp\left(-3.08\cot(\alpha)\frac{G_c}{L_{reg}}\right) \qquad [2\text{-}64]$$

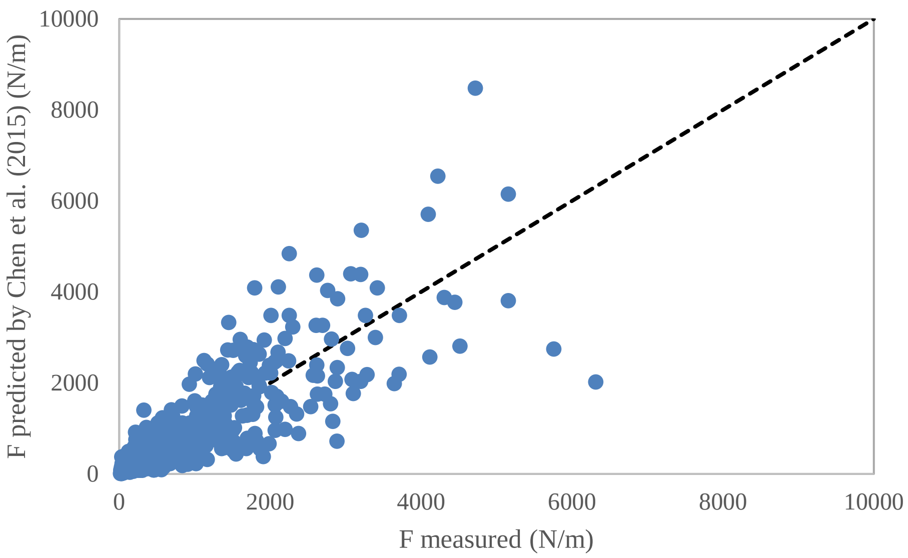

Figure 6-9. Comparison of the GWK data with the regular waves impact forces by Chen et al. (2015). The black line y = x shows the 45° line.

The procedure by Chen (2016) for irregular waves was not possible to tests, since the parameter range of the present work (deep/intermediate water) is out of range with Chen's parameter range and the given equations cannot be solved for the present range.

6.1.3 *Conclusions from the comparison with literature*

All the formulae from literature that – to some extent – fit the geometries tested in the current research have been tested against the measured data, and it can be concluded that none of them describe the data well. Most of the formulae give a (large) overprediction of the data, and all of the formulae present large scatter. Hence it is concluded that **new prediction formulae have to be deducted** to predict the impact forces on storm walls due to overtopping bores.

The existing prediction formulae use different denominators to make the force dimensionless: $\rho g d_{b0}^2$, $\rho g H_s^2$ and $\rho g H_s R_c$. None of them seem to work well for the current dataset. This will be investigated in more detail in the Section 6.4.1a).

6.2 *Measurements*

6.2.1 *Filtering and resonance*

This section deals with filtering of the impact signal. During the first analysis of the UGent-1 dataset, some unnatural recordings were noticed. Some force signals showed very high peaks followed by heavy oscillations, even showing negative values in the troughs of these oscillations. An example of one such impact signal is given in Figure 6-10.

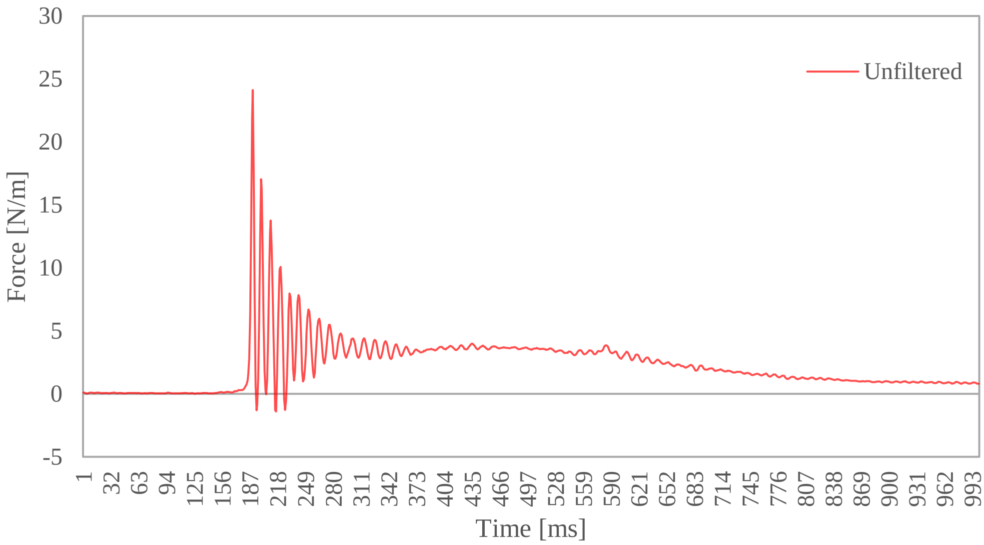

Figure 6-10. One impact during test 404 of the UGent-1 dataset.

This kind of signals only showed in the force recordings, not in the pressure recordings. Since load cells – unlike pressure cells – measure the response of the structure to the impact, it seems that the structure in the UGent-1 set-up resonated since frequency components in the force spectrum were close to the structure's eigenfrequency. To resolve this in the analysis of the force signal in the UGent-1 experiments, the natural frequency of the structure is determined by analyzing the inverse period of the tail of the oscillation, see Figure 6-11 and Figure 6-12. This leads to an eigenfrequency of the storm wall in the UGent-1 set-up of 1/11ms ≈ 90Hz.

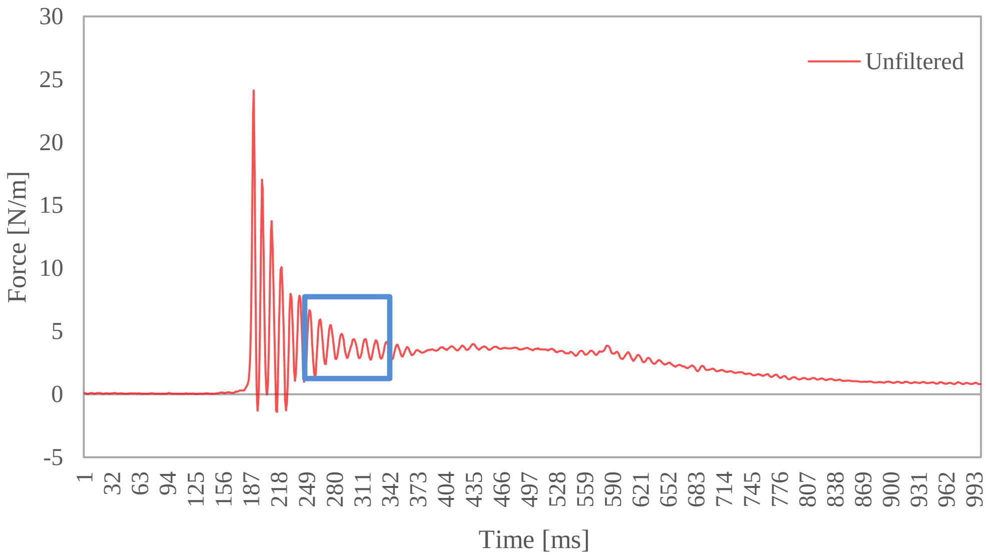

Figure 6-11. Analyzing the tail of the oscillation to determine the natural frequency of the storm wall in the UGent-1 set-up.

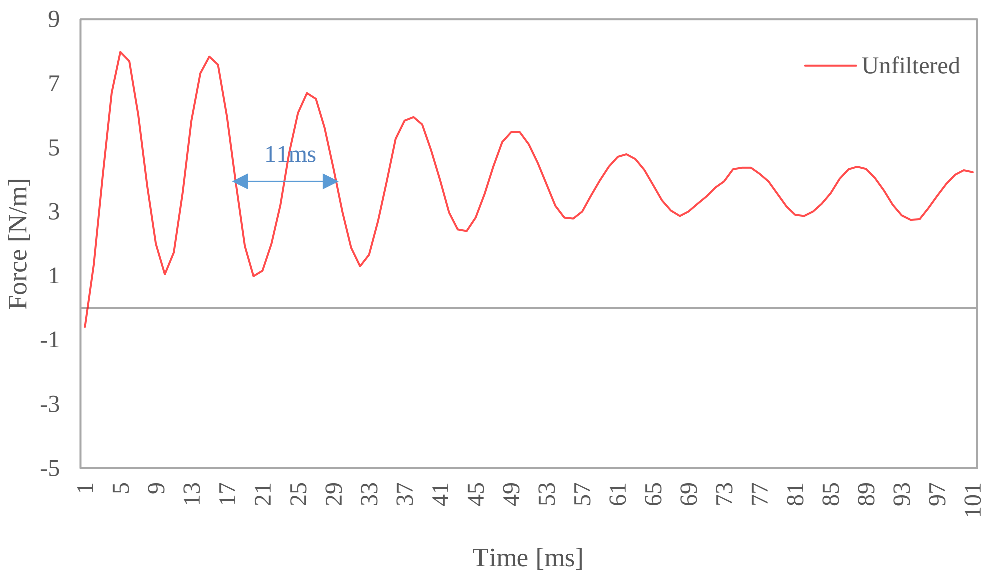

Figure 6-12. Detail of Figure 6-11. The wave period of the free oscillation is 11ms, which shows an eigenfrequency of the wall in the UGent-1 set-up of about 90Hz.

Now the energy spectrum of the force time series of one representative test from this test is plotted in Figure 6-13. It shows that most of the energy is located between 0 and 45 Hz.

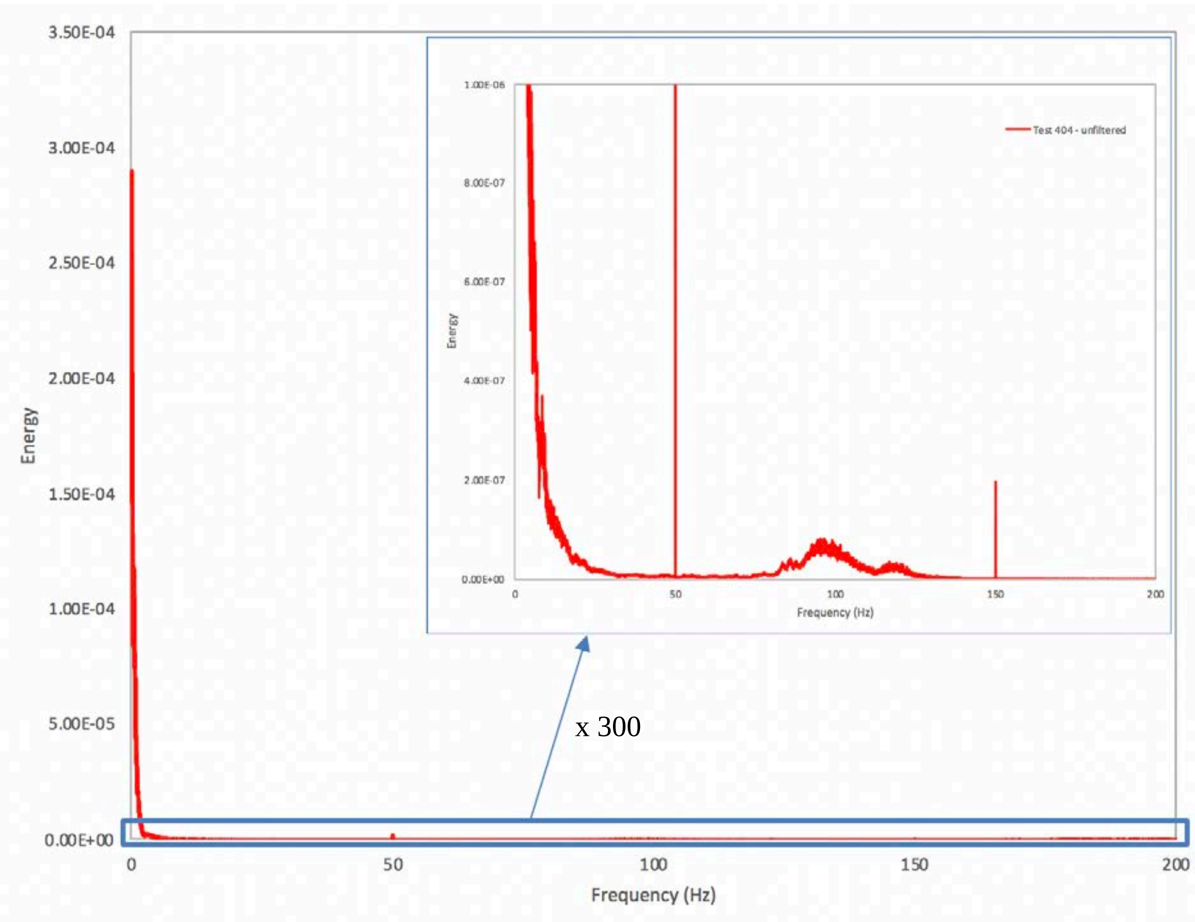

Figure 6-13. Energy spectrum of the force signal of one representative test (test 404) in the UGent-1 dataset. Zoomed by a factor 300 in the upper right corner.

When zooming in on the vertical axis by a factor 300, some peculiarities show: spikes at 50Hz and uneven multiples are noticed. Those spikes come from the electricity net. Also a bump of energy is noticed near 90Hz. Some frequency components of the force time series were near 90Hz which caused resonance of the structure that had an eigenfrequency of about 90Hz. The structure has experienced an oscillation causing an unnatural high value of the recording, which is not noticed in the pressure recordings. To avoid this resonating behavior, filtering has to be applied.

A band-stop filter (between 49.9Hz and 50.1Hz, between 149.9Hz and 150.1Hz, etc.) is always applied to remove the peak from the electricity net, and a low-pass filter of 50Hz also has to be applied. This low-pass filter degrades all values above 50Hz smoothly, so that the energy bump near the eigenfrequency is removed.

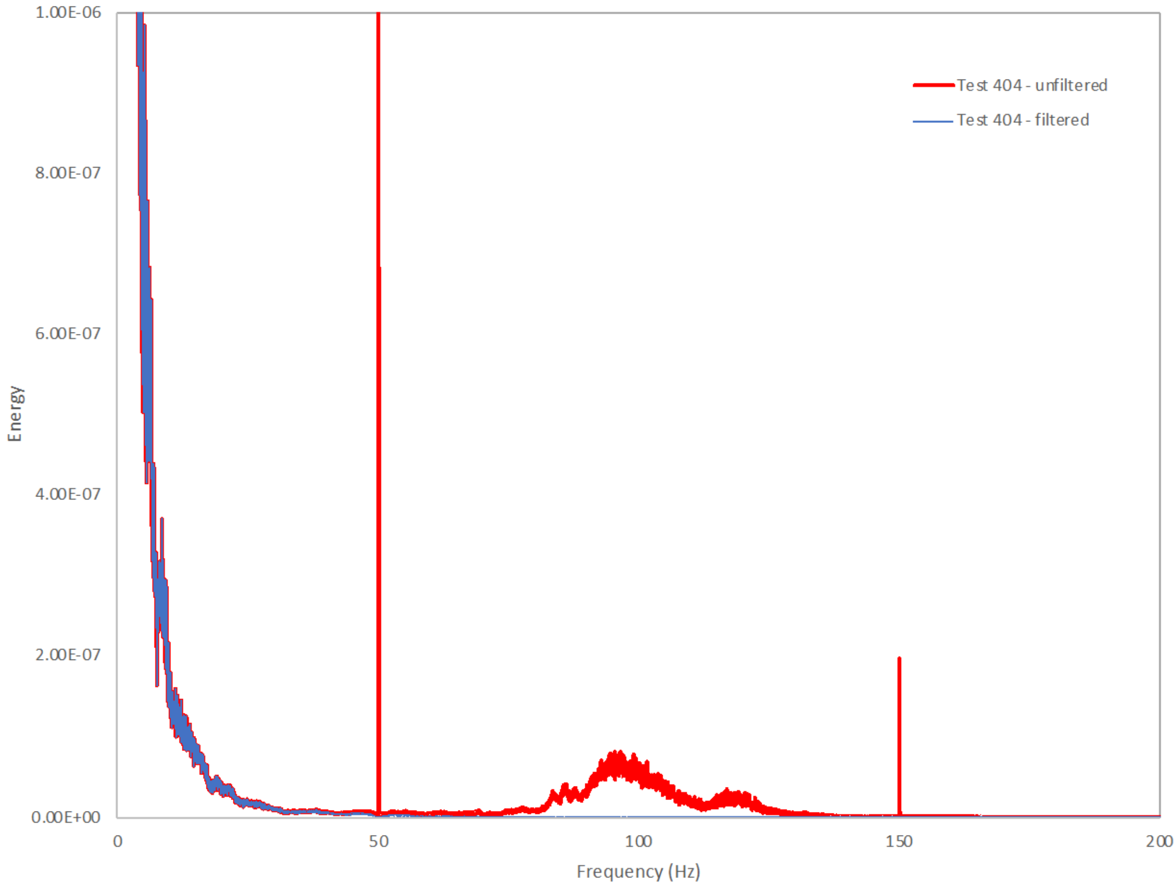

Figure 6-14. Filtering of the energy spectrum of the impacts in test 404 in the UGent-1 dataset.

Since this 90Hz energy is only a very small percentage of the full spectrum, it can be filtered out by the low-pass filter without losing actual impact energy. The realistic order of magnitude of the impact's maximum will be much closer to the filtered signal than to the unfiltered signal.

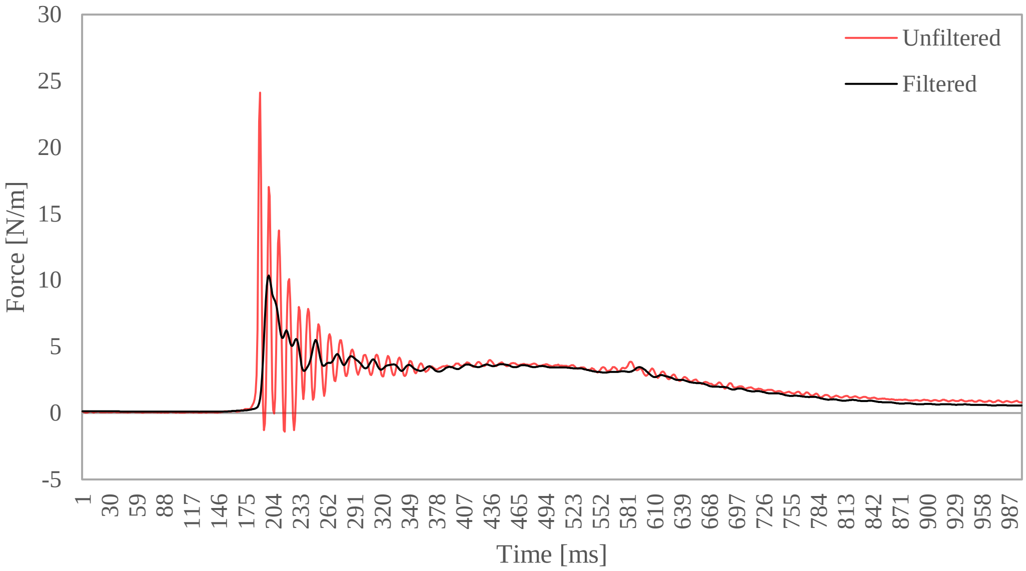

Figure 6-15. The same impact from test 404 of the UGent-1 dataset as plotted in Figure 6-10, where filtering of the signal (low-pass filter 50z and electricity net band-stop filter) have been applied.

The low-pass filter is applied to the whole UGent-1 dataset. The impacts that were not subject to resonance hardly change after filtering, see Figure 6-16.

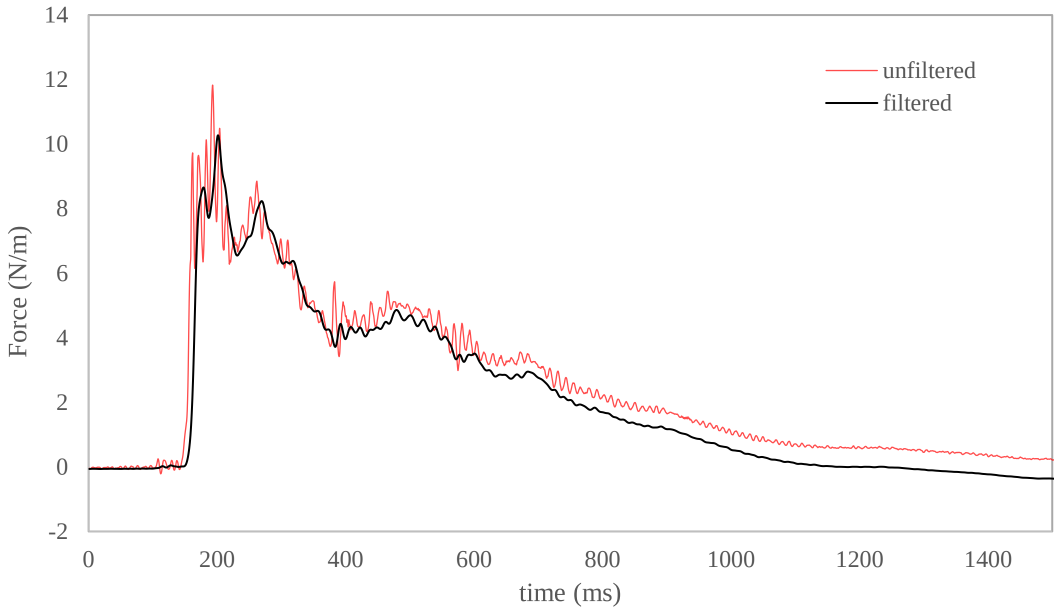

Figure 6-16. Filtering on a signal that was not affected by resonance does only influence the results minimally.

To conclude, it can be stated that filtering is required to filter out resonance and related oscillations and unrealistic high values. The value of the low-pass filter defines the peak value of the filtered signal, which is thereby subjective to this filter value. A value of about 50% of the eigen frequency is proposed, since detailed analysis has shown that thereby nearly all of the relevant energy remains untouched. By doing so, the filtered signal approximates the order of magnitude of the peak of the impact much better than the unfiltered signal with resonance. In this work, the filtered values of the UGent-1 tests are presented.

This knowledge has been applied for the Hydralab and the GWK test set-up too. Before any test was carried out, an impact was simulated with a hammer to measure the free oscillation of the wall. For the Hydralab set-up the eigenfrequency was 88Hz, where a spectral plot of a force signal mainly shows frequencies between 0 and 20Hz. Due to this large difference, no resonance of the structure occurred in those tests, so filtering of the signal was not necessary. Similar conclusions for the GWK tests were drawn. For the rest of this chapter, the unfiltered values of the Hydralab and GWK tests are used.

Prototype structures have lower eigenfrequencies than small scale structure due to their higher mass, so resonance in prototype situations could be expected at first sight. However, resonance issues are not to be expected for prototype structures. The eigenfrequency value derived for the small scale structure, 91Hz, is not the eigenfrequency of the storm wall itself, but the eigenfrequency of the whole system (a storm wall attached to a force sensor with a spring inside). The calculated eigenfrequency of the storm wall in model scale is much higher, order 1800Hz. A prototype storm wall in concrete of 1m high and 30cm thick has an eigenfrequency of about 170Hz, clearly below the model scale value, but still double of the derived value 91 Hz of the whole small scale system. Wave-induced impacts have frequencies between 0-50Hz, clearly below 170Hz, so prototype resonance effects are not to be expected.

6.2.2 *Shape of the impact recording*

The literature review has described different geometries where wave impacts have been recorded (Section 2.6). The geometries that fit those in the current research best were found in Chen (2016) and Streicher et al. (2018), however both sources have (very) shallow foreshores with breaking and broken waves, where in the current study non-breaking waves are considered. Nevertheless, a dike slope, a promenade and a storm wall were present in both sources and in the current research. For such geometries, the force recordings in literature describe two possible shapes: a church-roof shape with a large first dynamic peak of short duration and a longer but lower second quasi-static peak, and a twin-peak shape where the quasi-static peak is of the same magnitude or even larger than the dynamic peak. The twin-peak profiles were noticed most often by both authors. In Figure 6-17 to Figure 6-20, typical recordings from the three test campaings in the current research (UGent-1, GWK, Hydralab) are shown. For the UGent-1 research, only the geometry ‘smooth dike with promenade and wall’ is shown in Figure 6-17 and Figure 6-18 to compare with impacts on the same geometry in GWK (Figure 6-19) and Hydralab (Figure 6-20) and with Chen’s and Streicher’s findings.

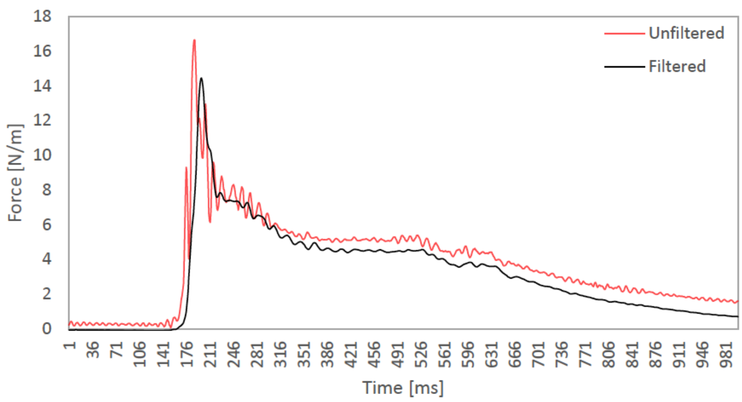

Figure 6-17. Impact with a church-roof shape of the UGent-1 dataset on geometry smooth dike with promenade and storm wall. The filtering is explained in Section 6.2.1.

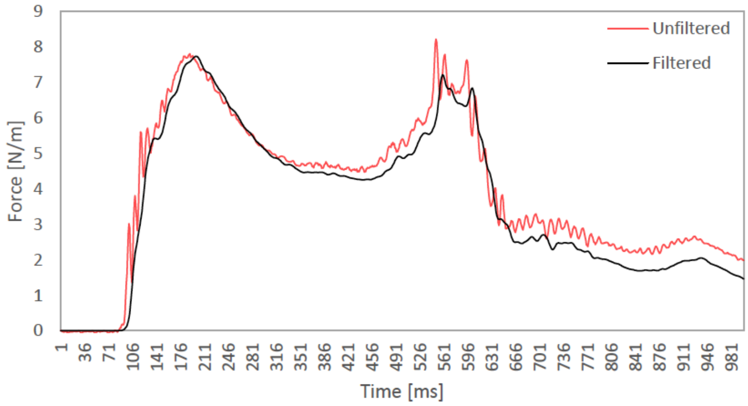

Figure 6-18. Impact with a twin-peak shape of the UGent-1 dataset on geometry smooth dike with promenade and storm wall. The filtering is explained in Section 6.2.1.

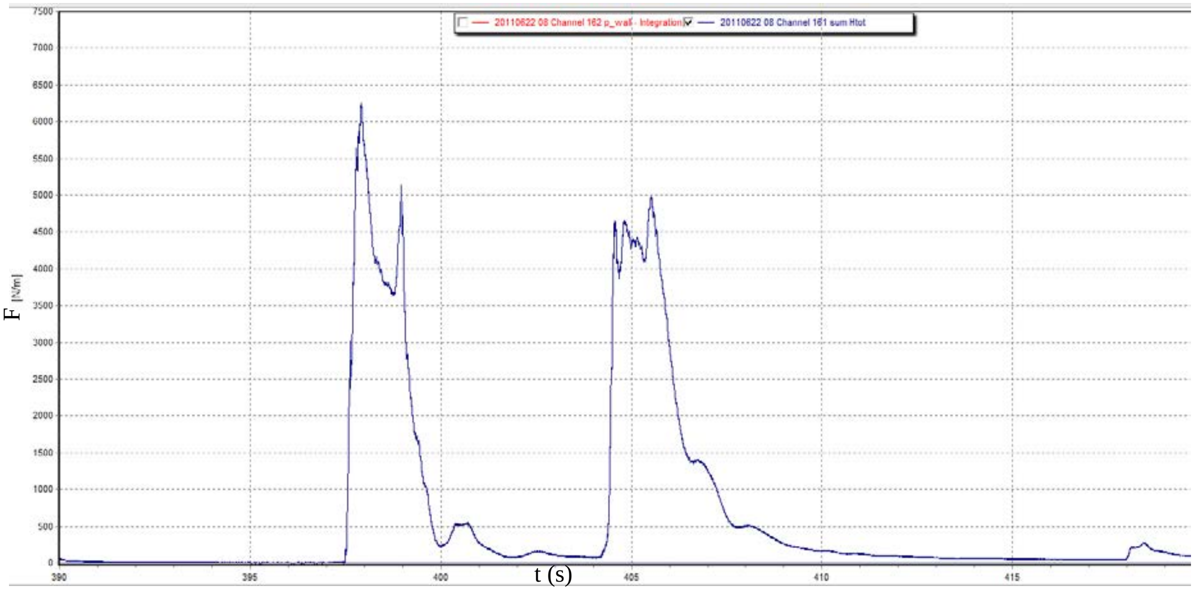

Figure 6-19. Force over time recording of 2 consecutive impacts from a test in the GWK tests.

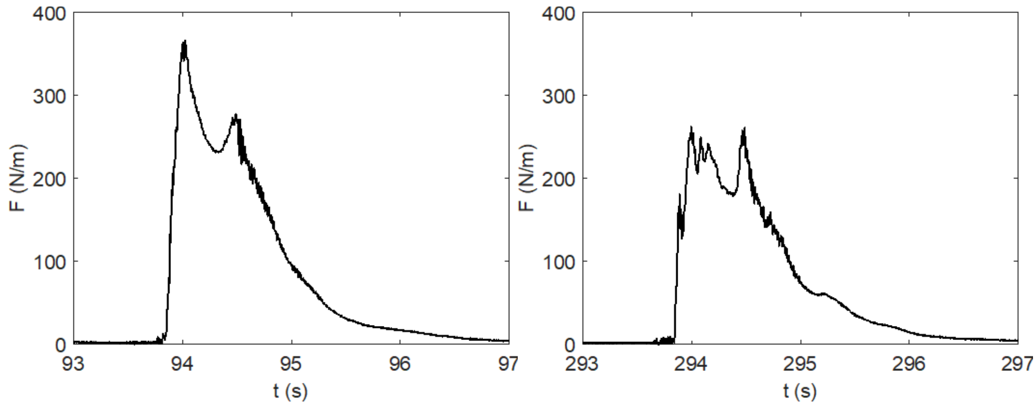

Figure 6-20. Two different impacts observed in a test during the Hydralab tests.

Just like in literature, the above Figure 6-17 to Figure 6-20 also show both church-roof and twin-peak impacts shapes recorded in the three different test campaigns. A visual observation tells that all the highest impacts in the UGent-1 dataset have a church-roof shape, but besides this top of the distribution, most impacts show a twin-peak shape. In the GWK dataset mostly twin-peaks shapes are noticed, where no big difference between the dynamic and the quasi-static peak exists. The impacts in the Hydralab experiments mostly have a twin-peak shape, with a few high peaks that more tend towards church-roof shape. These findings are in line with Chen (2016) and Streicher et al. (2018): mostly twin-peak shaped impacts with some exceptions that have church-roof profiles with a high dynamic peak. These are the highest impacts in the tests.

Besides dikes with promenade and storm wall, in the UGent-1 dataset also other geometries were tested. In Figure 6-21 to Figure 6-23, the highest impacts on these additional geometries in the UGent-1 dataset are shown: a storm wall located at the end of a smooth dike (without promenade): without bullnose (Figure 6-21) and with bullnose (Figure 6-22 and Figure 6-23). In Figure 6-22, the horizontal forces on the storm wall with bullnose are shown, where in Figure 6-23 the vertical forces are shown. The highest impacts on the additional geometries have a church-roof shape, lower impacts also show a twin-peak shape.

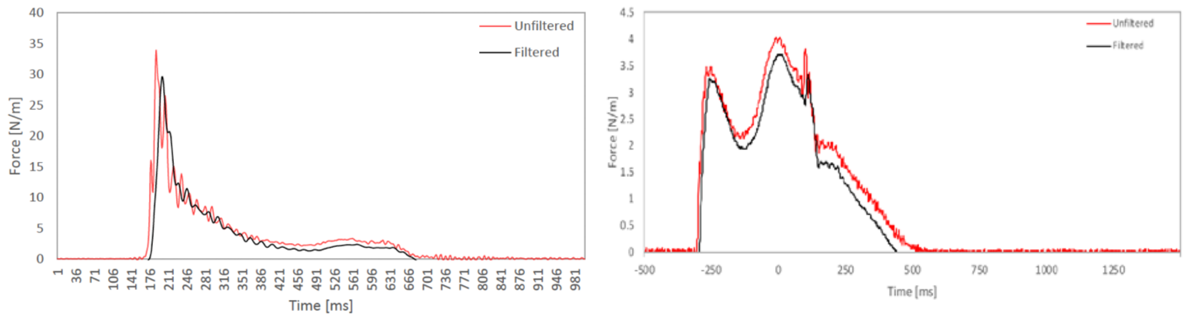

Figure 6-21. Typical impact on a storm wall on top of a smooth dike (no promenade). Church-roof (dynamic) impact on the left (30-35N/m model scale value), twin-peak (quasi static dominant) impact on the right (4N/m model scale value).

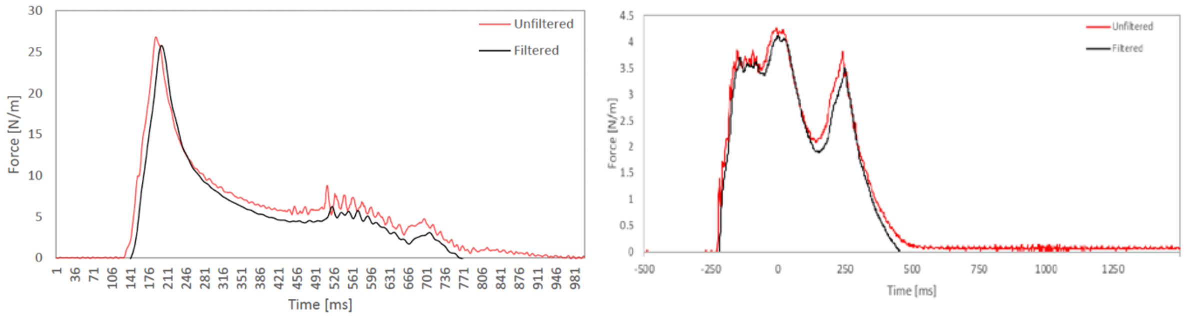

Figure 6-22. Typical impact on a smooth dike with storm wall and bullnose – horizontal measured force. Church-roof (dynamic) impact on the left (25N/m model scale value), twin-peak (quasi static dominant) impact on the right (4N/m model scale value).

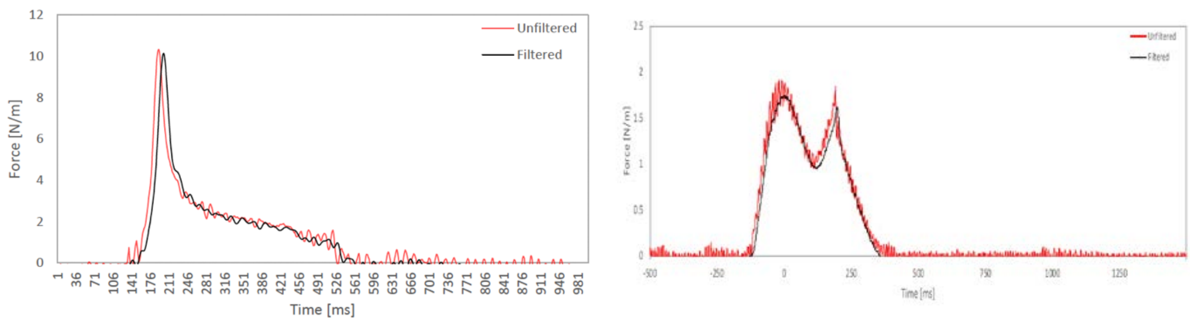

Figure 6-23. Typical impact on a smooth dike with storm wall and bullnose – vertical measured force. Church-roof (dynamic) impact on the left (10N/m model scale value), twin-peak (quasi static dominant) impact on the right (2N/m model scale value).

It can be seen from the above figures (Figure 6-17 to Figure 6-24) that the dynamic peak has a very short duration, and the quasi-static peak has a much longer duration. This has already been reported by several authors (Oumeraci et al. (1993), Pedersen (1996), Kortenhaus & Oumeraci (1998), Chen (2016), Streicher et al. (2018), …). The peak detection code written for this research to detect the maximum recorded value per impact did not make a difference whether it was due to the dynamic or the quasi-static impact. Only impacts with a peak value higher than the threshold value 1 N/m (UGent-1) or 4N/m (Hydralab) were taken into account, and peak values were sought in a window of 1s (UGent-1) or 2s (Hydralab), which is about half of the model scale wave period.

6.2.3 *Sensitivity of the different ways to measure the impacts*

In the UGent-1 test set-up, the impact recordings were carried out with a set of two force sensors, located on the left side and the right side from the center of the storm wall, see Figure 3-14 to Figure 3-16 and repeated here below in Figure 6-24.

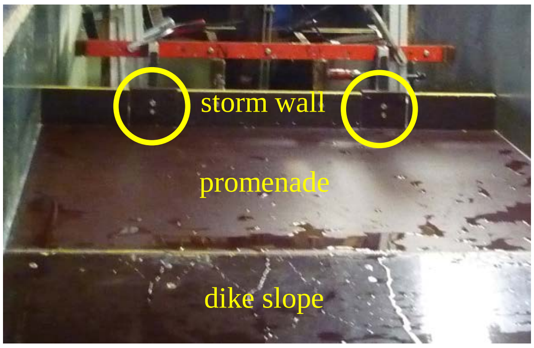

Figure 6-24. Repitition of Figure 3-15, indication of the two storm wall measurements in the UGent-1 test campaign.

In the GWK dataset, different storm walls have been installed: a set of horizontal plates with 3 x 4 force sensors, a vertical plate with 4 force sensors and a vertical plate with 8 PDCR (Figure 3-28, repeated in Figure 6-25). For some of the tests in GWK, the wall was fully closed, for the majority of the tests the wall was partially open (Figure 3-27 and repeated in Figure 6-25)

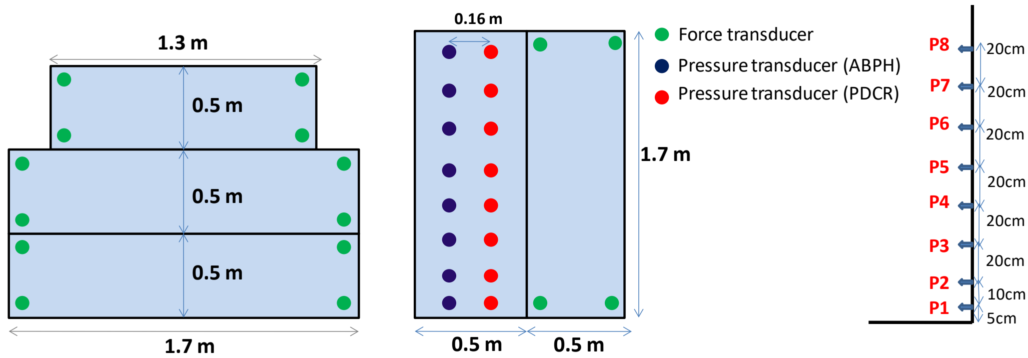

Figure 6-25. Repitition of Figure 3-28, indication of the measurement plates and equipment in the GWK test set-up.

Figure 6-26. Repitition of Figure 3-27, closed storm wall on the left, open storm wall on the right.

In the Hydralab experiments, a storm wall with 4 force sensors and a storm wall with 3 pressure sensors on a vertical line was installed (Figure 3-37, repeated in Figure 6-27).

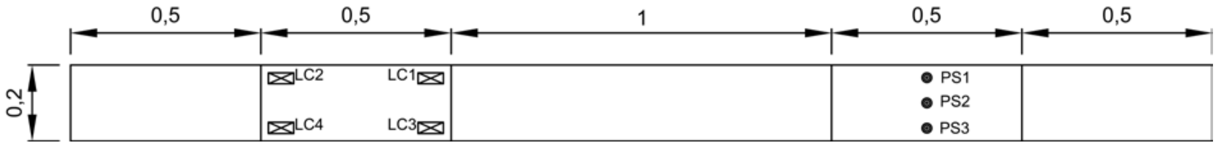

Figure 6-27. Repitition of Figure 3-37, indication of measurement plates in the Hydralab test set-up.

Hence, three different test set-ups habe been used to measure the impacts on a storm wall due to overtopped bores. In this section, the different ways used to measure these impacts are compared to each other.

a) *Location of measurements: left versus right (UGent-1)*

In the UGent-1 test campaigns, two storm wall sections were equipped to measure forces: one on the left side, one on the right side (Figure 6-24). Analysis of impacts on the left and right force sensor show a visual good correlation, see Figure 6-28. Two low exceedance values have been plotted, F_{max} which is the maximum measured force in the test and $F_{1/250}$ which is the average value of the highest 0.4% forces, where 0.4% is calculated from the number of incoming waves. The scatter is larger for F_{max} than for $F_{1/250}$, but both don't show a consistant deviation. This means no cross waves or deflections of the bore in the wave flume were detected. Both the left and the right force value are taken into account for the analysis later in this chapter.

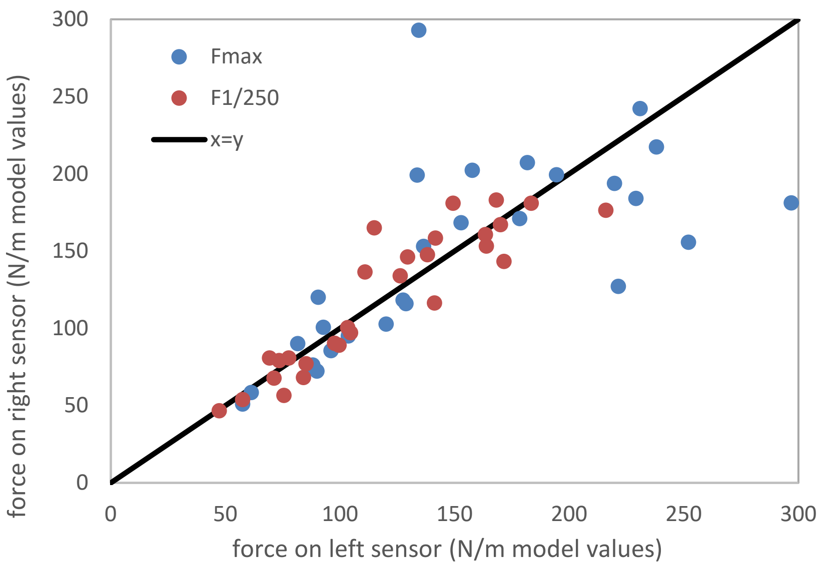

Figure 6-28. Comparison between the forces measured on the left and the right sensor in the UGent-1 dataset. The black line y = x shows the 45° line.

b) *Horizontal (left) plates versus vertical (right) plate (GWK)*

In the GWK test-campaign, the force transducres also were installed on a "left recording section" and a "right recording section". Unlike in the UGent-1 set-up the left and right wall in the GWK project were not equal to each other. The left recording section consisted of 3 individual horizontal plates (1.7m x 05m, 1.7m x 0.5m and 1.3m x 0.5m) and the right recording section of 1 vertical plate (0.5m x 1.3m), see Figure 6-29.

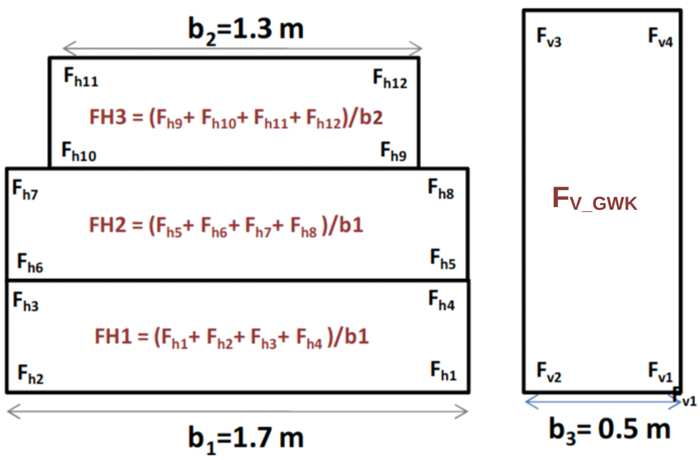

Figure 6-29. GWK test set-up: left storm wall consisting of horizontal plates, right storm wall consisting of a vertical plate.

The forces are expressed in force per meter width (N/m or kN/m) by dividing the measured forces through the width of the recording plate. For the left wall this means: $F_{H\_GWK} = F_{H1}+F_{H2}+F_{H3}$, with F_{H1}, F_{H2} and F_{H3} the sum of the 4 force sensors per plate divided by the width of the plate, as defined in Figure 6-29. For the right wall the total force is calculated in a similar way: $F_{V\_GWK} = (F_{V1}+F_{V2}+F_{V3}+F_{V4})/b_3$. Figure 6-30 shows all measured impacts from 21 tests on the left recording section in GWK (F_{H_GWK}) compared to the right recording section (F_V_GWK). It shows that, similar as in the previous section, forces on both walls are equal. Both the force values on the horizontal and the vertical wall are taken into account for the analysis later in this chapter.

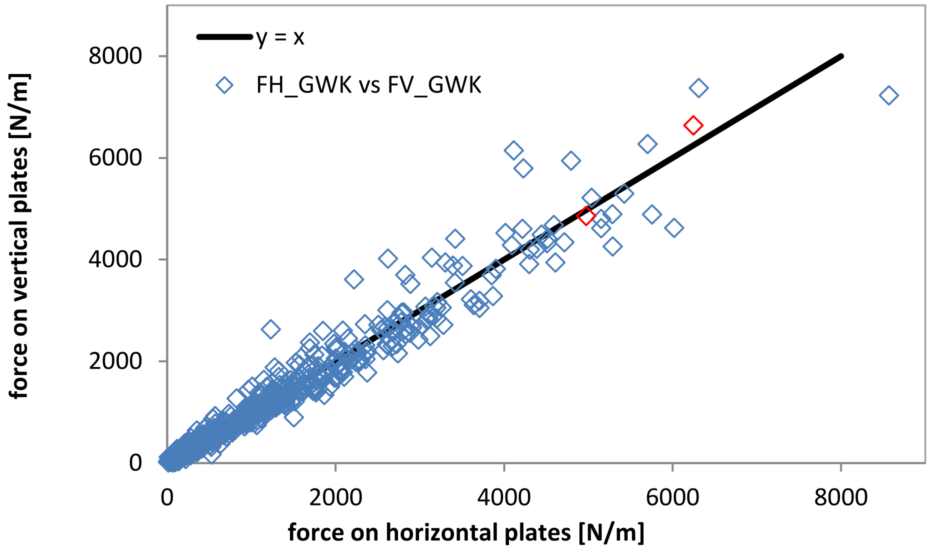

Figure 6-30. Comparison between the forces measured on the horizontal plates and the vertical plate in the GWK dataset. The two red markers are shown again in Figure 6-31 and Figure 6-34. The black line y = x shows the 45° line.

Figure 6-31 shows the two impacts indicated in red from Figure 6-30, where in the upper panel the forces on the vertical plates are shown, and in the lower panel the forces on the horizontal plate, both expressed in N/m.

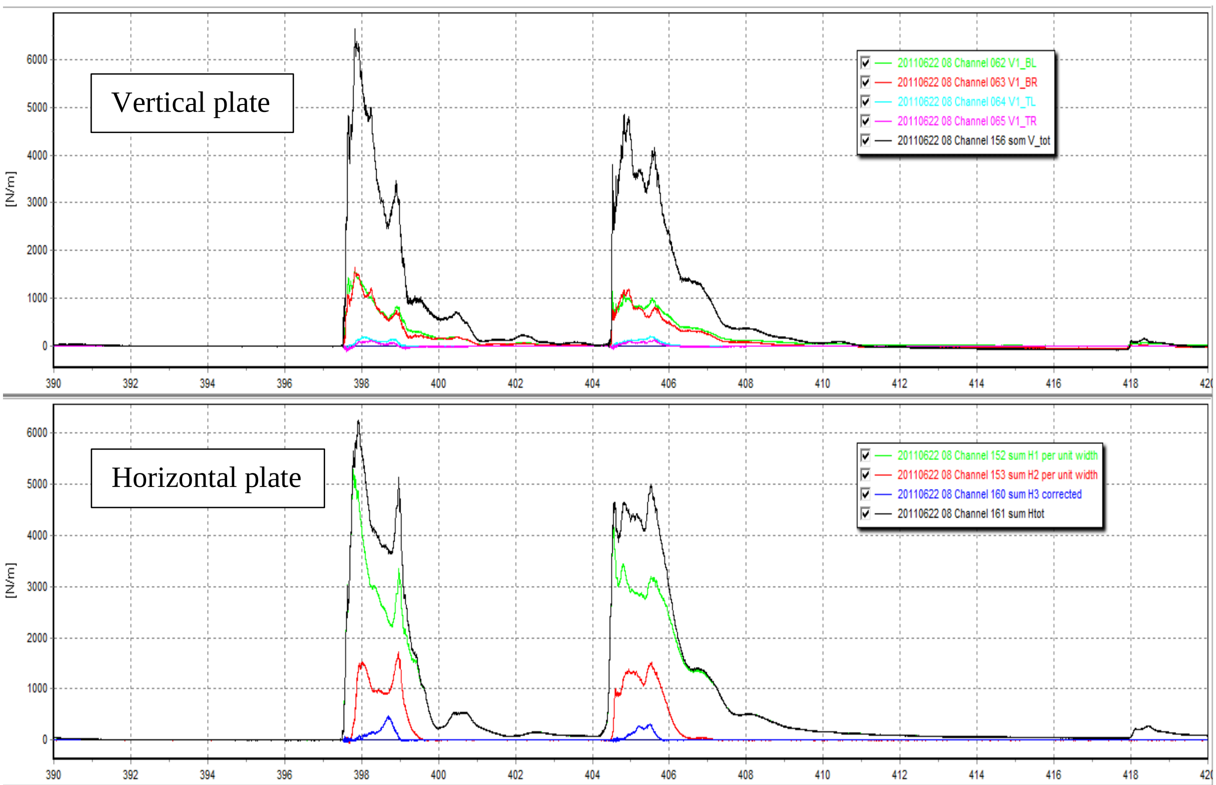

Figure 6-31. Example of 2 consecutive impact from test 20110622_08 in the GWK tests. The upper panel shows the force recordings on the vertical plate, the lower panel on the horizontal plate. Both panels express the force in N/m.

The first impact on the vertical plate has a maximum value (total force, black line) of 6600N/m, the second one 4850N/m. On the horizontal plate those values are 6300N/m and 5000N/m. Good agreement in magnitude (only 5% and 3% difference, respectively) and in shape can be observed from these graphs.

Besides the total force in black, Figure 6-31 also indicates the forces on the 4 individual sensors on the vertical plate (top panel) and the summed forces per meter of the 3 separate plates of the horizontal storm wall (lower panel). The recordings on the lowest plates or sensors show higher force values and a more pronounced church-roof signal than on the higher plates. The same was also detected in Figure 2-18 by Chen et al. (2014). This indicates that the lower part of the storm wall experiences most of the impact. This was to be expected since the overtopping waves travels on the promenade as a turbulent bore with a limited height only.

c) *Integrated pressures versus forces*

Besides forces, also pressures were measured in the GWK tests and in the Hydralab campaign. From the previous section, it’s already known that measuring forces at the left or the right side of the flume does not influence the results significantly. However, measuring pressures can be influenced by the location of the sensor in combination with the often only locally occurring impacts related to turbulent bores. Pressure sensors have a much smaller surface (ca. 1cm^2) and measure over a discrete vertical line, where force sensors measure over a surface of a certain width (ca. 1m^2 in GWK, 0.1m^2 in Hydralab). These wider recording surfaces smoothen out local variations due to turbulence.

In Figure 6-29 the procedure to compile the total force was shown. For pressures, a different procedure is required. When looking at the pressure values of the 8 individual pressure sensors (GWK experiements) at a certain moment in time, and plotting them over the height of the storm wall, Figure 6-32 shows.

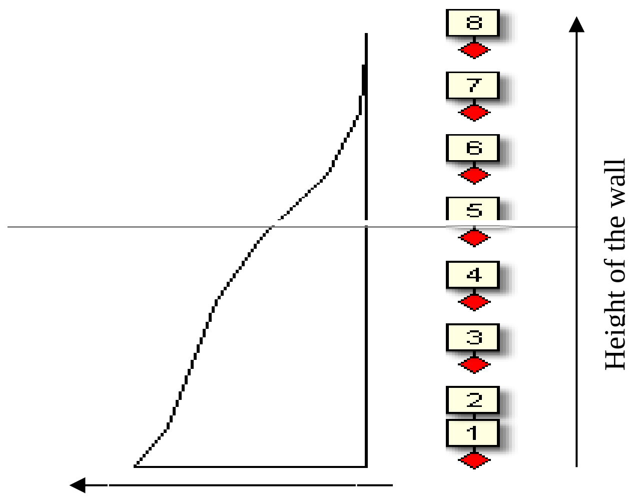

Figure 6-32. Envelope of the recordings of the 8 individual pressure sensors in the GWK experiments at a certain moment in time during an impact.

Pressure sensors have an output in Pa (N/m^2) and need to be integrated over the height of the wall to find a total impact force on the wall in N/m. This integration can be carried out by using rectangles (Eq. [6-1]) or trapezoids (Eq. [6-2]), see Figure 6-33. Both methods give similar results (when sufficient pressure sensors are installed over the height).

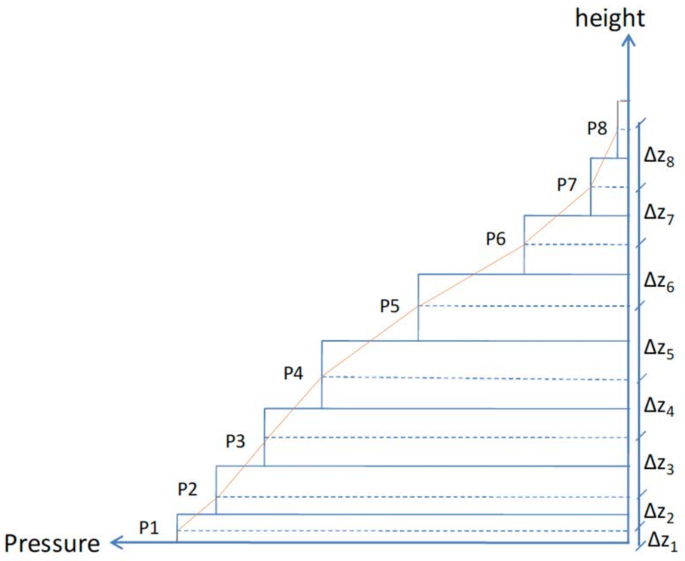

Figure 6-33. Rectangular integration (blue) and trapezoidal integration (orange) to obtain the total integrated pressure from 8 discrete pressure sensors in the GWK experiments.

$$P_{int\_rect} = P_1(t) \cdot \left[\Delta z_1 + \frac{\Delta z_2}{2}\right] + P_8(t) \cdot \Delta z_8 + \sum_{i=2}^{i=n-1} P_i(t) \cdot \left[\frac{\Delta z_i + \Delta z_{i+1}}{2}\right] \tag{6-1}$$

$$P_{int\_trap} = P_1(t) \cdot \Delta z_1 + P_8(t) \cdot \frac{\Delta z_8}{2} + \sum_{i=1}^{i=n-1} \left(P_i(t) + P_{i+1}(t)\right) \cdot \frac{\Delta z_{i+1}}{2} \tag{6-2}$$

Two consecutive impacts from a test in the GWK dataset, randomly chosen, are shown in in Figure 6-34, where both the integrated pressure (red) and the summed force (blue) are shown. Both signals show good agreement, however the peaks of the integrated pressure signal results into slightly higher values than the force values. The pressure signal however is a little less smooth and more spiky compared to the force signal.

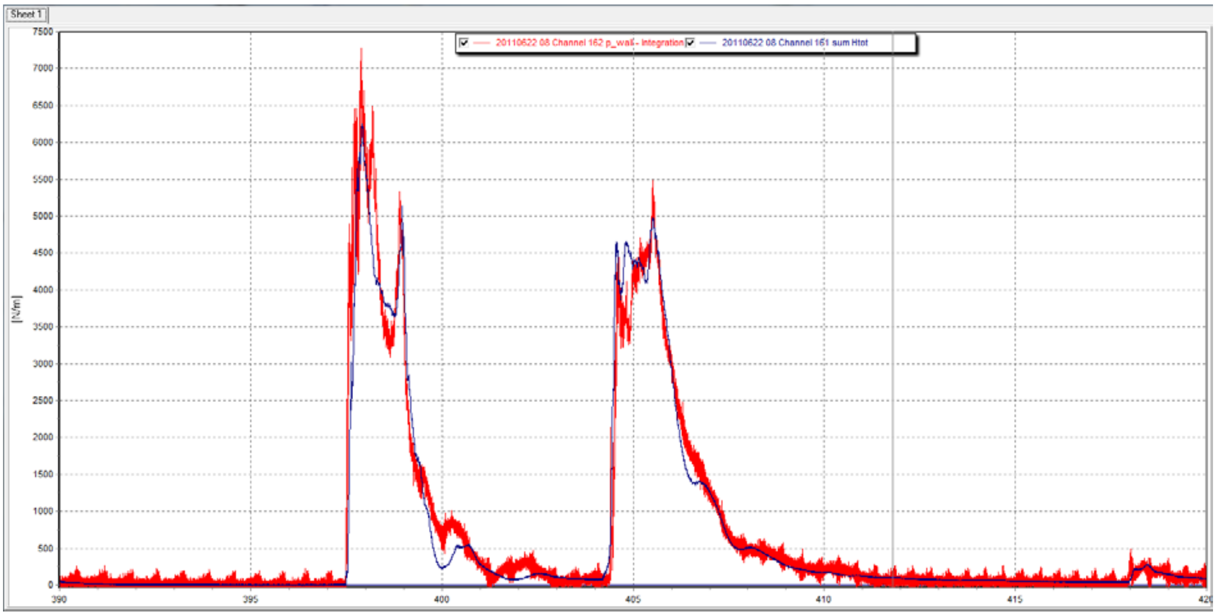

Figure 6-34. Force over time (blue) and pressure over time (red) recording of 2 consecutive impacts from test 20110622_08 in the GWK tests.

Figure 6-35 shows a comparison plot between the maxima of the total forces with the maxima of the integrated pressures for another randomly chosen test in the GWK experiments. Figure 6-36 shows a comparison for all GWK-tests with irregular waves. The integrated pressures are consistently a little higher than the forces. The difference becomes bigger for the higher impacts, and is on average about 25%.

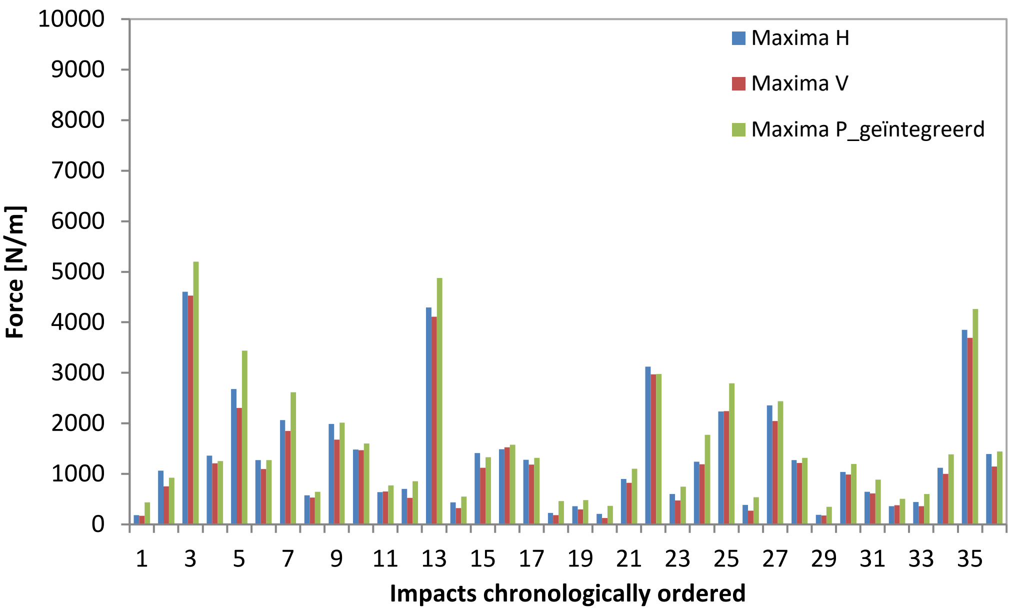

Figure 6-35. Comparison of all impacts in 1 GWK test: summed forces per meter on the horizontal plate (blue), summed forces per meter on the vertical plate (red) and integrated pressures (green).

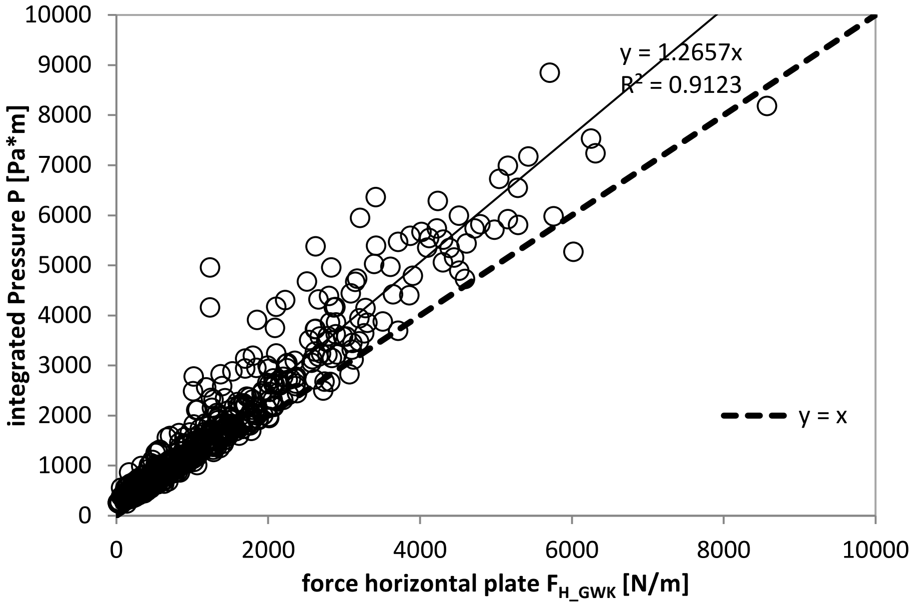

Figure 6-36. Comparion of the all forces with all integrated pressures in the GWK experiments (irregular wave tests). The black dashed line y = x shows the 45° line.

There are multiple reasons for this difference.

- As mentioned before, the pressure sensors have a smaller measuring surface. If a local peak value in the turbulent bore, which is characterized by spatial pressure variations, hits this smaller surface, a high value is recorded. In case of force sensors this high values is smoothened out since forces are measured over a larger area.

- Pressure sensors measure the impact, and are not dependent on the structure. Force sensors measure the response of the structure and might thereby be influenced by the structure's response (stiffness, reaction time, …). However the stiffness of the whole supporting structure was very high in all of the performed tests.
- Some energy might have been lost due to water evacuating through the gaps in between the measuring plates in GWK. The force sensors, measuring a certain area, are possibly a little more influenced by this than the smaller pressure sensors which are located further away from these gaps.
- In some tests, the overtopping reservoir was full and overflowing back towards the storm walls, so that a residual water layer behind the storm walls was noticed. This layer exerts a hydrostatic force component on the wall in the opposite direction (seaward), which reduces the measured total force. Pressure sensors were not influenced by this negative hydrostatic force.

Also in the Hydralab experiments pressures and forces were measured. The same conclusions as for the GWK experiments were found. An example of 4 consecutive impacts in a Hydralab test is given in Figure 6-37.

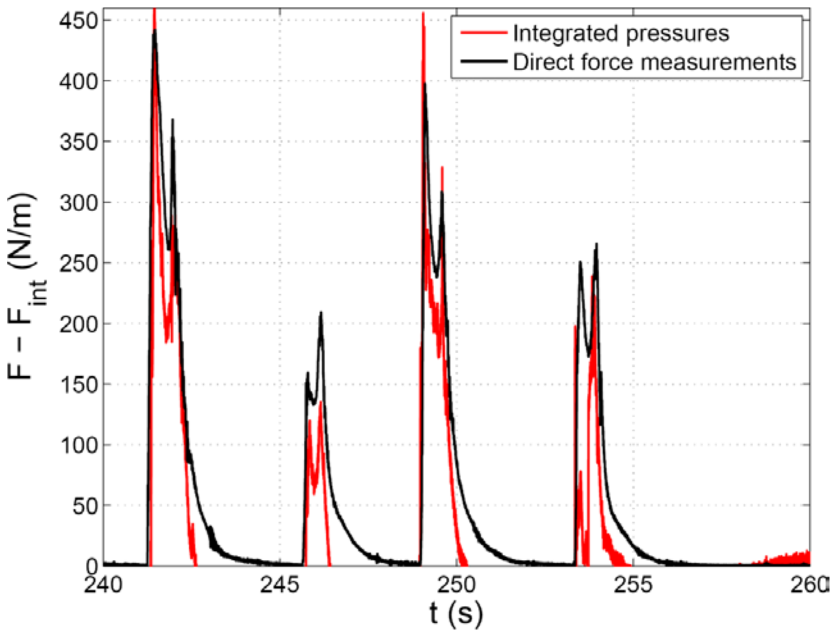

Figure 6-37. Force over time (black) and pressure over time (red) recording of 4 consecutive impacts from a test in the Hydralab campaign.

6.2.4 *Pressure/force distribution over the height*

Figure 6-31 already indicated that the lower sensors/walls register the largest part of the total force recording. Also in Figure 6-32, where the momentaneous pressure recordings are shown over the height of the wall, it can be seen that the lower sensors record higher values than the highest sensors. The integrated pressures over the wall height are shown during some important moments in the time recording, see Figure 6-38 to Figure 6-40. The red vertical line in the lower panel of the figure shows the time step in the integrated pressure profiel for which the upper panel shows the pressure values of the individual pressure sensors. The impact force for which these visualisations are made is the same as shown earlier, the first impact of two in in Figure 6-19, Figure 6-31 and Figure 6-34.

The green horizontal line plotted on the Figure 6-38 to Figure 6-40 shows the maximum value of the flow depth recorded at the third flow depth meter just before this impact occurred.

Since the bore front is a little ahead of the main body of the bore, due to its wedge shape as described by Chen et al. (2015), only the first two pressure sensors are touched by this bore front (Figure 6-38).

Figure 6-38. Start of the impact – upper panel shows the momentaneous pressure distribution over the wall height, the moment is indicated with a red line in the lower panel, which shows the integrated pressure over time.

Then the dynamic peak occurs, where the sensors near and below the bore height (sensors 1 to 5) show high values and the higher sensors show lower values due to a small layer of run-up which is running ahead of the main body (Figure 6-39). Most of the surface underneath the pressure envelope is registered up to 1 sensor above the flow depth, which indicates that the height of the storm wall is not of main importance in the dynamic impact.

Figure 6-39. Dynamic peak – upper panel shows the momentaneous pressure distribution over the wall height, the moment is indicated with a red line in the lower panel, which shows the integrated pressure over time.

In Figure 6-40 the maximum of the second peak, the quasi-static peak, is shown. A nice linear envelope shows, due to the maximum run-up height of the bore on the wall during this impact. At this moment, the run-down starts and the pressure values reduce. The height of the storm wall plays a significant role here.

Figure 6-40. Quasi-static peak – upper panel shows the momentaneous pressure distribution over the wall height, the moment is indicated with a red line in the lower panel, which shows the integrated pressure over time.

The example shown above has been investigated for more impacts always showing the same trend: when an impact is dynamic (church-roof type with highest 1st peak), the pressure sensors below the flow depth show large values and reduce for sensors located higher at the wall. When an impact has a higher 2nd peak (twin-peak type), the run-up dominates the pressure distribution and a linear shape shows. For what follows, the shape, rise-time or duration have not been further considered. The maximum value of the whole impact is used. The point of application seems to be near/below the depth of the incoming bore, although this should be investigated further in future work.

6.2.5 *Force distribution*

The previous sections have given some insight on the recorded signals of impacts, their comparison to other recordings and the need for filtering, all focused on individual impacts. This section investigates the distribution of all impacts in a storm. Chen (2016) uses a Pareto distribution to present her data, but states that also Weibull, Gamma and Exponential distributions perform well in describing the impacts. An example from the Hydralab dataset, which behaves similar than the UGent-1 and GWK dataset, is given in Figure 6-41. The vertical axis shows the measured forces, normalized by dividing through the test-average force value. The horizontal axis shows a theoretical generated (normalized) population based on estimated PDF-parameters. Similar to what Chen found, Weibull, Pareto and Exponential distributions describe the impacts well.

In a later stage of the current work, the impacts will be linked to the individual overtopping volumes, and those are described in literature by a Weibull probability distribution function. For that reason, a Weibull distribution is selected here to describe the impacts on storm walls.

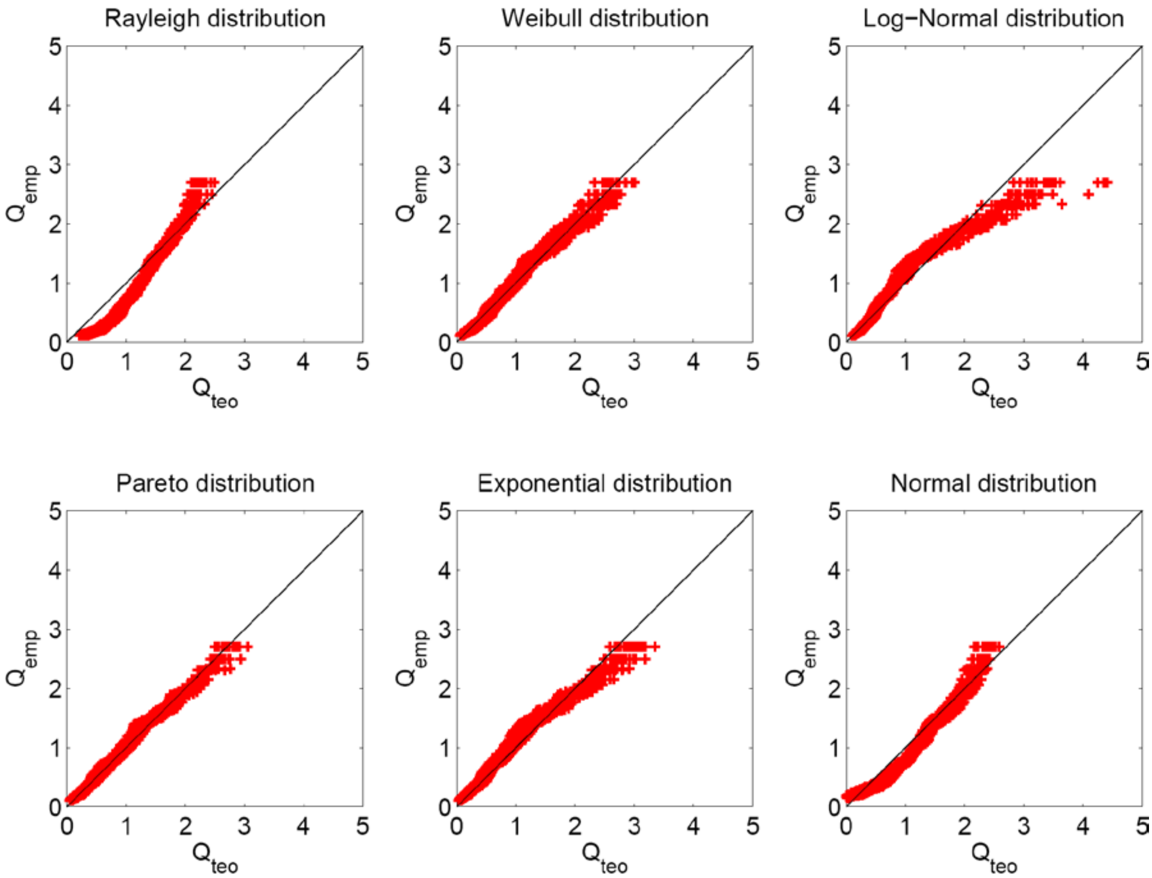

Figure 6-41. Different probability distribution functions for the impact forces. The measured normalized forces (Q = measured value divided by average measured value in one test) on the vertical axis, the theoretically estimated normalized forces on the horizontal axis.

More examples on a good representation of the normalized forces by a Weibull PDF are given in Section 6.4.2.

6.2.6 *Low exceedance value*

For design purposes, it's not the average value of a distribution of impacts that is relevant for the design of the wall. Structural design requires low-exceedance values since they are key for the stability of the structure. Den Heijer (1998) and Pedersen (1996) advise, however, to not use the maximum force F_{max} due to the stochastic behavior of impact forces and the dependency of the maximum force from the number of waves in a storm.

The low-exceedance values noted with a percentage as subscript are defined as: the value that is exceeded by the noted percentage of the waves, e.g $F_{0.1\%}$ is the value exceeded by 0.1% of the waves. Since this research works with about 1000 waves per model tests, $F_{0.1\%}$ is equal to F_{max}. Therefore, this parameter is thus also not used in the present work.

The low-exceedance values noted with a fraction as subscript ($F_{x/y}$) are defined as the average force value of the highest x/yth, related to the number of waves, impacts, e.g. $F_{1/250}$ is the average force value of the highest 1/250th of the total number of incoming waves in one test. For a time series of 1000 waves, $F_{1/250}$ is the average of the highest 4 impacts. For a test with 3000 waves, $F_{1/250}$ is the average of the highest 12 impacts.

Since it is advised in literature not to use F_{max}, $F_{1/250}$ is chosen in this work. This is based on the suggestion by Goda (1985) and the Coastal Engineering Manual (2001) who define design forces on breakwaters with $H_{1/250}$ instead of H_{max} for similar reasons. $F_{1/250}$ is a statistically more stable (i.e. less scattered) parameter. Design formulae that were set-up in the analysis of this work showed a (up to 50%) smaller standard deviation on the fitted parameters when $F_{1/250}$ was used instead of F_{max} (Van Doorslaer et al., 2015b).

In Section 6.2.1 the shape of the impact was discussed. Mostly, the highest impacts in the distribution, which determine both F_{max} as $F_{1/250}$, have a church-roof profile with a first high dynamic peak. The time duration to reach this dynamic peak is very short and the energy below its force curve over time is small in such a short time duration.

The difference between F_{max} and $F_{1/250}$ for the UGent-1 and Hydralab dataset are shown in Figure 6-42. F_{max} is on average 25 to 30% higher than $F_{1/250}$.

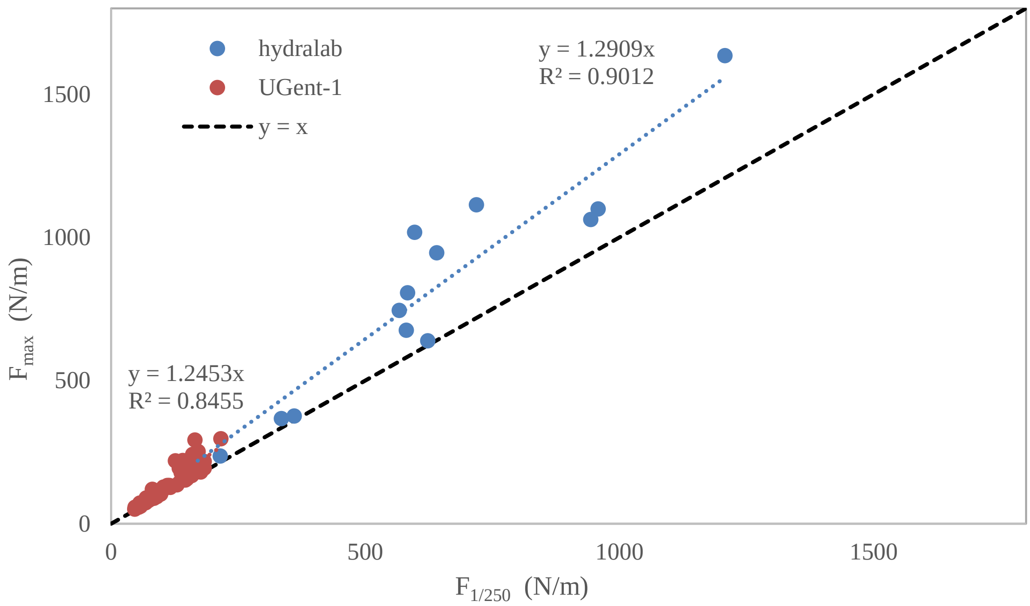

Figure 6-42. Comparison between F_{max} and $F_{1/250}$ in a dimensionless form.

6.2.7 *Summary and conclusion*

In Section 6.2 a detailed look was given to the impact signals and the different ways of recording the wave-induced forces and pressures at the storm walls. The most important findings are summarized here:

- When the spectral plot of a force time series shows energy at frequency components near the eigen frequency of the structure, like it was the case in the UGent-1 dataset, a **low-pass filter** has to be applied to filter out this energy. The **proposed filter value is about 50% of the eigen frequency**. A detailed analysis has shown that thereby only a very small fraction of the energy is removed and the relevant energy in the spectrum remains untouched. The force over time signals that didn't show resonance are hardly affected by this procedure, where for the affected signals the resonance is filtered out. The filtered signal gives a better approximation of the actual impact that would have occurred without resonance.
  Due to a larger scale and stiffer structure, the Hydralab and GWK data did not show resonance in the impact records, no low-pass filter had to be applied there.
- The impacts on the storm wall can have either a church-roof shape with a high first dynamic peak and a lower second quasi-static peak, or a twin-peak shape where the second quasi-static peak is of the same order of magnitude and sometimes even higher than the first dynamic peak. It is noticed that the **highest impacts** of a test usually show more a **church-roof** behavior where the lower impacts rather have a twin-peak shape.
- Measuring impacts on a **left or a right** recording section of the storm wall section has **not shown significant differences**.
- Measuring the impacts on **horizontal or vertical plates** of the same height **does not make a difference** when the forces are expressed per length of the wall (N/m or kN/m).
- Pressure sensors measure the impact, force sensors the total response of the structure. The applied pressure sensors give less clean signals, and need to be integrated over the height to obtain the total impact force. The applied force sensors give smoother signals and simply have to be summed in order to get the total force. **Integrated maximal pressure values seem to be consistently somewhat higher than the maximal force values.** Multiple reasons for this are possible, but local spatial variation in combination with a small measurement surface of the pressure sensors may be one of the main reasons.
  Pressure measurements start at a certain height above the promenade and have to be integrated by typically either rectangular or trapezoidal methods, where forces can be measured directly from the promenade without any loss. Also due to the smoother signal and easier installation (no row of sensors on a vertical line is requested, so also on small scale storm walls forces are easier to measure than pressures) the use of force sensors, if installed at a very stiff structure to avoid resonance effects, are usually preferable. The further **analysis in this manuscript will be performed with force sensors** because the difference between measured forces and pressure integrated forces is not significant and also more force data are available.
- The forces in a storm can be described by a **Weibull probability distribution** function.
- The **force envelope over the height of a storm wall during the dynamic impact is mostly concentrated over the height of the flow depth**. The height of the storm wall is of less importance here. The force envelope over the height during the quasi-static part of the impact is hydrostatic related to the run-up height, in which the height of the storm wall plays an important role.
- The low exceedance value chosen in this work is $\mathbf{F_{1/250}}$ to characterize extreme force values in a storm. F_{max} is statistically less stable, is dependent on the number of forces in a storm and

contains little energy in it's very narrow dynamic peak. On average F_{max} is 23% higher than $F_{1/250}$.

The studied storm walls have a rather limited height, and are principally overtoppable which means that a part of the incoming energy might go over the storm wall. For dynamic impacts (church-roof shape) the maximum value occurs before the maximum run-up at the wall is reached. Figure 6-39 shows that the force envelope over the height at that moment is concentrated near the flow depth height and the wall height is of less importance. For quasi-static impacts (twin-peak shape) the maximum impact value occurs at moment of maximum run-up (Figure 6-40) and is thus dependent on the wall-height. It may be possible that for those impacts, the maximum value could be higher for non-overtoppable walls. However, it are the high impacts (with church-roof signal) that define $\mathbf{F_{1/250}}$ wich means that this value is **not strongly dependent on the wall height**. In any case, the forces measured in this study are inseperably connected to the promenade width and the wall height. It's thereby strongly recommended to use the formulae deducted later in this chapter within their range of parameters.

6.3 *Methodology*

Three different test campaigns were carried out measuring impacts on this particular geometry in different wave flumes around Europe at different scales: small scale UGent-1 tests (Section 3.1), large scale GWK tests (Section 3.2) and midscale Hydralab tests (Section 3.3). Only non-breaking waves and smooth dikes were of interest in these test campaigns. Three different approaches are followed in the analysis and are sketched in Figure 6-43 and summarized below. Based on which information is available (only wave parameters: use approach 1; also flow parameters: use approach 2) or which information is requested (low exceedance value: use approach 1a; impact distribution: use approach 1b or 2) it's up to the user to select the preferred approach. The objective of all approaches however is to predict wave-induced impacts on storm walls.

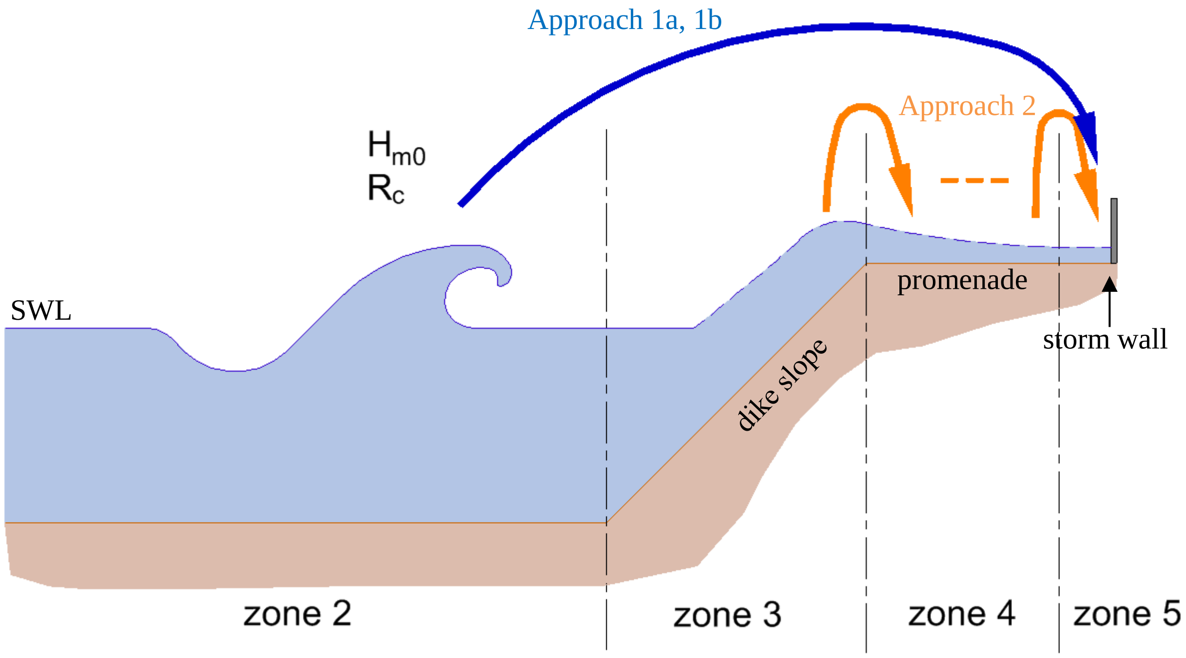

Figure 6-43. Different methodologies to calculate impact forces: a direct approach (blue arrow) to connect hydraulic and geometric parameters to the impact forces (approaches 1a and 1b), and an indirect approach (orange arrows) to link overtopping volumes to flow parameters to impact forces (approach 2). The dashed line indicates the exponential decay of flow parameters along the promenade.

Approach 1a: a direct link between impact forces (zone 5 in Figure 6-43) and hydraulic parameters (zone 2) is studied (blue arrow in Figure 6-43). As concluded in Section 6.2.6, the low exceedance value $F_{1/250}$ is used which is the average force value of the highest $1/250^{th}$ of the total number of incoming waves in one test. By following this blue arrow, the promenade width, the wall height and other parameters are not showing as variables in the formulae that will be deducted. The influence of those parameters is implicitly included in the measurements, for wider promenades the empirical coefficients of the derived equations in approach 1a would have been different, normally slightly lower. The validity of approach 1a is thereby restricted to the dimensionless parameter range as given in Table 3-13.

Approach 1b: the previous approach only provides the low exceedance value $F_{1/250}$, which is just one representative value out of all impacts that a storm wall or a building is facing during a storm with severe overtopping over the crest of the dike. Therefore, in the approach 1b, the distribution of all impacts during a storm is given. The parameters of the probability distribution (shape and scale parameter) are linked to the hydraulic and geometric parameters, so again the blue arrow is followed.

When the whole distribution of impacts is known, $F_{1/250}$ (or any other low exceedance value) can also be calculated and compared to Approach 1a. The same remark as for approach 1a is valid: the deducted formulae are only valid within the range of tested parameters (Table 3-13).

Approach 2: a more generic approach is followed which is less dependent on the specific geometry. In this approach, the distribution of individual overtopping waves is calculated, after which it's linked to the distribution of discharges on the crest of the dike (first orange arrow in Figure 6-43). Those discharges are then linked to the wave impacts on the storm wall (second orange arrow in Figure 6-43). As can be seen, both orange arrows do not perfectly connect to each other (see orange dashed line). That is due to the locations where the flow parameters on the promenade were measured. Eq. [2-55] by Hughes (2015) set up a relation between V and q at the beginning of the crest (first orange arrow), whereas the location where U and h were measured in the present research is located close to the storm wall (the second orange arrow explained further in this chapter). The decay of flow depth and flow velocity over the promenade between arrow 1 and arrow 2 is thereby not yet included. By comparing this Approach 2 to the previous approaches, the effect of the decay in flow parameters can be studied.

The reason why approach 2 is less dependent of the given structure, is that Eq. [2-55] (first orange arrow) can be replaced by different formulae for different structures, for example a dike slope with different roughness or different slope angle.

In Section 6.4 the three approaches will be worked out for the geometry 'smooth dike with promenade and wall'. At the end of that section the different approaches will be compared and discussed. In Section 6.5 the best approach will be used to describe wave impacts on the other geometries.

6.4 *Wave impacts on a smooth dike with promenade and wall*

The relevant geometry for the current section is shown in Figure 6-44

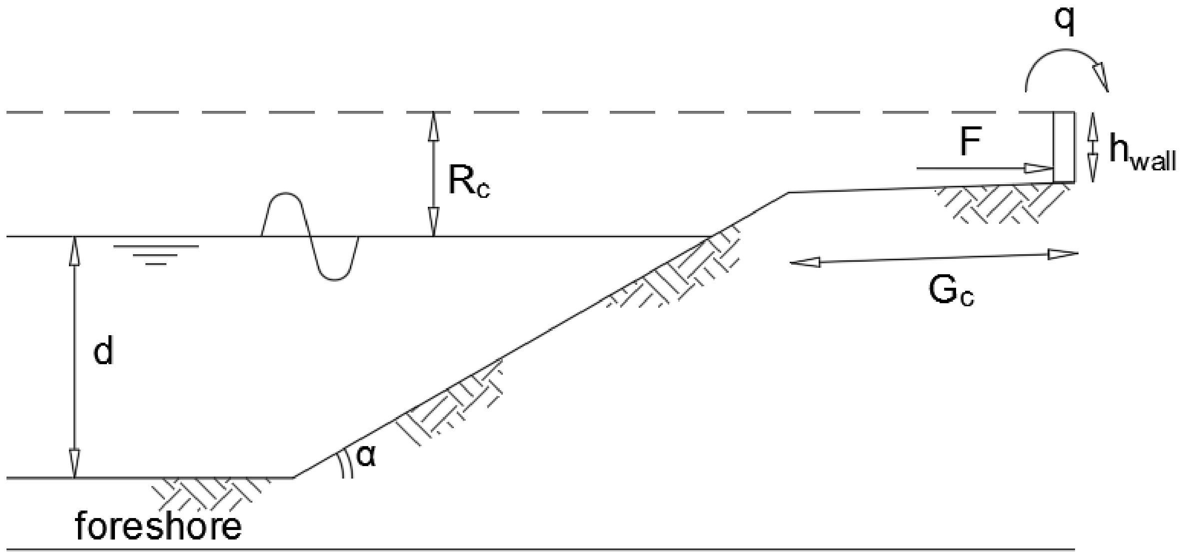

Figure 6-44. Smooth dike with promenade (G_c) and wall (h_{wall}) with indication of force measurement (F). Note that R_c is the difference between the SWL and the top of the storm wall: $R_c = A_c + G_c \cdot \tan(\text{promenade}) + h_{wall}$.

6.4.1 *Approach 1a: Empirical formula between incoming waves and impacts*

a) *Dimensionless force and shape of the prediction formula*

It is preferred to present the force in a dimensionless way. By dividing the force (expressed in N/m) through ρ (kg/m^3), g (m/s^2) and a unit in m^2 a dimensionless value is obtained. In literature d_{b0}^2, H_s^2 and R_cH_s are proposed for this final factor in the denominator. In section 6.1 these approaches were shown not to be successful, but it's not guaranteed that the respective factor in the denominator was the reason for that. d_{b0}^2, the flow depth at the beginning of the promenade measured in the tests by Chen et al. (2015), is not a handy parameter since it has been shown before that it's difficult to measure flow depths and the prediction formulae give very divergent results, also the location of the transition zone is questionable. For approach 1a, where the force is linked to the incoming wave parameters, the following values are possible (unit in m^2) and meaningful to make the force dimensionless: H_s^2, R_cH_s and R_c^2. The wave height and the freeboard are after all two of the main driving parameters according to the findings by Pedersen (1996). The (landward) freeboard R_c has the advantage over (the seaward freeboard) A_c that it also contains the wall height: $R_c = A_c + G_c \cdot \tan(\text{promenade}) + h_{wall}$. When plotting the impact data of the UGent-1 dataset on the geometry smooth dike with promenade and storm wall, the three proposed dimensionless values on the Y-axis are given in Figure 6-45 ($F/\rho g H_s^2$), Figure 6-46 ($F/\rho g H_s R_c$) and Figure 6-47 ($F/\rho g R_c^2$). A good fit was achieved by using a logarithmic vertical axis. On the horizontal axis, the dimensionless freeboard is given, since this is the governing parameter for wave overtopping and on this geometry it are the overtopped waves over the crest of the dike that give the impacts on the storm wall.

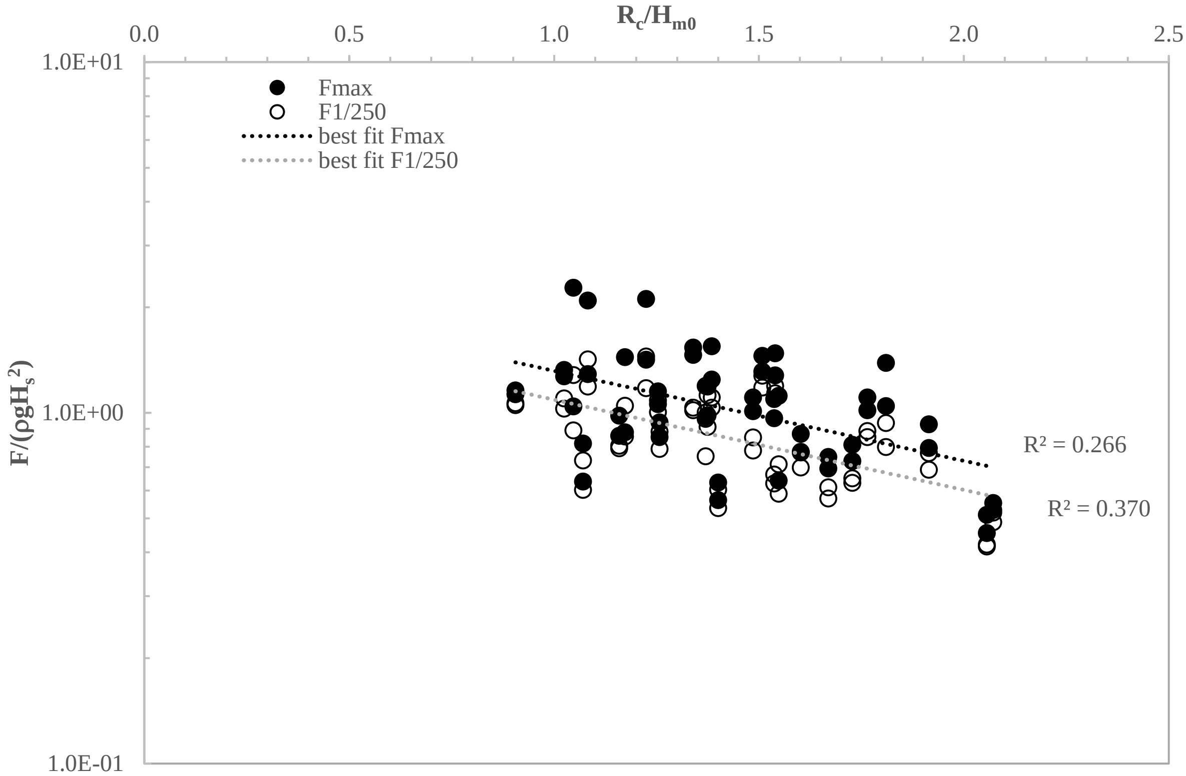

Figure 6-45. Dimensionless representation of the forces on a smooth dike with promenade and wall (UGent-1 experiments), force made dimensionless by dividing through $\rho g H_s^2$.

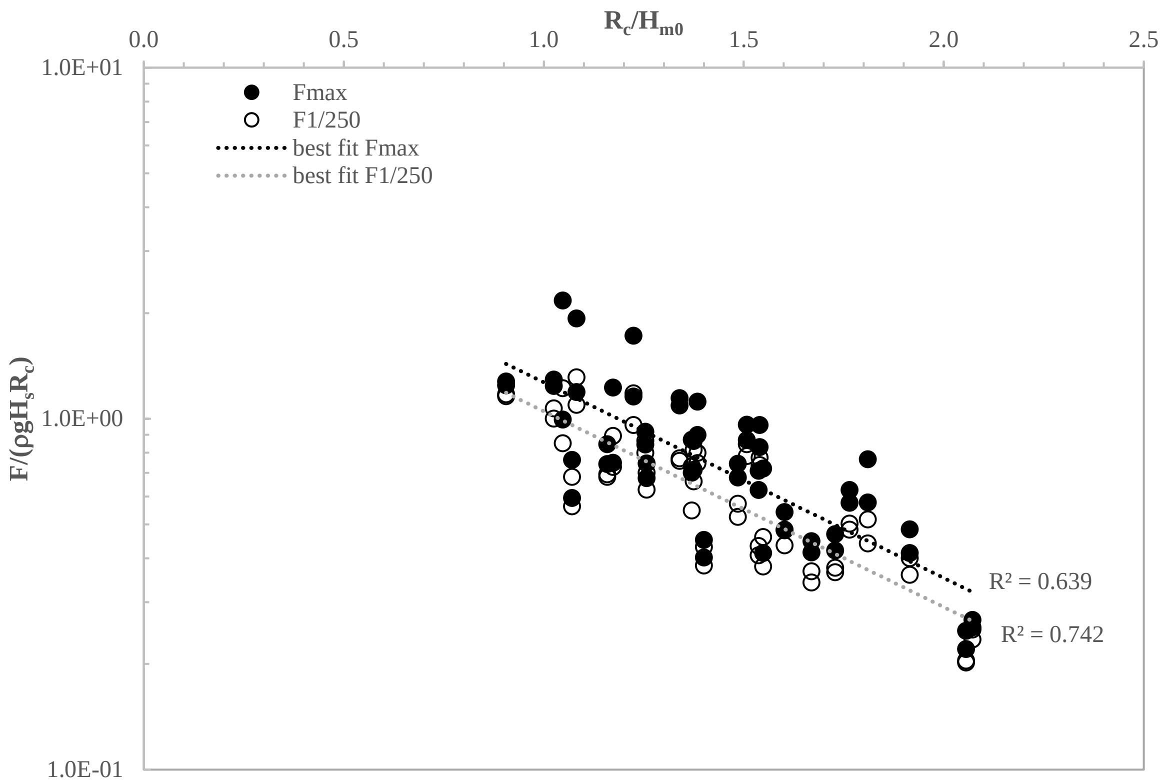

Figure 6-46. Dimensionless representation of the forces on a smooth dike with promenade and wall (UGent-1 experiments), force made dimensionless by dividing through $\rho g H_s R_c$.

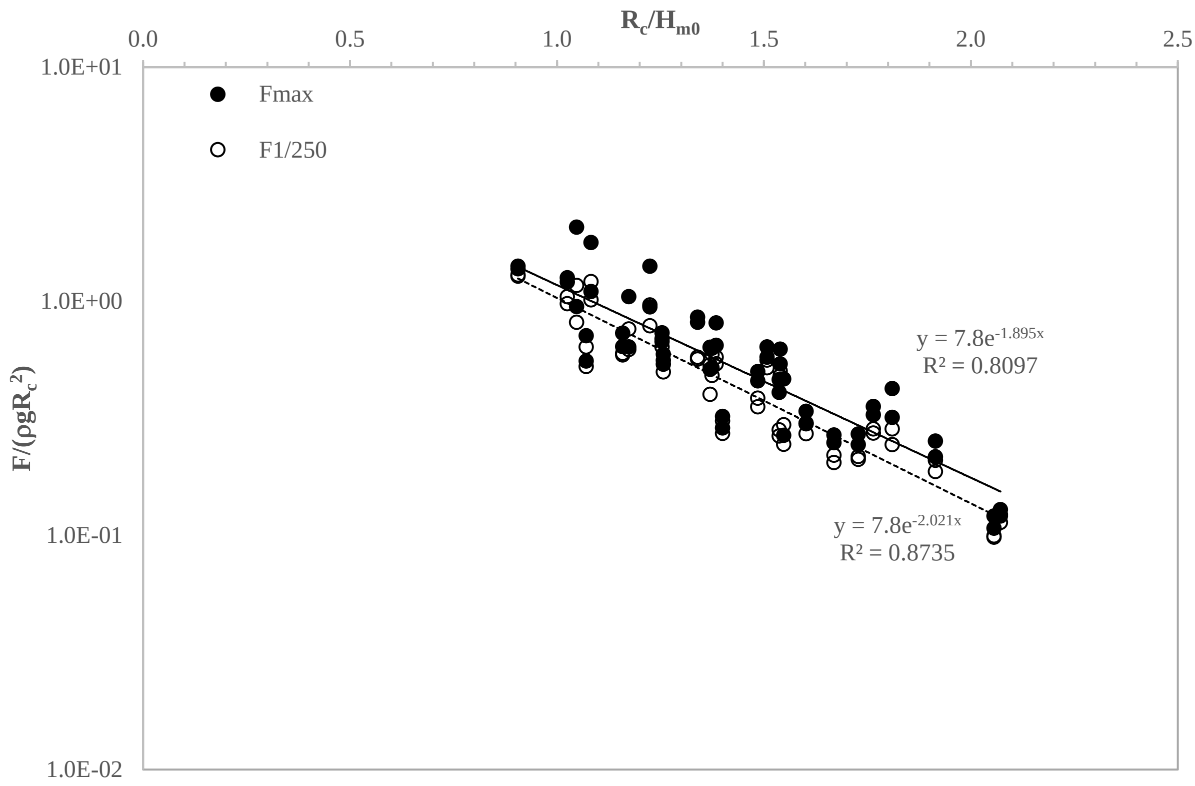

Figure 6-47. Dimensionless representation of the forces on a smooth dike with promenade and wall (UGent-1 experiments), force made dimensionless by dividing through $\rho g R_c^2$.

Figure 6-47 clearly gives the best relation between the dimensionless force and the dimensionless freeboard. The following dimensionless exponential form is proposed:

$$\frac{F}{\rho g R_c^2} = a_F \cdot exp\left(-b_F \frac{R_c}{H_{m0}}\right) \qquad [6\text{-}3]$$

This equation does not directly contain the wall height h_{wall} (although it's present in R_c) or promenade width G_c, since in the tests with force measurements those geometric values have not been varied and it's influence on the result could not be tested. It's advised to investigate this in the future.

The use of $F_{1/250}$ gives less scatter than using F_{max}, as can be seen from the R^2 values mentioned in the figures. As explained in Section 6.2.6, $F_{1/250}$ will be used for further analysis.

The shape of Eq. [6-3] and the influences of the wave height and freeboard in this formula are studied in Figure 6-48, which shows a parameter plot of Eq. [6-3] with only one parameter varying where the other is kept constant. The solid lines are in the ranges where data are available, as shown by 2 examples in Figure 6-49 and Figure 6-50. They confirm the proposed shape. The dotted lines are theoretical extrapolations (no data available) but are in line with the observations d, e and f by Pedersen (1996) listed in Section 2.6 and repeated here below:

d) Increasing wave heights result into increasing forces (for a constant freeboard): Figure 6-50. Increasing freeboards (for a constant wave height) give decreasing forces: Figure 6-49. The latter statement being true for decreasing water level (R_c increases): less water reaches the crest and the storm wall. However, for increasing wall heights (which also increases R_c), overtopping over the wall reduces which leads to increasing forces;
e) For overtopped wall heights, wave forces have a horizontal asymptote when the wave height increases. When overtopping occurs, the impact force does not keep on increasing. Non-

overtopped wall heights do not show this asymptote and impacts increase with increasing wave height;

f) The impact force is proportional to the wall height squared, but increasing the wall height beyond the threshold point between overtopping and no overtopping over the wall, does not further increase the wave load.

In the current tests where impacts were measured, the wall height was not varied, which makes investigating the influence of the wall height (statement f) not possible. However, the landward freeboard R_c contains the wall height (see Figure 6-44: $R_c = A_c + G_c \cdot \tan(\text{promenade}) + h_{wall}$). And according to Eq. [6-3] and Figure 6-48, the force is proportional to R_c squared. The proportionality to the wall height squared is thereby also valid for the present data.

The shape of Eq. [6-3] is supported by the data (in the range of the solid lines in Figure 6-48, see 2 examples plotted in Figure 6-49 and Figure 6-50) but also by the findings by Pedersen (1996) for the range of the extrapolated dotted lines. The proposed shape also gave the best correlation in Figure 6-47.

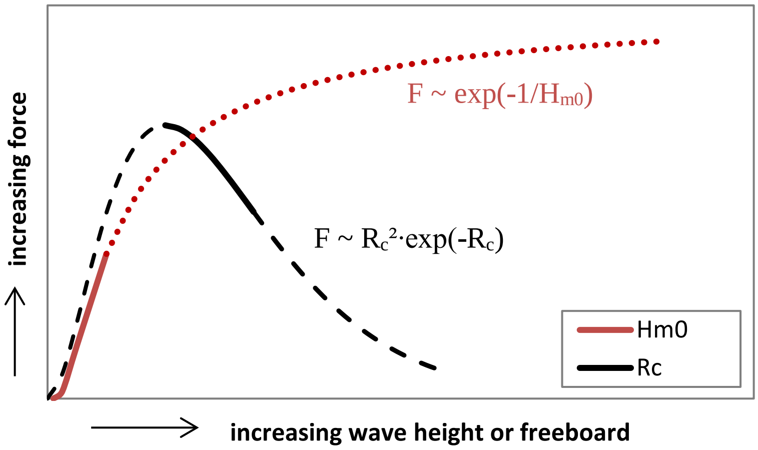

Figure 6-48. Generic influence of increasing R_c (black line, constant H_{m0}) and H_{m0} (red line, constant R_c) on the force F.

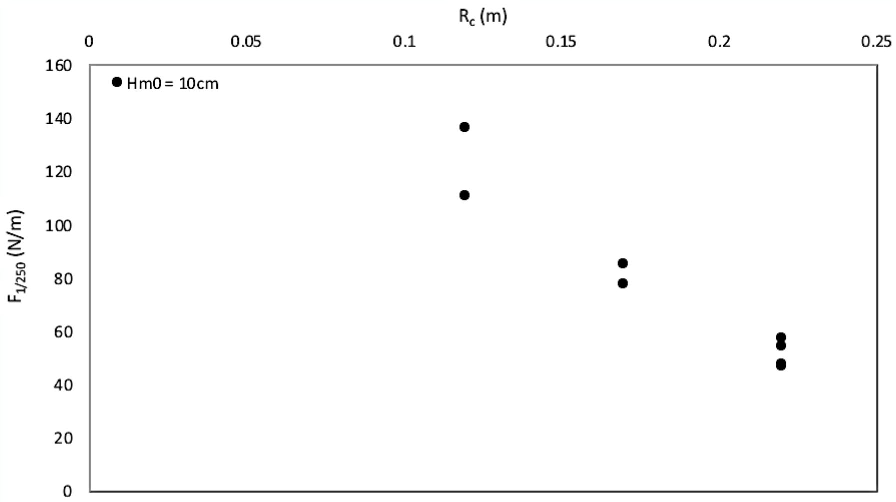

Figure 6-49. Force versus freeboard, for data of the UGent-1 dataset with constant wave height 10cm model values. See black full line in Figure 6-48.

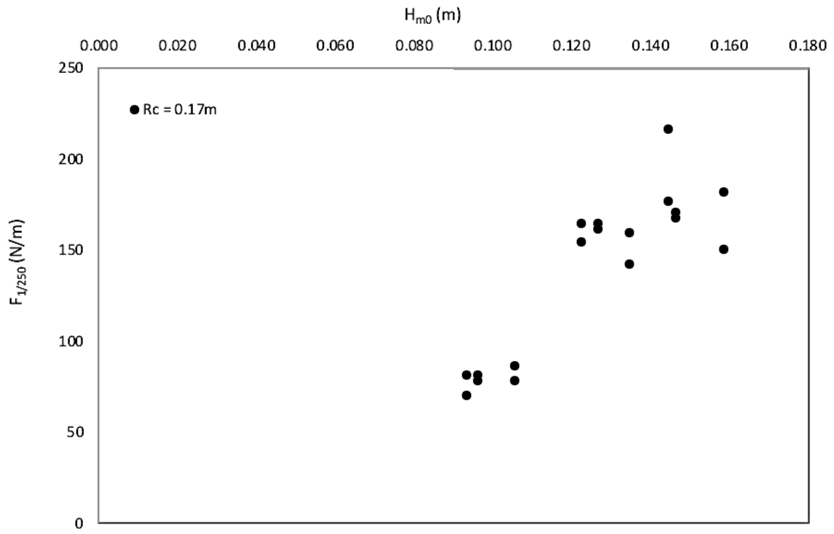

Figure 6-50. Force versus wave height, for data of the UGent-1 dataset with constant wave freeboard 17cm model values. See red full line in Figure 6-48.

Pedersen (1996) also made observations on the influence of the slope angle and the wave period on the forces (statements g and h):

g) Longer waves (higher wave periods) lead to higher impact forces.
h) The wave loading on the crown wall decreases with decreasing slope angle (flatter slope). Also Chen et al. (2015) implies a dependency on the slope angle in Eq. [2-64] for regular waves, but not anymore in her 7-step procedure for irregular waves.

The force data from UGent-1 dataset show possibly a very mild influence of the wave period (short wave periods are located on the lower end of the data cloud, see Figure 6-51), but not clear/strong enough to include in the formula. Regarding the slope angle, no influence is noticed at all (see Figure 6-52). Therefore, Eq. [6-3] does not include T_p nor α.

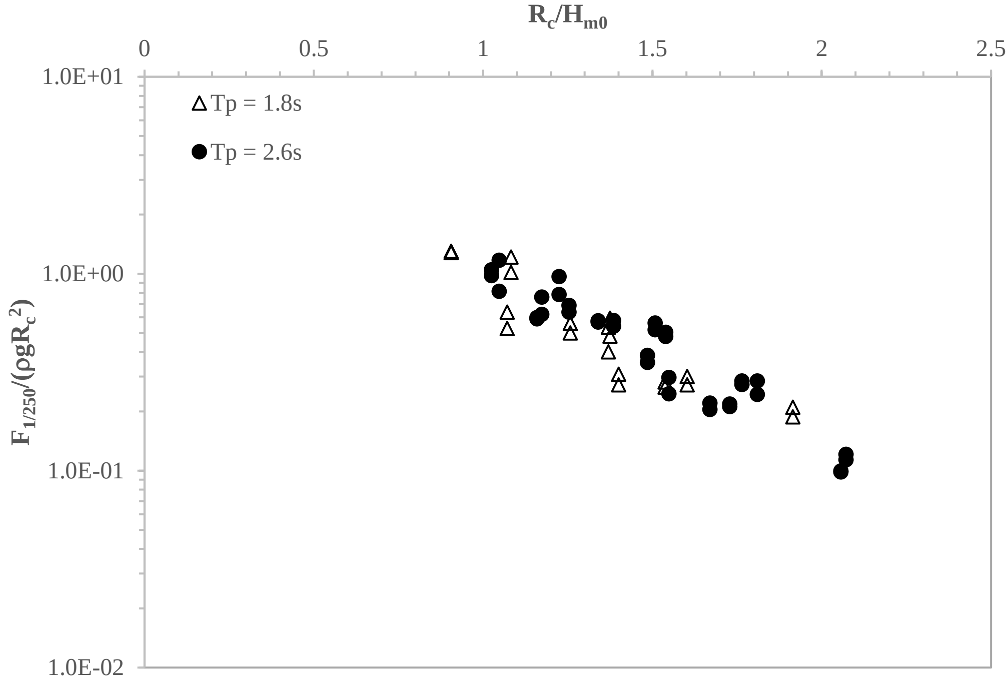

Figure 6-51. Log-linear plot of the dimensionless force as a function of the dimensionless freeboard. Data of UGent-1 dataset on smooth dike with promenade and wall. Data split up per wave period.

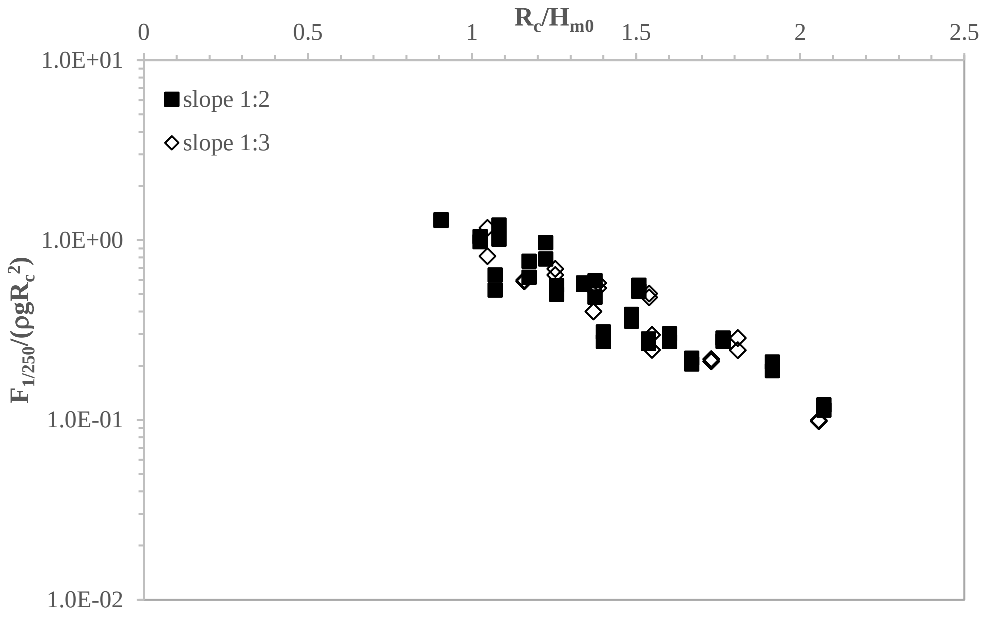

Figure 6-52. Log-linear plot of the dimensionless force as a function of the dimensionless freeboard. Data of UGent-1 dataset on smooth dike with promenade and wall. Data split up per slope angle of the dike.

The last statement i) in chapter 2 according to Pedersen (1996) observations is that the dynamic impact (first peak in the churchroof) dominates the quasi-static part; he only analyzed the dynamic peak. In the present peak-over-threshold analysis the maximum value is always selected, regardless if it comes from dynamic or quasi-static peaks. It is noticed however that the highest forces in the distribution (which determine $F_{1/250}$) mostly come from the dynamic impact. This confirms the findings by Pedersen (1996)

b) *Prediction formula*

Now that the shape of the relation between the impact force and the hydraulic parameters has been defined as Eq. [6-3], the parameters a_F and b_F can be fitted. It should be stressed that the promenade width and wall height have not been varied in the test set-up for impact measurements so these values are implicitly included in the results. The results are valid for the range of dimensionless values $G_c/L_{m-1,0}$ and h_{wall}/R_c as mentioned in Table 3-13. Outside of this range, results should be treated with great care.

It was already mentioned below Table 3-13, where the test set-ups of the different geometries are compared, that the GWK experiments will be treated seperatly since they have very short test durations and make it less reliable to define statistical parameters such as the low-exceedance value $F_{1/250}$. UGent-1 data and Hydralab data are plotted together since they have a comparable geometry, only tested at a different scale and a different wall height in prototype dimensions (see Table 3-13). A highly correlated linear trend between the dimensionless force and the dimensionless freeboard can be seen in the semi-logarithmic plot, see Figure 6-53.

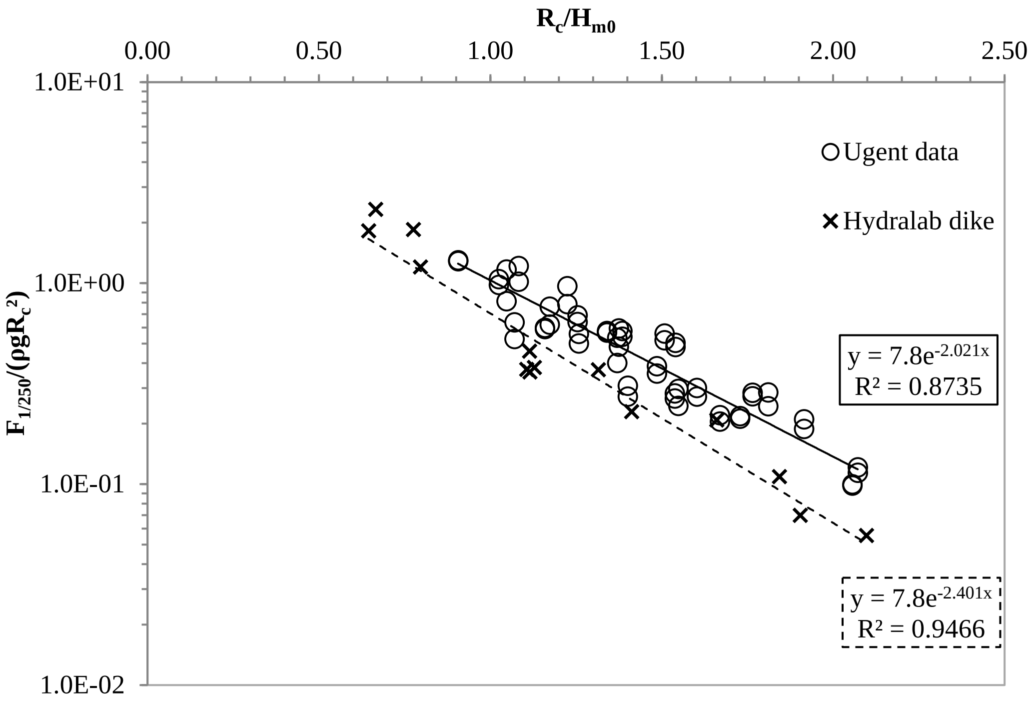

Figure 6-53. Log-linear dimensionless plot of all data of UGent-1 and Hydralab tests on a smooth dike with promenade and storm wall.

The coefficients for both datasets are given in Table 6-1, and are valid for the range of parameters as stated in the Hydralab and UGent-1 columns of Table 3-13.

Table 6-1. Coefficients for equation [6-3] to calculate impact forces. Relative standard deviation (σ' = σ/μ) between brackets. Also the most important parameter ranges A_c/H_{m0} and R_c/H_{m0} are given.

	UGent-1		Hydralab	
	a_F	b_F	a_F	b_F
$F_{1/250}$	7.8 (σ' = 0.029)	2.02 (σ' = 0.012)	7.8 (σ' = 0.077)	2.40 (σ = 0.038)
A_c/H_{m0}	0.2 to 1.2		0 to 1.2	
R_c/H_{m0}	0.9 to 2.0		0.65 to 2.0	

When referring to Figure 6-53, it can be seen that the two datasets follow the same trend but there is an offset between both. This difference may be due to two possible reasons:

- a difference in scale (Froude scale factor 6 in Hydralab versus 10 in UGent-1 related to a prototype situation). Bullock et al. (2001) and Steendam et al. (2018) claim that smaller scale has less air bubbles and thus larger impacts. Since no air bubble measurements have been carried out in the current research, it's unknown if the difference in scale between Hydralab and UGent-1 is large enough to give this difference;
- a model effect (different location of wave gauges, different steering of the wave paddle, UGent uses active wave absorption unlike for the Hydralab tests…). The geometry itself was built as similarly as possible, so little differences due to the geometry are expected.

At this stage, it cannot be said whether the scale or the model effect is dominating the difference between both results. In fact, the difference between the UGent-1 results and the Hydralab results is not very big, and as a conservative approach, the highest trendline of the two datasets is proposed as the (probabilistic) design line. The average trendline for impacts on storm walls at the end of a promenade at crest level of a smooth sloping dike (specific geometry, see Figure 1-9 or Figure 3-7) is:

$$\frac{F}{\rho g R_c^2} = 7.8 \cdot exp\left(-2.02\frac{R_c}{H_{m0}}\right) \qquad [6\text{-}4]$$

where R_c is defined as the landward freeboard (including the wall height). The range of important parameters for which this formula is valid is repeated here, the full range can be found in Table 3-13. Dike slope cot(α) between 2 and 3, the dimensionless crest width $G_c/L_{m-1,0}$ between 0.1 and 0.25, and the wall height between 35% and 70% of the freeboard ($0.35 < h_{wall}/R_c < 0.70$). The dimensionless freeboard R_c/H_{m0} was between 0.9 and 2 for these tests and A_c/H_{m0} between 0.2 and 1.2.

Approach 1a is easy and straightforward and can be summarized in Figure 6-54.

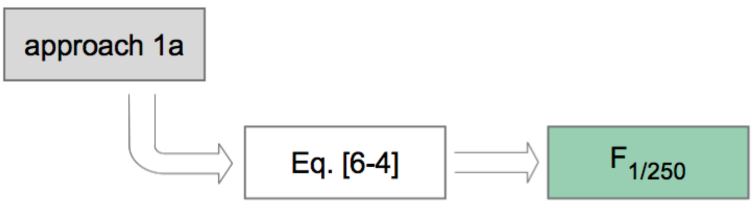

Figure 6-54. Flow chart of approach 1a to calculate $F_{1/250}$ for smooth dikes with a promenade and storm wall.

c) *Comparison with measurements*

Eq. [6-4] allows calculating the wave impact (low exceedance value $F_{1/250}$) on a storm wall at the end of a promenade. When the calculated force is compared to the measured data (dimensionless), a good correlation can be observed (Figure 6-55). Note that the coefficients for a_F and b_F from Table 6-1 are used. The followed approach works well, as expected, since the relative standard deviations given in Table 6-1 are small. However, this approach is only valid within the range of tested parameters (Table 3-13) for a dike slope (cot(α) = 2 to 3) with a promenade and a storm wall at its end.

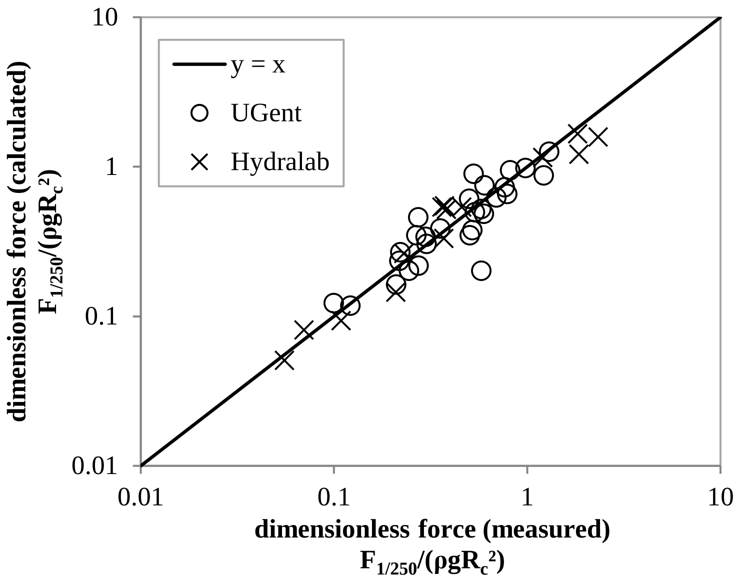

Figure 6-55. Comparison of measured forces and calculated (dimensionless) forces by approach 1a (empirical formula).

6.4.2 *Approach 1b : Force distributions linked to the incoming wave parameters*

a) *Prediction formula*

In approach 1b, not just one low exceedance value, but the entire distribution of all impacts during a test is studied. Empirical formulae for the statistical shape and scale parameters are provided, so that the full distribution and thereby any requested low exceedance value can be calculated. Just like in approach 1a, only the datasets of UGent-1 and Hydralab are used since they represent a storm of about 1000 waves.

The peak values of all impacts above a threshold value are listed for every experiment of the UGent and Hydralab tests. The threshold values (model scale values of 4N/m in the Hydralab tests and 1N/m in the UGent tests) are chosen so that all clear impacts are considered. An example for one experiment of UGent-1 is given in Figure 6-56, red markers for the left storm wall section, blue markers for the right storm wall section. About 660 impacts were registered, and like was proven in 6.2.3a), good agreement between measurments on the left and the right storm wall shows.

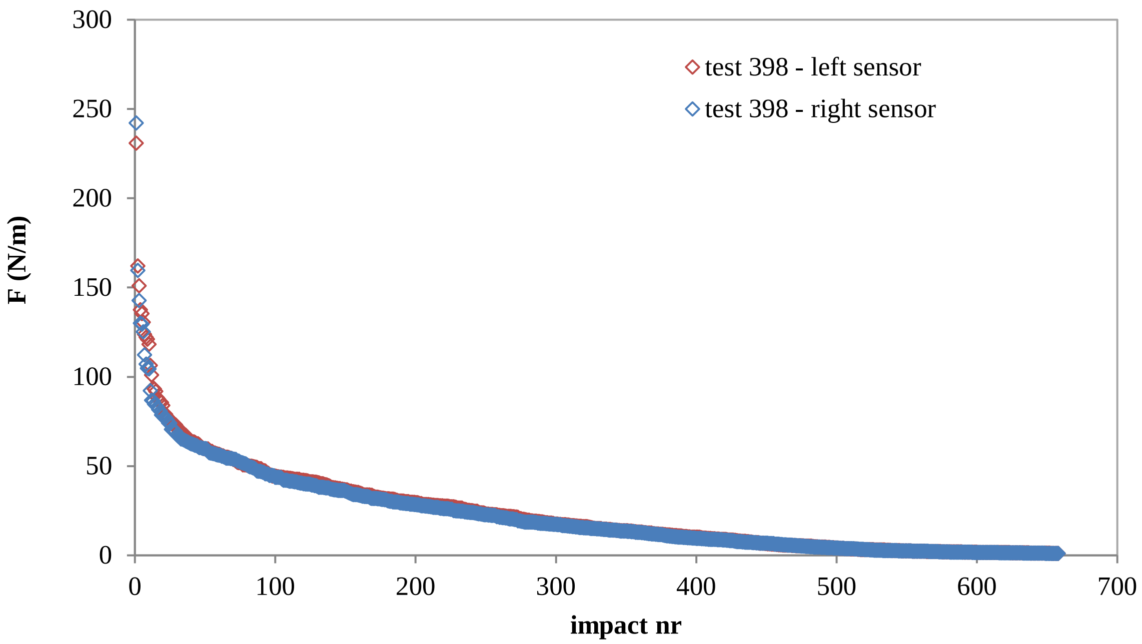

Figure 6-56. Distribution of all impacts in 1 test from the UGent-1 dataset, measured by 2 sensors but showing equal results.

The distribution of individual overtopping volumes by Victor (2012) is related to the number of overtopping waves. In approach 2, the distribution of these individual overtopping volumes will be linked to the distribution of impact forces. For that reason, the distribution of impact forces is also linked to the probability of overtopping waves P_{ov}, and not expressed as a function of the probability of impacts. Their relation is shown in Figure 6-57, where the force is made dimensionless by dividing through $\rho g R_c^2$ as explained in the beginning of Section 6.4.1. Since recordings on the left and the right part of the storm wall gave equal results, only one of both, the left, is plotted.

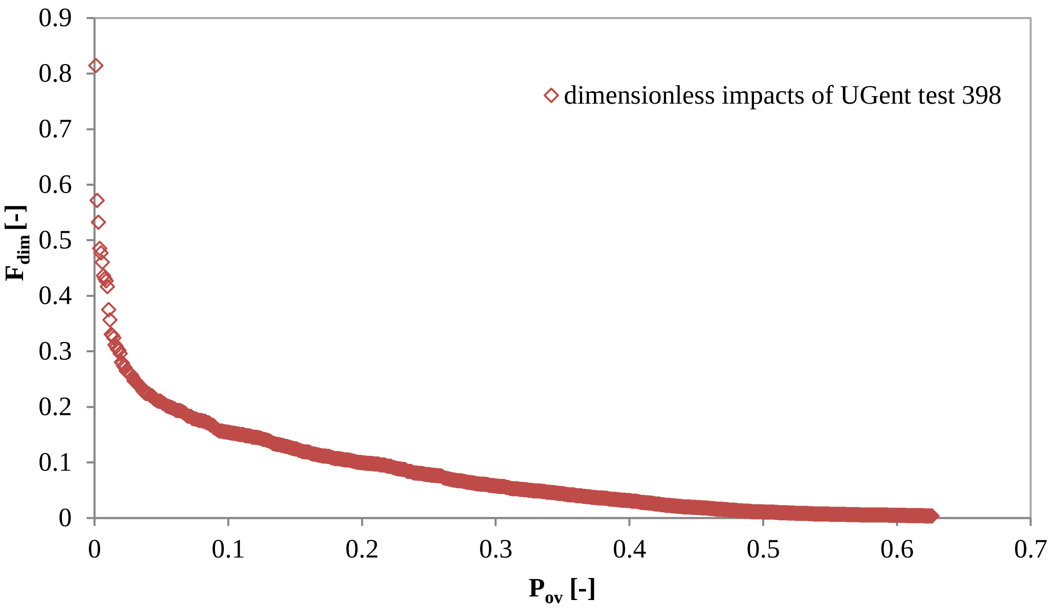

Figure 6-57. Distribution of dimensionless measured forces of test 398 of the UGent dataset.

Just like for individual wave overtopping, the (dimensionless) individual impacts on the storm wall can also be described very well by a two parameter Weibull distribution:

$$P_{ov} = exp\left(-\left(\frac{F_{dim}}{\lambda_F}\right)^{\kappa_F}\right) \quad [6\text{-}5]$$

$$P_{ov} = i/(N_{ow} + 1) \quad [6\text{-}6]$$

with P_{ov} being the exceedance probability of a certain overtopping volume according to Eq. [2-53] by Victor (2012), F_{dim} the dimensionless individual impact $F_{dim} = F/(\rho \cdot g \cdot R_c^2)$, i the rank number when impacts are ordered from the highest to the lowest and N_{ow} the number of overtopping waves. N_{ow} can be calculated by multiplying the number of waves (N_w) by the probability of overtopping (P_{ov}). λ_F is the scale parameter, κ_F the shape parameter of the Weibull distribution of impact forces.

The number of impacts (N_{im}) is smaller than the number of overtopping waves (N_{ow}) since not every overtopping wave is giving an impact on the structure. Consequently $P_{ov} < 1$ in Eq. [6-6], since $i < N_{ow}$. This can be seen in Figure 6-57 where P_{ov} only has force values up to $P_{ov} = 0.62$. 62% of the overtopping waves in test 398 gave an impact higher than the threshold value. For higher rank numbers ($i > N_{im}$), no force was recorded (F = 0N/m).

Rewriting Eq. [6-5] leads to

$$F_{dim} = \lambda_F\left(-ln(P_{ov})\right)^{\frac{1}{\kappa_F}} \quad [6\text{-}7]$$

$$log(\lambda_F) + \frac{1}{\kappa_F} log\left(-ln(P_{ov})\right) = log(F_{dim}) \quad [6\text{-}8]$$

Eq. [6-8] can be plotted in a scatter plot $log(F_{dim})$ versus $log(-ln(P_{ov}))$: see Figure 6-58. Where Hughes et al. (2012) only used the upper 10% values for his overtopping volumes, and van der Meer et al. (2011) and Victor (2012) used all values higher than the mean value, it is decided here to work with the impacts of the **highest 20% overtopped waves** ($0.2 \cdot N_{ow}$) to define the shape and scale factors. In tests with fewer impacts, coefficients κ_F and λ_F would be affected too much when only considering the 10% highest values if a few high wave impacts are outliers compared to the rest of its distribution. On the other hand, when considering all forces larger than F_{mean}, too many values could be considered and influence a good fit for the highest impacts. The choice of the impacts of the highest 20% overtopped waves is a good compromise, and leads to the most reliable shape and scale factors for the present data set. In the current research, always more than 20% of the overtopped waves had an impact ($N_{im} > 0.2 \cdot N_{ow}$).

The same test as in Figure 6-57 is now plotted according to Eq. [6-8] in Figure 6-58 as an example.

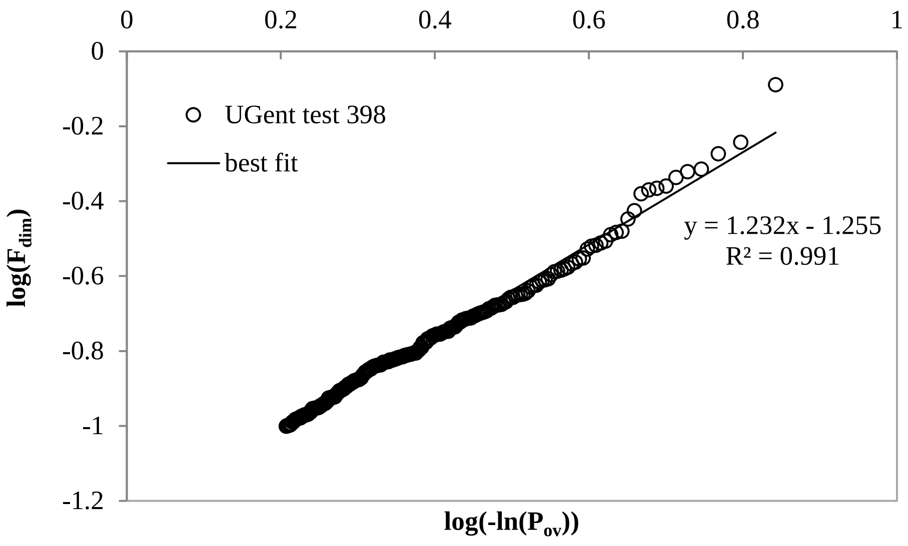

Figure 6-58. Weibull plot of test 398 in the UGent experiments.

The example from Figure 6-58 shows an excellent linear fit with the following trendline:

$$-1.255 + 1.232log\big(-ln(P_{ov})\big) = log(F_{dim}) \qquad [6\text{-}9]$$

from which κ_F and λ_F can be derived: $\log(\lambda_F) = -1.255$ and $1/\kappa_F = 1.232$. This leads to $\lambda_F = 0.0556$ and $\kappa_F = 0.812$ for this specific test.

This excellent linear fit ($R^2 = 0.991$) is another example to support Section 6.2.5 where a Weibull distribution of the impacts is promoted.

The derivation of λ_F and κ_F is done for all experiments in the UGent-1 and Hydralab dataset, and the list of scale and shape parameters is then linked to incoming hydraulic parameters, A_C and H_{m0}, per test (Figure 6-59 and Figure 6-60).

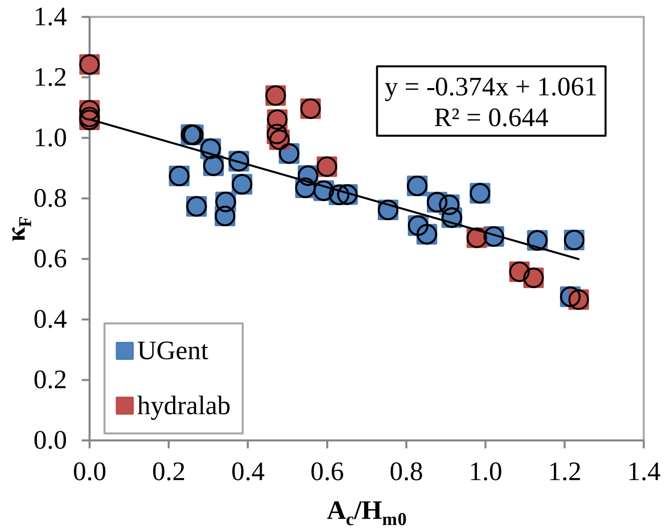

Figure 6-59. Weibull shape parameter of all tests (UGent-1 and Hydralab): Eq. [6-10].

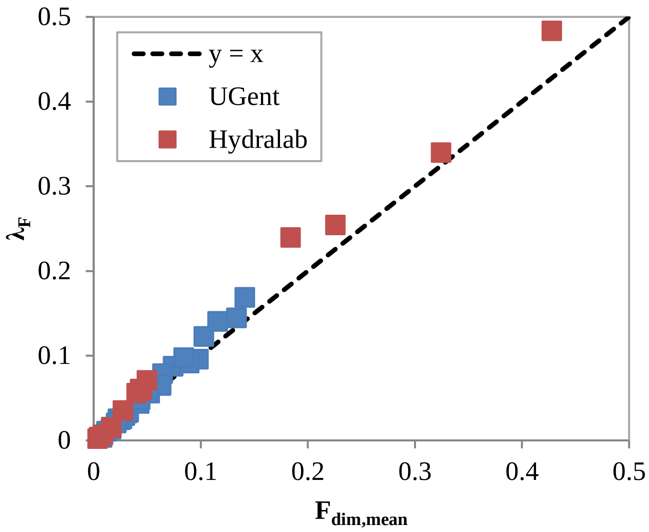

Figure 6-60. Weibull scale parameter of all tests (UGent-1 and Hydralab): Eq. [6-11].

This leads to Eq. [6-10] and [6-11] for the shape and scale parameters:

$$\kappa_F = 1.061 - 0.374 \cdot \frac{A_C}{H_{m0}} \qquad [6\text{-}10]$$

$$\lambda_F = \frac{F_{mean}}{\rho \cdot g \cdot R_c^2} \qquad [6\text{-}11]$$

where F_{mean} is the mean value of all forces during a test, again related to the number of overtopped waves: F_{mean} calculated as the mean value from impact 1 to 'impact' number N_{ow}, with zero values for the numbers N_{im} to N_{ow}. This choice is motived in Section 6.4.2.e). F_{mean} is calculated for all tests of the Hydralab and UGent-1 dataset, and then linked to the incoming hydraulic parameters in the same form as Eq. [6-3]. This gives the following formula.

$$\frac{F_{mean}}{\rho \cdot g \cdot R_c^2} = 1.80 \cdot \exp\left(-2.66 \frac{R_C}{H_{m0}}\right) \qquad [6\text{-}12]$$

With this Eq. [6-12], the scale factor λ_F of the Weibull force distribution can now be calculated by Eq. [6-11]. With the shape and scale parameters κ_F and λ_F, the Weibull force distribution for every test can be calculated by Eq. [6-5]. This was done for test 398 of the UGent-1 dataset, and was added to the data Figure 6-57 as a full black line, see Figure 6-61. Good agreement with the red marked data shows.

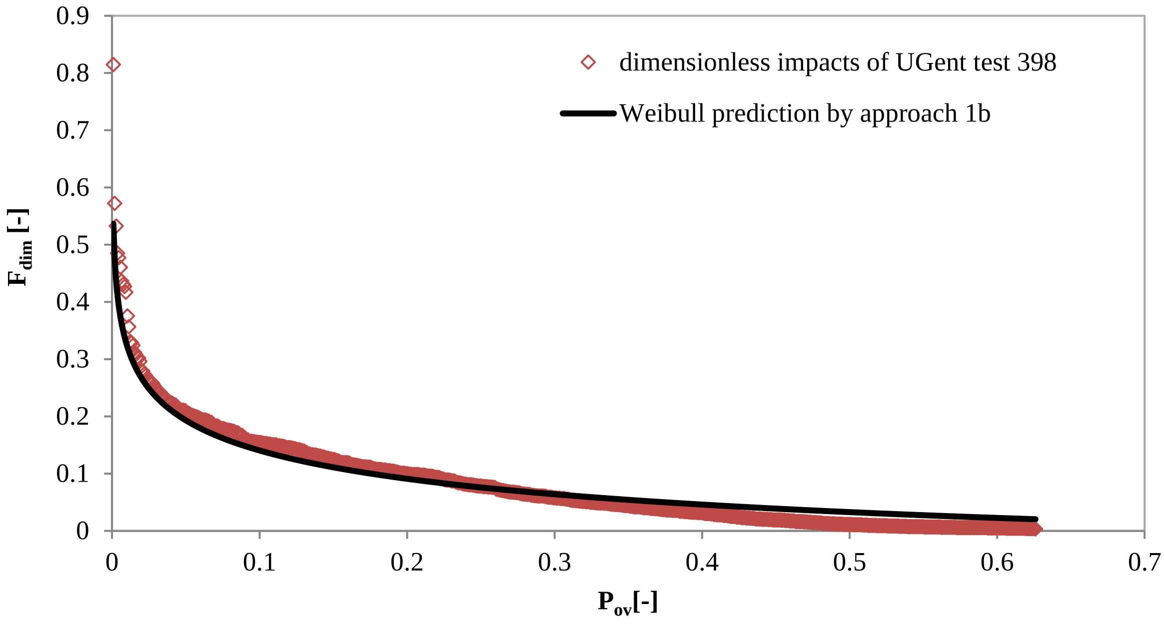

Figure 6-61. Comparison between the calculated Weibull PDF using Eq. [6-5], [6-10], [6-11] and [6-12] with the data of UGent-1 test 398.

b) *Number of impacts*

Note that the black line in Figure 6-61 is only drawn until i = N_{im}. It's already mentioned that the number of impacts (N_{im}) is smaller than the number of overtopping waves (N_{ow}), and certainly smaller than the number of incoming waves (N_w). To estimate the number of waves impacting a storm wall for a geometry like Figure 6-43, an empirical formula is derived. For all 42 tests of UGent-1 and Hydralab on the geometry 'smooth dike with promenade and storm wall', the number of impacts (values higher than its threshold) is linked to the dimensionless seaward freeboard A_c/H_{m0}, see Figure 6-62.

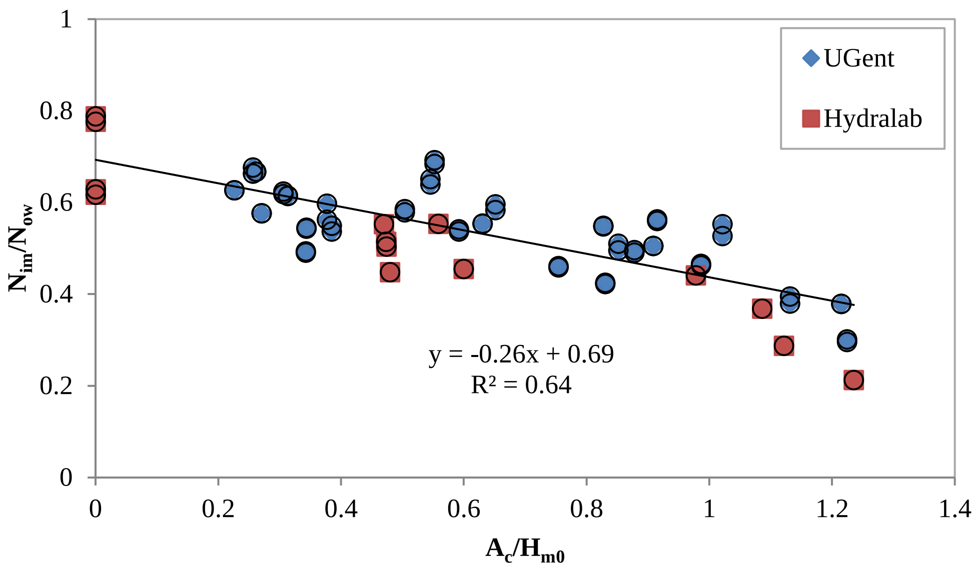

Figure 6-62. Relation between the relative freeboard and the relative number of impacting waves.

$$\frac{N_{im}}{N_{ow}} = 0.69 - 0.26\frac{A_C}{H_{m0}} \quad [6\text{-}13]$$

with N_{im} the number of impacts and N_{ow} the number of overtopping waves (N_{ow} = number of waves multiplied by P_{ov} by Eq. [2-53]) . Even for zero landward freeboards, not all waves give an impact larger than the threshold value, due to friction and/or a residual water layer on the promenade which mainly the small incoming waves cannot overcome.

This Eq. [6-13] is only required to limit the Weibull distribution plot of the impact numbers.

Approach 1b can now be summarized in the flowchart in Figure 6-63. The validity range for the developed formulae in approach 1b is A_c/H_{m0} between 0.2 and 1.2 and R_c/H_{m0} between 0.9 and 2.0.

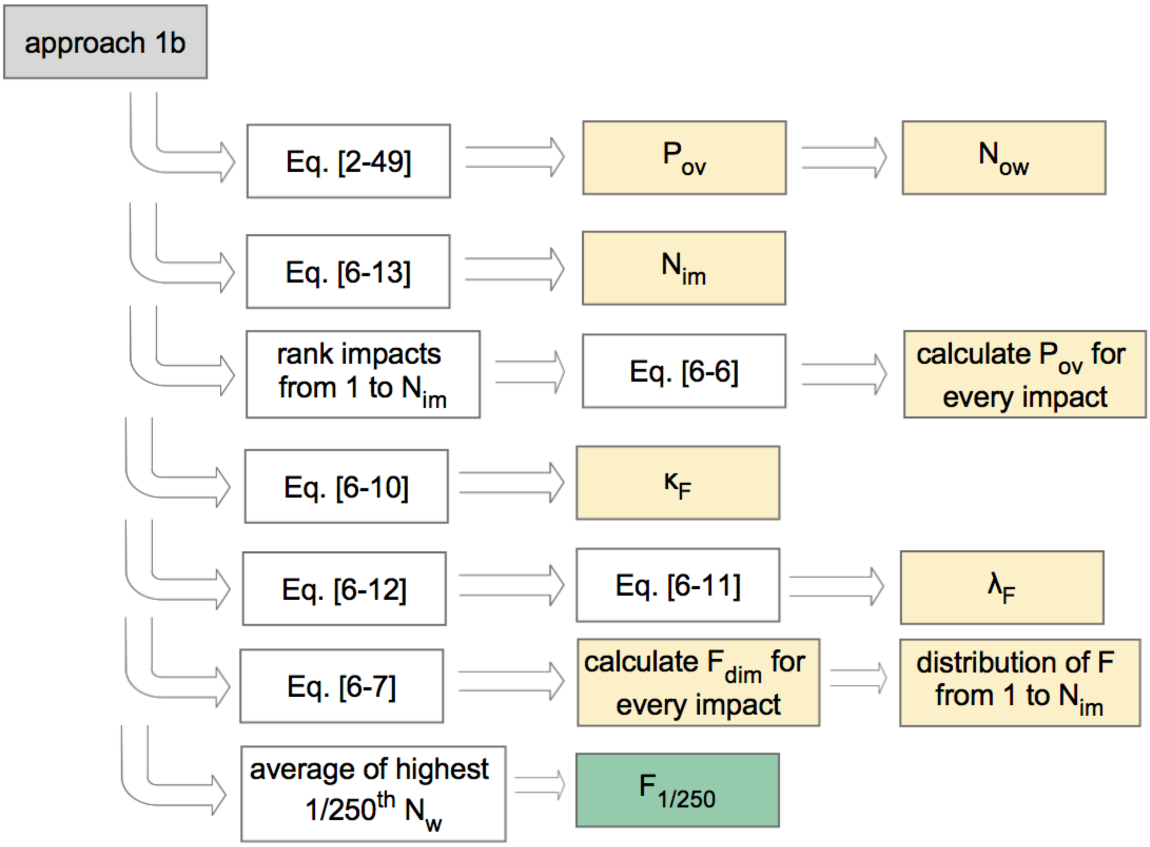

Figure 6-63. Flow chart of approach 1b to calculate $F_{1/250}$ for smooth dikes with a promenade and storm wall.

c) *Comparison with measurements*

Figure 6-58 and Figure 6-61 already showed that the data of UGent-1 test 398 are well represented by a Weibull distribution. In Figure 6-64 it is shown that this is the case for all tests of the UGent-1 and Hydralab dataset.

Using Eq. [6-10], [6-11] and [6-12] the scale and shape factor can be calculated, which leads to the full distribution of impacts by using Eq.[6-7]. From this distribution, $F_{1/250}$ can be calculated as the average value of the highest $1/250^{th}$ (related to the number of incoming waves) impacts. This obtained value is compared to $F_{1/250}/(\rho \cdot g \cdot R_c^2)$ from measured data. Good correlation shows in Figure 6-64, but for the largest forces the measurements are a little higher than the prediction formula. A Weibull distribution tends to underpredict the absolute maximum forces.

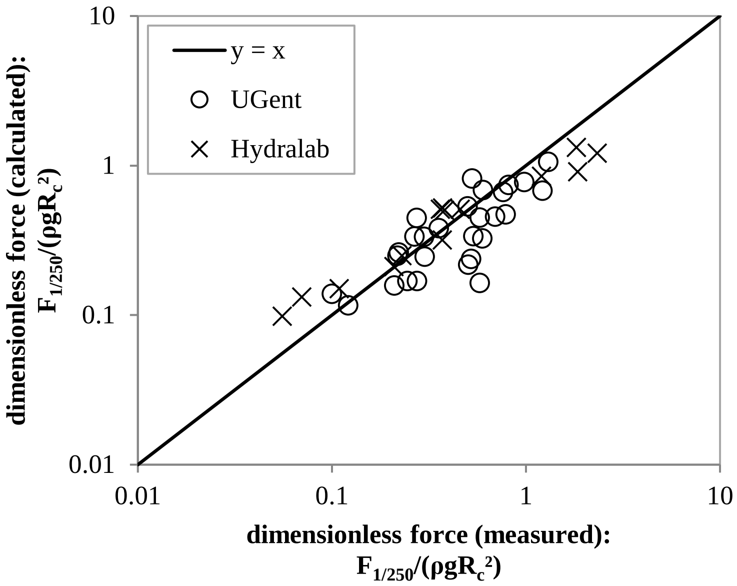

Figure 6-64. Comparison between measurements and calculation of (dimensionless) forces by means of approach 1b (Weibull distribution).

d) *Comparison to approach 1a*

Besides comparing to measurements, the predictions through approach 1a and 1b can also be compared to each other. Figure 6-65 showhs that the prediction of $F_{1/250}$ through both approaches agrees well. This was to be expected, since both approaches have been developed from the same data and use the same parameters (F, A_c and H_{m0}) to derive the empirical equations. Approach 1a gives slightly higher results, since it includes the highest forces where in a Weibull representation those could be slightly underestimated. There is however no difference to be seen between the Hydralab or UGent data.

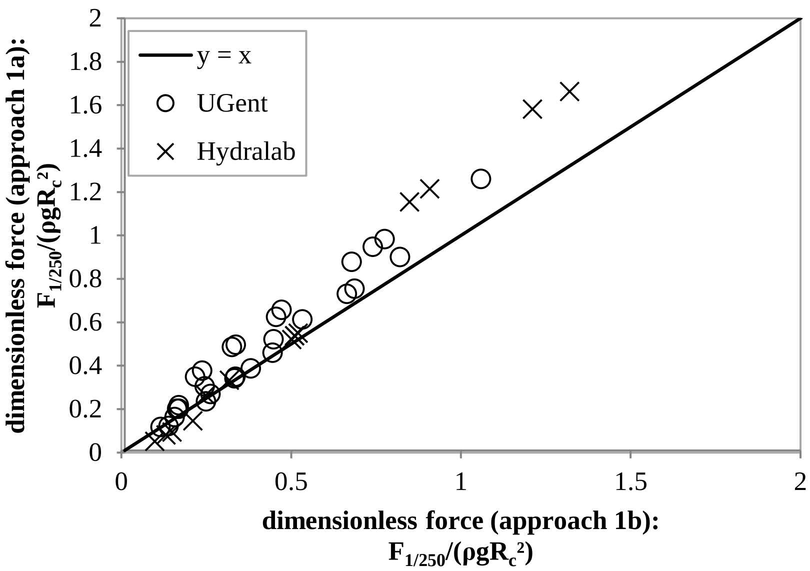

Figure 6-65. Comparison of dimensional forces $F_{1/250}$ by approach 1a (horizontal axis) and 1b (vertical axis).

e) *Discussion on low exceedance value $F_{1/250}$ and mean value F_{mean}*

In this section the definition of the low-exceedance value $F_{1/250}$ and the mean value F_{mean} are discussed. Both choices are at first sight not consistent, since $F_{1/250}$ is related to the number of incoming waves and F_{mean} related to the number of overtopped waves. Both definitions therefore require some extra explanation.

Approach 1a directly calculates $F_{1/250}$, representing the average impact of the highest $1/250^{th}$ of the number of incoming waves. Approach 1b calculates a distribution of impacts, related to the number of overtopping waves. Nevertheless, $F_{1/250}$ is also in this approach 1b calculated as the average value of the highest $1/250^{th}$ of the number of incoming waves, not overtopping waves. The definition $F_{1/250}$ is a definition of a low-exceedance value, that must be followed regardless of the approach followed. When an example storm of 1000 waves would have a probability of overtopping the dike of 70%, only these N_{ow} = 700 overtopped waves could create an impact and give a certain distribution with impact numbers from 1 to N_{ow} = 700. Nevertheless, F_{1250} has to be calculated as the average of the highest 4 impacts (1000 incoming waves ÷ 250) and not of 2 waves (700 overtopped waves ÷ 250 = 2.8 rounded down to 2).

For F_{mean} however the definition is different. F_{mean} defines the scale of the Weibull distribution, and the Weibull distribution is set up for the impacts of the highest 20% of overtopped waves, since only those can cause an impact. Therefore, F_{mean} is calculated as the average value of impact 1 to N_{ow} and not as the average of impact 1 to N_w. With that same example storm of 1000 incoming waves and 700 overtopped waves, F_{mean} this time has to be calculated as the average value of 700 impact values. Keep in mind here that not necessarily all 700 overtopping waves gave an impact higher than the threshold value, so at the lower tail of these 700 values some zero-values might be present. The reason why F_{mean} is still connected to the number of overtopping waves N_{ow} = 700, and not to the number of impacts, is that this last value is fully depending on which threshold value is chosen, and that value is not an objective number.

6.4.3 *Approach 2: Generic approach*

a) *Prediction formula*

As sketched in Figure 6-43, a different approach is followed here. The direct relation between the waves at the toe of the dike and the impacts is disregarded for now, and a more generic approach is followed: waves overtop and result in overtopping flows, after which the overtopping flow can result in an impact. These individual steps are linked to one another. Hughes (2015) has linked the overtopping wave volumes to the overtopping flow parameters (Eq. [2-55]). In this section, the overtopping flow parameters from Chapter 5 will be linked to the impact forces. This approach, unlike approach 1a and 1b, is based on the GWK experiments. The GWK database was the only one with good flow parameters measured. However, due to the short time series, the GWK dataset is not usable for extreme value analysis and statistics.

Figure 6-66 shows the trend between each of the 621 manually analyzed bore front velocities (between step gauge number 3 and the vertical plate of the pressure measurements) and its consecutive impact, measured over all 21 tests. This relation is of quadratic nature, also suggested by the formulae used in Cross (1967) and SPM (1977). Kinetic energy of waves also shows a quadratic relationship to the velocity of the waves ($E_{kin} \approx m \cdot U^2/2$).

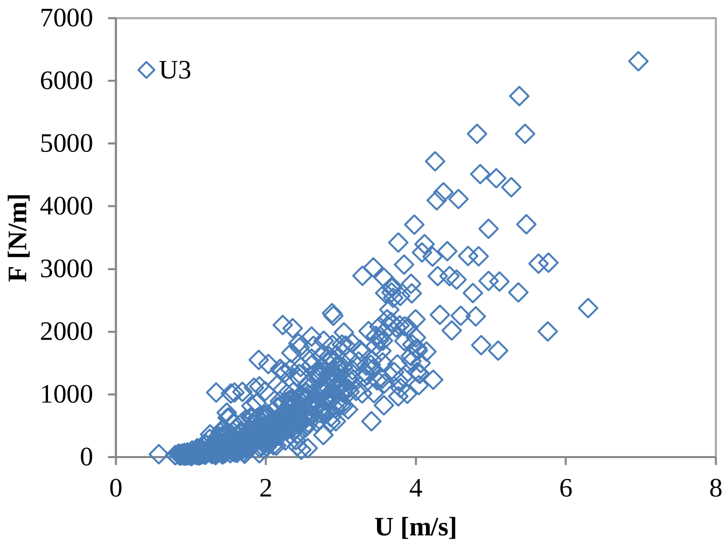

Figure 6-66. Relation between the bore front velocity (between the 3rd sensor and the plate) and the consecutive impact (model units, GWK).

The same graph is repeated in Figure 6-67, now with indication of the maximal velocities over the 21 tests (red squares) and the maximal impacts in the 21 tests (green circles). Green and red markers overlap 12 times. This shows that in 12 of the 21 tests, the highest impact is measured in the tests with the highest recorded velocity, but the other 9 values are not. It are thus not always the bores with highest recorded velocity that cause the highest recorded impact in a test.

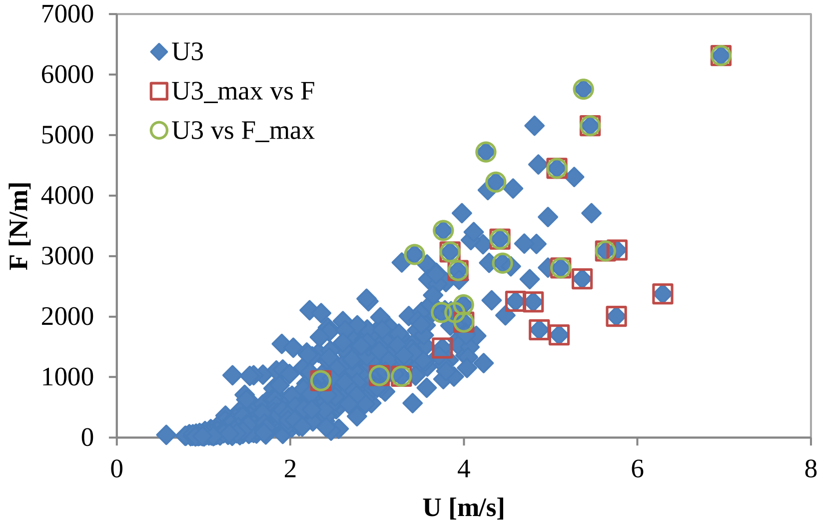

Figure 6-67. Relation between the bore front velocity and the impact, with indication of maximal velocities and maximal impacts for each of the 21 tests (model units, GWK).

Despite seeing a clear trend between the impacts and the velocity, there is a lot of scatter in Figure 6-66 and Figure 6-67. For a velocity of 5m/s, the impacts can be between 1500N/m and 6000N/m which is a factor of 4 and unsatisfying for giving design recommendations. This scatter was to be expected, since the mass of the incoming energy is neglected when only considering the flow velocity. The scatter is coming from the different flow depths at data with constant flow velocity. This is shown in detail in Figure 6-68, which zooms in on Figure 6-67 for U between 4.2m/s and 4.4m/s and its related forces. The size of circle and the value written on the right side of each circle, give the height of the flow depth in m. It shows that the lower forces occur for flow depths close to 0.40m, where the higher forces coincide with flow depths of up to 0.70 m. This explains most of the scatter: the variation in impacts measured for bores with nearly the same flow velocity is due to the difference in flow depth. Higher flow depths lead to higher forces for constant velocity.

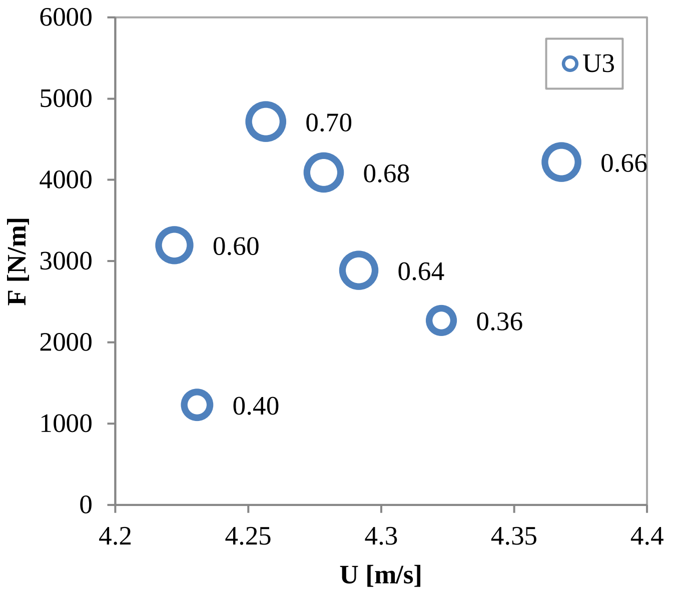

Figure 6-68. Detail of the force-velocity relationship for velocities between 4.2m/s and 4.4m/s. The size of the circle and the value both indicate the flow depth in m.

The same analysis can now be done for the flow depth. The relation between each of the 621 analyzed flow depths (measured at step gauge nr. 3) and the consecutive impact force during the 21 tests, is plotted in Figure 6-69. Chen et al. (2015) suggest a quadratic trend with the initial flow depth (d_{B0}^2 in Eq. [2-64]), and Cross (1967) and SPM (1977) both give the sum of a linear and a quadratic. The literature comparison in Section 6.1.2 already showed that those approaches not work, but the trend between impact force and flow depth also seems quadratic in Figure 6-69.

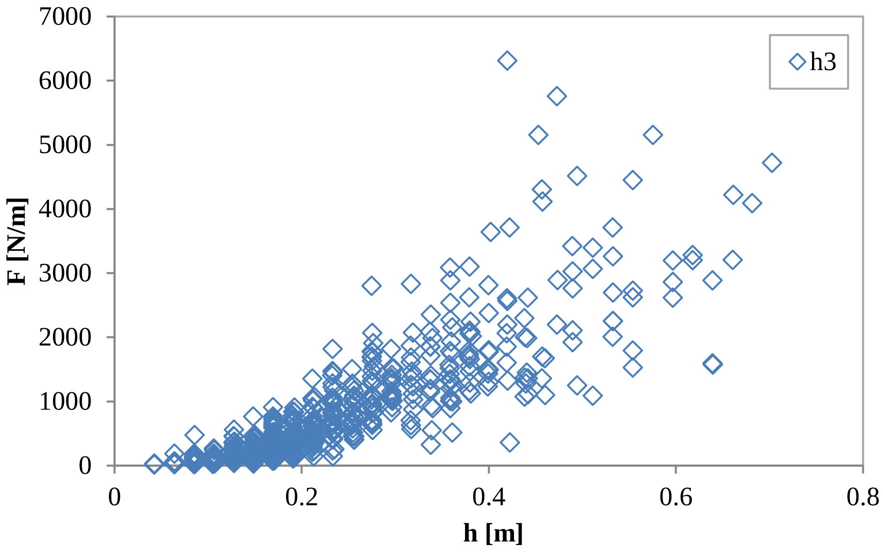

Figure 6-69. Relation between flow depth (at sensor 3) and the consecutive impact (model units, GWK).

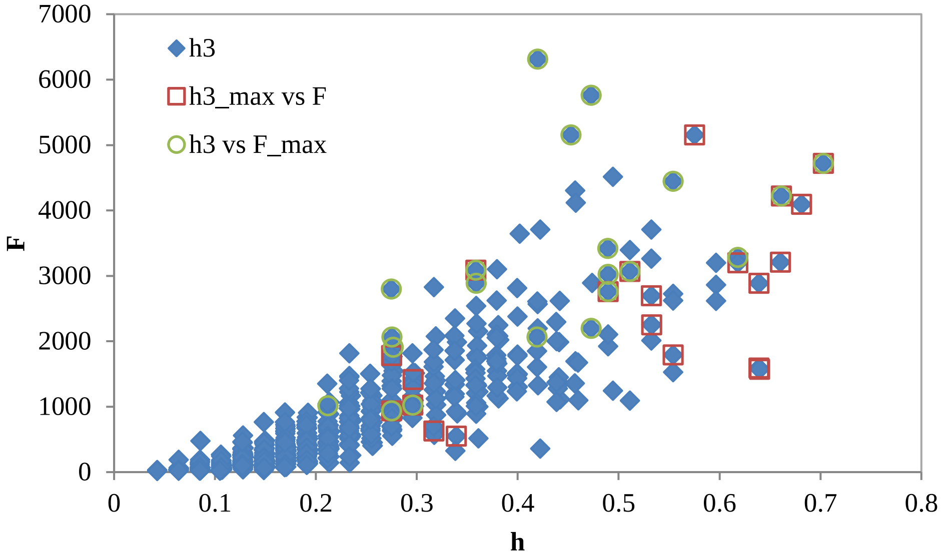

Figure 6-70. Relation between the flow depth and the impact, with indication of maximal flow depths and maximal impacts for each of the 21 tests.

Figure 6-70 shows the same graph as Figure 6-69, only now the maximum flow depths for the 21 tests have been highlighted with their corresponding impact (red squares), as well as the maximum force of each test with its corresponding flow depth (green circle). 7 green and red values overlap, so only in 7 of the 21 tests the maximum force comes from the maximum flow depth. It shows that the maximum recorded forces is not per se linked to the overtopped bore with the highest flow depth. For the flow velocity this value was 12, which could indicate that flow velocities are a bit more dominant in the process than flow depths.

The amount of scatter in Figure 6-69 and Figure 6-70 is similar as in Figure 6-66. For a fixed value of the flow depth, the variation in F (up to a factor of 6) comes from the variation in flow velocity. This is shown in Figure 6-71: larger circles (higher values in m/s shown in the figure) represent larger flow velocities. For a nearly constant flow depth, larger flow velocities lead to larger impacts.

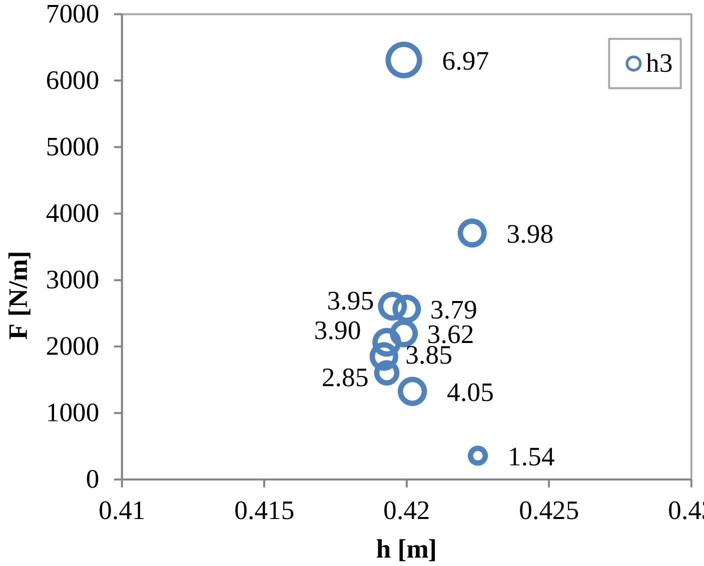

Figure 6-71. Detail of the force - flow depth relationship for flow depths between 4.1m/s and 4.3m/s. The size of the circle and the value both indicate the flow velocity in m/s.

Figure 6-66 to Figure 6-71 mainly show that a one parameter relationship is not enough to describe the impact forces at the storm wall. Therefore, in the following, the impact force is linked to a combination of flow depth and flow velocity.

Hughes (2015) links the overtopping wave volume to the discharges at the crest of that individual wave by means of Eq. [2-55].

$$q_{ind} = 7.405 \frac{V_{ind}\sqrt{tan\alpha}}{T_{m-1,0}} \qquad [2\text{-}55]$$

This discharge q_{ind} in $m^3/m/s$ can also be written as the multiplication of the flow depth h in m and the flow velocity U in m/s: U·h in m^2/s or $m^3/m/s$.

Where a one parameter plot (Figure 6-66 and Figure 6-69) show too much scatter, a two parameter plot gives a better relation with higher R^2 value, see Figure 6-72. Besides, when the impact F is linked to U·h (= q_{ind}), it can be combined with Hughes' equation [2-55] and a relation between the overtopping volumes V_{ind} and impact forces F is found.

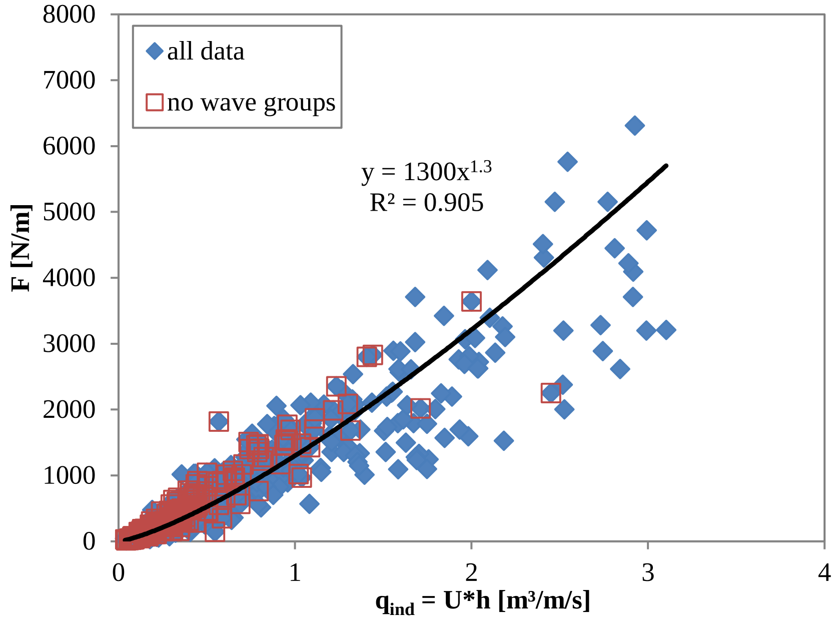

Figure 6-72. Relation between the initial overtopping discharge and the impact force (model units, GWK).

In Figure 6-72, all 621 analyzed incoming bores are plotted in the full (blue) diamonds. Waves often come in groups, thereby also the overtopped waves and consequently the impacting bores come in groups. To verify if the residual water layer and reflection from the previous bores was not disturbing the new incoming bores too much, only individual bores and the first bore of a group without obvious residual water layer were studied separately. They are plotted in the open (red) squares in Figure 6-73. No distinction is to be seen, the individual bores as the bores in group behave in the same way.

The relation between the impact force and the initial discharge (Figure 6-72) has a 15% higher R^2 value than the relation between the force and its individual flow parameters (Figure 6-66 and Figure 6-69). The flow parameters have an inseperable influence on the impact force, and lead to a good prediction line:

$$F = 1300 \cdot (U \cdot h)^{1.3} \qquad [6\text{-}14]$$

with σ'(1300) = 0.022 and σ'(1.3) = 0.017.

This equation directly links the flow parameters on the promenade to the impact forces at the storm wall, but has the following drawbacks:

- it is based on rather low impact values (only up to 7kN/m),
- the equation is not dimensionless,
- the force differs for different wall heights and promenade widths which is not considered here and is thus restricted to the geometry as tested, and
- the units are different on both axes suggesting no physical meaning of this correlation. The power-law is also not based on physics, but a best-fit in the statistical software SPSS.

The force is therefore made dimensionless as previously done in this work, by dividing it by $\rho \cdot g \cdot R_c^2$. The individual discharge is made dimensionless by dividing by $\sqrt{g \cdot R_C^3}$. Note that R_c is the landward freeboard including the wall height.

F and q_{ind} (=U*h) are individual values varying per overtopping event, where R_c and H_{m0} are constant values per test. Both sides of Eq. [6-14] are thus divided by a constant value per test. When different constants would have been used on both sides of the equation (e.g. R_c on the left side of the equation, H_{m0} on the right side), the link between the forces and the discharges would have been lost. To maintain this link, left and right side of the equation have to be divided by the same constant per test. Other attempts have been carried out but showed less correlation. For this reason, only one parameter (R_c) was used to make Eq. [6-14] dimensionless, which then resulted in the plot shown in Figure 6-73.

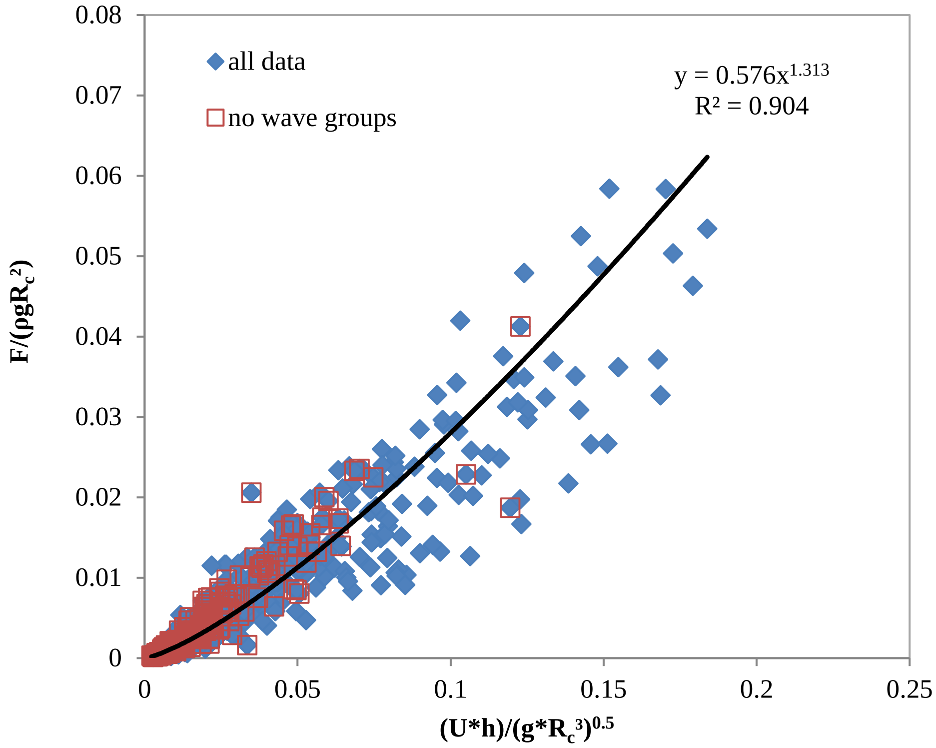

Figure 6-73. Dimensionless relation between initial overtopping discharges and impact forces.

$$\frac{F}{\rho \cdot g \cdot R_c^2} = 0.576\left(\frac{U \cdot h}{\sqrt{g \cdot R_c^3}}\right)^{1.313} \qquad [6\text{-}15]$$

The distribution of individual wave overtopping (Eq. [2-51] to [2-53] substituted to Eq. [2-46]) can now be transferred to a distribution of impact forces, by combining Eq. [2-55] (V to q) and Eq. [6-15] (q to F). From this distribution of forces, $F_{1/250}$ or any other low exceedance value can be calculated.

b) *Comparison with measurements: decay of flow depth*

Eq. [6-15] implies indirectly that all overtopping waves have an impact force, which is not the case due to loss of energy, friction and collision with reflected bores on the promenade. Therefore, the distribution of impacts from 1 to N_{im} (Eq. [6-13]) is plotted; beyond this number the force value is zero. Figure 6-61 is repeated, but now this theoretical equation Eq. [6-15] is added to the plot in dashed line, see Figure 6-74. The shape is promising, but a small offset is noticed.

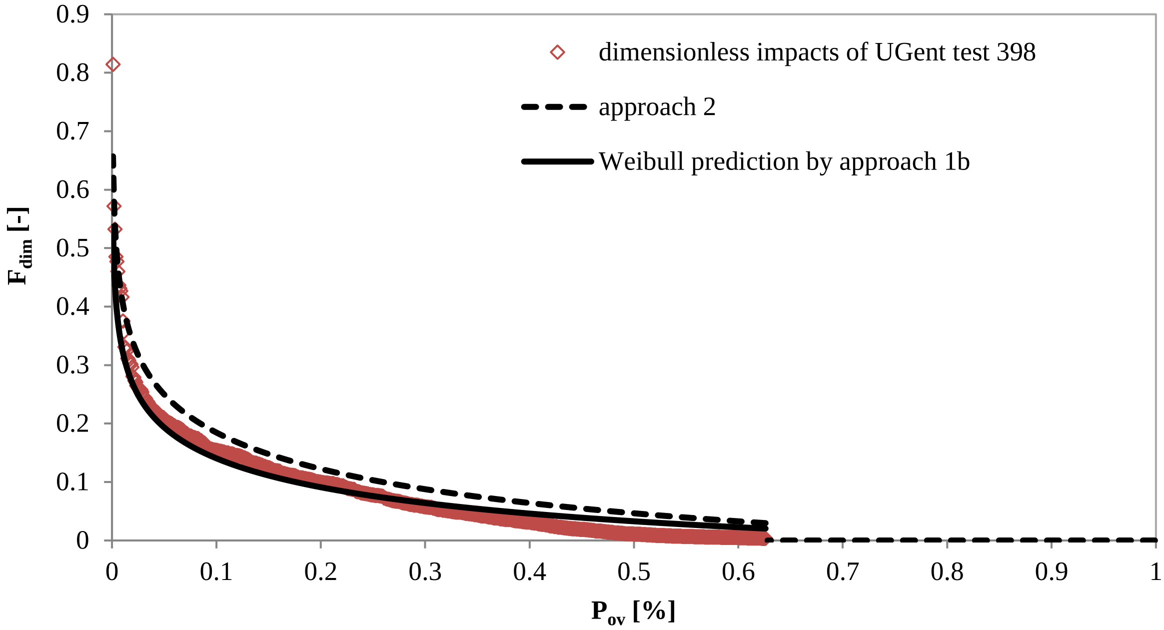

Figure 6-74. Comparison between measured (dimensionless) force distribution in red, Weibull prediction by approach 1b in full black line and the theoretical distribution by approach 2 in the dashed line.

Analogue to Figure 6-64, from this distribution calculated by approach 2, the low exceedance value $F_{1/250}$ can be calculated as the average value of the highest 1/250th (related to the number of incoming waves) impacts. This value is made dimensionless $F_{1/250}/(\rho \cdot g \cdot R_c^2)$ and compared to the measured $F_{1/250}/(\rho \cdot g \cdot R_c^2)$ of the tests in the UGent-1 and Hydralab experiments on smooth dike with promenade and storm wall: see Figure 6-76. This comparison between measurements and calculated values by means of approach 2 shows that this approach overpredicts the actual impacts.

The reason for this lies in the (exponential) decay of the overtopping flow parameters on the crest as explained in Chapter 2 and 5. For Eq. [2-55], Hughes (2015) used the overtopping flow parameters measured at seaward side of the crest, being at 10% from the beginning of the promenade length. To set up Eq. [6-14] and [6-15], the measurements at the landward side of the crest, located at 80% of the promenade length, have been used. At this location, both U and h have reduced compared to the beginning of the crest. This is explained in Figure 6-75. Eq. [2-55] represents the left orange arrow, Eq. [6-14] and [6-15] represent the right arrow, and q decreases between measurement location 1 and 3. A certain incoming overtopped volume V relates to a discharge q_1. By linking both equations as has been done so far, it’s this same discharge q_1 that is used to predict the related force F. But in reality, the discharge would have decreased to q_3 with a related lower value F. Without taking the decay (dashed arrow in Figure 6-75) into account, the force is overpredicted in this way.

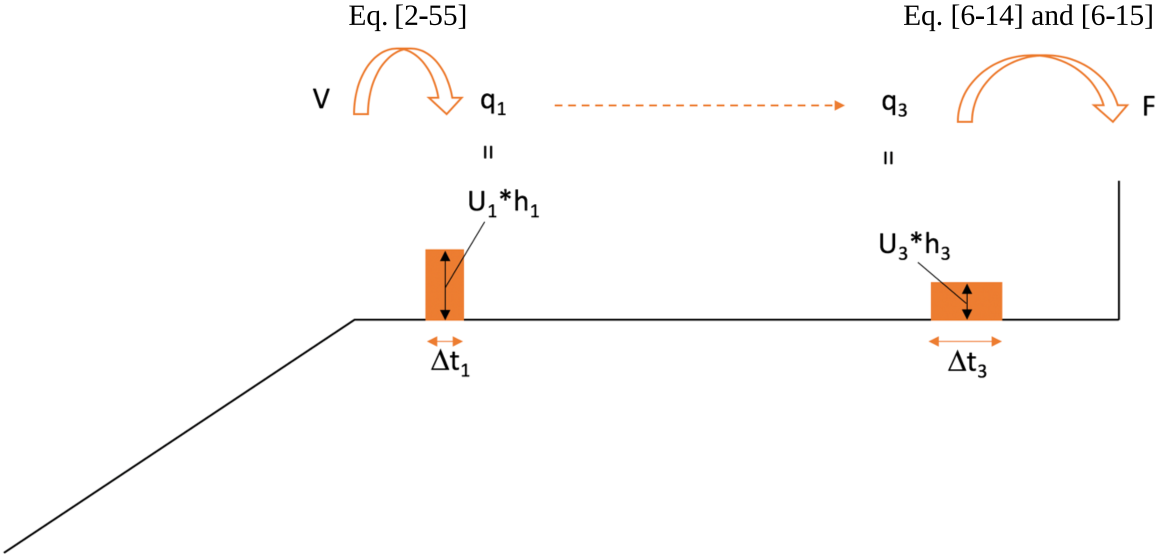

Figure 6-75. Schematic presentation of the overprediction of the force F when the decay (orange arrow) is not taken into account.

This decay is however difficult to measure due to the reasons mentioned in Section 5.1 and difficult to calculate theoretically since literature is indecisive. Eq. [2-55] is valid on the beginning of the crest, Eq. [6-14] and [6-15] are valid at the end of the crest. Between both literature (calculated by means of the coefficients from Table 2-2) predicts a reduction of U·h between 65 and 80% .

The decay that happened in the GWK experiments can also be calculated. This is done by comparing the calculated forces $F_{1/250}$ (by means of the combination of Eq. [2-55] and [6-15]) with the measured forces, see Figure 6-76.

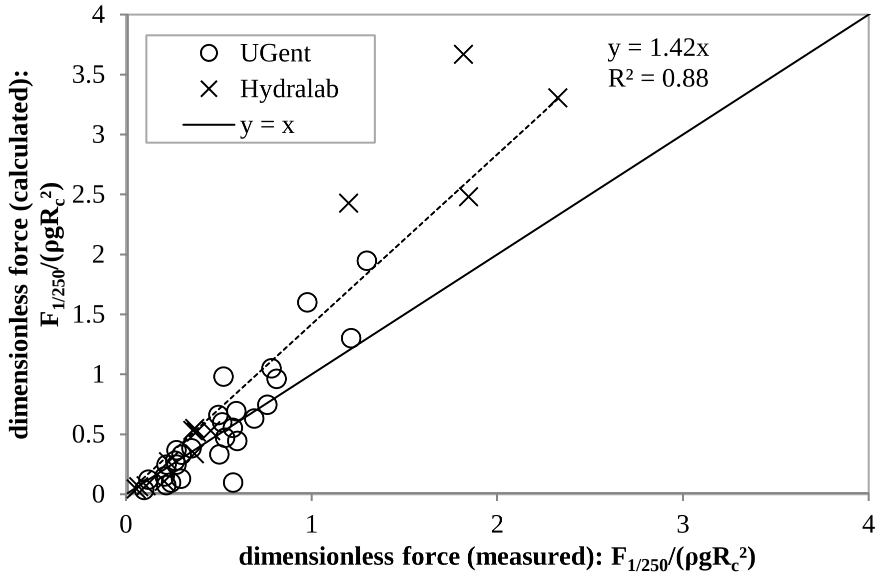

Figure 6-76. Comparison between measurements and calculation of $F^*_{1/250}$ by means of approach 2 (generic approach through overtopping volumes).

The calculated force $F_{1/250}$, with flow parameters at the beginning of the promenade, is 1.42 times the value $F_{1/250}$ from measurements at the wall. However, this deviation from the 45° degree line in Figure 6-76 is mainly due to some higher data points. The lower data points are predicted fairly well by Eq. [6-15].

When the coefficient 1.42 is inverted, the measured force at the wall is 0.70 times the calculated force. This means a decrease of the discharge (U·h) of 30%. To obey the mass conservation law the time duration of the combined flow depth and flow velocity signal will be equally longer (Δt_1 to Δt_3 in Figure 6-75). This 30% reduction is smaller than the 65% to 80% as predicted by the literature, but based on the own dataset and analysis.

By bringing this decay of discharge into account, Eq. [6-16] gives a better estimation than Eq. [6-15] of the higher impact forces based on the overtopping volumes. The comparison to the measured forces is plotted in Figure 6-77, where mainly the higher data (dimensionless force > 1) are now closer to the 45° line. Eq. [6-16] is a good description of impacts on the specific geometry tested (a smooth dike with promenade and wall with range of parameters listed in Table 3-8), and replaces Eq. [6-14] and [6-15].

$$\frac{F}{\rho \cdot g \cdot R_c^2} = 0.40\left(\frac{U \cdot h}{\sqrt{g \cdot R_c^3}}\right)^{1.313} \qquad [6\text{-}16]$$

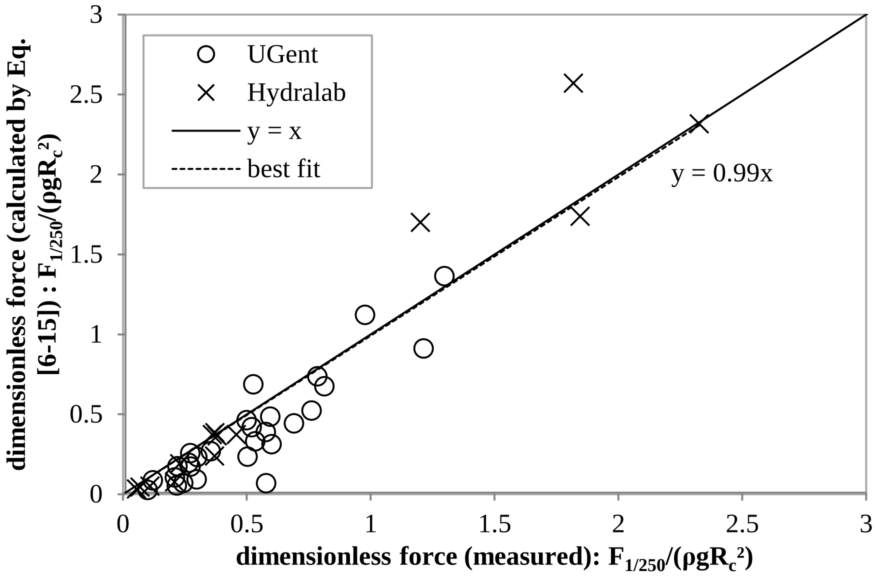

Figure 6-77. Calculated dimensionless forces by means of Eq. [82] compared to measured dimensionless forces.

As mentioned before, mainly the Hydralab data and UGent-1 data with largest forces are corrected properly by Eq. [6-16]. For a conservative calculation, Eq. [6-15] can be used for the smaller forces with dimensionless values below 1.

Approach 2 can be summarized by the flowchart in Figure 6-78. The validity range for the developed formulae in this approach is A_c/H_{m0} between 1.1 and 2.3 and R_c/H_{m0} between 2.2 and 4.4.

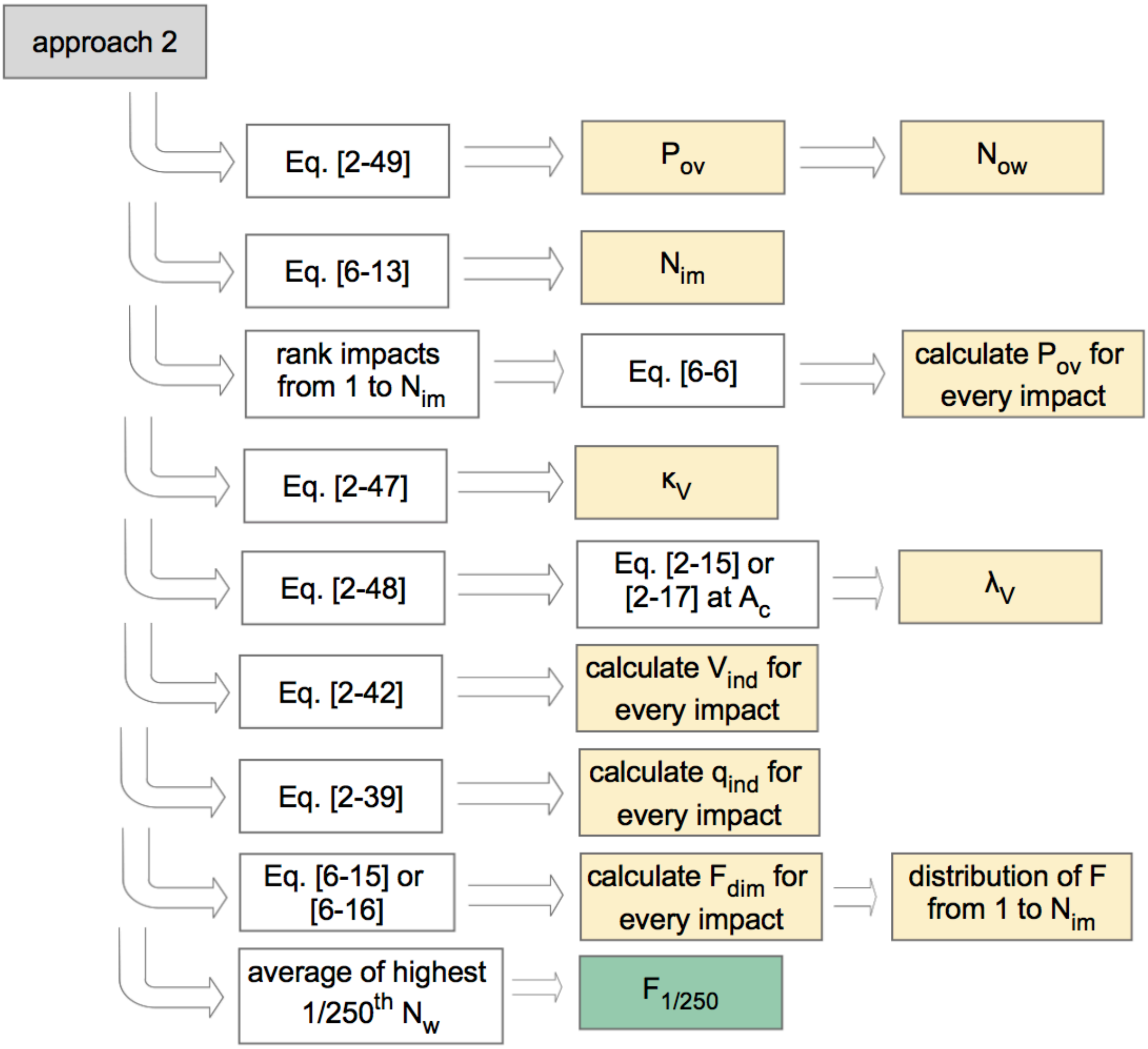

Figure 6-78. Flow chart of approach 2 to calculate $F_{1/250}$ for smooth dikes with a promenade and storm wall.

6.4.4 *Discussion on model/scale factor*

Eq. [6-4] in Section 6.4.1 was developed for UGent-1 and Hydralab datasets only, due to the reduced length of the time series in the GWK tests. When looking at the exponential coefficients (b-coefficient) in Table 6-1, a factor of 1.19 can be found between the $F_{1/250}$ values of the UGent-1 and the Hydralab dataset, with the Hydralab tests (larger scale than UGent-1) providing lower forces. The question was raised if this could have been due to scale and/or model effects? This section provides a comparison between the GWK data and the other two datasets. Attention has to be paid that the differences in the datasets are big. The parameter ranges between UGent-1/Hydralab and GWK are not overlapping. Therefore, the data don't allow an ideal comparison and separation between scale and model effects. However two attempts are made. To avoid the problem of the length of the time series, a good base for comparison is required.

A first attempt is to compare a low exceedance value per test. $F_{1/250}$ cannot be used for this analysis since the GWK tests did not have (more than) 250 incoming waves. Therefore, in a first step, the highest recorded force per test (noted as $F_{highest}$) is used in Figure 6-79. It is not noted as F_{max}, since it is likely that the highest recorded force in the GWK tests is lower than the maximum force in a longer storm duration. The comparison is plotted in a dimensionless way in Figure 6-79.

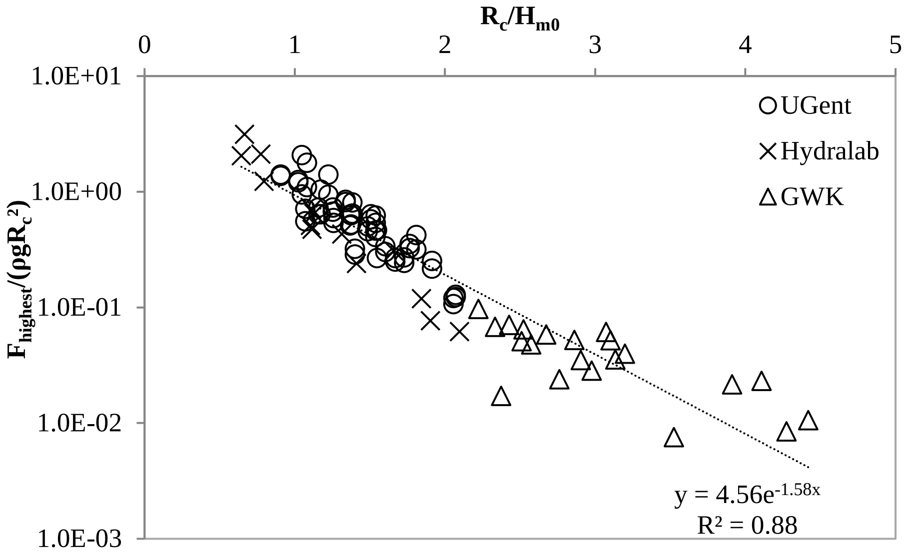

Figure 6-79. Comparison of the highest recorded (dimensionless) forces in the 3 test campaigns.

The Hydralab data are (slightly) below the UGent data. Based on the literature related to air bubbles and scale effects (small scale has less bubbles and consequently higher impacts), the expectation is that the GWK data (largest scale) should have lower forces. Figure 6-79 shows that this is not the case with the data comparison performed here. The data of the GWK tests are really well in line with the UGent-1 data, and actually well in line with the overall dataset. Where UGent-1 and Hydralab are very similar in test set-up and parameter range, GWK has a slightly different set-up with open storm walls and probably less reflection. GWK tests also had a larger A_c/H_{m0} range, which led to less overtopping over the storm wall and thus more impact energy measured on the wall. It can be assumed here that these model effects make the impacts on the wall higher than was expected based on the larger scale. It seems that this model effect eliminates any scale effect in the GWK set-up (if any scale effect can be noted at all).

A trendline can be fitted through the complete dataset (as is done in Figure 6-79), but also through the individual datasets (shown in Figure 6-80). With a constant 'a_F-coefficient" 4.56 from the overall trendline, the b_F-coefficients are respectively 1.54 (UGent-1), 1.88 (Hydralab) and 1.58 (GWK). The ratio b-coefficients of Hydralab/UGent-1 is 1.19 (scale effect dominant over model effect, due to similar test set-ups and parameter range), as was also the case for $F_{1/250}$. The ratio GWK/Hydralab is 0.84 (model effect dominant over scale effect). This comparison needs further investigations but shows that the scale and model effects both have an influence. The order of magnitude is limited to about +/-20% in the present datasets, which is smaller than the uncertainty on the formulae.

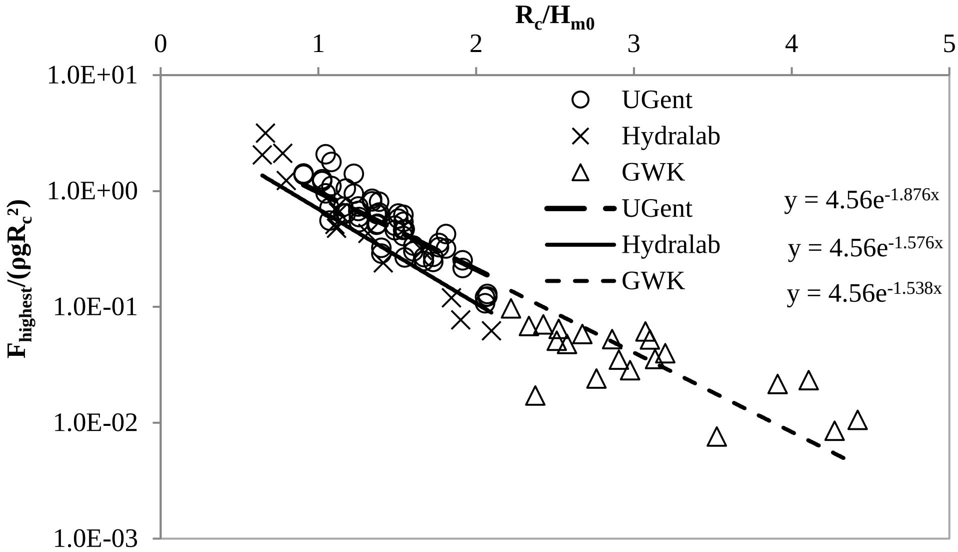

Figure 6-80. Plot of the dimensionless forces with trendlines through the individual datasets.

A second attempt for comparing the data, is by using a same low-exceedance value for all three datasets. The number of incoming waves in GWK varies between 37 and 204. For example 1/25th is a value that can be used for all datasets: rank all forces from high to low, take the average value of the highest 1/25th of the number of waves ranked forces. However, this will not be much of a difference for the GWK tests compared to Figure 6-79 (1/25th of e.g. 100 waves means the average of the highest 4 forces) but the values from UGent and Hydralab will reduce a lot more (1/25th of 1000 incoming waves means the average of the 40 highest impacts). This is no good base for comparison. Therefore, in this exercise, an exception is made in the way to calculate the average exceeding value which is exceptionally not related to the number of waves but to the number of impacts. The GWK tests showed in between 9 and 75 impacts, 1/9th of all impacts is used here. Figure 6-81 plots these data and gives very similar results than shown in Figure 6-79. When the trendlines per dataset are investigated separately, the same ratio's in b_F-coefficients are found: +/- 20%.

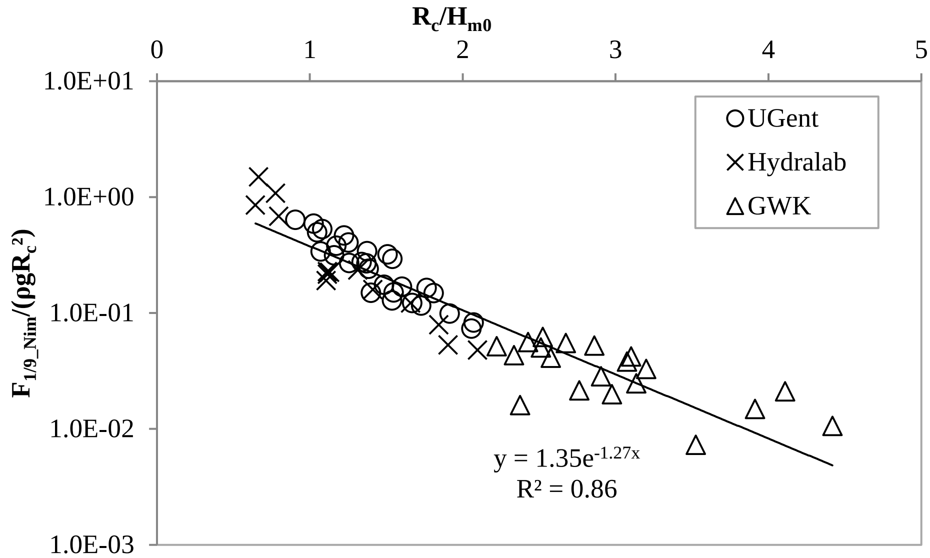

Figure 6-81. Comparison of the average of 1/9th of all impacts in the 3 datasets.

6.4.5 *Conclusion*

Three different approaches were given in this section 6.4. Approach 1a, a direct empirical relation between the wave conditions at the toe of the dike and the bore-induced impacts on the storm wall, is the most straightforward and most accurate methodology to calculate wave impact forces for the studied geometry: a storm wall at the end of a promenade at crest level of a smooth sea dike. The promenade has a prototype equivalent of 10m wide and a storm wall between 0.8m and 1.2m (UGent-1 scale 1:10, Hydralab scale 1:6). Section 6.2.7 has shown that the height of the storm wall is not dominant in the value $F_{1/250}$, which is determined by church-roof impacts impacting mainly the lower part of the storm wall. The impact force is made dimensionless by dividing through $\rho g R_c^2$, and the following formula is proposed as probabilistic formula:

$$\frac{F_{1/250}}{\rho g R_c^2} = 7.8 \cdot exp\left(-2.02\,\frac{R_C}{H_{m0}}\right) \qquad [6\text{-}4]$$

The approach 1a is recommended in this manuscript. The validity range for Eq. [6-4] is A_c/H_{m0} between 0.2 and 1.2 and R_c/H_{m0} between 0.9 and 2.0.

However, if the full distribution of all forces in a storm is of interest, approach 1b can be used. A Weibull distribution is proposed of which the shape and the scale parameters can be calculated using the incoming wave parameters. When information of the flow depths and flow velocities of the overtopped waves is available, possibly even for a different kind of structure, approach 2 can be used. It’s however shown that great care has to be taken where the flow parameters have been measured when combining equations, since not including the decay of the height of the flow parameters (proportional to their increase in time duration, conservation of mass) can lead to an overestimation of the impacts.

Based on the comparison of the results of the different test campaigns, carried out in different wave flumes at different scales, the scale and model effects were discussed. It’s difficult to isolate scale or model effects, but the order of magnitude seems to be around 20%.

This section has discussed the definitions of $F_{1/250}$, being the average impact of the highest $1/250^{th}$ of the number of incoming waves, and F_{mean}, calculated as the average value of impact 1 to the number of overtopped waves (N_{ow}). Also an equation is given to calculate the number of impacts N_{im}, useful for plotting the distribution from impact 1 to N_{im}.

6.5 *Wave impacts on other overtopping reducing measures*

As mentioned in Section 6.4.5 the preferred methodology is approach 1a for reasons of highest accuracy and simplicity. In that approach, the hydraulic conditions are directly linked to the impact forces in the following empirical formula with coefficients a_F and b_F based on experimental data:

$$\frac{F}{\rho g R_c^2} = a_F \cdot exp\left(-b_F\,\frac{R_C}{H_{m0}}\right) \qquad [6\text{-}3]$$

Section 6.4 was devoted to the geometry with a storm wall at the end of a promenade. However, the type of formula in [6-3] can also be used for the other geometries of a storm wall. For every different geometry, the parameters a_F and b_F will be given in this section.

The tests for these different geometries have only been carried out as part of the UGent-1 dataset, not in other research campaigns. Test set-up and test programs have been given in Section 3.1.

6.5.1 *Smooth dike with storm wall*

A sketch of this geometry was given in Figure 3-7 and is repeated here in Figure 6-82 with indication of the measured force.

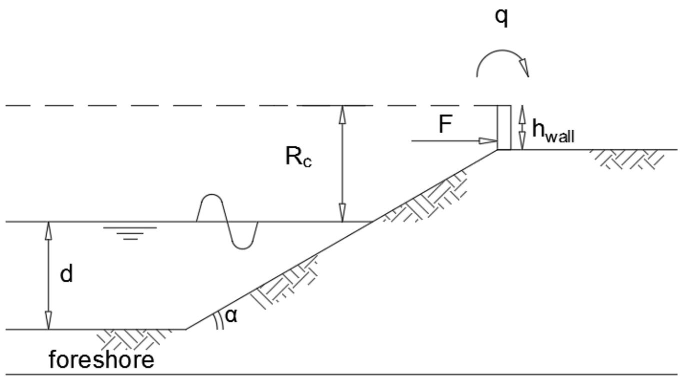

Figure 6-82. Geometry smooth dike with storm wall, with indication where the force is measured.

The test program on this geometry is given in Table 3-2. The analysis of the forces shows that the tested range of wave periods and dike slope angles α have no influence on the wave-induced forces, just as was concluded for the overtopping. A low scattered relationship with a_F = 4.45 (σ' = 0.03) and b_F = 1.49 (σ' = 0.013) is found, see Figure 6-83. This equation is valid for A_c/H_{m0} between 0.6 and 1.9 and R_c/H_{m0} between 1.1 and 2.6.

$$\frac{F_{1/250}}{\rho \cdot g \cdot R_c^2} = 4.45 \cdot \exp\left(-1.49 \cdot \frac{R_c}{H_{m0}}\right) \qquad [6\text{-}17]$$

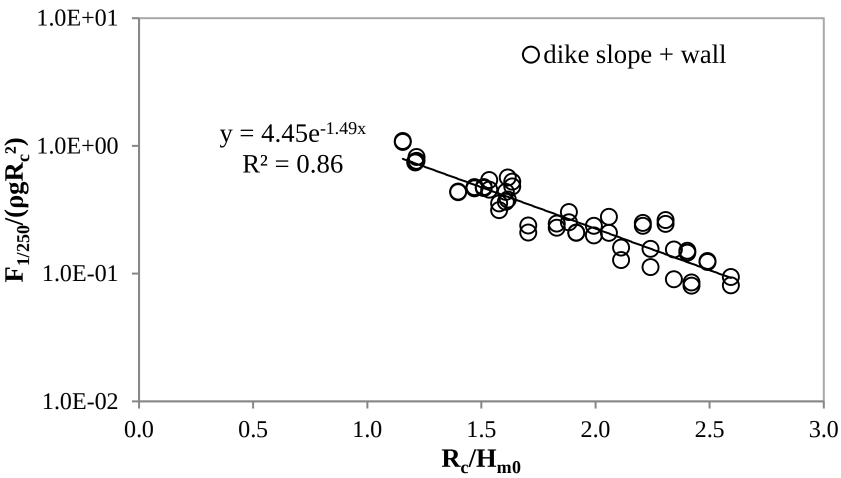

Figure 6-83. Impact forces on a storm wall without a promenade, UGent-1 data set.

6.5.2 *Smooth dike with storm wall and bullnose*

The overtopping can be further reduced by adding a bullnose to the storm wall (Figure 6-84), however, this implies larger impact forces on the storm wall. Tests have been carried out measuring both horizontal impact forces (F_h) and vertical impact forces (F_v). The test program is given in Table 3-3.

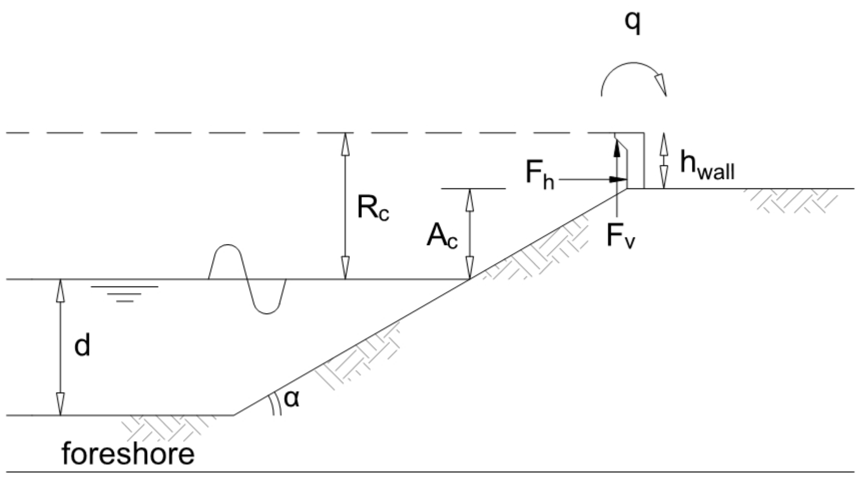

Figure 6-84. Geometry smooth dike with storm wall and bullnose, with indication where the force is measured.

Similar to the previous geometry, the dike slope angle (cot(α) = 2 or 3) and the wave period have no significant influence on the impacts and are thereby not included as a parameter in the formula. The angle ε of the bullnose and the kind of measurement (horizontal or vertical) both show a significant difference. Figure 6-85 shows the 4 different groups of data: a bullnose of 30° in full symbols, and a bullnose of 45° in open symbols; horizontal measurements in (black) circles and vertical measurements in (grey) triangles.

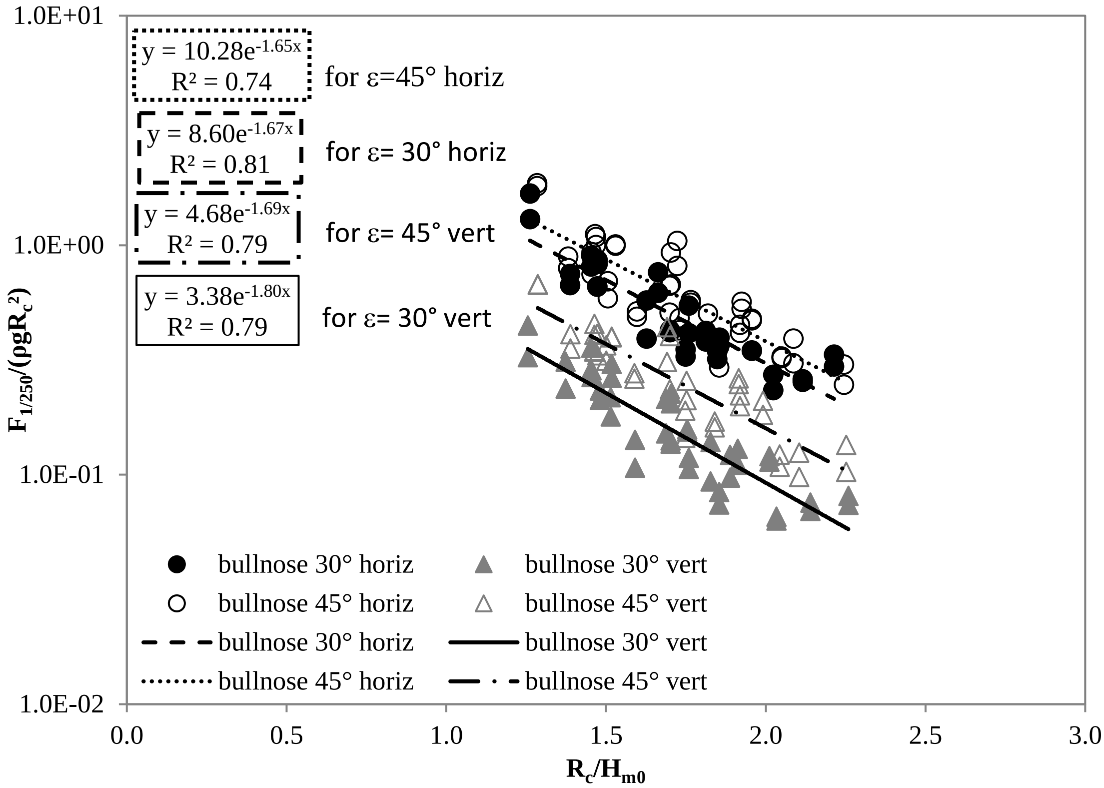

Figure 6-85. Impact forces on a storm wall with bullnose.

Consequently, 4 new coefficients a_F and b_F in Eq. [6-3] are identified. They are valid for for A_c/H_{m0} between 0.6 and 1.6 and R_c/H_{m0} between 1.3 and 2.2.

Table 6-2. Empirical coefficients a_F and b_F for a smooth dike with storm wall and bullnose

a_F	b_F	ε	Hor/vert	Eq.
10.28 (σ' = 0.045)	1.65 (σ' = 0.016)	45°	hor	[6-18]
8.60 (σ' = 0.044)	1.67 (σ' = 0.017)	30°	hor	[6-19]
4.68 (σ' = 0.036)	1.69 (σ' = 0.013)	45°	vert	[6-20]
3.38 (σ' = 0.036)	1.80 (σ' = 0.012)	30°	vert	[6-21]

Figure 6-85 shows that the 4 trendlines are quasi parallel. The b_F-coefficients in the exponential part of the formulae are thus all nearly equal. The difference in forces only shows in a different a-coefficient outside the formulae.

From a comparison of the a_F-coefficients, it is concluded that a 45° bullnose has about 20% higher horizontal forces (10.28/8.60 = 1.20) and about 40% higher vertical forces (4,68/3,38 = 1.38) than a 30° bullnose. The vertical forces of both bullnoses are less than half the horizontal forces on the same bullnose (4.68/10.28 = 0.45; 3.38/8.60 = 0.39).

6.5.3 *Smooth dike with promenade, storm wall and bullnose*

The final geometry tested was the smooth dike with promenade, storm wall and a bullnose. Again, horizontal and vertical forces have been measured, see Figure 6-86.

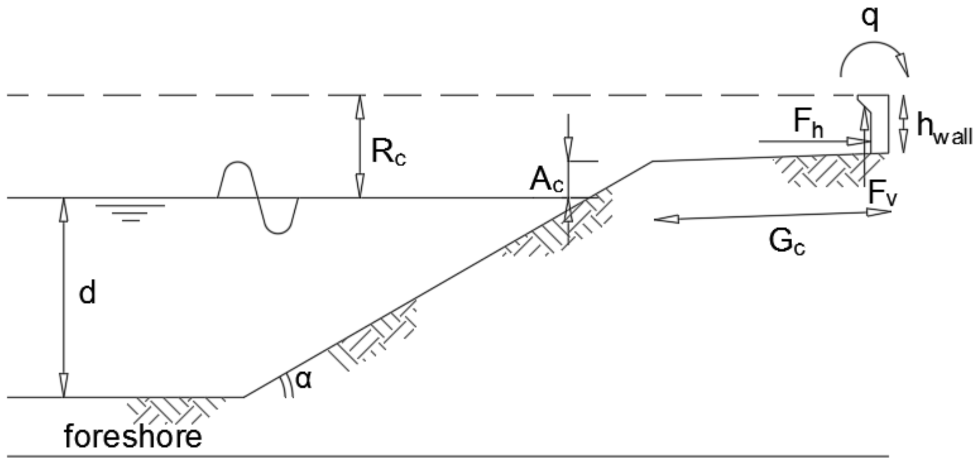

Figure 6-86. Geometry smooth dike with promenade, storm wall and bullnose, with indication where the force is measured.

The slope angle and wave period have again, just like for all other geometries, no significant influence on the impact forces. The angle of the bullnose (ε) and the measurement (horizontal or vertical) do, so the data in Figure 6-87 are split in four different groups. Separate formulae are given per group, which are valid for A_c/H_{m0} between 0.2 and 1.0 and R_c/H_{m0} between 0.9 and 1.8.

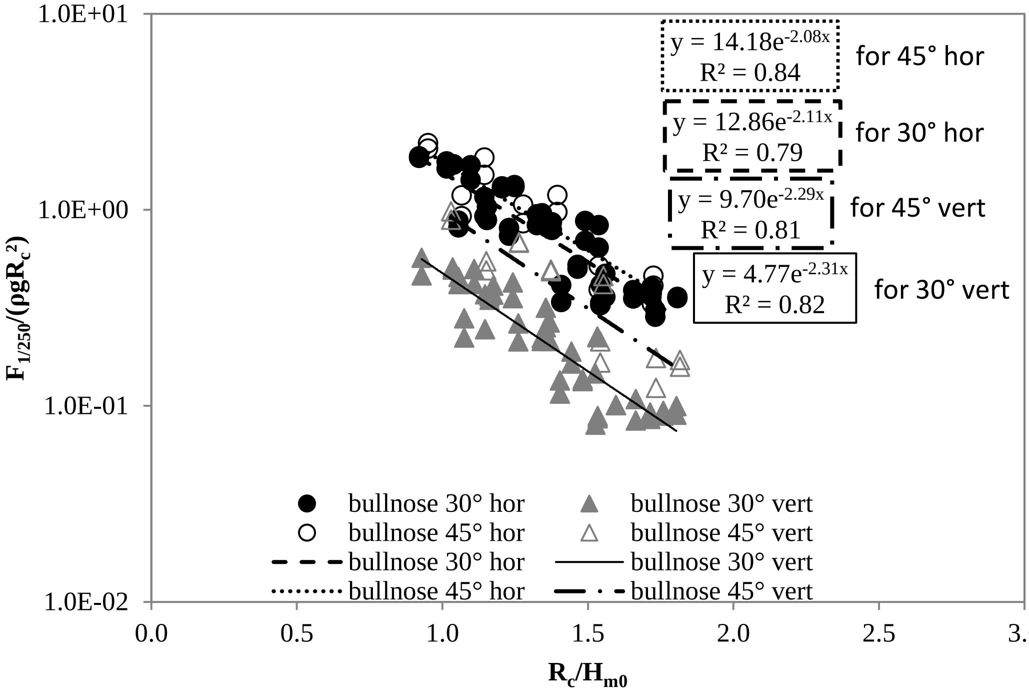

Figure 6-87. Impact forces on a storm wall with bullnose at the end of a promenade.

Table 6-3. Empirical coefficients a_F and b_F for a smooth dike with promenade, storm wall and bullnose

a_F	b_F	ε	Hor/vert	Eq.
14.18 (σ’ = 0.062)	2.08 (σ’ = 0.027)	45°	hor	[6-22]
12.86 (σ’ = 0.034)	2.11 (σ’ = 0.014)	30°	hor	[6-23]
9.70 (σ’ = 0.059)	2.29 (σ’ = 0.021)	45°	vert	[6-24]
4.77 (σ’ = 0.033)	2.31 (σ’ = 0.013)	30°	vert	[6-25]

The coefficients b_F are all close to each other, so the difference in the formulae are mainly in the constant value a_F.

Comparison of these a-coefficients shows that 45° bullnoses have 10% higher horizontal forces than 30° bullnoses, and double the uplift forces. The vertical forces are 0.68 (for 45° bullnose) to 0.37 (for 30° bullnose) times lower than the horizontal forces.

6.6 *Case study*

All obtained coefficients a_F and b_F for the different geometries are summarized in Table 6-4. Attention has to be paid to the validity range of the formule. The coefficients are only valid within the range of test parameters for the specific geometry. The most important tested range of parameters is given in Table 6-5, for the full overview, reference is made to Table 3-13.

Table 6-4. Overview of the coefficients a_F and b_F in Eq. [6-3] for the different geometries, usable in parameter ranges according to Table 6-5.

Geometry	ε (°)	direc tion	a_F	b_F	Eq. nr
Smooth dike with storm wall	-	hor	4.45	1.49	[6-17]
Smooth dike with storm wall and bullnose	30°	hor	8.60	1.67	[6-19]
Smooth dike with storm wall and bullnose	30°	vert	3.38	1.80	[6-21]
Smooth dike with storm wall and bullnose	45°	hor	10.28	1.65	[6-18]
Smooth dike with storm wall and bullnose	45°	vert	4.68	1.69	[6-20]
Smooth dike with promenade and storm wall	-	hor	7.80	2.02	[6-4]
Smooth dike with promenade and storm wall and bullnose	30°	hor	12.86	2.11	[6-23]
Smooth dike with promenade and storm wall and bullnose	30°	vert	4.77	2.31	[6-25]
Smooth dike with promenade and storm wall and bullnose	45°	hor	14.18	2.08	[6-22]
Smooth dike with promenade and storm wall and bullnose	45°	vert	9.70	2.29	[6-24]

Table 6-5. Range of parameters per geometry tested in the UGent-1 experiments on wave-induced impacts.

UGent-1 tests on wave impacts	Wall	Wall + bullnose	Promenade + wall	Promenade + wall + bullnose
$G_c/L_{m-1,0}$	n.a.	n.a.	0.13 – 0.25	0.13 – 0.25
h_{wall}/R_c	0.28 – 0.50	0.28 – 0.50	0.36 – 0.67	0.36 – 0.67
R_c/H_{m0}	1.15 – 2.60	1.26 – 2.26	0.91 – 2.07	0.92 – 1.82
A_c/H_{m0}	0.61 – 1.89	0.63 – 1.64	0.23 – 1.22	0.23 – 1.02
$\xi_{m-1,0}$	2.27 – 4.80	2.20 – 4.61	2.24 – 4.79	2.14 – 4.77
$s_{0,\ m-1,0}$	0.007 – 0.04	0.011 – 0.04	0.01 – 0.04	0.01 – 0.04

For these different geometries, an example is worked out to calculate the impacts on storm walls. The same boundary conditions are used as for the example in the case study on the reduction of overtopping.

Table 6-6. Boundary conditions for a case study on wave impacts.

cot(α)		2		
SWL	mTAW	7.00		
crest level	mTAW	9.00		
R_c	m	2.00		
$T_{m-1,0}$	s	8.2		
H_{m0}	m	2.00	1.33	1.00
R_c/H_{m0}	-	1.00	1.50	2.00
A_c	m	0.75		
A_c/H_{m0}	-	0.38	0.56	0.75

Over the dike crest, with A_c = 0.75m, an overtopping discharge for the 3 wave heights of respectively 496.7, 194.7 and 87.9 l/m/s overtopping would occur on the promenade for those geometries with promenade, after which those overtopped waves can impact the storm wall.

The overtopping values over the landward edge of the construction (over the storm wall, over the bullnose) as calculated in Section 4.3 have been added to Table 6-7, to indicate that reduction of overtopping leads to higher forces and vice versa.

Table 6-7. Forces and overtopping for the different geometries calculated by means of approach 1a.

			H_{m0} = 2m	H_{m0} = 1.33m	H_{m0} = 1m
Smooth dike with storm wall	$F_{1/250}$ (kN/m)	Eq. [6-17]	39.4	18.7	8.9
	q (l/s/m)	*Eq. [4-26]*	*55.2*	*4.7*	*0.4*
Smooth dike with storm wall and bullnose 45°	$F_{h,1/250}$ (kN/m)	Eq. [6-18]	77.5	34.0	14.9
	$F_{v,1/250}$ (kN/m)	Eq. [6-20]	33.9	14.6	6.3
	q (l/s/m)	*Eq. [4-27]*	*23.4*	*1.7*	*0.1*
Smooth dike with storm wall and bullnose 30°	$F_{h,1/250}$ (kN/m)	Eq. [6-19]	63.5	27.6	12.0
	$F_{v,1/250}$ (kN/m)	Eq. [6-21]	21.9	8.9	3.6
	q (l/s/m)	*Eq. [4-27]*	*38.7*	*3.7*	*0.3*
Smooth dike with promenade and storm wall	$F_{1/250}$ (kN/m)	Eq. [6-4]	40.6	14.8	5.4
	q (l/s/m)	*Eq. [4-29]*	24.0	1.2	0.05
Smooth dike with promenade and storm wall with bullnose 45°	$F_{h,1/250}$ (kN/m)	Eq. [6-22]	69.5	24.6	8.7
	$F_{v,1/250}$ (kN/m)	Eq. [6-24]	38.5	12.3	3.9
	q (l/s/m)	*Eq. [4-30]*	*10.1*	*0.3*	*0.01*
Smooth dike with promenade and storm wall with bullnose 30°	$F_{h,1/250}$ (kN/m)	Eq. [6-23]	61.2	21.3	7.4
	$F_{v,1/250}$ (kN/m)	Eq. [6-25]	61.2	21.3	7.4
	q (l/s/m)	*Eq. [4-30]*	*18.8*	*0.8*	*0.03*

When having a detailed look at different values in this table it becomes clear that the wall with bullnose reduces the overtopping discharge (e.g. wall 55.2 l/m/s → bullnose 45° 23.4 l/m/s for H_{m0} = 2m) but is subjected to larger horizontal impact forces (39.4 kN/m → 77.5 kN/m). Adding a promade to a dike with wall reduced the overtopping discharge (wall 4.7 l/m/s → promenade+wall 1.2 l/m/s for H_{m0} = 1.33m) and the impact forces (18.7 kN/m → 14.8 kN/m).

The vertical forces are significantly smaller than the horizontal forces on a wall with bullnose, but still need to be taken into account for structural design. Forces on a wall with bullnose 45° are higher than forces on a wall with bullnose 30°; more water is blocked which leads to higher impacts forces.

Finally, also approaches 1b and 2 have been worked out for the geometry smooth dike with promenade and storm wall. Approach 1b calculates the distribution of dimensionless impact forces by means of a Weibull PDF with shape and scale parameters linked to the incoming wave parameters. Approach 2 calculates the Weibull PDF of overtopping waves, transfers this to a PDF of discharges which are then linked to a PDF of impacts. From both PDF's, the value $F_{1/250}$ is calculated and compared to approach 1a in Table 6-8. The example for H_{m0} = 1.33m is also plotted in Figure 6-88.

Table 6-8. Comparison for the 3 approaches for the smooth dike with promenade and storm wall.

Smooth dike with promenade and storm wall		H_{m0} = 2m	H_{m0} = 1.33m	H_{m0} = 1m
$F_{1/250}$ (kN/m)	Approach 1a	40.6	14.8	5.4
	Approach 1b	34.8	10.6	3.3
	Approach 2 Eq. [6-15]	28.9	11.5	5.6

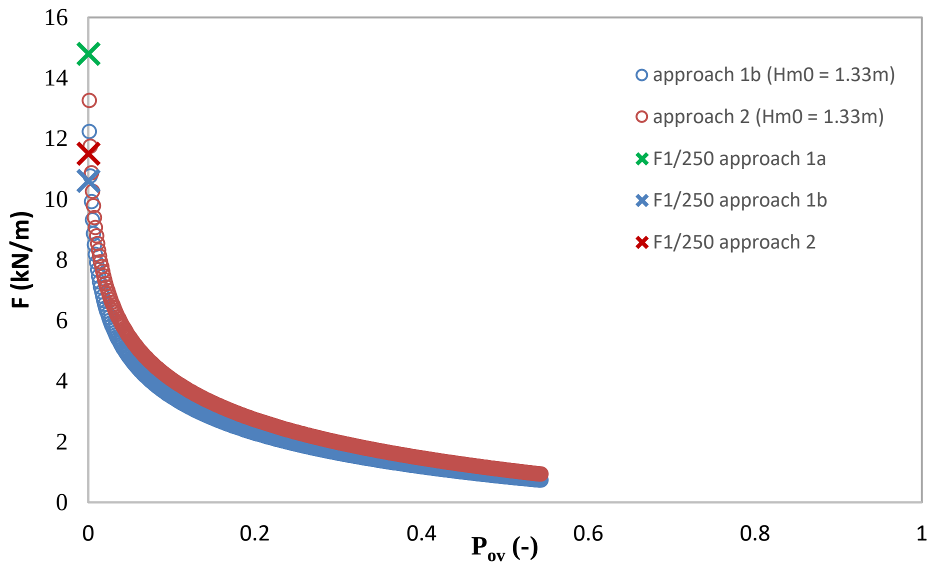

Figure 6-88. Comparison of PDF and $F_{1/250}$ by the different approaches.

This section has shown the calculation of impact forces by approach 1a for different geometries, and the comparison of different approaches for the geometry "smooth dike with promenade and storm wall". Both calculation examples show overall logic and well correlated results, and give a good estimate of the impact force within the tested parameter range (Table 6-5). Detailed experimental or numerical modelling would be advised before going to structural design of such storm walls, certainly when the geometrical or hydraulic conditions are outside of the tested parameter range.

7 Summary and conclusions

Reduction of wave overtopping, overtopping flows and consecutive impacts on overtopping reducing measures have been studied thoroughly in the present research. In this chapter the motivation, methodology and key results are presented.

The focus points of this research on **the reduction of wave overtopping by storm walls and promenades** and **wave induced forces on storm walls** were based on a typical Belgian sea dike with intermediate or deep water reaching the dikes. With dike slopes cot(α) 2 to 3 and the test program as mentioned in Chapter 3, this lead to non-breaking waves to analyze overtopping, overtopping flows and wave induced impacts. Also a small database for overtopping only was set-up for a milder dike slope cot(α) = 6 giving breaking waves, but the majority of data (+1100 tests) dealt with non-breaking waves. Within the tested range of parameters, the results are not restricted to the Belgian coast but can be used for river dikes, sea dikes, harbor basins, … with similar geometries.

In this manuscript, semi-empirical prediction formulae were set up by means of new tests using **experimental modelling**. A scale model was therefore built in different wave flumes and an extensive test program was carried out. Numerical modelling and the use of an Artificial Neural Network have not been used in this work since both had the disadvantage that this study works with new and rather complex geometries and the available numerical or Neural Network models were not yet validated or trained to these geometries.

Three main topics with several research questions have been answered in this work:

1. How to modify the crest of a dike to **reduce the overtopping discharges**? Is the available literature sufficient to account for overtopping reducing measures at crest level of dikes, or do new formulae need to be set up?
2. When a wave overtops a smooth dike, an **overtopped bore flows over the promenade**. How do the flow parameters look like and where is a good location to measure flow depths and flow velocities?
3. **When an overtopping flow on a crest promenade hits a storm wall, what is the related force** and how does the force signal look like? What are the prediction formulae linked to sea state conditions or overtopping flow parameters?

To answer these questions, a large database was collected with over **1100 new data points** from experiments in **four different test campaigns** in three different European laboratories:

- **UGent-1**, wave flume 30m x 1m x 1.20m of Ghent University. Small scale tests, over 1000 tests where wave overtopping was measured and over 200 tests where also forces were measured. All non-breaking waves.
- **UGent-2**: small wave flume 15m x 0.35m x 0.60m at Ghent University. Small scale tests, 50 tests where only wave overtopping was measured. Breaking waves.
- **Hydralab**: CIEM large wave flume 100m x 3m x 5m at UPC Barcelona. Middle scale tests, 14 tests on wave-induced forces. Non-breaking waves.
- **GWK**: large wave flume 300m x 5m x 7m at FZK Hannover. Large scale tests, 21 tests on overtopping flows and wave-induced forces. Non-breaking waves.

For completeness, a **fifth (existing) dataset** was added and reanalyzed in this work: **Harlingen**. Scheldegoot 55m x 1m x 1.2m at Deltares. Small scale tests, 38 tests on wave overtopping. Breaking an non-breaking waves.

The main parameter ranges of this research are summarized in Section 3.6, more specific in Table 3-11 to Table 3-13.

7.1 *Reduction of wave overtopping by means of storm walls and promenades at crest level of a dike*

In the first part of this PhD it was investigated how wave overtopping over sea dikes can be reduced dealing with the spatial restrictions in highly populated and economical/touristic areas. Overtopping reducing measures at crest level of the smooth dike were proposed in this work: a storm wall, a storm wall with bullnose, a promenade, a stormwall with/without bullnose at the end of a promenade or a stilling wave basin.

First, a smooth dike with storm wall was studied. The EurOtop (2007) procedure was followed to predict the newly developed data from the **UGent-1 database**, characterized by a **specific geometry of a high (emerged) storm wall** and **non-breaking waves**. It showed that about 2/3rd of the data were predicted well, but mainly the data with low freeboards were located outside of the 90% confidence band. Also other available literature (Coeveld et al. (2006) and Tuan (2013)) did not give an optimal prediction for UGent-1 data. Therefore, **a new procedure was developed** for non-breaking waves overtopping a smooth dike with storm wall at crest level. Since this storm wall, and all other overtopping reducing measures studied in this PhD, were located clearly above SWL and didn't really influence the breaking process anymore, it was decided to use the actual dike slope. Based on the UGent-1 database, a reduction factor for non-breaking waves was developed.

The same EurOtop (2007) procedure was also followed to predict the newly developed data from the **UGent-2 database, breaking waves** over a mild dike slope coat(α) = 6 with a storm wall at crest level. The available γ_v = 0.65 seemed to be too strong for these data, so **the same new procedure as for the UGent-1 database was followed to develop a reduction factor for the breaking waves of the UGent-2 database**. It's noted that UGent-2 contains less data and was set-up on a really small scale (1:50), so results must be taken with care.

The reduction factor for the UGent-1 (ξ_{0p} > 2, non-breaking) and UGent-2 (ξ_{0p} < 2, breaking) data was derived through a point-per-point analysis and in a relative way. Measurements over the geometry with overtopping reducing measure (e.g. storm wall) were compared to measurements over a reference geometry (a smooth dike with perpendicular waves). In this way, model effects were excluded. It was proven that **a reduction factor developed with a shape like EurOtop (2007)** (a straight line in a log-linear plot) **can also be used in the EurOtop (2016) equations** (with a curved line in a log-linear plot due to an exponent c).

7.1.1 *Reduction of average overtopping discharges due to a storm wall*

The new method, set up for geometries with a storm wall at crest level of a dike clearly above SWL, uses the actual dike slope to calculate the wave breaker parameter. Results of the UGent-1 data on slopes cot(α) 2 to 3 lead to $\xi_{m-1,0}$ > 2.1 so were all classified as **non-breaking (ξ_{0p} > 2)**. The reduction factor was derived and linked to the dimensionless wall height h_{wall}/R_c which was the best possible dimensionless parameter to describe the results. The reduction factor **γ_v was defined in Eq. [4-4]**.

Results of the UGent-2 data on slope cot(α) = 6 lead to breaker parameters $\xi_{m-1,0}$ < 1 and were thus classified as **breaking** waves **(ξ_{0p} < 2)**. For these tests, no influence of the wall height was clearly visible, and a (first estimate) reduction factor **γ_v = 0.92** was derived for breaking waves.

Finally, it was attempted to predict the data from the Harlingen dataset by this **new procedure**. Results showed that it **works good for "high walls", with their toe above SWL ($h_{wall}/R_c \leq 1$) but not good for submerged walls with toe below SWL ($h_{wall}/R_c > 1$)**. For this latter, the original procedure by EurOtop (2007) gives better results. This was also **summarized in a flowchart in Figure 4-26**.

7.1.2 *Reduction of average overtopping discharges due to other crest modifications*

Several **other crest modifications were studied in the UGent-1 database for non-breaking waves**: a bullnose was added to the storm wall, a promenade at crest level was included or a combination of promenade and storm wall with/without bullnose was studied. Also a Stilling Wave Basin (SWB) was presented, which also is a combination of storm walls with a kind of promenade in between. The wave period or slope angle dependency was studied for each geometry, and it was shown that **reduction factors can not always be simply multiplied**. A case study was worked out at the end of Chapter 4, showing that all measures have a (highly) overtopping reducing capacity. **An overview of the obtained reduction factors is given in Table 4-1.**

7.2 *Flow depths and flow velocities on the promenade at crest level of a dike*

In between the two main topics of this PhD manuscript – reduction of wave overtopping and wave induced forces – some attention was paid to the overtopped bore that causes the impact on a storm wall at the end of a promenade. This was done by measuring and analyzing the flow parameters (flow depth and flow velocity) from the large scale GWK-experiments.

The literature review (Section 2.4) has shown that numerous authors have been studying overtopping flow parameters in the past. Most of them give a similar shape of the equations, with an exponential decay of both the flow depth and the flow velocity over the width of the crest or promenade, but nearly all of them publish different coefficients, indicating a large variation amongst different studies (see Figure 2-13 and Figure 2-14). The location of measuring is of importance. It's suggested not to measure too close to the seaward edge of the promenade since a transition zone with very turbulent bores exists. Unfortunately, literature does not provide a width of this transition zone. In the recordings from GWK, recordings at a location close to the storm wall showed clean signals and were used for analysis.

A manual analysis needed to be carried out to **identify incoming from reflected bores**, leading to 621 flow parameters maintained for further analysis, spread over 21 (short duration) tests. The analysis of the flow parameters h and U showed that results were scattered, but still in line with the orders of magnitude calculated from literature. Flows of 0.10m flow depth had velocities between 1m/s and 3m/s, flows of 0.50m flow depth had velocities between 2m/s and 7m/s.

The analysis also showed that **the maximum flow depth and maximum flow velocity from a storm did not necessarily occur in the same wave,** again a confirmation from what was found in literature. Scatter plots of the flow parameters indicated that there is an increasing trend of the flow parameters with the increasing wave height and with a decreasing freeboard. However, **no highly correlated relation between the (individual) overtopped bores and the (test averaged) incoming wave parameters** could be deducted. A link with individual overtopping volumes and individual wave impacts is more meaningful and was analyzed in Chapter 6.

7.3 *Wave-induced impacts on a storm wall*

For the structural design of the overtopping reducing measure, **knowledge of the wave impacts on these structures is required**. Quite some literature on wave impacts is available, but mostly on violent impacts on deep water vertical structures such as caissons. Also tsunami-impacts and impacts on crown walls of breakwaters have been studied in the past. The only research that comes close to the present work is carried out by Chen (2016) and Streicher et al. (2018) but works with broken waves on (very) shallow foreshores, unlike the tests with non-breaking waves carried out for the present research. Comparison with literature was not satisfying so new formulae have been developed.

Impacts were recorded in **three different test campaigns**, in three different laboratories, at **three different scales**: UGent-1, GWK and Hydralab. UGent (scale 1/10) and Hydralab (1/6) experiments had a very similar test set-up. The GWK (scale 1/1) experiments were somewhat different, due to a higher crset of the dike (higher crest freeboard A_c) and much shorter test durations. Table 3-12 and Table 3-13 gave an overview and comparison of the three test campaigns.

7.3.1 *The analysis of wave-induced impact recordings*

The impact signals and different ways of measuring and analyzing them were studied in detail in this work. Some important findings are summarized below:

The eigenfrequency of the structure was verified, and if it was too close to the frequency signals of the impacts this created unwanted **resonance. A low-pass filter** then had to be applied in postprocessing to filter out high unnatural oscillations of the impact recording**.**

The shape of the impact recording varied between a church-roof shape (high 1st dynamic peak and (much) lower 2nd quasi-static peak) and a twin-peak shape (both peaks are closer to each other and the 2nd peak was sometimes even a little higher than the 1st peak). **The highest impacts in the distribution showed a church-roof shape**.

The impacts were recorded in different ways. Integrated maximal pressure values seemed to be consistently somewhat higher than the maximal force values. In this manuscript **the force sensors were used** to derive prediction formulae and the information of the pressure sensors was used to study the pressure distribution over the height of the wall. **For the dynamic impact, the highest pressure value was registered near the height of the incoming flow depth**. For the quasi-static impact, a nice hydrostatic trend from the highest run-up level could be noticed. The point of application of the highest impacts was located near the still water line.

Wave induced impacts are individual values. The analysis showed **that all impacts in a test are statistically best described by a Weibull PDF**. Literature advised to avoid F_{max} due to the stochastic behavior of impact forces and the dependency of the maximum force from the number of waves in a storm. Based on the work by Goda (1985), **the low exceedance value $F_{1/250}$ was proposed in this work**. This is the average force value of 1/250th of the total number of incoming waves in one test. This work **made the force dimensionless by dividing through $\rho g R_c^2$**.

7.3.2 *Three methodologies for prediction formulae of wave-induced impacts*

After the detailed study of the impact measurements, new formulae were set up by means of three different methodologies. A **first approach 1a** linked $F_{1/250}$ to the incoming wave parameters. **Approach 1b** described the full Weibull probability distribution function of the impacts, of which the shape and scale parameters were also linked to the incoming wave parameters. From this distribution, the value $F_{1/250}$ could be calculated. A completely different **approach 2** was also investigated, where overtopping volumes were linked to overtopping flows and eventually to impacts on the storm wall. This all was **summarized in a flow chart for every approach:** Figure 6-54 for approach 1a, Figure 6-63 for approach 1b and Figure 6-78 for approach 2.

In this work, **approach 1a was proposed as the most reliable and straightforward methodology** to calculate wave impacts on structures. The shape of approach 1a was given in Eq. [6-3]:

$$\frac{F}{\rho g R_c^2} = a_F \cdot exp\left(-b_F \frac{R_C}{H_{m0}}\right) \qquad [6\text{-}3]$$

Through curve fitting, the coefficients a_F and b_F were defined, for the structure with promenade and storm wall, but also for the other reducing geometries with storm walls. The coefficients are summarized in Table 6-4. It's important to note that these coefficients are only valid for the geometries and the parameter ranges that belong to the tests on those geometries, summarized in Table 6-5. Mainly the ratios A_c/H_{m0} (0.2 to 1.2) and R_c/H_{m0} (0.9 to 2.0) are important. More information on the geometries and parameter ranges can be found in Chapter 3.

By comparing the results from the three test campaigns, from different laboratories at different scale, **scale and model effects were studied**. It seemed to be **difficult to separate** these effects, and results were not fully as could be expected from literature related to air bubbles in bores and salt versus fresh water. However, the conclusion was that the **order of magnitude of both effects was about 20%**, and both effects seemed to balance each other.

8 Recommendations for further research

The previous chapter has shown that the research objectives stated in the beginning of this work have been met. However, based on the analysis and the conclusions in this work, there are a number of items that can be investigated further. Those will be listed in the current chapter.

Now that an extended database has been developed, an Artificial Neural Network can be trained. For overtopping, this is currently ongoing work by the University of Bologna and latest update was recently presented at ICCE 2018 (Zanuttigh et al., 2018). The database can also be used to validate numerical models. Also this is ongoing work by De Finis et al. (n.d.). By means of an ANN or a numerical model, the geometrical boundaries can be stretched and more constructions or parameter variations can be tested.

<u>Reduction of wave overtopping</u>

The reduction of wave overtopping discharges was summarized in flowchart Figure 4-26. The split between the EurOtop (2007) procedure and newly developed procedure is based on the location of the wall: $\mathbf{h_{wall}/R_c}$. Since another difference between the Harligen dataset and the UGent-1/2 datasets is the relative height of the wall over the structure's height, it is worth investigating if this improves the **decision making tool** in which procedure to follow.

Another main question is how the new procedure really works for **non-breaking waves on geometries with a storm wall at crest level**. Few tests in UGent-2 were carried out indicating only a small influence $\gamma_v = 0.92$ is present, but the boundary conditions of this dataset were limited and the scale was very small. Does the wall height have an influence on mild slopes after all? How do slopes 1:3 or 1:4 behave in hydraulic conditions with shorter waves ($\xi_{0p} < 2$), but a storm wall at crest level of this dike? Those questions can't yet be answered by the new procedure.

A last recommendation for future research on the reduction of wave overtopping is the difference in behavior of a bullnose/parapet for horizontal oriented wave run-up on a dike versus vertical wave run-up on a caisson breakwater. Both have been investigated individually, but it's interesting to study the relationship with the incoming flow.

<u>Flow parameters</u>

Chapter 5 has shown the difficulties related to flow depth and flow velocity measurements. It would be of interest to continue the study on the flow parameters. The exponential decay should be studied more in depth, better knowledge on the **interaction between incoming and reflective bores** with a **separation methodology** is an absolute must, and also the effect of (reflection by) a storm wall on the flow parameters should be tested. Some of these questions could be solved by running a number of tests on an empty promenade followed by a repetition of those tests on a promenade with storm wall. (High Speed) Video analysis might be helpful here, but most promising to study the flow parameters would be with **numerical models**. In this way, a full flow field can be studied in detail and it might even be possible to analyze the acceleration of the overtopped bore at the moment of the impact. Force is mass times the acceleration, which might lead to new insights and physical relationships.

<u>Wave induced forces</u>

For wave induced forces also a few recommendations are proposed. It is advised to widen the test program to **study the influence of varying wall heights and promenade widths** on the wave-induced forces. The height of the wall should also be increased up to a point where wave overtopping over the wall no longer occures, in order to evaluate a possible reduction of the impacts related to loss of energy through overtopping over the wall.

The **effect of 3D tests** (waves with obliquity and spreading) should be investigated on a promenade, since the reflection pattern can be different compared to perpendicular incoming waves. Possible also artificial roughness elements can be added, since different air entrainment could lead to different results. It's a question if a reduction (or increasing?) factor like γ_β or γ_f could be added to the developed prediction formulae?

If possible, also measurements of individual overtopping volumes would be of interest. This information could replace Eq. [2-55] with an empirical relation determined specifically for this test set-up.

Related to the force and pressure recordings, it is recommended to further investigate the **differences between dynamic and quasi-static impact**. The amount of energy below each of those impacts and its relation to the structural strength of the construction that is impacted, as well as the rise time and duration of each phase in the impact, is of interest for structural engineers. Also a more precise location of the **point of application of the impact** related to the incoming flow depth would be of interest for the structural design.

Table 6-4 provided an overview of all a_F and b_F coefficients to be used in Eq. [6-3] for the different geometries. The b_F-values seem to be close to each other and can maybe be grouped. Also the a_F-values can maybe be grouped depending on the presence of a bullnose, or make a_F and b_F a function of the promenade width and wall height and/or presence of the bullnose. It would be beneficial to study this in combination with a wider parameter range (promenade width and wall height) to be tested.

To conclude, when new measurements on different scales become available, it would be of interest to **investigate scale and model effects further**, in order to try to separate both influences. Therefore, the test set-ups in the different scales have to be as comparable as possible, since any variation in any possible parameter (geometrical, hydraulic, recording equipment, …) can interfere with other influences and make a separation between scale effects and model effects impossible.

9 Bibliography

Allsop, W., Besley, P. and Madurini, L. (1995). Overtopping performance of vertical walls and composite breakwaters, seawalls and low reflection alternatives. *Final report of Monolithic Coastal Structures (MCS) project.*

Altomare, C., Verwaest, T., Suzuki, T. and Trouw, K. (2014). Characterization of wave impacts on curve faced storm return walls within a stilling wave basin concept. In *Proceedings of the 34th International Conference on Coastal Engineering (ICCE 2014)*. Seoul, Korea.

Altomare, C., Crespo, A. J. C., Domínguez, J. M., Gómez-Gesteira, M., Suzuki, T. and Verwaest, T. (2015). Applicability of Smoothed Particle Hydrodynamics for estimation of sea wave impact on coastal structures. *Coastal Engineering*, *96*, 1–12. https://doi.org/10.1016/j.coastaleng.2014.11.001

Amanti, P. and Franco, L. (2001). Performance of overspill basin on top of breakwaters. In *International conference on ocean engineering* (pp. 41–46). Madras, India.

Audenaert, S. and Duquet, V. (2012). *Wave overtopping over sea dikes and wave impacts on storm walls (In Dutch. Original title: Golfovertopping over zeedijken – krachten op stormmuur)*. Master thesis. Ghent University.

Beels, C. (2005). *Experimental research to reduce wave overtopping over smooth dike slopes (In Dutch. Original title: Experimenteel onderzoek naar de reductie van golfoverslag bij dijken)*. Master thesis. Ghent University.

Bellotti, G., Van Doorslaer, K., Romano, A., Baelus, L., Caceres, I., De Rouck, J. and Franco, L. (2014). Forces on (flood)walls and buildings by wave overtopping. In *Proceedings of the Hydralab IV Joint User Meeting*.

Boderé, T. and Vanhouwe, G. (2010). *Reduction of wave overtopping at smooth dike slopes. A combinaton of a promenade and a storm wall. (In Dutch. Original title: Reductie van golfoverslag bij een gladde dijk: combinatie van een berm en een stormmuur)*. Master thesis. Ghent University.

Bosman, G., Van Der Meer, J. W., Hoffmans, G., Schüttrumpf, H. and Verhagen, H. J. (2008). Individual overtopping events at dikes. In *Proceedings of the 31st International Conference on Coastal Engineering (ICCE 2008)* (pp. 2944–2956). Hamburg, Germany: World Scientific Publishing Company.

Bullock, G. N., Crawford, A., Hewson, P., Walkden, M. J. and Bird, P. A. (2001). The influence of air and scale on wave impact pressures. *Coastal Engineering*, *42*(4), 291–312. https://doi.org/10.1016/s0378-3839(00)00065-x

Burcharth, H. F. (1993). *The design of breakwaters.* Aalborg.

Burcharth, H. F. and Andersen, T. L. (2006). Overtopping of rubble mound breakwaters with front reservoir. In *Proceedings of the 30th International Conference on Coastal Engineering (ICCE 2006)* (pp. 4605–4615). San Diego, USA: World Scientific Publishing Company.

Cappietti, L. and Aminti, P. L. (2012). Laboratory Investigation on the Effectiveness of an Overspill Basin in Reducing Wave Overtopping on Marina Breakwaters. In *Proceedings of the 33rd International Conference on Coastal Engineering (ICCE 2012)*. Santander, Spain. https://doi.org/10.9753/icce.v33.structures.20

Castellino, M., Sammarco, P., Romano, A., Martinelli, L., Ruol, P. and Franco, L. (2018). Large impulsive forces on recurved parapets under non-breaking waves. A numerical study. *Coastal Engineering*, *136* (May 2017), 1–15. https://doi.org/10.1016/j.coastaleng.2018.01.012

Chen, X. (2016). *Impacts of overtopping waves on buildings on coastal dikes*. PhD Thesis. TU Delft.

Chen, X., Hofland, B., Altomare, C., Suzuki, T. and Uijttewaal, W. (2015). Forces on a vertical wall on a dike crest due to overtopping flow. *Coastal Engineering*, *95*, 94–104. https://doi.org/10.1016/j.coastaleng.2014.10.002

Chen, X., Hofland, B., Altomare, C. and Uijttewaal, W. (2014). Overtopping flow impact on a vertical wall on a dike cest. In *Proceedings of the 34th International Conference on Coastal Engineering (ICCE 2014)*. Seoul, Korea.

Coeveld, E. M., Busnelli, M. M., van Gent, M. R. A. and Wolters, G. (2006). Wave overtopping of rubble mound breakwaters with crest elements. In *Proceedings of the 30th International Conference on Coastal Engineering (ICCE 2006)*. San Diego, USA: World Scientific Publishing Company.

Cornett, A., Li, Y. and Budvietas, A. (1999). Wave overtopping at chamfered and overhanging vertical structures. In *Proceedings International Workshop on Natural Disasters by Storm Waves and Their Reproduction in Experimental Basins* (p. 14).

Cross, R. (1967). Tsunami surge forces. *Journal of the Waterways and Harbors Division*.

Cumberbatch, E. (1960). The impact of a water wedge on a wall. *Journal of Fluid Mechanics*, *7*, 353–374.

Dalrymple, R. A., Knio, O., Cox, D. T., Gomez-Gesteira, M. and Zou, S. (2001). Using a Lagrangian Particle Method for Deck Overtopping. *Waves*.

De Finis, S., Romano, A. and Bellotti, G. (no date). Numerial and laboratory analysis of post-overtopping wave impacts on a storm wall for a dike-promenade structure. *Submitted for Journal of Coastal Engineering*.

De Rouck, J., Van Doorslaer, K., Versluys, T., Ramachandran, K., Schimmels, S., Kudella, M. and Trouw, K. (2012). Full scale impact tests of an overtopping bore on a vertical wall in the large wave flume (GWK) in Hannover. In *Proceedings of the 33rd International Conference on Coastal Engineering (ICCE 2012)*. Santander, Spain.

De Rouck, J., Verhaeghe, H. and Geeraerts, J. (2009). Crest level assessment of coastal structures - General overview. *Coastal Engineering*, *56*(2), 99–107. https://doi.org/10.1016/j.coastaleng.2008.03.014

Den Heijer, F. (1998). *Wave overtopping and forces at water retaining structures - report H2014 (in Dutch. original title: golfoverslag en krachten bij waterkerende constructies).*

EurOtop. (2007). *Wave overtopping of sea defences and related structures: Assessment manual*. Pullen, T., Allsop, M. W. H., Bruce, T., Kortenhaus, A., Schuttrumpf, H., van der Meer, J. W.

EurOtop. (2016). *Manual on wave overtopping of sea defences and related structures An overtopping manual largely based on European research, but for worldwide application*. van der Meer, J. W., Allsop, W., Bruce, T., De Rouck, J., Kortenhaus, A., Pullen, T., Schüttrumpf, H., Troch, P., Zanuttigh, B. Retrieved from http://www.overtopping-manual.com/index.html

Formentin, S. M., Zanuttigh, B. and van der Meer, J. W. (2017). A Neural Network Tool for Predicting Wave Reflection, Overtopping and Transmission. *Coastal Engineering Journal*, *59*(1). https://doi.org/10.1142/s0578563417500061

Formentin, S. M., Zanuttigh, B., van der Meer, J. W. and Lara, J. (2014). Overtopping flow characteristics at emerged and overwashed dikes. In *Proceedings of the 34th International Conference on Coastal Engineering (ICCE 2014)*. Seoul, Korea. https://doi.org/10.9753/icce.v34.structures.7

Franco, L., de Gerloni, M. and van der Meer, J. W. (1994). Wave overtopping on vertical and composite breakwaters. In *Proceedings of the 24th International Conference on Coastal Engineering (ICCE 1994)* (pp. 1030–1045). Kobe, Japan: American Society of Civil Engineers (ASCE).

Gallach Sanchez, D. (2018). *Experimental study of wave overtopping performance of steep low-crested structures*. PhD thesis. Ghent University. Retrieved from https://biblio.UGent.be/publication/8569975

Geeraerts, J. and De Rouck, J. (2008). Reduction of wave overtopping at seadikes: stilling wave basin – 3D research. In *Proceedings of the 31st International Conference on Coastal Engineering (ICCE 2008)* (pp. 3157–3163). Hamburg, Germany: World Scientific Publishing Company.

Geeraerts, J., De Rouck, J., Beels, C., Gysens, S. and De Wolf, P. (2006). Reduction of wave overtopping at seadikes: stilling wave basin (SWB). In *Proceedings of the 30th International Conference on Coastal Engineering (ICCE 2006)* (pp. 4680–4691). San Diego, USA: World Scientific Publishing Company.

Gier, F., Schüttrumpf, H., Lorke, S., Mönnich, J., Beton, B. and van der Meer, J. W. (2012). Stability of Interlocked Pattern Placed Block Revetments. In *Proceedings of the 33rd International Conference on Coastal Engineering (ICCE 2012)*. Santander, Spain.

Goda, Y. (1985). Random seas and design of maritime structures. Tokyo: WORLD SCIENTIFIC.

Goda, Y. (2009). Derivation of uni fi ed wave overtopping formulas for seawalls with smooth , impermeable surfaces based on selected CLASH datasets. *Coastal Engineering, 56*(4), 385–399. https://doi.org/10.1016/j.coastaleng.2008.09.007

Günbak, A. and Ergin, A. (1983). Damage and repair of the Antalya harbour breakwater. In *Conference on Coastal Structures*. Alexandria, Egypt.

Hamilton, D. G. and Hall, K. R. (1992). Preliminary analysis of the stability of rubble mound breakwater crown walls. In *Proceedings of the 23rd International Conference on Coastal Engineering (ICCE 1992)* (pp. 1217–1230). Venice, Italy: American Society of Civil Engineers (ASCE).

Hughes, S. A. (1993). *Physical Models and Laboratory Techniques in Coastal Engineering*. World Scientific Publishing Company.

Hughes, S. A. (2015). Hydraulic Parameters of Overtopping Wave Volumes. In *Coastal Structures and Solutions to Coastal Disasters 2015: Resilient Coastal Communities - Proceedings of the Coastal Structures and Solutions to Coastal Disasters Joint Conference 2015*. https://doi.org/10.1061/9780784480304.075

Hughes, S. A., Thornton, C., van der Meer, J. W. and Scholl, B. N. (2012). Improvements in describing wave overtopping processes. In *Proceedings of the 33rd International Conference on Coastal Engineering (ICCE 2012)*. Santander, Spain. https://doi.org/10.9753/icce.v33.waves.35\

IPCC. (2014). *Climate Change 2014 Synthesis Report Summary Chapter for Policymakers*. *Monika Rhein*. Gian-Kasper Plattner.

Jensen, B., Jacobsen, N. G. and Christensen, E. D. (2014). Investigations on the porous media equations and resistance coefficients for coastal structures. *Coastal Engineering*, *84*, 56–72. https://doi.org/10.1016/j.coastaleng.2013.11.004

Jensen, O. (1984). *A monograph on rubble mound breakwaters*. Horsholm, Danmark.

Kortenhaus, A., Geeraerts, J. and Hassan, R. (2006). *Wave run-up and overtopping of sea dikes with and without stilling wave basin under 3D wave attack (DIKE-3D). Final Report, Braunschweig, Germany*.

Kortenhaus, A., Haupt, R. and Oumeraci, H. (2001). Design aspects of vertical walls with steep foreland slopes. In *ICE* (pp. 221–232).

Kortenhaus, A. and Oumeraci, H. (1998). Classification of Wave Loading on Monolithic Coastal Structures. In *Proceedings of the 26th International Conference on Coastal Engineering (ICCE 1998)* (Vol. 1, pp. 867–880). Copenhagen, Denmark: American Society of Civil Engineers (ASCE). https://doi.org/10.9753/icce.v26.

Kortenhaus, A., Pearson, J., Bruce, T., Allsop, W. and van der Meer, J. W. (2003). Influence of Parapets and Recurves on Wave Overtopping and Wave Loading of Complex Vertical Walls. In *Coastal Structures*. https://doi.org/10.1061/40733(147)31

Lorke, S., Bruning, A., van der Meer, J. W., Schüttrumpf, H., Bornschein, A., Gilli, S., … Schlutter, F. (2010). On the effect of current on wave run-up and wave overtopping. In *Proceedings of the 32nd International Conference on Coastal Engineering (ICCE 2010)* (pp. 1–15). Shanghai, China.

Lorke, S., Scheres, B., Schüttrumpf, H., Bornschein, A. and Pohl, R. (2012). Physical Model Tests on Wave Overtopping and Flow Processes on dike crests influenced by wave-current interaction. In *Proceedings of the 33rd International Conference on Coastal Engineering (ICCE 2012)* (pp. 1–13). Santander, Spain. https://doi.org/10.9753/icce.v33.waves.34\

Mansard, E. P. D. and Funke, E. R. (1980). The measurement of incident and reflected spectra using a least squares method. In *Proceedings of the 17th International Conference on Coastal Engineering (ICCE 1980)* (pp. 154–172). Sydney, Australia: American Society of Civil Engineers (ASCE).

Martinelli, L., Ruol, P., Volpato, M., Favaretto, C., Castellino, M., Girolamo, P. Deand Franco, L. (2018). Experimental investigation on non-breaking wave forces and overtopping at the recurved parapets of vertical breakwaters. *Coastal Engineering*, *141*(September), 52–67. https://doi.org/10.1016/j.coastaleng.2018.08.017

Mertens, T., De Wolf, P., Verwaest, T., Trouw, K., De Nocker, L. and De Coudere, K. (2008). An integrated master plan for Flanders future coastal safety. In *Proceedings of the 31st International Conference on Coastal Engineering (ICCE 2008)* (pp. 4017–4028). Hamburg, Germany: World Scientific Publishing Company.

Molines, J. and Medina, J. R. (2015). Calibration of overtopping roughness factors for concrete armor units in non-breaking conditions using the CLASH database. *Coastal Engineering*, *96*, 62–70. https://doi.org/10.1016/j.coastaleng.2014.11.008\

Oumeraci, H., Allsop, W., De Groot, M., Crouch, R. and Vrijling, J. (1999). *PROVERBS: probabilistic design tools for vertical breakwaters. MAST – EU Project*.

Oumeraci, H., Klammer, P. and Partenscky, H. W. (1993). Classification of breaking wave loads on vertical structures. *Journal of Waterway, Port, Coastal and Ocean Engineering*, *119*(4), 381–397.

Owen, M. W. (1980). Design of seawalls allowing for wave overtopping. Technical report, HR Wallingford

Pearson, J., Bruce, T., Kortenhaus, A. and van der Meer, J. W. (2004). Effectiveness of recurve wave walls in reducing wave overtopping on seawalls and breakwaters. In *Proceedings of the 29th International Conference on Coastal Engineering (ICCE 2004)* (pp. 4404–4416). Lisbon, Portugal: World Scientific Publishing Company.

Pedersen, J. (1996). *Wave forces and overtopping on breakwaters crown walls: an experimental study.* Aalborg.

Ramachandran, K., Genzalez, R. R., Oumeraci, H., Schimmels, S., Kudella, M., Van Doorslaer, K., Trouw, K. (2012a). Loading of vertical walls by overtopping bores using pressure and force sensors - A large scale model study. In *Proceedings of the 33rd International Conference on Coastal Engineering (ICCE 2012)*. Santander, Spain.

Ramachandran, K., Genzalez, R. R., Oumeraci, H., Schimmels, S., Kudella, M., Van Doorslaer, K., Trouw, K. (2012b). Loading of vertical walls by overtopping bores using pressure and force sensors – a large scale model study. In *Proceedings of the 4th International Conference of the Application of Physical Modelling in Coastal and Port Engineering and Science (Coastlab12)*. Ghent.

Romano, A., Bellotti, G., Briganti, R. and Franco, L. (2015). Uncertainties in the physical modelling of the wave overtopping over a rubble mound breakwater: The role of the seeding number and of the test duration. *Coastal Engineering*, *103*, 15–21. https://doi.org/10.1016/j.coastaleng.2015.05.005\

Schüttrumpf, H. (2001). *Wave run-up at sea dikes - experimental and theoretical research (In German. Original title: Wellenüberlaufströmung bei Seedeichen-Experimentelle und theoretische Untersuchungen)*. PhD thesis. T.U. Braunschweig. Retrieved from http://www.digibib.tu-bs.de/?docid=00001216

Schüttrumpf, H., Müller, J. and Oumeraci, H. (2002). Overtopping flow parameters on the inner slope of seadikes. In *Proceedings of the 28th International Conference on Coastal Engineering (ICCE 2002)* (pp. 2116–2127). Wales, United Kingdom: World Scientific Publishing Company. https://doi.org/10.1142/9789812791306_0178\

Schüttrumpf, H. and Oumeraci, H. (2005). Layer thicknesses and velocities of wave overtopping flow at seadikes. *Coastal Engineering*, *52*(6), 473–495. https://doi.org/10.1016/j.coastaleng.2005.02.002

Schüttrumpf, H. and van Gent, M. R. A. (2003). Wave Overtopping at Seadikes. In *Coastal Structures*. https://doi.org/10.1061/40733(147)36

SPM. (1977). *The Shore Protection Manual*. U.S. Army Coastal Engineering Research Center.

Stansby, P. K. (2003). Solitary wave run-up and overtopping by a semi-implicit finite-volume shallow water Bousinesq model. *Hydr. Res.*, *41*(6), 639–647.

Steendam, G. J., van der Meer, J. W., Van Steeg, P. and Joosten, R. (2018). Wave impacts at small and real scale for the stepped sloped seawall design at Den Oever. In *Proceedings of the 36th International Conference on Coastal Engineering (ICCE 2018)*. Baltimore, USA.

Streicher, M., Kortenhaus, A., Gruwez, V., Hofland, B., Chen, X. and Hughes, S. A. (2018). Prediction of dynamic and quasi-static impacts on vertical sea walls caused by an overtopped water wedge. In *Proceedings of the 36th International Conference on Coastal Engineering (ICCE 2018)*. Baltimore, USA.

Streicher, M., Kortenhaus, A. and Hohls, C. (2016). Analysis of post overtopping flow impacts on a vertical wall at the Belgian Coast. In *Proceedings of the 6th International Conference of the Application of Physical Modelling in Coastal and Port Engineering and Science (Coastlab16)*. Ottawa, Canada.

TAW. (2002). *Technical report wave run-up and wave overtopping at dikes*. Technical Advisory Committee on Flood Defence, Delft, The Netherlands.

Trouw, K., Mertens, T., Vermander, J., Verwaest, T., Bolle, A., Van Doorslaer, K. and De Rouck, J. (2012). Design of storm return walls for the masterplan for coastal safety: from conceptual to detailed design. In *Proceedings of the 4th International Conference of the Application of Physical Modelling in Coastal and Port Engineering and Science (Coastlab12)*. Ghent.

Tuan, T. Q. (2013). Influence of Low Sea-Dike Crown-Walls on Wave Overtopping Discharge. *Coastal Engineering Journal*, *55*(4), 1350013-1-1350013–1350023. https://doi.org/10.1142/s0578563413500137

USACE (2001). *Coastal Engineering Manual*. United States Army Corps of Engineers

van der Meer, J. W. (1993). *Wave run-up and overtopping at dikes - report H2458 (in Dutch. original title: Golfoploop en golfoverslag bij dijken) - part I*.

van der Meer, J. W. (1997). *Wave run-up and overtopping at dikes - report H2458 (In Dutch. Original title: golfoploop en golfoverslag bij dijken) - Part II*.

van der Meer, J. W. and Bruce, T. (2014). New Physical Insights and Design Formulas on Wave Overtopping at Sloping and Vertical Structures. *Journal of Waterway, Port, Coastal and Ocean Engineering*. https://doi.org/10.1061/(ASCE)WW.1943-5460.0000221

van der Meer, J. W., Hardeman, B., Steendam, G. J., Schüttrumpf, H. and Verheij, H. (2010). Flow depths and velocities at crest and landward slope of a dike in theory and with the wave overtopping simulator. In *Proceedings of the 32nd International Conference on Coastal Engineering (ICCE 2010)*. Shanghai, China.

van der Meer, J. W. and Janssen, J. P. F. M. (1994). Wave run-up and wave overtopping at dikes and revetments. *Wave Forces on Inclined and Vertical Wall Structures*, (485), 1–27.

van der Meer, J. W., Provoost, Y. and Steendam, G. J. (2012). The wave run-up simulator, theory and a first pilot test. In *Proceedings of the 33rd International Conference on Coastal Engineering (ICCE 2012)*. Santander, Spain.

van der Meer, J. W., Thornton, C. and Hughes, S. A. (2011). Design and operation of the US Wave Overtopping Simulator. In *Coastal Structures*. WORLD SCIENTIFIC. https://doi.org/10.1142/9789814412216_0014

van der Meer, J. W., Verhaeghe, H. and Steendam, G. J. (2009). The new wave overtopping database for coastal structures. *Coastal Engineering*, *56*(2), 108–120. https://doi.org/10.1016/j.coastaleng.2008.03.012

Van Doorslaer, K. (2008). *Reduction of wave overtopping over dikes by means of a parapet (in Dutch. Orinal title: Reductie van golfoverslag over dijken door middel van een parapet*. Master thesis. Ghent University.

Van Doorslaer, K. and De Rouck, J. (2009a). Innovative crest design to reduce wave overtopping: Parapet and Stilling Wave Basin. In *Book of abstracts "An overview of marine research in Belgium anno 2009", 10th VLIZ Young Scientists' day* (p. 142). Ostend, Belgium.

Van Doorslaer, K., De Rouck, J. and Gysens, S. (2009b). Reduction of wave overtopping: from research to practice. In *Proceedings of the 4th International Short Conference on Applied Coastal Research (SCACR 2009)* (pp. 337–346). Barcelona.

Van Doorslaer, K. and De Rouck, J. (2010a). Reduction of wave overtopping on a smooth dike by means of a parapet. In *Proceedings of the 32nd International Conference on Coastal Engineering (ICCE 2010)*. Shanghai, China.

Van Doorslaer, K., De Rouck, J., Boderé, T., Vanhouwe, G. and Troch, P. (2010b). The influence of a berm and a vertical wall above SWL on the reduction of wave overtopping. In *Proceedings of the 3rd International Conference of the Application of Physical Modelling in Coastal and Port Engineering and Science (Coastlab10)*.

Van Doorslaer, K., De Rouck, J., Trouw, K., van der Meer, J. W. and Schimmels, S. (2012). Wave forces on storm walls, small and large scale experiments. *International Conference on Coastal and Port Engineering in Developing Countries (PIANC - COPEDEC VIII - 2012)*, 1–11. https://doi.org/10.13140/2.1.2319.1362

Van Doorslaer, K., De Rouck, J., Audenaert, S. and Duquet, V. (2015a). Crest modifications to reduce wave overtopping of non-breaking waves over a smooth dike slope. *Coastal Engineering*, *101*, 69–88. https://doi.org/10.1016/j.coastaleng.2015.02.004

Van Doorslaer, K., Romano, A., Bellotti, G., Altomare, C., Cáceres, I., De Rouck, J., van der Meer, J. W. (2015b). Force Measurements on Storm Walls Due to Overtopping Waves: A Middle-Scale Model Experiment. In *Coastal Structures*. https://doi.org/10.1061/9780784480304.069

Van Doorslaer, K. and De Rouck, J. (2016a). Wave overtopping over sea dikes and impact forces on storm walls. In *International conference on coastal and port engineering in developing countries (PIANC - COPEDEC IX - 2016)*. Rio De Janeiro.

Van Doorslaer, K., De Rouck, J. and van der Meer, J. W. (2016b). The reduction of wave overtopping by means of a storm wall. In *Proceedings of the 35th International Conference on Coastal Engineering (ICCE 2016)* (Vol. 35). Antalya, Turkye.

Van Doorslaer, K., Romano, A., De Rouck, J., and Kortenhaus, A. (2017). Impacts on a storm wall caused by non-breaking waves overtopping a smooth dike slope. *Coastal Engineering*, *120*(November 2016), 93–111. https://doi.org/10.1016/j.coastaleng.2016.11.010

Van Gent, M. R. A. (2001). *Low exceedance wave overtopping event. Internal report DC030202/H3803*.

Van Gent, M. R. A. (2002). *Low exceedance wave overtopping event. Internal report DC030202/H3803*.

van Gent, M. R. A., van den Boogaard, H. F. P. P., Pozueta, B. and Medina, J. R. (2007). Neural network modelling of wave overtopping at coastal structures. *Coastal Engineering*, *54*(8), 586–593. https://doi.org/10.1016/j.coastaleng.2006.12.001

Veale, W., Suzuki, T., Verwaest, T., Trouw, K. and Mertens, T. (2012). Integrated Design of Coastal Protection Works for the town of Wenduine, Belgium. In *Proceedings of the 33rd International Conference on Coastal Engineering (ICCE 2012)*. Santander, Spain. https://doi.org/10.9753/icce.v33.structures.70

Verhaeghe, H., De Rouck, J. and van der Meer, J. W. (2008). Combined classifier-quantifier model: A 2-phases neural model for prediction of wave overtopping at coastal structures. *Coastal Engineering*, *55*(5), 357–374. https://doi.org/10.1016/j.coastaleng.2007.12.002

Victor, L. (2012). *Optimization of the Hydrodynamic Performance of Overtopping Wave Energy Converters: Experimental Study of Optimal Geometry and Probability Distribution of Overtopping Volumes*.

Wong, P., Losada, I. J., Gattuso, J.-P., Hinkel, J., Khattabi, A., McInnes, K. L., Levy, A. (2014). *Coastal systems and low-lying areas*. Cambridge University Press (CUP).

Zanuttigh, B., Formentin, S. M. and van der Meer, J. W. (2016). Prediction of extreme and tolerable wave overtopping discharges through an advanced neural network. *Ocean Engineering*. Elsevier BV. https://doi.org/10.1016/j.oceaneng.2016.09.032

Zanuttigh, B., Formentin, S. M., van der Meer, J. W. and Van Doorslaer, K. (2018). Reduction of the wave overtopping discharge at dikes with crown walls and bullnoses. In *Proceedings of the 36th International Conference on Coastal Engineering (ICCE 2018)*. Baltimore, USA.

Zijlema, M., Stelling, G., and Smit, P. (2011). SWASH: An operational public domain code for simulating wave fields and rapidly varied flows in coastal waters. *Coastal Engineering*, *58*(10), 992–1012. https://doi.org/10.1016/j.coastaleng.2011.05.015